SDC 91-165
December 1991

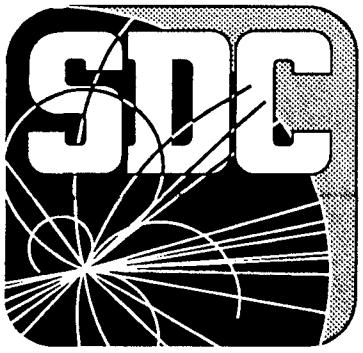

Proceedings of the Solenoidal Detector Collaboration Meeting at the SSC Lab

November 13-16, 1991
Superconducting Super Collider Laboratory
Dallas, TX

PLENARY SESSIONS

WEDNESDAY, NOVEMBER 13

Report by Spokesman	G. Trilling(LBL)
Report by Technical Manager	M. Gilchriese(LBL)
SDC Experimental Facilities	R. Stefanski(SSCL)
FNAL Test Beam Efforts	D. Green(Fermilab)

FRIDAY, NOVEMBER 15

Muon Group Report - Issues for the Technical Proposal	G. Feldman(Harvard)
SDC Computing	L. Price(Argonne)
Physics in the Proposal	K. Einsweiler(LBL)
Front End Electronics, Triggering, and DAQ	A. Lankford(Irvine)

SATURDAY, NOVEMBER 16

Report from Committee on Absorber Configuration	J. Siegrist(SSCL)
Report from Tracking Evaluation Committee	T. Kondo(KEK)

LPBautz:12/09/91

CALORIMETRY
(PARTIAL)

THURSDAY, NOVEMBER 14

Report of the Committee on Absorber Configuration	J. Siegrist(SSCL)
Preliminary Results from Hanging File Calorimeter	A. Byon-Wagner((FNAL)
Single Particle Calorimeter Simulations	L. Price(ANL)
e/h Simulation	D. Green(FNAL)
Single Particle and Jet Response of Several Calorimeter Models	C. Hearty(LBL)
Analytic Characterization of a Two Compartment Calorimeter	D. Groom(LBL)
Impact of the Hadron Calorimeter Absorber Choice on the Solenoid	R. Kephart((FNAL)
Calorimeter Cost Comparison Lead vs. Steel in HAC1	D. Scherbarth (Westinghouse)

FRIDAY, NOVEMBER 15

SDC Forward Calorimetry	W. Frisken(LBL/York)
Impact of EM Calorimeter Thickness on Resolution	C. Hearty(LBL)

ELECTRONICS

(PARTIAL)

WEDNESDAY, NOVEMBER 13

Options for Electronic Location Inside and Outside the SDC	C. Bebek(LBL)
Detector Layouts with Various Electronic Layouts and Placement	T. Thurston(SSCL)

THURSDAY, NOVEMBER 14

Silicon Strip Front End Electronics	H. Sadrozinski(UC/SC)
Muon Front End Analog Electronics (See paper under MUON SYSTEM)	J. Oliver(Harvard)
1st and 2nd Level Muon Triggers Based on the Jet Chamber System (See paper under MUON SYSTEM)	H. Sakamoto(KEK)

FRIDAY, NOVEMBER 15

Data Acquisition Status Report and Discussion of Sub-Detector Crates	E. Barsotti(FNAL)
SDC Second Level Trigger Using ASP	J. Brisson(CEN Saclay)
Report on Location of Electronics Inside or Outside Muon Steel	Electronics Working Group
Technical Assessment of the Electronics for the Central Tracking Options	Electronics Working Group

LPBautz:12/13/91

MUON SYSTEM

(PARTIAL)

NOVEMBER 13-14

Design of a JET-cell Chamber System for the SDC Muon Detector	KEK Muon Chamber Group
Concept for the Intermediate Region and BW3 vs. IW3	H. Iwasaki(KEK)
1st and 2nd Level Muon Triggers Based on the Jet Chamber Design	H. Sakamoto(KEK)
Forward Muon System	A. Skuja(Maryland)
SDC Muon Simulation at University of Illinois	Errede, et al.
Muon Matching Studies	S. Errede(Illinois)
BW3 - BW2 Radial Separation Studies	J. Wiss(Illinois)
Muon System Alignment Studies	J. Wiss(Illinois)
Muon Momentum Resolution	V. Slonim(Colorado)
Preliminary Proposal for SDC Muon Scintillator System	R. Thun(Michigan)
Possibility of Constructing a First Level Muon Trigger with Adjustable Pt Threshold	V. Molchanov(Protvino)
Muon Front End Analog Electronics	J. Oliver(Harvard)
Muon System Front End Electronics - Preliminary Conceptual Design Report	J. Oliver(Harvard)
Drift Tube Development at Minnesota	K. Heller(Minnesota)
Prototypes	R. Loveless(Wisconsin)

LPBautz:12/13/91

TRACKING

(PARTIAL)

WEDNESDAY, NOVEMBER 13

Silicon Tracking Conceptual Design Report	A. Seiden(UC/SC)
Modular Straw Outer Tracking System Conceptual Design Report	H. Ogren(Indiana)
Conceptual Design Scintillating Fiber Outer Tracking	D. Koltick(Purdue)
Conceptual Design Report for the Straw-Fiber Tracking System for the SDC	S. Reucroft (Northeastern)
Progress towards the Conceptual Design Report for the SDC Intermediate-Angle Tracking Detector	A. Sill(Rochester)

THURSDAY, NOVEMBER 14

Pattern Recognition in Silicon and Straw Tracking System	B. Hubbard(UC/SC)
Pattern Recognition in a Silicon and Scintillating Fiber SDC Tracking System	D. Adams(Rice)

LPBautz:12/12/91

APPENDIX

LIST OF PARTICIPANTS

PLENARY SESSIONS

WEDNESDAY, NOVEMBER 13

Report by Spokesman	G. Trilling(LBL)
Report by Technical Manager	M. Gilchriese(LBL)
SDC Experimental Facilities	R. Stefanski(SSCL)
FNAL Test Beam Efforts	D. Green(Fermilab)

FRIDAY, NOVEMBER 15

Muon Group Report - Issues for the Technical Proposal	G. Feldman(Harvard)
SDC Computing	L. Price(Argonne)
Physics in the Proposal	K. Einsweiler(LBL)
Front End Electronics, Triggering, and DAQ	A. Lankford(Irvine)

SATURDAY, NOVEMBER 16

Report from Committee on Absorber Configuration	J. Siegrist(SSCL)
Report from Tracking Evaluation Committee	T. Kondo(KEK)

LPBautz:12/09/91

Report by Spokesman

G. Trilling(LBL)

COLLABORATION MEETING

(November 13, 1991)
G. H. Trilling

Future meeting schedule

Status of new applicants

International news

HEP funding issues..relevance to SDC

PAC meeting

Comments on proposal

Major goals for this meeting

FUTURE SDC MEETINGS (1992)

Pisa	Jan. 8 (PM) to Jan. 11 (Noon)
SSCL	Feb. 26 - 29 (Special meetings Feb. 24 - 25)
Fermilab	April 13 - 15
KEK	May 25 - 28

INTERNATIONAL NEWS

Visit of Korean delegation to SSCL Oct. 30 - Nov. 1
- Physicists, government officials, industrialists
- Working group (Gilchriese (SDC), Sanders(GEM) for detectors)
- Potential support for both SSC and one detector
- Group views detector involvement as way to build up HEP in Korea

Visit by US SDC group to Beijing and IHEP
- Group strongly involved in radiation damage tests in collaboration with Fermilab

Taiwanese visit to SSCL expected in near future

Japanese visits: Schwitters/Happer/Friedman/Weinberg/Wojcicki
- Bromley
- Admiral Watkins/Happer
- President Bush visit postponed; new Prime Minister may go to Washington in near future

First East Asian/Pacific - U.S. Symposium on SSC Physics, Experiments, &Technology (Beijing May 21 - 24, 1992)

STATUS OF NEW APPLICANTS

~~VOTING UNDER WAY~~ NEW MEMBERS

LAFEX (Brazil)

University of Montreal

APPLICATIONS

IHEP - Protvino (USSR)

ITEP - Moscow (USSR)

University of Kansas

University of Oklahoma

CONCLUSION

If this group values the SDC program, and believes that doing SSC physics as soon as possible is the right goal, it needs to do its best to educate the councils of organized wisdom (HEPAP, new subpanel..), and,

make sure that HEPAP and the subpanel recognize the immediate and growing importance of the SSC detector efforts,

strongly resist pressures to solve base program shortfalls by subtraction from the SSC budget,

support the principle that the salaries of PRD physicists working on the SSC experimental physics program are a proper responsibility of the base program,

urge that the continued vitality of university and national laboratory groups engaged in the design and construction of SSC detectors be a continuing high priority of the U.S.HEP base program.

PAC MEETING
(October 3, 1991)

Discussed calorimeter & tracking volume decisions

Presented FY1992 budget request of $19.9M as minimum required

Presented detector cost estimate of $580M(FY1991 $)

Separate presentations on:
Tracking (Seiden), Calorimetry (Green), Muon system (Bensinger), Electronics (Lankford)

PAC CONCLUSIONS:
Support for $19.9M budget request
Concern about detector cost
Generally positive comments about SDC progress

Next PAC meeting: December 15-17
(This is the fourth this year).

HEP FUNDING ISSUES
(and their impact on the SSC program)

FY1993 HEP base program must take a 10% cut in "as spent" dollars relative to FY1992.

HEPAP Subpanel to be convened to recommend FY1994-FY1997 program under each of 3 scenarios:
Same funding as FY1993 in "as spent" dollars
Same funding as FY1993 in "constant" dollars
2-3% real growth per year after FY1993

RELEVANCE TO SSC/SDC EFFORT

HEPAP has misconception that SSC transition occurs only at SSC commissioning time or at most two or three years earlier. *In fact the SSC physics program (SDC) has already started, and and capabilities of the detectors are being defined NOW.*

Planned sharp rise in FY1993 base program support of physicists working in SSC/PRD has been eliminated.

Ability of base HEP program to help support activities relevant to the SSC detector effort may be much reduced.

It is extremely important that the new subpanel, in its planning exercises consider *both* the base program research *and* the simultaneously increasing level of SSC detector effort.

There may be moves in Congress or elsewhere to relieve base program tightness by subtraction of SSC funds. This would call into serious question the HEP community's commitment to SSC, and could undermine our strong efforts in international collaboration.

Technical Proposal Schedule

October 1	Assign coordinating editors
November 13	Detailed outline + final writing assignments and/or draft text
December 13	Zeroth draft submitted to chapter editors(and overall editors for comments)
January 3	Submit first draft to overall editors
January 31	Submit second draft to overall editors
February 21	Deliver final draft to SSCL for duplication of 150 copies
February 26-29	Review of final draft by collaboration and editors
March 23	Final printout of text with figures
March 25	Assemble, print and bind 40 copies
April 1	Submit 40 copies to SSCL

HOW TO FUND SDC DETECTOR?

Examine carefully the cost/physics balance for all pieces.
Can we still make reductions without running unacceptable risk.
This meeting is our last opportunity to do this before the T.P.

Get as much of this detector as possible from non-US sources.
We are beginning the process of defining responsibilities.
Can we fit U.S. SDC responsibilities (including installation & project management) into the allotted $275M +/- $50M?

There may well be shortfall between U.S. responsibilities for SDC/GEM and total U.S. funds available.
Potential methods of resolution:
Staging, further descopes, elimination of one detector...

CONCERN ON PROPOSAL PREPARATION
Chapter on Physics Performance

Since physics discovery is the total justification of this very expensive detector, we need to provide strong evidence that our proposed instrument can really tackle the challenges of the SSC era, while indicating that a lesser one could not do so.

In the continuing competition for support, comparisons will be made between GEM and SDC performance claims. We need to demonstrate that our detector has a strong physics capability, and that the SDC has a strong ability to assess that capability.

Kevin Einsweiler needs help in the preparation of the Physics Performance chapter.

Technical Proposal Production

Overall editors: D. Groom, W. Chinowsky, G. Trilling and M. Gilchriese

The SDC Technical Proposal - Coordinating Editors
1. Introduction - G. Trilling
2. Overview of the Detector - M. Gilchriese
3. Physics Performance - K. Einsweiler
4. Central Tracking System - A. Seiden
5. Superconducting Solenoid - A. Yamamoto
6. Calorimeter System - L. Nodulman
7. Muon System - G. Feldman
8. Electronics, Data Acquisition,Trigger and Control Systems - F. Kirsten
9. On-line Computing - A. Fry
10. Off-line Computing - L. Price
11. Safety - J. Elias
12. Experimental Facilities - T. Thurston
13. Installation and Commissioning - M. Harris
14. Test Beam Program - J. Siegrist
15. Cost and Schedule Summary - M. Gilchriese

SOME MAJOR GOALS FOR THIS MEETING

Presentation and discussion of tracking CDR's
Reduction of options and definition of future directions for tracking

Decision on central calorimeter absorber configuration

Definition of dimensions and scope of detector for purposes of proposal
Final attempt to optimize cost/benefit and reduce cost

Agreement on proposal chapter outlines and full definition of all writing responsibilities

Report by Technical Manager

M. Gilchriese(LBL)

Technical Proposal Production

Overall editors: D. Groom, W. Chinowsky, G. Trilling and M. Gilchriese

The SDC Technical Proposal - Coordinating Editors	Page Allocation
1. Introduction - G. Trilling	5
2. Overview of the Detector - M. Gilchriese	20
3. Physics Performance - K. Einsweiler	100
4. Central Tracking System - A. Seiden	100
5. Superconducting Solenoid - A. Yamamoto	25
6. Calorimeter System - L. Nodulman	100
7. Muon System - G. Feldman	100
8. Electronics Systems - F. Kirsten	150
9. On-line Computing - A. Fry	15
10. Off-line Computing - L. Price	50
11. Safety - J. Elias	10
12. Experimental Facilities - T. Thurston	20
13. Installation and Commissioning - M. Harris	20
14. Test Beam Program - J. Siegrist	10
15. Cost and Schedule Summary - M. Gilchriese	5
TOTAL	730

Technical Proposal Schedule

October 1	Assign coordinating editors
November 13	Detailed outline + final writing assignments and/or draft text
December 13	Zeroth draft submitted to chapter editors(and overall editors for comments)
January 3	Submit first draft to overall editors
January 31	Submit second draft to overall editors
February 21	Deliver final draft to SSCL for duplication of 150 copies
February 26-29	Review of final draft by collaboration and editors
March 23	Final printout of text with figures
March 25	Assemble, print and bind 40 copies
April 1	Submit 40 copies to SSCL

Section	Coordinating Editor	Status
1. Introduction	Trilling	OK
2. Overview of the Detector	Gilchriese	OK
3. Physics Performance	Einsweiler	Heard from
4. Central Tracking System	Seiden	Preliminary
5. Superconducting Solenoid	Yamamoto, Fast	OK
6. Calorimeter System	Nodulman	OK
7. Muon System	Feldman	OK
8. Electronics Systems	Kirsten	OK
9. Online Computing	Fry	OK
10. Offline Computing	Price	OK
11. Safety	Elias	Heard from
12. Experimental Facilities	Thurston	Heard from
13. Installation and Commissioning	Harris	Heard from
14. Test Beam Program	Siegrist	OK
15. Cost and Schedule Summary	Gilchriese	OK

SDC Meeting

SSC Laboratory

November 13, 1991

M. G. D. Gilchriese

- **Status of Technical Proposal and related documents**
- **Detector issues and decisions at this meeting**
- **Status of underground/surface facilities -> R. Stefanski**

Design Decisions

- Technical Proposal must represent a consistent and coherent design with minimum number of options
- "Freeze" parameters with minimal number of well defined options and then reduce options - see schedule
- Many changes will occur later(after submission of Technical Proposal).

Other Documents Related to Technical Proposal

- Cost/schedule book. Coordinators: W. Edwards, D. Etherton
  - See schedule of events. This is very tight and requires detailed knowledge of detector parameters => design decisions!
- SDC Project Management Plan: Coordinators: T. Elioff, T. Kirk
  - First draft by December 2
- Preliminary hazards analysis. Coordinator: J. Elias
  - Schedule and preliminary assignments established

Decisions and Reviews

Tracking system - initial cut	This meeting
Central calorimeter absorber configuration	This meeting
Electronics inside or outside detector	This meeting
Radius of barrel toroid	This meeting
Freeze basic layout of muon system	This meeting
Central calorimeter design frozen	????
Electronics baseline(+ options) frozen	Feb. 1, 1992??
Forward calorimeter option(s) selected	Feb. 1, 1992
Barrel muon chamber selected	Feb. 1, 1992
Tracking system option(s) selected	Feb. 1, 1992

Milestone	Date
Costing Milestones:	
Kickoff Technical Proposal Costing/Scheduling	10/24/91
Submit Revised WBS & Dictionary	11/08/91
Release Costing/Scheduling Procedures Book	11/11/91
Submit Descoped Cost Estimate & Contingency	11/22/91
Descope Roll-up #1	11/27/91
Prelim. Draft Cost Book Complete	12/20/91
Submit 2nd Descope Iteration WBS & Dictionary	1/08/92
Submit 2nd Iteration Cost Estimate & Contingency	1/17/92
Descope Roll-up #2	1/22/92
Independent Reviews Completed	2/19/92
Final Roll-up	3/02/92
Final Cost Book Complete	3/04/92
Submit Cost Book	4/01/92
Scheduling Milestones:	
Kickoff Technical Proposal Costing/Scheduling	10/24/91
Release Costing/Scheduling Procedures Book	11/11/91
2nd Iteration of Subsystem Schedules Submitted	11/22/91
2nd Iteration of Subsystem Schedules Reviewed	12/02/91
Integration of 2nd Iteration Schedules Complete	12/07/91
Prelim. Draft Schedule Book Complete	12/20/91
Submit 3rd Iteration of Subsystem Schedules	1/20/92
Review 3rd Iteration Schedules	2/17/92
Integrate 3rd Iteration Schedules	3/02/92
Submit Schedule Book	4/01/92

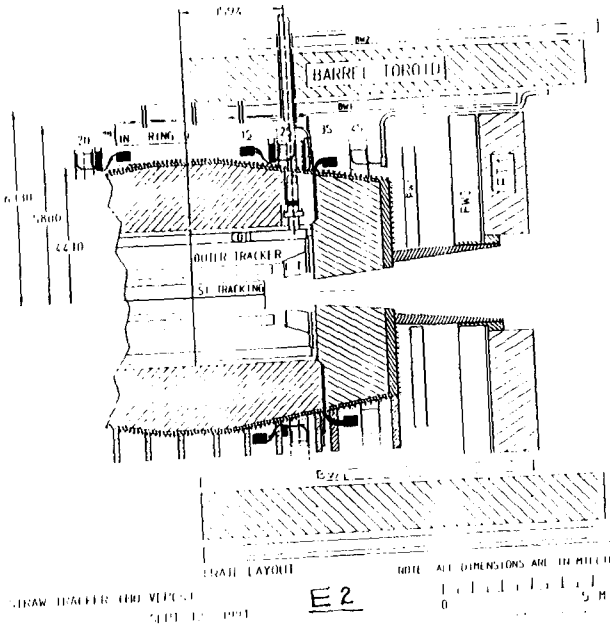

0033

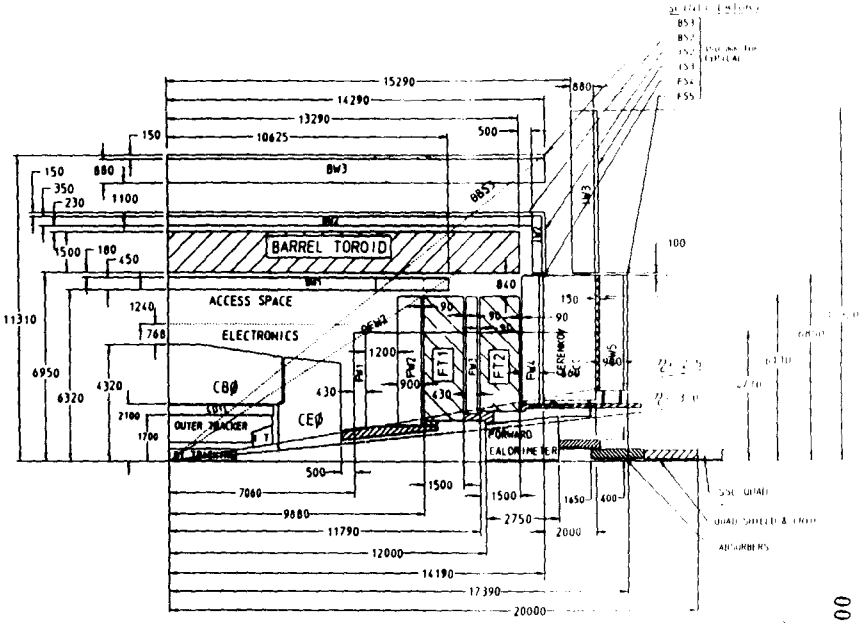

NOTE ALL DIMENSIONS ARE IN MILLIMETERS

SDC DETECTOR DIMENSIONS
LBL DWG# 2300375 9/30/91 D SHUMAN

0031

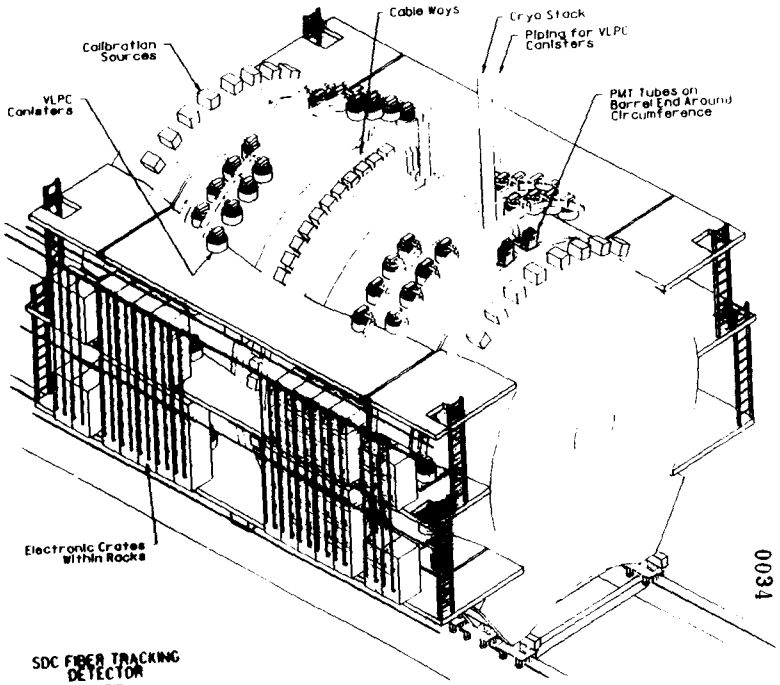

SDC FIBER TRACKING DETECTOR

0034

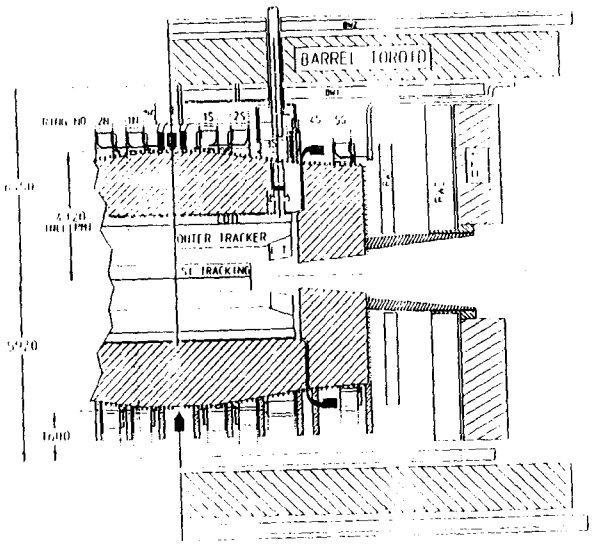

SECTION SHOWING OCTANT 1 CABLEWAY

NOTE ALL DIMENSIONS ARE IN MILLIMETERS

0032

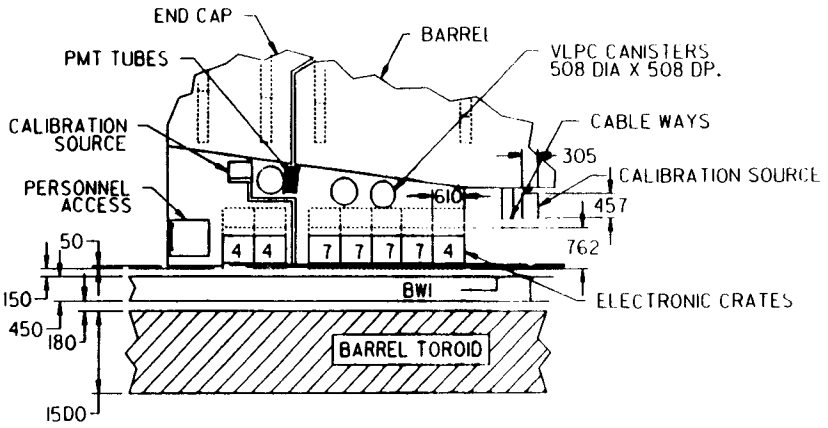

CALORIMETER - DETAIL B
FIBER TRACKER OPTION

SDD000064

0037

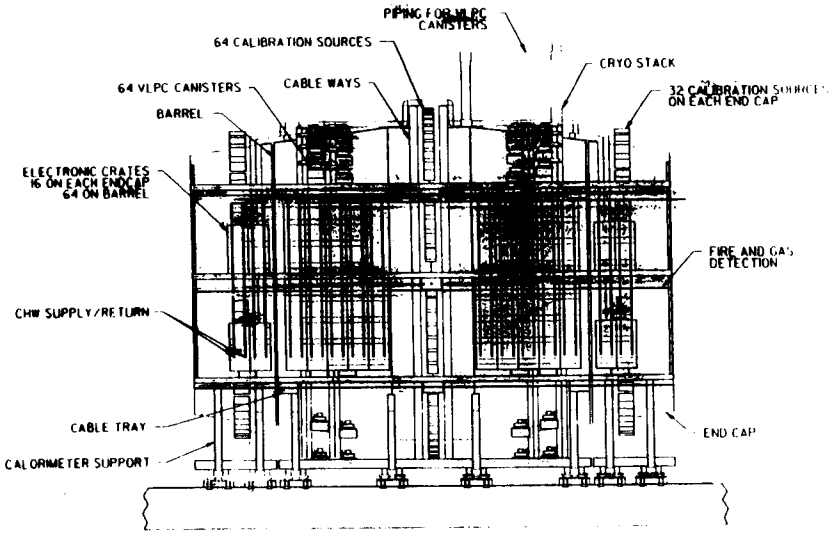

CALORIMETER ELEVATION VIEW - SIDE
FIBER TRACKER OPTION

SDD000068

0035

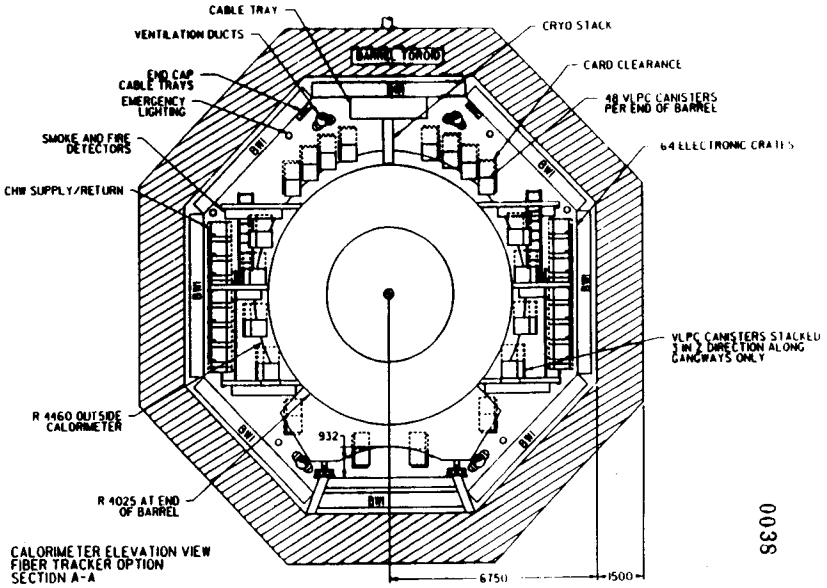

CALORIMETER ELEVATION VIEW
FIBER TRACKER OPTION
SECTION A-A

SDD000047

0038

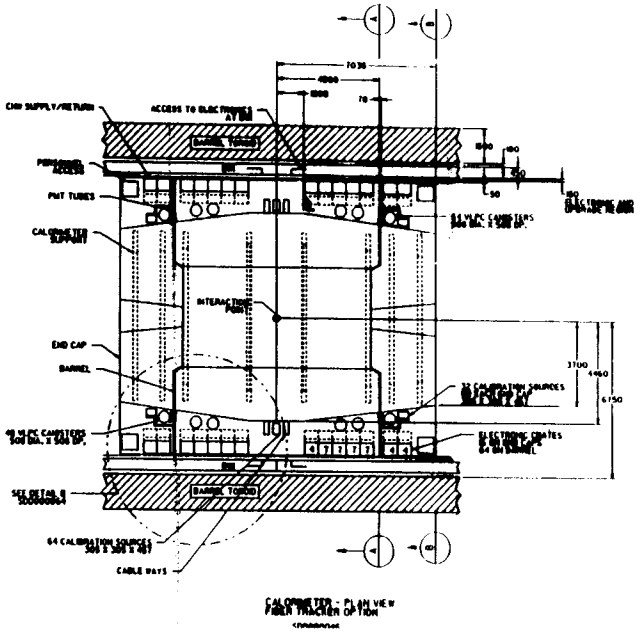

0036

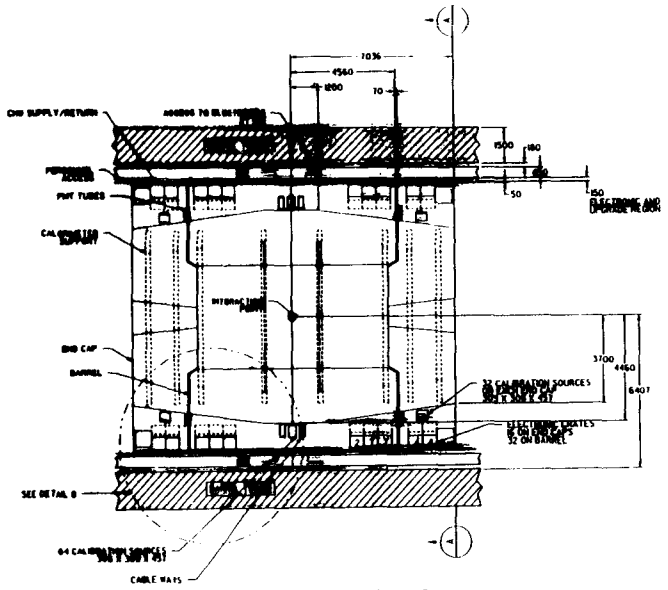

0041

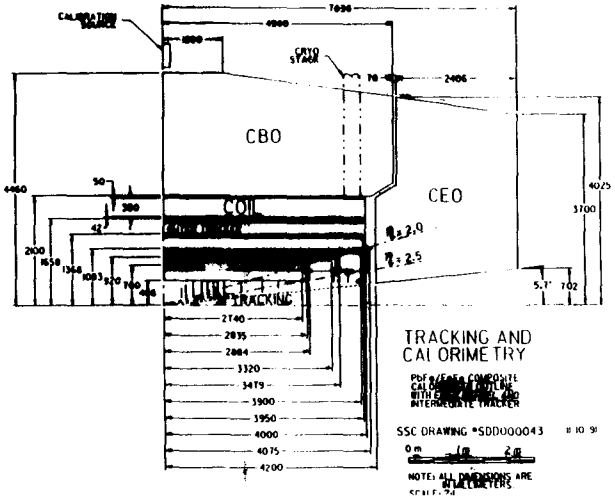

0039

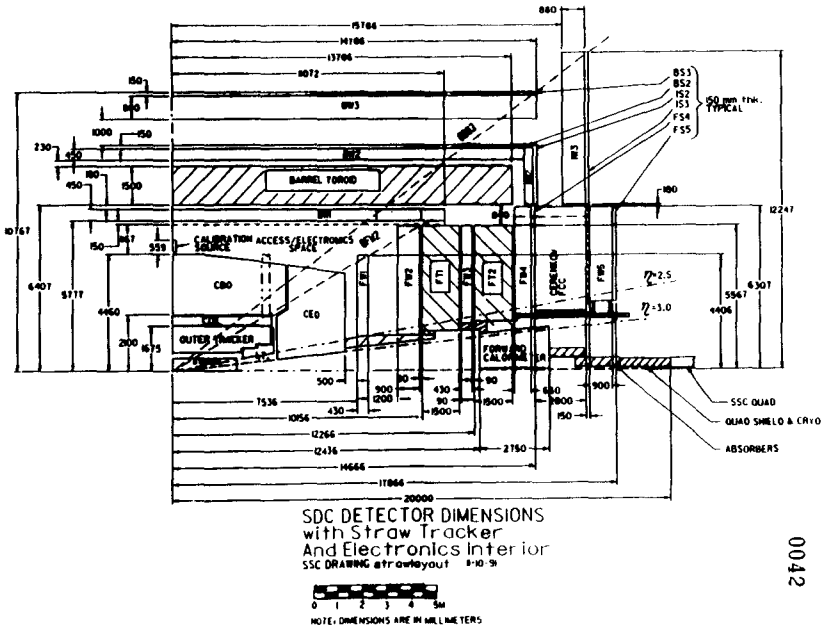

0042

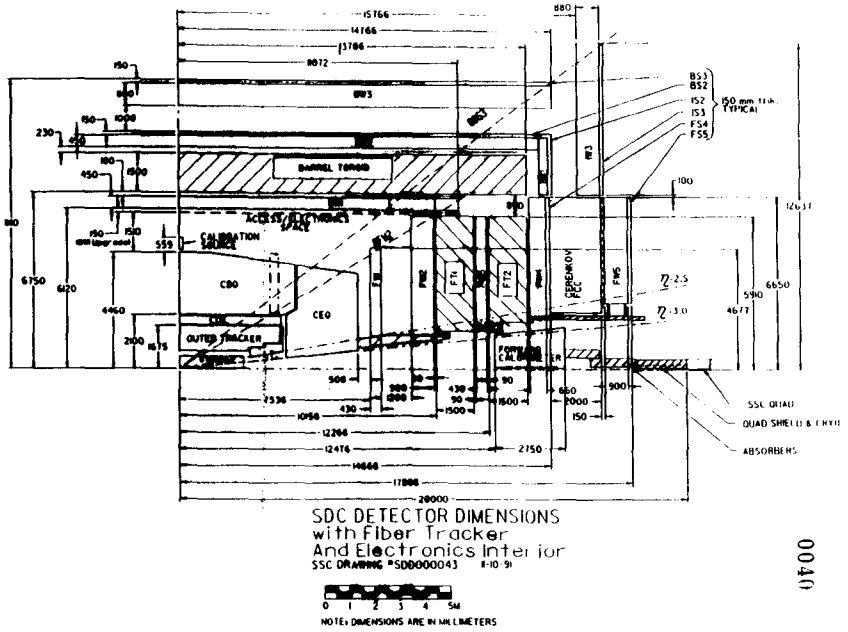

0040

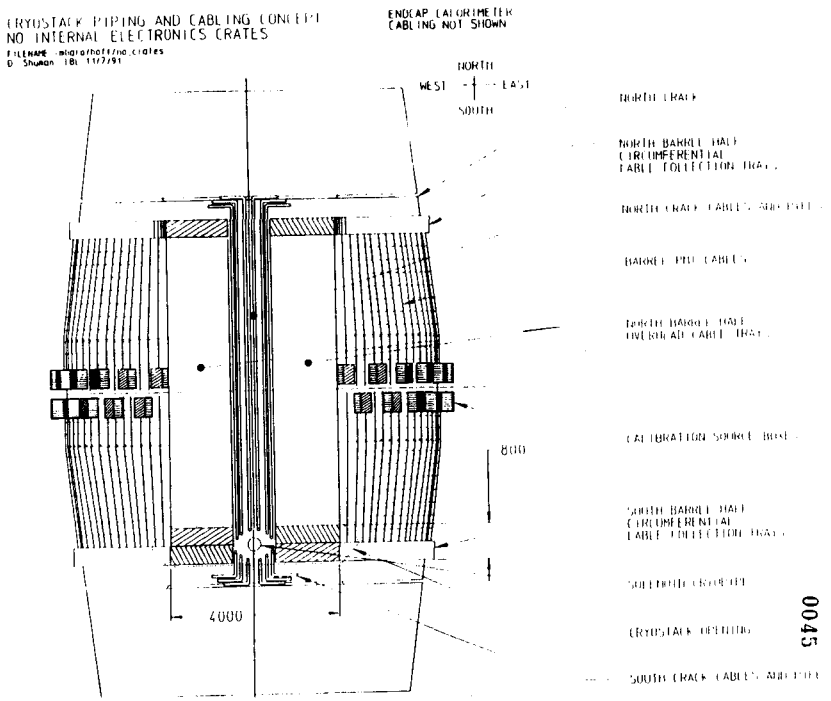

0045

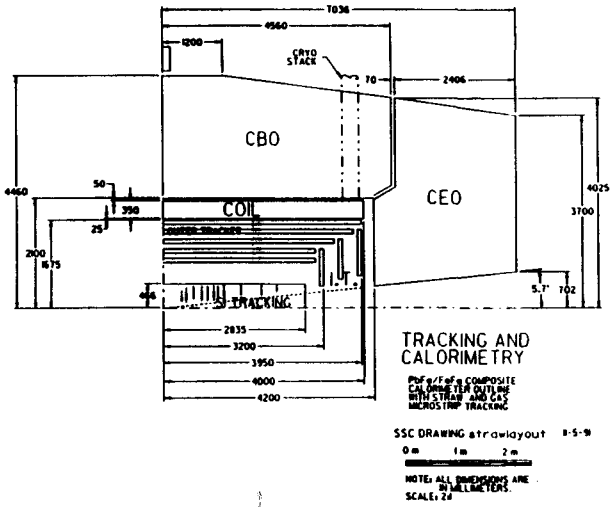

0043

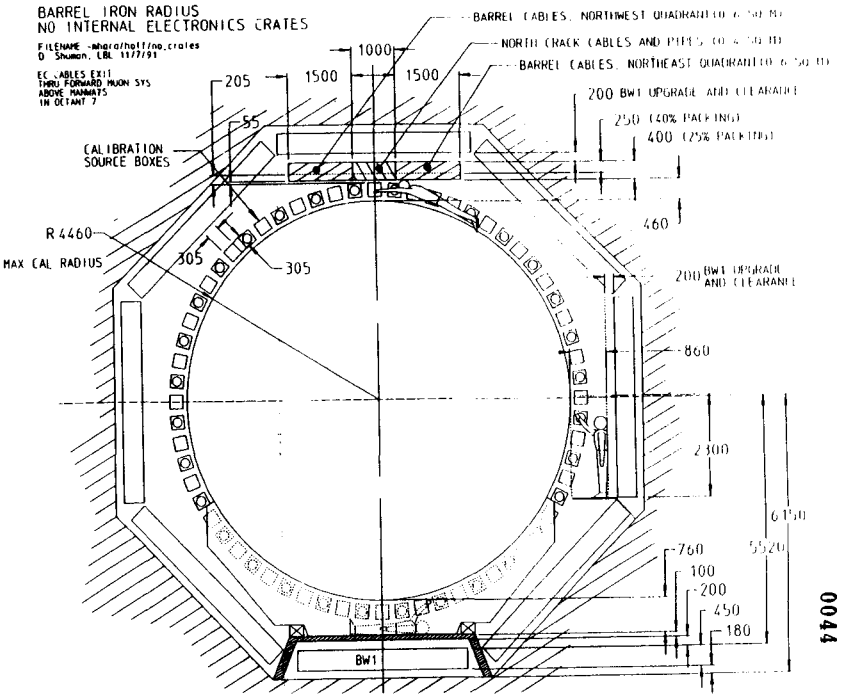

0044

ACCESS SPACE OPTIONS

0046

ORNL COLLABORATION MEETING OPTION

DET. OVERALL WIDTH 22.39/25.87 m
STEEL OUTSIDE WIDTH 6.66 m
STEEL INSIDE WIDTH 3.66 m
$$ =

64 CRATES — STRAWS

28 CRATES — FIBERS — 96 VLPC CANNISTERS

DET. OVERALL WIDTH 22.62/25.34 m
STEEL OUTSIDE WIDTH 6.90 m
STEEL INSIDE WIDTH 3.90 m
$$ =

OCTOBER EC MEETING OPTION

DET. BARREL OVERALL WIDTH 22.53/24.49m
STEEL OUTSIDE WIDTH 16.50m
STEEL INSIDE WIDTH 13.50m
$$ =

64 CRATES — STRAWS

28 CRATES — FIBERS — 96 VLPC CANNISTERS

OUTSIDE ELECTRONICS OPTION

DET. BARREL OVERALL WIDTH 21.02/23.91 m
STEEL OUTSIDE WIDTH 15.30m
STEEL INSIDE WIDTH 12.30m
$$ =

0 CRATES — STRAWS

0 CRATES — FIBERS — 96 VLPC CANNISTERS

DET. BARREL OVERALL WIDTH 21.62/22.71 m
STEEL OUTSIDE WIDTH 15.90m
STEEL INSIDE WIDTH 12.90m
$$ =

Cost Comparison

- **Distributed crates vs racks vs electronics outside**
- **Muon system derivatives - see plot**
- **Length scaling not yet clear**
- **Differences in cable costs have large uncertainty(contingency?) - size, readout method,.....**

Calorimeter length increased

Option	R(inner)(m)	R(outer)(m)	(L/2)(m)	Δmuon(M)	Δcable(M)
dist. Fiber	6.950	8.450	13.290	0.15	.....
dist. Straw	6.830	8.33	13.13	-1.6	.....
rack Fiber	6.750	8.250	13.766	0	.....
rack Straw	6.407	7.907	13.766	-3.4	0
out Straw	6.150	7.650	13.766	-5.9	+(2-7)
out Fiber	6.450	7.950	13.766	-2.9	+????

- **Better estimate needed but**
- **Integration easier and muon system slightly cheaper with straws**
- **Incremental cable(and other) costs to remote electronics uncertain but may cancel cost savings in muon system.**

0044

Muon System Cost Sensitivities

Muon System Radius Cost Sensitivity

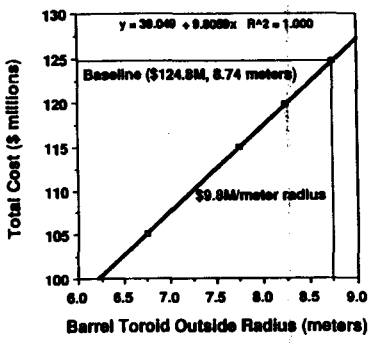

Muon System Barrel Length Cost Sensitivity

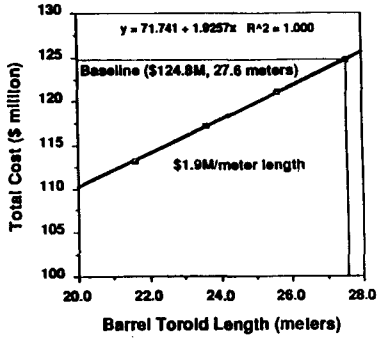

0045

SDC Experimental Facilities

R. Stefanski(SSCL)

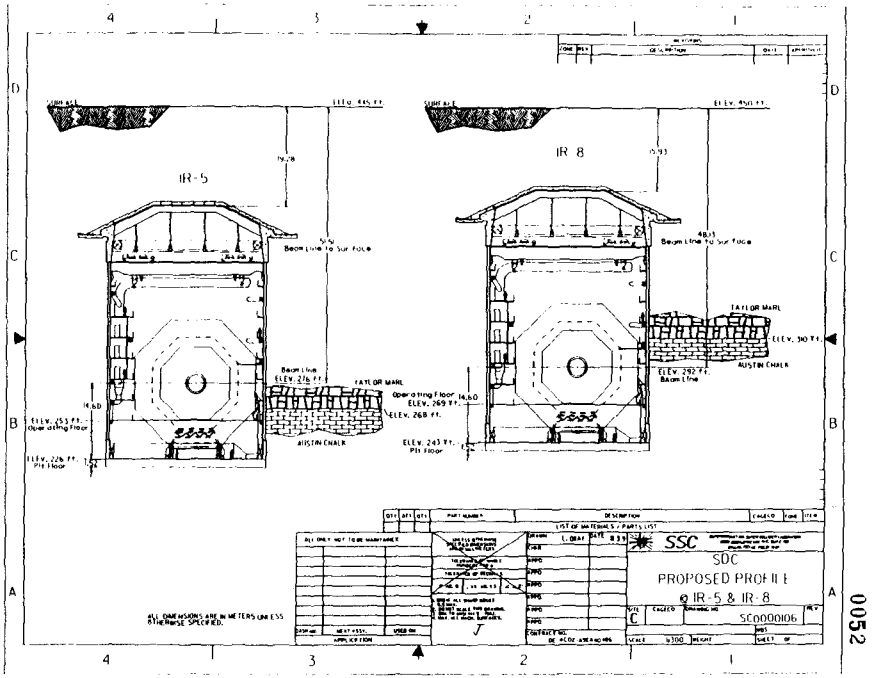

0052

SSC Laboratory **Physics Research Division**

Detector Requirements

- In the long term (10 years) the detector floor must remain aligned in respect to the beam within a reasonable limit estimated as of the order of ±25mm. The compensation for such movement would be carried out using jacks.
- In the short term (1 year) the floor must remain stable in the lower millimeter range so as not to affect alignment of the tracking components. This implies that there will be no appreciable change in detector position during beam running. Realignment, if necessary, will be carried out during long access periods.
- The low beta quads have alignment requirements of less than a millimeter. A stable floor is also required to meet this requirement.
- For the smaller, special purpose detectors, the site should be consistent with the schedule for choosing those detectors. Furthermore, construction of small cavern-like halls is better done in chalk.

10/15/91

0051

SSC Laboratory **Physics Research Division**

SDC Presentation

- Large detector will move to East Complex pending DOE approval.
  - Preparation for Title I design and critical path building must begin in earnest.
  - Muon Assembly building will be discussed this morning.
  - Will have presentation on SDC hall shortly.
- SEFUR (SDC Experimental Facilities User Requirements)
  - Draft version transmitted to CCD and PB/MK on 11/8.
  - Will be used as a start for facilities design.
  - Periodic updates may be generated as needed, or will replaced with PB/MK reports.
- Change Control Board Action.
  - Establish baseline for detectors in project.
  - Will include surface facilities and halls, and small detectors.
  - Schedules: late availability of halls.
- Test beams
  - CERN beams. Need a guess by late December.
  - Trying to accelerate SSC test beam program to Jan '96.

11/9/91

0053

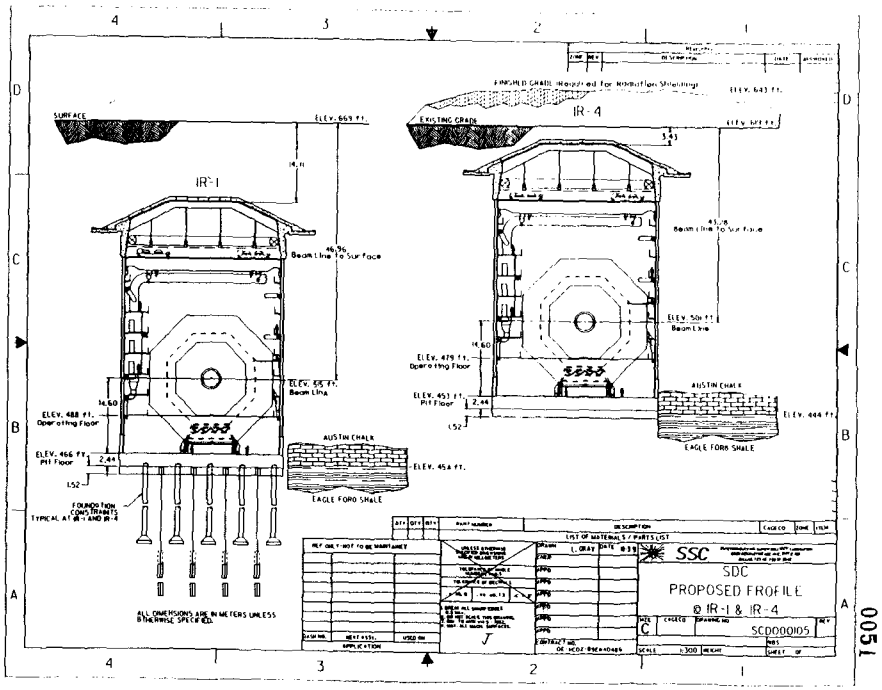

0054

FNAL Test Beam Efforts

D. Green(Fermilab)

FNAL T-861 EFFORTS

1. SCINTILLATOR FIBER TRACKING - NWU
   FIBER + ELEC + MAPS
2. SM - MP
   PS
3. EM CAL - MP
4. EM/H CAL - MP
   a. COF PLAG c. WL TESTS
   b. HANGING FILE
5. MU TRACKING - NWU
6. π BKGND IN MU - NWA
   DATA TAKEN

0056

PS/SM

T841 PRESHOWER RESULTS AND FUTURE ANALYSIS

Λ(τ) 1) DETERMINE SHOWER WIDTH VERSUS DEPTH IN RADIATION LENGTHS. (See plots)
PS (2RL) FWHM = 4.7 mm
SM (6RL) FWHM = 11 mm

π/e 2) PI / EL SEPARATION USING ENERGY IN PS, VERSUS DEPTH, ENERGY. (See plots)
(pion tail increases with RL, not shown in plot)

TRACK MATCH 3) TRACK/SHOWER MATCHING RESOLUTION VERSUS DEPTH, ENERGY. <= 1 mm sigma

"MASSLESS GAPS" 4) CORRECTING EM CALORIMETER ENERGY RESOLUTION WITH MATERIAL UPSTREAM USING PS ENERGY. FOR INSTANCE:
18%/SQ(E) without material in front,
22%/SQ(E) with 1RL Al + 1 RL Pb (can we fix?)

5) PRESHOWER + SHOWER-MAX + EM + HAD COMBINED PERFORMANCE?

Dan Green, Nov. 8, 1991
I have plots showing preliminary results for items 1, 2, and 4.
Philip Melese 212-570-8826
FNAL::MELESE

APO READOUT

Average Electron shower profile (energy weighted hit fiber distribution about the shower centroid, averaged over 700 showers).
Preshower results at various depths in R.L.

Λ(τ) - PS

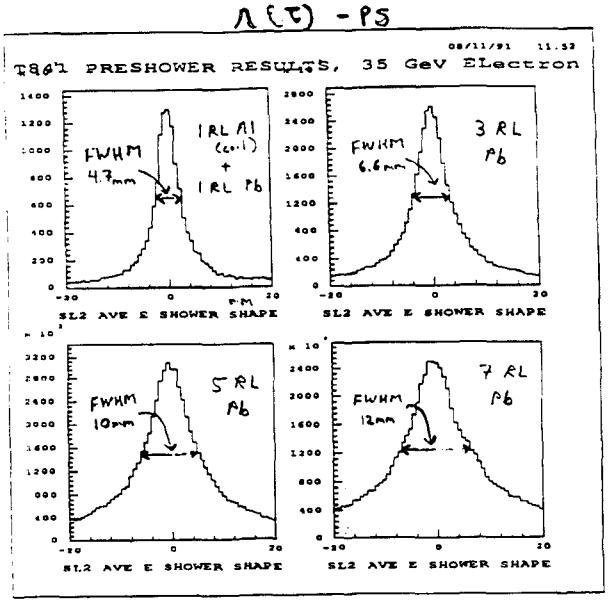

Preliminary!

0058

Distributions of dE(τ) - PS
Energy Deposited in Preshower
At various depths in Radiation Lengths (RL
35 GeV Electrons (π⁺ superimposed)

π/e REJECTION

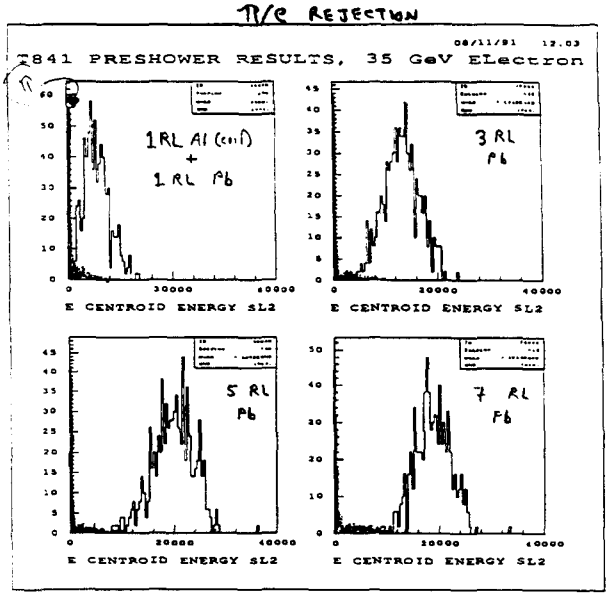

Preliminary!

P. Melese
Registered

Scatter plot of Preshower Energy versus EM Calorimeter Energy. Slight anticorrelation may improve EM resolution by adding PS Energy information.

PS - ENERGY MATCH

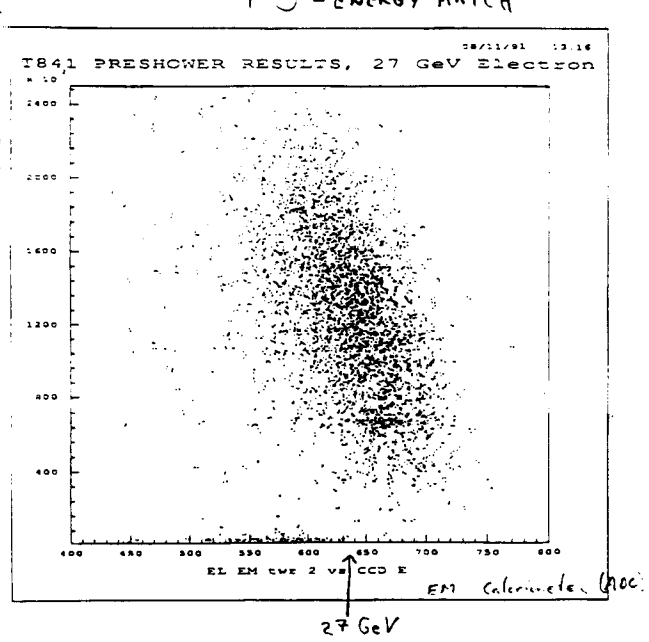

MP - SM TESTS

SHOWER MAXIMUM BEAM TEST MEASUREMENTS

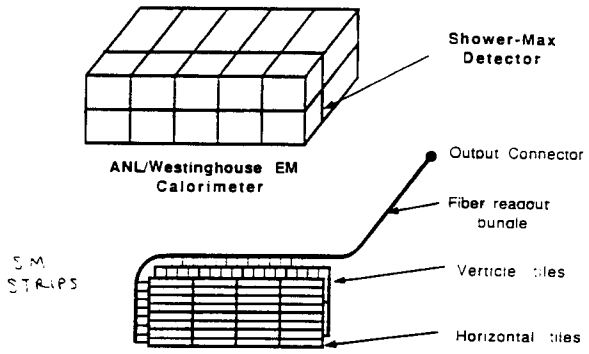

We are equiping 8 out of the 10 towers of both calorimeters with 4 x 4 arrays of tiles read out with wavelength-shifting fibers. In both calorimeters the fibers go to a 64 channel connector.

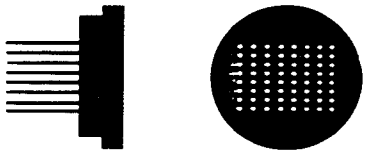

64 Channel Fiber connector to connect to APD and MCPMT readout.

SM

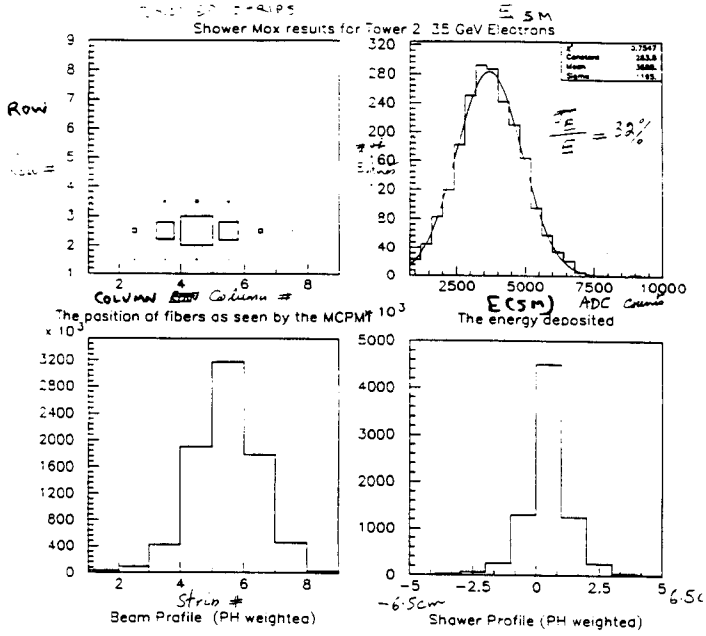

Each strip = 1.275 cm

SHOWER PROFILE

SM/PS
Data sets and plans

The data were taken at 35, 27, 20 and 15 GeV electron/pion beam at Fermilab. These data were taken at center of each tower to study the variation in response of different design of tiles. Moreover a 1.0 cm vertical and horizontal scan was done for some of the towers. In addition to this data were taken with with different radiation length of Pb in front of the pre shower detector. This will enable us to study the shower shape in preshower detector and compare the results from ShowerMax detector.

- More data will be taken at higher beam energies (50, 100 GeV). We also plan to use APD's to readout the ShowerMax. At present we are using APD's to readout preshower detector.

Second ShowerMax module will be installed along with second EM module and the hadron calorimeter in the third week of November.

MP TEST BEAM

EM CAST Pb — ANL/WSTC

How good are the pieces?

- Absorber Thickness
  - $\sigma = 1\%$ ⇒ SMALL CONSTANT TERM
- Optical System
  - Testing system β SOURCE SCAN
  - Light Yield 3 p.e./mip-layer
  - Transverse uniformity σ - 1%
  - Longitudinal uniformity $\sigma = 8\%$
    - Scintillator thickness $\sigma = 3.6\%$
    - Fibers + splices $\sigma = 3.8\%$
  - May want to mask *

QC FINAL PASS

< 2% FOR

< 0.5% CONSTANT TERM

CAST Pb TEST MODULE

SDC TILE/FIBER CALORIMETER

Truncated EMC Module for Testbeam

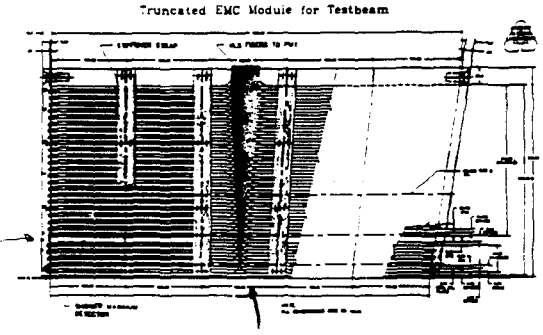

CAST Pb IN Fe BULKHEAD STRUCTURE

Figure 4.12 Truncated EM Test Module Design

Pb Thickness Uniformity

EM Test Module No. 1

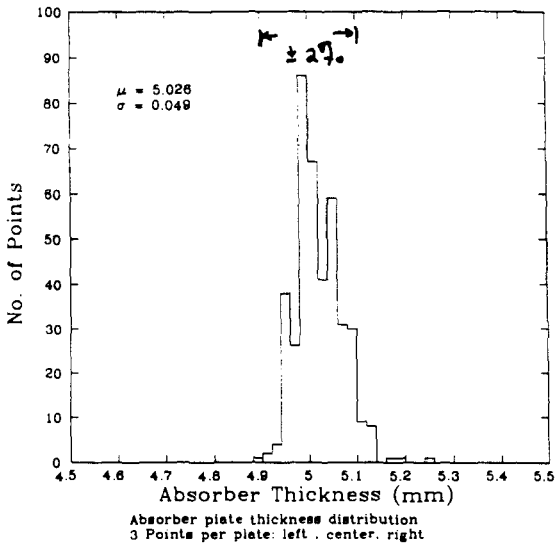

Absorber plate thickness distribution
3 Points per plate: left , center, right

MP - EM

How good is the whole calorimeter?

- Testbeam measurements
  - September 1-6, 1991
  - 3 towers instrumented
- Beamline setup
  - Momentum tagging to $\sigma = 1.5\%$
  - 2 gas Cerenkov counters to tag electrons
  - Beam 30-50% electrons
  - Tunable 15-35 GeV. Can go to 100-150 GeV but rarely
  - PWC's

Data at (10), 19, 25, 33 GeV

- Resolution
  - Matches calculation of $18\%\sqrt{E}$ *
  - No evidence of constant term (< 4%)
- Uniformity
  - Undersize scintillator emphasizes dip at bulkhead
  - ...Which is mostly correctable "CRACK SCAN"
- Light yield
  - Light to Tower 1 attenuated by neutral density filter

0067

MP

EM RESOLUTION

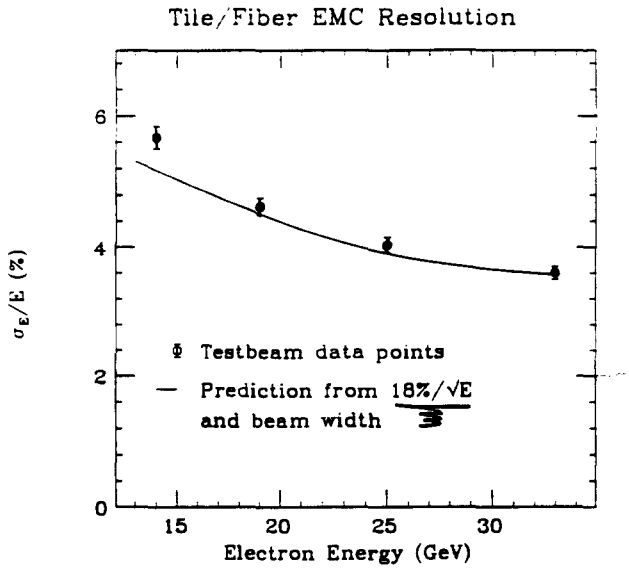

0065

MP: SCAN ACROSS TOWER BOUNDARY

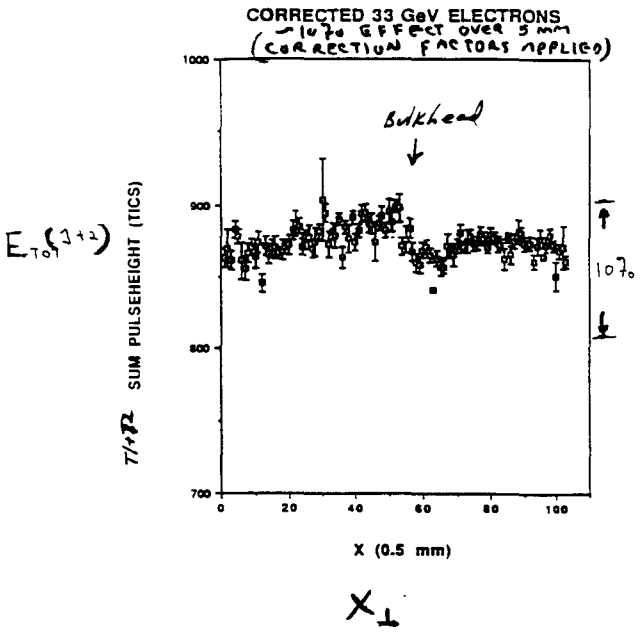

E_{TOT}(1+2)

T/+2

$X_\perp$

0069

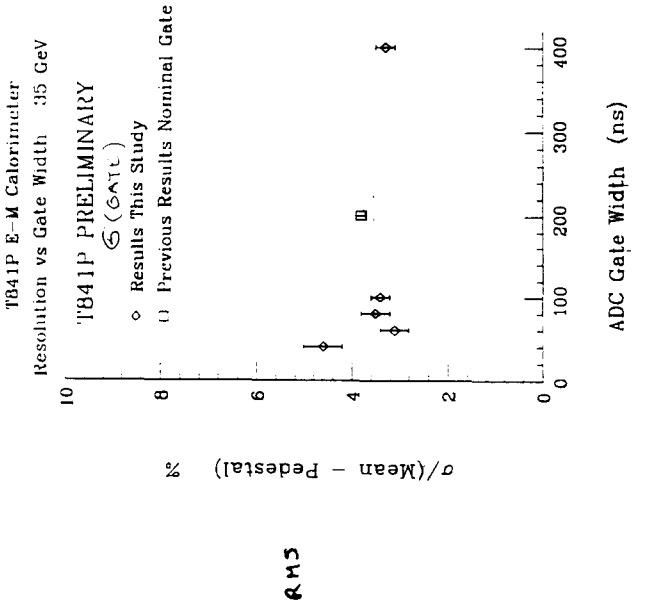

RMS

0070

MT: COF ENDPLUG PROTOTYPE

(CONSTANT TERM < 1.6%)

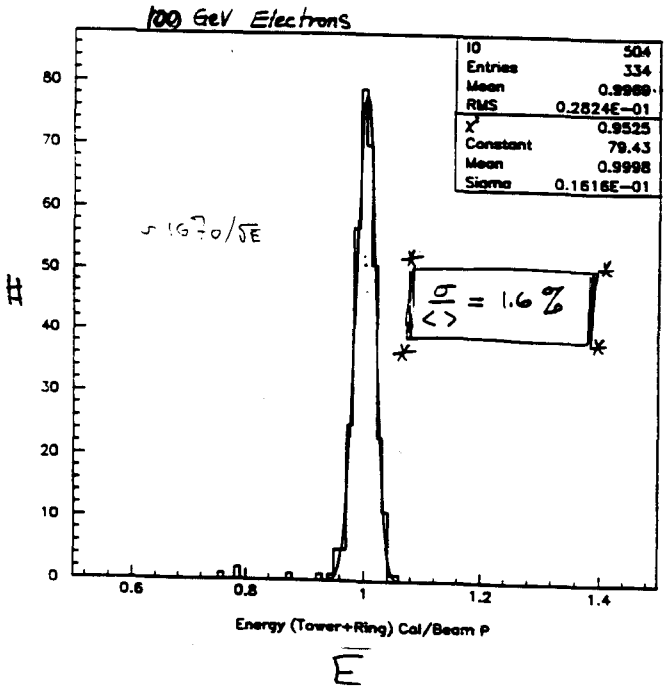

E

0071

M.I.T. CDF ENDPLUG PROTOTYPE

$\sigma/E = \sqrt{\left(\frac{3.175}{4.8}\right)^2} = 0.813$ TO $\sigma/\sqrt{E}$

1 mm SCINT ⇒ 400 PE/GeV

G4 PE/MIP/TILE

OR $\sigma/\sqrt{E} \rightarrow 12$

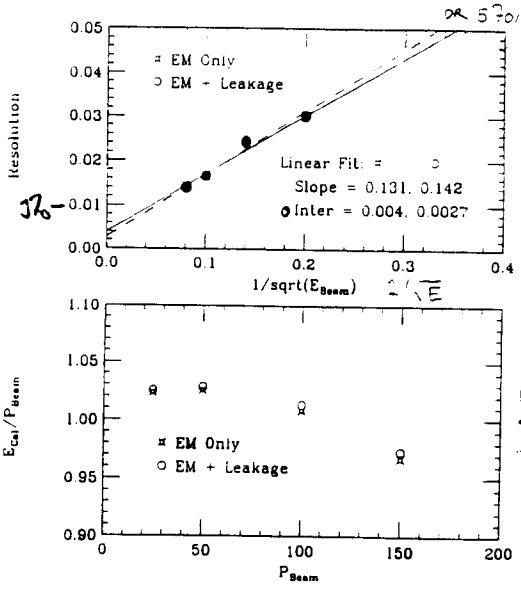

EGS4 RESULT

LINEARITY

LEAKAGE

0072

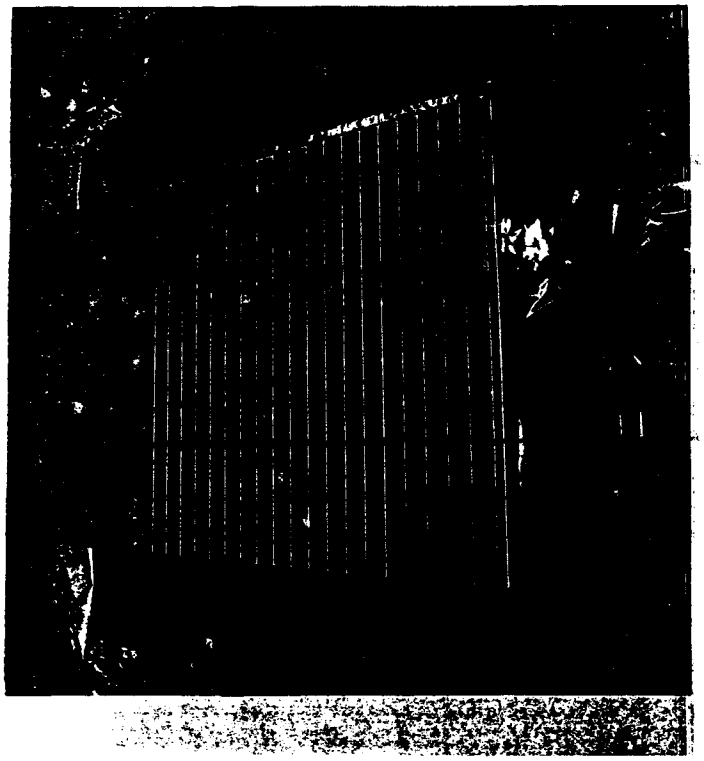

0073

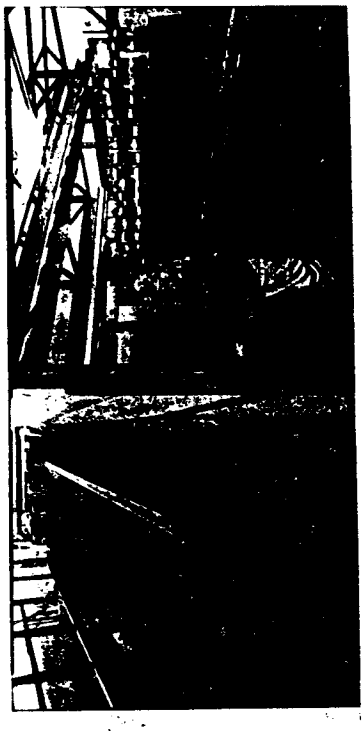

0074

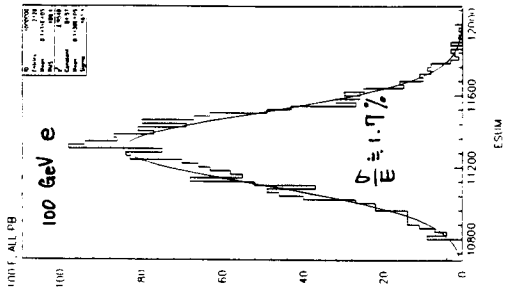

(1/8" Pb + 3mm Scin) * 4p

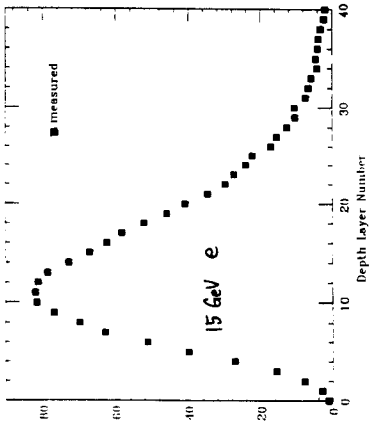

0075

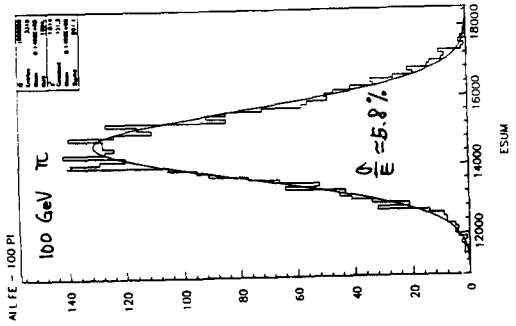

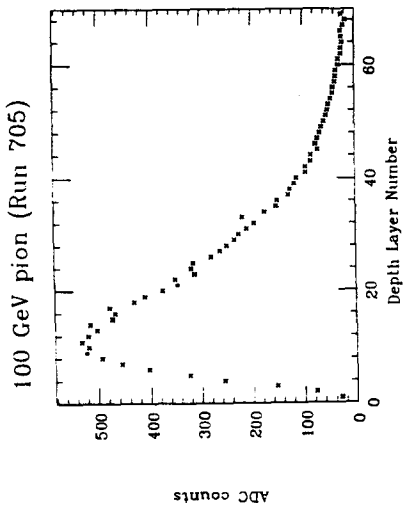

(1" Fe + 3mm Scin) * 69

0076

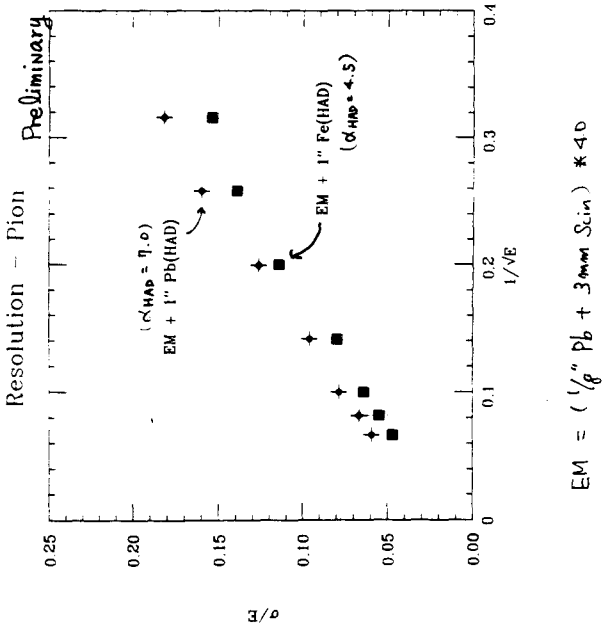

EM = (1/8" Pb + 3mm Scin) * 40

0077

9-24-91 HJL

MUON BEAM TESTS

- Tevatron Muon Beam
  - Locate downstream of E665 in the New Muon Lab
  - Beam can be tuned from 100 GeV to 650 GeV with useful flux for these tests
- Apparatus
  - Scintillator trigger
  - Six multi-sampling drift chambers
    3 cells/module
    6 sense wires/cell
    Sense wire length 11 in.
    Staggered wires (0.25 mm)
    2.75 in. cell/1.375 in. drift
    Two track resolution < 3 mm
    Window 1/2 mil aluminized Kapton
  - Fe absorber (25 in.)
    Last 8 in. magnetizable
  - Čerenkov counter has 2 mirrors, each 50 cm^2
- Data Acquisition System
  - FAST BUS TDC's and ADC's
  - On-line VAX 3500
  - Log to 8 mm tape

0078

[illegible] [200k Trigs on Tape]

[illegible] [2x10^6 Trigs on Tape]

ENERGIES

Oct 4 ≈ 490 GeV

Nov 5 ≈ 90, 360, 480, 550 GeV

Material : Al, Lucite, G-10, Pb

Oct 4: DC2, DC3, DC4, DC5 z-coord.
DC1, DC6 y-coord

Nov 5: DC2, DC3, DC4, DC5, DC6 z-coord
DC1 y-coord

Summary of 1990 Run — Oct. 90

R#	D L	D S	B Y	B N	NO	Material: DC4 upstream 1A	3A	4L	4G	DC4 dstrm 6A	6L	DC5 ustrm 1A	1L	Trig 15	12	# of events with extra track(s): DC4 (%) ~25-30% a	b	DC5 (%) b	DC4&5 (%)	Clean Incident (%)
1	0		0	0		no material										--	--	JUNK		-
2	0		0	0										0		24	13		9	89
3	0	0		0						1/16" Al		1" Al				22	12		9	89
4	0	0		0						↓		↓			0	19	10		7	85
5	0	0								0		0 ←		0		23	→ 24		12	89
6	0	0									0		0	0		20	→ 18		8	88
7		0	0		0	no material				1/16" Lucite		1" Lucite		0		26	14		10	86
8		0		0	0									0		27	12		10	87
9		0		0		0								0		27	13		9	89
10		0	0			0	1" Al							0		26	13		10	89
11		0		0		0									0	28	11		8	88
12		0		0		0									0	28	12		9	85
13		0		0			0	3/16" Al							0	--	--			-
14		0	0				0							0		28	14		11	86
15		0		0			0							0		27	14		9	88
16		0		0			0								0	28	11		7	93
17		0		0				0	1/4" Lucite						0	26	11		8	92
18		0		0				0						0		30	14		10	89
19		0		0					0	1/4" G-10				0		30	19	2	11	89
20		0	0						0					0		28	16		10	89

10K/each run Statistical Error ~ ±2% Systematic Error ~ +5%

FNAL T8 SUMMARY

1. VIGOROUS PROGRAM IN PLACE

   NOW TAKING DATA

2. PROSPECTS OF AN EXTENSION OF THE FIXED TARGET RUN

   a) SCIFI ?

   b) HAC IN MP?

   c) MORE HF WORK; CLADDING?

   d) MORE ν BKGND DATA

3. TEST BEAM DATA OFTEN CRUCIAL IN SSC DECISION MAKING — E.G. CALORIMETRY

Nov 5 Run — 55 GeV (only Fe absorber)

Muon Group Report - Issues for the Technical Proposal

G. Feldman(Harvard)

Muon Group Report

Issues for the Technical Proposal

1. Review of ϕ chambers, especially in BW1.

2. Review of the amount of iron at the $\eta = 1.5$ corner.

3. Review of the BW3–IW3 arrangement.

Gary Feldman
November 15, 1991

We use ϕ measurements in the muon system for three reasons:

1. To provide track matching, i.e., which track in the central tracker was the muon?

2. To provide the second level trigger.

3. To improve momentum resolution at very high momenta.

Track Matching

Rob Gardner presented an idealized calculation from the U. of Illinois. They studied high p_t $b\bar{b}$ production.

There was perfect θ and ϕ resolution in the inner tracker, and no background or δ-rays in the muon system.

For all configurations with some phi information, there was a maximum of 1.5% confusion.

Table 2 : Layout Description[1.3]

Layout	BW1	BW2	BW3
1	2ϕ , 2θ	2θ	2θ
2	2θ	2ϕ , 2θ	2θ
3	2θ	2θ	2ϕ , 2θ
4	2ϕ , 2θ	2ϕ , 2θ	2ϕ , 2θ
5	1ϕ , 2θ	2θ	2θ
6	2θ	1ϕ , 2θ	2θ
7	2θ	2θ	1ϕ , 2θ

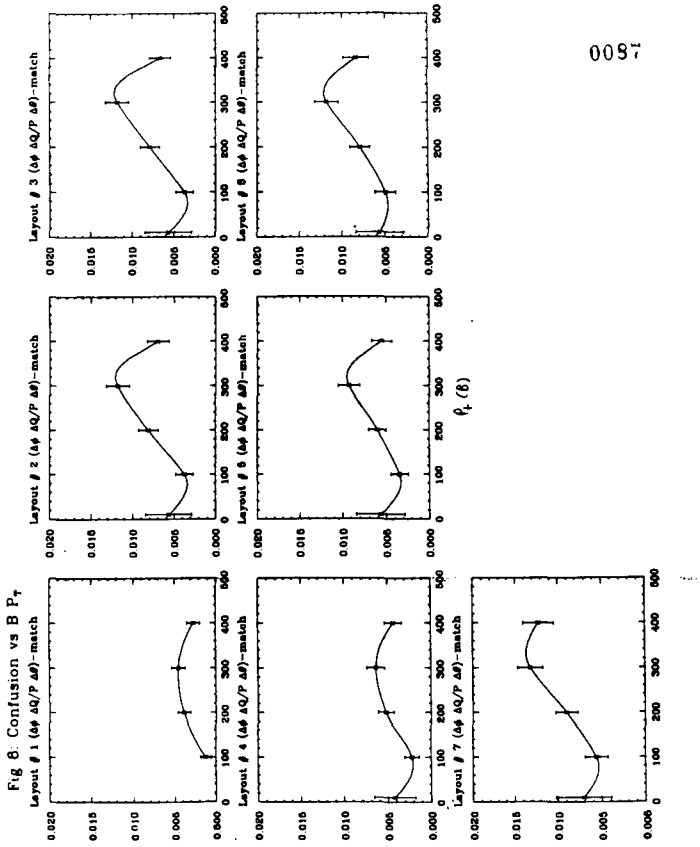

Fig 8. Confusion vs B P_T

Test beam data, which are not yet analyzed in detail, show that 20 to 30% of high energy muons are accompanied by other (soft) tracks.

The present descoped design has ϕ measurements in only one place, 4 layers in BW3. The muon group was concerned that, given this and possibly other backgrounds, one position is not sufficient. We therefore recommend that 4 layers of ϕ be added back into BW1.

There was considerable discussion between 2 and 4 layers. Two layers gives no redundancy and does not provide for both left-right ambiguity resolution and projective wires.

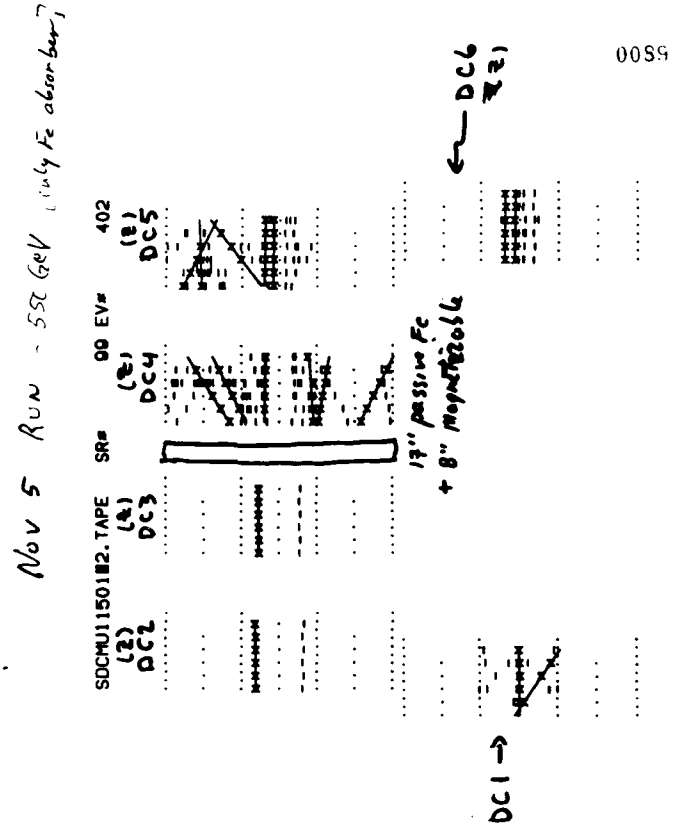

This requires 85 cm thickness for BW1 allowing for all chamber options.

History: LOI had 28 barrel layers; we descoped to 18, and are now recommending rescoping to 22.

Amount of Iron at η = 1.5 Corner

Conclusion is that improvement is not cost effective. Leave as is.

BW3–IW3 Arrangement

Conclusion is that there is no strong physics argument either way and it should be treated as an engineering problem.

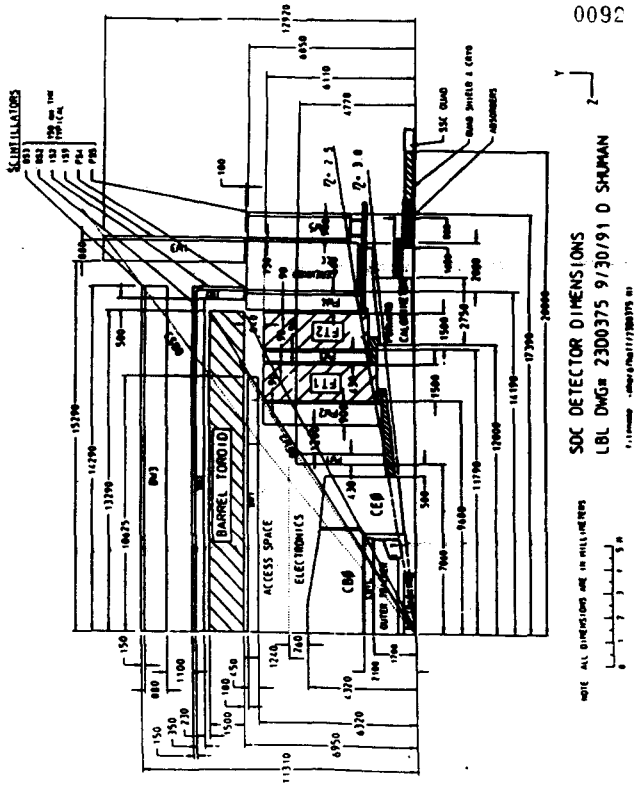

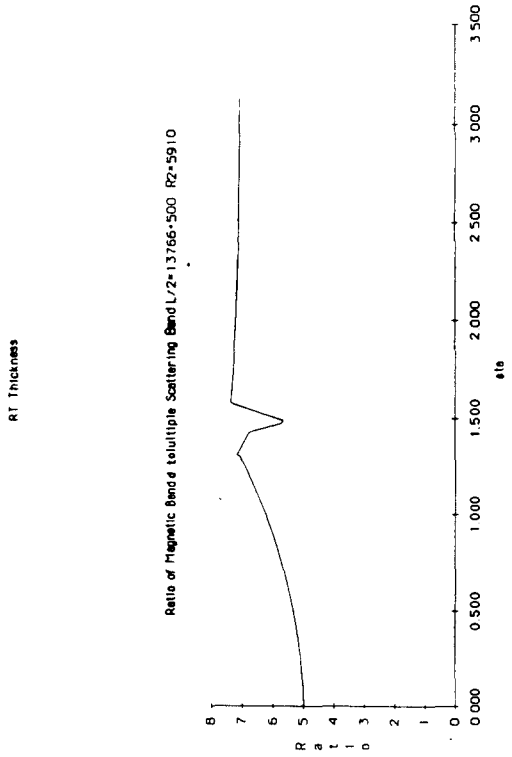

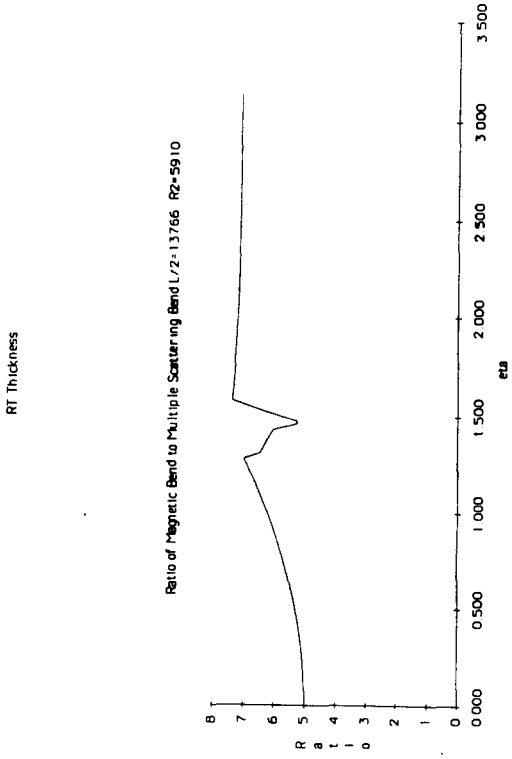

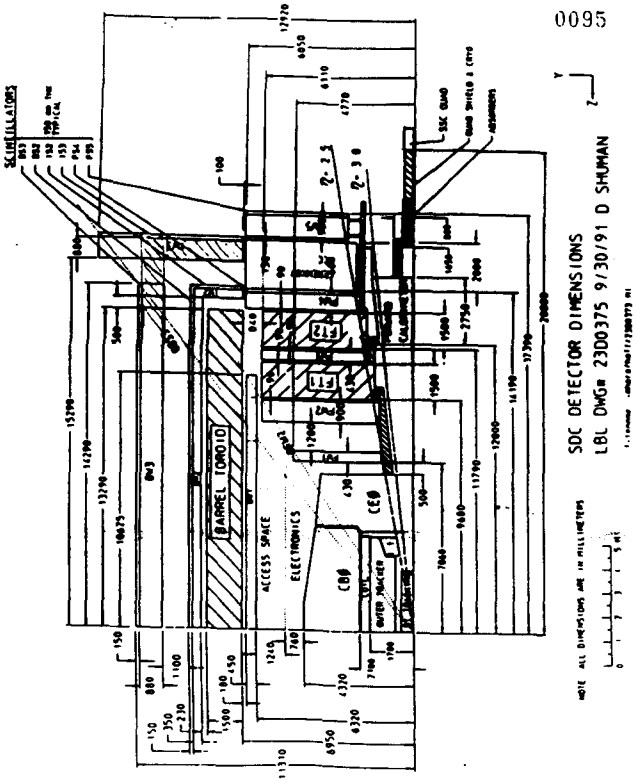
SCINTILLATORS
BARREL TOROID
ACCESS SPACE
ELECTRONICS
CEB
SDC DETECTOR DIMENSIONS
LBL DWG# 23D0375 9/30/91 D SHUMAN
NOTE ALL DIMENSIONS ARE IN MILLIMETERS

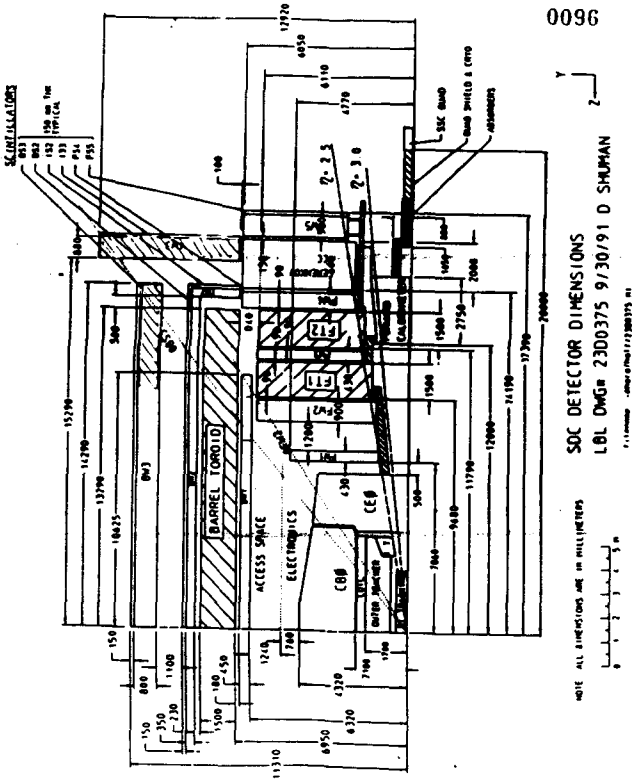
SCINTILLATORS
BARREL TOROID
ACCESS SPACE
ELECTRONICS
CEB
SDC DETECTOR DIMENSIONS
LBL DWG# 23D0375 9/30/91 D SHUMAN
NOTE ALL DIMENSIONS ARE IN MILLIMETERS

SDC Computing

L. Price(Argonne)

SDC COMPUTING

SDC Collaboration Meeting

L. E. Price
November 15, 1991

Recent Activities

- Workshop October 28-November 1
- Organization of SDC computing at SSCL
- Writing of SDC Proposal computing section Draft 0.

Assumptions/Principals

- Operating systems
  - Unix and subsequent evolution → POSIX
- Programming Languages (FORTRAN 90, C++)
- User interface, Frameworks
- Data storage and access
  - Database model
- Software engineering standards
- Distribution of computing
- Programming for analysis
- Standards

Online Computing

user4:[fry.memo.tex.tp]tp.tex

OUTLINE OF CHAPTER 9 - ONLINE COMPUTING
*** DRAFT ***
A.Fry 91.11.06

9 Online Computing System

9.1 Overview

9.2 Operational Concepts
9.2.1 Purpose and Goals
9.2.2 Modes of operation

9.3 Functional Requirements
9.3.1 Acquiring and recording data
9.3.2 Insuring data integrity
9.3.3 Physics processing
9.3.4 Software Tools

Irwin

9.4 Relationships and Impact on other systems
9.4.1 Front-end electronics
9.4.2 Level I and II Trigger systems
9.4.3 DAQ and Level III
9.4.4 offline computing
9.4.5 Test-beam system(s)
9.4.6 Slow controls
9.4.7 User Code

Bell while

9.5 Implementation
9.5.1 Methodology
9.5.2 Operability and Reliability
9.5.3 Functional Implementation
Fig. 1 Functional Event-like data flow
Fig. 2 Primary control paths
Fig. 3 Online process
Fig. 4 Hardware diagram
9.5.4 Run Control
9.5.5 Configuration Control and Monitor
9.5.6 Data Logging
9.5.7 Data Monitoring
9.5.8 Condition Monitoring
9.5.9 Calibration
9.5.10 Interlocks and Failsafe systems
9.5.11 Physics Processing
9.5.12 Alarms and Limits
9.5.13 Database
9.5.14 Documentation
9.5.15 Software Tools and Standards — Irwin

9.6 Schedule

9.6.1 Testbeam January 1996
9.6.2 Data Format
9.6.3 Sub-detector installation
9.6.4 Level III, Data routing and logging

Roe

9.6.5 Cosmic Ray runnning March 1999
9.6.6 Detector turn on October 1999

9.7 Organization

0102

0103

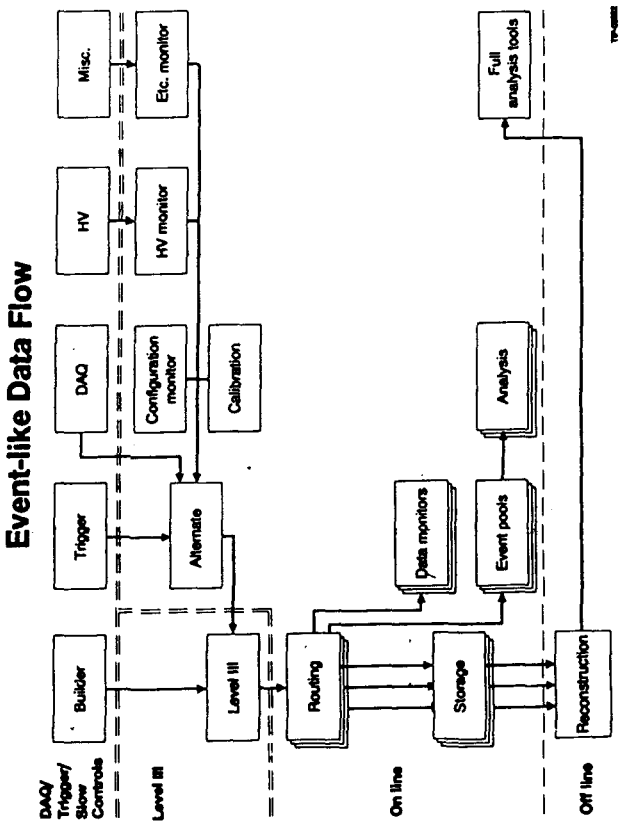

0104

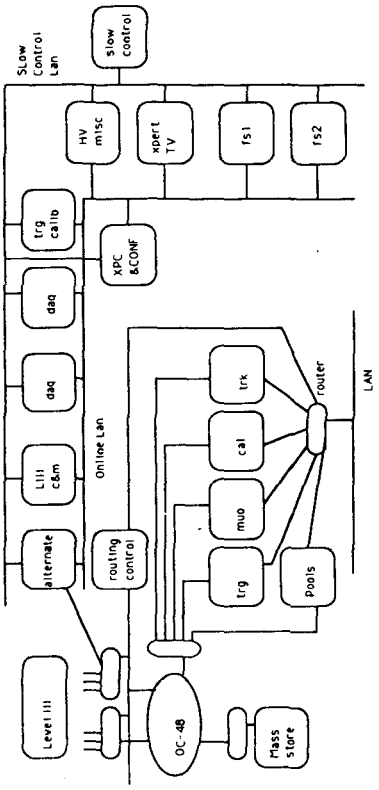

Offline Computing

0105

- Components
  - Production reconstruction
  - Data storage
  - Event filtering and analysis
  - Simulation
- Requirements
  - Data recording rate: 100 MB/sec
  - Annual storage: 2×10^{15} bytes = 2000 Terabytes
  - Production Processing: 10^5 MIPS
  - "Near real time" reconstruction
  - Master DST at SSCL: 100 TB
  - Working DST: 10^8 events, 1-10 TB
    - Probably copies at regional centers
  - Database organization of data
    - Metadata: keys and index files widely distributed
    - Hierarchical storage
    - Longer access delay times for less filtered data samples
    - Ability to read slected portions of event

Online documentation on data formats, etc., accessible across network

Communications

LAN

MAN

WAN

Conferencing

Simulation

Processing: 10^4 - 10^5 MIPS

- Design

Systems at SSCL

Regional Centers

Local institutions

SDC Technical Proposal

COMPUTING SECTION DRAFT OUTLINE

10.1 Executive Summary (Larry Price) [2]

10.2 Computing Model and Operational Concepts (Dave Miller, Bob Ennis) [4]

10.3 Functional Requirements (Andy White) [11]
- 10.3.1 overview (Block Diagram & External Interfaces)
- 10.3.2 Data Reconstruction (Andy White)
- 10.3.3 Data Storage Management (Andy White)
- 10.3.4 Analysis (Drew Baden)
- 10.3.5 Software (Irwin Gaines)
- 10.3.6 Communications (Ed May)
- 10.3.7 System Services (Chris Day, Glenn Kubena, E. Poole)
- 10.3.8 Simulation (Shuichi Kunori, Soren F.)
- 10.3.9 Performance Goals (Glenn Kubena)

10.4 Relationship of Computing to Detector Subsystems (Irwin Gaines) [2]

10.5 Generic SDC Computing Model (Tony Elam) [2]

10.6 Hardware Design (Larry Price, Brian Scipioni, Ken Liao, K.Amako) [6]
- 10.6.1 Overview
- 10.6.2 Architecture
- 10.6.3 Hardware Development Process
- 10.6.4 Upgrades and scalability

10.7 Software Design (Drew Baden, Chris Day, Harald Johnstad, Glenn Kubena) [6]
- 10.7.1 Overview
- 10.7.2 Architecture
  - 10.7.2.1 Software Architecture Overview
  - 10.7.2.2 Software Infrastructure/Framework
  - 10.7.2.3 Common Application Services
  - 10.7.2.4 Functional Components
- 10.7.3 Development Process
  - 10.7.3.1 Software Engineering and Other Tools
  - 10.7.3.2 Code Management
  - 10.7.3.3 Data Modelling
  - 10.7.3.4 Programming Languages
  - 10.7.3.5 Validation & Verification
- 10.7.4 Software Sources

10.8 Organization & Policy (Larry Price) [1]

10.9 SDC Interactions with the Computing Industry (Larry Price, Tony Elam) [1]

10.10 Computing for SDC Outside of SSCL (K.Amako, Andy White, (Europe)) [4]

10.11 R&D Required (Drew Baden) [3]

10.12 Technology Forecast (Terry Watts, Tony Elam) [2]

10.13 Schedule and Milestones (Larry Price, Phil Liebold, Larry Cormell) [3]

10.14 Manpower and Cost (Larry Price, Phil Liebold, Larry Cormell) [3]

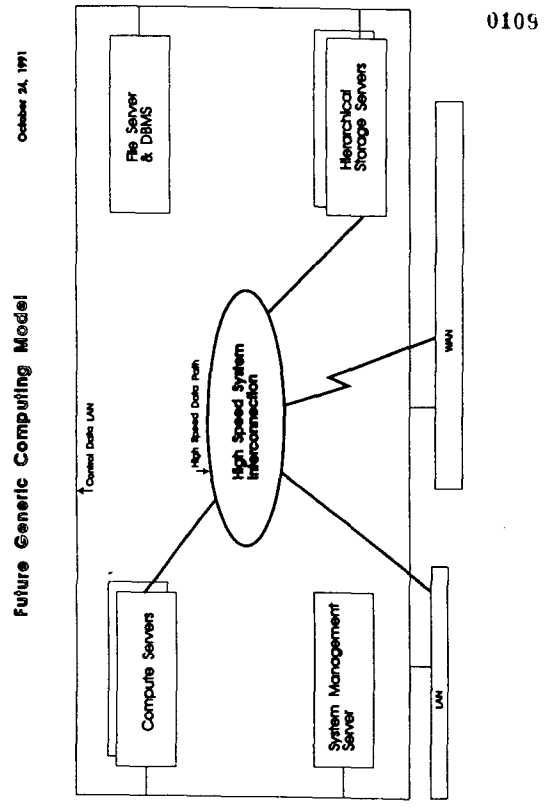

Small Cluster Options.

November 5, 1991

Option 1a.

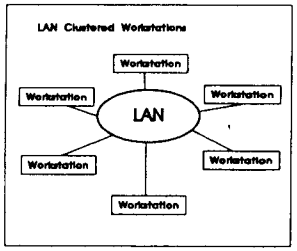

Option 1b.

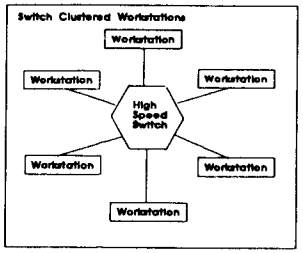

Option 1c.

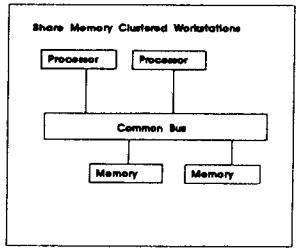

0112

SDC Conceptual Architecture Diagram

October 24, 1991

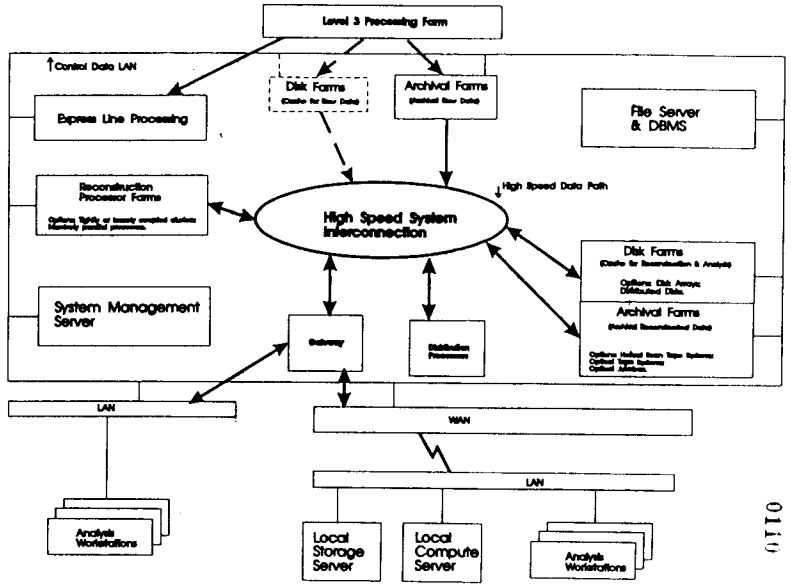

0110

Hardware Option 2.

November 5, 1991

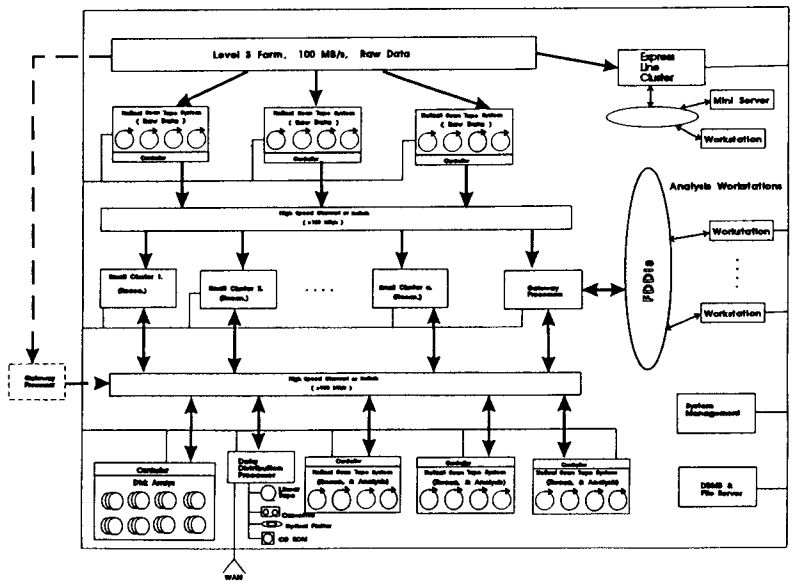

0113

Hardware Option 1a, 1b, 1c.

November 5, 1991

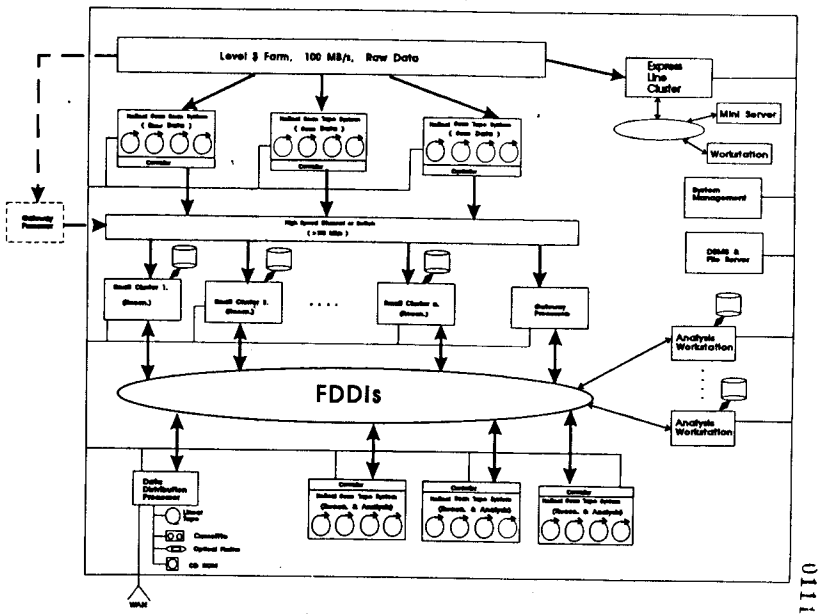

0111

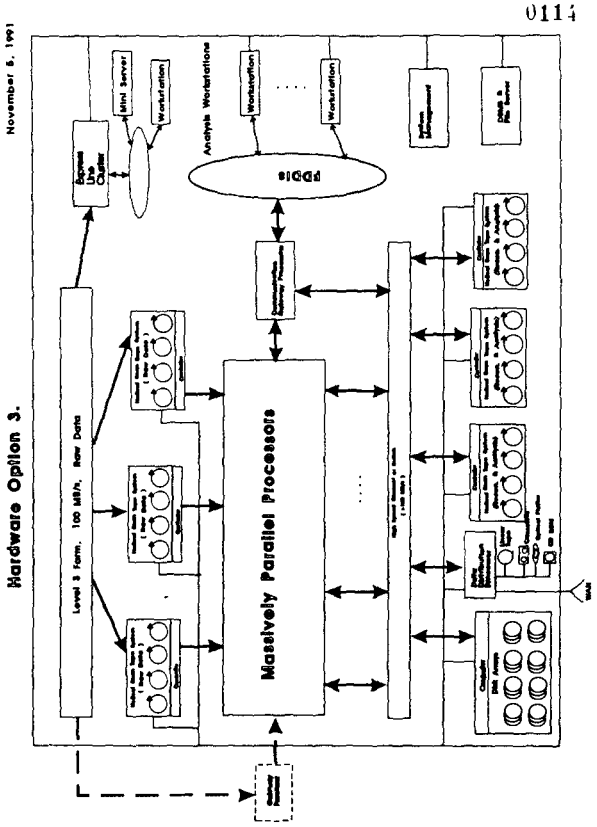

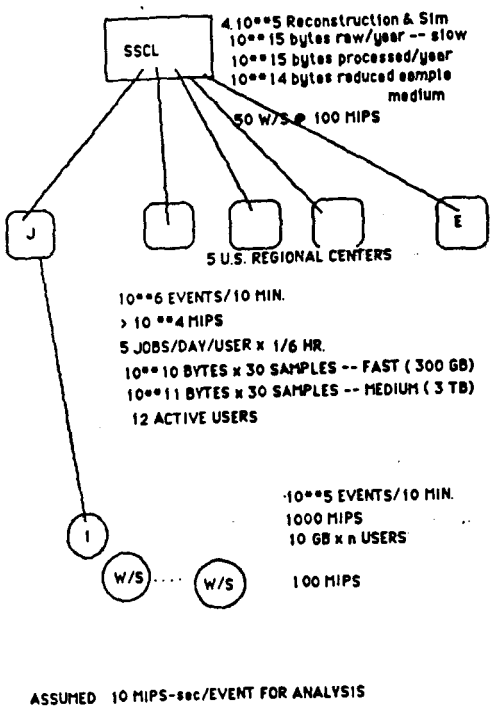

Fig. 7. First assessment of SDC Offline Computing rates and resources.

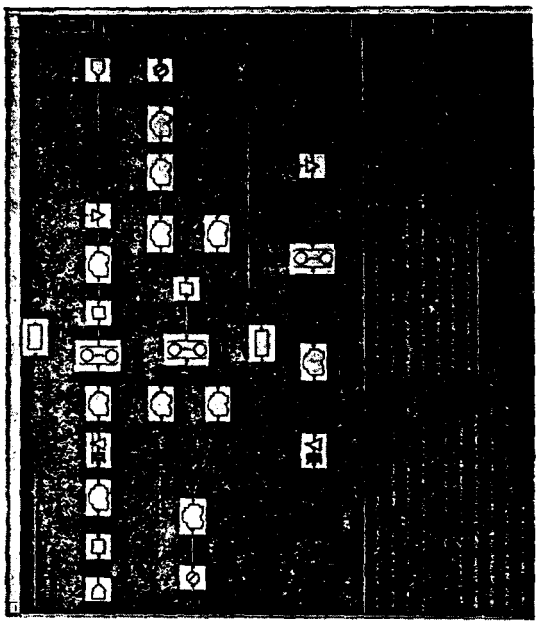

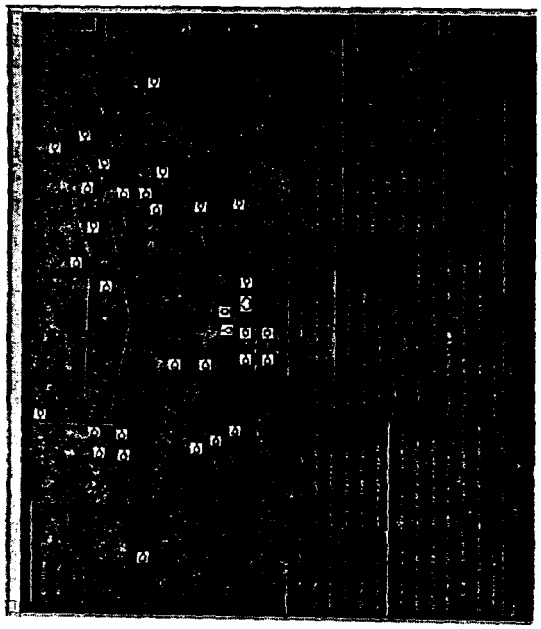

Software

0115

- Requirements
  - Kernal software provided by systems group
  - Physics/detector software provided by subsystem groups
  - Modularity
  - Portability
  - Languages
  - Data Modeling
  - Software development process
    - Software Engineering
    - Code management
    - Life cycle
      - Requirements Analysis
      - Design
      - Coding
      - System Integration
      - Acceptance Test
      - Operation and Maintenance
  - User Interface
    - X-windows, Motif
  - Database access to data
  - Standards
  - Operating System
  - Histogramming
  - Application Graphics
  - Design

0118

0120

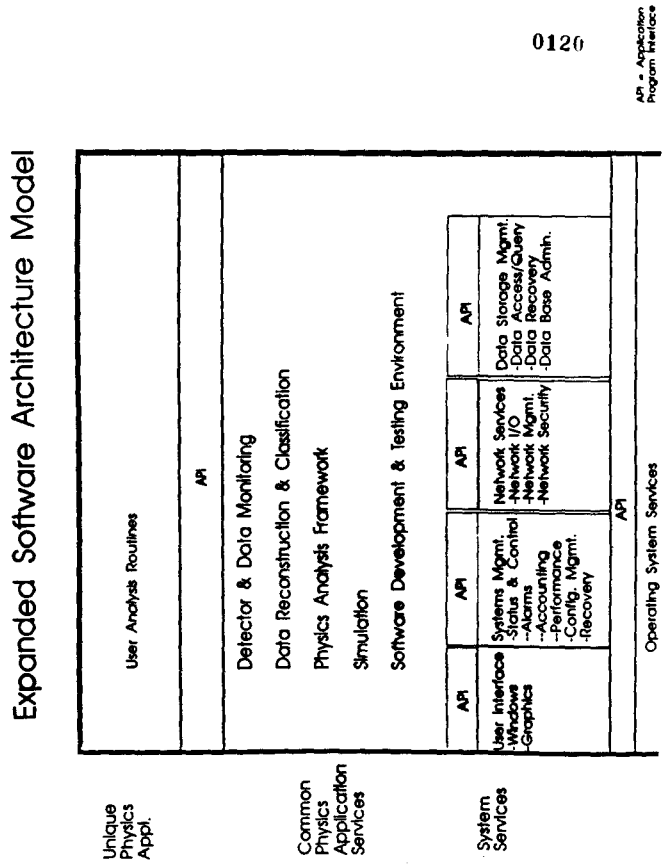

R&D Plans

0121

- Database project HPCC: ANL, LBL, UIC, UMd, SSCL, ...
- Software design and engineering SSCL + others LBL
- Architecture and performance modeling IBM, SSCL
- Online Computing U. Mich.

SDC Computing activities at SSCL

- People
  - Gaines
  - White
  - Roe
  - Frederiksen
  - Johnstad
  - Fry
  - Traversat
  - Song (B. Scipioni)
  - Nixdorf (L. Cormell)
  - Liu (M. Marquez)
- Projects
  - Software development methods
    Adams evaluation
  - Data storage and access
    - Database project
    - Advanced storage devices
      Architecture / Performance evaluation
      Cost

Schedule for SDC computing development

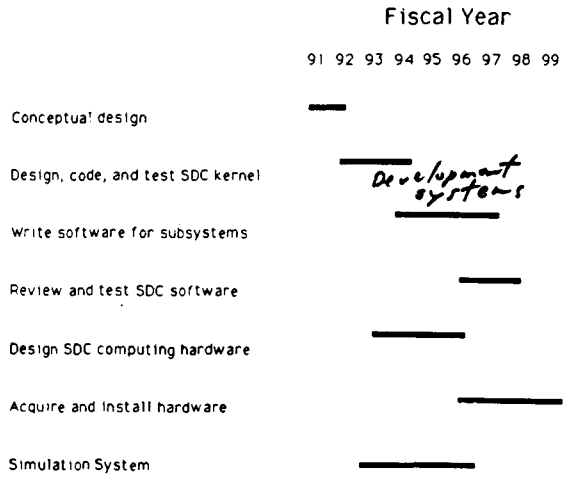

Schedule and Milestones

Hardware	
Baseline design	92
Modeling	92-95
Final design	96
Procure trial devices	94-96
Prototype system	96
Production system	98-99
Analysis system	96-99
Distribution system	
Software	
Identify software development systems	92
Core system	
Requirements Analysis	92
Functional specification	92
Design	92-93
Coding	94
Testing	95
Physics/Detector systems	
Requirements Analysis	94
Functional specification	94
Design	94-95
Coding	95-97
Testing	97-98
Simulation	
Requirements Analysis	92
Functional specification	92
Design	93-95
Coding	94-96
Testing	96-98

Data modeling tools

Data structure specification

Computing Milestones

Hardware

Fix baseline design		1/11/92
Baseline cost estimate		3/1/92
Final Design		1/96
Acquire Production System	10%	1/98
	100%	6/99
Analysis System		

Software

Identify software development systems	kernel 10/92
	user code 10/93

Core System:

Requirements Analysis	6/92
Functional Specification	10/92
complete Design	10/93
Complete Coding Release 1.0	10/94
Complete testing	10/95

Physics / Detector systems

Requirements Analysis	5/94
Functional Specification	10/94
complete design	10/95
complete coding Release 1.0	10/97
Complete testing	10/98

Simulation:

Requirements Analysis		3/92
Functional Specification		1/93
Complete design	1.0	1/94
	2.0	1/95
Complete coding	1.0	1/95
	2.0	1/96
Complete testing	1.0	1/96
	2.0	1/97

Cost

Current Computing Activities

- SDCSIM
- USE of PDSF
- SDC$_N$*EWS*

SDC Computing Costs

Cost Elements	M$
Production system:	
Tertiary storage system Raw data Pass 1 output DST	3.7
Communications link to online	0.2
Network/switch Input to production farm Output of production farm	0.05
Production computing farm (10^5 MIPS)	6
Production disk system(s)	1.5
Printers	0.02
Software	2

Data distribution system: Processors Disks Distribution media devices	1
Express line system: Processors Disks Network	1
Simulation system (10^5 MIPS)	6 ?
Local analysis system:	
Networks	0.5
Workstations	0.5
Batch processors	0.5
Storage 1 TB disk, 9 TB tertiary system	0.5
Printers	0.05
Software	0.15
External Networking	
Video conferencing (2 centers)	0.15
NREN Connections	0.1
	$ 23.92 M
Effort	
SDC Computing Support (25 FTE-yr)	2.5
Hardware (23 FTE-yr)	2.3
SDC Software: (60 FTE-yr)	6.0
Computer systems for development	0.5
Development software	0.5

Effort			FTE-yr
SDC Computing Support group	4(1992) - 10 (1999)		25
Hardware			
Requirements analysis			3
System design			6
System modeling			2
Procurement			2
Installation			5
Testing			5
Software			
Core system (Production and analysis)			
Requirements analysis			5
Design			10
Coding			5
Testing			5
Reviews			2
Documentation			3
Physics/Detector systems (Written by SDC collaboration, including SSCL)	100	SSCL:	20
Simulation software	50	SSCL:	10

T.9 FTE-yr

T. SONG 2/14/91

PHYSICS DETECTOR SIMULATION FACILITY NETWORK

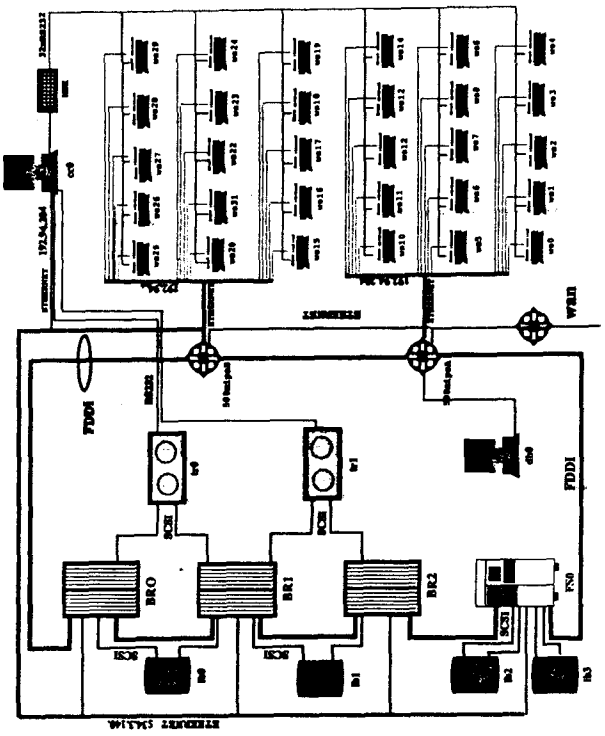

PLANNED PDSF WITHOUT OPTION

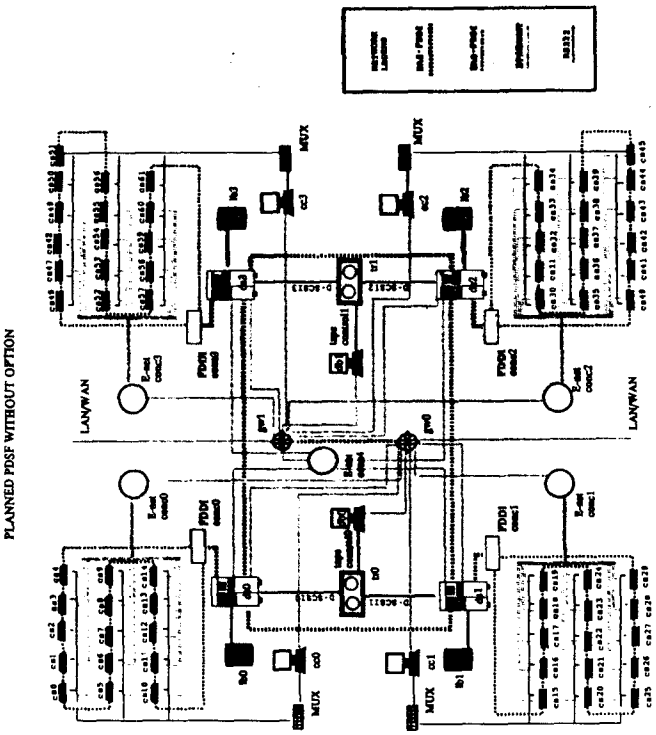

Physics in the Proposal

K. Einsweiler(LBL)

Physics in the Proposal

Physics section:

- self-contained overview of SDC goals
- contains global (no detailed detector model) simulations for major physics topics
- establishes requirements which lead into detailed studies & design choices in Detector sections

Detector sections:

- bear burden of proving that the particular implementation chosen by SDC meets requirements
- expected to contain detailed simulation results (SDCSIM/GEANT) within detailed detector model

⇒ significant coordination required to match sections

I) Electroweak Symmetry Breaking

i) low mass Higgs ($80 < m < 140$)
→ $t\bar{t}H$, WH (resist direct $H \to \gamma\gamma$)
↳ $\to \gamma\gamma$

ii) intermediate mass Higgs ($130 < m_H < 180$)
→ $H \to ZZ^* \to 4\ell$

iii) heavy Higgs ($180 < m_H \lesssim 800$)
→ $H \to ZZ \to 4\ell$, $2\ell 2\nu$, ($2\ell 2j$?)

iv) forward jet tagging
- improved background rejection
- testing $H \leftrightarrow t, Z, W$ coupling

v) susy extensions ($\Rightarrow H^\pm, h^0, H^0, A^0, \ldots$)
- many BR modified

vi) Gauge Boson Pairs ($W\gamma$, $Z\gamma$, WW, WZ, ZZ)
- check boson properties

vii) Strong Breaking (Technicolor, ...)
- high mass WW, ZZ scattering

II) Top Physics

i) mass measurement
ii) leptonic branching ratios
iii) non-standard decays (e.g. $t \to H^+ b$)
iv) V-A coupling + other detailed tests

III) susy Searches

i) squarks + gluinos
ii) charginos, neutralinos, ...

IV) Heavy Boson Searches

i) W', Z'
→ measure m, Γ, asymmetry

V) Compositeness

i) quark + lepton substructure

VI) Standard "QCD"

i) jet cross sections
ii) γ, W, Z cross sections
iii) heavy quark production (b, c)
+ jet fragmentation

→ no explicit discussion of b physics (e.g. rare decays, CP violation, ...)

These considerations are reflected in detailed performance goals: 0138

Trigger:
- topological requirements
- thresholds & acceptances

Tracking:
- acceptance
- resolution
- efficiency
- vertexing capability

Calorimeter:
- acceptance
- EM, HAD resolutions
- segmentation & depth
- linearity & dynamic range

Muons:
- acceptance
- resolution
- efficiency

Translate into specifics ...

Physics Section: very small number of people currently active 0139

⇒ anyone interested in contributing please contact me

Detailed simulations which cross detector boundaries:

(1) electron ID in particular:
simulation of E/p performance and shower profile analysis in presence of material in tracking volume

(2) τ ID "untouched" issue

τ is heavy ⇒ special relationship to Higgs
i.e. violations of universality ⇒
"beyond minimal standard Model" physics
e.g. $H^{\pm} \to \tau\nu$, $H \to \tau\tau$

⇒ would like to measure "inclusive τ" spectrum, as one currently does with e, μ 0140

signature = isolated hadron(s)
(very low mass jet with charged multiplicity = 1 or 3)

impact:

Trigger: isolated hadron like a "loose electron"
⇒ high P_T necessary to get above QCD background
(tracking triggers can't select "high" P_T tracks, e.g. $\gtrsim$ 50–100 GeV)

Tracking: 2-track resolution, mass resolution for "tight" jet

calorimeter: segmentation requirements

Physics – Detector Interface: 0141

Trigger: define list of triggers to be discussed & derive associated rates and thresholds (e & μ)

Tracking: { tracking & muons hard to parametrize ⇒ more support needed in detector section ... }

provide detailed simulations of reconstruction efficiency & resolution for:

i) e, μ in $H \to 4\ell$
(m_H = 140, 400 GeV ?)

ii) non-isolated μ in $t\bar{t} \to \mu\nu + X$

iii) b-tagging in $t\bar{t} \to b\bar{b} + X$

iv) jet fragmentation ?

v) τ identification ?

Physics in the Proposal

Physics section:

- self-contained overview of SDC goals
- contains global (no detailed detector model) simulations for major physics topics
- establishes requirements which lead into detailed studies & design choices in Detector sections

Detector sections:

- bear burden of proving that the particular implementation chosen by SDC meets requirements
- expected to contain detailed simulation results (SDCSIM/GEANT) within detailed detector model

⇒ significant coordination required to match sections

II) Top Physics

I) Electroweak Symmetry Breaking

i) low mass Higgs ($80 < m < 140$)
→ $t\bar{t}H$, WH (resist direct $H \to b\bar{b}$)
↳ $\to b\bar{b}$

ii) intermediate mass Higgs ($130 < m_H < 180$)
→ $H \to ZZ^* \to 4\ell$

iii) heavy Higgs ($180 < m_H \lesssim 800$)
→ $H \to ZZ \to 4\ell$, $2\ell 2\nu$, ($2\ell 2j$?)

iv) forward jet tagging
- improved background rejection
- testing $H \leftrightarrow t, Z, W$ coupling

v) SUSY extensions ($\Rightarrow H^\pm, h^0, H^0, A^0, \ldots$)
- many BR modified

vi) Gauge Boson Pairs ($W\gamma$, $Z\gamma$, WW, WZ, ZZ)
- check boson properties

vii) Strong Breaking (Technicolor, ...)
- high mass WW, ZZ scattering

VI) Standard "QCD"

Front End Electronics, Triggering, and DAQ

A. Lankford(Irvine)

8.0 Front-End Electronics, Triggering, and DAQ

8.1 Overview - Kirsten

8.2 Triggering - Smith

8.3 Calorimetry - Lankford, Levi, Jared, Foster, LeDu
- Introduction
- SCA-based system
- Digital PMT system
- Shower Max

8.4 Straw Tubes - Williams

8.5 Muon Chambers - Chapman

8.6 Scintillating Fibers - Baumbaugh

8.7 Intermediate Tracker - Nickerson

8.8 Silicon "off-detector" Elex - Nickerson

8.9 Data Acquisition & Control - Gaines, Barsotti

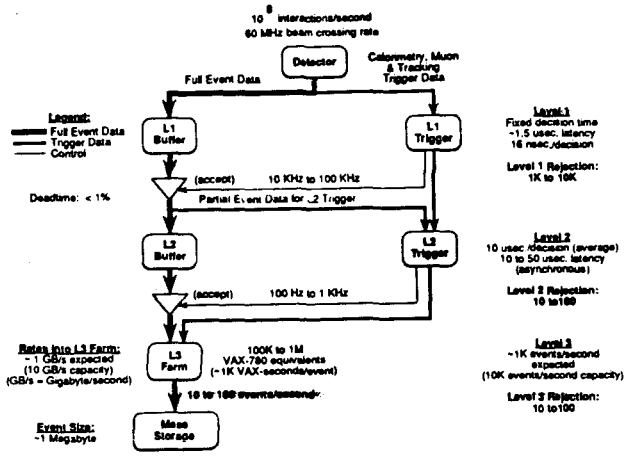

8.1 Overview

8.1.1 Functional Overview
- of complete system
- Basic functionality
- Signal flow paths
- Control flow paths
- How this system differs from previous systems

8.1.2 Physical Overview

8.1.3 Front End Channel, Card, and Crate Counts
- including
  - event sizes, data rates, trigger-data channels

8.1.4 Generic Front-End Design
- including trigger protocols, DAQ/TRIG interfaces

8.1.5 Front End Special Requirements

8.2 Triggering

8.2.1 Introduction

8.2.2 Trigger Philosophy

8.2.3 Trigger Structure

8.2.4 Trigger Definitions
- Jets
- electrons / photons
- muons
- neutrinos

8.2.5 Level 1 Trigger Information
- organized by subsystem

8.2.6 Level 1 System Layout

8.2.7 Trigger Interface to F.E. and DAQ
- including L1 Pipeline Length

8.2.8 Level 2 Trigger Information

8.2.9 Level 2 Trigger Processing

8.2.10 Level 3

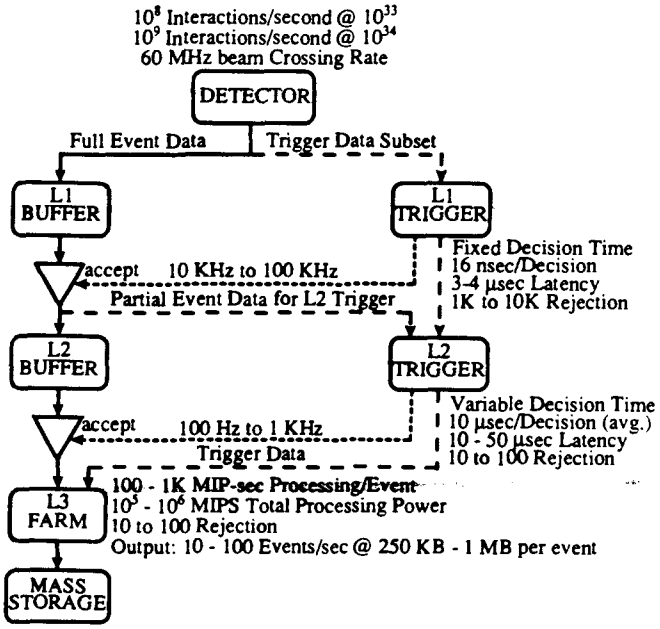

FIG. 1. Trigger and data acquisition dataflow for the SDC.

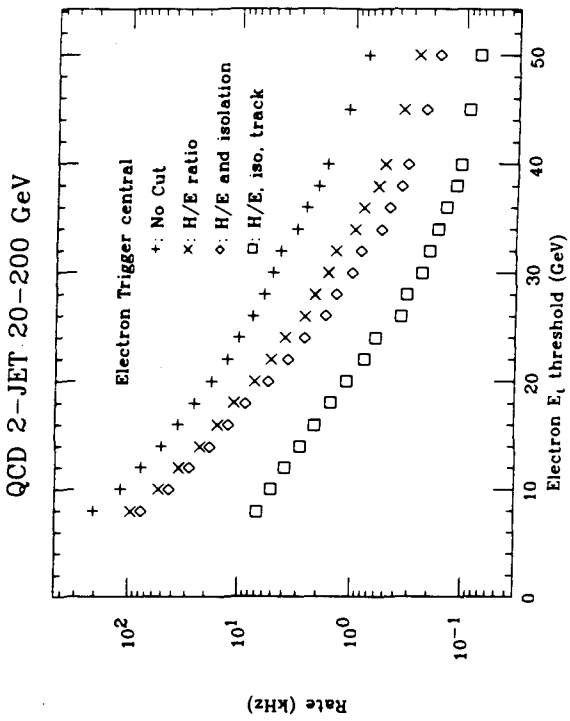

Figure 45

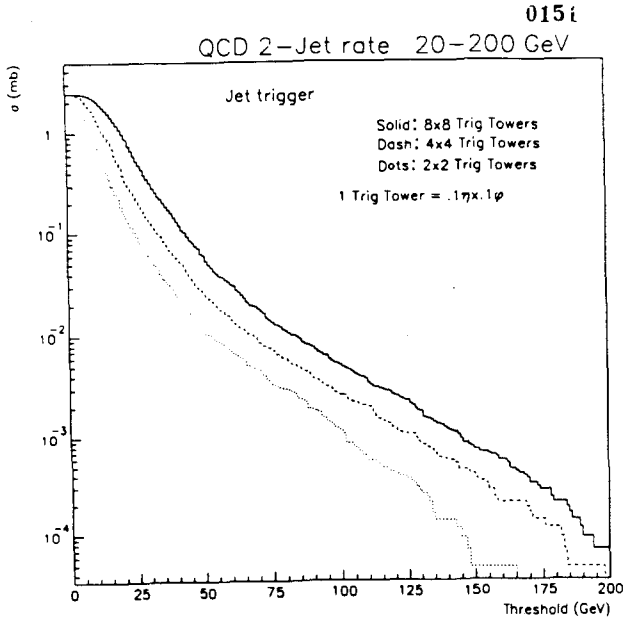

Figure 2: The level 1 inclusive jet trigger rate versus the E_T threshold for various tower sizes.

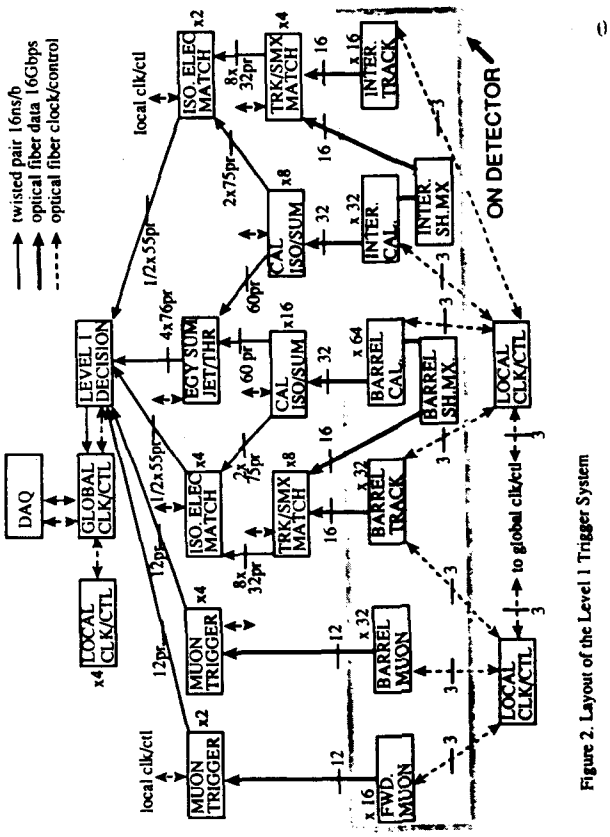

Figure 2. Layout of the Level 1 Trigger System

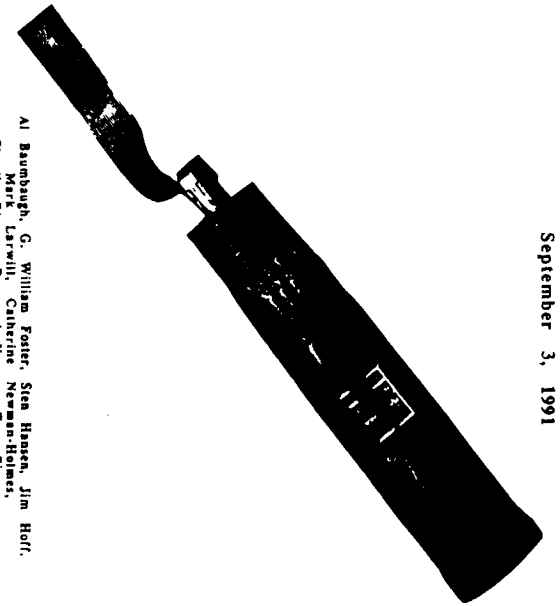

Al Baumbaugh, G. William Foster, Stan Hansen, Jim Hoff,
Mark Larwill, Catherine Newman-Holmes,
Claudio Rivetta, Raymond Yarema, Tom Zimmerman
Fermi National Accelerator Laboratory

September 3, 1991

BASELINE IMPLEMENTATION OF THE DIGITAL PHOTOTUBE READOUT SYSTEM FOR THE SDC CALORIMETER

Level 1 Clock and Control Distribution System

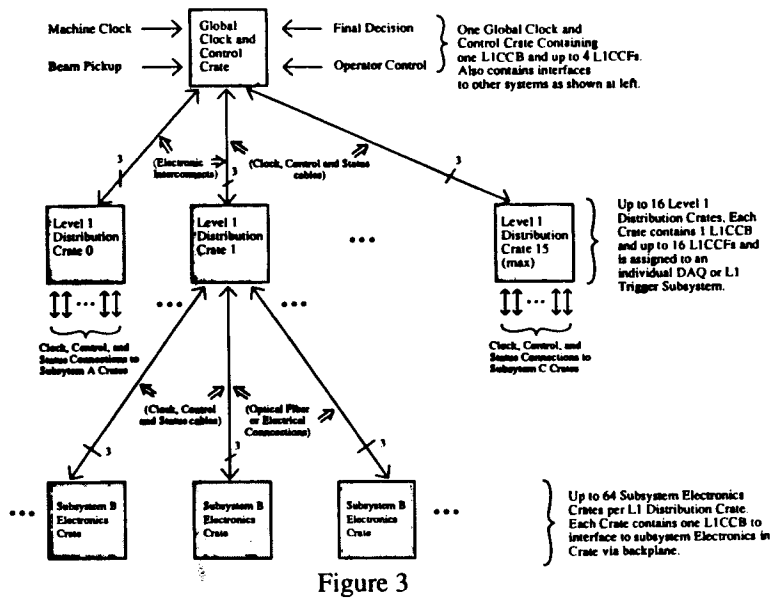

Figure 3

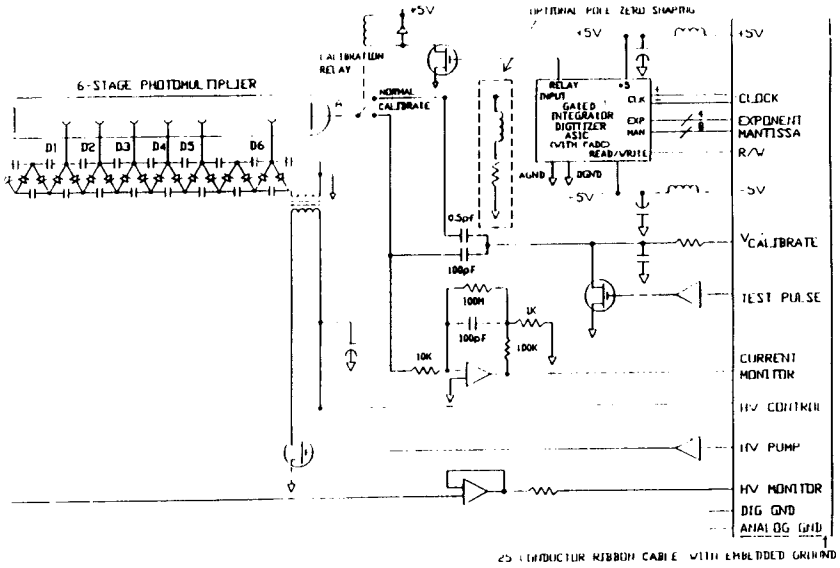

SDC SCINTILLATING TILE
PHOTOMULTIPLIER TUBE CIRCUIT SCHEMATIC

fig. 12 PMT BASE DIGITIZER MODULE circuit diagram. It contains the Phototube, Cockroft-Walton "charge pump" HV supply, current monitor, charge injection circuit, and

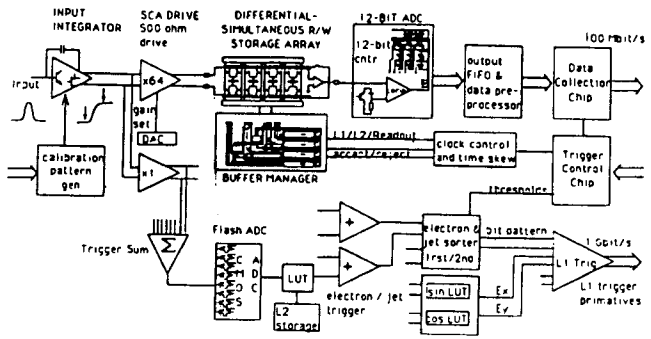

10. Calorimeter front-end block diagram

frequency cutoff may be realized in the preamplifier and

Development of devices which could operate at

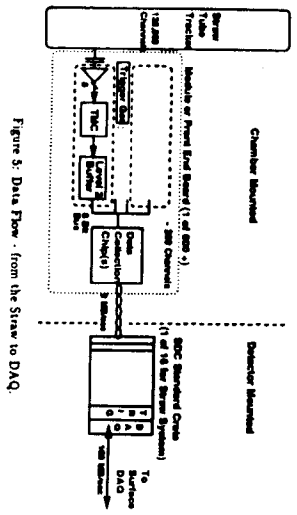

Figure 5: Data Flow - from the Straw to DAQ.

Front end read out components

today status

1024 "Phi"bit

1024 "phi" x 30 "eta"

Level 1 Trigger

8bit

FMC

slow

Level 2 Trigger

Photo Detector → Preampli Shaper → Pipeline → ADC → Buffer

Photo Detector	Preampli Shaper	Pipeline	ADC	Buffer
APD ? Avalanche Photo Diode or MAPMT ? Multianode Photomultiplier	Shaping 6 ns *depends of the Photo detector*	3 to 4 µsec Analog Digital ?	Dynamic range 12 bit or more? Speed Multiplexing ?	Technique (FIFO or RAM ?) Size ? DAQ ?

or...

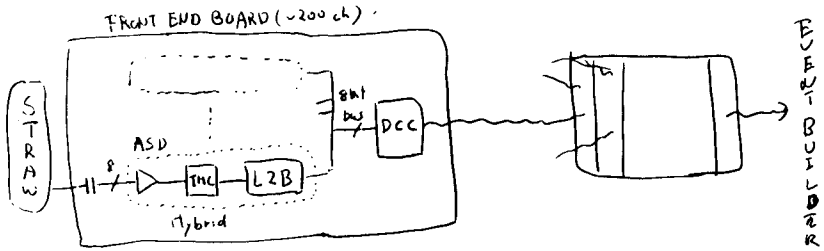

Front end read out partition

- Read out organized per octant inside the detector
- In tegration with the rest of the calorimeter (EM + HD)
- Assume 256 read out channels per Front end board → 128

END CAP	Elem.	El. Ch.	FE card
EM towers	180	720	3
HD towers	60	240	1
SM xtrips	544	544	2
SM y strips	544	544	2

BARREL	Phi	Eta	Elem.	El. Ch.	FE card
EM towers	16	28	448	1792	7
HD towers	8	14	112	448	2
SM xtrips	128	7	896	896	4
SM y strips	4	224	896	896	4

1328 Channels
---> 1 crate
2 ⇒ 4 wedges/crate
= 2 rectns /crate

4032 Channels
---> 2 crates
4 ⇒ 2 wedges/crate

BARREL

END CAP

96

TOTAL= 48 crates
---> 16 "End cap" crates
---> 32 "Barrel" crates

ONE HALF "OCTANT"

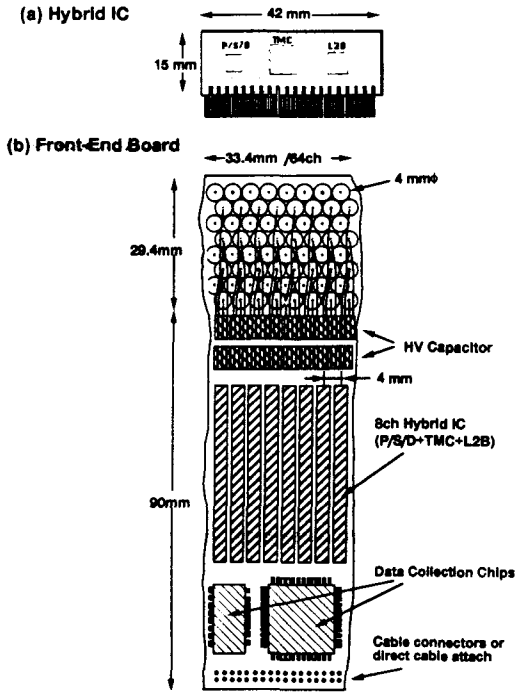

Front-End Electronics Mounting Example

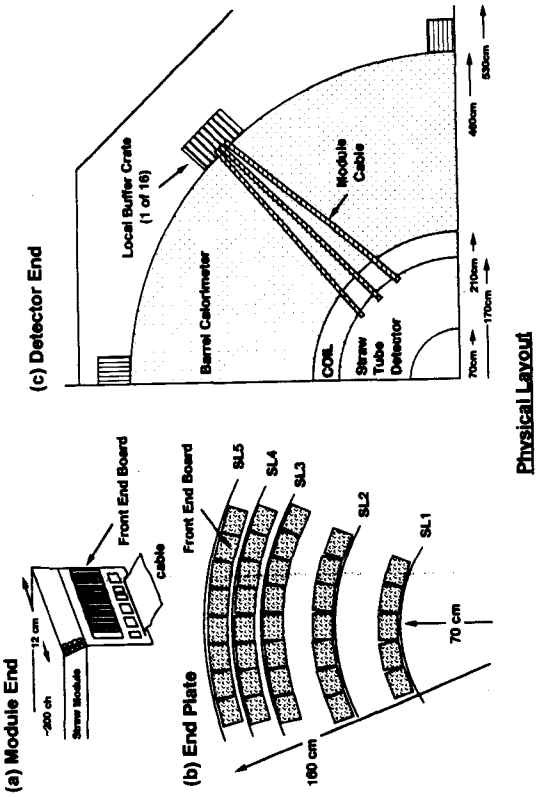

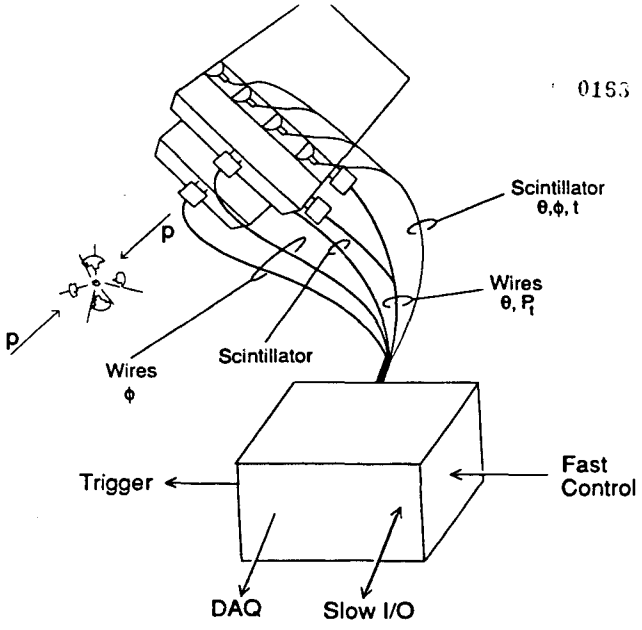

FIG. 2. An octant section from the barrel portion of the SDC muon system beyond the toroid for the option that includes two scintillator stations radially.

the muon system at modest transverse momentum, falling dramatically with momentum. The output rate from the first trigger of these muons has yet to be determined and is a

SDC Data Acquisition
Event Data Fragment Sources & Locations
(October 28, 1991)

Front-End/Trigger System	# Crates/ DAQ CPUs	# Sources	Crate Type	Location
Inner Tracking Silicon Strips & Inner Tracking Silicon Pixels	10	10	SDC DAQ Std.	Counting Room
Intermediate Tracking Gas Microstrips	10	10	SDC DAQ Std.	Counting Room
Central Calorimeter (SCAsl, Central Calorimeter Shower Max & Outer Tracking Straw Tubes[1]	96	256	SDC DAQ Std.	On Detector
Central Calorimeter (Flash ADCs)[2]	96	96	Special	On Detector
Forward Calorimeter	2	2	SDC DAQ Std.	Counting Room
Muon	64	64	SDC DAQ Std.	On Detector
Level 1 Trigger (<= 1 KB/crate)	40	40	SDC DAQ Std.	Counting Room
Level 2 Trigger (<= 1 KB/crate)	30	30	SDC DAQ Std.	Counting Room
Totals:	288	413		

Notes:
1. Each of the 96 crates has one Data Collector module with one Calorimetry and one Shower Max source. Event data are transmitted directly to the Event Builder Subsystem from the Data Collection modules. 64 of the 96 crates have Straw Tube event data read out over the crate's bus and transmitted to the Event Builder Subsystem by the crate's DAQ CPU module.
2. Central Calorimeter (Flash ADCs) was not counted in totals

Descoped Quantities
Crates With DAQ CPUs & Front-End/Trigger System Event Data Sources

0165

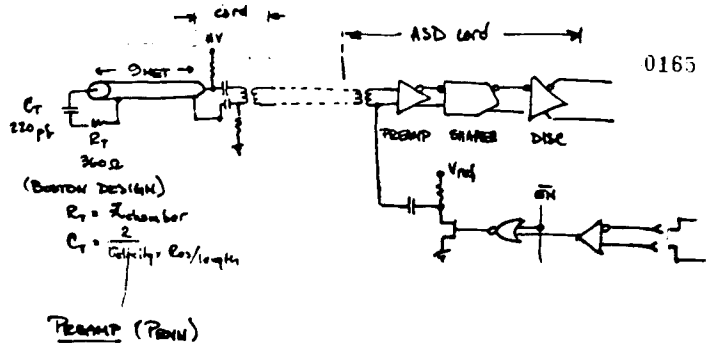

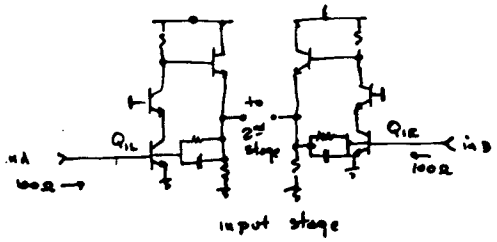

NOISE CALCULATIONS (SPICE)

DOMINANT NOISE SOURCES

1. INPUT TRANSISTORS Q_{1L}, Q_{1R} BASE RESISTANCE & SHOT
2. WIRE RESISTANCE OF CHAMBER (@ 80Ω/METER)
3. TERMINATION RESISTOR

0166

SDC Fiber Tracker Electronics Block Diagram

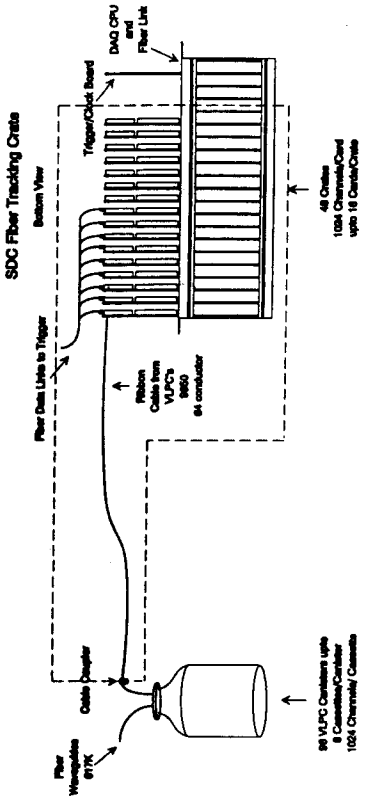

10/31/91

0167

SDC Fiber Tracker Reciever Board

9U X 400 mm (14.437" X 15.750") Printed Circuit Board

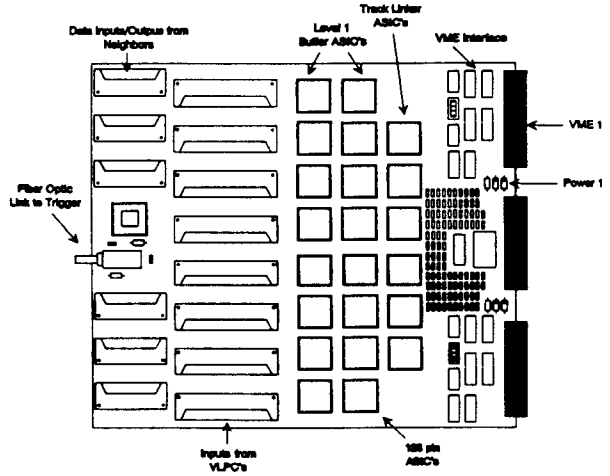

0165

SDC Tracking/Trigger Segment Finder ASIC

Stores all "Hit" information locally while trigger is formed

Provides serial readout of selected events

Provides "Track Segments" for trigger

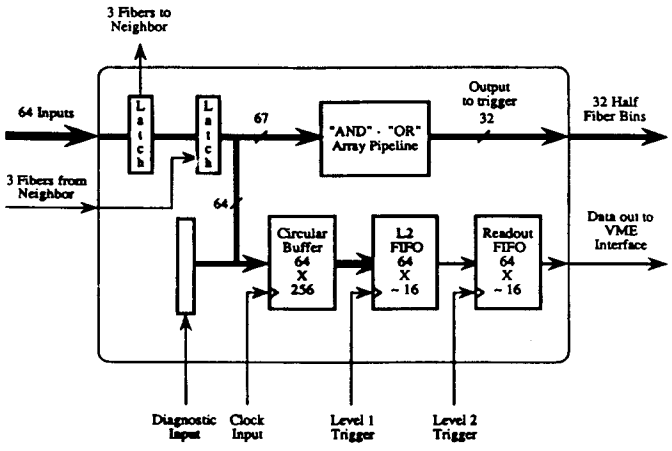

Track Segment Finding Algorithm

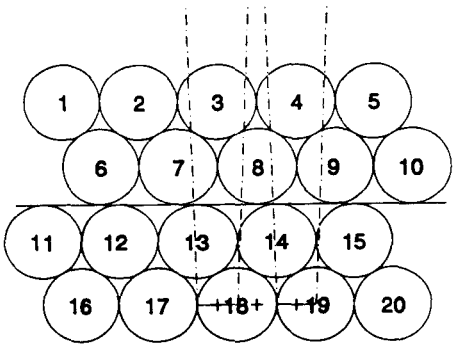

Acceptance cones for 10 GeV tracks
in half fiber bins, centered on 1/4 fiber dia.

SDC Data Acquisition System
Technical Proposal Outline
(11/14/91)

8.9 Data Acquisition and Slow Control

8.9.1 Data Acquisition System Overview

8.9.2 Data Acquisition System Requirements
- 8.9.2.1 Data flow and event collection requirements
- 8.9.2.2 Data monitoring requirements
- 8.9.2.3 Slow control requirements
- 8.9.2.4 Partitioning and stand-alone operation requirements
- 8.9.2.5 ...abilities requirements

8.9.3 Relationship of Data Acquisition to other Subsystems
- 8.9.3.1 Relationship to front-end system
- 8.9.3.2 Relationship to trigger system
- 8.9.3.3 Relationship to slow controls system
- 8.9.3.4 Relationship to On-line computing system
- 8.9.3.5 Relationship to level 3 processor system

8.9.4 Data Acquisition System Architecture
- 8.9.4.1 Logical block diagram
- 8.9.4.2 Physical block diagram and layout
- 8.9.4.3 Data flow paths
- 8.9.4.4 Control paths and slow control system
- 8.9.4.5 Partitioning and stand alone operation
- 8.9.4.6 Major DAQ components and channel counts
  - a) Event data read-out modules
  - b) Subsystem crate
  - c) Event builder subsystem
  - d) Event data flow control
  - e) On-line processor subsystem
  - f) Control computing interface
  - g) Rack protection subsystem
  - h) Software systems

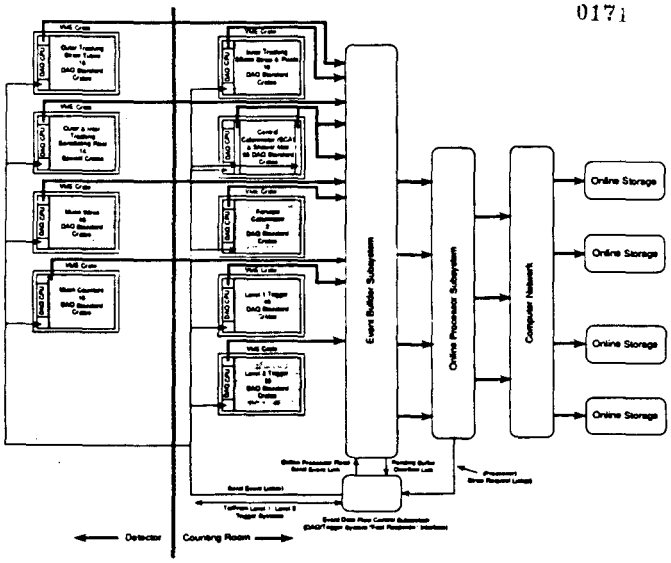

Update

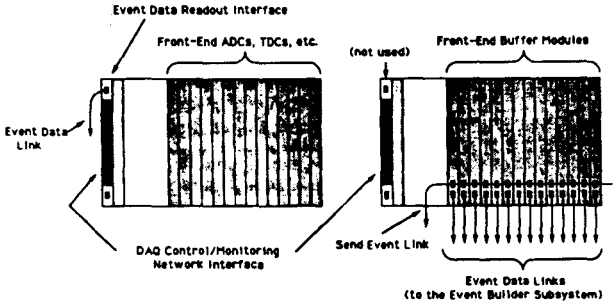

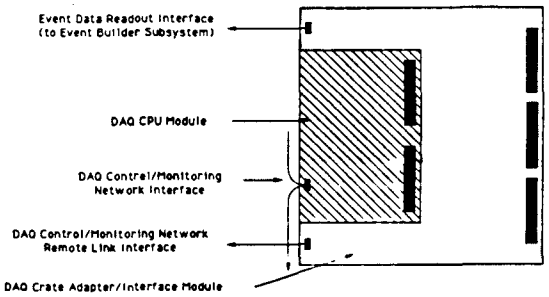

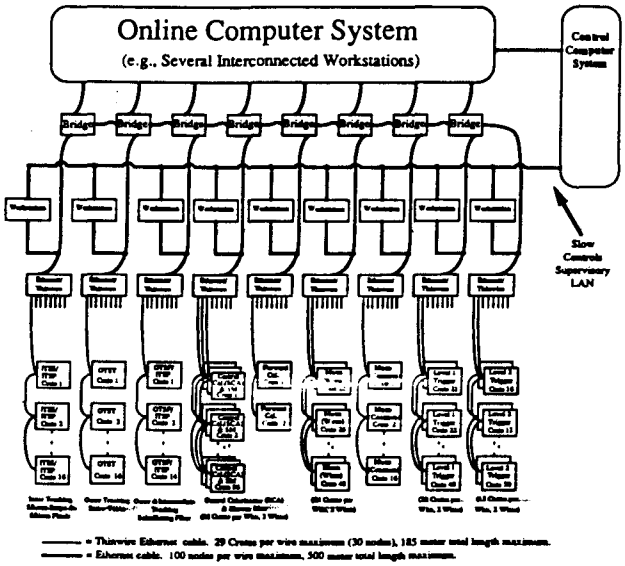

8.9.5 Additional DAQ Component Details

8.9.5.1 Front-end & trigger system event data readout & control/monitoring interface
- a) Crates, backplanes and power supplies
- b) DAQ CPU modules
- c) DAQ event data readout bus slave interface
- d) DAQ crate adapter/interface module
- e) Event data links
- f) DAQ control/monitoring network
- g) Remote DAQ control/monitoring network interface, links & repeaters

8.9.5.2 Event builder subsystem
- a) Input interface & data balancing/input queueing network
- b) switching network
- c) Interface to online processor subsystem

8.9.5.3 Event data flow control subsystem
- a) Interface to trigger subsystem
- b) Interface to other DAQ subsystems
- c) Event data flow and trigger inhibiting

8.9.5.4 Online processor subsystem
- a) Processing and software development environment
- b) Interface to other DAQ subsystems

8.9.5.5 Software systems
- a) Run control
- b) Runtime user interface
- c) Control and monitoring interface

8.9.5.6 Stand-alone DAQ systems

8.9.6 Commissioning the Data Acquisition System (Installation, Integration & Testing)

8.9.7 Status, Ongoing and Future R&D, Milestones & Critical Path Items

SDC DAQ Milestones

Completion of DAQ requirements	Nov, 91
Completion of DAQ system design, incl. technical choices	1993
Completion of DAQ component design	1994
Portable DAQ for use in test beams/labs	1994
Prototypes of all DAQ components	1995
Delivery of partial DAQ systems for subsystems	Jan, 97
Muon subsystem	?
Calorimeter subsystem	?
Tracking subsystem	?
Installation of complete DAQ system	Jan, 99
Certification of full, working DAQ system	July, 99

LOCATION OF ELECTRONICS

INSIDE OR OUTSIDE MUON STEEL

SCENARIOS

1) OUTSIDE MUON SYSTEM
2) RACK-MOUNTED CRATES ALONG VERTICAL WALLS OF BW-1
3) CRATES MOUNTED ON SURFACE OF CALORIMETER
4) REVISED LAYOUT ON CALORIMETER

ISSUES

1) ELECTRONICS PERFORMANCE
2) RELIABILITY
3) EASE OF MAINTAINANCE
4) EASE OF DESIGN
5) COST

CONCLUSIONS

1) THE INNER RADIUS OF THE MUON SYSTEM SHOULD BE CHOSEN SO AS TO ALLOW LOCATION OF ELECTRONICS IN CRATES EITHER ON THE BACK OF THE CALORIMETER OR IN RACKS ADJACENT TO BW-1.

2) THE ELECTRONICS SHOULD BE PLACED ON THE BACK OF THE CALORIMETER, PROVIDED THAT A LAYOUT WHICH ALLOWS ADEQUATE ACCESS TO PMT'S IS DEVELOPED.

Report from Committee on Absorber Configuration

J. Siegrist(SSCL)

Conclusion on Reentrant ENDCAP

- more uniform B
- Longer detector (≥ 2 m$)
- reduced coil forces
  - However, flat iron design gives coil forces $<<$ LAr
  - other methods to reduce coil risk?
- Additional breaks in EM coverage un Appearing. Work in progress to understand (B field, etc.)

Choose 'flat' option $\simeq$ Model A or B

CALORIMETER

Absorber

Configuration

Decision

16-NOV-91

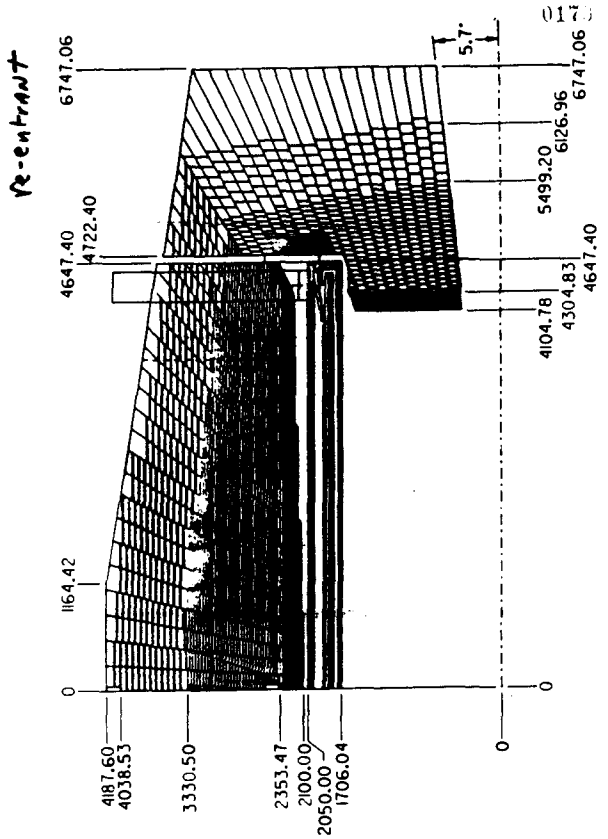

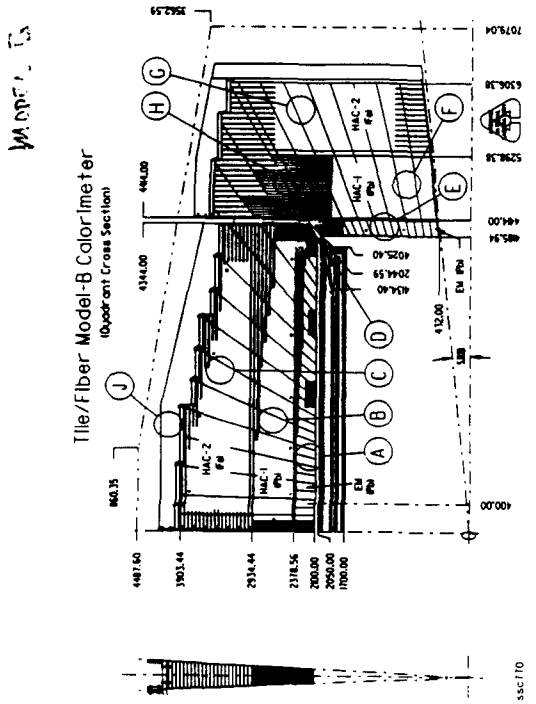

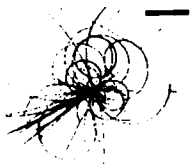

Calorimeter Configurations

	Model A	Model B	Reentrant
Endcap EM			
Longitudinal segs.	2	2	2
Xverse seg.	.05	.05	.05
Pb thickness (mm)	6.3	8	6.3
Scint. thickness (mm)	4	4	4
absorber layers	18	15	18
X0	21	21	21
Endcap HAD 1			
Xverse seg.	.05	.1	.05
abs. thickness (mm)	51 Fe	31.5 Pb	51 Fe
scint. thickness (mm)	2.5	2.5	2.5
absorber layers	21	24	21
λ	6.4	4.4	6.4

Calorimeter Configurations

	Model A	Model B	Reentrant
Total Depth eta=0	9 λ	9 λ	9 λ
Total Depth eta=3	11 λ	11 λ	>11 λ
Barrel EM			
Longitudinal segs.	1	1	1
Xverse seg.	.05	.05	.05
Pb thickness (mm)	3.2	4	3.2
Scint. thickness (mm)	4	4	4
absorber layers	36	29	36
X0	21	21	21
Barrel HAD 1			
Xverse seg.	.05	.1	.05
abs. thickness (mm)	25.4 Fe	21 Pb	25.4 Fe
scint. thickness (mm)	2.5	2.5	2.5
absorber layers	32	24	32
λ	4.8	3	4.8

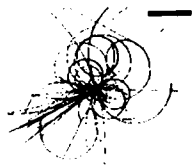

Calorimeter Configurations

	Model A	Model B	Reentrant
Endcap Had2			
xverse seg.	.1	.1	.1
abs. thickness(mm)	102 Fe	102 Fe	102 Fe
scint. thickness	2.5	2.5	2.5
abs. layers	7	10	7
λ	4.3	6.1	4.3
total depth barrel	11λ	11λ	11λ
resolution (e,π)			
stochastic			
constant			

Calorimeter Configurations

	Model A	Model B	Reentrant
Barrel Had2			
Xverse seg.	.1	.1	.1
abs. thickness(mm)	51 Fe	51 Fe	51 Fe
scint. thickness	2.5	2.5	2.5
abs. layers	12	18	12
λ	3.6	5.5	3.6
total depth barrel	9λ	9λ	9λ
resolution (e,π)			
stochastic			
constant			

E/pi vs E, AMBBy, 22.3 9.59 98.1 179

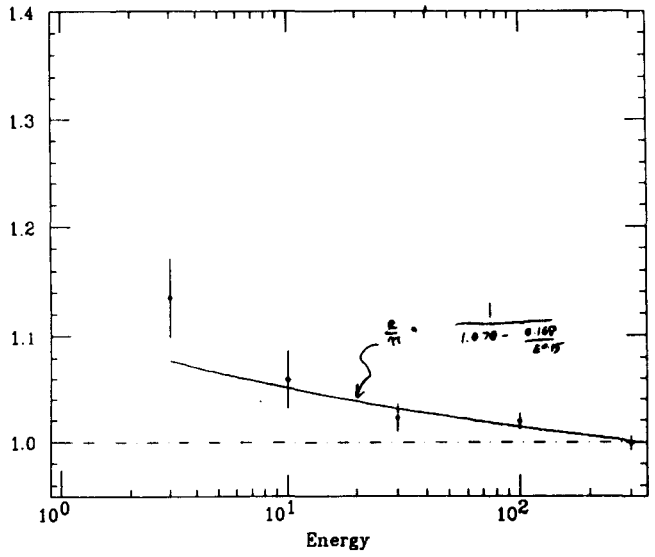

0195

Absorber Configuration Issues

Main Issues: A B Re-entrant

- Had Resolution, Constant term
- Energy Scale Error
- Cost
- Coil forces
  Field Uniformity
  Tracker Volume
  Coil/tracker supports
- Access and Supports
- Integration Issues
- Impact of Multiple Scattering on L1 muon trigger
- Technical Risk

0197

E/pi vs E, AMABy, 23.2 9.52 86.7 170

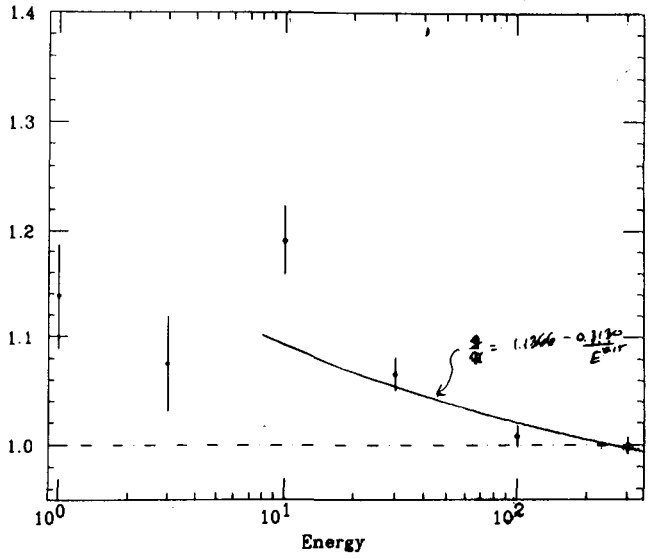

0196

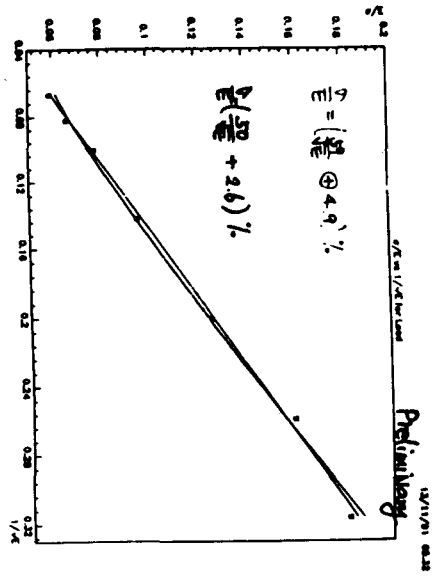

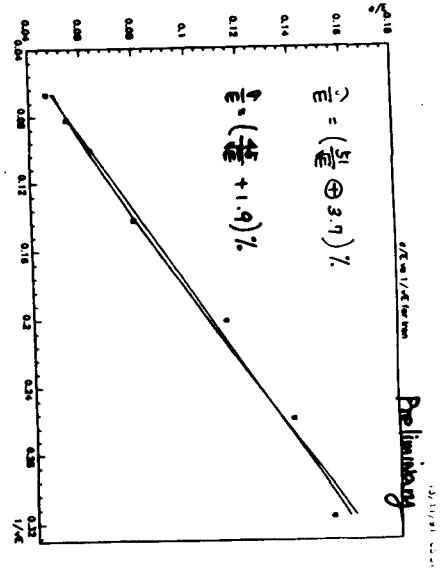

0198

Summary of Single Particle Response

case	e/h	<---------σE/E----------> e/h calib		300 GeV calib	
A Barrel	1.57	0.66	0.054	0.73	0.060
B Barrel	1.17	0.55	0.042	0.58	0.051
B Homo.	1.08	0.65	0.000	--	--
A Endcap	1.47	0.83	0.051	0.83	0.074
B Endcap	1.12	0.79	0.049	0.80	0.052

Barrel e- resolution $0.115/\sqrt{E} + 0.003$

Jet Response

Single particle response (E_{meas}/E_{true}, sigma_E/E) parameterized as a function of energy.

- Isajet twojet events, various Et ranges, |eta|<1.2 for barrel studies.
- fixed cone (R=0.7) cluster algorithm. Seed = highest Et track in jet. Iterate to find stable centroid. (Perfect resolution for everything but neutrinos and muons).
- same cone used for all calorimeter cases.

Calorimeter response to a jet is the sum of the responses to the single particles in the cone:

$$E^{jet}_{t\,meas} = \sin\theta_c \cdot \sum_{i=1}^{n} E^{i}_{meas} \quad ; \text{ sum over non-}\nu,\mu \text{ in cone}$$

$$E^{i}_{meas} = E^{i}_{t\,true} \cdot \left[\left\langle \frac{E_{meas}}{E_{true}} \right\rangle + X\left(\frac{\sigma_{Et}}{Et}\right)\right] \quad ; X = \text{Gaussian rand. num}$$

$$E^{jet}_{t\,true} = \sin\theta_c \cdot \sum_{i=1}^{n} E^{i}_{true} \quad ; \text{ (non-}\nu,\mu\text{)}$$

Cases Studied -- Barrel

In addition to models A and B calibrated via e/h or at 300 GeV, simulate other cases for comparison:

- linear model B:
  $\sigma e/E = 0.57/\sqrt{E} \oplus 0.042$ (π-)
- good resolution:
  $\sigma e/E = 0.40/\sqrt{E} \oplus 0.030$ (π-)
- very good resolution:
  $\sigma e/E = 0.40/\sqrt{E}$ (π-)

All of these have e- resolution of $0.115/\sqrt{E}$ and have < Et-meas/Et-true> = 1.

Interpretation

Understand jet resolution by studying:
- compositeness
- dijet mass resolution (Z')
- H--> jet jet e+e-
- missing-Et

Compositeness

- Linearity (after correction) most important.
  - determine using single particle test beam data + MC jets (need to know fragmentation functions and be able to extrapolate single particle response)
  - use gamma-jet events?

Bigger correction ==> bigger error (?)

- non-Gaussian tails must be small and understood.

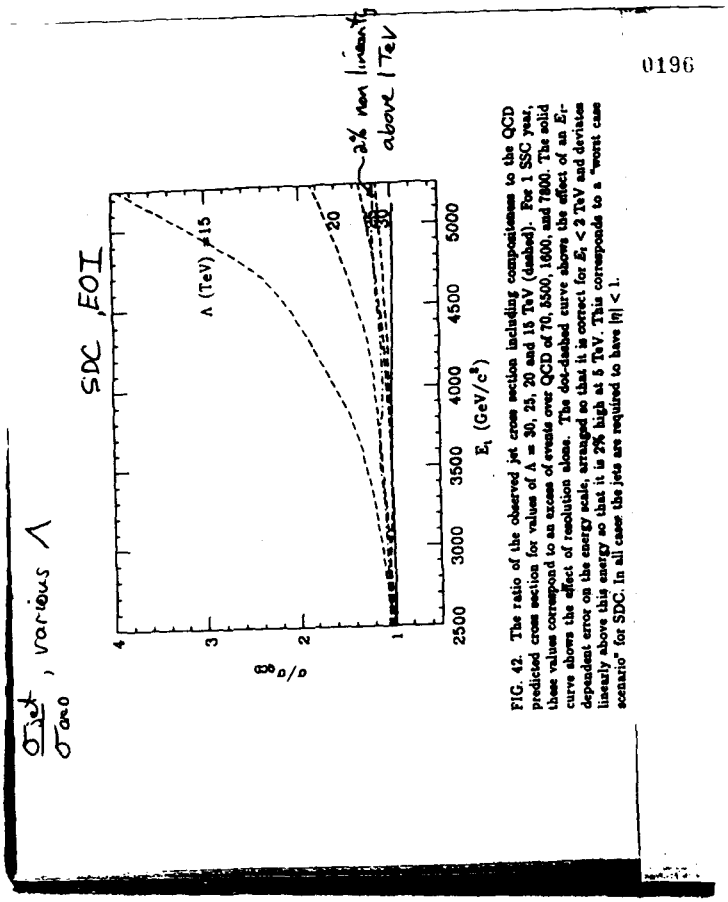

FIG. 42. The ratio of the observed jet cross section including compositeness to the QCD predicted cross section for values of Λ = 30, 25, 20 and 15 TeV (dashed). For 1 SSC year, these values correspond to an excess of events over QCD of 70, 5500, 1600, and 7800. The solid curve shows the effect of resolution alone. The dot-dashed curve shows the effect of an E_T-dependent error on the energy scale, arranged so that it is correct for $E_T < 2$ TeV and deviates linearly above this energy so that it is 2% high at 5 TeV. This corresponds to a "worst case scenario" for SDC. In all cases the jets are required to have $|\eta| < 1$.

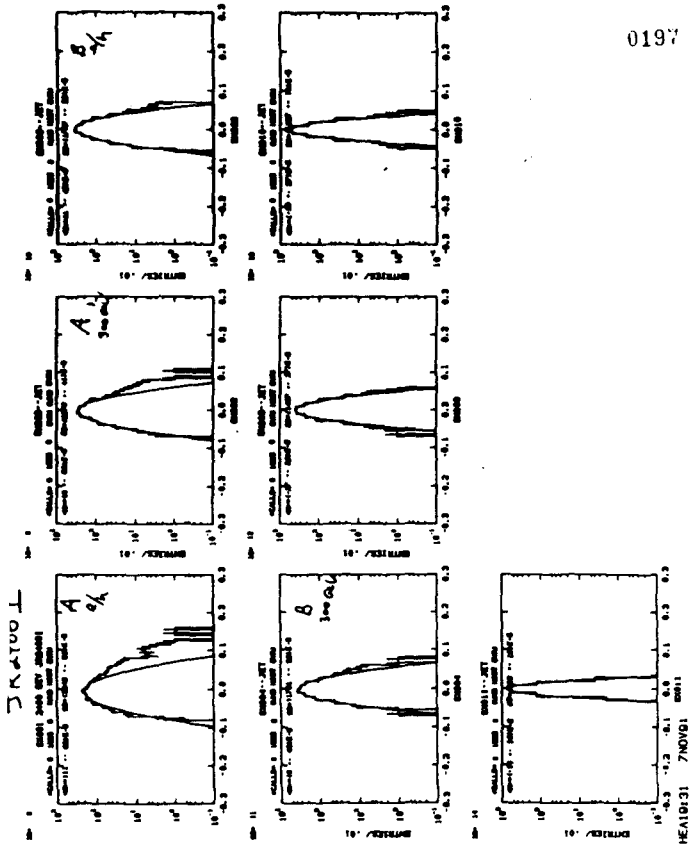

Dijet Mass Resolution

- Use Isajet Drell-Yan events to make heavy vector boson of fixed mass.

Mass of two-jet event:

- $\vec{P}jet = \sum Ei\,\hat{n}i$, cones defined above. (use true particle direction or nearest .05 bin center).

- event mass is the mass of the 4-vector sum of the two jets.

- excludes pileup, combinatorics and leakage.

- includes calorimeter resolution, underlying event, fragmentation fluctuations, gluon radiation and neutrinos.

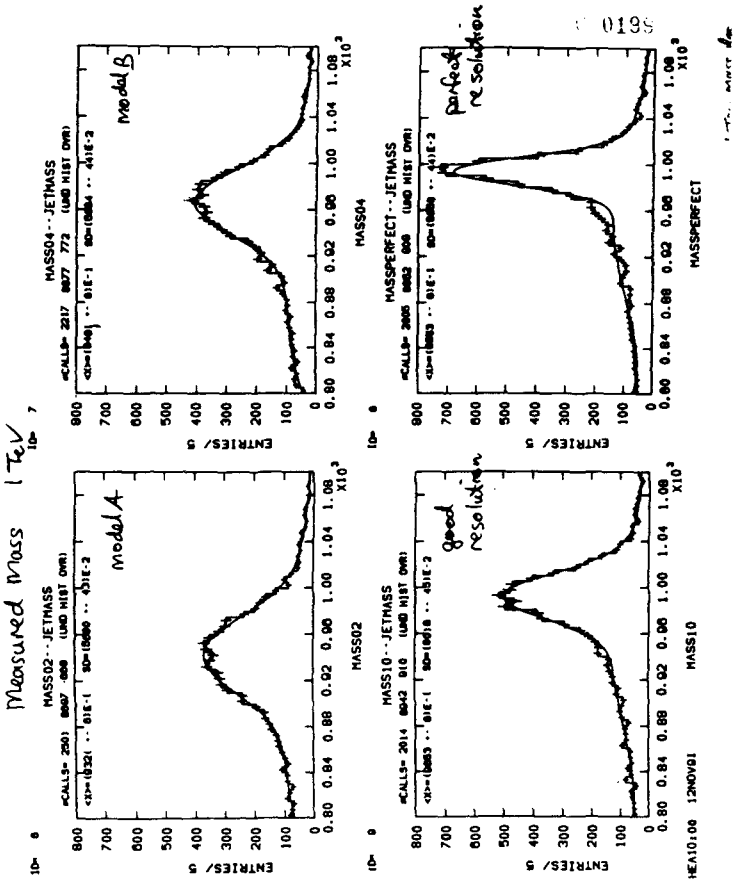

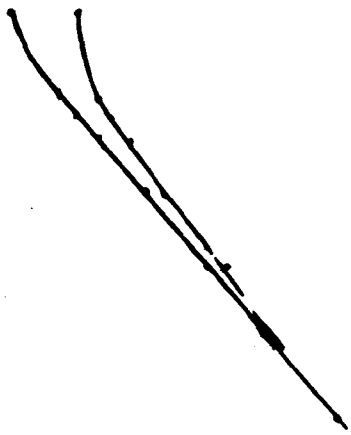

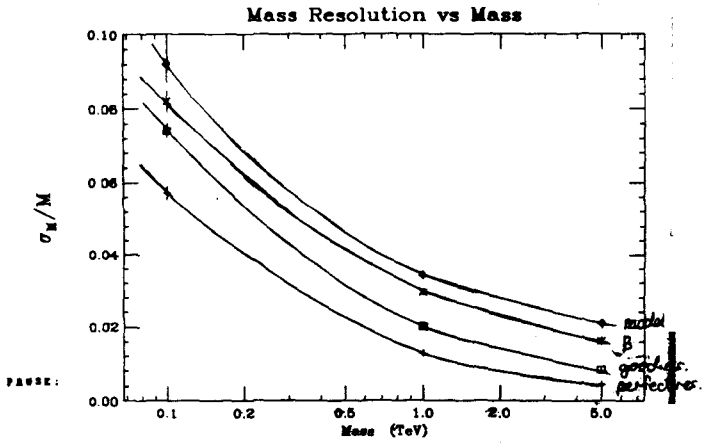

PRESENT WORK

RESOLUTION

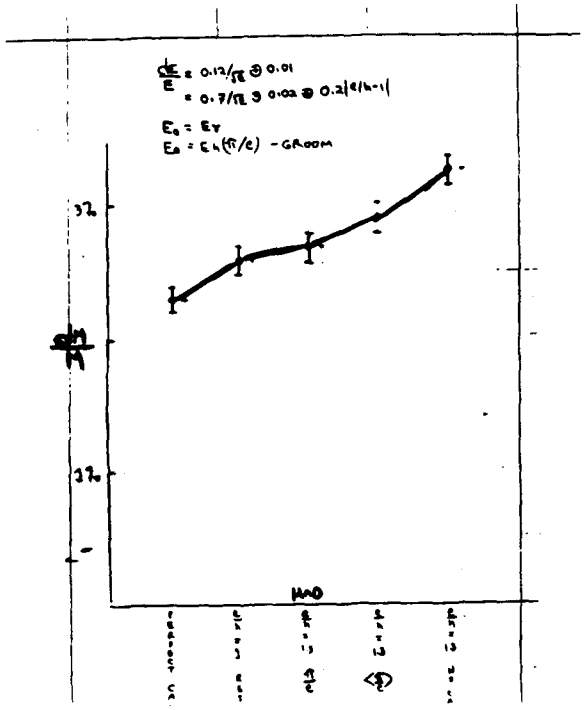

Jet resolutions JRxxxI Barrel NOV 7/9,

Fit all 5 energies — fit resfitx fortran, resooxA fortran — 0203

case	
model A, barrel, e/h	(.058 ± 0.08) ⊕ (.030 ± .004)
" " 300 GeV	(0.61 ± 0.02) ⊕ (.016 ± .002)
B " e/h	(0.49 ± 0.02) ⊕ (.015 ± .002)
B " 200 GeV	(0.51 ± 0.02) ⊕ (.011 ± .002)
Tune B	(0.48 ± .014) ⊕ (0.010 ± 0.001)
good res σ_{jet} 0.003, 4%	(0.357 ± .009) ⊕ (0.007 ± .001)
V. good res (no const.)	(0.347 ± .005) ⊕ (0.002 ± .001)

- constant term (& stochastic term) are better for jets than for pions
- small pion nonlinearity (<10%, E ≥ 10 GeV) ⇒ small increase in constant term (model B, e/h vs linear model B)

  larger nonlinearity ⇒ larger const term (model A e/h vs model A, 300 GeV)

0204

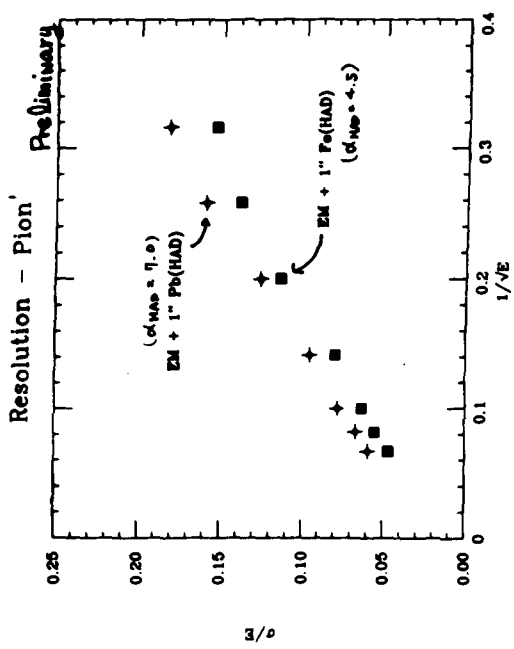

0205

HAD RES

MODEL A, nominal	.61 ⊕ .02 (JETS)
	.51 ⊕ .04 π, HFC
	.66 ⊕ .05 π, CALOR
MODEL B	.51 ⊕ .01 (JETS)
	.57 ⊕ .04 π, HFC
	.55 ⊕ .02 π, CALOR

JET Linearity .04

A, R: $E_{meas} - E_{true}$ ~ .93 - .95

B: ~ .97 - .99

MASS Resolution @ 1 TeV

A: .034

B: .032

0206

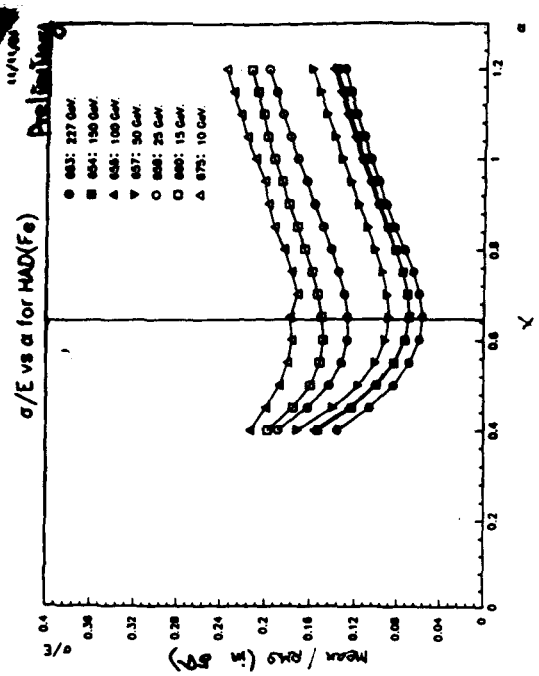

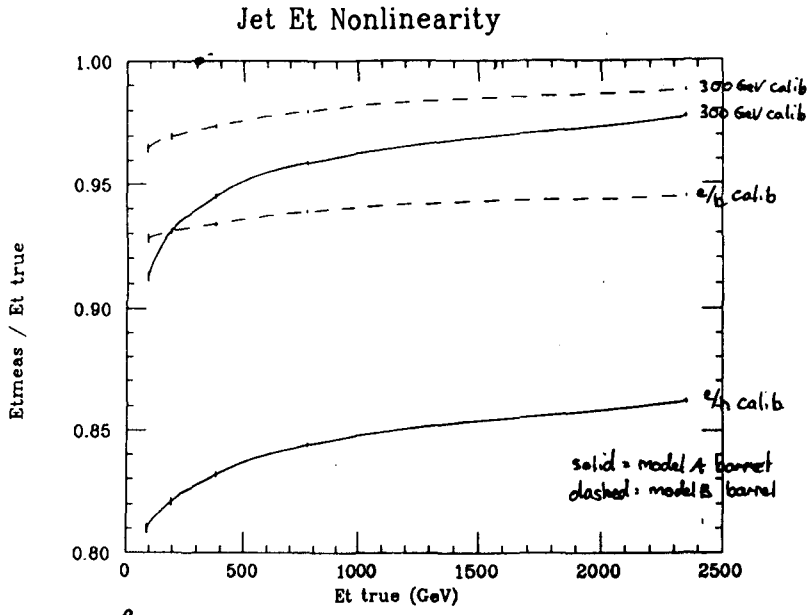

$e/\pi \neq 1 \Rightarrow$ nonlinearity in measured jet E_t

0209

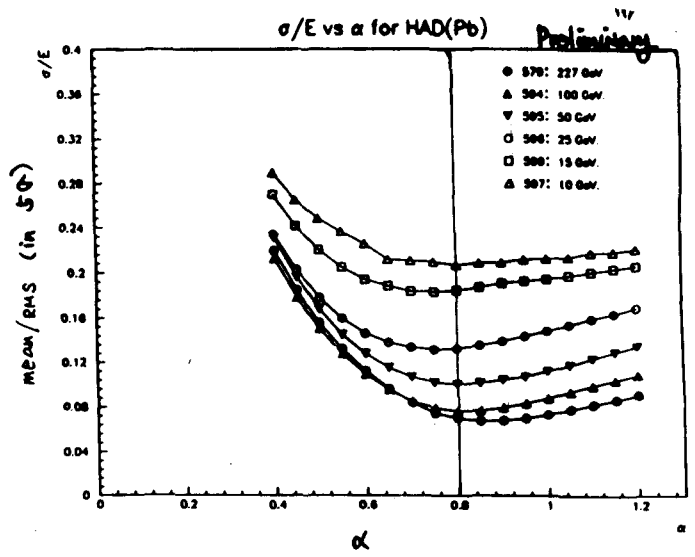

$E = E(EM) + \alpha \cdot W_{\pi} \cdot E(HAD)$

$W\left(\frac{e}{(\pi)}\right) = 1.1$

0207

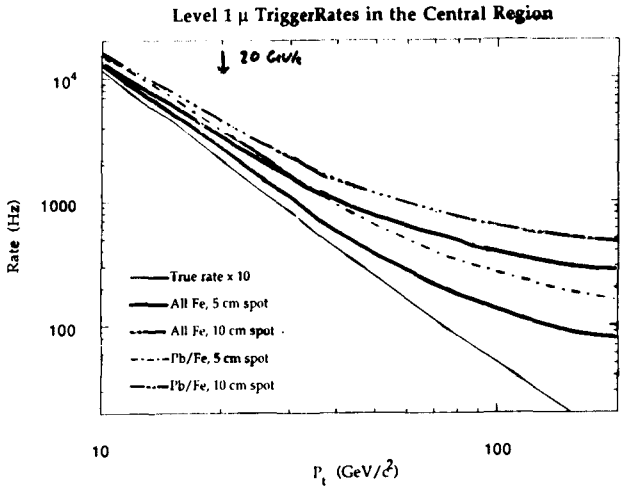

0210

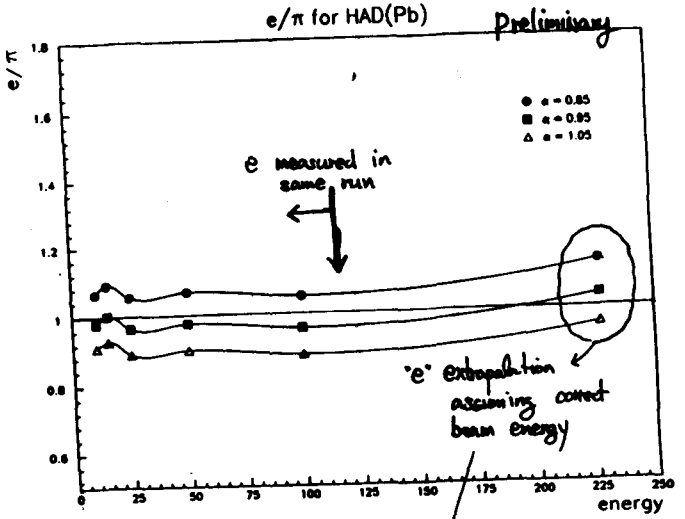

errors from beam energy incorr
leakage
saturation (ADC)

0208

Recommendation

The Calorimeter group recommends adoption of an iron hadronic calorimeter in both the barrel and endcap .

- **physics performance of lead and iron comparable**
- **lead version cost + 8 M$**
- **re-entrant version has additional breaks in the EM coverage**

A new consensus baseline (14-Nov resolution) has been adopted

7 11/14/91 jls

0213

$\Delta W = 250$ t

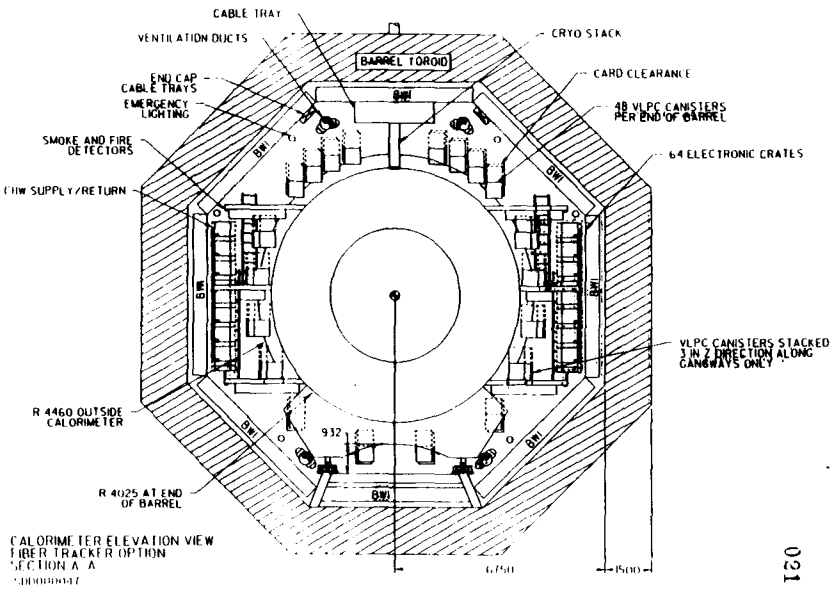

CALORIMETER ELEVATION VIEW
FIBER TRACKER OPTION
SECTION A-A

0211

CALORIMETER COST COMPARISON

LEAD VS. STEEL IN HAC1

- **Baseline Cost (Descope 20) Has Lead in HAC1 of Barrel and End Cap**
- **Replacing Lead with Steel in Barrel and End Cap Saves 7.9 M$, Relative to Descope 20**
- **Replacing Lead With Steel in End Cap Only Saves 2.8 M$**
- **Contingencies Included in These Cost Comparisons**

Viewgraph 8
DWS
11.11.91

Westinghouse
Science & Technology Center

0214

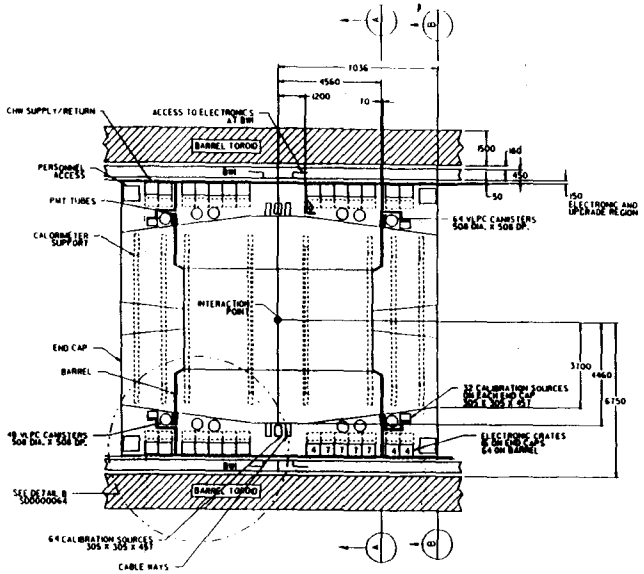

CALORIMETER - PLAN VIEW
FIBER TRACKER OPTION

0212

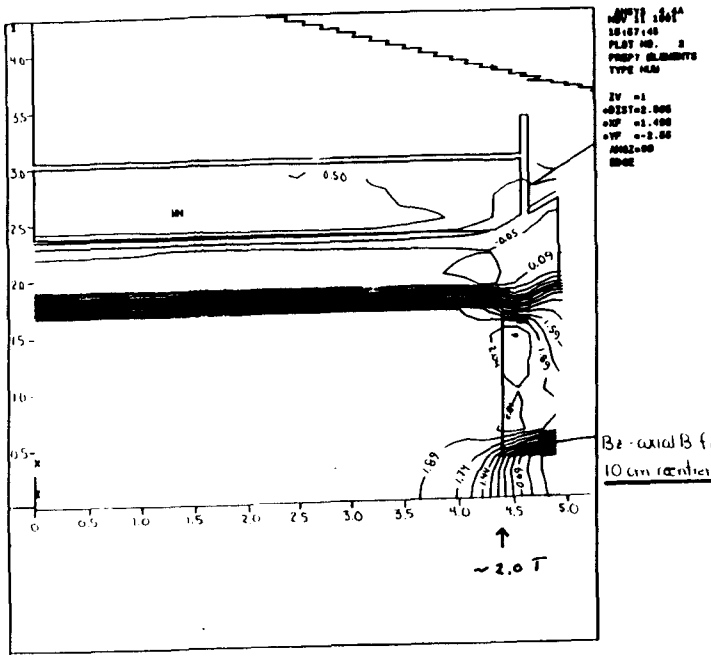

0217

CALORIMETER COST COMPARISON

LEAD VS. STEEL IN HAC1

Total Cost Delta in Favor of Steel	**7.9 M$**
Delta Caused Directly by Absorber Material	**5.8 M$**
Delta Caused by Tile Count **Δ Tile Count = 58,964** **$32.72 Per Tile**	**1.9 M$**
Delta in Support System and Weight Bearing Tooling	**0.2 M$**

Viewgraph 7
DWS
11.11.91

Westinghouse
Science & Technology Center

0215

So why do I care about Iron location? Answer = Coil forces + stress levels (more on this)

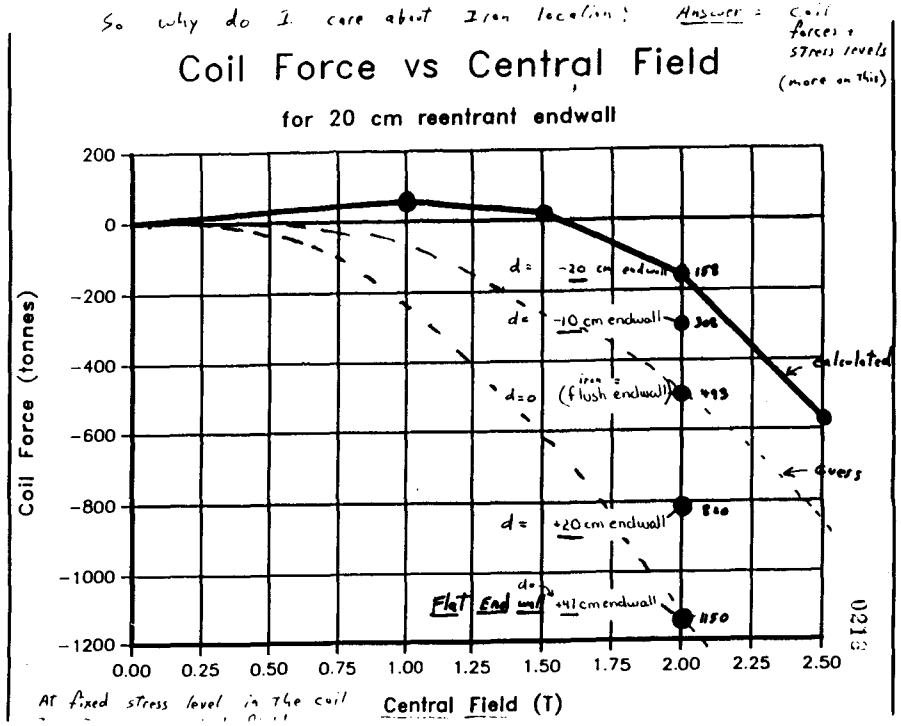

At fixed stress level in the coil

0213

Conclusion on Hadron Response

- Model A more non-linear for single particles, & is more sensitive to choice of weights
- With proper choice of weights, performance is comparable
- Model B is far from the best Pb calorimeter that can be built because of cost
- Physics performance is comparable for Afb
- Both models Afb will require considerable test beam study up to the highest energy beams available, and inside study

0216

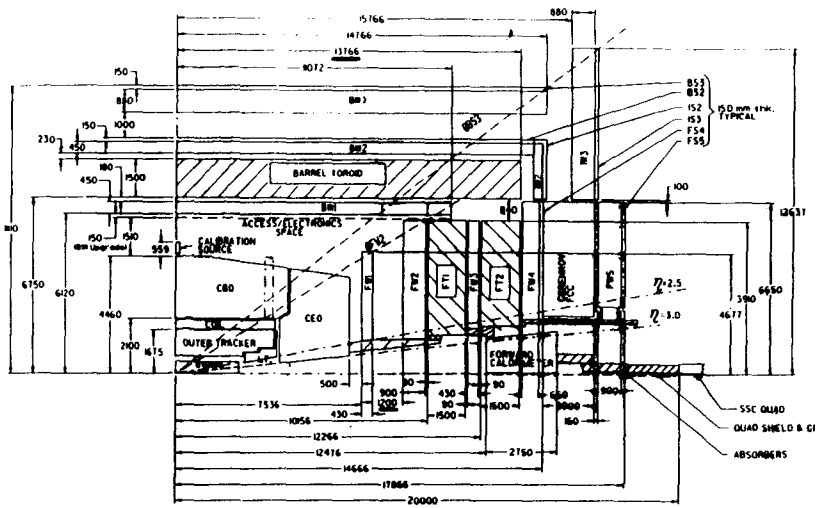

SDC DETECTOR DIMENSIONS
with Fiber Tracker
And Electronics Interior
SSC DRAWING #SD0000043 8-10-91

0 1 2 3 4 5M

NOTE: DIMENSIONS ARE IN MILLIMETERS

0221

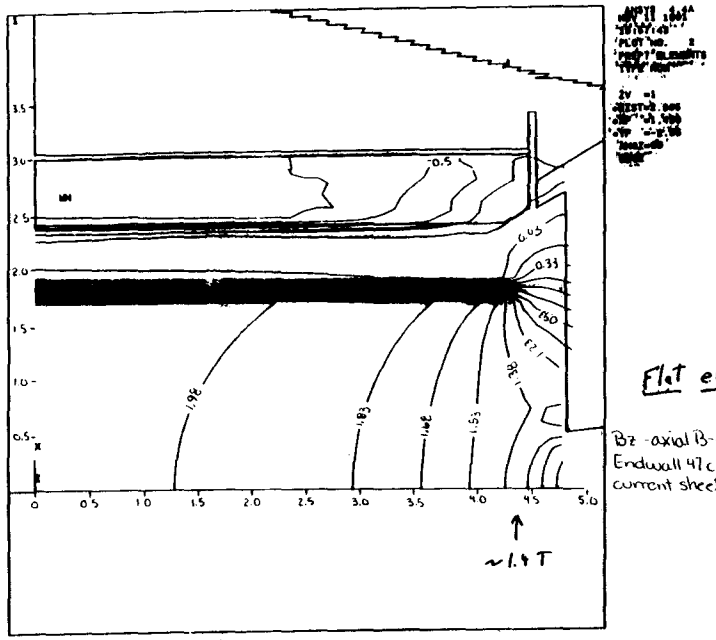

0215

ΔL ~ 80 cm

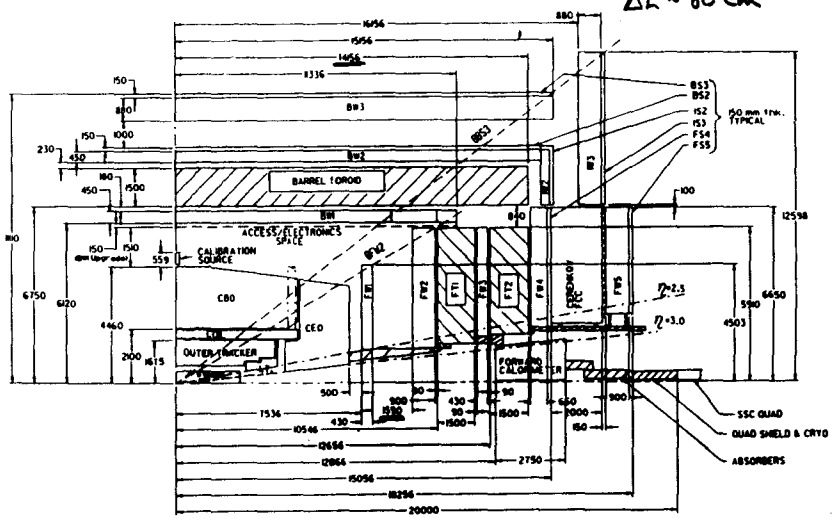

SDC DETECTOR DIMENSIONS
with Reentry Calorimeter
SSC DRAWING #SD0000075 8-12-91

0 1 2 3 4 5M

NOTE: DIMENSIONS ARE IN MILLIMETERS

0220

Muon System Cost Sensitivities

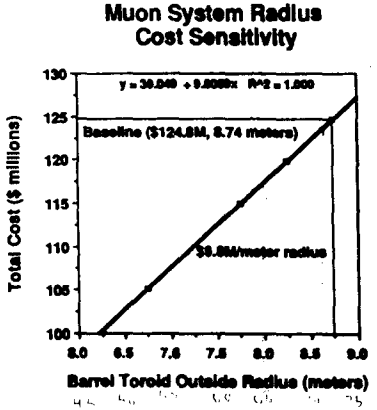

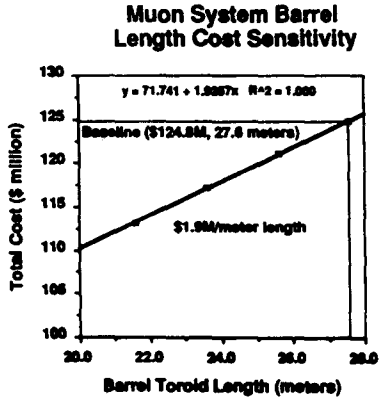

Δ$ ~ 1.5-2 M$

0221

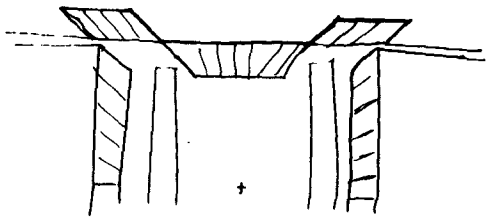

0225

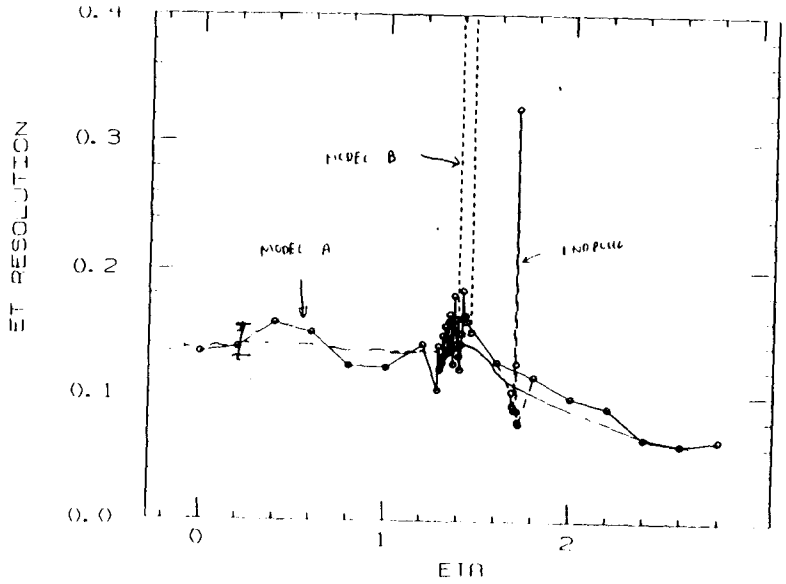

0223

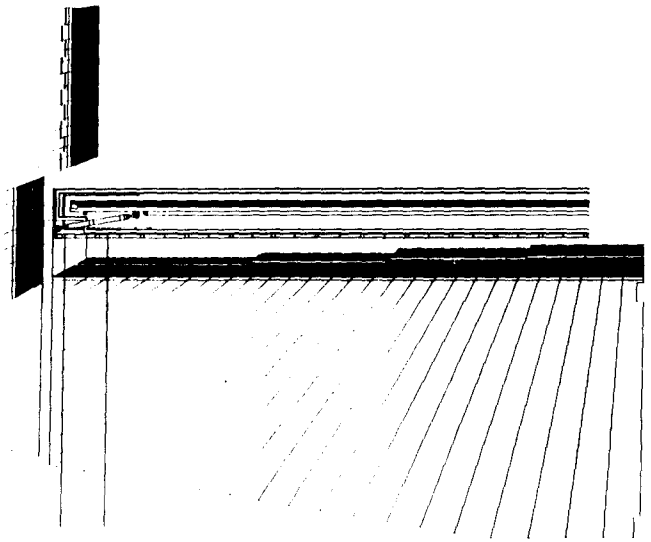

0226

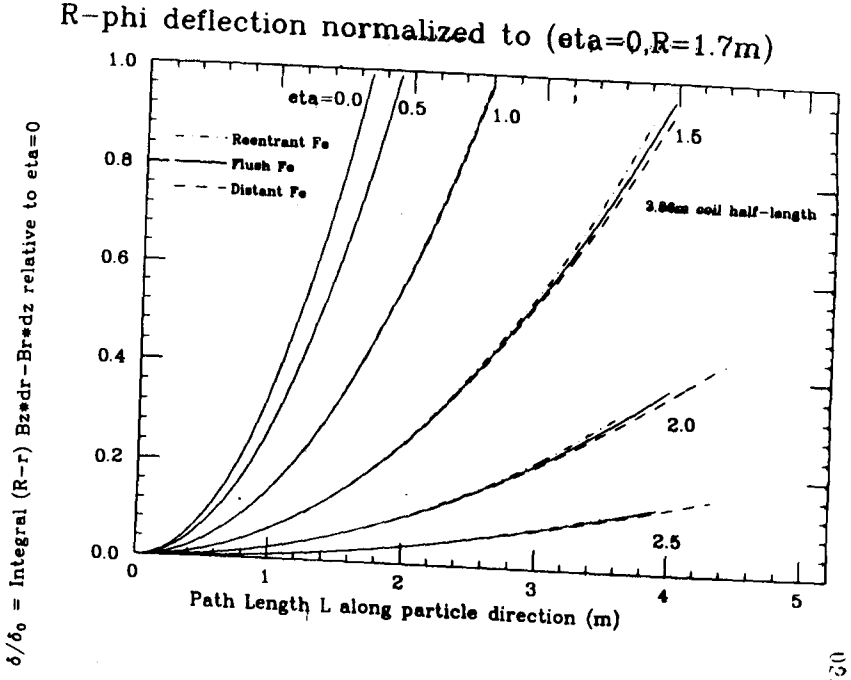

0224

14-Nov Consensus Design

Barrel EM

Longitudinal segs.	1
Xverse seg.	.05
Pb thickness (mm)	3.2
Scint. thickness (mm)	4
absorber layers	36
X0 (inc. coil)	22 (1.1 λ)

Barrel HAD 1

Xverse seg.	.05
abs. thickness (mm)	25.4 Fe
scint. thickness (mm)	2.5
absorber layers	32
λ	4.9

Barrel Had2

Xverse seg.	.1
abs. thickness(mm)	51 Fe
scint. thickness	2.5
abs. layers	13
λ	4.0
total depth barrel	10λ

resolution (e,π)
stochastic (12%, 50%)
constant (1% , 4%)

Punch : Depth - 6X0

14-Nov Consensus Design

Endcap EM

Longitudinal segs.	2
Xverse seg.	.05
Pb thickness (mm)	6.3
Scint. thickness (mm)	4
absorber layers	22
X0	25 (.9 λ)

Endcap HAD 1

Xverse seg.	.05
abs. thickness (mm)	51 Fe
scint. thickness (mm)	2.5
absorber layers	21
λ	6.4

Endcap Had2

xverse seg.	.1
abs. thickness(mm)	102 Fe
scint. thickness	2.5
abs. layers	8
λ	4.9
total depth barrel	12λ

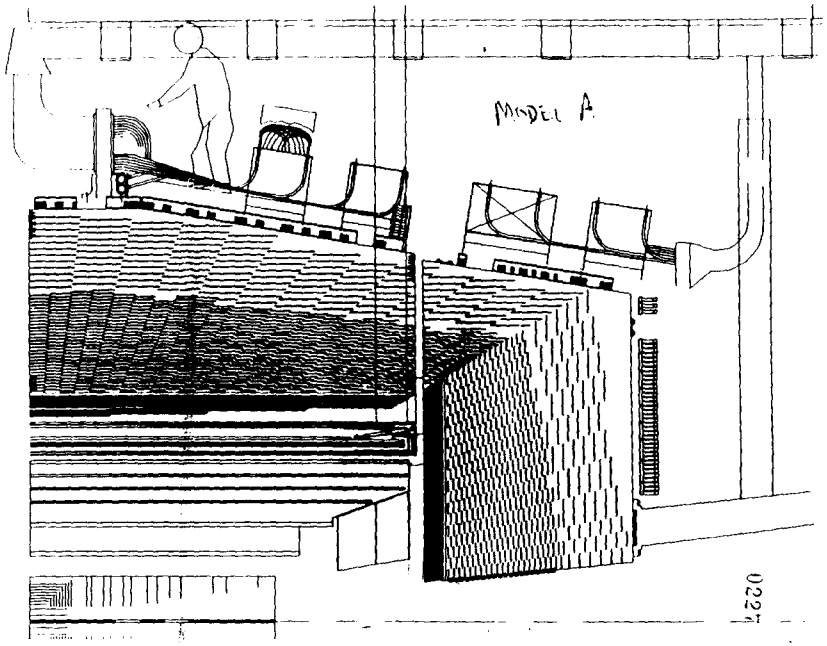

Consensus design description

- move to 10 λ depth
  - weighting schemes complicated by back leakage
  - efficiency for high Et events improved
  - cost Δ < 2 mf
- Exact endcap configuration (model A vs B) under study
- Hcal-Hcal boundary under study via HFC data
- Hcal xverse seg. under study (2.5)

Trigger Segmentation

11.25°
~~4.45°~~

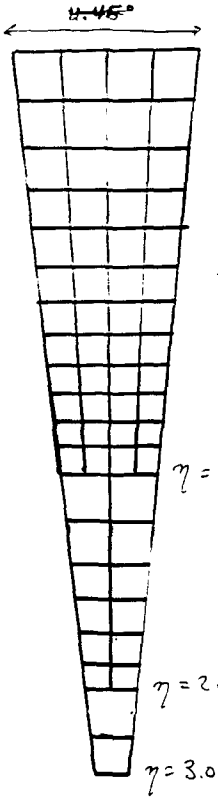

62 towers/wedge

Assumes barrel-end transition at $\eta = 1.4$

$\frac{1}{2}$ Barrel = 28 towers
$(28 \times \Delta\eta = .05)$

Criterion:
Divisible in .2 × .2 elements

Proposed for compatability with SM and trigger

14 Nov 1991

Report from Tracking Evaluation Committee

T. Kondo(KEK)

Nov 16, 91 T. Kondo

Schedule of SDC Tracking Group

version 9

NOV.12

9:00-18:30	Cost and schedule (chaired by D.Etherton)	} COS
20:00	Tracking Evaluation Commiittee (ciosed)	

NOV.13 Conceptual Design Report

14:00-14:40	A.Selden	Silicon tracker	} CDR
14:40-15:20	H.Ogren	Modular straw tracker	
15:50-16:30	D.Koltick	Fiber tracker	
16:30-17:10	S.Reucroft	Straw-fiber tracker	
17:10-17:50	A.Sill	Gas microstrip tracker	

Nov.14 Pattern Recognition Report

8:30-9:00	M.Corden	SI + Straw-fiber	} Pattern Recogniti
9:00-9:30	B.Hubbard	SI + outer (all straw)	
9:30-10:00	F.Luehring	SI + all straw	
10:30-11:00	D.Adams	SI + all fiber	
11:00-11:30	H.Ziok	SI + outer (all straw)	
11:30-12:00	T.Thurston	Integration comparison of fiber and straws	
13:30-14:30	D.Etherton	Review of cost & schedule	
	H.H.Williams	Front end electronics	
	W.Ford	Tracking Requirements	
14:30-16:30	Questions and Answers to each CDR		
	1. Modular straw tracker		} Q & A
	2. Straw-fiber tracker		
	3. Fiber tracker		
17:00-0:00	Tracking Evaluation Commiittee (ciosed)		

Nov.15

9:00-19:00	Tracking Evaluation Commiittee (ciosed)

0234 SDC-91-133

Silicon Tracking
Conceptual Design Report
1991

D R A F T

Si CDR ③

0235

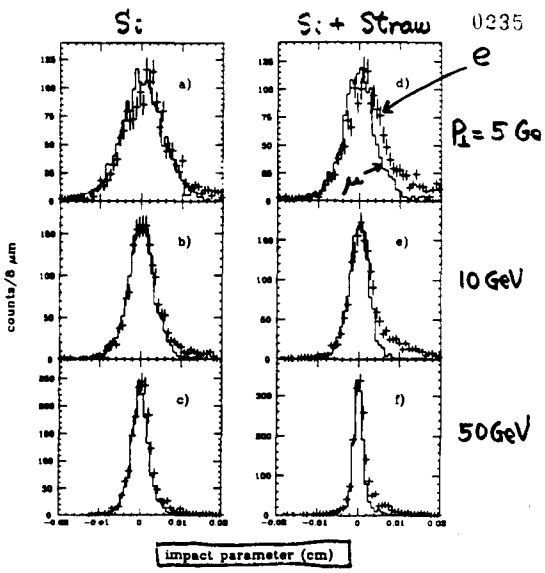

Fig. 5. Impact parameter distributions for e^- (crosses) and μ^- (histograms) single track events generated from $z = 0$ at fixed $P_\perp$ and uniformly in η over the range $|\eta| < 2.5$. Impact parameter determined from the silicon system alone for $P_\perp = 5$, 10 and 50 GeV/c tracks (a)–(c), respectively] and for the combined silicon and straw tube system (d)–(f)]

Si CDR ④

0236

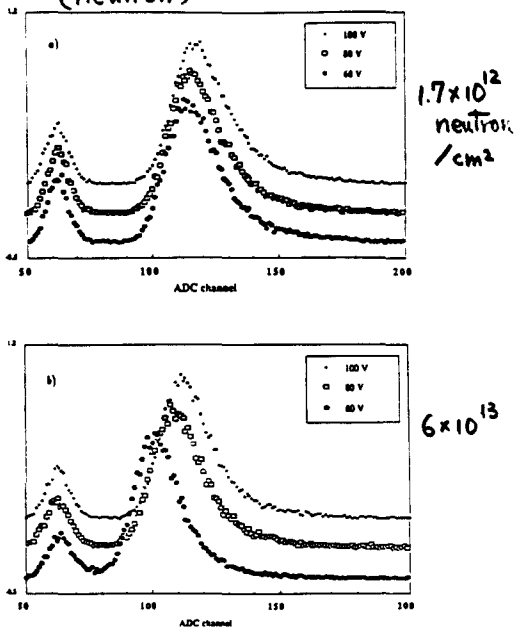

Fig. 21. Beta spectrum from irradiated diode. a) fluence = 1.7 10^{12} n/cm^2 b) fluence = 6.0 10^{13} n/cm^2.

Si CDR

0237

Silicon Readout

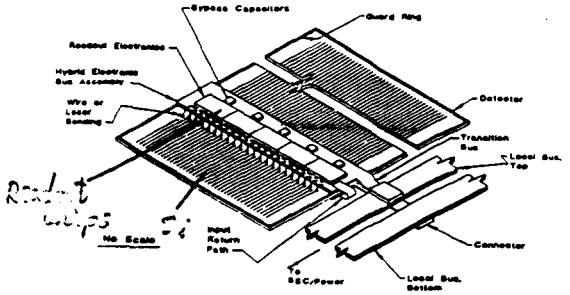

Fig. 30. Conceptual layout of a detector module.

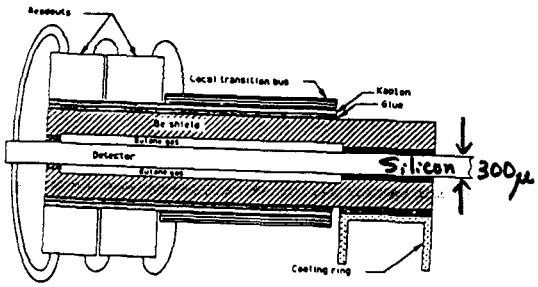

Fig. 31. Cross section through a detector module.

47

Straw CDR (6)

0236

IUHEE-91-10
SDC-91-00125
November 7, 1991

SDC

MODULAR STRAW

OUTER TRACKING SYSTEM

CONCEPTUAL DESIGN REPORT

B. Adrian, D. Alexander, B. Corliss, F. Ellis, E. Erdos, W. T. Ford, D. Johnson, M. Lohner, P. Rankin, G. Schultz and J. G. Smith
University of Colorado

R. Foster, G. Hanson, F. Luehring, B. Martin, H. Ogrea, D. R. Rust and E. Wente
Indiana University

Y. Arai
KEK

J. W. Chapman, A. Dunn and J. Mann
University of Michigan

J. Mayhall, T. Ryan and J. Shaffer
Oak Ridge National Laboratory

H. M. Newcomer, R. Van Berg and H. H. Williams
University of Pennsylvania

R. L. Swensrud and D. T. Hackworth
Westinghouse Science and Technology Center

DRAFT

Straw CDR (7)

0239

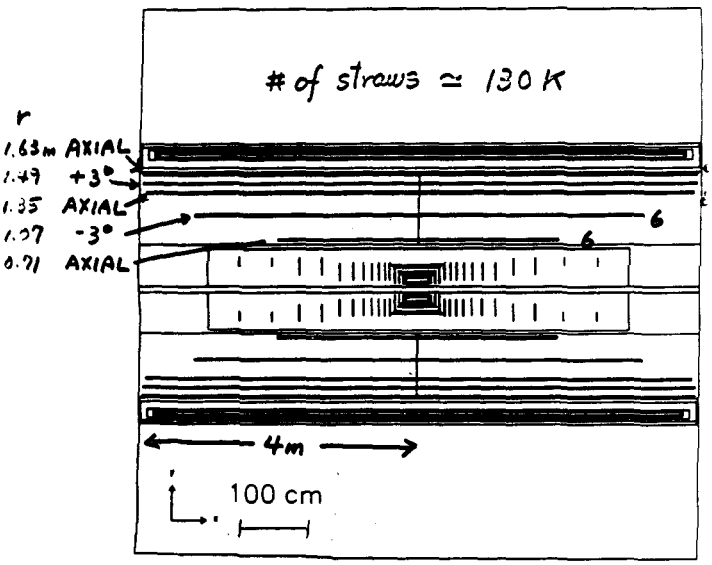

Fig. II.2. A side view of the proposed tracking system design. The figure shows the beam pipe, the descoped silicon tracker, a five superlayer straw tube system, and the solenoidal magnet.

Straw CDR (8)

0240

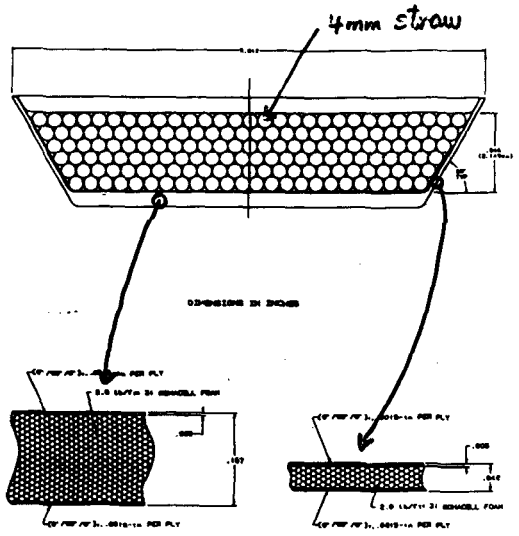

Fig. VI.29. Details of the cross-sectional view of the non-trigger module.

Straw CDR (9)

Double V (Wire) position

0241

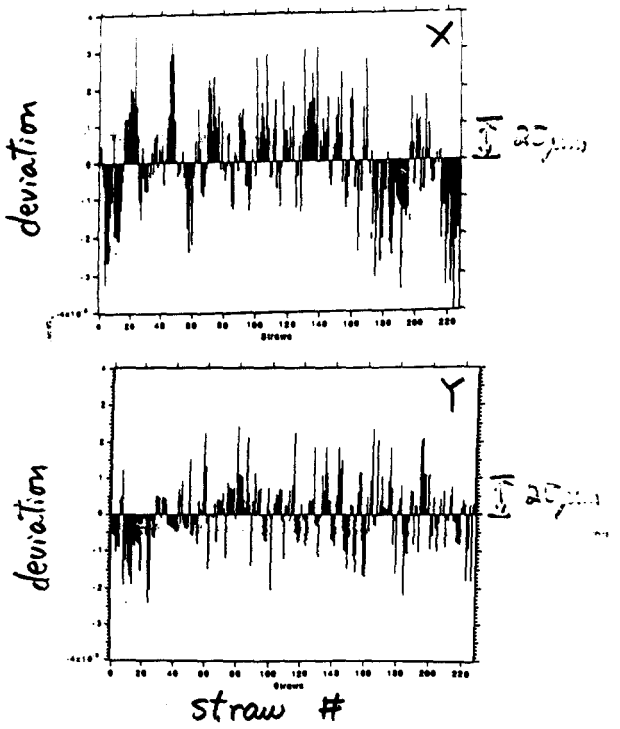

Fig. IV.5. The deviation of the theoretical close packed fit in x position (a) and y position (b) for an 8 layer trapezoid.

Straw CDR (10)

0242

Superlayer

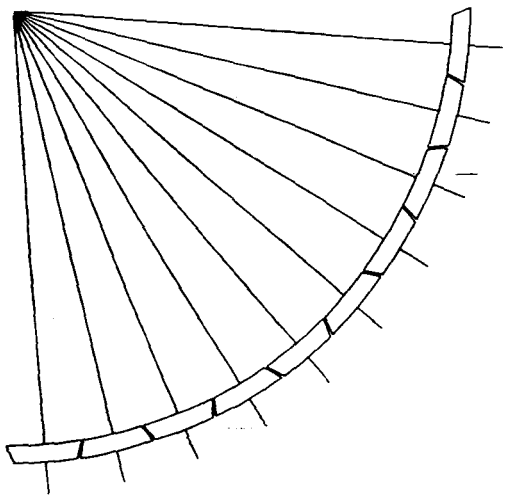

Figure 4: Schematic cross-section of a superlayer arc.

Straw CDR (11)

0243

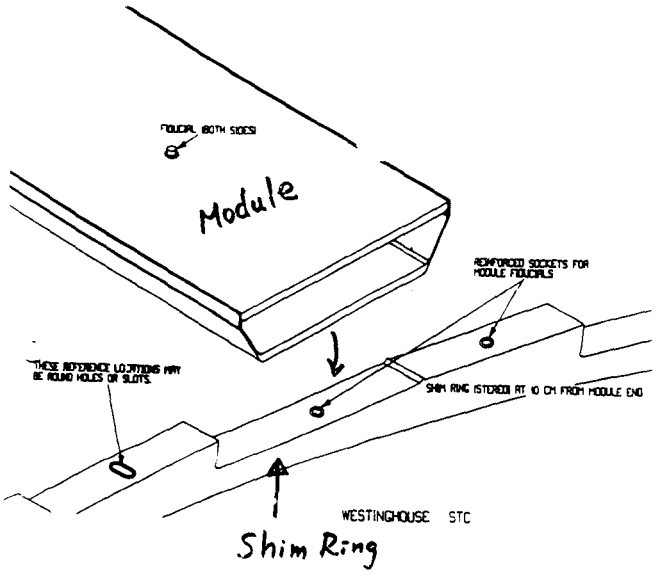

Fig. VI.17. Conceptual drawing of module and shim ring fiducials.

Straw CDR (12)

0244

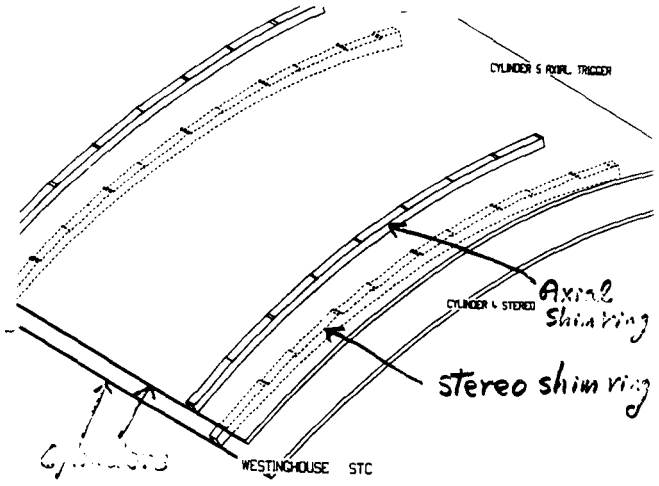

Fig. VI.13. Detail of the stereo and axial shim rings.

straw CDR (13)

0245

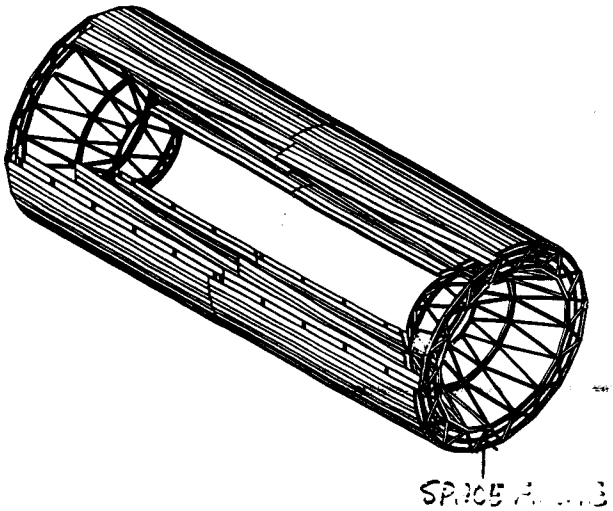

Fig. VI.1. Completely assembled central tracker.

148

Fiber CDR (14)

0246

Conceptual Design
Scintillating Fiber Outer Tracking

Fiber Tracking Group (FTG)

B.Abbot[k], D.Adams[i], M.Adams[c], E.Anderson[m], T.Armstrong[i], M.Atac[a,b], A.Baumbaugh[b], B.Baumbaugh[g], M.Binkley[b], F.Bird[n], J.Bishop[g], N.Biswas[g], A.D.Bross[b], C.Buchanan[a], N.Casons, R.Chaney[o], D.Chrisman[a], D.Cline[a], C. Collins[a], M.Corcoran[i], R.Davies[k], J.Elias[b], G. Eppley[i], E.Fenyves[o], D.Finley[b], G.W.Foster[b], R. Fox[n], H.Goldberg[c], H.Hammack[o], A.Hasan[i], S.Heppelmann[i], K.Hess[n], J. Hylen[b], J.Jaques[g], J.Kaufmann[i], R.Kehoe[g], C.Kelley[c], M. Kelly[g], V.Kenney[g], R.Kephart[b], D.Koltick[k], J.Kolonko[a], K.Kondo[p], J.Kubic[a], L.Leedom[f], R.A.Lewis[i], R.Leitch[h], C.Linkis[f], J.LoSecco[g], B.Lowery[o], J.Marchant[g], R.McCracken[m], R.McIlwain[k], S.Margulies[c], H.Mendez[c], F.Mierd, H.Miettinen[i], R.Moore[i], R.J.Mountains, R.Nelson[a], B.Ohi, T.Okusawa[f], J.Orgeron[o], H.Paik[d], J.Park[a], J.Passaneau[i], K.Pennington[n], M.Perroff[m], J. Piles[a], A.Pla-Dalmau[b], S.Reucroft[f], C.Rivetta[b], R.Ruchti[g], R.Scalise[i], J.Schmitz[k], W.Shephard[g], E.Shibata[k], J.Skeens[i], G.A.Smith[i], J.Solomon[c], K.Takikawa[p], T.Thurston[n], S.Tkaczyk[b], W.Tooshacker[i], Balamurali V[g], D.Vandergrift[n], K.Vasavada[d], R.Wagner[b], J.Warchol[g], M.Wayne[g], J.Whitmore[i], and T.Yasuda[f]

University of California at Los Angeles[a]
Fermi National Accelerator Laboratory[b]
University of Illinois at Chicago[c]
Indiana University - Purdue University at Indianapolis[d]
Massachusetts College of Pharmacy and Allied Health Sciences[e]
Northeastern University[f]
University of Notre Dame[g]
Oak Ridge National Laboratory[h]
Pennsylvania State University[i]
Philadelphia College of Pharmacy and Science[j]
Purdue University[k]
Rice University[l]
Rockwell International Science Center[m]
Superconducting Super Collider Laboratory[n]
University of Texas at Dallas[o]
Tsukuba University[p]

Draft Presented to the SDC Collaboration
Tracking Review Committee
November 12, 1991

Compiled and Edited by
D.Adams, A.Baumbaugh, F.Bird, R.Chaney, C.Collins, W.Gall, K.Hess, D.Koltick, R.Leitch, A.Odese and R.Ruchti

D. Koltick
Nov. 13, 1991

Fiber CDR (15)

0247

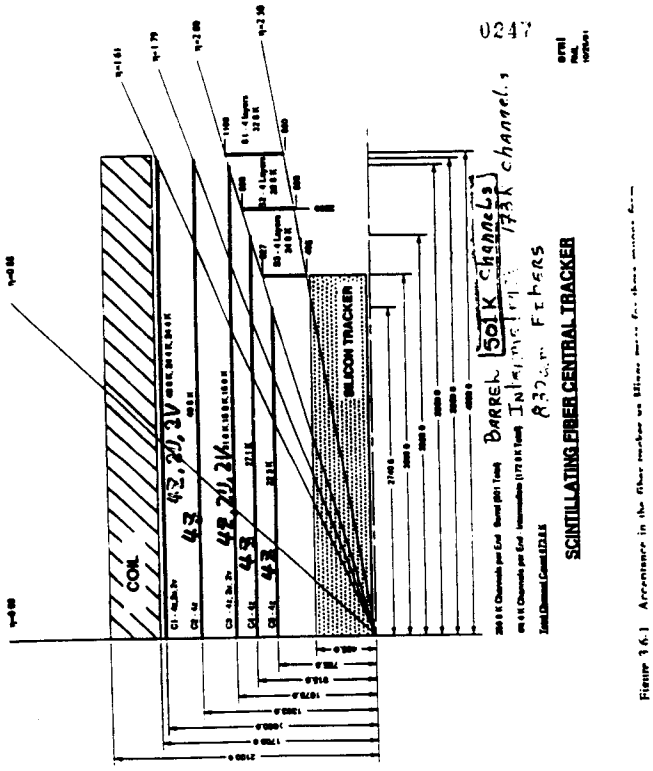

Figure 3.6.1 Acceptance in the fiber tracker as lines move for three vertex [illegible]

Fiber CDR talk (16)

0248

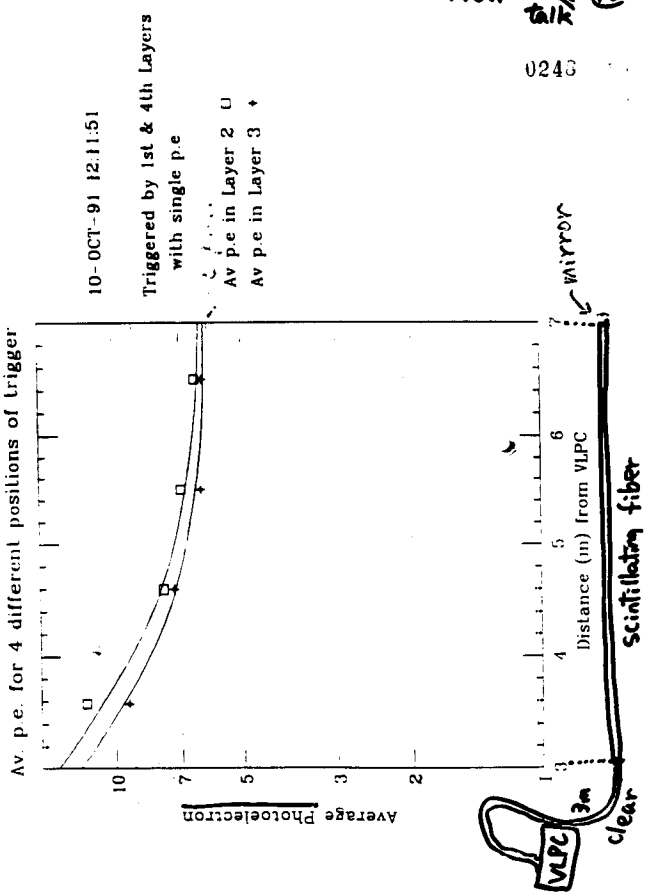

CALORIMETRY

(PARTIAL)

THURSDAY, NOVEMBER 14

Report of the Committee on Absorber Configuration	J. Siegrist(SSCL)
Preliminary Results from Hanging File Calorimeter	A. Byon-Wagner((FNAL)
Single Particle Calorimeter Simulations	L. Price(ANL)
e/h Simulation	D. Green(FNAL)
Single Particle and Jet Response of Several Calorimeter Models	C. Hearty(LBL)
Analytic Characterization of a Two Compartment Calorimeter	D. Groom(LBL)
Impact of the Hadron Calorimeter Absorber Choice on the Solenoid	R. Kephart((FNAL)
Calorimeter Cost Comparison Lead vs. Steel in HAC1	D. Scherbarth (Westinghouse)

FRIDAY, NOVEMBER 15

Jet Tagging	K. Einsweiler(LBL)
Implications of Missing Et on FCAL Specifications	M. Barnett(LBL)
SDC Forward Calorimetry	W. Frisken(LBL/York)
Impact of EM Calorimeter Thickness on Resolution	C. Hearty(LBL)

LPBautz:12/11/91

4) Provide the integrated mechanical design of the packaging for the electronics and cabling.

Fibers:

1) Measure properties of production quality VLPC's under conditions appropriate for SSC application, including dark current, pulse rate, noise, speed, etc..., using SDC type electronics.

2) Demonstrate fibers with VLPC's in a large scale test.

3) Demonstrate that the fibers have sufficient radiation hardness.

4) Demonstrate the light collection efficiency in scintillating fiber/clear fibers with two optical couplers in series using fibers properly chosen to match actual expected lengths.

Common Issues for Straws or Fibers:

1) Provide a table of parametric resolutions.

2) Provide simulations of efficiencies and resolutions using practical and realistic pattern recognition programs.

3) Understand the trigger performance in the region $1.6 < \eta$.

4) Provide a method to reduce the L1 fake rate that does not significantly impact the overall efficiency.

5) Address performance of the system when used for pattern recognition in the absence of the silicon system.

6) Understand improving of the capabilities of the system as the luminosity rises beyond the design luminosity of 10^{33} up to 10^{34} (e.g. pattern recognition, trigger, and radiation damage issues).

Near Future Schedule

- Engineering review meeting on modular straw design

  December 4 (tentative)
  organizer : W.Miller, H.Frisch

- Pisa Meeting

  - CDR presentation of gas microstrip intermediate tracker
  - alternative proposals for intermediate tracker
  - high luminosity performance of silicon and straw systems
  - simulation reports
  - tracking requirements summary
  - discussion on η division between barrel and intermediate trackers

- Final CDR deadline : January 20, 1992

- Tracking committee meeting

  - final recommendation on the baseline design for Technical Proposal
  - 2 days in the week of January 27th

Recommendation III

The committee was impressed by the great deal of effort and the rapid progress of the fiber tracker design. This group has gone a long way towards developing a tracking concept capable of meeting the physics and technical requirements established by the collaboration for the outer tracker. This design has a number of unique capabilities and should be pursued. The fiber system has also great potential and looks very promising for possible high luminosity designs.

Nevertheless the committee felt that the fiber tracker uses some new and presently risky technologies that must be better understood before the design could be considered acceptable. The committee felt that significantly more may be known with regard to its feasibility as a result of continued R&D. The design report lacked information in a number of

key areas (discussed below) and did not yet give a credible demonstration that the technical goals could be satisfied.

1) The principal concern of the committee was the lack of robustness in the pattern recognition due to the limited number of superlayers. The arrangement of fibers has the limitation of providing only two space points and three in xy. Adding more fibers would increase the cost and add unacceptably to the tracking volume material. The information content of the fiber superlayers (points) is significantly less than the information content of the straw superlayers (segments). The capability of the system is a fundamental issue that must be resolved.

2) The committee focused much attention on the relatively new VLPC technology. These devices are not widely available and not fully characterized. This technology will remain unacceptably risky until such time as a broader effort in the use of the VLPC's is undertaken. VLPC's should be made available to all collaborators willing to test them. These issues can be settled by the ongoing R&D. The committee expressed concern whether this R&D could be satisfactorily completed within a reasonable period.

Recommendation IV

In addition to previous recommendations the following issues must be adequately addressed. If answers cannot be provided by the next review a timetable should be produced.

Straws:

1) Demonstrate a four meter straw with the prototype readout at radiation levels (e.g. rate and current draw) corresponding to SSC operation.

2) Demonstrate a four meter module loaded with straws and read out.

3) Demonstrate electronics robustness to noise and oscillation at operating conditions in a large scale test.

Recommendation I

The present balance as described in the draft CDR's between the inner silicon and the outer barrel trackers is approximately correct and the combined descoped system appears to be marginally sufficient to meet the SDC tracking requirements. Additional simulations of the combined system are needed to establish the performance and to finalize the exact tracker structure.

Recommendation II

1) The Committee was impressed by both straw designs. The two designs have different strengths. However, the Committee believes that the number of layers, the number of straws/layer, the radial distribution of layers, and the stereo configuration are not yet optimum in either design.

2) The Committee saw no strong justification for the inclusion of fiber layers in a predominantly straw design. We believe the Z measurement requirements can be met by an all-straw design avoiding the complexity of another readout technology.

3) The Committee would like to see an all-straw design for the Technical Proposal with robust capabilities in the following areas:

   a) Good pattern recognition and efficient linkage to the silicon system to exploit fully the large magnetic volume for measurements of momentum and position.

   b) A L1 trigger that uses more than a single axial superlayer and is both highly efficient and has good fake rejection.

   c) Measurements of the Z coordinate and polar angles that are well matched to the requirements of extrapolation to the outer detectors.

   d) The understanding of the capabilities of the system, e.g. pattern recognition, trigger, and radiation damage, as the

luminosity rises beyond the design luminosity of 10^{33} up to 10^{34}.

4) On the mechanical design, the Committee notes:

   a) A modular approach provides a credible way to make stereo straws.

   b) Any credible design must address the issue of replacing the inner layers for higher luminosity operation.

The Immediate Goal

(Nov.12,1991)

Among the issues to be considered,

1. relative balance between inner and outer trackers
2. selection of options for outer tracker
3. relative balance between outer and intermediate trackers
4. selection of technology for intermediate tracker

committee has made recommendations on #1 and # 2.

SDC Tracker Preliminary Cost/Schedule Review Meeting

- Nov.12, 1991, D.Etherton

- **Preliminary cost estimates including contingency and readout electronics**

Silicon tracker	~~$55.2M~~ 42	(mistake??)
Fiber Intermediate	$13.6M	
Gas Microstrip	$21.7M	
Modular Straw	$49.8M	[~$47M]
Fiber	$50.3M	[~$55M]
Straw-Fiber	$45.1M	[~$52M]

[ ] = adjusted by D.Etherton's prediction

- **conclusion :**

no clear winner for the barrel outer tracker

ACCESS / INTEGRATION T. Thurston

SUMMARY OF ACCESS CONSIDERATIONS

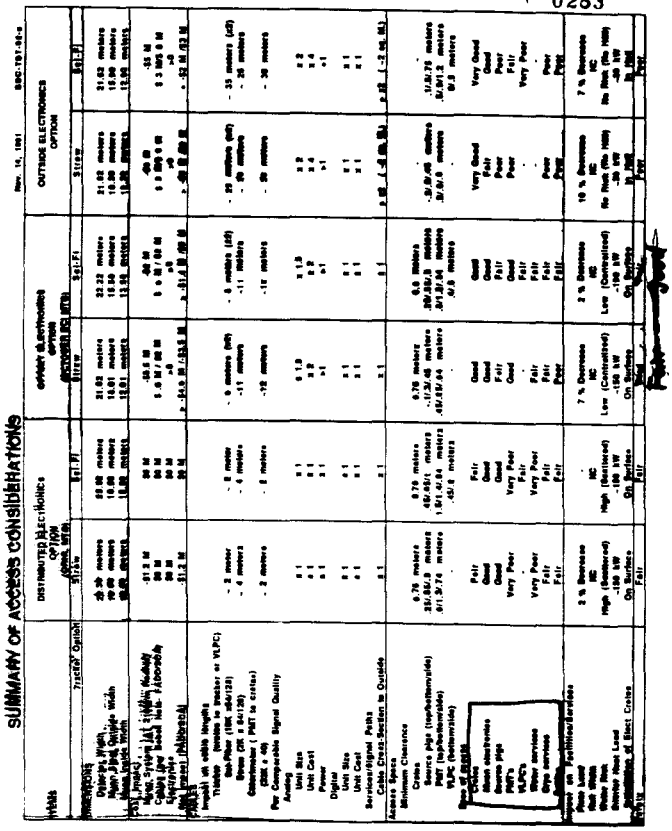

RECOMMENDATIONS

by

TRACKING EVALUATION COMMITTEE

November 15, 1991

Pattern Recognition Status

- results are coming out
- bad, good, supergood } news exist
- lots of assumptions cuts
- need of tuning
- all (except F. Luehring) relies on silicon !

Tracking Evaluation Committee

members: M.Edwards/J.Dainton
J.Elias
W.Ford
H.Frisch (vice chairperson)
A.Goshaw
G.Hanson
(R.Hollebeek)
T.Kondo (chairperson)
M.Levi (vice chairperson)
(H.Lynch)
G.Oakham
R.Ruchti
A.Seiden
(Y.Unno)
A.Weinstein

consultants;

engineering: W.Miller
R.Swensrud
D.Vandergriff
M.Harris/T.Thurston

cost/schedule: D.Etherton
W.Edwards

pattern recogn: K.O'shaughnessy
M.Corden
D.Adams
F.Luehring

G.Trilling, M.Gilchriese

Charge of Committee

- Recommend by Feb.1,1992 a preferred configuration(s) to be described in the SDC Technical Proposal.
- If at all possible, select a single, baseline configuration.
- If options are necessary, the recommendation shall include a schedule and description of the criteria for selection subsequent to submitting the Technical Proposal.
- Evaluate the draft CDRs
- Recommend by Nov.17 the minimal number of options to be documented and reviewd by Feb.1,1992. ← THIS TIME
- Recommend the relative balance among the silicon, barrel, and intermediate tracker.
- Preliminary recommendation by Nov.17
  Final recommendation by Feb.1,1992.

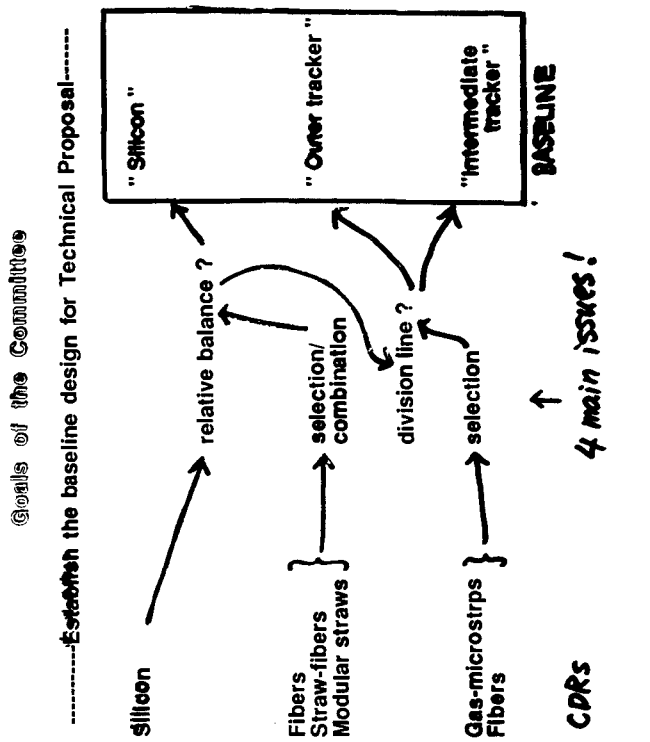

Road Technique

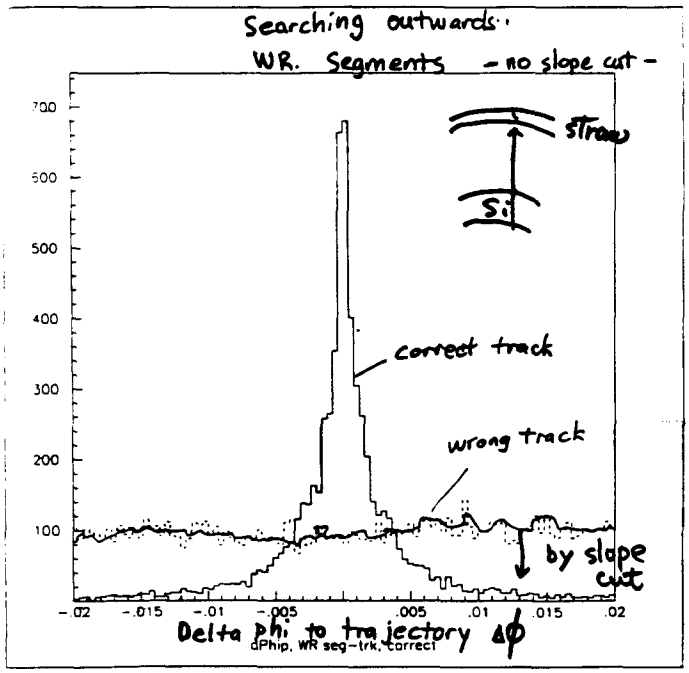

Reconstruction Efficiency

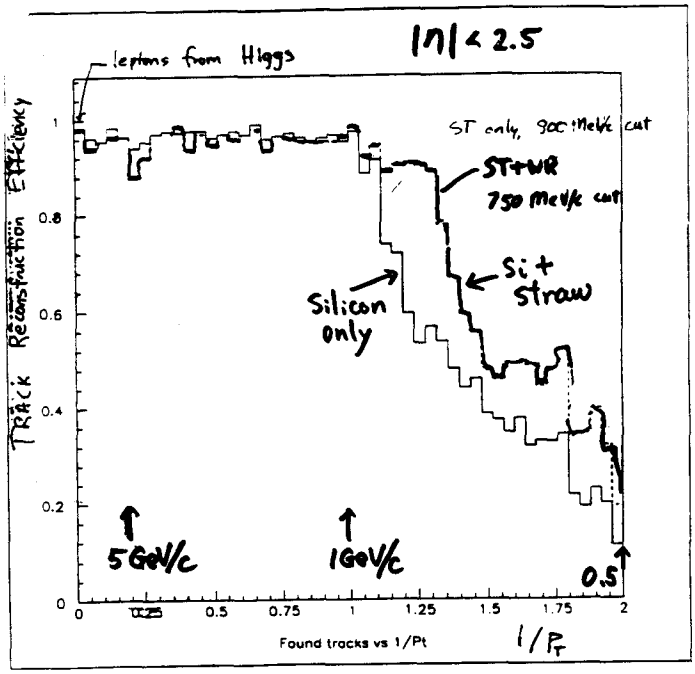

D. Adams (23)

Si + Fiber

	Track-finding e	Track-finding μ	Reconstruction e	Reconstruction μ
Si alone	0.99	1.00	0.94	1.00
Si + Scifi	0.92	0.99	0.70	0.97

Table 4. Track finding and track reconstruction efficiencies for electrons and muons in the silicon alone and silicon with scintillating fibers.

	particle	Resolution Si → Si + Scifi	
dpT/pt**2 (/Tev/c) w/rvc	e	1.1	0.35
	mu	0.8	0.16
w/o rvc	e	2.3	0.41
	mu	1.6	0.16
phi0 (rad) w/rvc	e	0.00007	0.00005
	mu	0.00004	0.00003
w/o rvc	e	0.00027	0.00009
	mu	0.00021	0.00007
r0 (mm) w/o rvc	e	0.027	0.013
	mu	0.022	0.012
tan(lambda)	both	0.011	0.0067
z0 (mm)	both	2.6	1.1
z-showermax (mm)	both	26.	1.
z-muon (mm)	both	62.	3.

resolution improvements

Table 5. Resolutions for various track parameters calculated as the RMS differences between reconstructed and Monte Carlo values. Momenta are evaluated with and without a radial vertex constraint (rvc). The last two parameters (z-showermax and z-muon) are not evaluated directly but are estimated from tan(lambda). See the text for details.

H. Ziock (27)

Si + straw

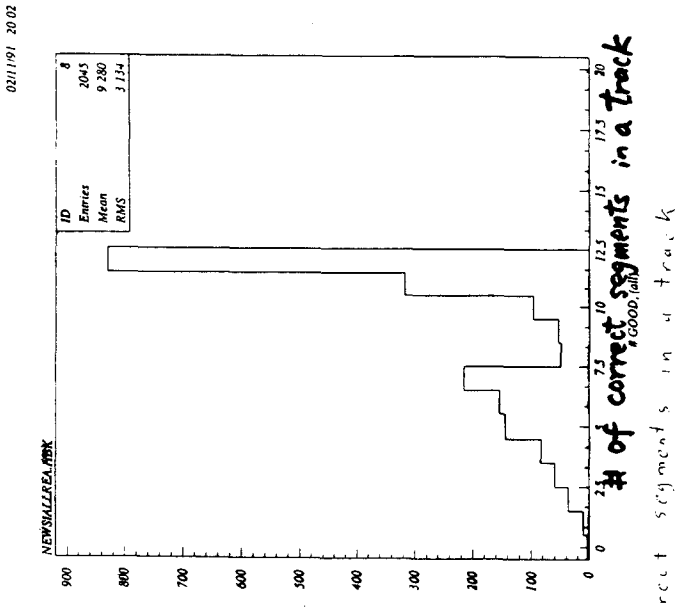

ITD group (37)

0269

TILE_WITH_ELECTRONICS

Steve Markfield SiII (35)

OCCUPANCY

0270

Number of hits/event/plane. ~150

'Event' means the composite consisting of 6 bunch-crossings worth of minimum bias events + 1 Higgs event →

Mean number of hits / plane / bunch-crossing:
~20
Maximum ~33

Define occupancy as: $\frac{\text{\# hits/plane(}ring\text{)/crossing}}{\text{\# }\mu\text{strips/plane(}ring\text{)}}$

Ring	Mean occupancy(%)	Max occupancy(%)
1	.047	.078
2	.035	.059
3	.02	.036
4	.018	.031
5	.014	.023
Mean	*.029*	*.049*

Low occupancy ⇒ low probability of 'masking' of hits by events from other bunch-crossings

M. Cordon (39)

0271

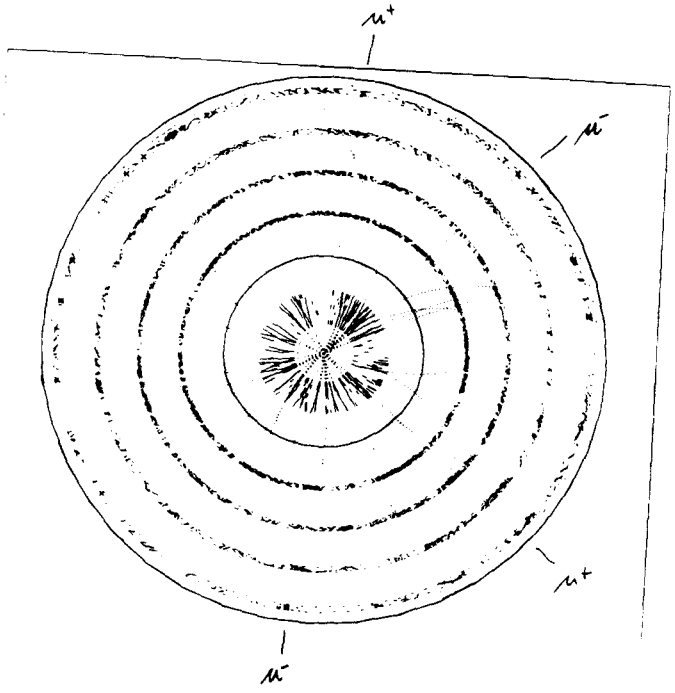

M. Cordon (40)

0272

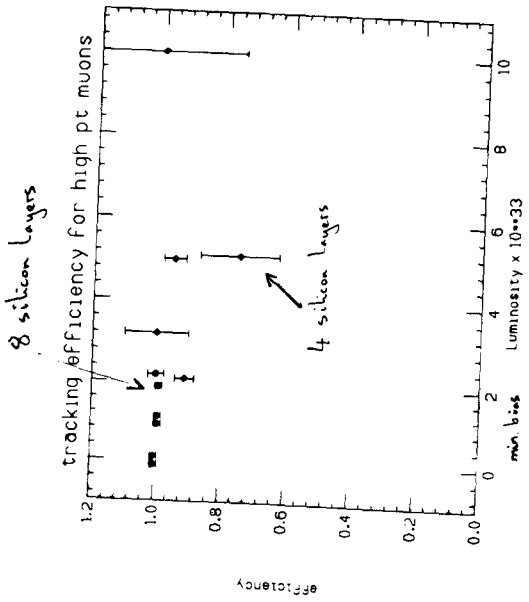

M. Corden (33)

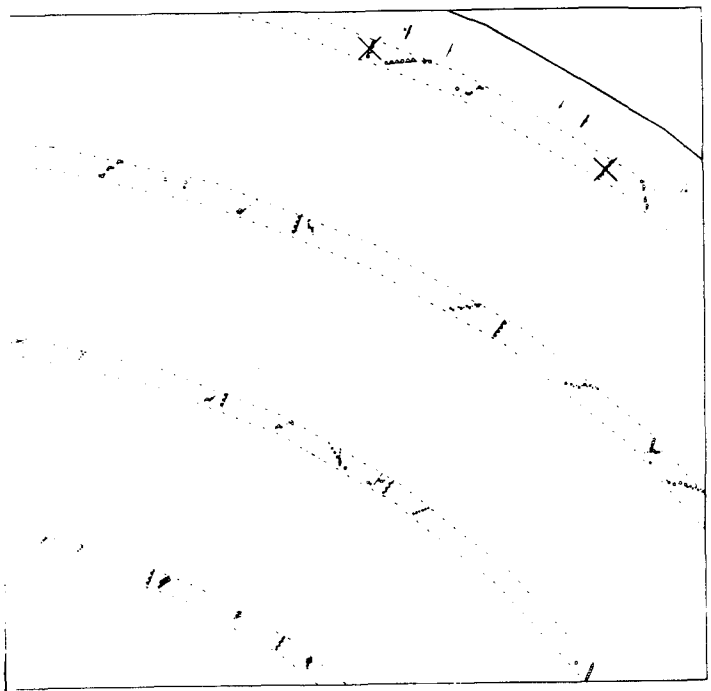

Straw-Fiber (34) CDR

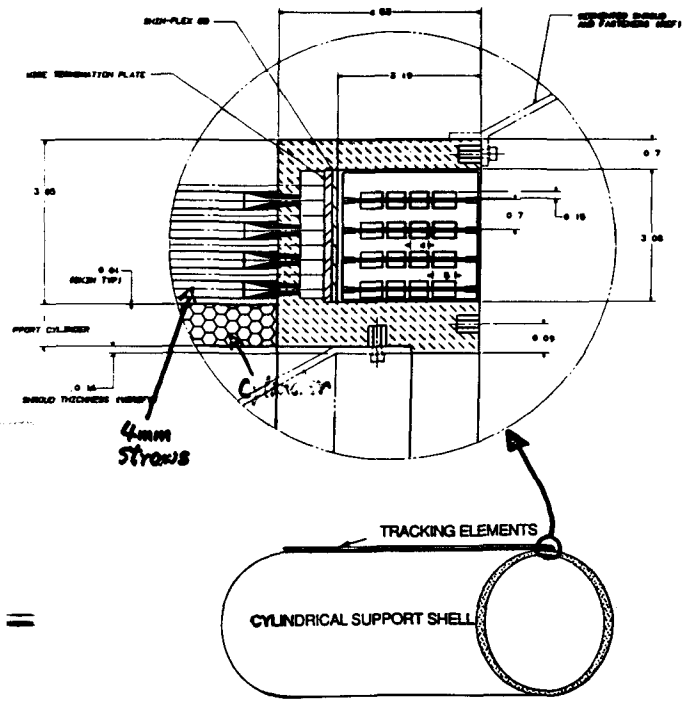

ITD group (35)

Steve Maxfield (36)

Progress Towards the Conceptual Design Report for the SDC Intermediate-Angle Tracking Detector

SDC ITD Group

(Liverpool, Rutherford Appleton Labs, Bristol, Oxford, Carleton, Montreal, Rochester, Texas A&M, Purdue)

M. Edwards, Editor

Editorial Committee:
Gerald Oakham, Carleton
Alan Sill, Rochester
Eugene Barasch, Texas A&M
Mike Edwards, RAL

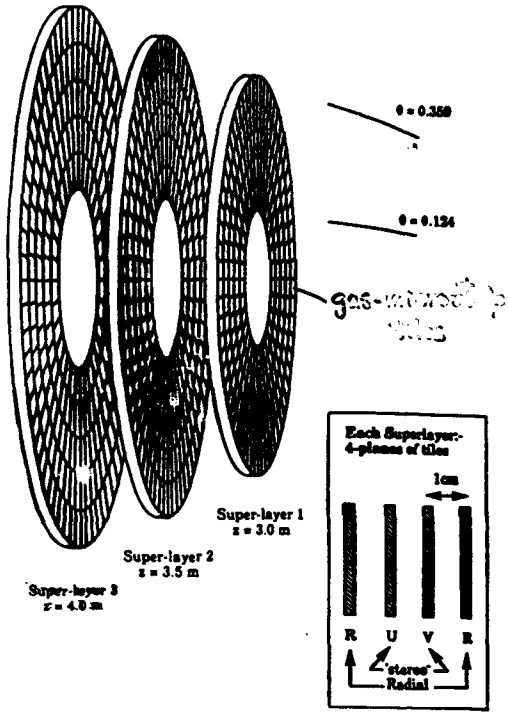

Contributors*

A.T. Goshaw, S. Oh, W. Robertson, M. Yin
Duke University

V. Hagopian, E. Hernandez, K. Hu, K. Johnson
Florida State University

Y. Arai, H. Ikeda
KEK

J. Dainton
Liverpool University

J. Chapman, A. Dunn, J. Mans
University of Michigan

G. Alverson, A. Grimes, M. Glaubman,
I. Leedom, S. Reucroft, T. Yasuda
Northeastern University

G. Alley, H. Brashear, C.L. Britton, Jr., M. Emory
T. Gabriel, R.M. Leitch, T. Ryan, D. Vandergriff
Oak Ridge National Laboratory

W.L. Dunn, M. van Haaren, F. O'Foghludha, A.M. Yacout
Quantum Research Services, Inc.

M. Edwards
Rutherford Appleton Laboratory

M. Corden, M. Mermikides, D. Xiao
Supercomputer Computations Research Institute

W. Fraszer, R. Henderson, R. Openshaw, M. Salomon
TRIUMF

M. Newcomer, R. van Berg, H.H. Williams
University of Pennsylvania

Contacts: A.T. Goshaw and S. Reucroft

* We acknowledge the efforts of the following: S. Majewski, C. Zorn, *CEBAF*; S. Blake, T.S. Elleman, J. Paulos, *North Carolina State University*; H. Dautet, R. McIntyre, *EG&G, Canada*; C. Hurlbut, *Bicron*; F. Amirani, *Mitsui*; T. Shimizu, *Kurary*.

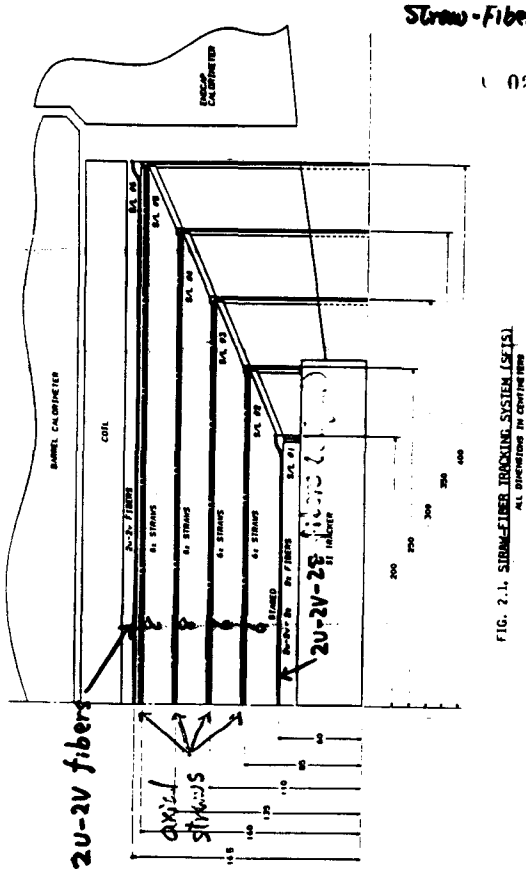

FIG. 2.1: STRAW-FIBER TRACKING SYSTEM (SCFS)

HYBRID (Duke)

Measurement of the resolution of straw tube drift cells in a 2.7m long superlayer with simulated SSC background rates.

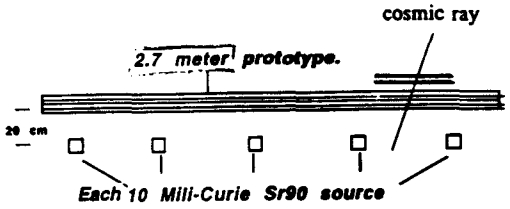

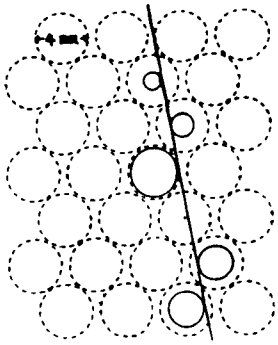

singles rate 1-2 MHz

current draw ~5 μA/wire

gain ~ 105

HYBRID (Duke)

High rate test of straw tube position resolution.

⟹ σ = 120 μm / straw tube

⟹ σ/√8 = 42 μm / 8 deep superlayer

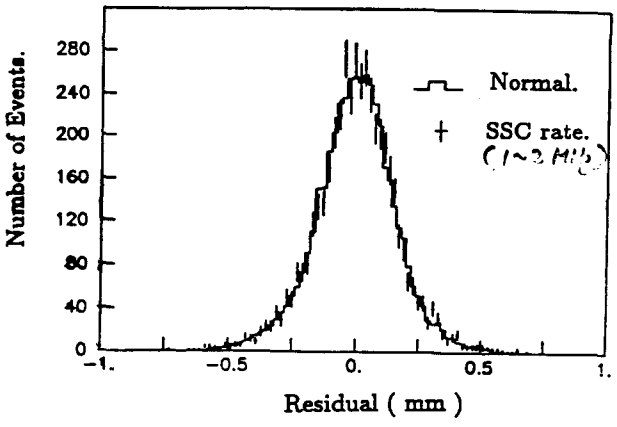

Koltick (25)

0257

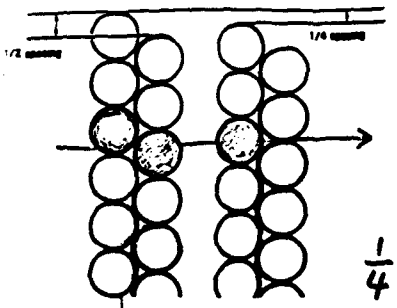

CENTER TO CENTER 85C
ACTIVE AREA 77%
CLADDING WALL 26%
GAP 29%

1/4 staggering

IDEAL RESOLUTION
FOR 1/4 SPACED FIBERS

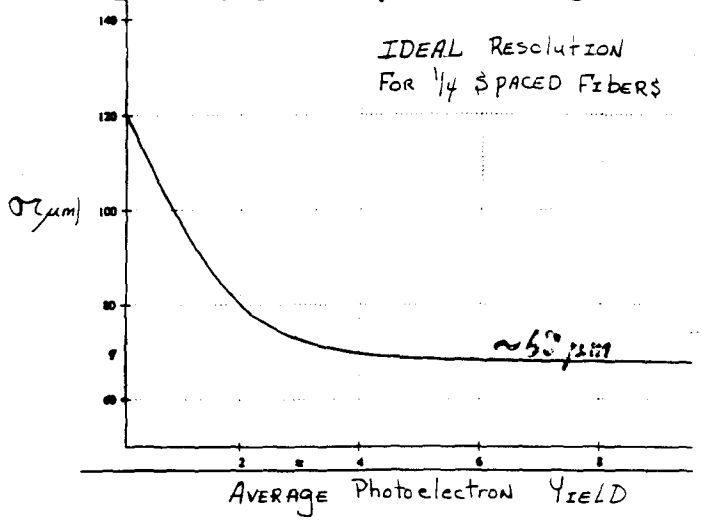

Koltick (26)

0258

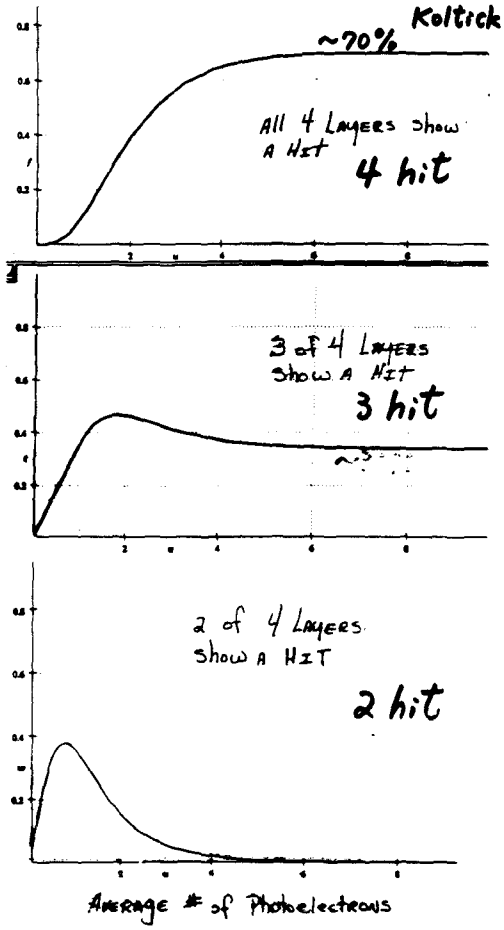

Williams (27)

0259

ULPC warm amps

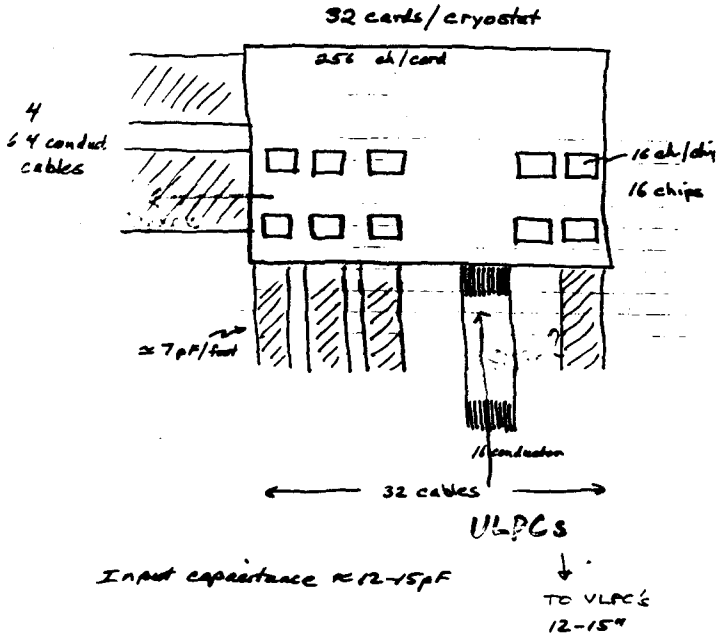

0260

Conceptual Design Report

~~Hybrid~~ for the

Straw-Fiber Tracking System for SDC

Submitted to the

Solenoidal Detector Collaboration

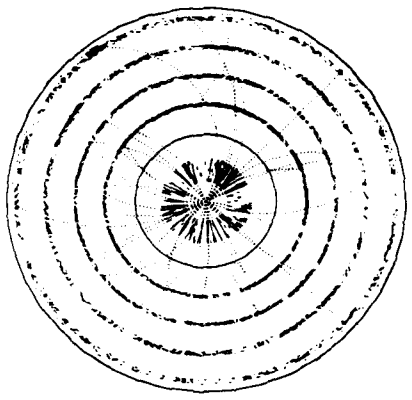

8 November 1991

0253

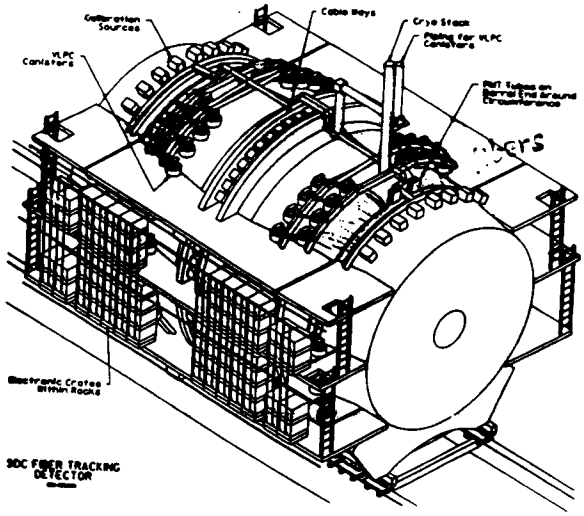

Figure 4.5.1-2. Isometric view of the calorimeter showing the placement of VLPC cryostats.

Level 1 Trigger Rate (P_t = 10 GeV)

0254

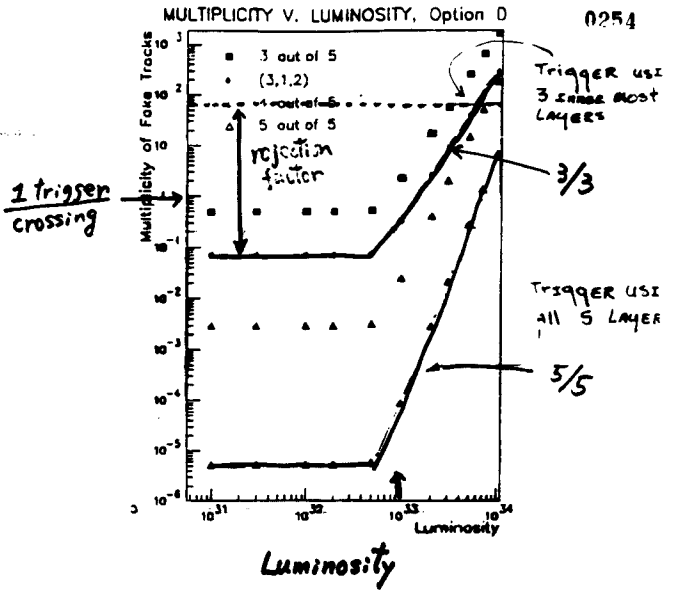

Figure 3.8-1. Trigger accidental rates (per crossing) [3-5] for various combinations of fastest superlayers. The open diamonds correspond the the three-layer case C345 illustrated in the text and the open triangles are the full five-layer system.

3-11

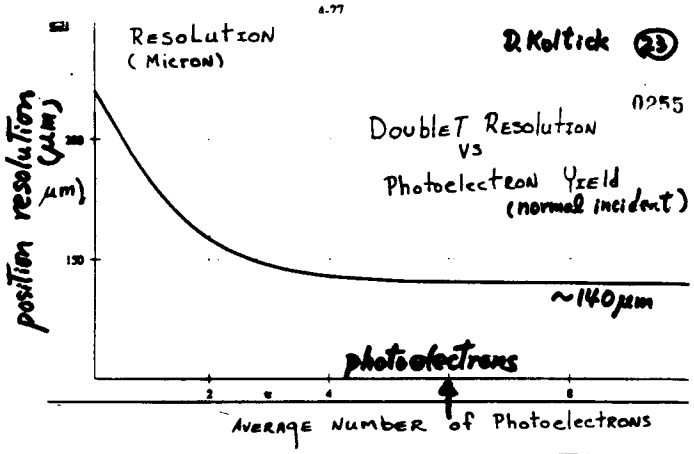

Resolution vs Photoelectron Yield

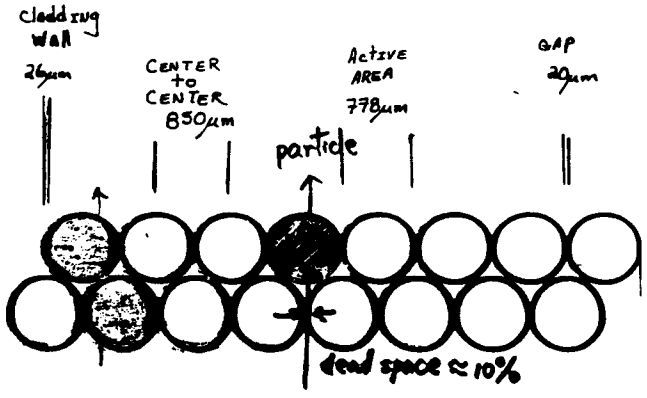

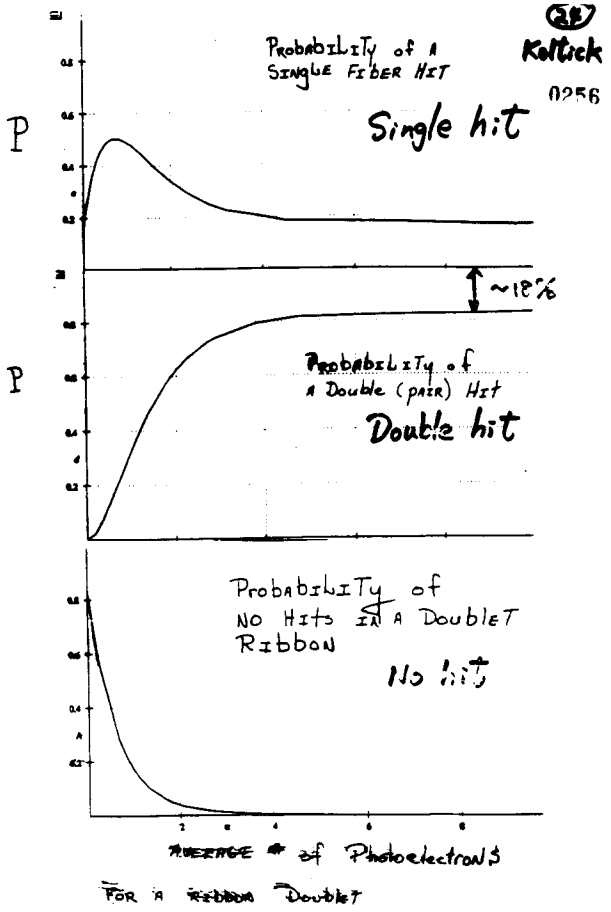

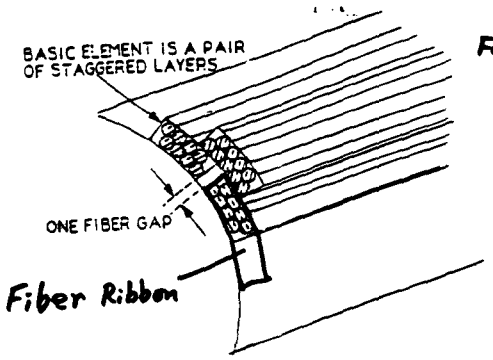

Figure 4.1-2 Axially mounted superlayer

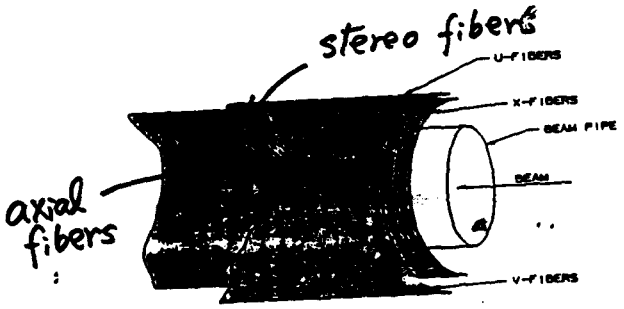

Figure 4.1-3 Stereo mounted superlayer

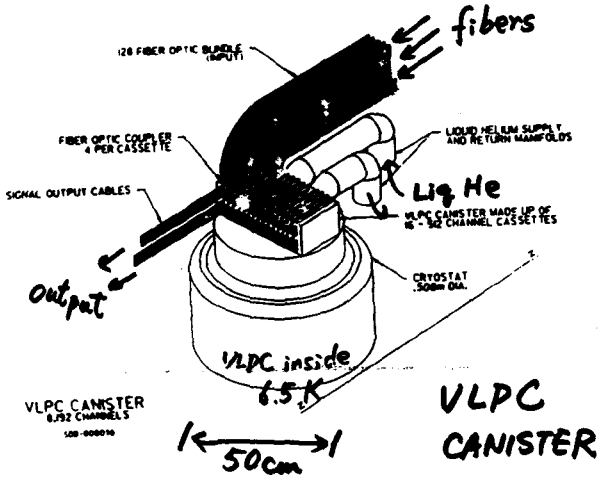

Figure 4.4-1 Detail of the Fiber Cables Connecting Into The VLPC Cryostat.

thus access is restricted. Figure 7.2.1.1-1 shows a comparison of the spectral quantum efficiencies for current VLPCs, as well as the progress of the VLPC development.

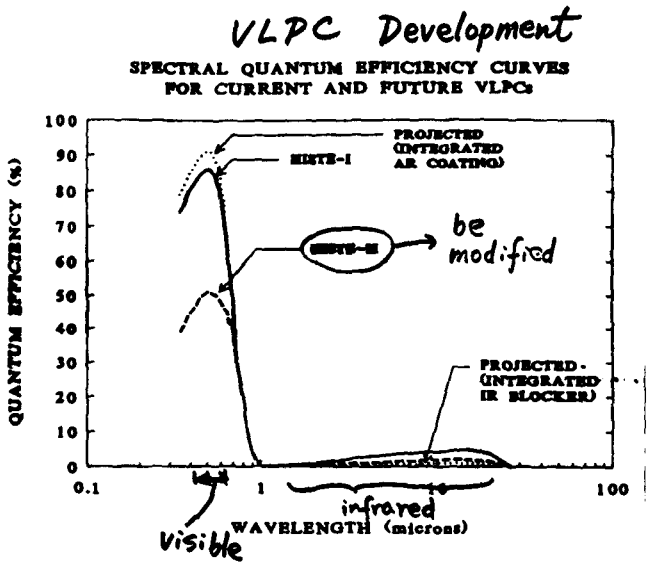

Figure 7.2.1.1-1 Spectral quantum efficiency development for VLPC devices.

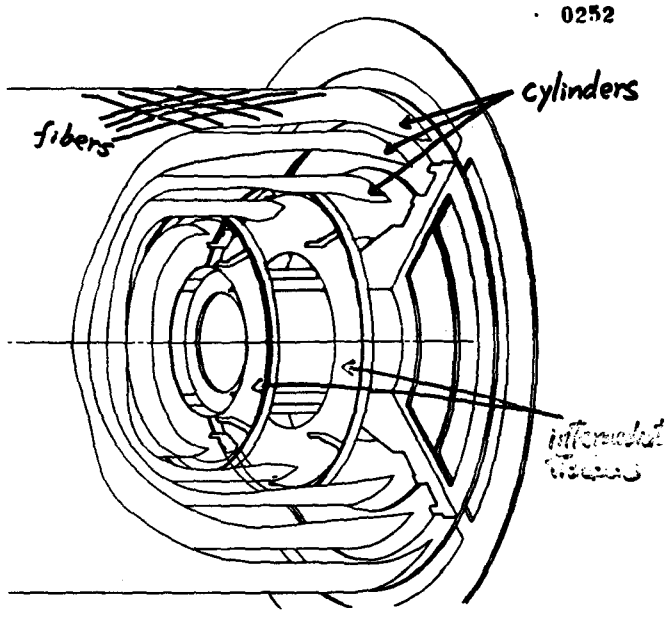

Figure 4.3-6 A cut-away view of the support structure. The intermediate tracker and barrel cylinders are held accurately in place by 4 thin support panels. The panel support is then connected to the main outer support ring which also supports the silicon tracker.

Report of the Committee on Absorber Configuration

J. Siegrist(SSCL)

Report of the Committee on Absorber Configuration

Report of the Committee on Absorber Configuration

Recommendation

The committee recommends that the hadronic calorimeter absorber be iron, and that the endcap not be reentrant. The basis for this decision is:

- the two proposed absorber configurations have comparable physics capabilities and satisify the SDC requirements.
- the lead absorber configuration cost is approximately $8M greater than the iron configuration.
- the reentrant geometry has addition breaks in the EM calorimetry.

1. Description of options

Elevation views of the configurations that have been considered are shown in fig. 1 (model A, iron HAC1), fig. 2 (model B, lead HAC1), and fig. 3 (model C, iron HAC1 with reentrant endcap). The calorimeter parameters are summarized in table 1. Models A and B have the same EM compartments but differ in the absorber used in HAC1 and in the HAC1 thickness. The HAC2 unit cell is the same in both cases, but the number of cells is selected to give a total thickness of nine interaction lengths in the barrel and eleven in the endcap.

The reentrant endcap design places the iron of the hadronic calorimeter within the current sheet, thereby terminating the solenoidal field. This version has a different geometry than model A, but the response is expected differ from this option only near eta=1.6. The physics analyses have, therefore, concentrated on models A and B only.

Issues that have been considered include:

- performance (hadron, jet and mass resolution and linearity)

- impact on EM calorimeter
- impact on other systems
- cost and engineering

These issues are briefly discussed below; additional information is contained in the attached notes. The report concludes by outlining the consensus design.

2. Physics Performance

The response of the two configurations to electrons and pions has been studied in the hanging file testbeam calorimeter and with CALOR89. Monte Carlo methods have been used to study the resulting jet and mass resolutions and linearity. Conclusions are:

- model A requires a larger correction to achieve linearity and is more sensitive to the relative weighting of the EM and hadronic compartments.
- model B is not an optimal design for a lead absorber calorimeter due to cost constraints.
- either calorimeter will require extensive test beam calibration to the highest available energy and *in situ* study.
- the performance of models A and B is comparable in single particle, jet and mass resolution and both satisfy the SDC requirements.
- no physics processes have been identified that require better performance. The possibility that new physics will place more stringent requirements on the calorimeter is a technical risk.

3. Impact on EM Calorimeter

Model C has a break in the EM calorimeter not present in either of models A or B. Although detailed studies of the impact of this break

are still underway, the conclusion of the calorimeter group is that such discontinuities are undesirable and are likely to lead to a loss of fiducial volume.

4. Impact on Other Systems

muon

Lead produces more multiple scattering per interaction length than iron. The momentum resolution for muons at the level one trigger is, therefore, slightly worse for model B and results in an increase in the level one trigger rate. The rate is less than 5 khz for either configuration for a 20 GeV pt threshold --- an acceptable level.

As indicated in fig. 5, the reentrant endcap requires the muon steel to be 1.2 m longer to allow the endcap to be retracted enough for access to the tracking detectors.

tracking

The field uniformity is noticably better with the reentrant endcap than for either other case; the field at the end of the tracking volume is within 0.1T of the nominal 2T, compared to 1.3T in model A and 1.0T in model B. The tracking group has, however, concluded that all three cases are acceptable.

The neutron fluence in the tracking volume is approximately three times higher for the lead HAC1. When an endcap moderator is used, the fluences for models A and B are 3x10**11 and 1x10**12 n/cm**2.

solenoid

The forces on the solenoid differ substantially between the three cases studied. The compressive loads are 308, 1150 and 1700 t, for the reentrant endcap, model A and model B. The solenoid group has indicated that a new alloy developed for this purpose will enable even the largest of these values to be tolerated. The lower values represent a larger safety factor. If necessary, it may be possible to increase the safety factor by increasing the conductor thickness or reducing the nominal field.

5. Cost and Engineering

Both the iron and the lead hadronic calorimeters are technically feasible. The lead casting method has a larger technical risk, which is reflected in a larger contingency in the cost. The cost of model B is estimated to be $8M greater than that of model A. Using lead only in the barrel HAC1 would increase the cost by $5M. The largest contribution to this difference is fabrication of the absorber.

The Model B barrel calorimeter is heavier than Model A by 211 tonnes (10%); each endcap is 136 tonnes heavier (19%). The support structure would reflect this difference.

Detailed engineering has not been done for Model C, and, therefore, no cost estimate difference is available for the calorimeter itself. The increased length of the muon steel is estimated to cost $1.5M--$2.0M.

6. Consensus Design

The calorimeter group has reached a consensus on the design summarized in Table 2. The design is similar to that of model A, with the calorimeter thickness increased from nine to ten interaction lengths at eta=0. The reduction in leakage simplifies the calibration and weighting of the hadronic calorimeter, which is likely to be complex. The thicker calorimeter will have better efficiency for high Et jet events due to more complete containment. The cost increase is estimated to be less than $1M.

Other parameters that are still under study include the endcap EM configuration, which is different for models A and B; the optimal location for the HAC1/HAC2 boundary; and the transverse segmentation of the HAC1 compartment.

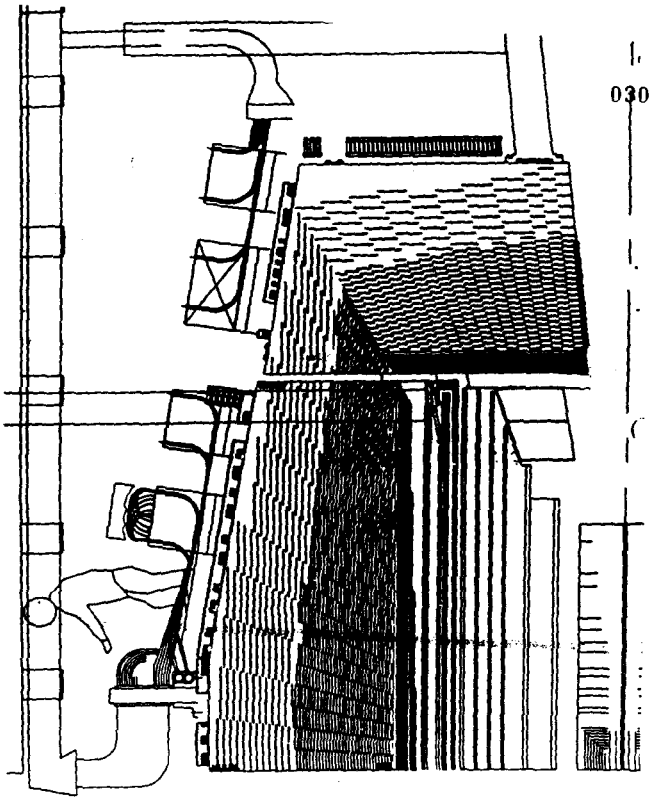

Figure 1. Model A, Iron Hadronic Calorimeter

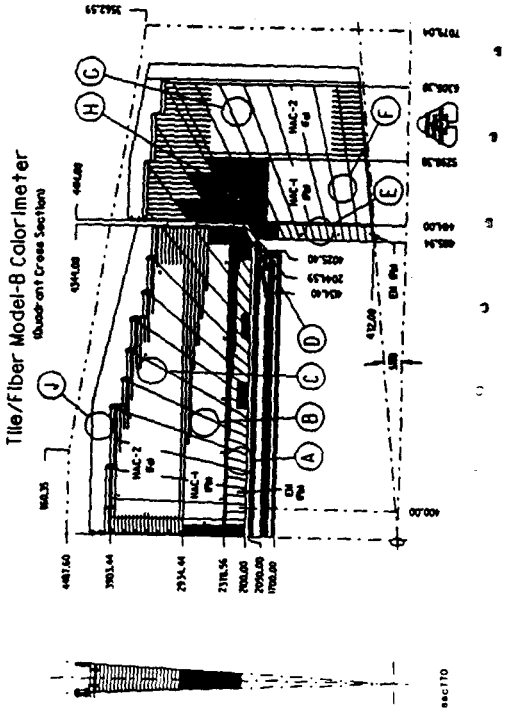

Figure 2 Model B, lead HAC1 section

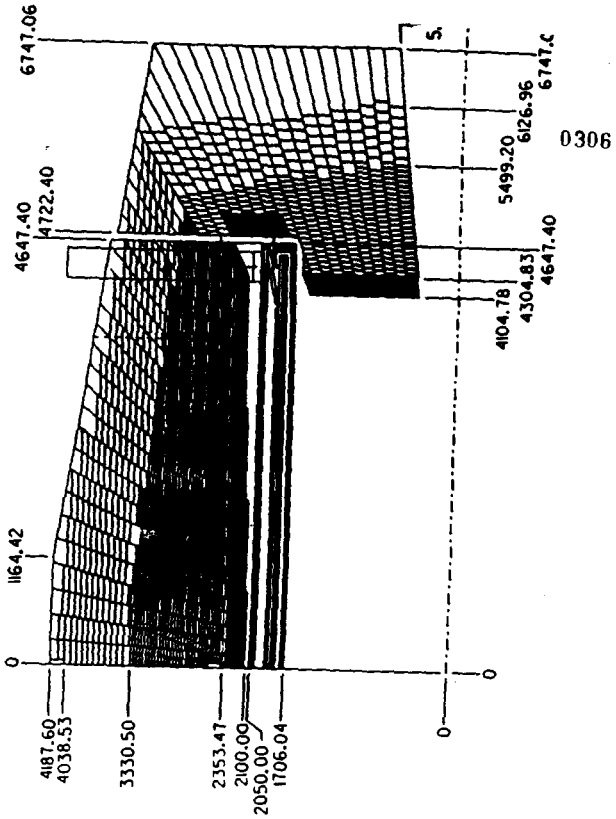

Figure 3 Model C Reentrant Endcap, iron hadronic calorimeter

Table 1. Parameters of the three options considered

Calorimeter Configurations

	Model A	Model B	Reentrant
Total Depth eta=0	9 λ	9 λ	9 λ
Total Depth eta=3	11 λ	11 λ	>11 λ
Barrel EM			
Longitudinal segs.	1	1	1
Xverse seg.	.05	.05	.05
Pb thickness (mm)	3.2	4	3.2
Scint. thickness (mm)	4	4	4
absorber layers	36	29	36
X0	21	21	21
Barrel HAD 1			
Xverse seg.	.05	.1	.05
abs. thickness (mm)	25.4 Fe	21 Pb	25.4 Fe
scint. thickness (mm)	2.5	2.5	2.5
absorber layers	32	24	32
λ	4.8	3	4.8

Calorimeter Configurations

	Model A	Model B	Reentrant
Endcap EM			
Longitudinal segs.	2	2	2
Xverse seg.	.05	.05	.05
Pb thickness (mm)	6.3	8	6.3
Scint. thickness (mm)	4	4	4
absorber layers	18	15	18
X0	21	21	21
Endcap HAD 1			
Xverse seg.	.05	.1	.05
abs. thickness (mm)	51 Fe	31.5 Pb	51 Fe
scint. thickness (mm)	2.5	2.5	2.5
absorber layers	21	24	21
λ	6.4	4.4	6.4

Calorimeter Configurations

	Model A	Model B	Reentrant
Barrel Had2			
Xverse seg.	.1	.1	.1
abs. thickness(mm)	51 Fe	51 Fe	51 Fe
scint. thickness	2.5	2.5	2.5
abs. layers	12	18	12
λ	3.6	5.5	3.6
total depth barrel	9λ	9λ	9λ
resolution (e,γ) stochastic			
constant			

Calorimeter Configurations

	Model A	Model B	Reentrant
Endcap Had2			
xverse seg.	.1	.1	.1
abs. thickness(mm)	102 Fe	102 Fe	102 Fe
scint. thickness	2.5	2.5	2.5
abs. layers	7	10	7
λ	4.3	6.1	4.3
total depth barrel	11λ	11λ	11λ
resolution (e,γ) stochastic			
constant			

Table 2 Parameters of the consensus design

SDC / SSCL Physics Research Division

14-Nov Consensus Design

Barrel EM

Longitudinal segs.	1
Xverse seg.	.05
Pb thickness (mm)	3.2
Scint. thickness (mm)	4
absorber layers	36
X0 (inc. coil)	22 (1.1 λ)

Barrel HAD 1

Xverse seg.	.05
abs. thickness (mm)	25.4 Fe
scint. thickness (mm)	2.5
absorber layers	32
λ	4.9

Barrel Had2

Xverse seg.	.1
abs. thickness(mm)	51 Fe
scint. thickness	2.5
abs. layers	13
λ	4.0
total depth barrel	10λ

resolution (e,π)
stochastic (12%, 50%)
constant (1% , 4%)

8 11/15/91

jls

0311

SDC / SSCL Physics Research Division

14-Nov Consensus Design

Endcap EM

Longitudinal segs.	2
Xverse seg.	.05
Pb thickness (mm)	6.3
Scint. thickness (mm)	4
absorber layers	22
X0	25 (.9 λ)

Endcap HAD 1

Xverse seg.	.05
abs. thickness (mm)	51 Fe
scint. thickness (mm)	2.5
absorber layers	21
λ	6.4

Endcap Had2

xverse seg.	.1
abs. thickness(mm)	102 Fe
scint. thickness	2.5
abs. layers	8
λ	4.9
total depth barrel	12λ

9 11/15/91

jls

0312

From: CSA::GILG 20-SEP-1991 16:12:35.60
To: @CAL_ABSORBER
CC: @TECHNICAL_BOARD
Subj: Calorimeter absorber configuration

Please reply to me and to Jim Siegrist::SSCVX::siegrist) if you are willing to serve on the committee presented below. We must put this group together very quickly. Please respond ASAP.

0313

PREAMBLE

Scintillating tile/fiber calorimetry has been selected as the choice for the central calorimeter of the SDC detector. We now have before us three basic choices for the configuration of the absorber in the hadronic section of the calorimeter: (1) a lead section(HAC1) followed by an iron section(HAC2) in both the barrel and endcap regions; (2) an iron HAC1 and iron HAC2 in the barrel and iron HAC1 and HAC2 in the endcap regions; and (3) a lead HAC1 and iron HAC2 in the barrel region with both iron HAC1 and HAC2 in the endcap region. In the case of the iron loaded endcap, the possibility of having a resonant endcap to provide a more uniform field must be considered. We must move as rapidly as possible to select a single absorber configuration.

CHARGE

The hadronic absorber evaluation committee is charged to evaluate the relative calorimetric performance and physics capability, as well as cost and engineering feasibility of the configurations described above. The Technical Board will make a recommendation for the optimal absorber configuration, based on the committee's evaluations and on its analysis of the impact of the absorber choice on the other detector subsystems. The committee is charged to prepare the appropriate reports and presentations for the collaboration meeting of November 13-16. If sufficient data are in hand at that time, the Technical Board will be requested to make a recommendation for the hadronic absorber configuration. If not, another date will be set to formulate a recommendation.

MEMBERSHIP OF THE COMMITTEE

Chairman.....J. Siegrist(SSCL)
Calorimeter options.....D. Green(FNAL), G. W. Foster(FNAL), L. Nodulman(ANL), J. Proudfoot(ANL)
Physics performance.....C. Hearty(LBL), M. Shapiro(LBL)
Cost/schedule.....M. Edwards, D. Etherton and MSTC personnel
Engineering.....L. Bartoszek(FNAL), N. Hill(ANL), W. Pope(LBL) M. Harrie/T. Thurston(SSCL, ex officio)
Others.....G. Abrams(LBL), J. Erwin(Saclay), W. Frisken(York), K. Takikawa(Tsukuba), B. Wicklund(ANL)

Appendix A: Comm. tee membership and charge

Preliminary Results from Hanging File Calorimeter

A. Byon-Wagner((FNAL)

Preliminary Results from Hanging File Calorimeter

Nov. 14, 1991

presented by A. Byon-Wagner

BEAM TEST OF RECONFIGURABLE-STACK CALORIMETER

A. Byon-Wagner, G. W. Foster, J. Freeman, D. Green, R. Tokarek, Y. Zhou, A. Beretvas
Fermi National Accelerator Laboratory

V. Hagopian
Florida State University

D. E. Groom, R. Kadel, R. Donahue
Lawrence Berkeley Laboratory

R. Gustafson, M. Shappirio, C. Leggett
University of Michigan

J. Huston
Michigan State University

L. Cremaldi, D. Summers, B. Moore
University of Mississippi

V. E. Barnes, A. Laasanen
Purdue University

P. de Barbaro, H. Budd, A. Bodek, W. Sakamoto
University of Rochester

C. Zhao
University of Wisconsin

If I missed anybody, I apologize!

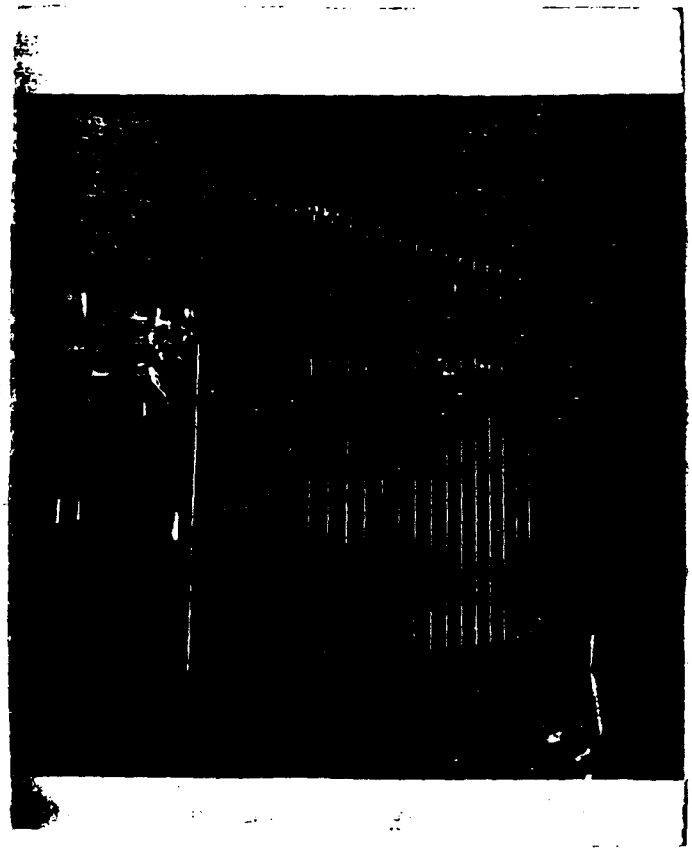

File grooving	Groom
PMT	Groom, Huston
Frontend / Trigger	Willis, Bill, Pawel
DAQ	Willis, Zhao
Online Monitoring	Bill
Muon Calibration	Pawel
Source Calibration	Virgil, Alvin
Beam Tuning	Tokarek
HFC Offline	Groom, Pawel, Andy
SWDC Analysis	Kadel
Monte Carlo	Groom/Donahue, Bill, Brent

Equipments (PMT, electronics, computer) from FSU, Purdue, LBL, U of M, Rochester

critical Inputs from Bill, Groom, Virgil, Gustafson, Ari, Reidy, Freeman

Tile Uniformity : Example of "good tile"

1m x 1m x 3mm SCSN-81

0323

Photo Statistics in each counter measured at test beam

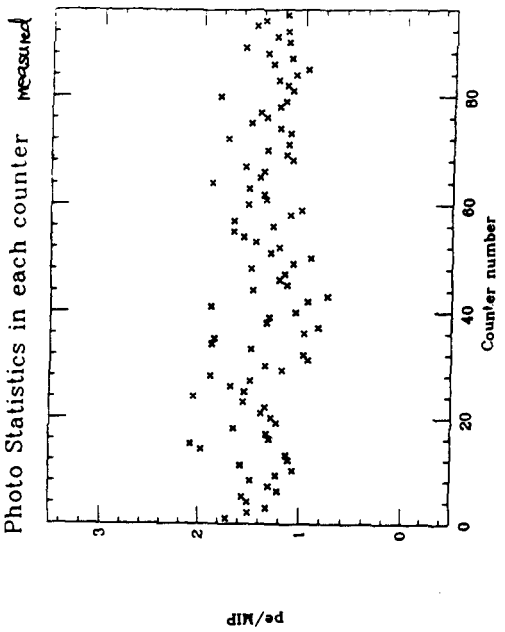

0324

Tile Uniformity : Example of "not so good" tile

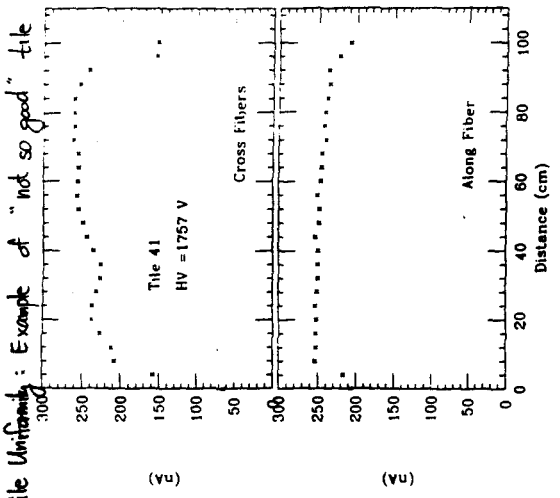

10

0325

* Some numbers in M-Test

time between spill = 40 sec

beam spill time = 19 ~ 23 sec

# of particles / spill = 10K (10 GeV π)
25K (26 GeV π)
100K (50 ~ 100 GeV)
3M (225 GeV)

time required to change beam energy = 2 min
" " π to e = 3 min
" to switch beam from CDF = <5 min

Typical particle contents in π - beam

	π	e
> 100 GeV	> 99%	< 1%
50 GeV	~ 70%	~ 30%
25 GeV	50%	50%
10 GeV	30%	70%

0326

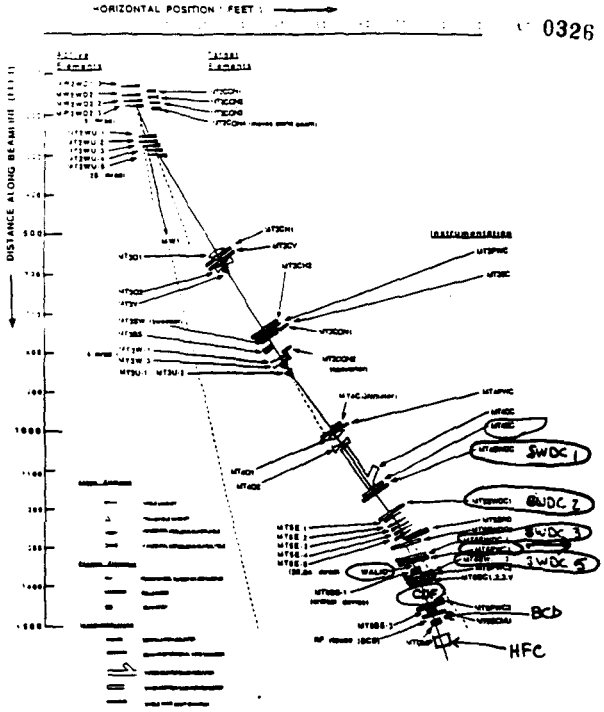

Single Wire Drift Chamber (beam momtum analysis)

15

0327

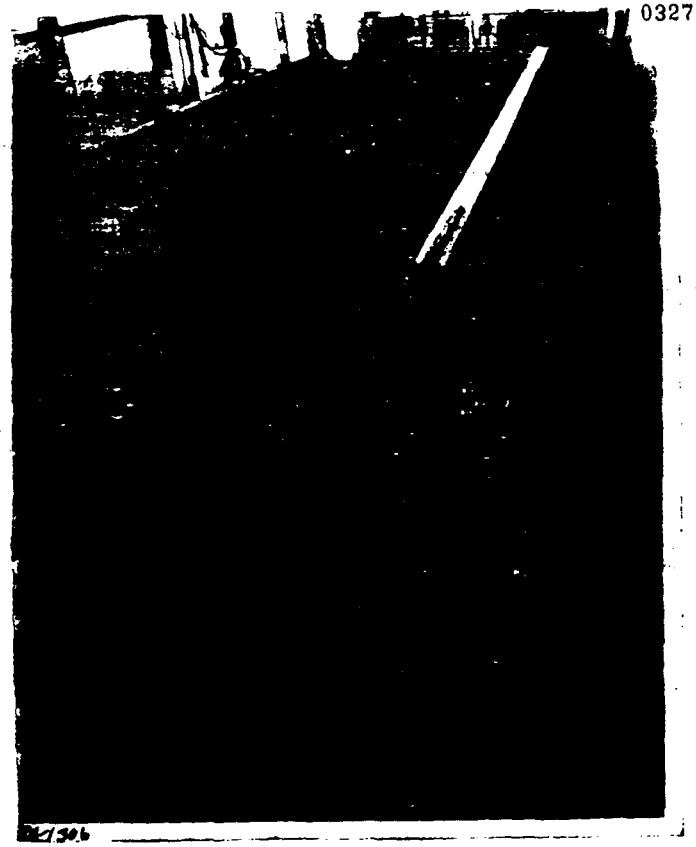

0328

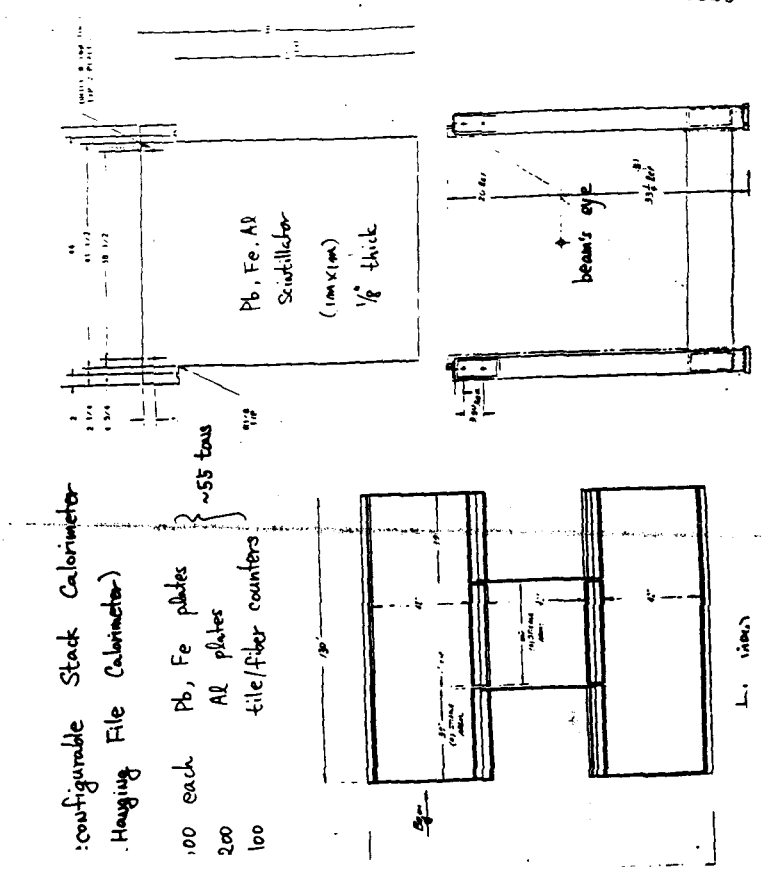

0329

Trigger on B1·B2 (HFC trigger counters)

Latch in

MT4SC
CDF Tr
S1·S2 (CDF beam counters)
C3 (BCD trigger counter)
C4 (")
BCD Veto (BCD veto counter)
HFC Veto (HFC " ")
muon counter

0330

What we can do in 1 shift ("good shift")

Run #	# Events	Time	Run Type
R000505F01.FSP	682	7-OCT 06:44	pedestal
R000507F01.FSP	11780	7-OCT 07:12	227-pi
R000508F01.FSP	12028	7-OCT 07:20	150-pi
R000509F01.FSP	13144	7-OCT 07:25	100-pi
R000610F01.FSP	13082	7-OCT 07:32	50-pi
R000611F01.FSP	24118	7-OCT 07:39	25-pi
R000612F01.FSP	39990	7-OCT 07:51	8-pi
R000613F01.FSP	682	7-OCT 08:09	pedestal
R000617F01.FSP	682	7-OCT 11:36	pedestal
R000618F01.FSP	7998	7-OCT 11:36	mu
R000621F01.FSP	558	8-OCT 06:39	pedestal
R000622F01.FSP	3596	8-OCT 06:57	mu
R000623F01.FSP	9734	8-OCT 07:10	227-pi
R000624F01.FSP	14880	8-OCT 07:14	227-pi
R000625F01.FSP	15748	8-OCT 07:22	150-pi
R000626F01.FSP	11904	8-OCT 07:32	100-pi
R000627F01.FSP	13850	8-OCT 07:47	50-pi
R000628F01.FSP	1550	8-OCT 07:53	25-pi
R000629F01.FSP	13082	8-OCT 07:55	25-pi
R000630F01.FSP	12710	8-OCT 08:05	8-pi
R000646F01.FSP	806	20-OCT 06:16	pedestal
R000649F01.FSP	4526	20-OCT 06:19	mu
R000650F01.FSP	682	20-OCT 06:56	pedestal
R000651F01.FSP	1178	20-OCT 07:00	mu
R000652F01.FSP	9486	20-OCT 07:08	227-pi
R000653F01.FSP	26184	20-OCT 07:22	227-pi
R000654F01.FSP	24490	20-OCT 07:34	150-pi
R000655F01.FSP	26970	20-OCT 07:47	100-pi
R000656F01.FSP	496	20-OCT 07:57	pedestal
R000657F01.FSP	25844	20-OCT 07:59	50-pi
R000658F01.FSP	30442	20-OCT 08:13	25-pi
R000659F01.FSP	744	20-OCT 08:44	pedestal
R000660F01.FSP	32048	20-OCT 08:53	15-pi
R000643F01.FSP	558	20-OCT 10:08	pedestal
R000644F01.FSP	2804	20-OCT 10:10	mu
R000646F01.FSP	20212	20-OCT 10:36	mu

>90% ■ usage of beam-time

R. W. Kadel
Nov 11, 1991

Magnetic Analysis M - TEST

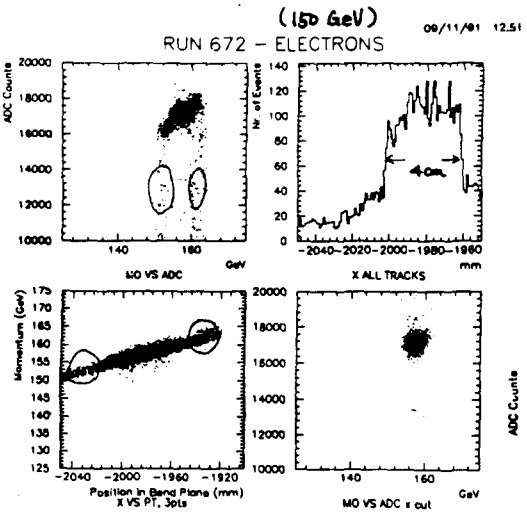

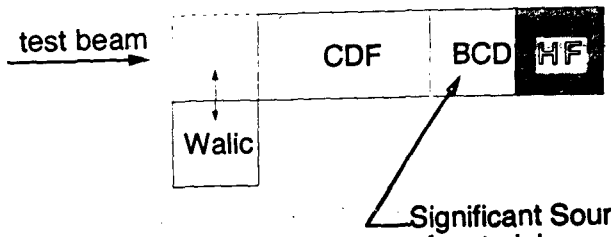

Run 672 Electrons **(Total Triggers 16740)**

Total Trks Reconstructed 6730 (40%

2054 (12%

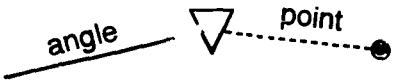

4676 (28%

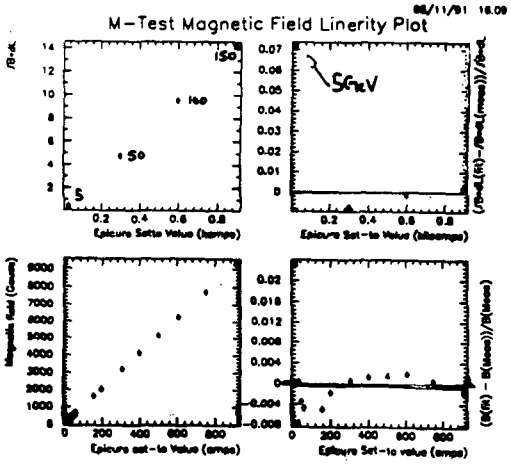

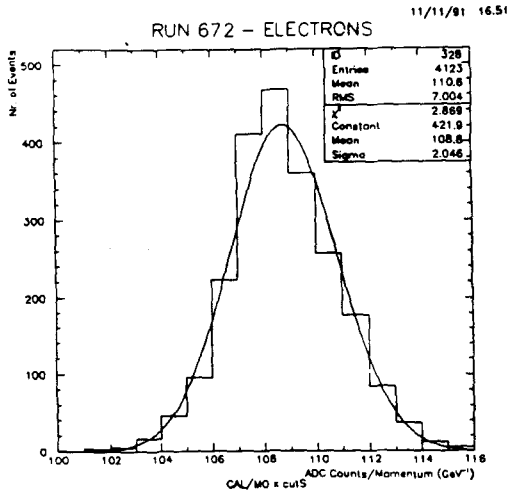

cut on position in Bend plane → 2% spread

tight cut on upstream trigger counters → ~0.5% spread

Run Plan of of Reconfigurable-Stack Calorimeter - T841T
August 16, 1991

** 1 calendar week = 4 successful data points + 5 shifts of muon calibrations

1. System Debugging (2 weeks: Aug 19 - Aug 31)
2. Checkout configurations (1 week: Sep 1 - Sep 7)
   - Muon running : demonstrate calibration procedures
   - EM resolution tests (1/8" lead)
3. Reference configurations : comparison with published data (2 weeks: Sep 8 - Sep 21)
   - 1/2", 1" Pb
   - 1", 2" Fe
4. CDF configurations : (2 weeks: Sep 22 - Oct 5)
   - Pb EM + 2" Fe + 1/4" Pb [1] (Pb upstream or downstream of scintillator)
   - Pb EM + 2" Fe + 1/4" Pb + 1/8" Al (test of cladding)
   - CDF Central Calorimeter 1/8" Pb EM + 1" Fe hadronic
5. SSC HADRON configurations (3 weeks: Oct 6 - Oct 12)
   - Lead insert tests: 1" Fe + 1/4" Pb (Pb upstream or downstream of scintillator or buried in middle of Fe plates)
   - Cladding tests: 1" Fe + 1/8" Al (Al upstream or downstream of scintillator) or 1" Fe + 1/4" Pb + 1/8" Al
   - High-lead tests: 1/2" Fe + 1/2" Pb or 1/4" Fe + 1/4" Pb (Pb upstream or downstream of scintillator)
6. SSC Hybrid/back-catcher configurations (2 weeks: Oct 13 - Oct 26)
   - 1 λ Pb + Fe/scintillator Hadron
   - 2 λ Pb + Fe/scintillator Hadron
   - 3 λ Pb + Fe/scintillator Hadron
   - 4 λ Pb + Fe/scintillator Hadron
7. Measurement of albedo loss (1 week: Oct 27 - Nov 2)
8. Data to tune up Hadronic Cascade Montecarlos (remainder of run: Nov 3 - Dec 15)
   - Run with "dead" plastic inserted into stack
   - Additional configurations to clarify any discrepancies between the Montecarlos and hanging-file data.

[1] CDF cladding is Pb EM + 2" Fe plates + X

We do Run by Run beam momenta calculation

For now –

"Beam Energy"
= "Nominal Beam Energy"
= What Epicure set says the energy is

• EM • (7/8" Pb • Scin)•20 • (1"Fe • Scin)•35

R000721F01.FSP	1900	2-NOV	227-pi
R000723F01.FSP	1400	2-NOV	150-pi
R000724F01.FSP	2300	2-NOV	100-pi
R000735F01.FSP	1400	4-NOV	50-pi
R000736F01.FSP	1300	4-NOV	25-pi
R000737F01.FSP	1100	4-NOV	10-pi

• EM • (1"Fe • 1/8"Al • Scin • 1/8"Al)•21 • (1"Fe • Scin)•34

R000748F01.FSP	550	6-NOV	227-pi
R000749F01.FSP	800	6-NOV	150-pi
R000750F01.FSP	1800	6-NOV	100-pi
R000751F01.FSP	800	8-NOV	50-pi
R000752F01.FSP	900	8-NOV	25-pi
R000753F01.FSP	600	6-NOV	10-pi

• (1/4"Pb • 2Scin)•20 • (2"Fe • 2Scin • 1/8"Al)•27

R000811F01.FSP	1550	12-NOV	227-pi
R000815F01.FSP	1300	12-NOV	100-pi

configurations measured so far

• (1" Fe • Scin)•68

R000697F01.FSP	1700	24-OCT	227-pi
R000704F01.FSP	1100	1-NOV	150-pi
R000705F01.FSP	3000	1-NOV	100-pi
R000706F01.FSP	2900	1-NOV	50-pi
R000707F01.FSP	550	1-NOV	25-pi
R000708F01.FSP	950	1-NOV	8-pi

• EM • (1" Pb • Scin)•52

R000679F01.FSP	2800	11-OCT	227-pi
R000694F01.FSP	2300	13-OCT	100-pi
R000695F01.FSP	2500	13-OCT	50-pi
R000696F01.FSP	3300	13-OCT	25-pi
R000697F01.FSP	1200	13-OCT	10-pi
R000699F01.FSP	1700	13-OCT	15-pi

• HV lowered by 30V for all channels

R000824F01.FSP	1900	18-OCT	100-pi
R000825F01.FSP	2000	18-OCT	50-pi
R000826F01.FSP	800	18-OCT	25-pi

• EM • (1" Fe • Scin)•55

R000653F01.FSP	2200	20-OCT	227-pi
R000654F01.FSP	2100	20-OCT	150-pi
R000655F01.FSP	3400	20-OCT	100-pi
R000657F01.FSP	2500	20-OCT	50-pi
R000658F01.FSP	1800	20-OCT	25-pi
R000660F01.FSP	850	20-OCT	15-pi
R000675F01.FSP	500	21-OCT	8-pi

• EM •(1"Fe • 1/8"Al • Scin • 1/8"Al)•55

R000784F01.FSP	2300	8-NOV	227-pi
R000785F01.FSP	1200	8-NOV	150-pi
R000787F01.FSP	3000	8-NOV	100-pi
R000788F01.FSP	1300	8-NOV	50-pi
R000789F01.FSP	800	8-NOV	25-pi
R000790F01.FSP	500	8-NOV	10-pi
R000791F01.FSP	800	8-NOV	15-pi

continue –

0339

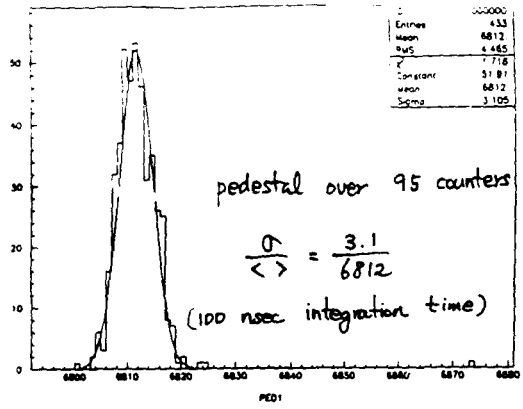

* 120 counts / GeV in EM
  → 3 counts ≃ 25 MeV

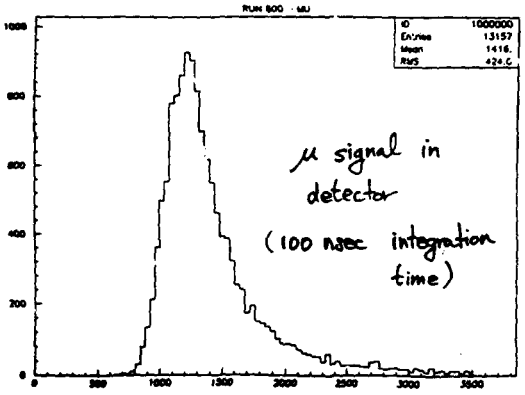

0340

* Front end

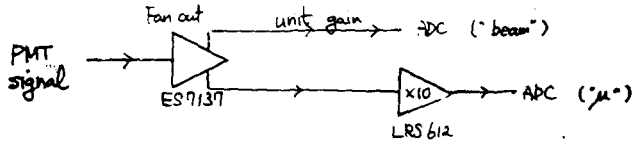

0341

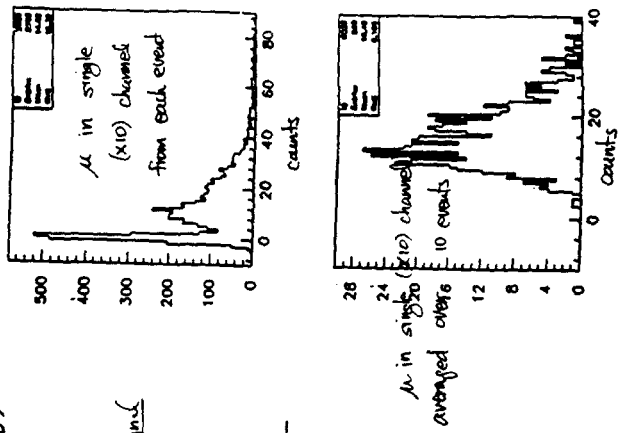

Muon Calibration (Paul de Barbaro)

Calibration constant = "trimmed" mean of (x10) muon signal / ratio of (x10/x1) signals

Calibrated signal = measured ADC counts / calibration constant

0342

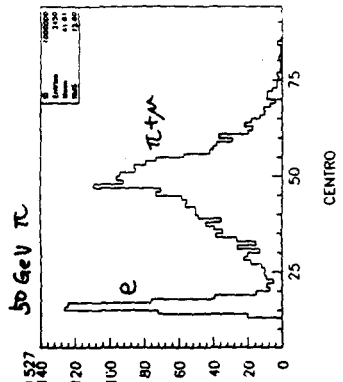

< Raw data >

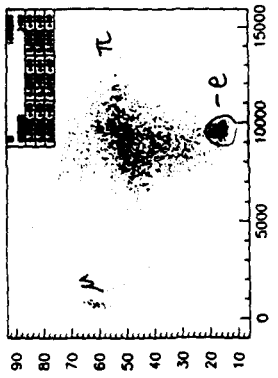

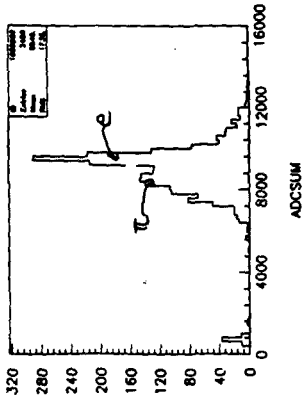

Linearity & Calibration

Electron – 10/13, 10/20, 11/4, 11/8

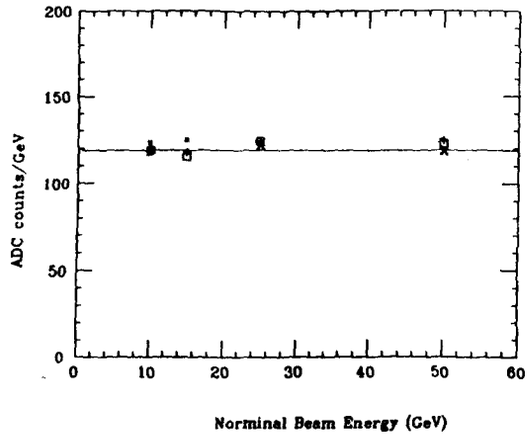

over 4 weeks → ~120 counts/GeV in EM

0345

2ℓ

RUN 705 (100 GeV π)

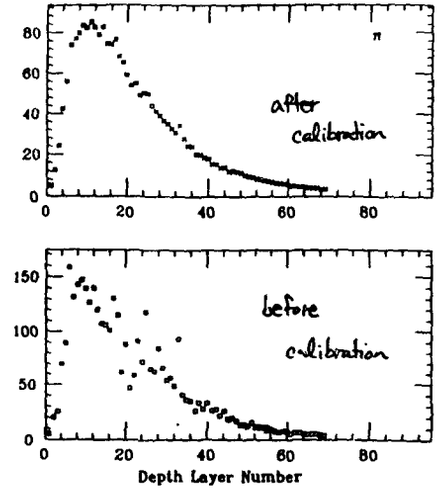

(1" Fe + Scin) * 69

0346

100 GeV electron (R673)

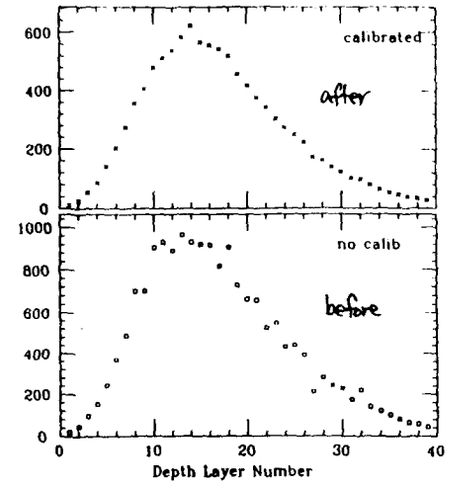

(1/8" Pb + Scin) * 40

0343

10 GeV electron (R670)

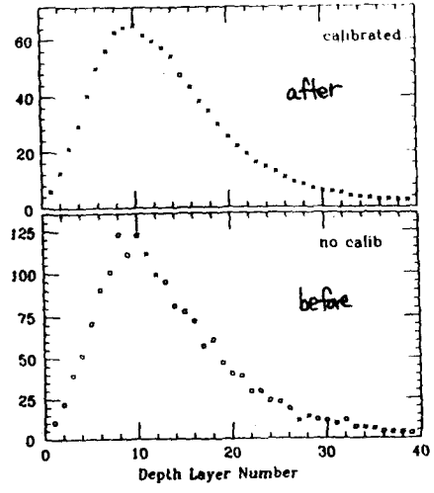

in (1/8" Pb + Scin) * 40

0344

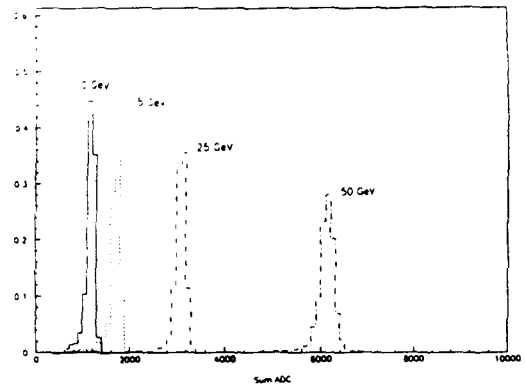

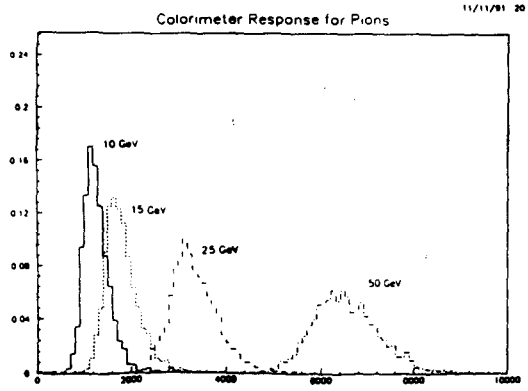

Calibration Methods

muon

source

minimize resolution

shower development (smoothing!)

at 100 GeV $\left(\frac{\sigma}{E}\right)_{\text{meas}} = 1.75\%$

$\left(\frac{\sigma}{E}\right)_{\text{expected}}$ = 1.3 ⊕ Photoshd. ⊕ Beam 0.5

120 counts/GeV } ⇒ 104 pe/GeV
1.3 pe/MIP }
1.5 counts/MIP

9.8%

$\therefore \left(\frac{\sigma}{E}\right)_{\text{expected}} = 1.3 \oplus \frac{9.8}{\sqrt{100}} \oplus 0.5$

= 1.70 %

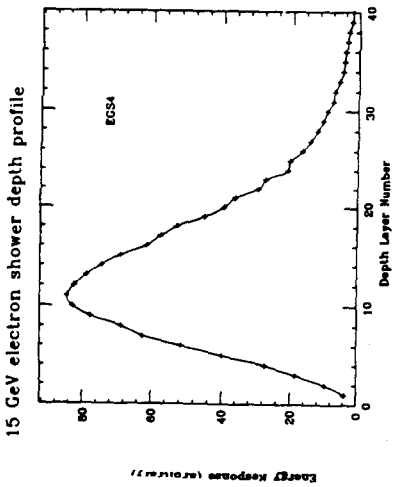

100 GeV electron

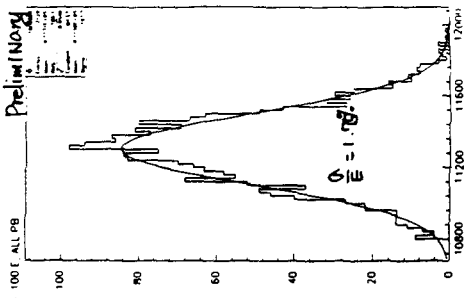

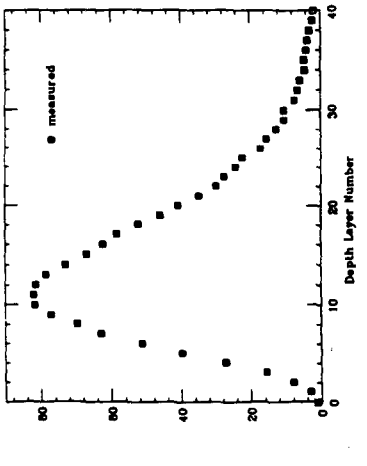

EM = (1/8" Pb + 3mm Scint.) * 40

0351

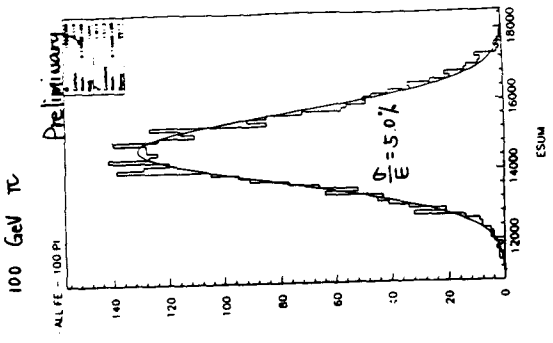

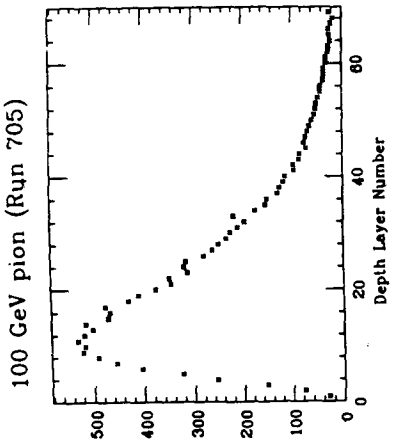

(1" Fe + 3mm Scin) * 69

0352

* Possible errors / contributions to resolution

Photostatistics , P_beam

gain drift , calibration

non-uniformity in tile

plate thickness / flatness

upstream beam scraping (especially low energy)

0353

total energy $E = E(EM) + \alpha \cdot E(HAD)$

$$E(HAD) = (\Sigma ADC) * \frac{\left(\frac{dE}{dx}\right)_{HAD}}{\left(\frac{dE}{dx}\right)_{EM}}$$

weighting factor for plate thickness

0354

- DHS (2.5 cm Fe + 0.5 cm Scin) 50 × 60 cm²
- HFC (1" Fe + 0.3 cm Scin) 100 × 100 cm²

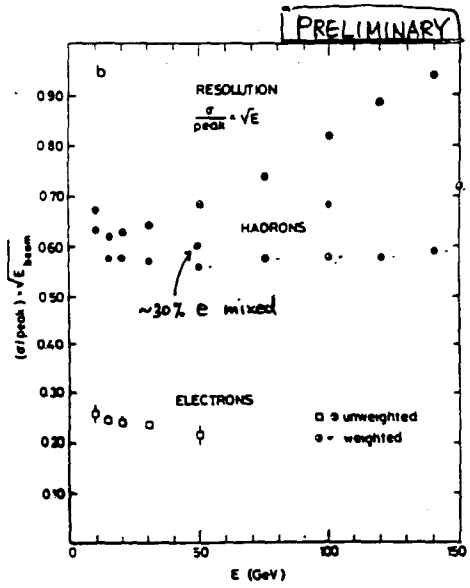

Fig. 4. a) Calorimeter response to hadrons and electrons in terms of numbers of equivalent particles (nep) per incident energy (GeV) against the energy of the incident particle, E_{beam} in GeV. b) The width of the energy distributions. $(\sigma/\text{peak})\sqrt{E_{beam}}$ against incident energy, E_{beam} in GeV.

0355

0356

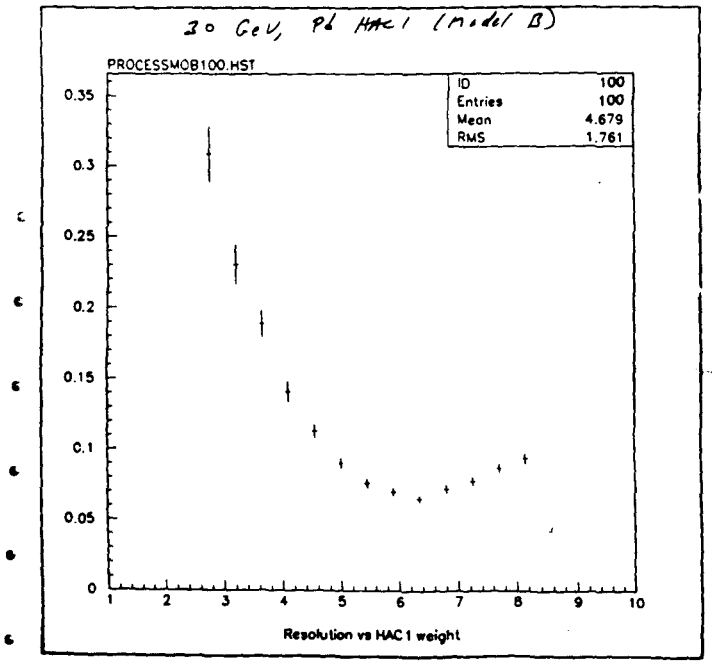

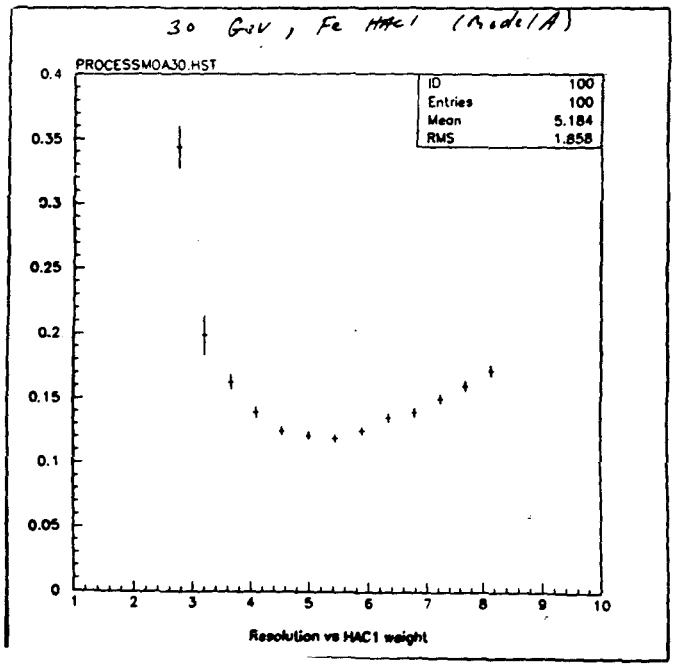

0357

0358

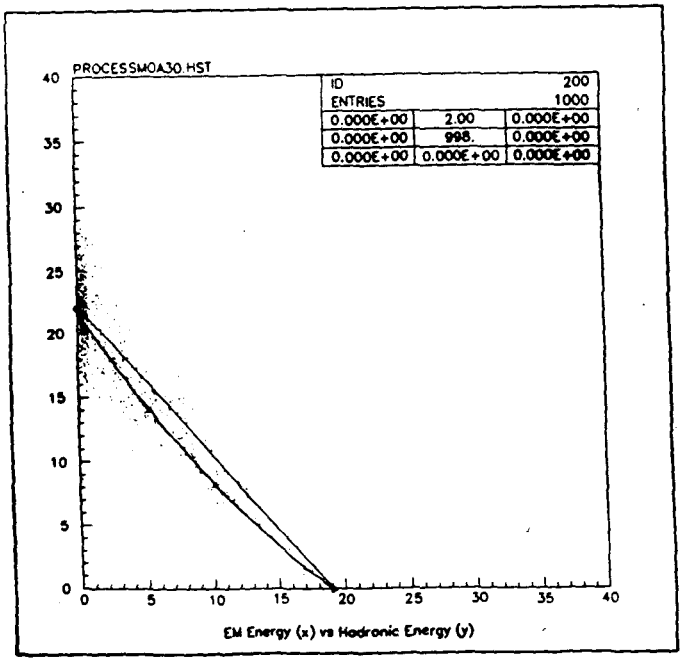

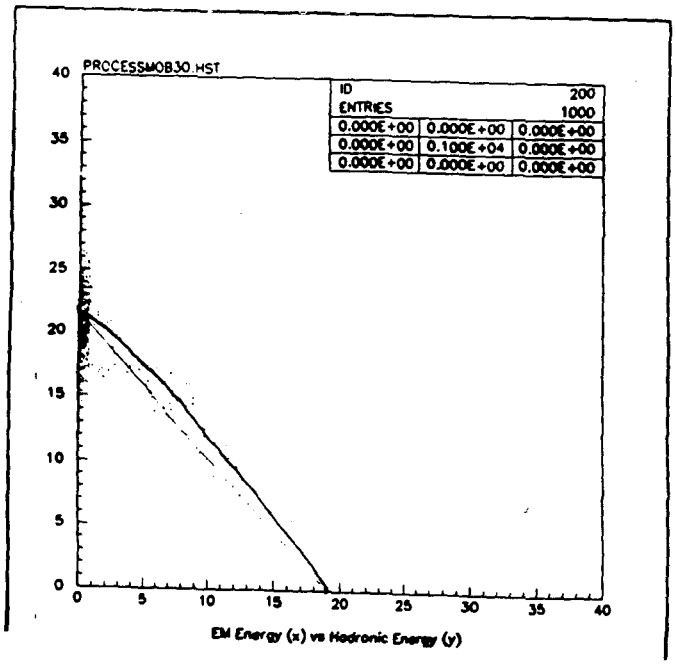

0359

Possible errors in e/π

1. extrapolation of electron energy at 227 GeV
2. leakage
3. Saturation ~3% of events at 227 GeV
   ~1% " 150 GeV
   0% " ≤100 GeV
4. contamination of e in π (<1%)
5. μ contamination small at 10 GeV
   negligible > 10 GeV
6. uncertainty in beam energy (< 1%)
7. upstream beam scraping (at low energy)

0360

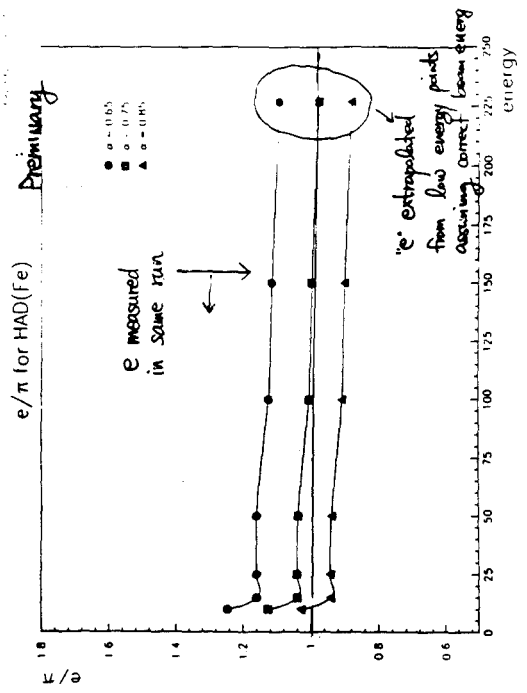

0361

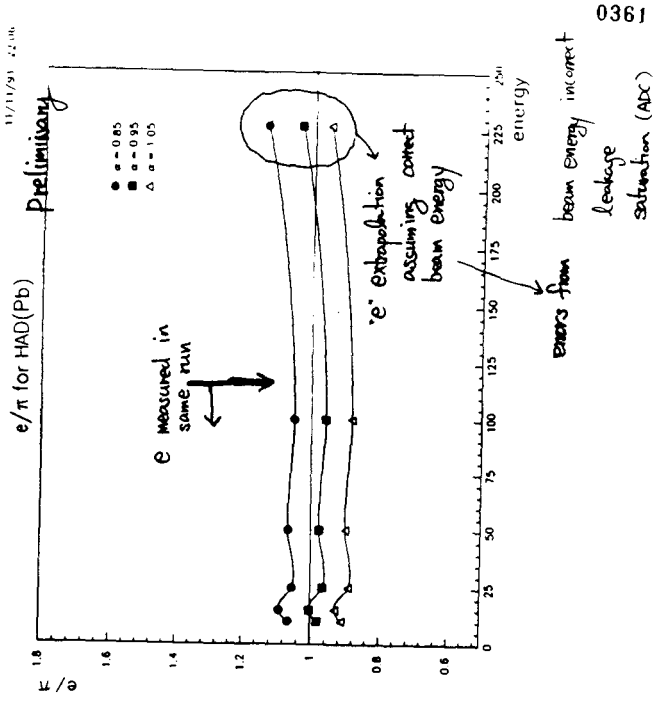

0362

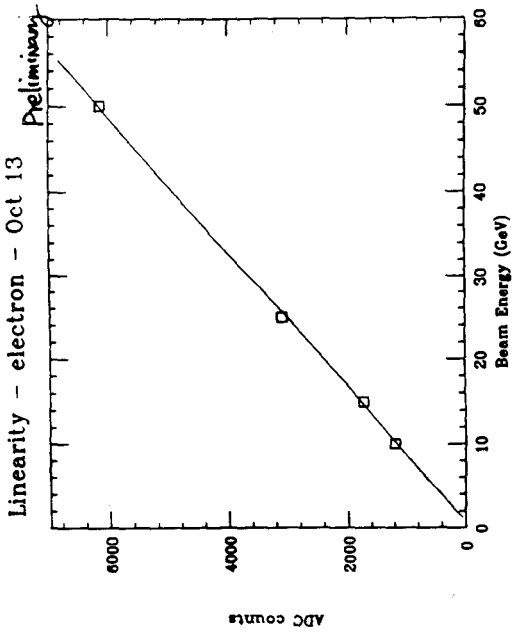

Bernardi et al NIM A262 (1987)

(1cm Pb + 0.25 cm Scin) #81

$\left(\frac{\sigma}{E}\right)_e = \frac{(23.5 \pm 0.2)}{\sqrt{E}}$ %

$\left(\frac{\sigma}{E}\right)_\pi = \frac{(44.2 \pm 1.3)}{\sqrt{E}}$ %

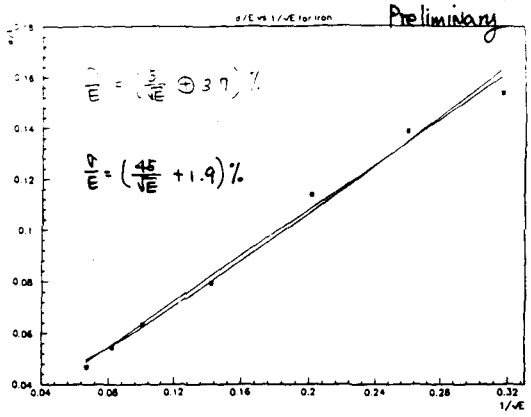

$\frac{\sigma}{E} = \frac{35}{\sqrt{E}} \oplus 3.7$ %

$\frac{\sigma}{E} = \left(\frac{45}{\sqrt{E}} + 1.9\right)$ %

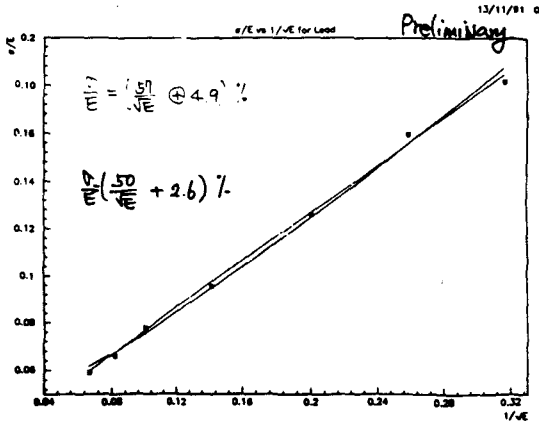

$\frac{\sigma}{E} = \frac{55}{\sqrt{E}} \oplus 4.9$ %

$\frac{\sigma}{E} \left(\frac{50}{\sqrt{E}} + 2.6\right)$ %

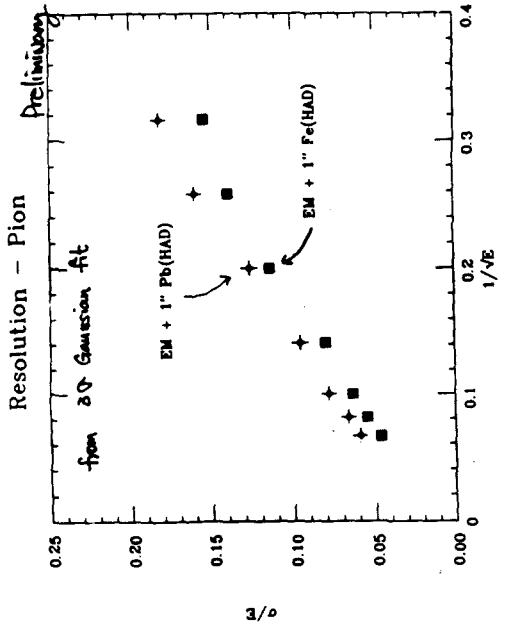

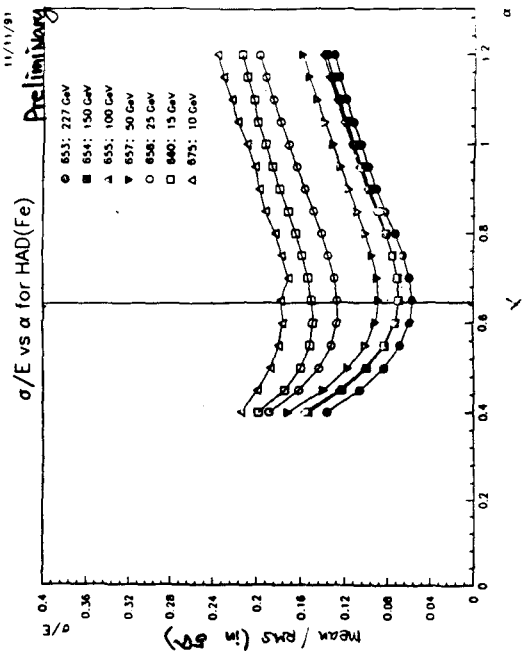

$W\left(\frac{\lambda_E}{\lambda_I}\right) = 6.46$

$W\left(\frac{dE}{dx}\right)_{Pb} = 7.1$

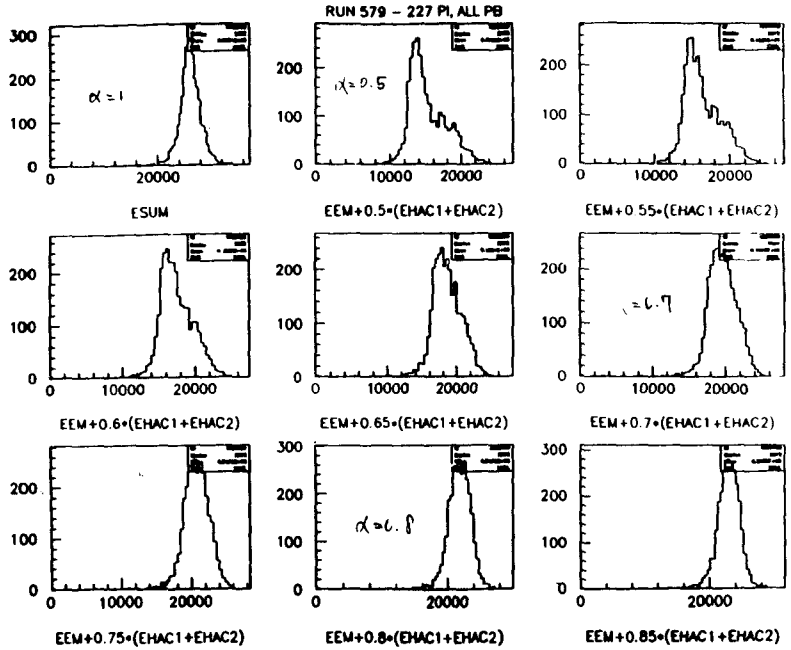

0369

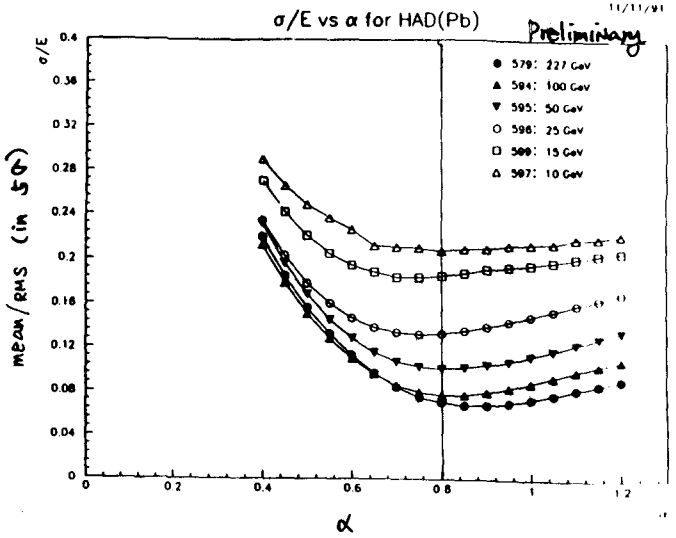

$E = E(EM) + \alpha \cdot W_{Pb} \cdot E(HAD)$

$W\left(\frac{dE}{dx}\right) = 7.1$

0367

The energy deposited in a calorimeter due to dE/dx is

material	dE/dx	density	thickness(cm)	Total (MeV)
Pb 1/8in	11.13	11.35	.318	28.56
Pb 7/8in			2.22	
Pb 1 in			2.54	32.64
Fe 1 in	1.48	7.87	2.54	29.58
Scintillator	1.95	1.032	.3	.604
Al 1/8in	1.82	2.70	.318	1.39

Total Energy/ Energy in scintillator

1/8° lead = (.604 + 4.06)/.604 = 7.75

1° lead = (.604 +32.64)/.604 = 55.04

7/8° lead = (.604 +28.56)/.604 = 48.27

1° iron = (.604 +29.58)/.604 = 49.97

1°Fe+1/8°Al+Scint+1/8°Al = (.604+1.39+29.58+1.39)/.604 = 54.58

1/8°Pb+1/8°Al+Scint+1/8°Al = 12.96

If α = proportion to 1/8° lead Pb = 1

MAD(1/8° lead) = 7.10
MAD(7/8° lead) = 6.23
MAD(1°Fe+1/8°Al+Scint+1/8°Al) = 7.04
MAD(1/8°Pb+1/8°Al+Scint+1/8°Al) = 1.59

$W\left(\frac{dE}{dx}\right)$

$E = \Sigma ADC(EM) + \left(\Sigma ADC(HAD) * \alpha \cdot W\left(\frac{dE}{dx}\right)\right)$

0370

$W\left(\frac{dE}{dx}\right)_{Fe} = 6.46$

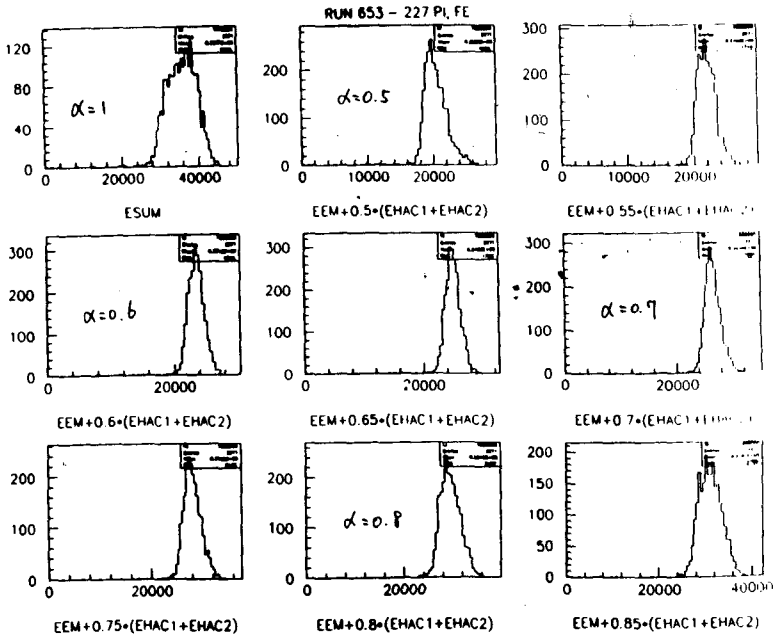

0368

Single Particle Calorimeter Simulations

L. Price(ANL)

0372

SINGLE PARTICLE

CALOR SIMULATIONS

L. Price

P. K. J. L

11/14/91

0373

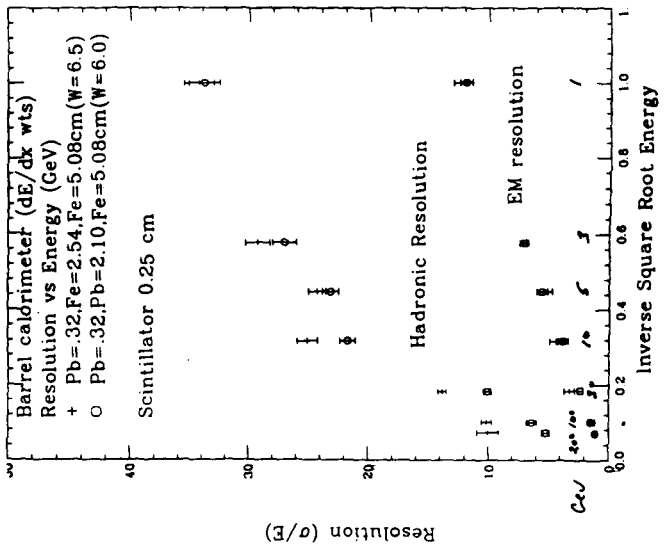

0374

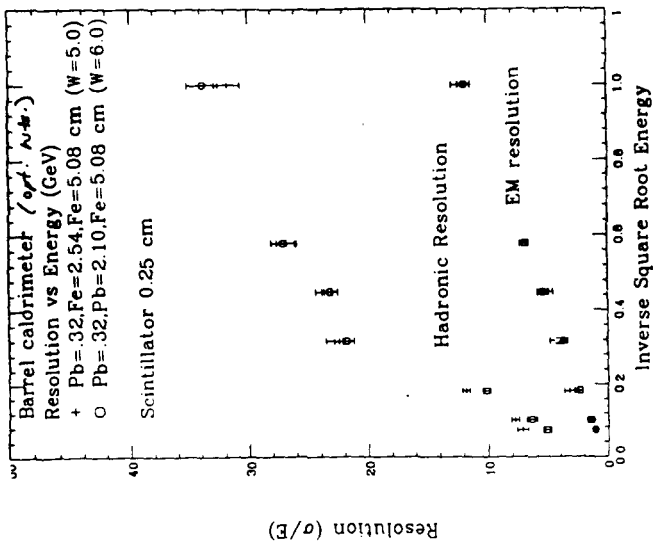

0375

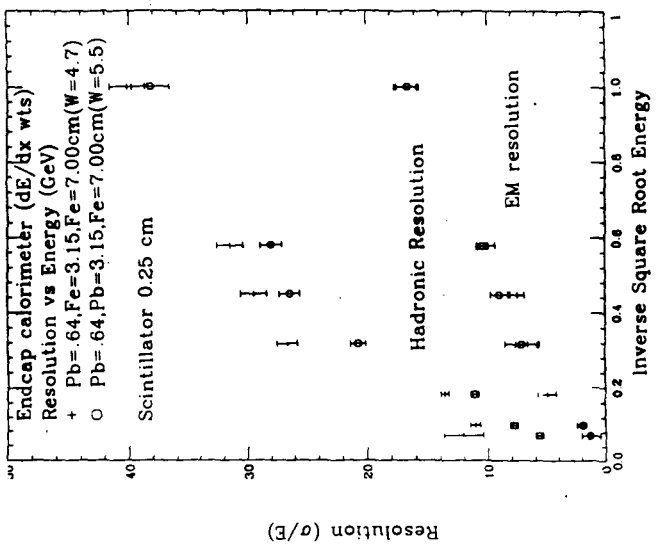

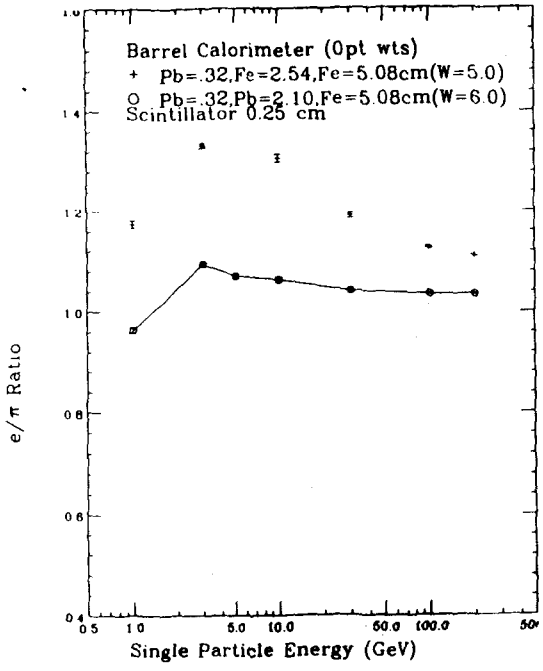

0378

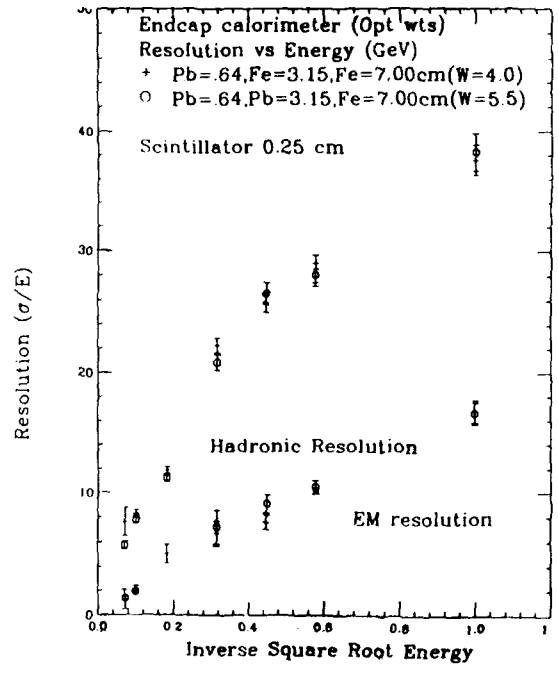

0376

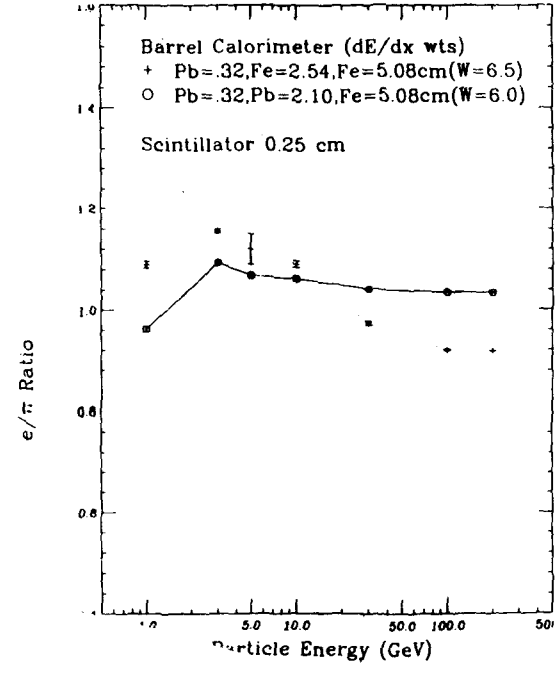

0377

e/h Simulation

D. Green(FNAL)

DRG
11/91

e/h SIMULATION

1. STUDY 10 TeV DIJET AS MOST SENSITIVE TO RESOLUTION OF CALORIMETER - LoI 0.1 TeV, 3.0 TeV
2. GENERATE M_{JJ} = 10 TeV
3. CLUSTERING WITH $R = \sqrt{\Delta\eta^2 + \Delta\phi^2}$
   LANDAU/VAVILOV EVENT OUT OF CONE (CARLSON) = 0.6
4. PARAMETRIZATION OF γ AND π ENERGY DEPOSITION INTO 2 COMPARTMENTS EM (Pb) AND HAD (Fe)

EM HAD

EFFECTS ON M_{JJ} RESOLUTION

- • — FRAGMENTATION FLUCTUATIONS
- o — CALORIMETER RESOLUTION
  $dE_H/E_H \sim 0.5/\sqrt{E} \oplus 0.03$
  $dE_\gamma/E_\gamma \sim 0.2/\sqrt{E} \oplus 0.01$
- ▽ — $J \to Q \to q\bar{q}V$

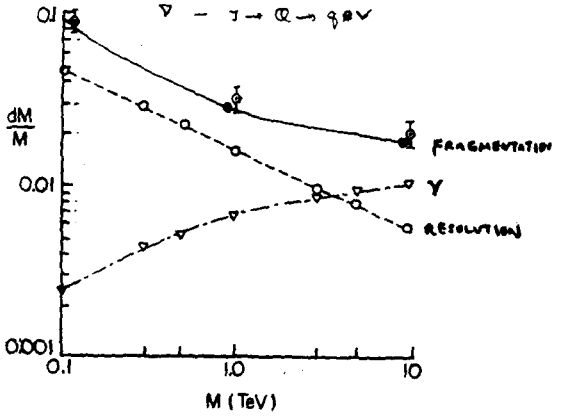

LHC STUDY - CHECK OF CONCLUSIONS

$H \to b\bar{b}$

PERFECT DETECTOR (NO RESOLUTION)

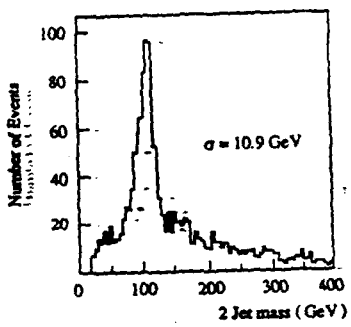

ONLY MARGINALLY WIDENED BY A POOR CALORIMETER RESOLUTION OF $100\%/\sqrt{E} \oplus 4\%$

(EM, HAD COMPARTMENTS)

4.0. LONGITUDINAL γ

$$\frac{dE}{b(d\tau)} = \left[(b\tau)^{a-1} e^{-b\tau}\right] E_0/\Gamma(a)$$

$b \sim 0.5$
$\tau = z/X_0$, $y = E_0/E_c$
$\tau_{max} = (a-1)/b = 1.0[\ln y + 0.5]$

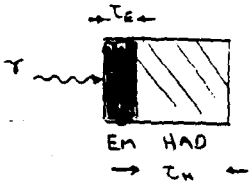

PICK $dN/d\tau_0 = e^{-\tau_0}$ • CONVERSION POINT FLUCTUATION
$\tau = \tau_E - \tau_0$

$$\frac{E_{em}(\tau)}{E_0} = \Gamma(a, b\tau)/\Gamma(a)$$

$$\frac{E_{HAD}(\tau)}{E_0} = \gamma(a, b\tau)/\Gamma(a) = \frac{1 - \Gamma(a, b\tau)}{\Gamma(a)}$$

• LEAKAGE

(3)

4. b. TRANSVERSE γ

• 2 EXPONENTIALS IN r

$$\frac{dE}{dr} \sim \left[e^{-r/r_1} + g e^{-r/r_2} \right] r / (r_1^2 + g r_2^2)$$

$g \sim 0.0066$

$r_1 \sim [0.046 + 0.015 t]$ (cm) • CDF

$r_2 \sim [0.33 + 0.058 t]$ (cm)

4. c. LONGITUDINAL h

EM – f_0, HAD – $(1-f_0)$

$D = z/\lambda_0$

$$dE \sim \left\{ \begin{array}{l} f_0 [(bt)^{a-1} e^{-bt} d(bt)] + \\ (1-f_0)[D^{a-1} e^{-dD} d(dD)] \end{array} \right\} E_0 / \Gamma(a)$$

$a = 0.62 + 0.32 \ln E_0$

$b = 0.22$

$d = 0.91 - 0.024 \ln E_0$

$f_0 = 0.46$

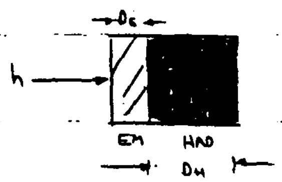

$D_E \sim 0.72$

$D_H \sim 8.3$

(4)

4. d. PROB. INT. $D_0 = e^{-D_0}$ • INTERACTION POINT FLUCTUATIONS

IF D_0 IS IN EM THEN:

$D = D_E - D_0$,
$t = t_E - t_0$

$$\frac{E_{EM}(h)}{E_0} \doteq \frac{[f_0 \Gamma(a, bt) + (1-f_0)\Gamma(a, dD)]}{\Gamma(a)}$$

$$\frac{E_{HAD}(h)}{E_0} \sim \left\{ \begin{array}{l} f_0 (1 - \Gamma(a,bt)/\Gamma(a)) \\ + (1-f_0)(1 - \Gamma(a,dD)/\Gamma(a)) \end{array} \right\} (\pi/e)$$ IGNORING LEAKAGE OUT OF HAD

IF D_0 IS IN HAD, THEN:

$D = D_H + D_E - D_0 \sim \infty$, IGNORE LEAKAGE

$$\frac{E_{EM}(h)}{E_0} = 0$$

$$\frac{E_{HAD}(h)}{E_0} \simeq [f_0 + (1-f_0)] (\pi/e)$$

$$\pi/e \doteq \left[1 - |1 - h/e| \left(\frac{1\,GeV}{E_0}\right)^{0.15} \right]$$ • GROOM

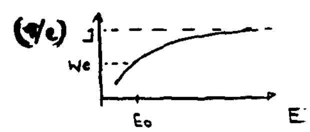

• NONLINEARITY ADDED EXPLICITLY

CONTAINS NON-LINEARITY DUE TO $f_0(E)$ – ENERGY SCALE AND NONCOMPENSAT.

(5)

4. e) TRANSVERSE h

SUM OF 2 EXPONENTIALS

OR

$dE/dz \sim a_1 e^{-|z|/b_1} + a_2 e^{-|z|/b_2}$

$a_1 = 0.7$, $a_2 = 0.3$

EITHER ONE IS CLOSE ENOUGH

$b_1 = 2$ cm, $b_2 = 7$ cm

5. ENERGY SMEARING

5. a. $d(E_{EM}(\gamma)) = [a_E / \sqrt{E_{EM}(\gamma)} \oplus b_E] E_{EM}(\gamma)$

$a_E \sim 0.13$
$b_E \sim 0.01$ • GOOD EM

$d(E_{HAD}(\gamma)) = [a_E' / \sqrt{E_{HAD}(\gamma)} \oplus b_E'] E_{HAD}(\gamma)$

$a_E' \sim 0.37$ • $\sqrt{t}$ SCALING

$b_E' \sim 0.02$

5. b. IF INTERACTION IS IN EM

$d(E_{EM}(h)) \sim [a_E / \sqrt{E_{EM}(h)} \oplus b_E] E_{EM}(h)$

$d(E_{HAD}(h)) \sim [a_H / \sqrt{E_{HAD}(h)} \oplus b_H \oplus b(e/h)] E_{HAD}$

$a_H \sim 0.70$,
$b_H \sim 0.02$, $b(e/h) \sim 0.2 |e/h - 1|$ "CONSTANT TERM" ADDED EXPLICIT

5. c. IF INTERACTION IS IN HAD

$d(E_{HAD}(h)) \sim [a_H / \sqrt{E_{HAD}(h)} \oplus b_H \oplus b(e/h)] E$

"CALOR 89" Pb vs Fe

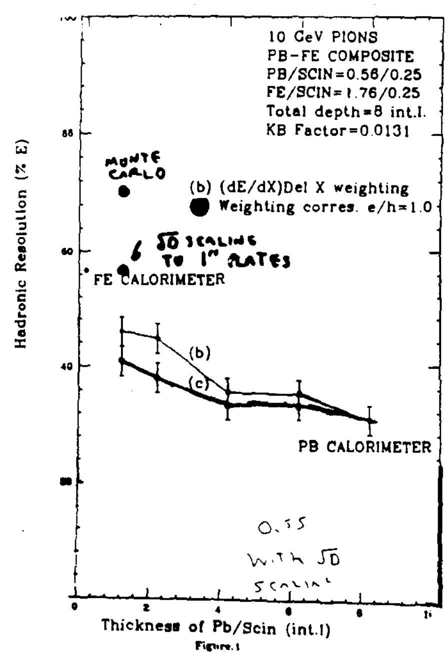

Figure 1

e/h FOR HOMOGENEOUS CALORIMETERS

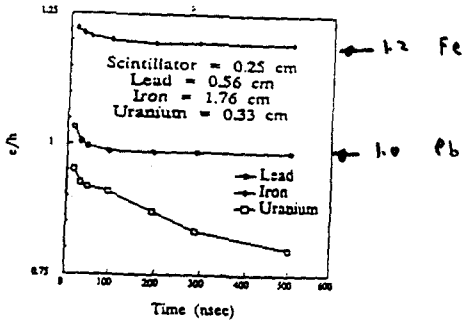

Figure 5. e/h for lead, iron and uranium calorimeters with nominal compensating geometries as a function of signal integration time.

"CONSTANT TERM" AND e/h

b(e/h)

$\pm 0.2 \left| e/h - 1 \right|$

WIGMANS ~0.23

GROOM ~0.14

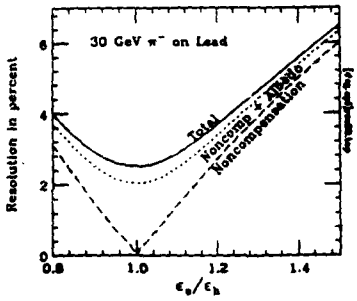

FIG. 4. Contributions to the resolution at 30 GeV as a function of the degree of noncompensation.

$E(h) = [f_0 - (1-f_0)h/e]E$

$\frac{dE(h)}{E} = df_0 |1 - h/e|$

$df_0 \propto f_0/\langle n_{\pi^0} \rangle$

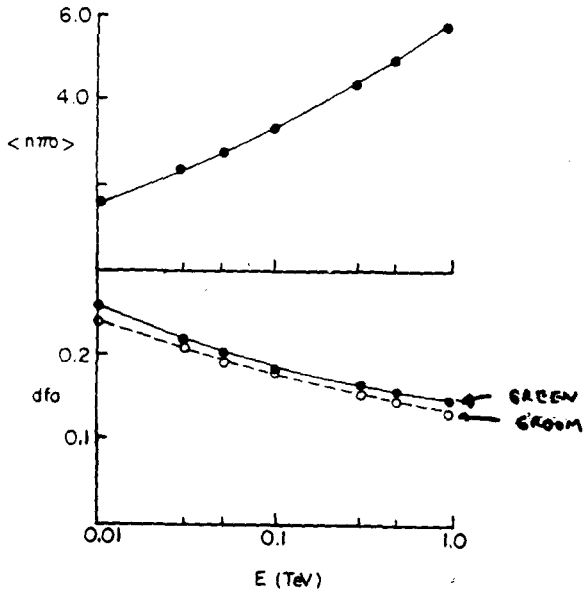

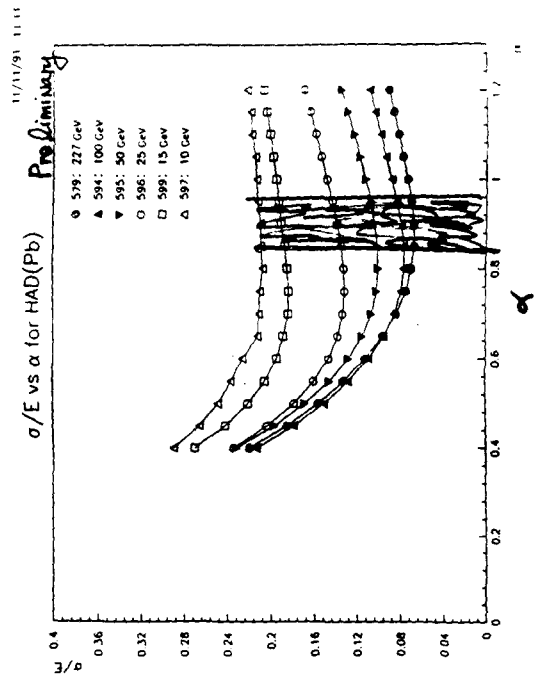

$E = E(EM) + \alpha_{HAD} E(HAD)$

$\alpha_{HAD} \propto \alpha \cdot w(\frac{dE}{d\alpha})$

$w(\frac{dE}{d\alpha})_{Pb} = 7.1$

$w(\frac{dE}{d\alpha})_{Fe} = 6.46$

for 1" sampling

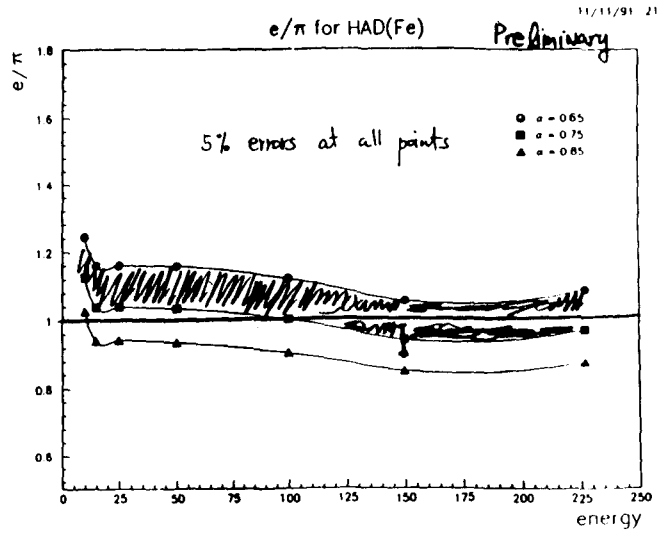

0394

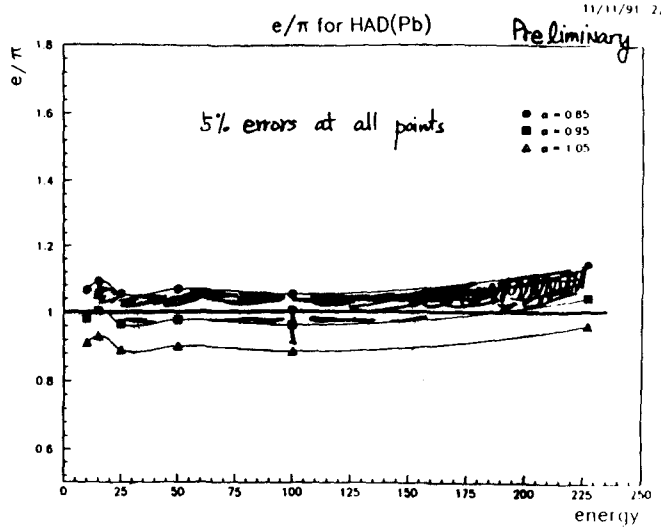

0392

α 70/SE 0.02 0 0.2 e/h = 1.3 - 3 |

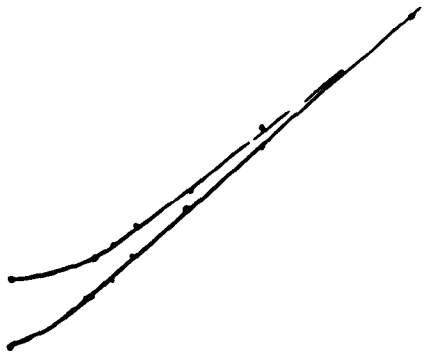

0395

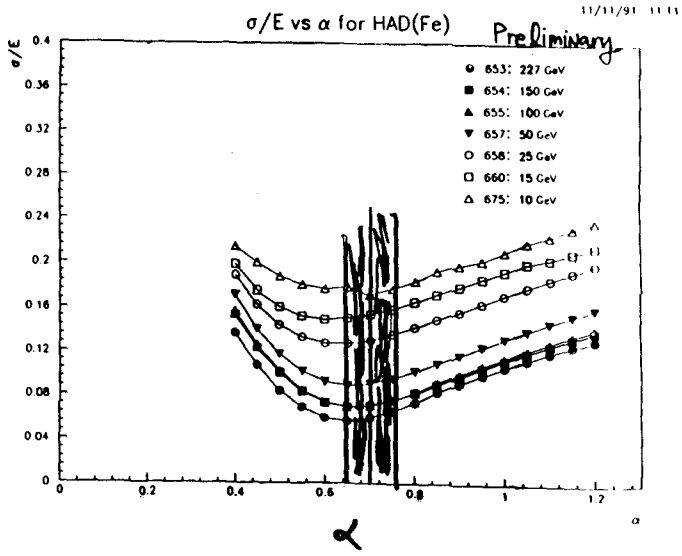

α

0393

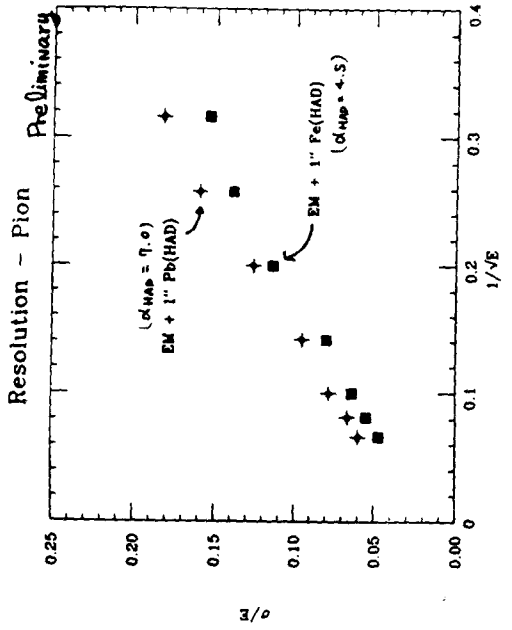

EM = (1/8" Pb + 3mm Scint.) * 40

G. CALIBRATION:

Ga π/e : FOR e/h = 1.3 :

$(\pi/e) = [1 - 0.12/E^{0.15}]$, $\frac{\pi}{e} \approx 0.77$

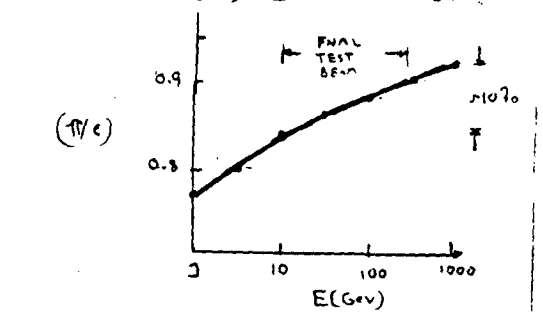

Gb. ONE HAS ROUGHLY ONLY THE RELATIVE HAD/EM TO ADJUST (ENERGY INDEPENDENT)

$E_{HAD}(h) = E_{HAD}(h)/\langle\pi/e\rangle$

$\langle\pi/e\rangle \sim 0.88$

"LoI" MONTE CARLO

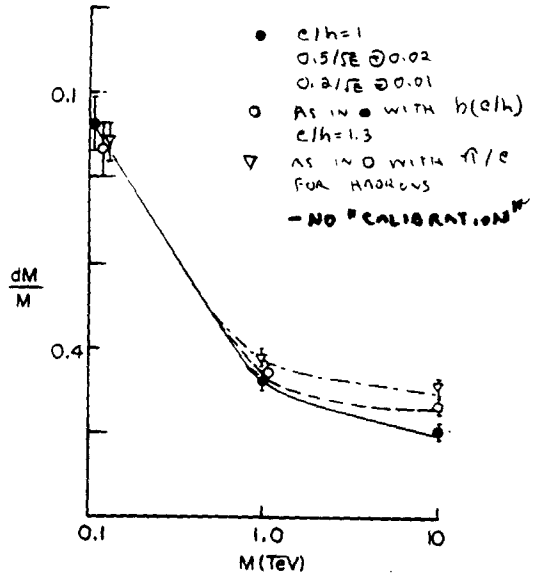

PRESENT WORK

RESOLUTION

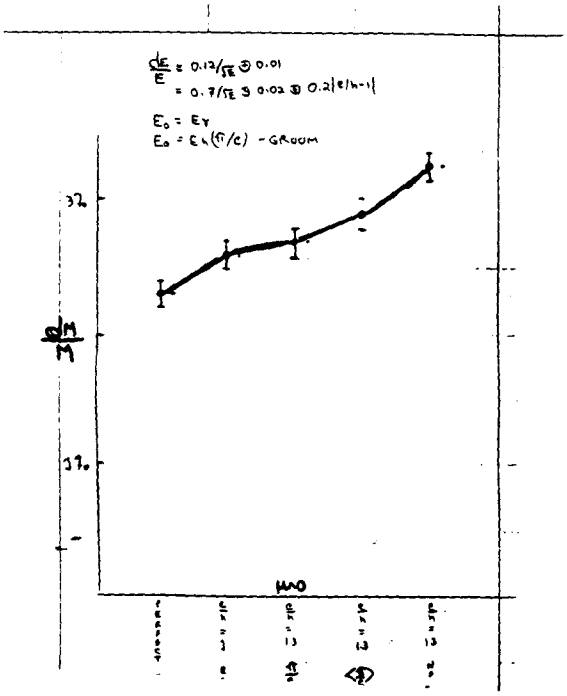

0400

PRESENT WORK

LINEARITY

BEST M_{JJ} RESOLUTION IS ONLY 9% OF M

M_{REC}/M_{GEN}

1.0

0.9

0.8

0401

PRESENT WORK - PERFECT CALORIMETER

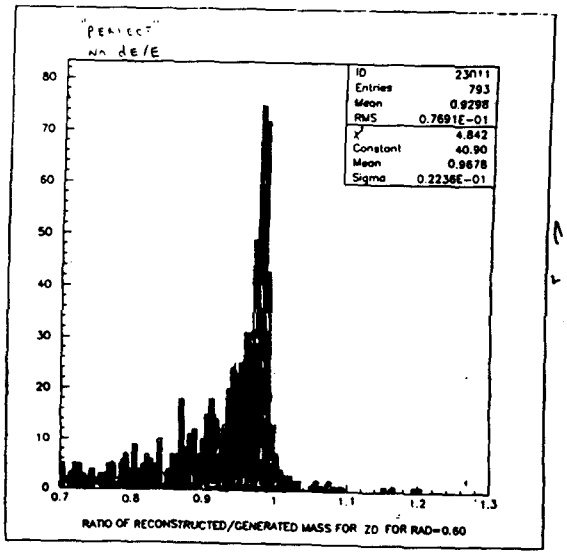

0402

$\frac{dE}{E} \neq 0$

$e/h = 1$

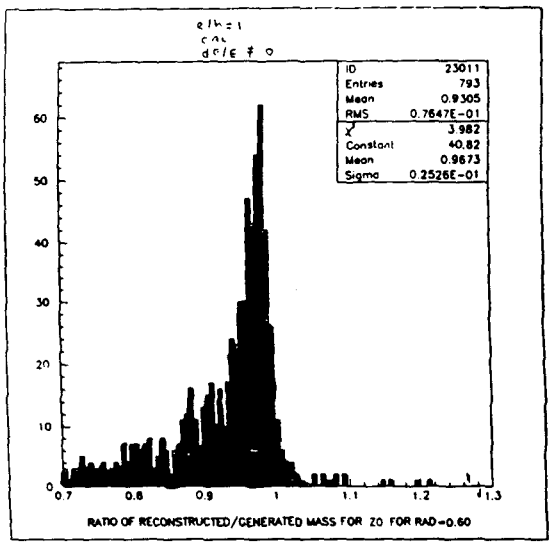

0403 $\frac{dE}{E} \neq 0$

$e/h \neq 1$

NO CALIBRAT

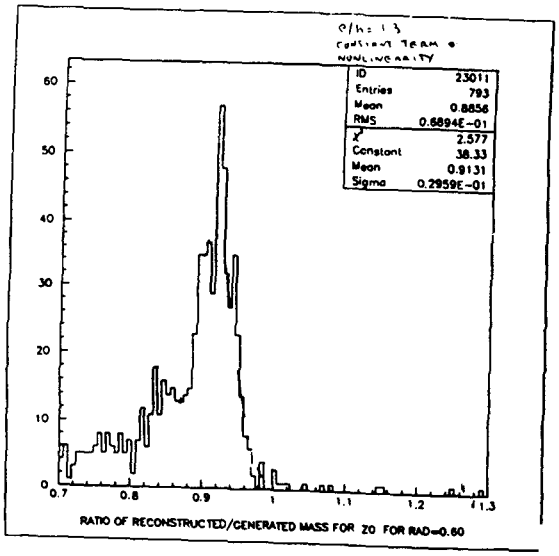

ESTIMATED SIZE OF EFFECT FOR $e/h \neq 1$

a. $E_{meas}(h)/E_0 \sim \left[f_0 + \left(\frac{h}{e}\right)(1-f_0)\right]$ ⇒ RESOLUTION AND NONLINEARITY

$$\frac{dE_{meas}(h)}{E_0} \sim df_0\,|1-h/e| = 0.2\,|1-h/e|$$

$$\sim \frac{f_0}{\langle n_{ch}\rangle}\,|1-h/e|$$

$$\pi/e \sim [f_0 + (1-f_0)\,h/e]$$

$$\sim [1-(1-h/e)(1-f_0)]$$, FOR SEVERAL GENERATIONS

$$= [1-|1-h/e|(E_1/E)^{0.13}]$$, $f_0(E_1) \xrightarrow[E\to\infty]{} 1$

$$\to 1\,|_{E\to\infty}$$ - NOT A CONSTANT

b. $P_J = P_1 + P_2 + P_3 + \cdots$, ERROR PROPAGATION

$M \sim 2P$, $dM/M \sim dP/\sqrt{2}P$

$dP/P = a/\sqrt{P} \oplus b$

$$dP_J/P_J = \sqrt{\textstyle\sum_i [a^2 z_i/P_J + b^2 z_i^2]}$$, $P_i = z_i P_J$

$$dM/M = a/M \oplus \sqrt{\textstyle\sum_i b^2 z_i^2/2}$$

$$\sim a/M \oplus b z_3/\sqrt{2}$$

• $dM/M \sim a/M \oplus b z_3/\sqrt{2} \oplus 0.2|e/h-1|z_3/\sqrt{2}$

SINGLE

ERROR PROPAGATION

$$\sum_J D(z)$$, $D(z) \sim 7(1-z)^5/z$

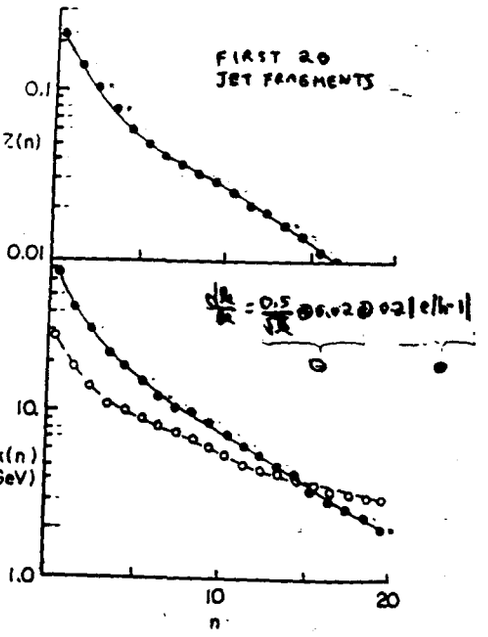

• FOR 10 TeV DOMINANT ERROR DUE TO CALOR IS LEADING FRAGMENT CONSTANT TERM

b. $a = 0.7$, $b = 0.02$, $e/h = 1.3$

$\left(\frac{dM}{M}\right)_{FRAG} \cong 2.3\%$, STERMAN-WEINBERG CALCULATION OF SOFT g BREAM

$e/h = 1 \Rightarrow \left(\frac{dM}{M}\right)_{RES} = 0.007 \oplus 0.003$ ($z_1 \sim 0.2$)

$= 0.0076$

$\left(\frac{dM}{M}\right) = 0.024$

$e/h = 1.3 \Rightarrow \left(\frac{dM}{M}\right)_{e/h} = 0.2(.3)(.2)(.709)$

$= 0.0085$

$\left(\frac{dM}{M}\right) = 0.0255$

"OBSERVE" IN MONTE CARLO : $\left(\frac{dM}{M}\right)_{FRAG} = 2.3\%$

⊕ CAL ABS ± 12% ⇒ 2.6%

⊕ $e/h \neq 1$ CONSTANT TERM ± 1% ⇒ 2.8%

⊕ NONLINEARITY ⇒ 3.2%

$\pi/e = 1.65$?

CLOSE TO CALCULABLE

e/h SIMULATION

1. $q \to J$ SO J RESOLUTION IS THE RELEVANT QUESTION

2. JETS ARE HARD TO DEFINE ACCURATELY
   FRAG - OUT OF CONE, BREAM
   γ - LOST
   UNDERLYING LEADING INTO CONE

3. GO TO HIGHEST M AVAILABLE (LOI, 2, ?' , $e/h < 1.3$ IS OK)

4. PUT IN "CONSTANT TERM" AND NONLINEARITY EXPLICITLY (WORSE THAN HF DATA)

5. CORRECT WITH J ENERGY INDEPENDENT NUMBER OR USE HAC TOWER TO ESTIMATE

6. MY CONCLUSION
   DESIGN TO COST
   J NOT DEGRADED BY Fe
   PUT YOUR $ INTO EM WHERE IT MAY DO SOME GOOD - E.G. $H \to \gamma\gamma$

Single Particle and Jet Response of Several Calorimeter Models

C. Hearty(LBL)

Single-Particle and Jet Response of Several Calorimeter Models

Christopher Hearty
LBL

SDC Collaboration Meeting, SSCL
Nov. 14, 1991

CALOR89 Data

For each calorimeter model, Tom Handler has generated electron and pion showers at six energies: 1, 3, 10, 30, 100 and 300 GeV.

100 showers of each type at each energy.

- Integration time = 16ns
- Birk's constant = 0.0132

(e/pi depends on these and on absorber/scint ratio and on calorimeter thickness)

These data are used to derive single particle responses of various cases.

	Barrel	Endcap	Barrel	Endcap
	10 cm Al, 4 mm scint	—	10 cm Al, 4 mm scint	
EM	36 layers {1/4" pb, 4 mm scint.	18 layers {1/4" pb, 4 mm scint, 4 cm Fe end cap	(same as model A)	(same as model A)
HAD1	32 layers {1" Fe, 2.5 mm scint	21 layers {2" Fe, 2.5 mm scint	24 layers {21 mm pb, 2.5 mm scint	24 layers {31.5 mm pb, 2.5 mm scint
HAD2	12 layers {2" Fe, 2.5 mm scint	7 layers {4" Fe, 2.5 mm scint	18 layers (same as model A)	10 layers, (same as model A)
	4.1	11.2	9.0	11.1

For each configuration, both π^- and e^- showers of energy
1, 3, 10, 30, 100, 300 GeV
100 showers each case

Each shower should be characterized by "ADC counts" in each cell of EM, HAD1 and HAD2

+ homogeneous model B
≡ 81 layers of 21mm pb + 2.5mm scint.

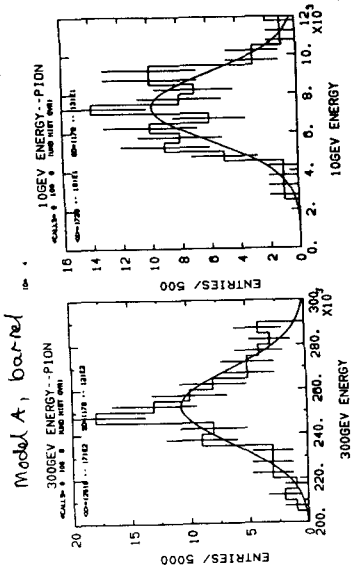

Model A, barrel

within the statistics of 100 events, π^- response appears Gaussian

Single Particle Response

Goal is to find a set of weights for each case:

$E_{meas} = W_{mg}E_{mg} + W_{EM}E_{em} + W_{h1}E_{h1} + W_{h2}E_{h2}$

where Ei is the energy deposited in the scintillator in that section.

The weights are independent of particle type and energy.

Linearity and resolution depend on the weights.

Method Used to find Weights

- goal is achieve linearity, rather than best possible single particle resolution (linearity ==> better jet resolution).
- MG and EM weights selected to give best e- linearity ≥10 GeV
- ratio W_{h2}/W_{h1} selected to give best resolution for 300 GeV pions. (i.e., make Hac2 look like Hac1).
- two different values found for W_{h1}:
  - fit measured e/π for E≥ 10 GeV to extract e/h and Wh1 (use Groom's formula for e/π vs E).
  - Select W_{h1} to give $e/\pi=1$ at 300 GeV (using all pions)

Test Case: Homogeneous Model B

Divide 81 layers into 3 sections:

EM, HAC1, HAC2

Code gives weights (e/h method):

89.2 91.5 92.4 (expect same value for all sections)

- e/h = 1.08
- $\sigma_E/E = (0.37 \pm 0.01)/\sqrt{E}$ (e-)

  $= (0.65 \pm 0.02)/\sqrt{E}$ (π-)

(no constant term)

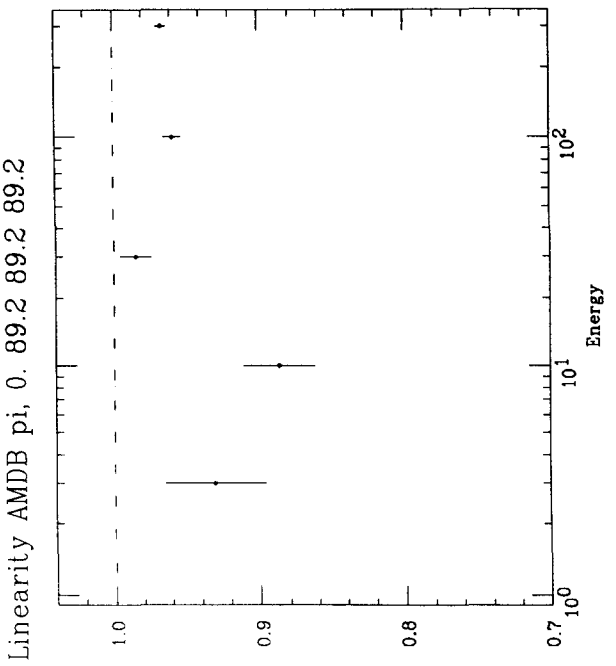

0417

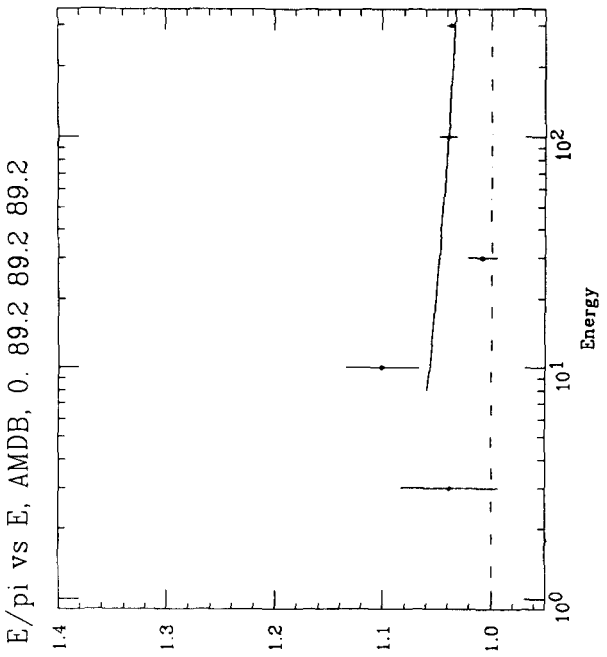

0418

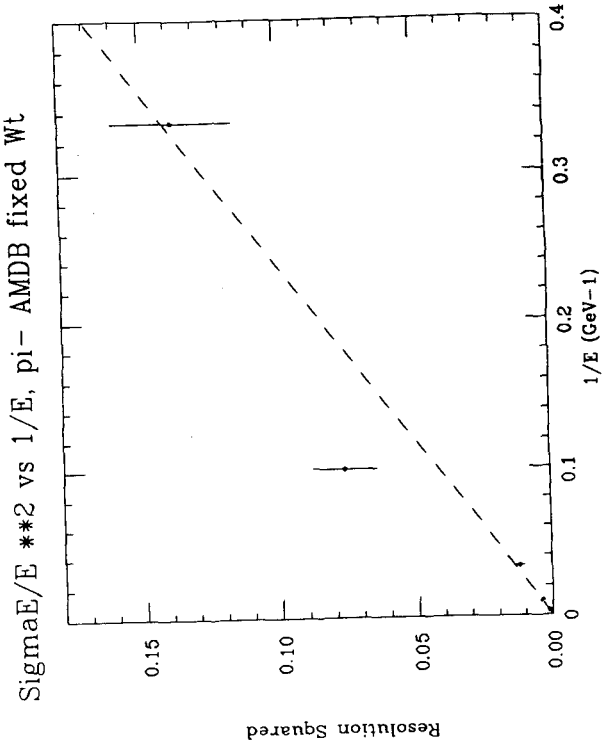

0419

Nonhomogeneous Model B

- e/h weighting gives hac1 weight = 90.6
  - very close to correct (homogeneous case) value.
  - e/h = 1.17
- $\sigma_{e}/E = (0.55\pm0.03)/\sqrt{E} \oplus (0.042\pm0.005)$ (pions)

==> EM section results in lower stochastic term but induces a constant term.

(calibration at 300 GeV gives slightly worse π- resolution).

0420

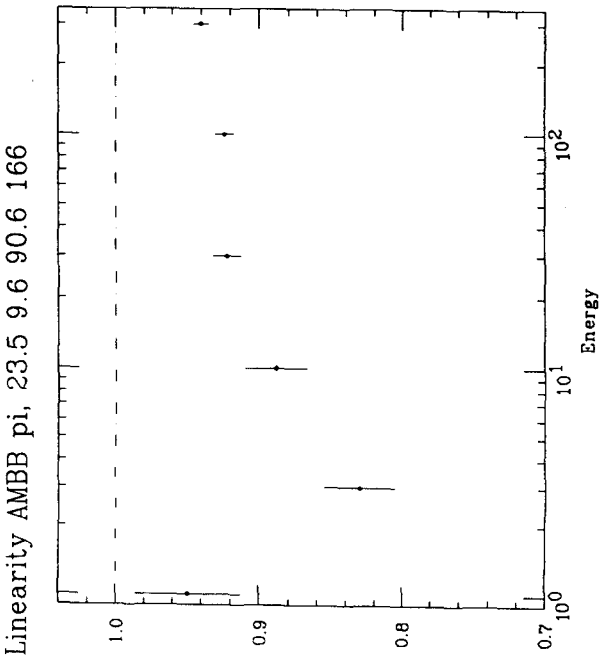

Linearity AMBBy pi, 25.3 9.59 98.1 179

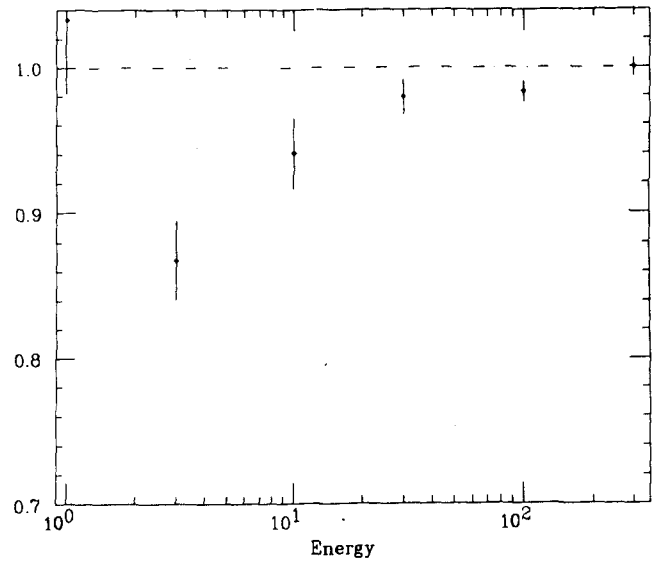

0423

E/pi vs E, AMBB, 23.5 9.6 90.6 166

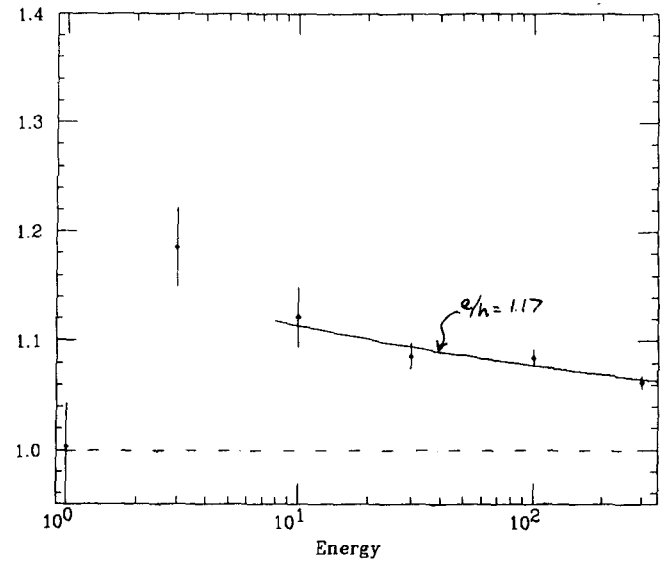

0421

E/pi vs E, AMBBy, 22.3 9.59 98.1 179

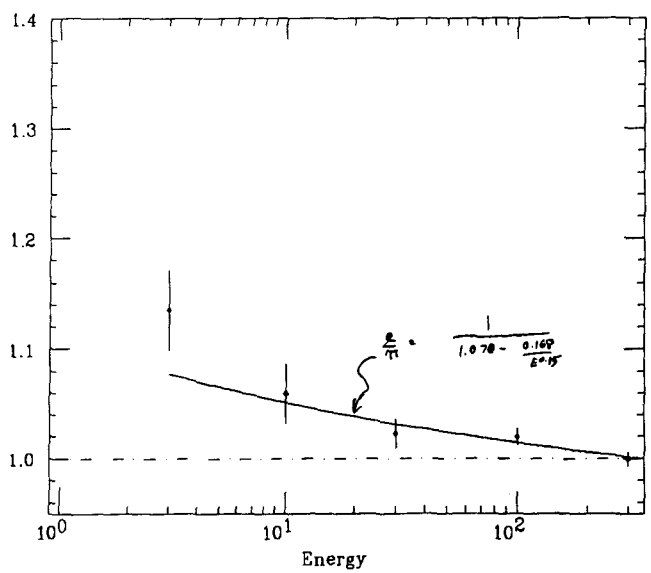

0424

SigmaE/E **2 vs 1/E, pi, AMBB

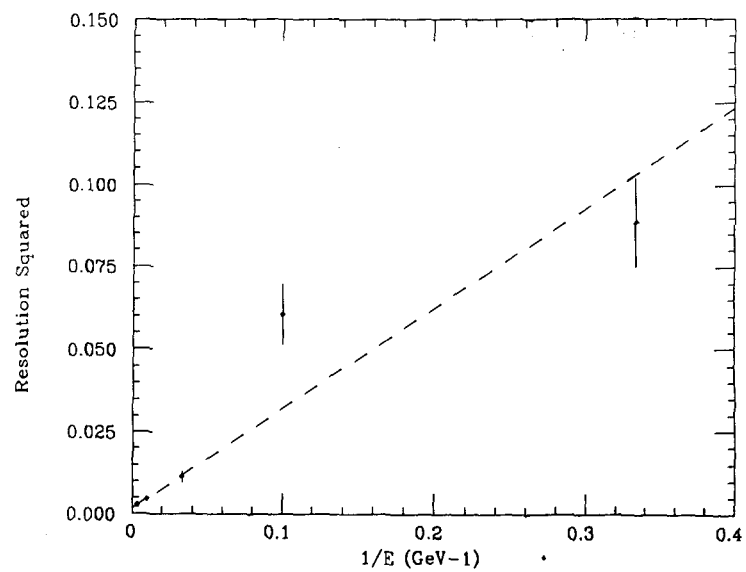

0422

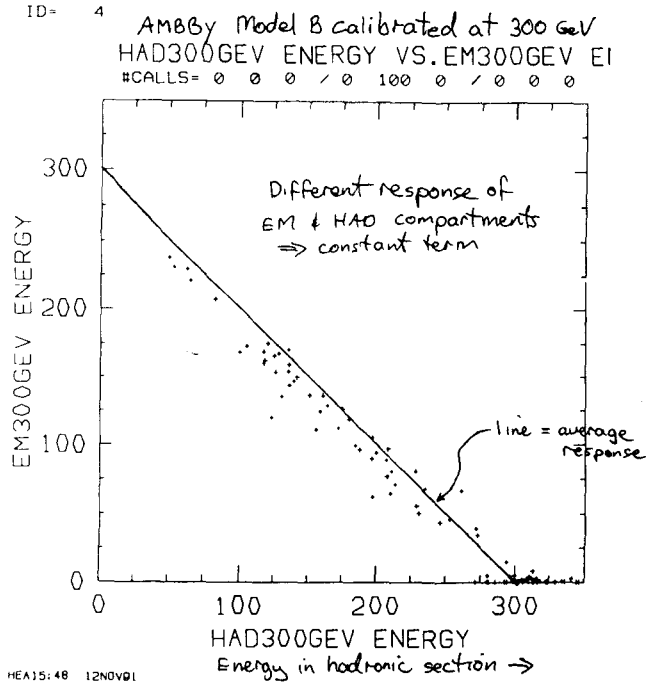

0427

ambby

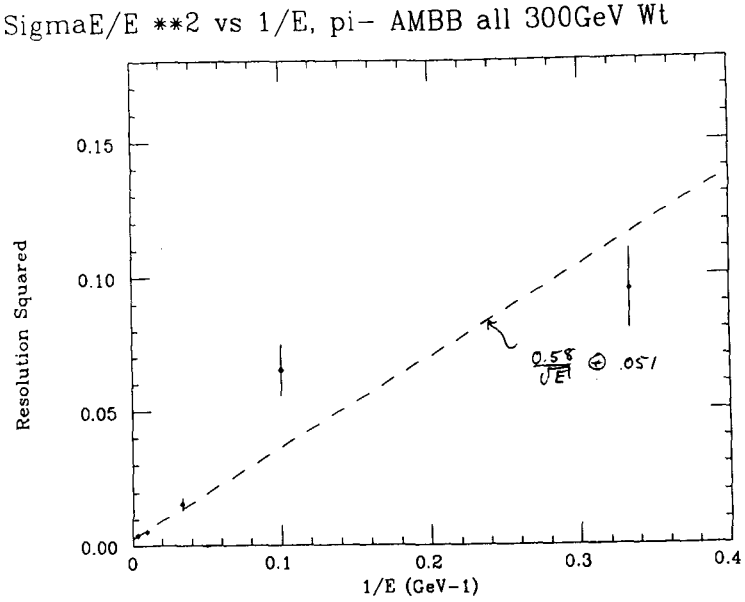

0425

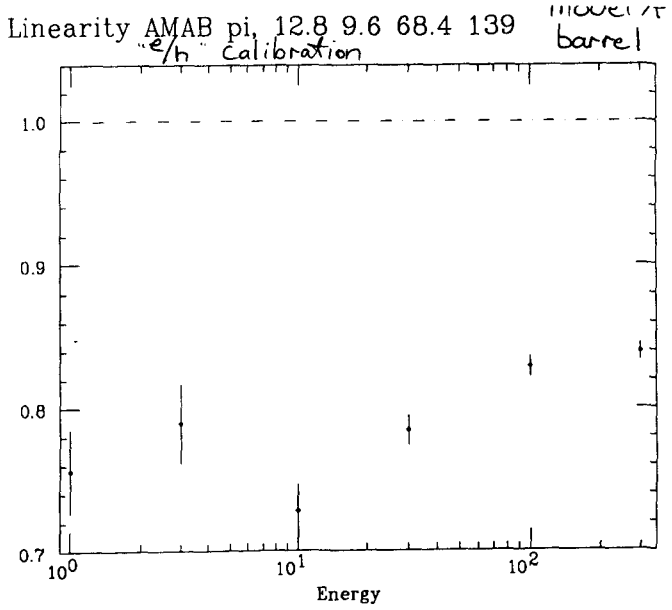

0428

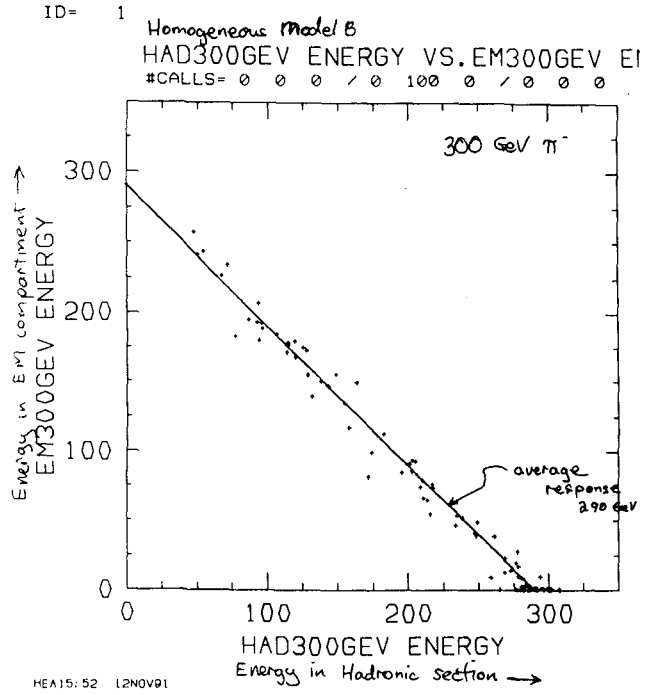

0426

homogeneous

Linearity AMABy pi, 23.2 9.52 86.7 170 Model A barrel
Calibrate at 300 GeV

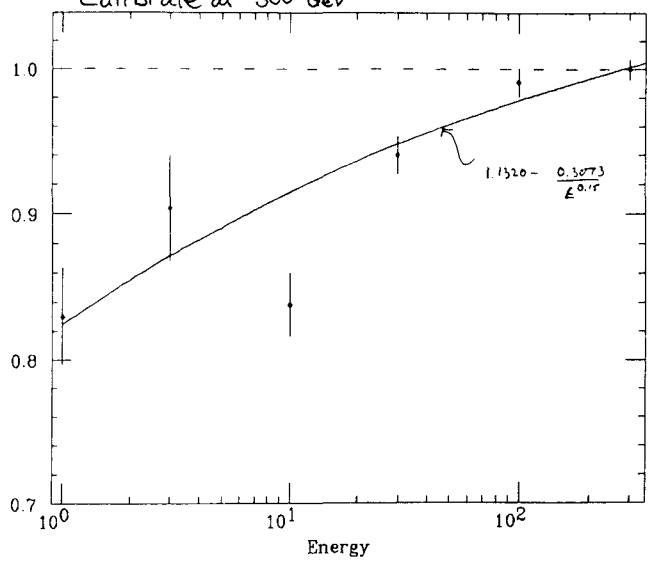

0431

E/pi vs E, AMAB, 12.8 9.6 68.4 139
"e/h" calibration

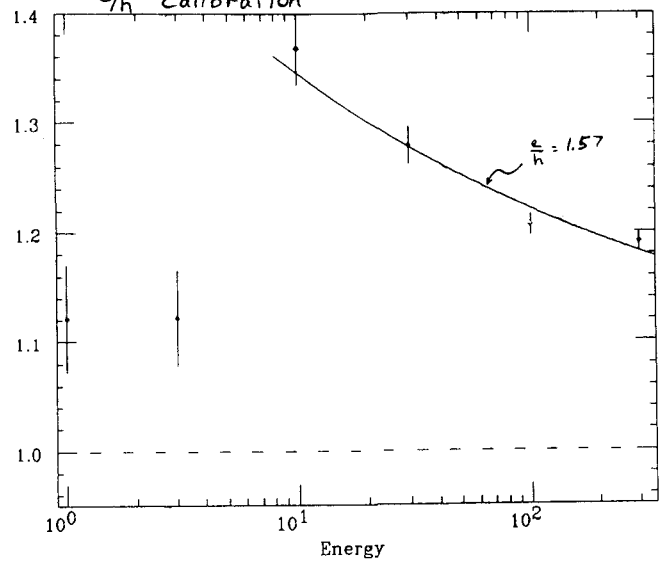

0429

E/pi vs E, AMABy, 23.2 9.52 86.7 170

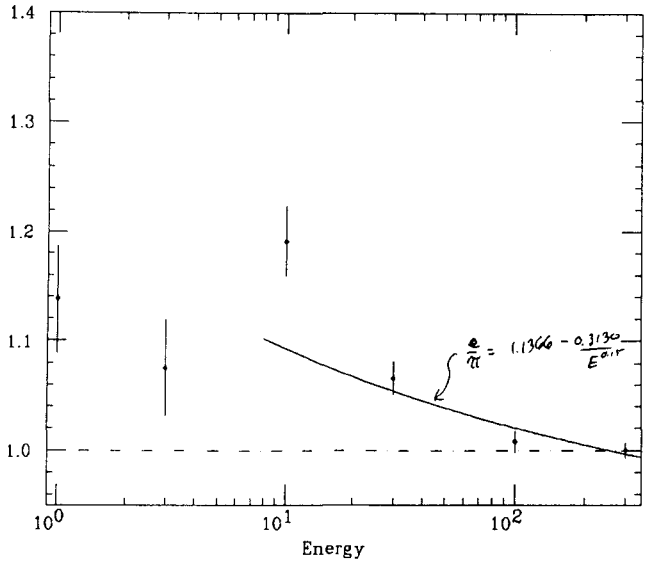

0432

SigmaE/E **2 vs 1/E, pi−, AMAB

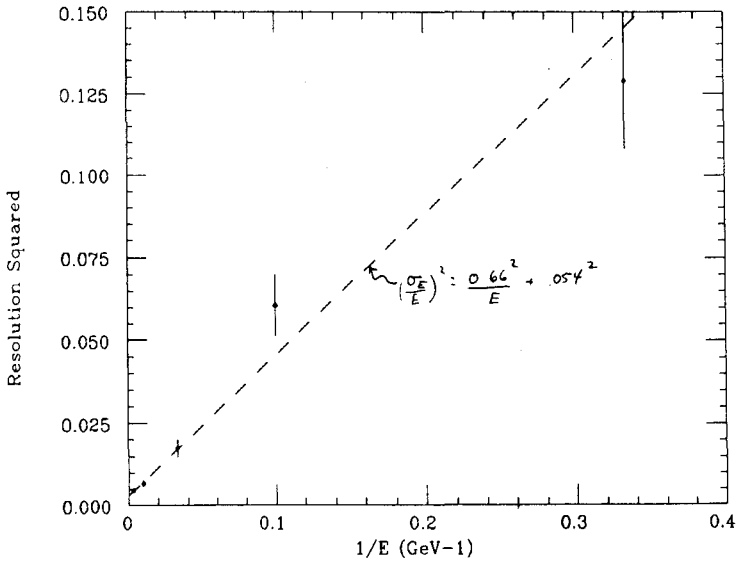

0430

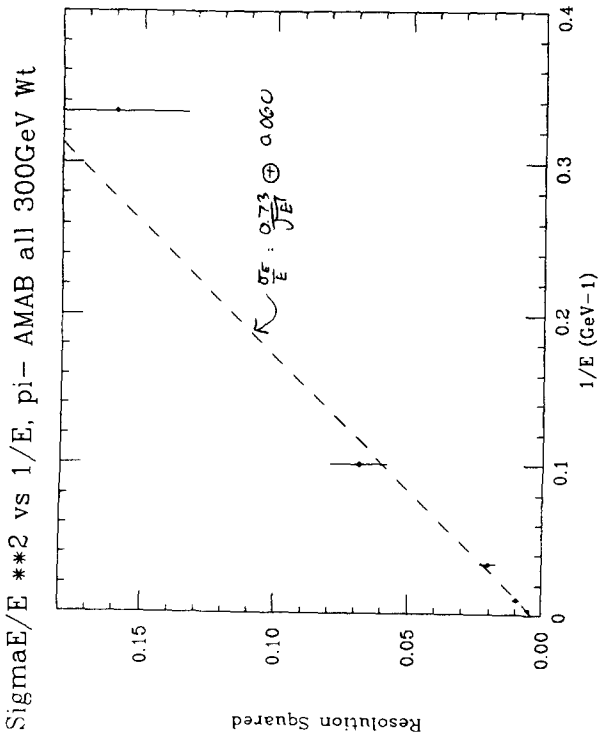

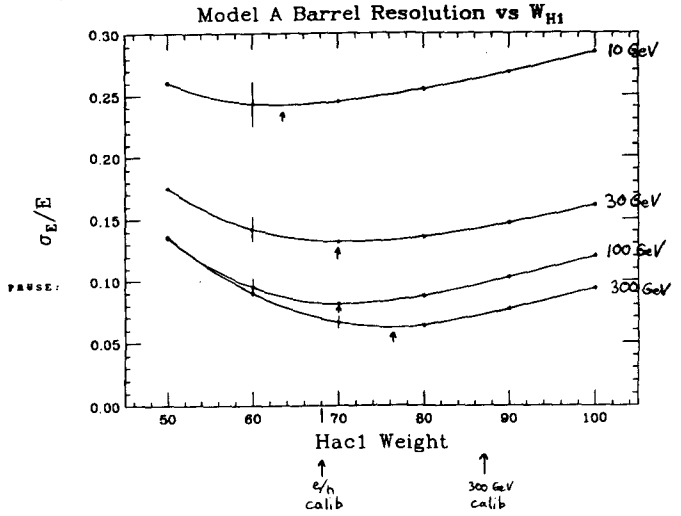

Summary of Single Particle Response

case	e/h	<---------σE/E----------> e/h calib		300 GeV calib	
A Barrel	1.57	0.66	0.054	0.73	0.060
B Barrel	1.17	0.55	0.042	0.58	0.051
B Homo.	1.08	0.65	0.000	–	–
A Endcap	1.47	0.83	0.051	0.83	0.074
B Endcap	1.12	0.79	0.049	0.80	0.052

Barrel e- resolution 0.115/√E + 0.003

Summary of linearity & resolution, e^- & π^-, various cases:

case	linearity (e^-)	resolution (e^-)	π^-
amb, e/h	(1) .92 .94 .96 .97 .98 .985 .99 .99 .995 .995 100 (12)	.145/√E ⊕ .0052; .15 @ 1 GeV	electron divided by e/h=1.57, E≥10; 0.75 E ≤ 10
amb; all 300 GeV/c (amaby)	same	same	
amb; e/h norm	(1) .95 .97 .985 .99 .99 .99 .995 .995 200 GeV .995 100 (12)	same	E≥3 GeV; 1.0 1 GeV; 0.9 2 GeV
amae; e/h	(1) .99, .99 1.00	.147/√E ⊕ .0095; .17 @ 1 GeV	e/h = 1.466 E≥3; 1.0 1 GeV 0.85; 2 GeV 0.79
ambe; e/h	1.00	.081/√E ⊕ .009; .17 @ 1 GeV	e/h = 1.118, E≥3; 1 GeV 1.0; 2 GeV 0.97
ambby: with 300 GeV	(as ambb)	(as ambb)	1 GeV 1.03; 2 GeV .95
amaeby: with 300 GeV	(as amae)	(amae)	1 GeV 0.91; 2 GeV 0.87
ambeby: with 300 GeV	ambe	ambe	

Jet Response

Single particle response (E_{meas}/E_{true}, sigma_E/E) parameterized as a function of energy.

- Isajet twojet events, various Et ranges, |eta|<1.2 for barrel studies.

- fixed cone (R=0.7) cluster algorithm. Seed = highest Et track in jet. Iterate to find stable centroid. (Perfect resolution for everything but neutrinos and muons).

- same cone used for all calorimeter cases.

Calorimeter response to a jet is the sum of the responses to the single particles in the cone:

$$E^{jet}_{t\,meas} = \sin\theta_c \cdot \sum_{i\ in\ cone} E^i_{meas} \quad ; \text{ sum over non-}\nu,\mu$$

$$E^i_{t\,meas} = E^i_{t\,true} \cdot \left[\left\langle \frac{e_{meas}}{e_{true}} \right\rangle + X\left(\frac{\sigma_{E_t}}{E_t}\right)\right] \quad ; X = \text{Gaussian rand num}$$

$$E^{jet}_{t\,true} = \sin\theta_c \cdot \sum_{i\ in\ cone} E^i_{true} \quad ; \text{ (non-}\nu,\mu)$$

Cases Studied -- Barrel

In addition to models A and B calibrated via e/h or at 300 GeV, simulate other cases for comparison:

- linear model B:
  $\sigma e/E = 0.57/\sqrt{E} \oplus 0.042$ (π-)

- good resolution:
  $\sigma e/E = 0.40/\sqrt{E} \oplus 0.030$ (π-)

- very good resolution:
  $\sigma e/E = 0.40/\sqrt{E}$ (π-)

All of these have e- resolution of $0.115/\sqrt{E}$ and have < Et-meas/Et-true> = 1.

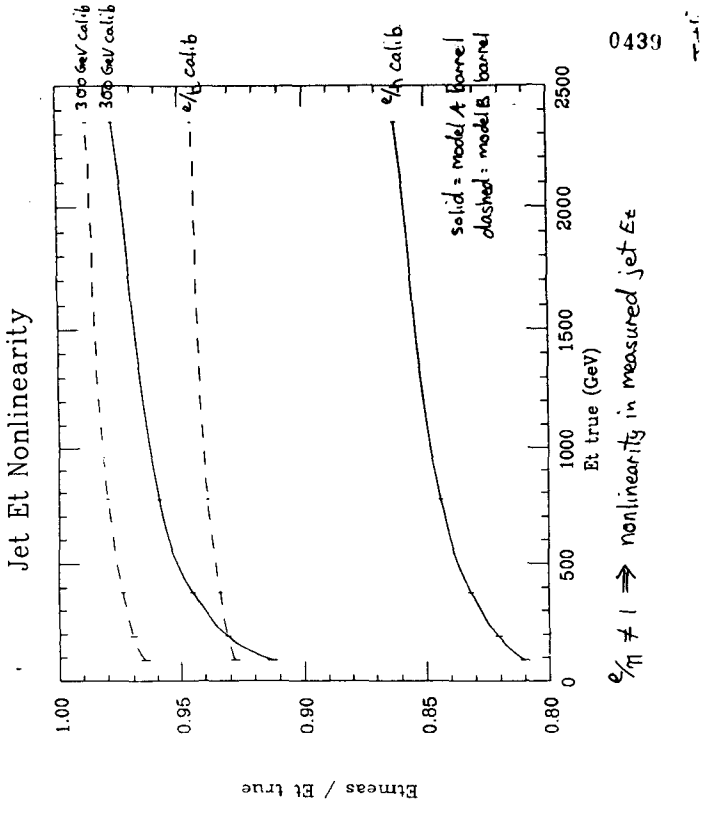

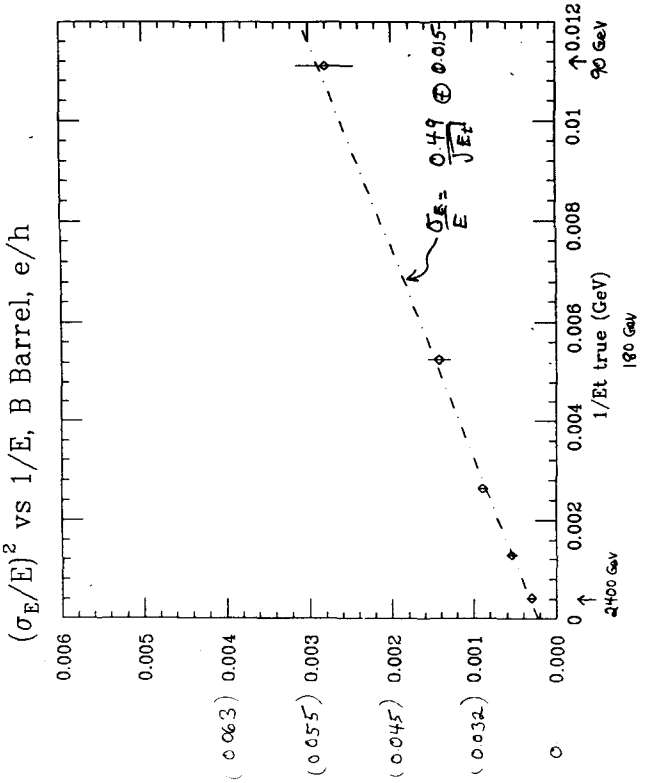

$(\sigma_E/E)^2$ vs 1/E, A Barrel, e/h

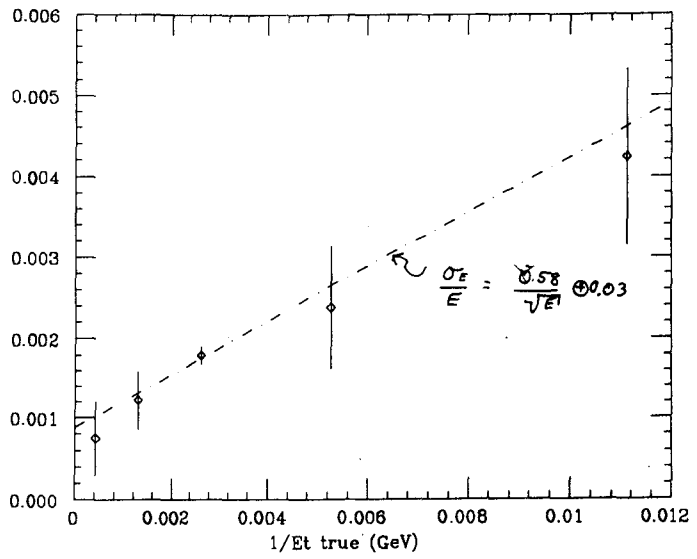

0443

$(\sigma_E/E)^2$ vs 1/E, B Barrel, 300GeV

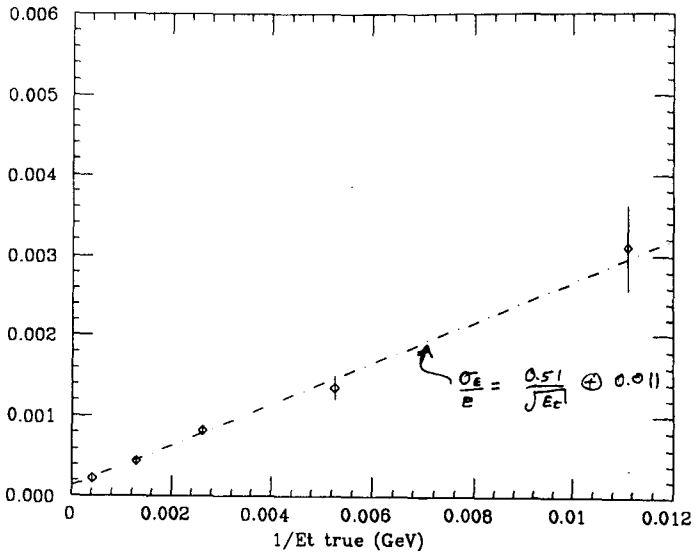

0441

$(\sigma_E/E)^2$ vs 1/E, A Barrel, 300GeV

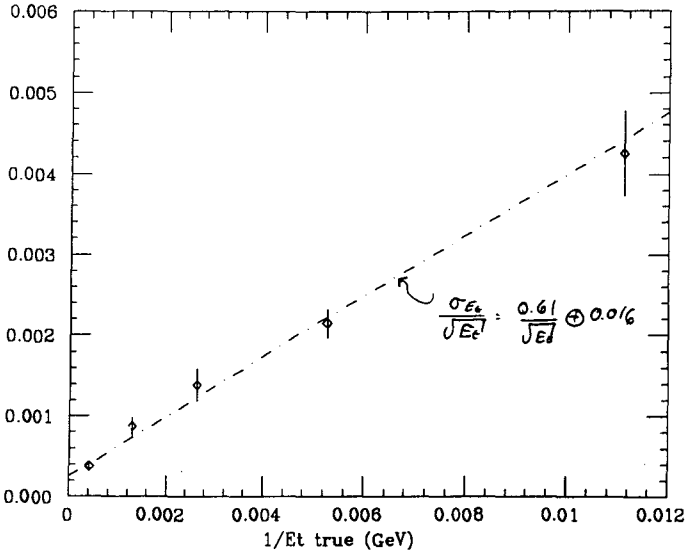

0444

$(\sigma_E/E)^2$ vs 1/E, Linear Model B

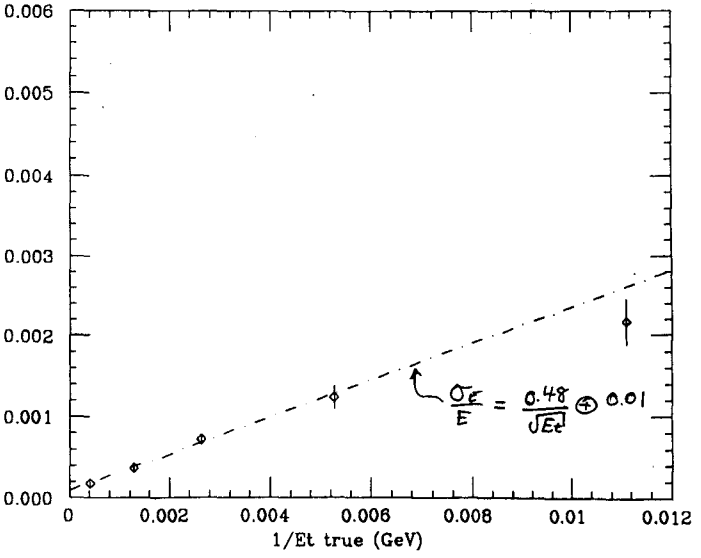

0442

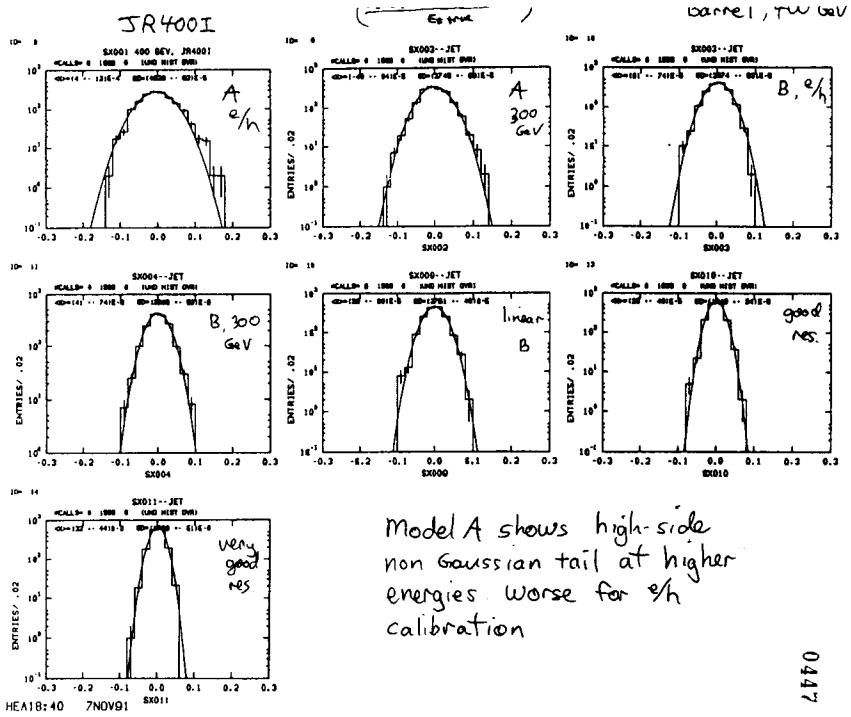

0447

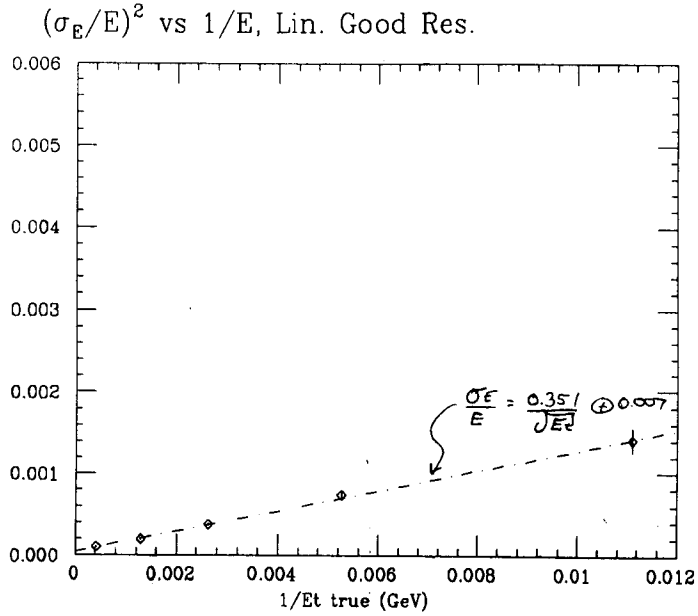

0445

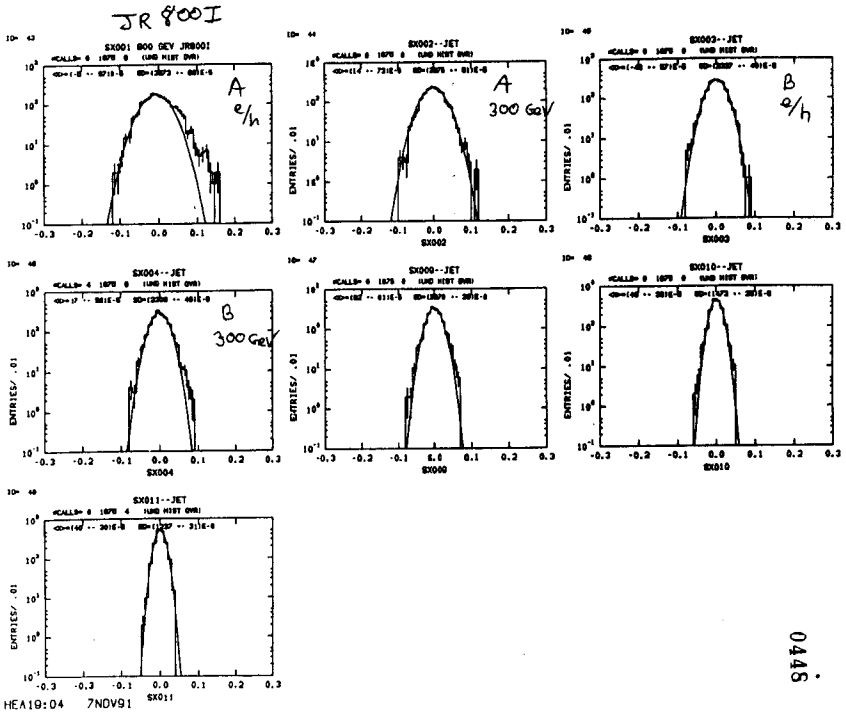

0448

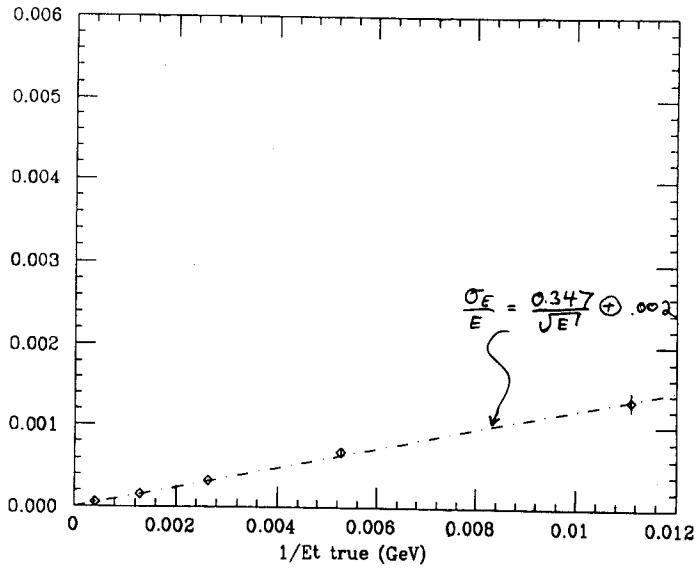

0446

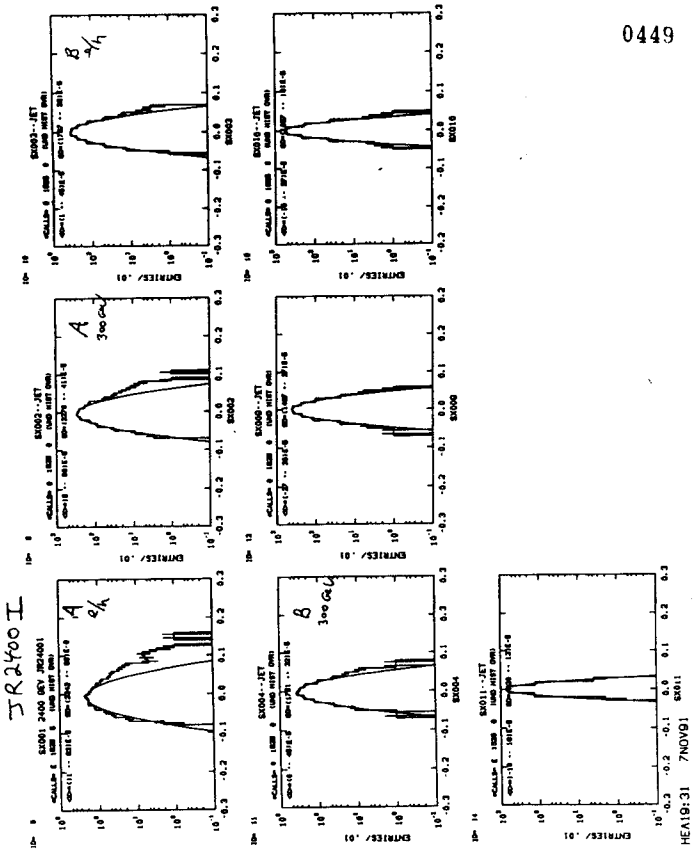

Jet resolutions JRxxxI Barrel

Fit all 5 energies — Resfitx fortran, Res00xA topdraw

case	
model A, barrel, e/h	(0.58 ± 0.08)/√E ⊕ (.030 ± .004)
" " 300 GeV	(0.61 ± 0.02)/√E ⊕ (.016 ± .002)
B " e/h	(0.49 ± 0.02)/√E ⊕ (.015 ± .002)
B " 300 GeV	(0.51 ± 0.02)/√E ⊕ (.011 ± .002)
Tiner B	(0.48 ± .014)/√E ⊕ (0.010 ± 0.001)
good res. $\frac{\sigma_{jet}}{E}$ 0.003; 4% ⊕	(0.357 ± .009)/√E ⊕ (0.007 ± .001)
V. good res (no const.)	(0.347 ± .005)/√E ⊕ (0.002 ± .001)

- constant term (& stochastic term) are better for jets than for pions
- small pion nonlinearity (<10%, E ≥ 10 GeV) ⇒ small increase in constant term (model B, e/h vs linear model B)

larger nonlinearity ⇒ larger const term (model A e/h vs model A, 300 GeV)

Comparison to Actual Jet Et

"Isajet" jet Et = Σ Et ; sum over all particles with correct jet label.

Emeas/Eisajet has long low-side tail from gluon radiation with Gaussian distribution near one from soft fluctuations, underlying event, initial state radiation and neutrinos.

- for compositeness study, compare measured Et to predicted Et ==> these effects matter only to the extent they are not modeled correctly.
- for mass measurements, tail causes loss of events from peak, other fluctuations degrade resolution.

$\frac{E_{t\,true}}{E_{t\,isajet}}$ at E_t = 100 GeV

- $E_{t\,true}$ = E_t in cone, excluding μ, ν, including underlying event
- $E_{t\,isajet}$ = Σ E_t, particles with correct jet label

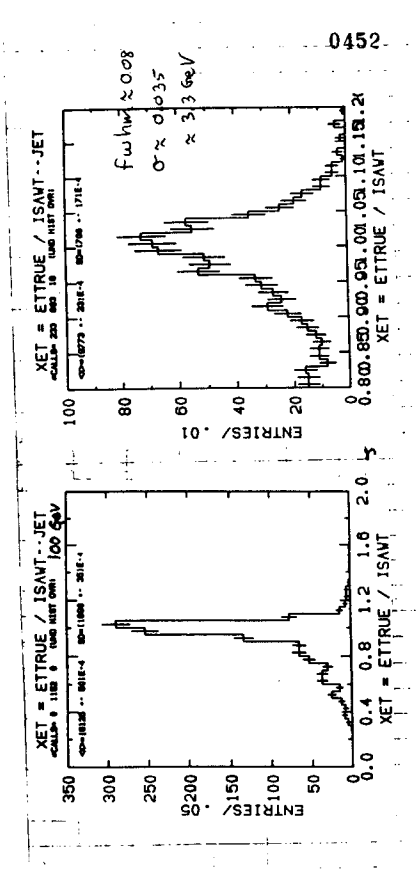

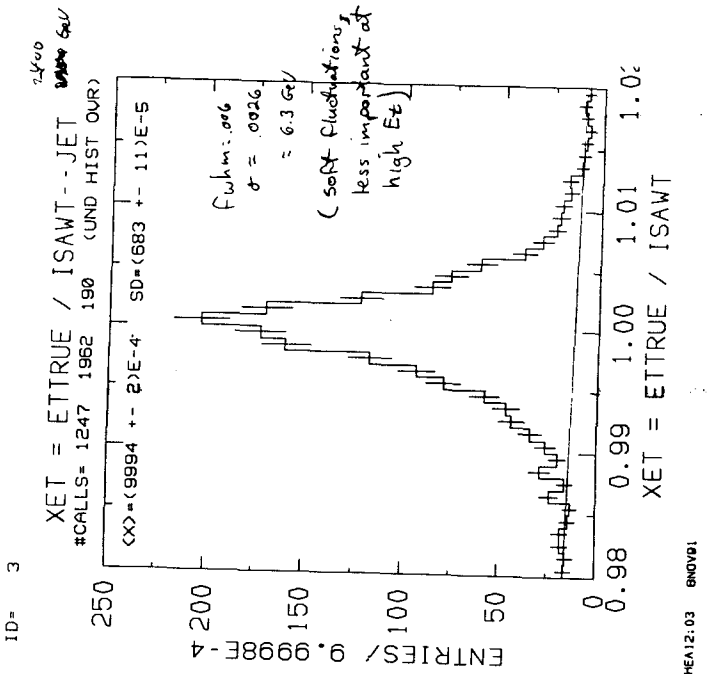

Jet Resolution -- Endcap

- 2.0 < |eta| < 2.5
- single particle resolution flat in Ez across endcap.
- σ_e/E approximately constant, Et≥200 GeV:

  model A: $\sigma_e/E \approx 0.030$
  model B: $\sigma_e/E \approx 0.022$

Interpretation

Understand jet resolution by studying:
- compositeness
- dijet mass resolution (Z')
- H--> jet jet e+e-
- missing-Et

Compositeness

- Linearity (after correction) most important.
  - determine using single particle test beam data + MC jets (need to know fragmentation functions and be able to extrapolate single particle response)
  - use gamma-jet events?

Bigger correction ==> bigger error (?)

- non-Gaussian tails must be small and understood.

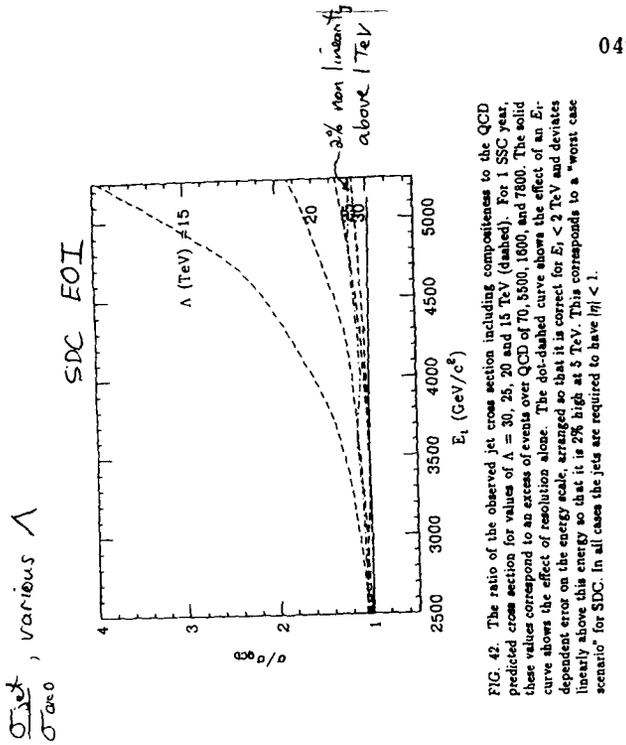

FIG. 42. The ratio of the observed jet cross section including compositeness to the QCD predicted cross section for values of Λ = 30, 25, 20 and 15 TeV (dashed). For 1 SSC year, these values correspond to an excess of events over QCD of 70, 5500, 1600, and 7800. The solid curve shows the effect of resolution alone. The dot-dashed curve shows the effect of an E_t-dependent error on the energy scale, arranged so that it is correct for $E_t < 2$ TeV and deviates linearly above this energy so that it is 2% high at 5 TeV. This corresponds to a "worst case scenario" for SDC. In all cases the jets are required to have $|\eta| < 1$.

Dijet Mass Resolution

- Use Isajet Drell-Yan events to make heavy vector boson of fixed mass.

Mass of two-jet event:

- $\vec{P}$jet = $\sum E_i \hat{n}_i$, cones defined above. (use true particle direction or nearest .05 bin center).
- event mass is the mass of the 4-vector sum of the two jets.
- excludes pileup, combinatorics and leakage.
- includes calorimeter resolution, underlying event, fragmentation fluctuations, gluon radiation and neutrinos.

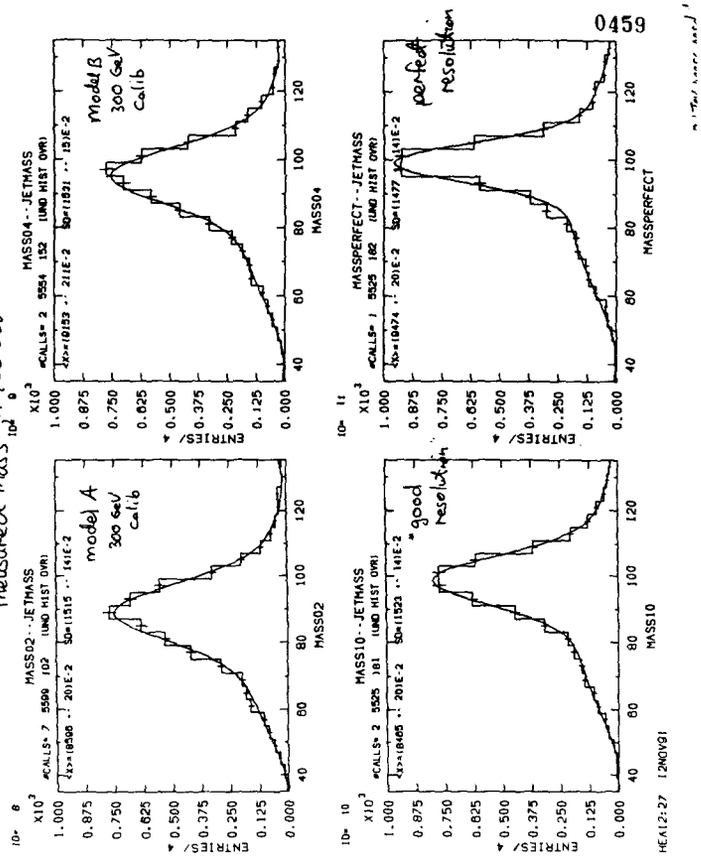

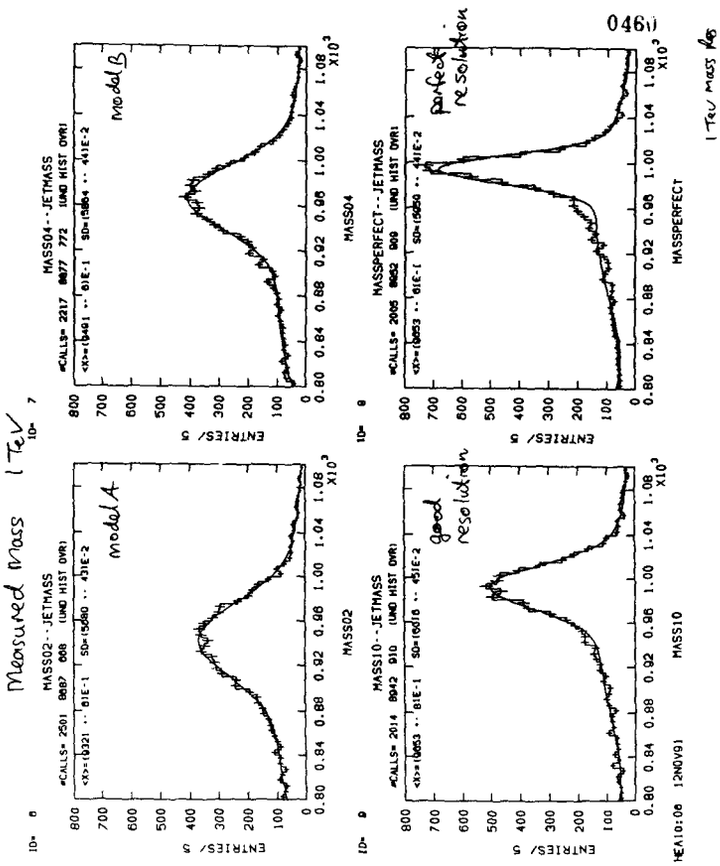

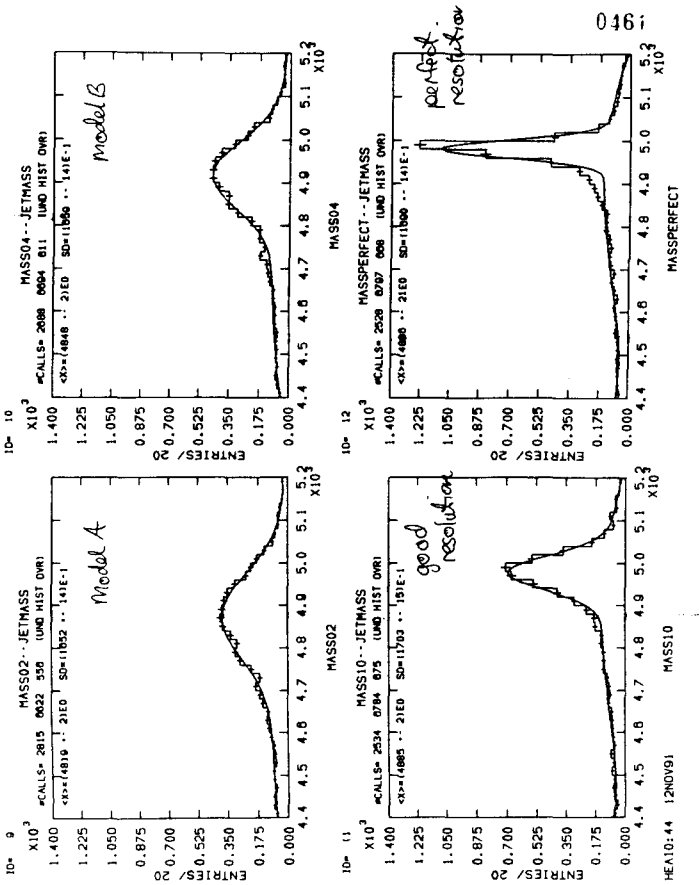

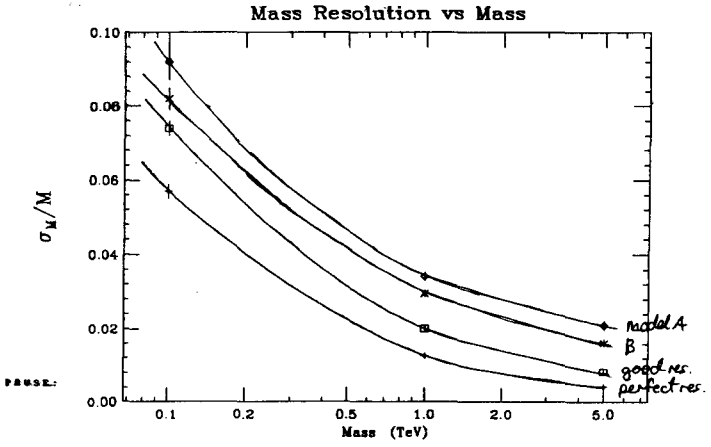

SUMMARY

<u>pion resolution</u>

barrel

model A: (0.66±0.03)/√E ⊕ (0.054±0.005)
model B: (0.55±0.03)/√E ⊕ (0.042±0.005)

endcap

model A: (0.83±0.03)/√E ⊕ (0.051±0.005)
model B: (0.79±0.03)/√E ⊕ (0.049±0.005)

<u>pion linearity (barrel and endcap)</u>

A: < Et-meas/Et-true> ≥ 0.85 - 0.90, E≥10
B: < Et-meas/Et-true> ≥ 0.95, E≥10

<u>Jet Resolution</u>

barrel

model A: (0.61±0.02)/√E ⊕ (0.016±0.002)
model B: (0.51±0.02)/√E ⊕ (0.011±0.002)

endcap

model A: $\sigma_e/E \approx 0.030$
model B: $\sigma_e/E \approx 0.022$

<u>Jet Linearity, barrel</u>

A: < Et-meas/Et-true> ≈ 0.93 - 0.95
B: < Et-meas/Et-true> ≈ 0.97 - 0.99

<u>Mass Resolution at 1 TeV</u>

A: 0.034 ± 0.001
B: 0.030 ± 0.001
good res. 0.020 ± 0.001

Analytic Characterization of a Two Compartment Calorimeter

D. Groom(LBL)

THREE CONCLUSIONS

1. If $\frac{\langle h_1 \rangle}{\langle e_1 \rangle} \neq \frac{\langle h_2 \rangle}{\langle e_2 \rangle}$, there is no systematic and/or correct way to combine R_1 & R_2
   (but we can fool ourselves with average values & Monte Carlos)

2. This is particularly bad for jets, where there are systematic energy determination errors.

3. $\frac{\langle h \rangle}{\langle e_1 \rangle} \approx \frac{\langle h_2 \rangle}{\langle e_2 \rangle}$ is more important than $\frac{\langle h \rangle}{\langle e \rangle} = 1$!

AND ONE OBSERVATION

The "e" part of "e/h" can be decreased by $\gtrsim 10\%$ with 1/16 cladding in Pb/scint system ($\sim 3\%$ in Fe/scint)

Impact of the Hadron Calorimeter Absorber Choice on the Solenoid

R. Kephart((FNAL)

Impact of the hadron calorimeter absorber choice on the solenoid

Many issues to consider:

Physics "Performance" issues

(Field Uniformity) vs (Tracking)	(Calorimeter Performance) vs (absorber material + geometry)	(Muons)
• Pattern recognition • $\Delta p/p$ resolution • Triggering • Tracking volume vs uniformity (cost) • Central field value	• Em hermeticity, resolution • e/h • hadron resolution	• multiple Scattering Fe vs Pb • Phys return geometry
	Discussed by others ⇒	

I will focus on Coil Engineering issues. (Particularly on Iron geometry vs Coil design)

Coil Engineering issues (Fe/Pb + Geometry)

1) Electromagnetic Forces on Coil

a) Compressive force {function of B_r}

b) Radially outward forces {function of B_z}

① Support cylinder stress levels

- Hoop stress $\propto \frac{\beta^2 t}{(2\mu_0)t}$ } Total stress*
- axial stress*

② Conductor stresses

- hoop } Total stress*
- axial*

③ Conductor/support cylinder epoxy joint stress

c) decentering forces

① axial*

② radial* (centering vs decentering magnitude vs cold mass)

What if there is no Iron near the end of the current sheet?

≃ HAC1 = Pb ≃ -A CASE ⇒

- Non-uniform field
- Compressive force on Coil ≈ 1700 T
- small decentering forces <5T/in

magnetic field contour of B_z (weight = Type 1, (r,z/2)=(1.7m,10m).

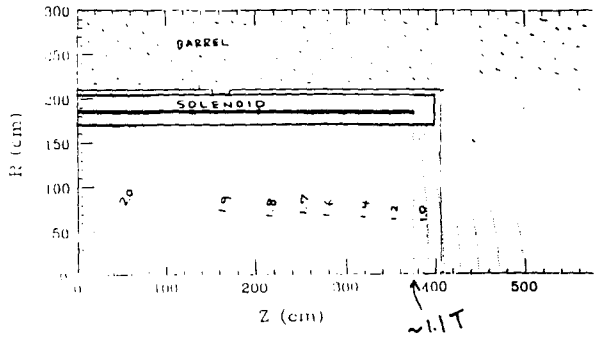

Engineering Issues

1) high conductor stresses (≥ yield of available Al (high RRR)) ← material

2) reliance on conductor/support cylinder epoxy bon ← process

3) must build ~ full diameter prototype coil to evaluate the design. (If problems occur what will we do?) ≡ RISK

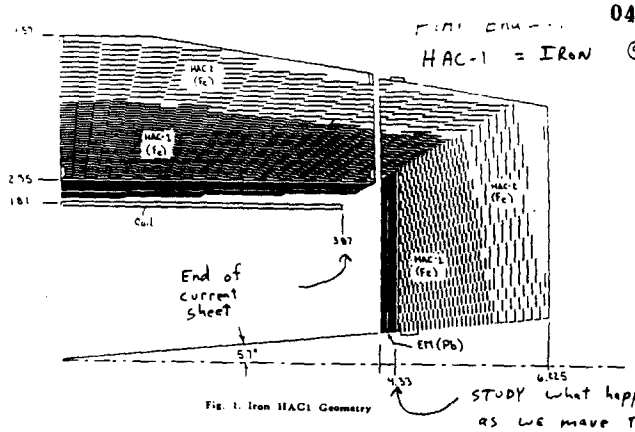

Fig. 1. Iron HAC1 Geometry

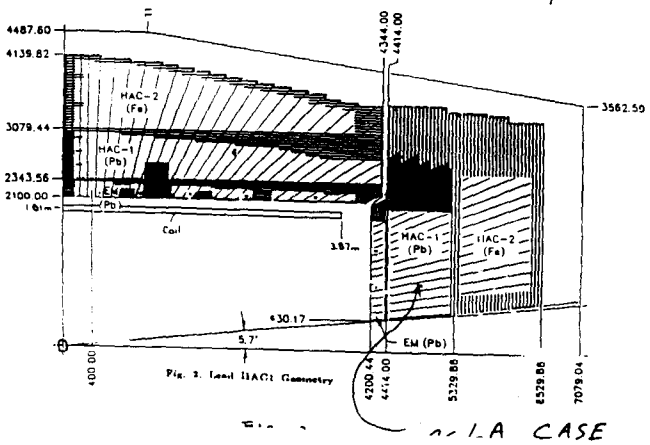

Fig. 2. Iron HAC1 Geometry

ANSYS
Refined Generic Models

Purpose: To study the effect of barrel and endplug proximity on the coil compressive and decentering forces. With 20 cm reentrant endplug, model corresponds to that used by Bill Foster in EGS simulation.

Approach: ANSYS 2-d axisymmetric finite element model, vector potential formulation

Endplug: Modeled as iron/scint, with hac1 and hac2 regions based on Fermilab calorimeter conceptual design. Iron and air modeled as discrete finite elements

Barrel: Modeled as iron/scint, with hac1 and hac2 regions based on Fermilab calorimeter conceptual design. Iron and air modeled as discrete finite elements

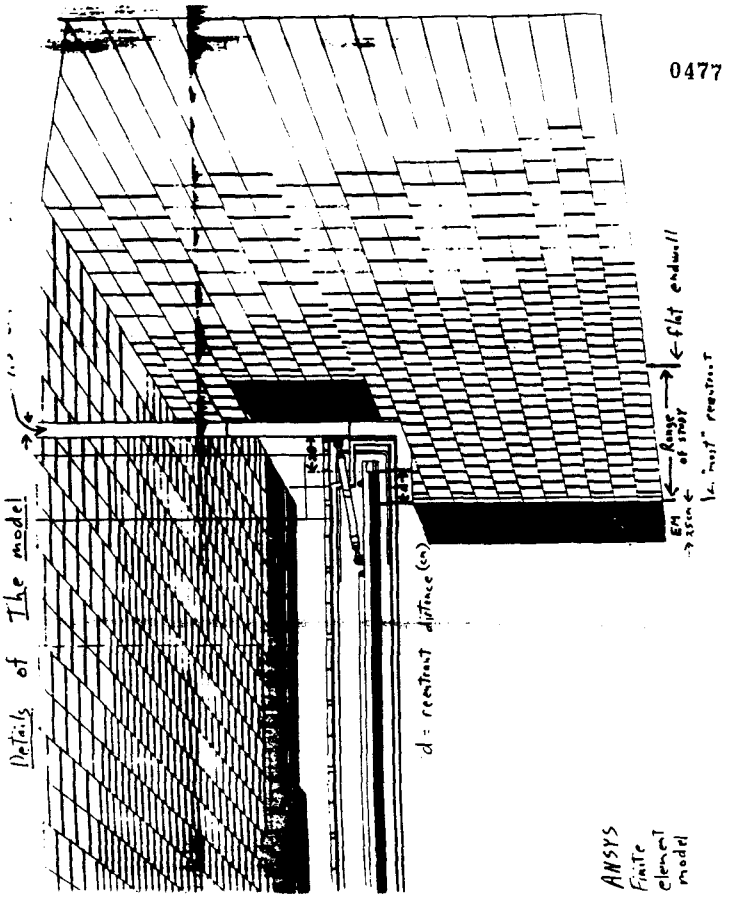

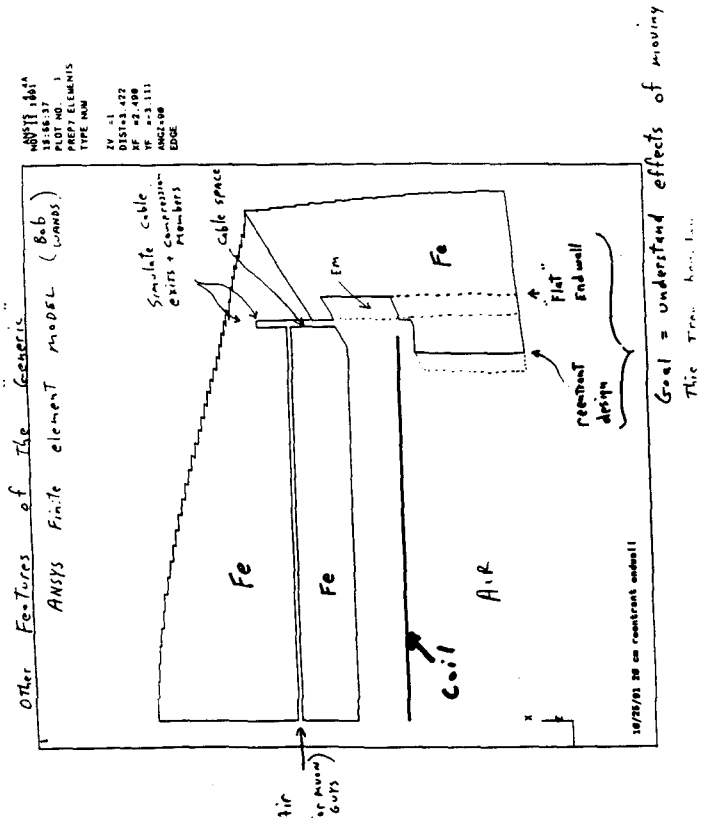

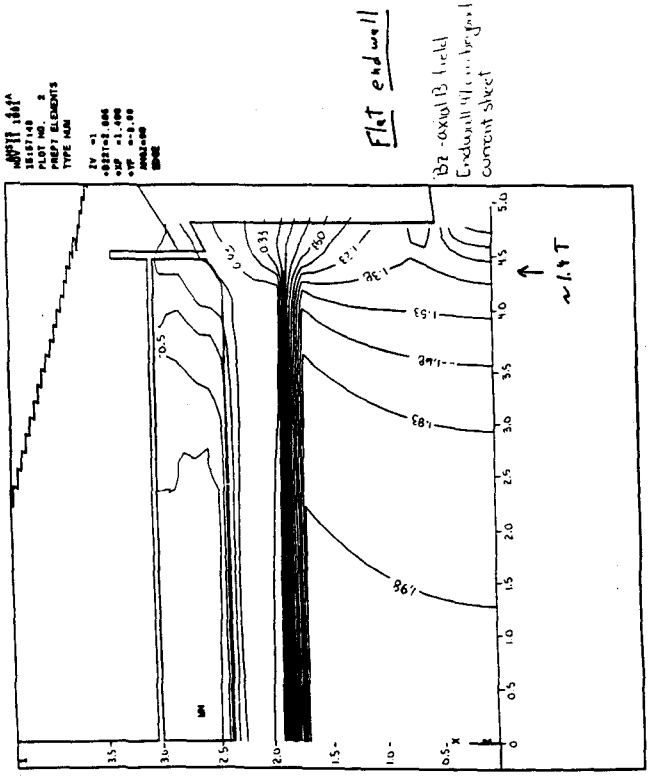

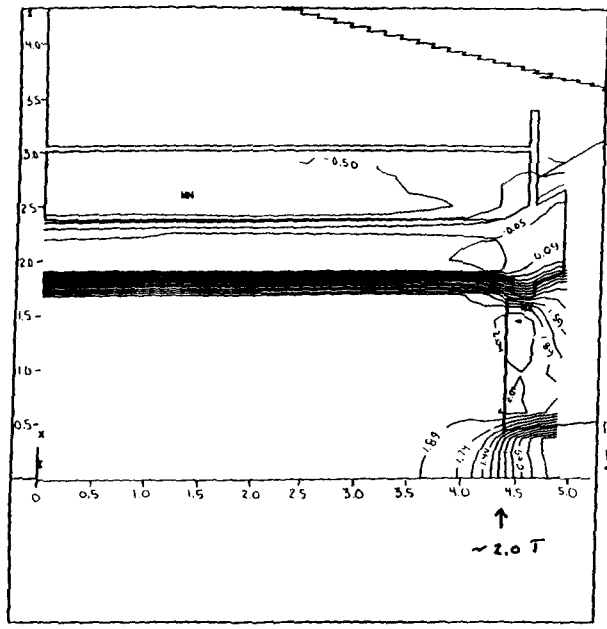

Bz - axial B field
10 cm recessed endwall

0482

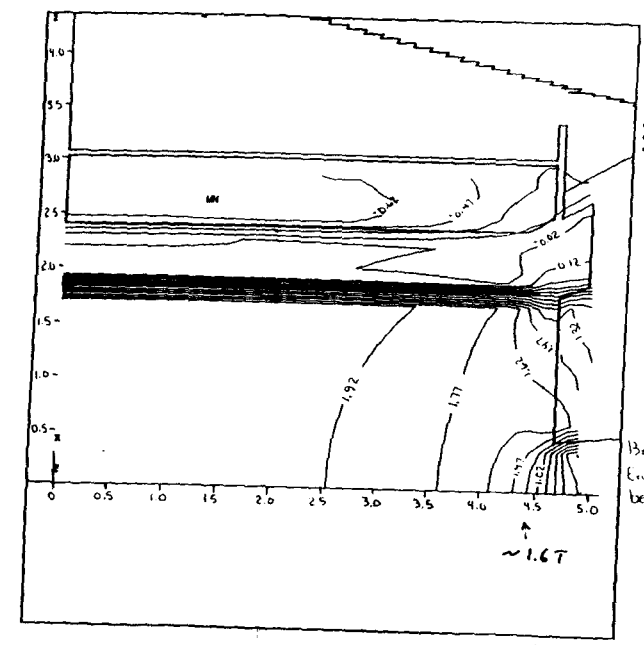

Bz - axial B field
Endwall current
beyond current sheet

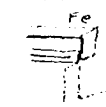

- Flat iron Endwall
- recessed Fe

0480

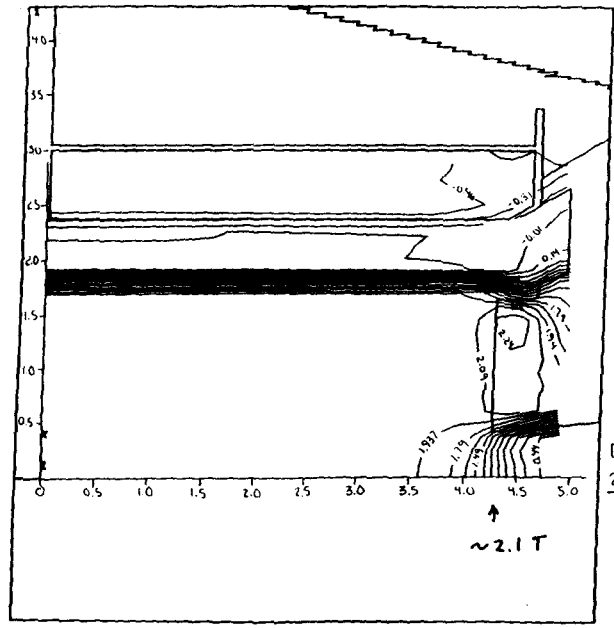

Bz - Axial B field
20 cm recessed endwall
(Too far)

0483

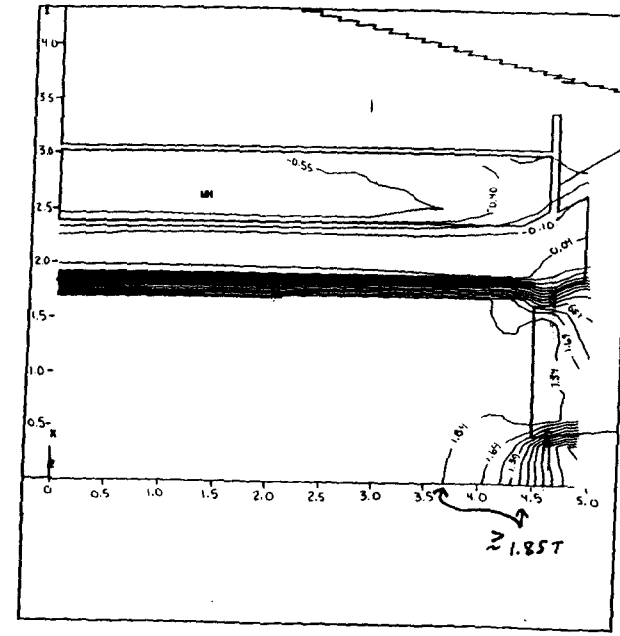

Bz - axial B field
Endwall flush with
current sheet

0481

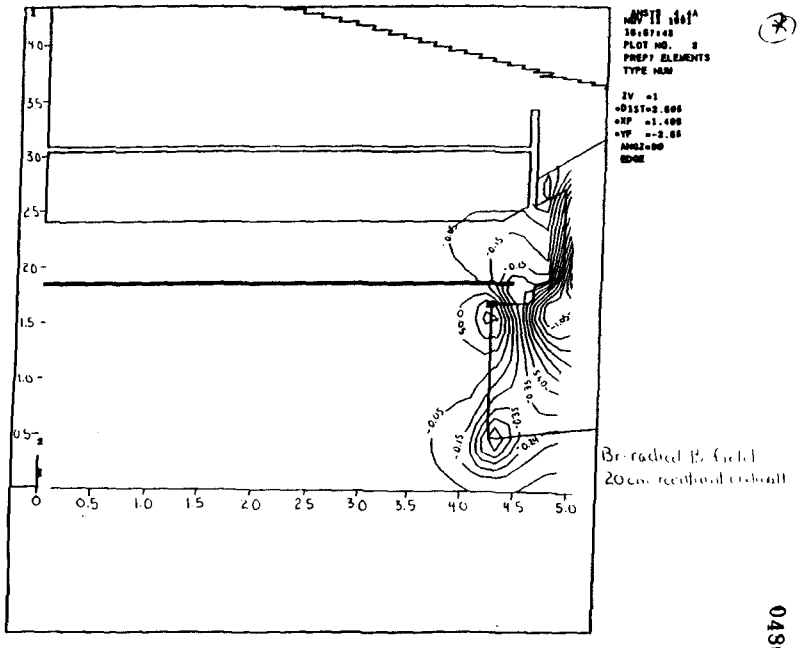

Br radial B field
20 cm reentrant endwall

0486

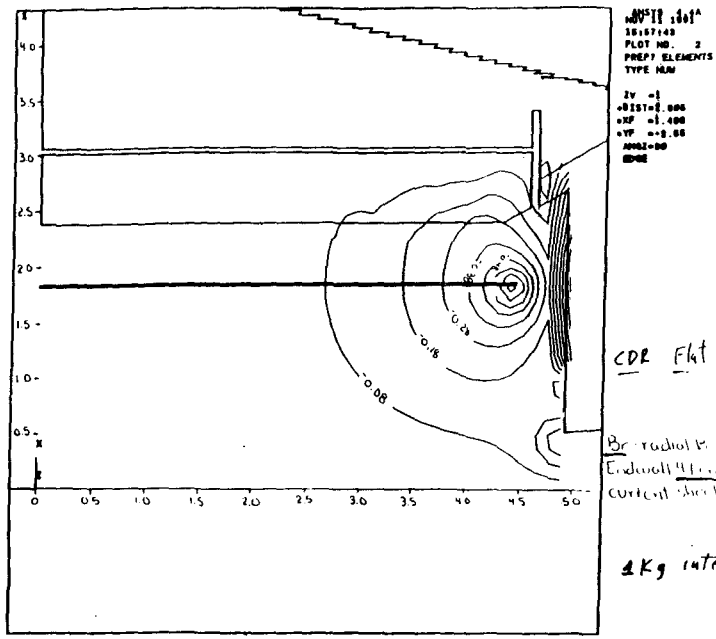

CDR Flat ENDWALL

Br radial B field
Endwall 4 cm tapered
current sheet

1 Kg intervals

0484

So why do I care about Iron location? Answer - forces & stress levels (more on this)

Coil Force vs Central Field

for 20 cm reentrant endwall

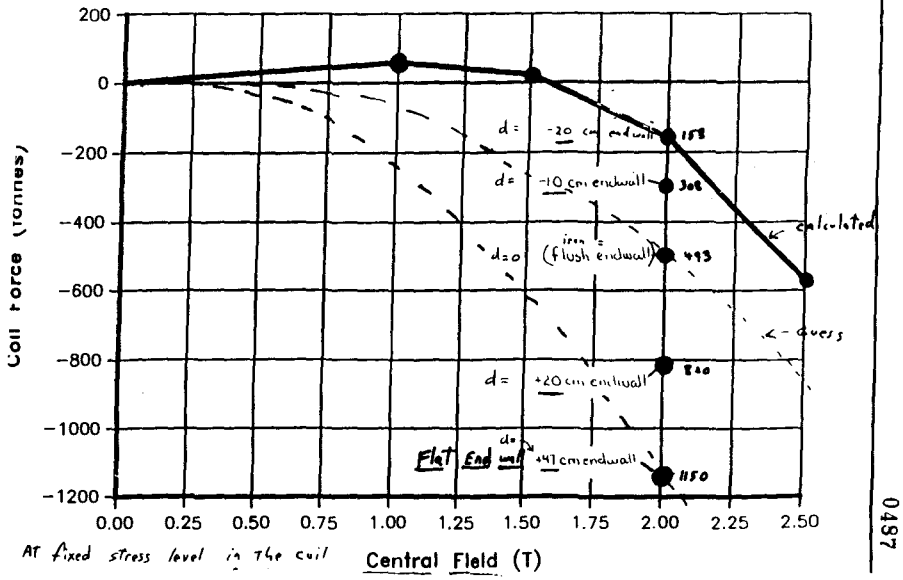

At fixed stress level in the coil

0487

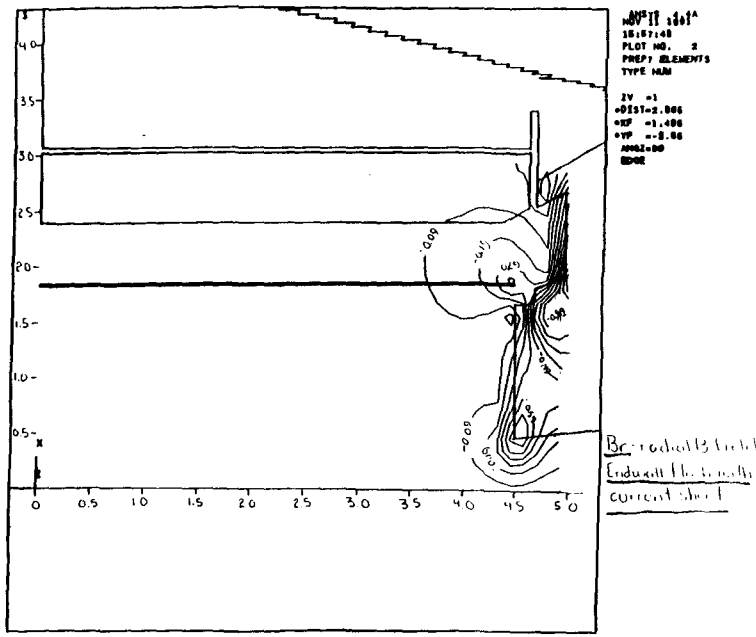

Br radial B field
Endwall 4 cm tapered
current sheet

0485

so what are the estimated stress levels in the coil? as for No Iron ⇒ $F_{coil} = 1700T$

conductor stress levels are ≃ 60 MPa

1 MPa = Kg/mm²

1 ATM = 0.1 MPa = 15 PSI

(24)

Table 3-6. Mechanical stability of the SDC coil.

Element	Material	El. Limit	Hand Cal.	FEA	
		9ksi PSI			9ksi PSI
Conductor	pure Al (3N8)	66 MPa	59 MPa	59 Mpa	
Insulation	GFRP/KGEPP	>100 MPA	30	30	
Cylinder	A-5083	169 MPa	59 MPa	55	
Cyl., Bonding	Epoxy	(18 x 1/3) / 6	<4	<1	} reliability of 6

Table 3-4. Yield strength of pure Al as a function of RRR.

RRR	Reduction	Y.S.(@77 K)	U.S. (@4.2 K)	Elongation
626	0	31 MPa	147 MPa	53.7 %
530	10% + cure	76	155	42.6
485	10 %	79	153	46.1

Note CDF, TopAZ, etc solenoids were built with much higher purity Aluminum (RRR = 1850 for CDF)
⇒ sacrificed some stability for conductor strength, but still NOT Good enough for SDC's needs.

AN you make such a material? YES (62)

( ) COLD WORK REDUCTION

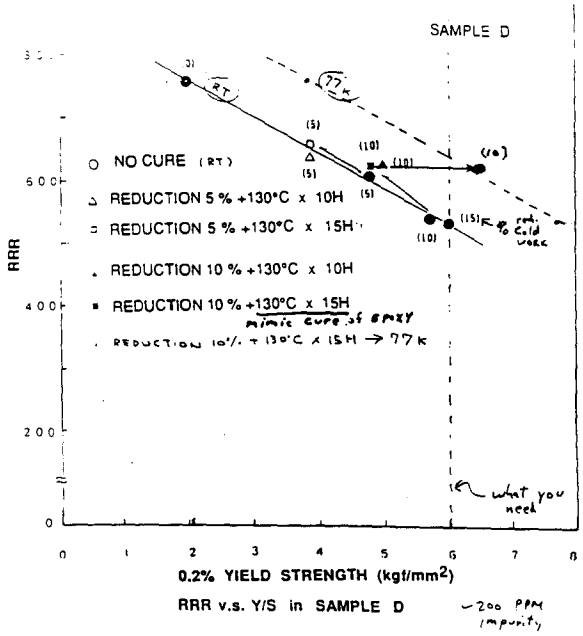

RRR v.s. Y/S in SAMPLE D ~200 PPM impurity

1) worry: can we control amount of cold work?
2) worry: can we reliably control the alloy?
3) worry: will it Room Temp anneal? etc

Fig. 7-2.

IT is a new material

(63)

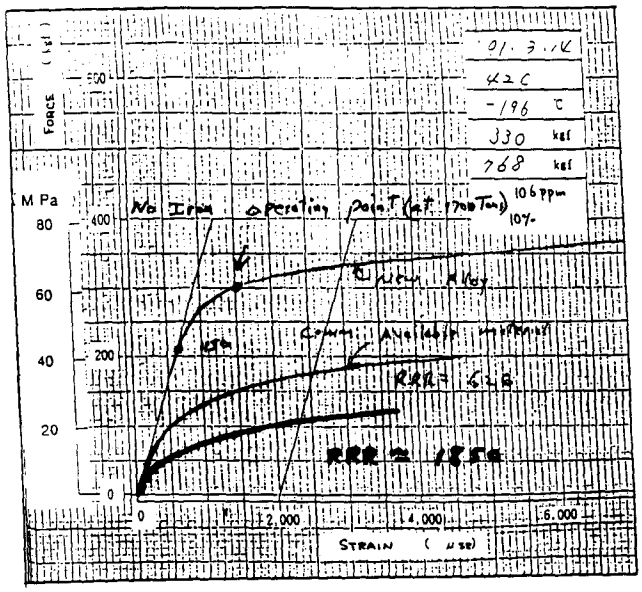

A STRESS- STRAIN CURVE OF HIGH STRENGTH PURE Al (4N)

Fig. 7-3

EGGS - look at "worst case" d = -20 cm reentrant design.

How badly does it screw up EM resolution/hermeticity?

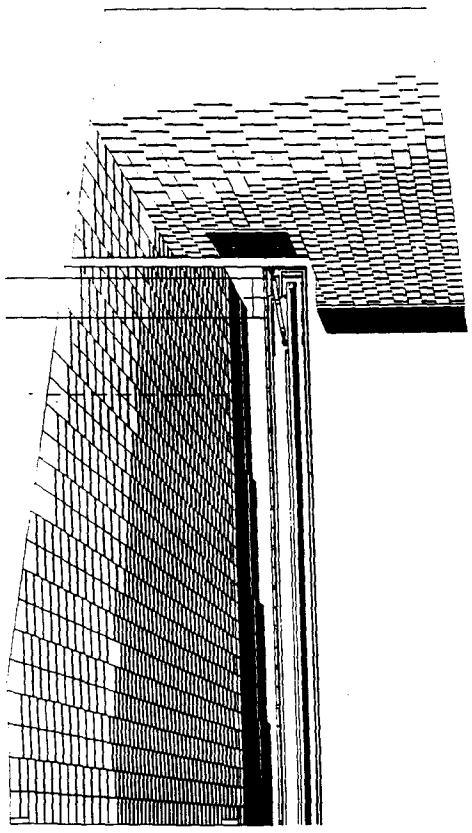

0492

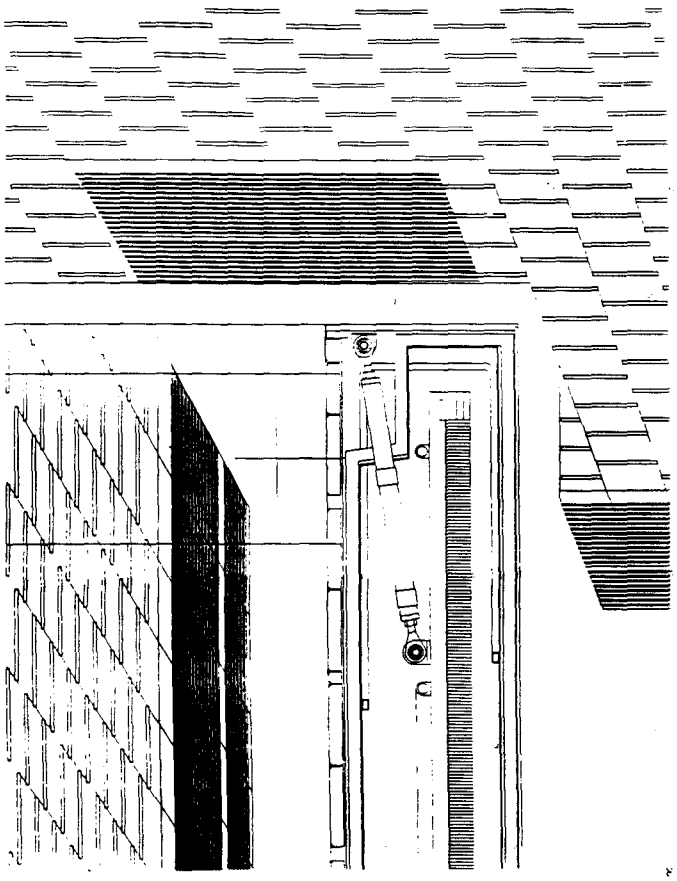

0493

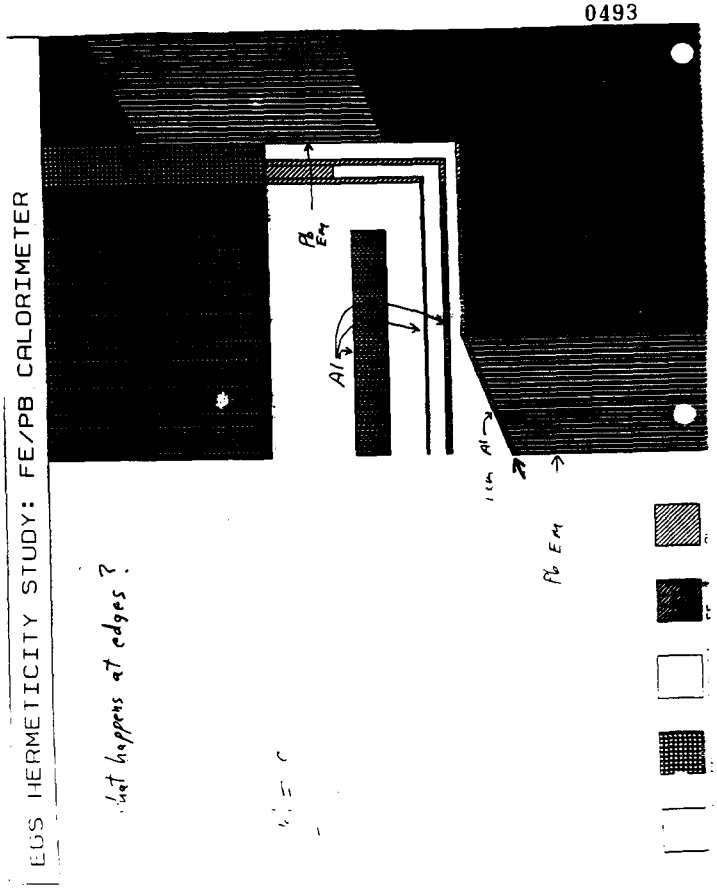

0494

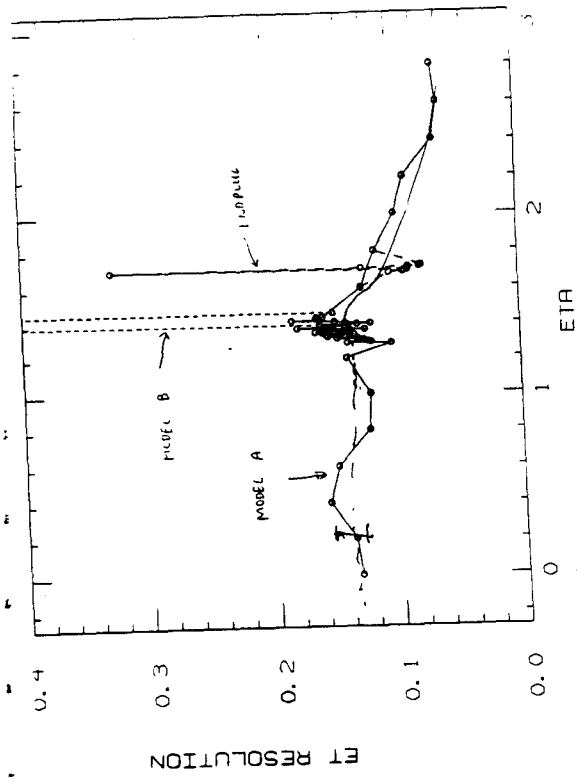

0495

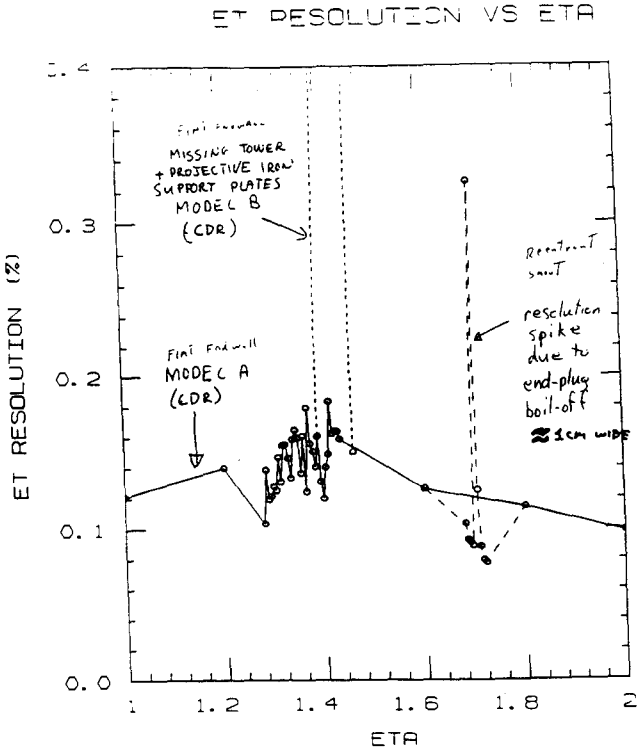

Preliminary Result: Conclude that Edge has little effect on overall EM resolution + hermeticity [MARC TURCOT (SSC GEANT, B=0

EM Decentering Forces

0496

	AXIAL	Radial	wei.
~No Iron (HAC-1 = Pb)	< 5T/20mm	< 5T/20mm	20
d = 17, 20, 0, −10 } not done YET		} Expected to be small	
d = -20 cm reentrant	7GT/20 mm	5 T/20mm	20T

(1) PRINCIPLE difference is the axial decentering force for the reentrant iron cases. (~2X CDF)

(2) NEW radial support requirements are determined by coil weight. for ~all designs

How much material is required for supports. (ie effects on EM calorimetry ... still under STUDY ... but NOT a major problem)

0497

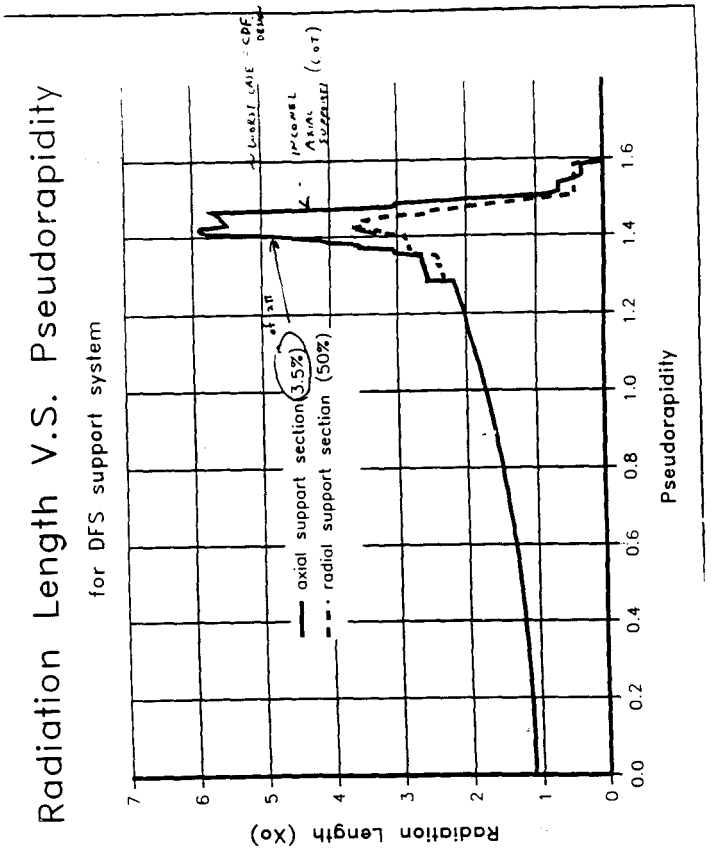

0498

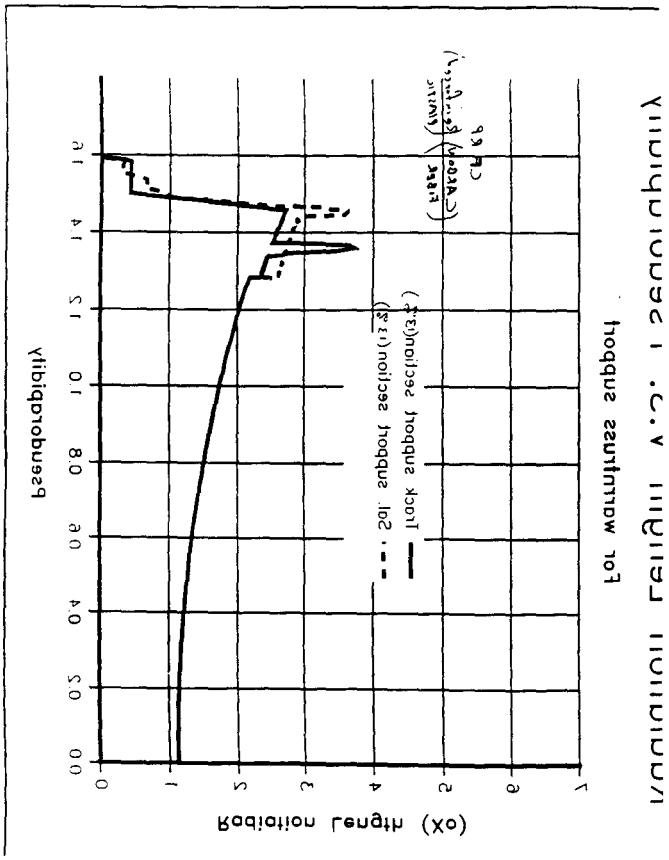

0499

Conclusions

1) Fe absorber for HAC-1 in the endwall region can reduce the forces on the SC coil and lead either to more conservative designs or higher central field values. Iron in close proximity to the end of the current sheet results in very uniform fields in the Tracking Volume.

2) We are assembling the tools to study various iron geometries in detail. These geometries may have a smaller impact on EM hermeticity and resolution than previously thought.

Calorimeter Cost Comparison Lead vs. Steel in HAC1

D. Scherbarth(Westinghouse)

CALORIMETER COST COMPARISON

LEAD VS. STEEL IN HAC1

D. W. Scherbarth (Dave)

Viewgraph 1
DWS
11.11.91

0501

CALORIMETER COST COMPARISON

COST COMPARISON METHOD

- Cost and Design Data Base for Model B Was Used
- Two Descopes Created
  - Descope 20, With Lead HAC1
  - Descope 21, With Steel HAC1
- Descope 21 is NOT Model A, as Described in CDR, But a Version of Model B, in Which Steel Has Replaced Lead in HAC1

Viewgraph 2
DWS
11.11.91

Westinghouse
Science & Technology Center

0502

CALORIMETER COST COMPARISON

SIMILARITIES BETWEEN DESCOPE 20 (LEAD) AND DESCOPE 21 (STEEL)

- All Parameters For EM and HAC2
- Volume, or Envelope, of HAC1
  - Barrel; 74.7 m^3
  - End Caps; 45.7 m^3
- Depth (λ) of HAC1
  - Barrel; 2.8 λ @ $\eta = 0$
  - End Cap; 4.6 λ @ $\eta = 3$
- Transverse Granularity of HAC1 = 0.05 x 0.05
- Total Depth
  - Barrel; 9 λ @ $\eta = 0$
  - End Cap; 11 λ @ $\eta = 3$

Viewgraph 3
DWS
11.11.91

Westinghouse
Science & Technology Center

0503

CALORIMETER COST COMPARISON

DIFFERENCES BETWEEN DESCOPE 20 (LEAD) AND DESCOPE 21 (STEEL)

	Descope 20 (Lead)	Descope 21 (Steel)	Δ (20-21)
BARREL HAC1			
Absorber Matl.	Lead	Steel	
Cell Depth (cm)	2.55	3.129	
Abs. Thk. (cm)	2.1	2.54	
Tile Thk. (cm)	0.25	0.25	
Tile Clearance (cm)	0.2	0.339	
Tile Volume (m^3)	6.53	5.97	0.56
Tile Quality	133,632	108,910	24,722
Total Mass (Tonnes)	693	482	211
END CAP HAC1			
Absorber Matl.	Lead	Steel	
Cell Depth (cm)	3.6	5.877	
Abs. Thk. (cm)	3.15	5.08	
Tile Thk. (cm)	0.25	0.25	
Tile Clearance (cm)	0.2	0.547	
Tile Volume (m^3)	2.87	1.94	0.93
Tile Quantity	88,384	54,142	34,242
Total Mass (Tonnes)	448	312	136

Viewgraph 4
DWS
11.11.91

Westinghouse
Science & Technology Center

0504

CALORIMETER COST COMPARISON

STEEL VS. LEAD

Steel Absorber is Cheaper Than Lead in HAC1

- **Base Cost Per Lb for Lead Is Slightly Lower**
  - **Lead: $3.88/lb**
  - **Steel: $4.30/lb**
- **Contingencies are Higher for Lead**
  - **Lead: 31%**
  - **Steel: 24%**
  - **Total Calorimeter: 27%**
- **Steel HAC1 is Lighter Than Lead HAC1 by 345 Tonnes**

Westinghouse
Science & Technology Center

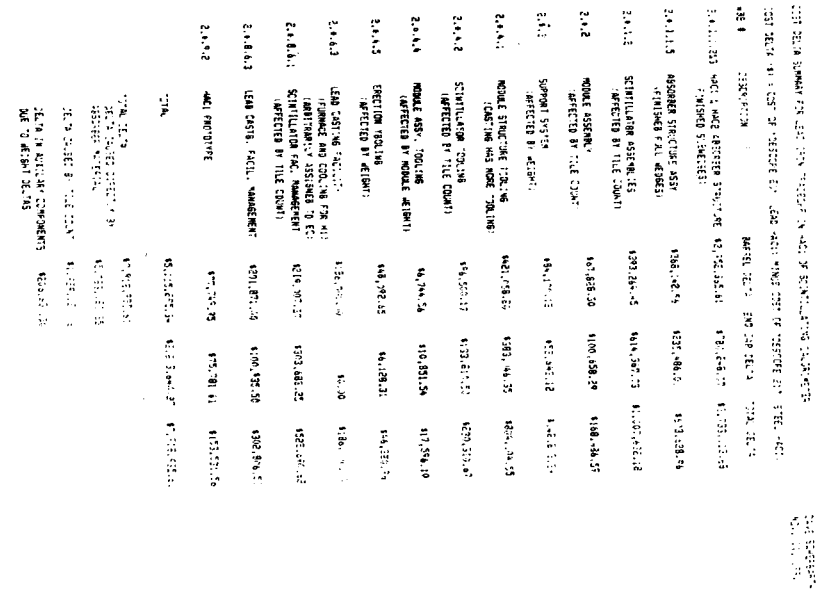

CALORIMETER COST COMPARISON

LEAD VS. STEEL IN HAC1

- **Baseline Cost (Descope 20) Has Lead in HAC1 of Barrel and End Cap**
- **Replacing Lead with Steel in Barrel and End Cap Saves 7.9 M$, Relative to Descope 20**
- **Replacing Lead With Steel in End Cap Only Saves 2.8 M$**
- **Contingencies Included in These Cost Comparisons**

Westinghouse
Science & Technology Center

CALORIMETER COST COMPARISON

LEAD VS. STEEL IN HAC1

Total Cost Delta in Favor of Steel	**7.9 M$**
Delta Caused Directly by Absorber Material	**5.8 M$**
Delta Caused by Tile Count **Δ Tile Count = 58,964** **$32.72 Per Tile**	**1.9 M$**
Delta in Support System and Weight Bearing Tooling	**0.2 M$**

Westinghouse
Science & Technology Center

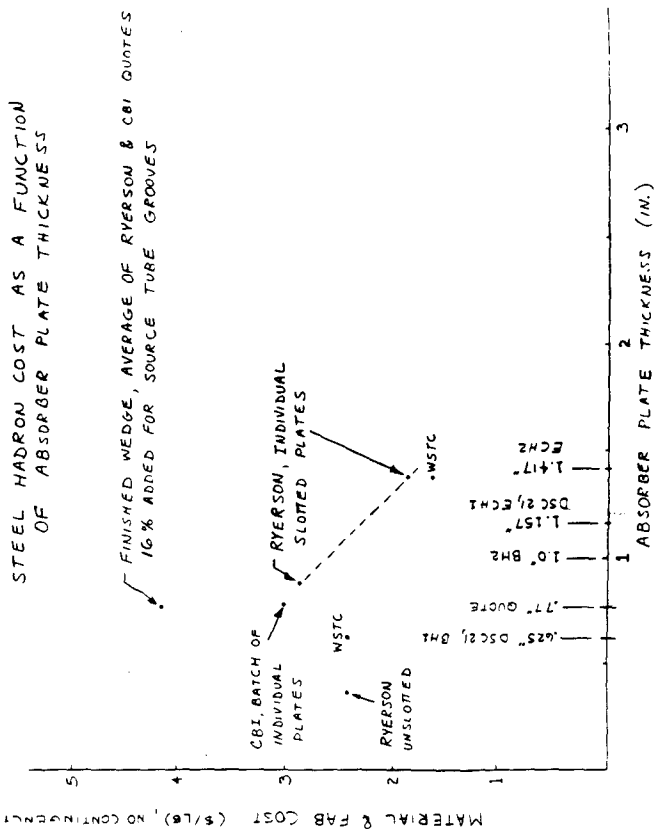

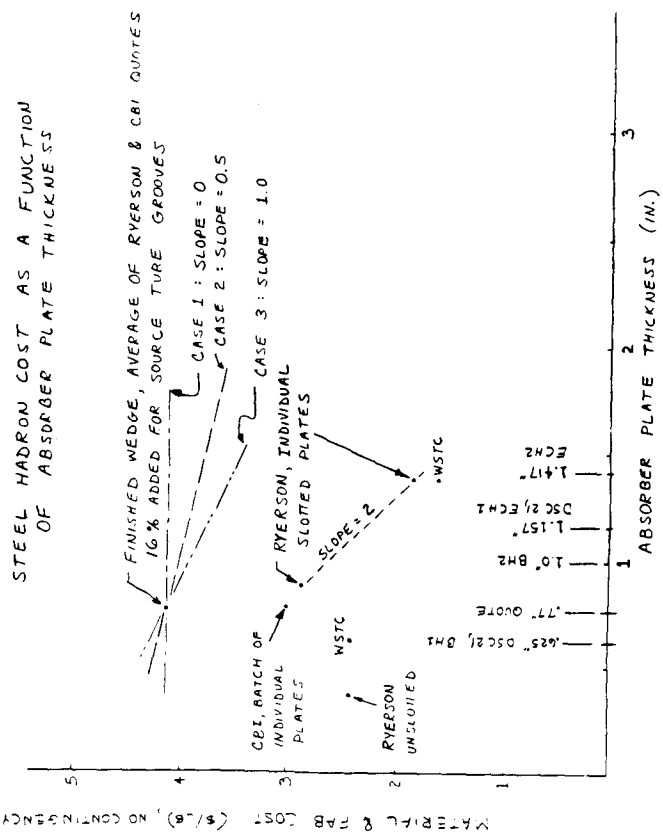

MATERIAL & FABRICATION COSTS FOR STEEL HADRON ABSORBERS

CASE NO	SLOPE (Δ/R/IN)	$/LB OF FINISHED STEEL WEDGE AT VARIOUS LOCATIONS AND PLATE THK.				TOTAL COST Δ* (M$)
		DESCOPE 21 BHAC1 .625"	QUOTE .77"	DESCOPE 20 & 21 BHAC2 1"	DESCOPE 21 E.C. HAC1 1.157"	DESCOPE 20 & 21 E.C. HAC2 1.417"	
1	0	4.14	4.14	4.14	4.14	4.14	7.9
2	0.5	4.21	4.14	4.03	3.95	3.82	7.9
3	1.0	4.29	4.14	3.91	3.75	3.49	7.9

* POSITIVE COST Δ MEANS STEEL IS CHEAPER THAN LEAD

MODEL COMPARISON

Model type	A	B
Long. Barrel EM Channels	2	2
Long. End Cap EM Channels	2	2
Shower Max Tiles / Tower	8	12
Shower Max MAPMT	64	64
Hac 1 Trans. Granularity	0.5x0.5	0.5x0.5
Hac 2 Trans. Granularity	0.1x0.1	0.1x0.1
Total Standard PMT's	34,624	33,936
Total 64 anode MAPMT's	1,440	2,041
Total Tiles	510,000	609,040
Hac 1 Absorber	Steel	Lead

SOURCE TUBES

LEAD

Casting into matrix, requires tooling for positioning and routing.

Manifold must be designed for access to source tester.

IRON

Machined grooves add 18% to steel costs.

Compound bends are difficult.

Manifold issues same as lead.

STRUCTURAL REQUIREMENTS

Lead

Heavier, more $ for structure.

Potential reduction in access due to more structure.

Iron

Lighter, less $ for structure, better access.

Integration Issues

Who designs the supports?

Who determines the location on barrel?

What is the interface boundary between barrel and support design teams?

R&D ISSUES FOR LEAD & IRON

Lead

Can mold techniques be used in production?

Can tolerances be relaxed from prototype?

Can source tubes be routed and cast successfully into lead matrix?

Iron

Three fabrication techniques must be narrowed to one method.

Can source tubes be routed out of steel with compound bends?

Integration

How to the interfaces between EM, Hac1, Hac2 actually connect?

SCHEDULE CONTINGENCY

Lead

Higher technical and schedule risk. Potential for limited vendor sources with required capability.

Iron

Lower technical and schedule risk. Large number of vendor sources.

SAFETY ISSUES

What are requirements from DOE on Lead handling?

Lab personnel requirements?

Contractor requirements, liability?

Potential for DOE oversight on contractor activity?

SOURCE CALIBRATION TECHNIQUE

EDGE ILLUMINATION

Easier routing.

Uniformity?

Tile response?

FACE ILLUMINATION

More complex routing required.

Improved response.

Improved uniformity.

Engineering Issues

LEAD RADIATOR EM

Cast

Limit 4 mm thickness.

Source tubes cast in place.

Additional cost of precision tooling, fixtures, molds, etc.

Creep concerns.

Stacked

Need proof of principle.

Compression and creep concerns.

Stability in cantilevered position.

Cost of cladding lead to make stable.

Source tubes require grooves in lead.

Jet Tagging

K. Einsweiler(LBL)

Jet Tagging

0521

Idea: 2 basic Higgs production mechanisms for large m_H:

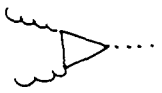

gg fusion

WW/ZZ fusion

$Br(H \to ZZ \to 4l)$	$\sim 1.4 \times 10^{-3}$	increasing backgrounds
$Br(H \to ZZ \to 2l 2\nu)$	$\sim 8.8 \times 10^{-3}$	
$Br(H \to ZZ \to 2l 2j)$	$\sim 30 \times 10^{-3}$	
$Br(H \to WW \to l\nu l\nu)$	$\sim 30 \times 10^{-3}$	
$Br(H \to WW \to l\nu jj)$	$\sim 200 \times 10^{-3}$	

→ Try to find forward quark jets from WW/ZZ fusion process

0522

1) improve signal to noise { ~ no tag jets in background }

$H \to ZZ \to 4l$	small $q\bar{q} \to ZZ$ background
$H \to ZZ \to 2l 2\nu$	$q\bar{q} \to ZZ$ + large Z+jets
$H \to ZZ \to 2l 2j$	$q\bar{q} \to ZZ$ + overwhelming Z+jets
$H \to WW \to l\nu l\nu$	$q\bar{q} \to WW$ + overwhelming $t\bar{t}$
$H \to WW \to l\nu jj$	$q\bar{q} \to WW$ + overwhelming $t\bar{t}$, W+jets

2) test $W, Z \leftrightarrow H$ and $t \leftrightarrow H$ coupling (vital to understand nature of symmetry breaking ...)

0523

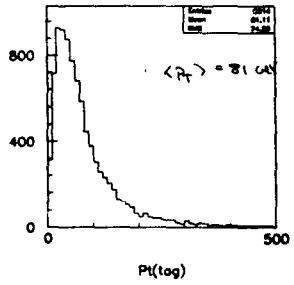

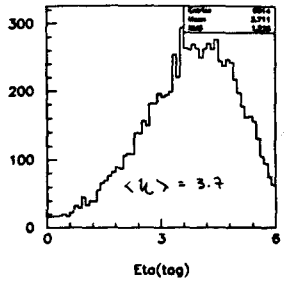

P_T, η for tag parton

jet finding will be done in P_T (E_T)

"noise" for jet definition = underlying events which are ~ uniform P_T vs η ⇒ natural

likely cut for jet ID will be ~ 50 GeV

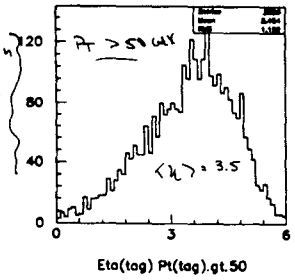

natural tagging region at 40 TeV ~ $\eta = 2.5 \to \eta = 5$

0524

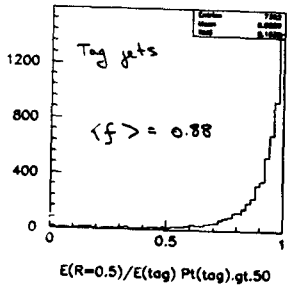

Alternative:

fraction of parton energy contained in particles flowing with $\Delta R < 0.5$ relative to parton direction

⇒ Tag jets behave well with $R = 0.5$ cone definition for clustering

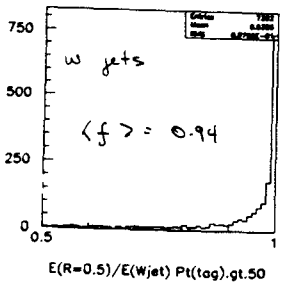

In addition: Highly boosted jets from W decay are extremely narrow ($\Delta R \lesssim 0.1$)

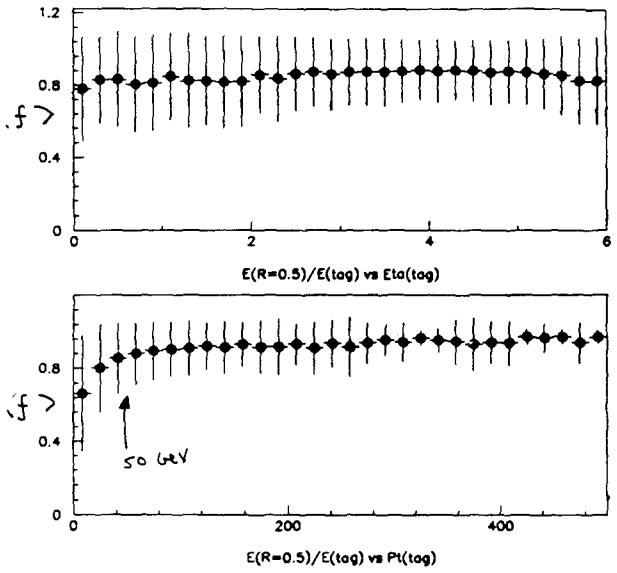

→ mean fraction of E inside cone is independent of η

→ slight decrease in clustering efficiency for $P_T \lesssim 50$ GeV

Defines analysis strategy:

1) define "base" calorimeter = $|\eta| < 6$

segmentation = $.05 \times .05$ | 128 ϕ cells, 240 η cells |

→ study $\times 2, \times 4, \times 8, \times 16$

2) do naive jet finding

(cluster in E_T, defined by summing all particles except μ, ν)

- cone $\Delta R = 0.6$
- seed ($E_T > 5$ GeV) defines cone axis
- collect all cells with $E_T > 1$ GeV in cone
- define jet 4-vector = sum of individual "massless" cell 4-vectors → jet acquires mass

→ jet axis not iterated → for large segmentation must be careful

$\Delta R = 0.6$ (0.6 carefully chosen...)

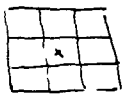

$\Delta\eta \times \Delta\phi = 0.4$

$\Delta\eta \times \Delta\phi = 0.8$

3) divide detector into 2 regions:

(i) "central" = $|\eta| < 2.5$, contains (mainly) H decay products → order clusters in P_T

(ii) "tag" $2.5 < |\eta| < 5.0$, contains (mainly) tag jets + initial state radiation → order in E to enhance tag jets in sample...

processes: use HERWIG V5.3

- $qq\,H \to qq\,WW$
- $gg \to H \to WW$
- $gg \to t\bar{t} \to WW$ + jets
- $q\bar{q}, gg \to W$ + jets

} 1 leptonic W, 1 hadronic W decay required

Here:

- discuss only tag region (not feasibility of complete analysis)
- ignore easier final state:

$H \to ZZ \to \ell\ell\nu\nu$

| ~ no $t\bar{t}$ background ~ 2 tjets easier to get rid of... |

---

today:

1) review acceptances and ability to distinguish "true" tag jets from initial state radiation

2) study resolutions in | η, ϕ P_T, E | versus segmentation in $\Delta\eta \times \Delta\phi$

| → particle level → no geometry |

First: Event topology for different processes

	$qq \to WW$	$gg \to H$	W+jets	$t\bar{t}$
$\langle$#jets$\rangle$ in tag region with P_T(cluster) > 50	0.90	0.45	0.40	0.50
$\langle$#jets$\rangle$ in tag region, P_T > 50 - NOT tag - NOT W decay = initial state radiation)	0.02	0.34	0.40	0.30

⇒ lots of radiation in this region

characteristic feature of tag jet: very large E

(but there are strong correlations between E_{jet}, η_{jet}, especially after a P_T cut

look at "single tag" and "double tag":

1) single tag $E > 3$ TeV

(with $P_T > 50$ ⇒ unbiassed beyond $\eta \sim 5$)

2) double tag: · 2 jets $E > 1.5$ TeV
· opposite η in detector

	$qq \to WW$	$gg \to H$	W+jets	$t\bar{t}$
single tag	0.176	0.068	0.090	0.055
ejection =		2.6	2.0	3.2
uble tag	0.059	0.0063	0.0055	0.0068
ejection =		9.4	10.7	8.7

Further optimization possible for P_T, E cuts + tag region definition

but: tagging useful; not a panacea

Note: if tag region extends to $\eta = 4$ ⇒ ~ factor 2.5 loss

Comment:

⇒ there is significant unresolved disagreement on these numbers: FNAL 91/149-T V. Barger et al.

· they do a matrix element analysis of single tagging (background matrix element not available for double tag)

· rough agreement on signal (in particular, ϵ vs cut on E_{tag})

· significant disagreement on $t\bar{t}$ background:

Parton shower (this analysis):

$$\frac{\epsilon(E_{tag} > 3\ \text{TeV})}{\epsilon(E_{tag} > 1\ \text{TeV})} \sim 4\text{-}5$$

Barger et al ratio ~ 100

⇒ conclude jet tagging is very effective

Resolutions: (Preliminary ...)

⇒ study effect of segmentation by comparing "True" value to "observed" value for different segmentations

1) initial segmentation 128×240 ⇒ can divide many times by 2 before you get into trouble

study: $.05 \times .05$, $.1 \times .1$, $.2 \times .2$, $.4 \times .4$, $.8 \times .8$ } range for FCal ?

2) what is "True" value ?

· use tag parton direction for $qq \to WW$

· observe that with HERWIG, there is a significant smearing due to "fragmentation"

⇒ if define parton 4-vector as sum of all particles "produced" by it, this differs from initial parton direction ...

choose 4 variables

$\Delta\phi$
$\Delta\eta$
$\Delta P_T/P_T$
$\Delta E/E$

0533

look at jets from tag partons only
($qq \to qqH \to qqWW$)
with P_T (cluster) > 50 GeV

91/11/12 09.01

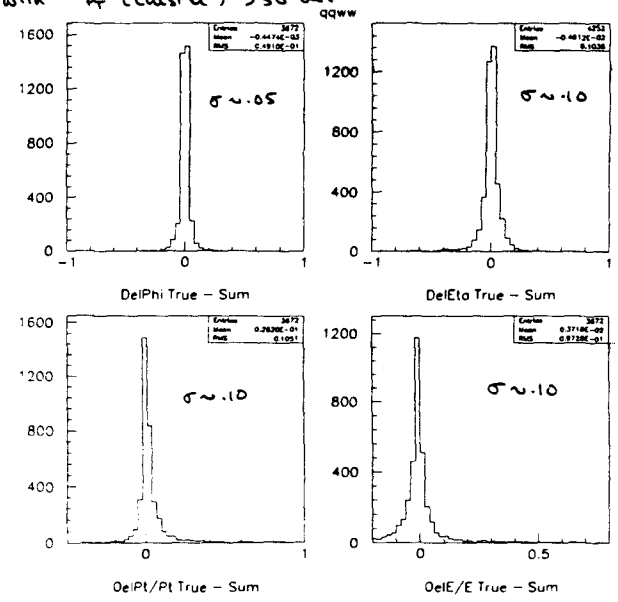

0534

Comments:

→ although E of jets is very high, P_T is not ⇒ fragmentation effects + underlying event effects are large

| in general, this is true of FCal: high P_T jets are all central |

⇒ don't expect good intrinsic E resolution

(see: $\frac{\Delta E}{E} \sim 8\%$ ⇒ sets floor for required E resolution ...)

→ segmentation studies:

expect that as long as jet hits several cells, the measurement will still be centroid ⇒ soft function of segmentation. Once jet "swallowed" by one cell ⇒ poor resolution

"Typical" Tag Jet

0535

91/10/11 17.48

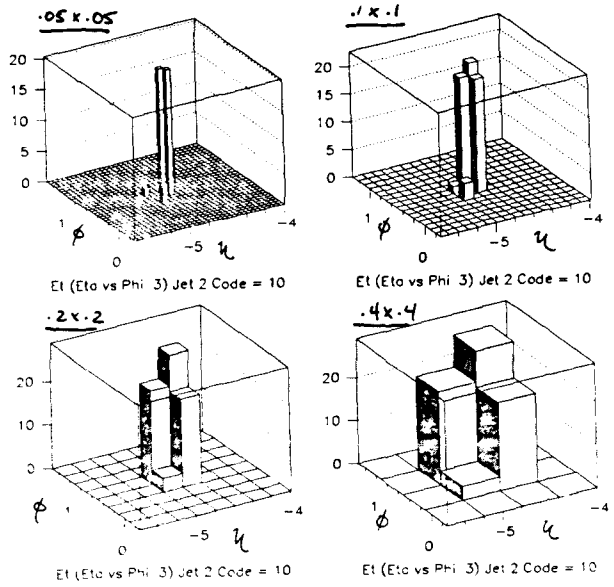

$\Delta\phi$ $\{\equiv \phi_{TRUE} - \phi_{CLUSTER}\}$

0536

⇒ segmentation

Note: using ϕ_{SUM} = sum of all particles arising from parton ⇒ slightly narrower distributions

91/11/12 09.01

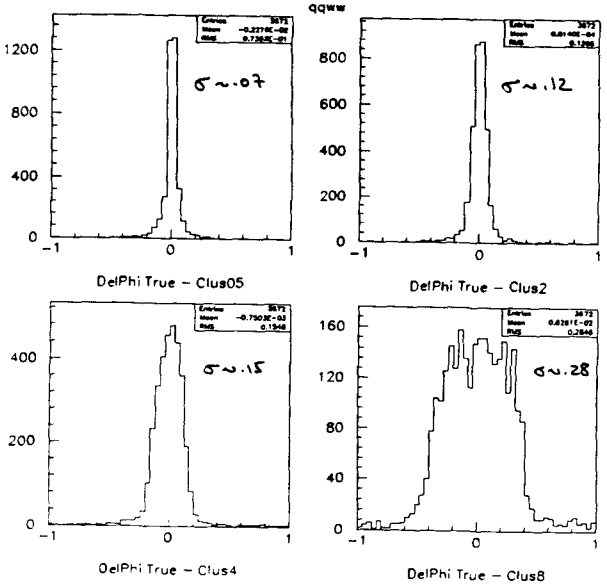

$\Delta\eta \equiv \eta_{TRUE} - \eta_{CLUSTER}$ 0537

vs segmentation

91/11/12 09.02

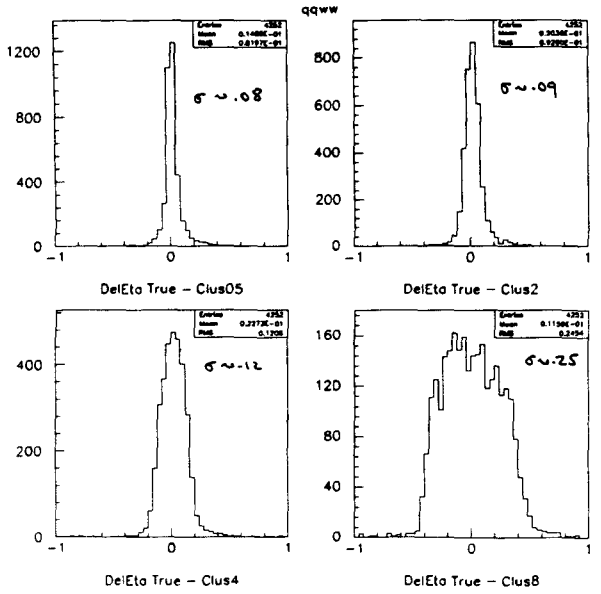

$\frac{\Delta P_T}{P_T} \equiv \frac{P_T(TRUE) - P_T(CLUSTER)}{P_T(TRUE)}$ 0538

vs segmentation note: angular errors due to segmentation: $P_T \sim \sin\theta$ large, $E \sim \cos\theta$ small

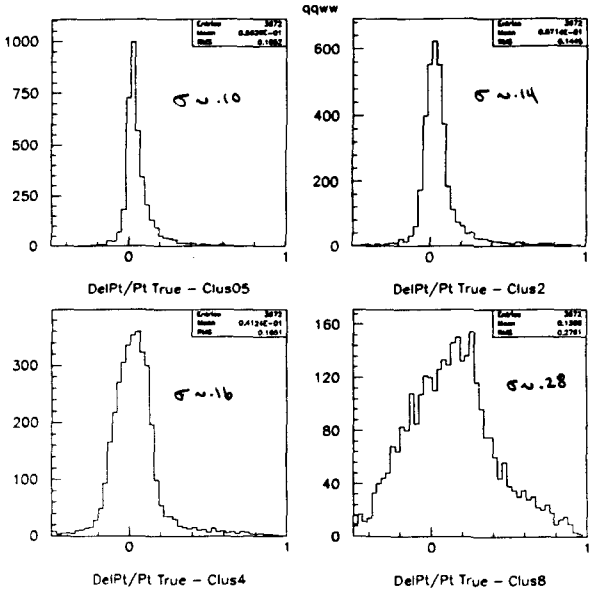

$\frac{\Delta E}{E} \equiv \frac{E_{TRUE} - E_{CLUSTER}}{E_{TRUE}}$ 0539

vs segmentation

Note: expect ~no effect from $\Delta\theta$. For .8x.8 get "edge" jets ⇒ large error

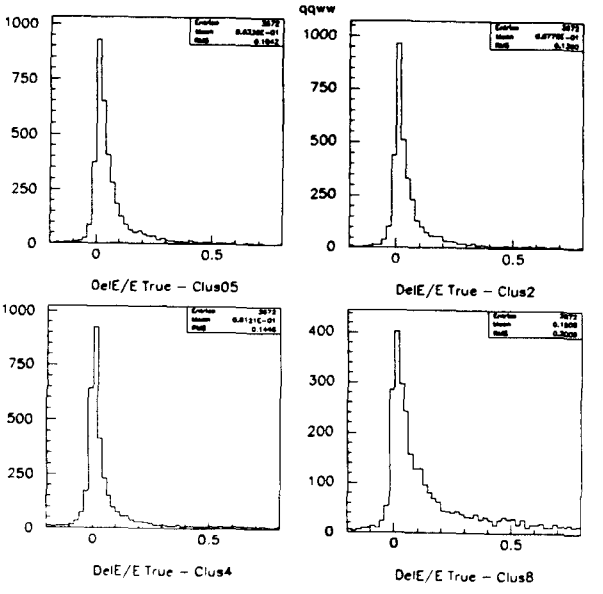

relative error

$\Delta\phi \equiv \phi|_{.05x.05} - \phi|_{.1x.1}$ 0540

.2x.2
.4x.4
.8x.8

91/11/12 09.02

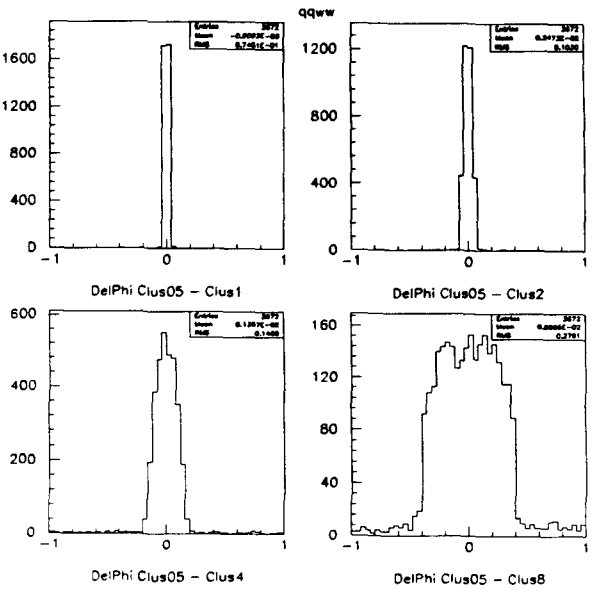

$\Delta\eta$

0541

91/11/12 09.02

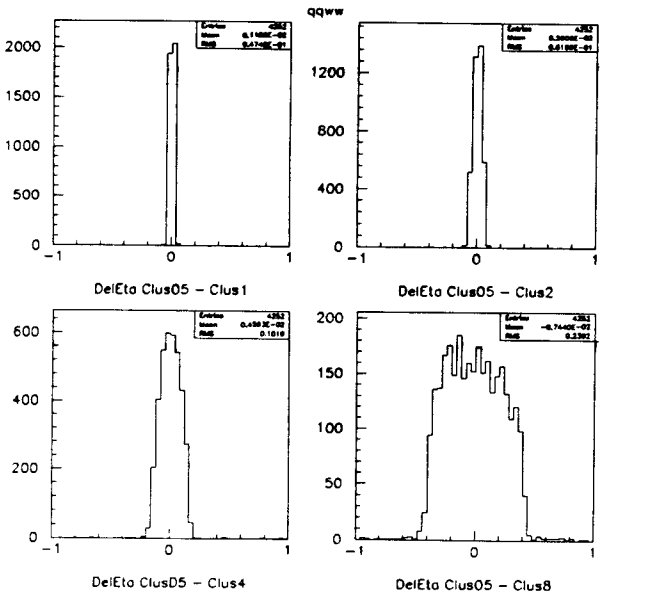

$\frac{\Delta P_T}{P_T}$

0542

91/11/12 09.02

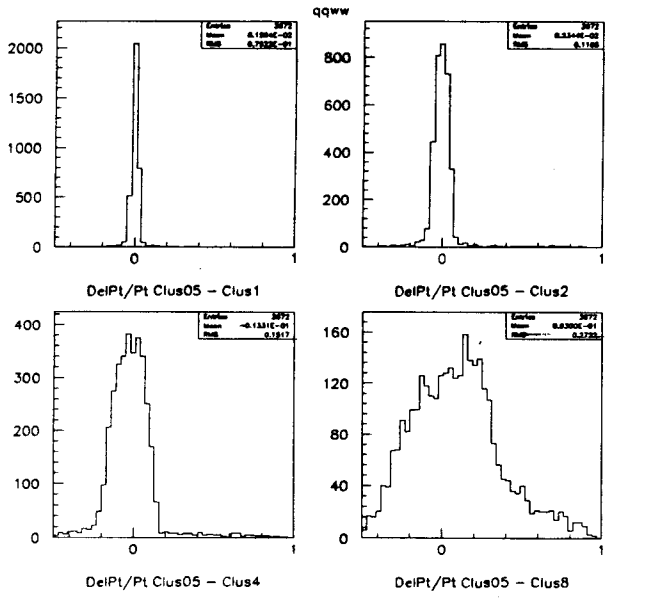

$\frac{\Delta E}{E}$

0543

91/11/12 09.02

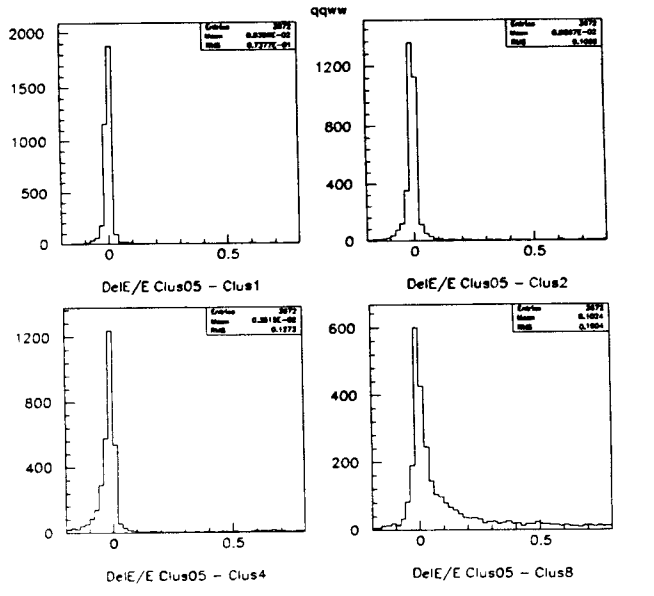

"Conclusions"

0544

1) important variable in this case is probably $\frac{\Delta P_T}{P_T}$. To be quantitative, need full signal/noise analysis ... Otherwise, if want: segmentation effects ~ fragmentation effects

$\Rightarrow \Delta\eta \times \Delta\phi \sim .2 - .4$

but clearly hadronic shower sizes must be included ...

2) geometry issues:

2 "extremes" = . backstop at z=16m
. reverse cone

Naive concepts:

i) backstop with $\Delta\eta = .5$ at 16 m

η =	R =	ΔR =
5.5	13.2 cm	8.4 cm
5.0	21.6 cm	13.9 cm
4.5	35.5 cm	23.1 cm
4.0	58.6 cm	38.0 cm
3.5	96.6 cm	62.6 cm
3.0	159.2 cm	

ii) inverse cone:

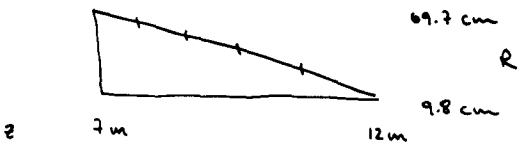

η =	z =	R =	ΔR =
5.5	12 m	9.8 cm	5.1 cm
5.0	11 m	14.9 cm	7.4 cm
4.5	10 m	22.3 cm	10.7 cm
4.0	9 m	33.0 cm	15.3 cm
3.5	8 m	48.3 cm	21.4 cm
3.0	7 m	69.7 cm	

comments:

→ differences are probably not large because large η cells are at large z for both designs

but cells are small on scale of hadronic showers ⇒ suspect that apparent advantage of $\Delta\eta = .2$ vs $\Delta\eta = .4$ in particle level simulation will disappear ⇒ .4 will appear natural (16 ϕ cells × 6-7 η cells)

→ no simulation done for "Cartesian" calorimeter:

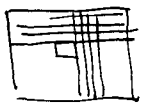

but segmentation effects (= angular measurement errors) will be more severe for given cell size. //

Next step:

repeat simulation with realistic geometry

- full GEANT? (large CPU time due to large ϵ in forward)
- just include shower parametrization tuned to realistic geometry?

Implications of Missing Et on FCAL Specifications

M. Barnett(LBL)

M. Barnett

0548

IMPLICATIONS OF MISSING E_T ON FCAL SPECIFICATIONS

What are $A + B$ in

$$\frac{\sigma}{E} = \frac{A}{\sqrt{E}} \oplus B \quad ?$$

What are $\Delta\eta$ and $\Delta\phi$ to do missing E_T physics. ?

Results shown:

- Rick Field using ISAJET.
- Michael Barnett using Parton Monte Carlo.

Both have important deficiencies

0550

Geometry of Forward Calorimeter

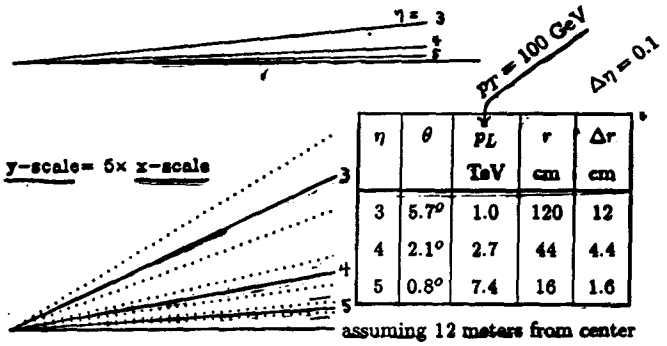

η	θ	p_L TeV	r cm	Δr cm
3	5.7°	1.0	120	12
4	2.1°	2.7	44	4.4
5	0.8°	7.4	16	1.6

assuming 12 meters from center

Want to Measure E_T

$$E_T = E \sin\theta \approx E\theta$$

Error on E_T, $\frac{\Delta E_T}{E_T}$, is $\frac{\Delta\theta}{\theta} \oplus \frac{\Delta E}{E}$ where $\frac{\Delta\theta}{\theta} \approx \Delta\eta$.

So $\Delta\eta = 0.2$ corresponds to $\frac{\Delta\theta}{\theta} \approx 20\%$,

and $\frac{\Delta E}{E} < 10\%$ won't help $\frac{\Delta E_T}{E_T}$.

0551

Segmentation

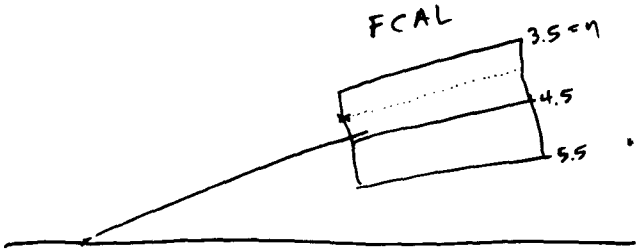

0552

Why choose a light gluino (300 GeV) as the test case ?

1. It yields little $E_T^{missing}$ so is difficult.
2. It has the biggest possible background — ordinary QCD multi-jet events.

Signal - 3 jets + $E_T^{missing}$

Detector Background -

3 jets with one or more badly mismeasured.

Rick Field - ISAJET

$\phi > 40°$

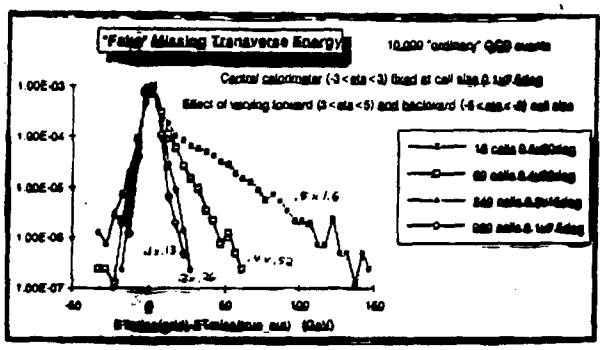

$m(\tilde{g}) = 300$ GeV

3 jets with $E_T > 70$ GeV;

$\phi(\text{jet} - E_T^{\text{miss}}) > 40°$

$|\eta|<4$. vs. full coverage

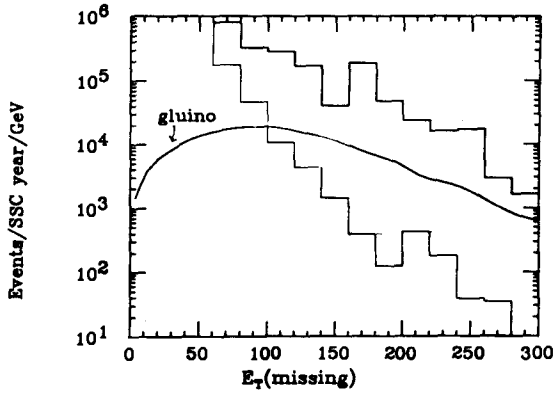

why light gluino?
1. small E_T^{miss}
2. big background.

$m(\tilde{g}) = 300$ GeV

3 jets with $E_T > 70$ GeV; $\phi > 40°$

$\frac{\sigma}{E} = \frac{80\%}{\sqrt{E}} \oplus 10\%$

cut vs no cut. fine vs one η cell

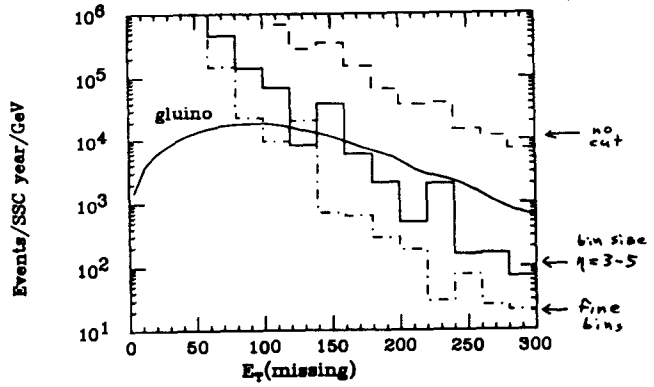

why light gluino?

$m(\tilde{g}) = 300$ GeV

3 jets with $E_T > 70$ GeV; $\phi > 40°$

$\frac{\sigma}{E} = \frac{200\%}{\sqrt{E}} \oplus 10\%$

$\phi>40$. 200% two η cells (one)

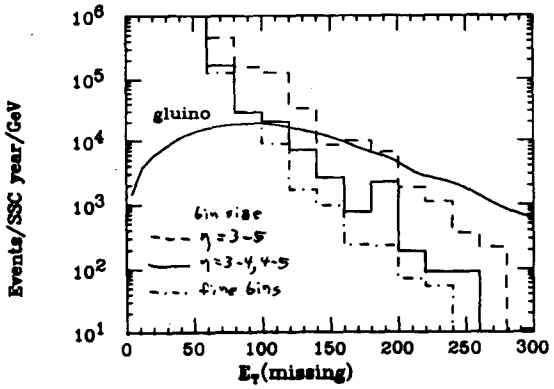

$m(\tilde{g}) = 300$ and 500 GeV

3 jets with $E_T > 70$ GeV; $\phi > 40°$

$\frac{\sigma}{E} = \frac{80\% \text{ or } 200\%}{\sqrt{E}} \oplus 10\%$

~~[illegible]~~. $\phi>40$. 80% vs 200% fine bins

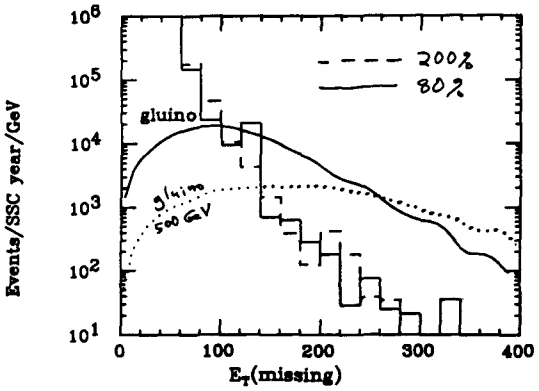

For $m(\tilde{g}) = 500$ GeV, should change cuts (for example, 3 jets > 100 GeV and 4th jet > 70 GeV).

$m(\tilde{g}) = 300$ GeV

3 jets with $E_T > 70$ GeV; $\phi > 40°$

$\frac{\sigma}{E} = \frac{80\% \text{ or } 200\%}{\sqrt{E}} \oplus 10\%$

s>70. $\phi>40$. 80% vs 200% one η cell = 3-5

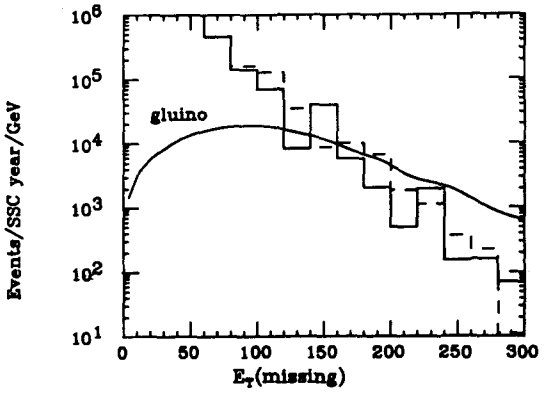

Preliminary Remarks: *R. D. Field*

- Cell size and rapidity coverage appear to be the important factors.
- Smearing does not seem to be much of an effect. However, I must do more work here.
- Summary of cell sizes in forward ($3 < \eta < 5$) and backward ($-5 < \eta < -3$) region:
  1. 960 cells $\Delta\eta\Delta\phi = \underset{0.13}{0.1} \times 7.5°$ is excellent. Going to smaller cells does not buy you anything since at this cell size fake missing E_T is dominated by the rapidity cut (i.e., $|\eta| < 5$).
  2. 240 cells $\Delta\eta\Delta\phi = \underset{0.26}{0.2} \times 15°$ is still very good.
  3. 60 cells $\Delta\eta\Delta\phi = \underset{0.5}{0.4} \times 30°$ is boaderline. It might be okay if one can still identify "jets" so you can make your "no missing E_T in the direction of jets" cut. If you go to larger cells you will not be able to identity jets.
- With forward cells larger that $\Delta\eta\Delta\phi = 0.4 \times 30°$ you produce so much fake missing E_T that you can no longer use missing E_T in an effective way to eliminate the QCD background. In this case you cannot use missing E_T as a handle on the "new" physics.

I will examine more carefully the effects of smearing and run the plots out to higher missing E_T.

Sincerely, *Rick*

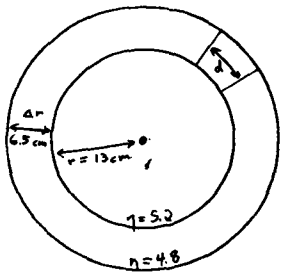

Suppose that the forward calorimeter goes from $\eta = 3$ to 6.8 and starts at 12 meters from interaction point.

The following are the coarsest possible cell sizes for which missing E_T physics remains possible.

Measuring missing E_T does not require fine segmentation; however, segmentation is essential to find jets in order to make cuts that reduce backgrounds below signal.

η of cell	$\Delta\eta$	Δ(radius)	radius$\times\Delta\phi$	for $\Delta\phi$
3.0 – 3.2	0.2	22 cm	21 cm	0.20 = 11 degrees
3.6 – 3.8	0.2	12 cm	12 cm	0.20 = 11 degrees
4.2 – 4.4	0.2	6.5 cm	6.4 cm	0.20 = 11 degrees
4.4 – 4.8	0.4	9.7 cm	9.5 cm	0.39 = 22 degrees
4.8 – 5.2	0.4	6.5 cm	6.4 cm	0.39 = 22 degrees
5.2 – 6.0	0.8	7.3 cm	7.0 cm	0.79 = 45 degrees

This conclusion based on a parton Monte Carlo study.

Conclusions

- In $\frac{\sigma}{E} = \frac{A}{\sqrt{E}} \oplus B$

  if $B = 10\%$ (in FCAL),

  missing E_T results are insensitive to $A = 80\% - 200\%$.

  Non-gaussian tails (à la CDF) have been included.

- Segmentation must be adequate to identify jets so that critical cuts can be made. It must be adequate to identify the angle between the missing E_T and any jets in the FCAL. This implies $\Delta\phi \approx \Delta\eta \approx 0.2 - 0.4$.

- Improved studies would be valuable.

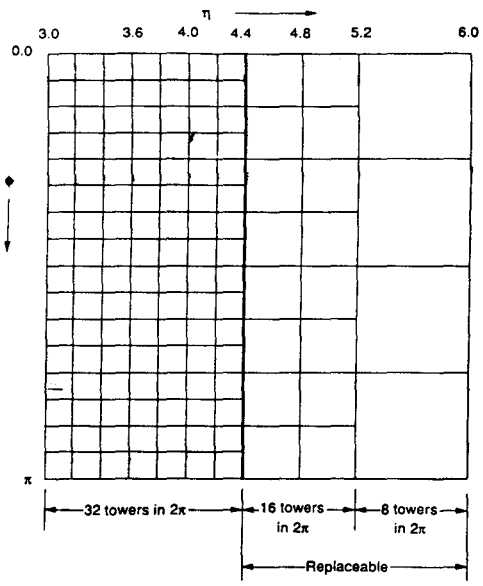

Cross section of towers at z = 16 meters

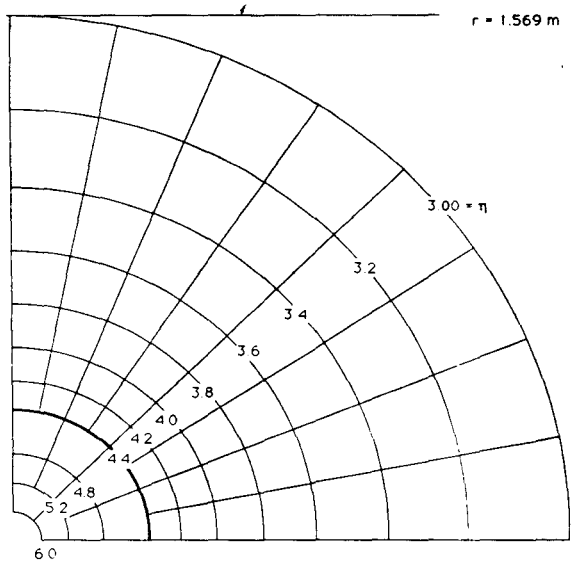

SDC Forward Calorimetry

W. Frisken(LBL/York)

SDC FORWARD CALORIMETRY

Presented by Bill Frisken, LBL/York U.
SSCL, Nov. 14/1991

OUTLINE:

1. INTRODUCTORY REMARKS: The FCal Environment

2. FCal PERFORMANCE REQUIREMENTS

3. INTEGRATION/SSCINTERFACE ASPECTS

4. R&D PLANS
   - SHORT TERM---> FEBRUARY 92
   - LONGER TERM

MOST OF THIS MATERIAL IS FROM

SDC FORWARD CALORIMETRY WORKSHOP

Held at LBL October 31 and Nov1 1991

Contents:

1. INTRODUCTORY REMARKS: The FCal Environment

- Luminosity, event rate

  $L=10^{33}$--->10^{34}

  $R=10^{8}$--->10^{9} per second

- Radiation dose at high eta.

  Show transparency----->>>>>

- Radioactivation of SDC and SSC components

  See D.E. Groom at Capri/91----->>>>>

- Crowded? in principal not, but everyone planned to use that space.....

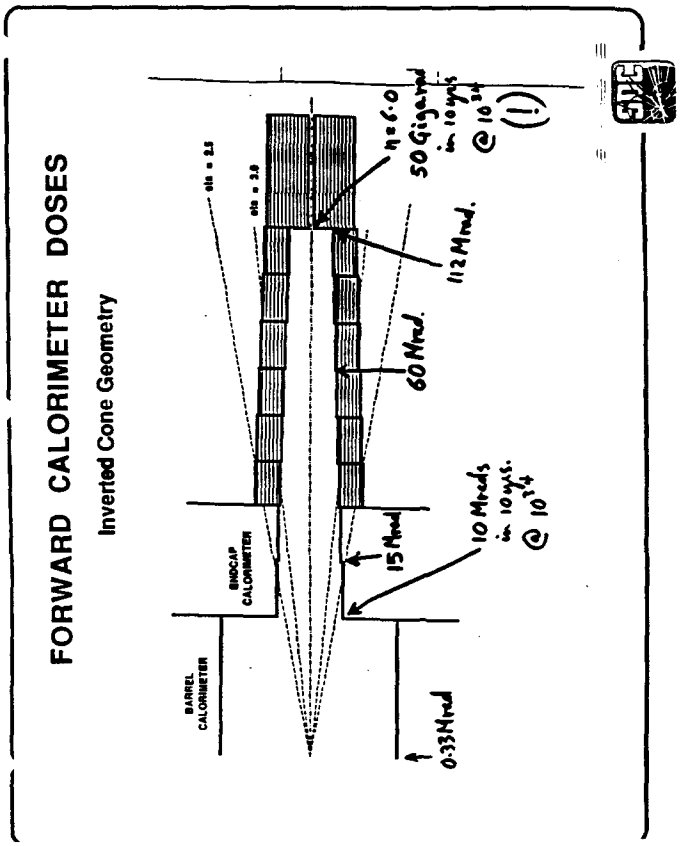

Capri 14-18 October 1991
Don Groom Det Act-1

EXTENSION OF SSC-SR-1033 APPROACH TO THE RADIOACTIVATION OF LHC AND SSC DETECTORS

Don Groom
Lawrence Berkeley Laboratory, Berkeley, California
Solenoidal Detector Collaboration

1. The SSC-SR-1033 approach
2. Plan to include radioactivation
3. Extension of model to "star density"
4. Relationship of star density to activation and dose

→ Slow decays of surface dose: absorb

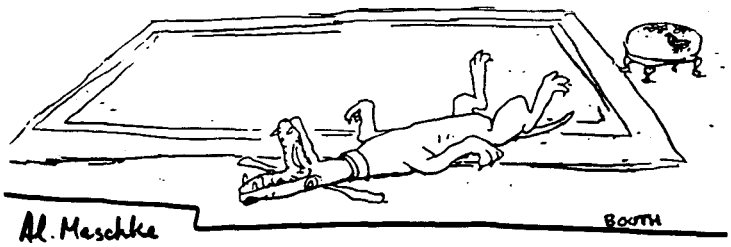

Al. Maschke

Optimum = Cool down wait time ≈ Planned Access

1 Sv. = 10^2 rem : 1 μSv = 0.1 mrem.

Table 1

Detector radioactivation at the LHC and SSC under nominal operating conditions (6×10^8 interactions s^{-1} at the LHC, 10^8 s^{-1} at the SSC). Other machine assumptions may be found in RPP.[5] Following Stevenson[6] and Höfert,[7] we assume a 30-day irradiation time followed by a 1-day cooldown; these doses are smaller by factors of two or three than would be obtained with longer irradiations. For solid lead or iron at a depth z given in the table, the dose, in Sv hr^{-1}, is $B \cosh^{3+m} \eta / r^2$, where r is the total distance to the interaction point in meters. It is a surface dose; that is, half the dose experienced by a piece of scintillator buried in the absorber. For example: in one version of the SDC detector, the endcap starts 4.2 m from the IP. If a solid lead calorimeter section at $\eta = 3$ were cut open at a depth of 25 cm after the radiation history given above, the surface dose at would be

$$8.08 \times 10^{-8} \cosh^{3.672} 3.0 / 4.45^2 = 200\ \mu\text{Sv hr}^{-1}$$

Similarly, at $r = 18$ m and $\eta = 5$, the surface dose from a SSC iron calorimeter is 400 μSv hr^{-1}.

10^{33}

	Iron				Lead			
z (cm)	α	A	B_{LHC}	B_{SSC}	α	A	B_{LHC}	B_{SSC}
0–2	0.257	0.0708	3.65×10^{-5}	7.41×10^{-6}	0.264	0.0970	7.47×10^{-5}	1.52×10^{-5}
2–4	0.299	0.0899	4.52×10^{-5}	9.21×10^{-6}	0.352	0.1000	7.31×10^{-5}	1.50×10^{-5}
4–6	0.343	0.0985	4.83×10^{-5}	9.87×10^{-6}	0.409	0.0987	6.98×10^{-5}	1.43×10^{-5}
14–16	0.518	0.0913	4.03×10^{-5}	8.37×10^{-6}	0.557	0.0904	5.85×10^{-5}	1.22×10^{-5}
24–26	0.653	0.0663	2.70×10^{-5}	5.67×10^{-6}	0.675	0.0637	3.84×10^{-5}	8.08×10^{-6}
34–36	0.747	0.0459	1.77×10^{-5}	3.74×10^{-6}	0.783	0.0382	2.16×10^{-5}	4.58×10^{-6}
44–46	0.831	0.0305	1.12×10^{-5}	2.38×10^{-6}	0.865	0.0244	1.31×10^{-5}	2.80×10^{-6}
54–56	0.885	0.0209	7.42×10^{-6}	1.59×10^{-6}	0.932	0.0152	7.87×10^{-6}	1.89×10^{-6}
64–66	0.946	0.0135	4.62×10^{-6}	9.95×10^{-7}	1.009	0.0089	4.40×10^{-6}	9.53×10^{-7}
74–76	1.009	0.0084	2.75×10^{-6}	5.96×10^{-7}	1.076	0.0052	2.45×10^{-6}	5.33×10^{-7}
84–86	1.072	0.0051	1.61×10^{-6}	3.50×10^{-7}	1.132	0.0032	1.46×10^{-6}	3.20×10^{-7}
94–96	1.135	0.0031	9.38×10^{-7}	2.05×10^{-7}	1.217	0.0016	6.77×10^{-7}	1.49×10^{-7}

6. References

1. "Report of the Task Force on Radiation Levels in the SSC Interaction Regions," ed. by D. E. Groom, SSC Central Design Group Report SSC-SR-1033 (June 1988).
2. A. Ferrari, A. King, and G. R. Stevenson, oral tradition (1991).
3. D. E. Groom, in *Proc. of the Workshop on Calorimetry for the Superconducting Super Collider*, Tuscaloosa, Alabama, 13–17 March 1989, ed. R. Donaldson and M. G. D. Gilchriese, World Scientific (June 1990), pp. 59–75.
4. T. A. Gabriel and R. T. Santoro, Particle Accelerators 4, 169-186 (1973).
5. T. A. Gabriel, Nucl. Instrum. Meth. 91, 67-72 (1971).
6. G. R. Stevenson, CERN Divisional Report TIS-RP/90-18/CF; also published in *Proc. of the ECFA Large Hadron Collider Workshop*, Aachen (4–9 October 1990), CERN 90-10 (1990).
7. M. Höfart and A. Bonifas, *Measurement of Radiation Parameters for the Prediction of Dose Rates from Induced Radioactivity*, CERN Divisional Report TIS/RP/90-10/CD (1990).
8. Particle Data Group, J. Hernández *et al.*, Phys. Lett. B239, 1 (1990), p. III.25; see also the erratum.

2. FCal PERFORMANCE REQUIREMENTS

- Physics drivers:
  - + Jet tagging (Einsweiler)----->>>>>>>
  - + Missing Et (Barnett)----->>>>>>>>
  - + Geant shower studies (Hauptman)----->>>>>>
  - + Trigger expectations of FCal (All)
    - -Smooth transition of lateral seg into Endcap
    - -Reasonable time shaping (see speed, below)
- Radiation Resistance
  - + Survival strategy (eta depend.) to be designed in.
  - + Same for the recycling and disposal of sampling medium and (eventually) absorber.

FCal PERFORMANCE REQUIREMENTS (continued)

- Rate/Speed/Pileup
  - + No special problem for FCal, (dN/deta=const.) except in that the lateral segmentation
    - -is made coarser by factor of 2*2 to 4*4
    - -can be further compromised by moving in too close.
  - + Signal duration should be less than or equal to the time for a shower to build up and decay in the calorimeter (typically 10 to 60 nanosec),
  - + Signal rise time << 16ns

FCal PERFORMANCE REQUIREMENTS (continued)

- Eta coverage (Detector range = fiducial range + 1 lambda)
  - + A function of integrated luminosity. Fiducial range 3.0 < eta < 5.0 at startup. As low mass high crossection physics is cleaned up, retreat gracefully to 3.0 < eta < 4.0
  - + Detector range at startup: 2.5 < eta < 6.0
  - + At high Luminosity (later): 2.5 < eta < 4.5
- Energy resolution
  - + High Et jets have very high energy. The missing Et measurement needs sigma(E)=10% at 1 TeV, ie insensitive to the stochastic term.
  - + Quadrature sum of energy independent contributions to sigma(E) due to tower-to-tower and segment-to-segment fluctuations to be kept below 10%. Requires good maintenance of (inter) calibration in the face of the severe FCal radiation environment.
  - + Hermeticity and adequate depth (see below) is required to avoid non gaussian tails.

- Eta/phi segmentation
  - +There are two segmentation drivers:
    - -trigger--->smooth transition to ECal segments.
    - -jet recognition: needed in the missing Et cut strategy, and of course to find forward jets associated with WW/ZZ fusion -->Higgs
  - +This requires deta*dphi=0.2*0.2 at eta=3.0, relaxing to 0.4*0.4 at eta=5.0
  - +dphi=0.2 (0.4) means 32 (16) phi bins.
- Depth, compartments in depth.
  - + Depth specification requires much further study of showers in the tail of the response distribution (slow work).
  - + Default position is 10 lambda (2.5 meters in Z), with a HAC2 segment.
  - + The 10% constant term requirement on sigma(E) may require an electromagnetic compartment (but with hadronic lateral segmentation). This would be technology dependent.

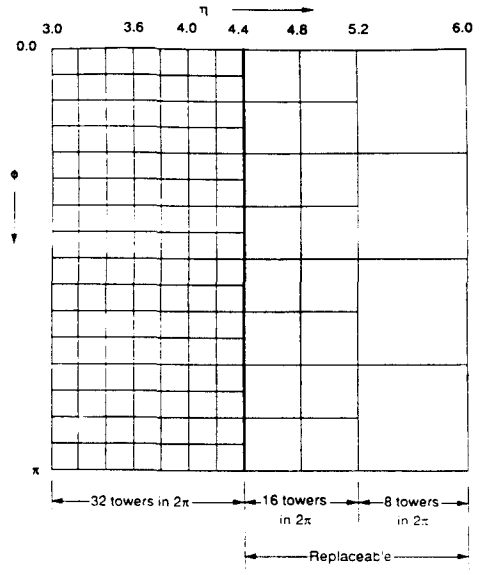

Cross section of towers at z = 16 meters

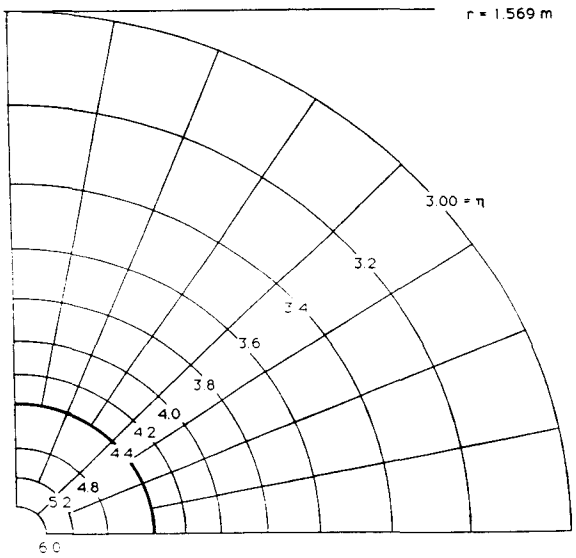

3. INTEGRATION/SSCINTERFACE ASPECTS

- The Endcap/FCal interface
- FMuon space
- SSC machine elements (Q1+energy shield, etc.)
- Radioactivation and access

Geometry/Integration Frisken/Wenzel

Figure 1. shows the LOI description of FCal (no input from any FCal proponent. Not shown is that the part nearest the beam centerline could be replaceable.

Note expanded lateral scale in Wenzel sketches.

Figures 2,3. The region with eta<4 could be closer to the IP.

- •smoother transition to Endcap Calorimeter
- •better FMuon space/shielding
- •lower (half) total mass.
- •all of the above become stronger as the high eta part is moved away from the IP, toward higher Z.
- •Grazing incidence of showers (feared to lead to "counter Et" (energy reflected to opposite phi) was studied. Non problem (Hauptman)

Figures 4,5,6. Variations on the preferred Forward Cone geometry. The stepped ("Aztec") cones shown here are a particufarly good match to the semiprojective geometry concept. This segmentation can be projective in phi, and box-wise projective in eta. It gives a large saving in parts inventory, and makes a particularly smooth match to the Endcap Calorimeter. Needless to say, cost considerations would speak MUCH more loudly for use of this concept in the Endcap calorimeter.

Notice that "semiprojective geometry" in the Endcap would NOT imply more longitudinal compartments, thanks to the flexibility offered by the tile/fibre readout scheme.

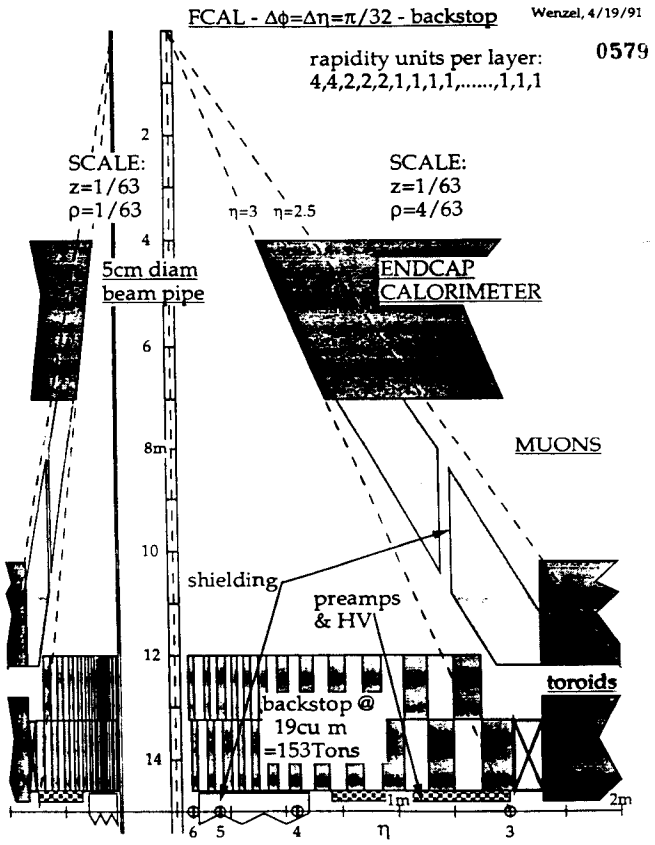

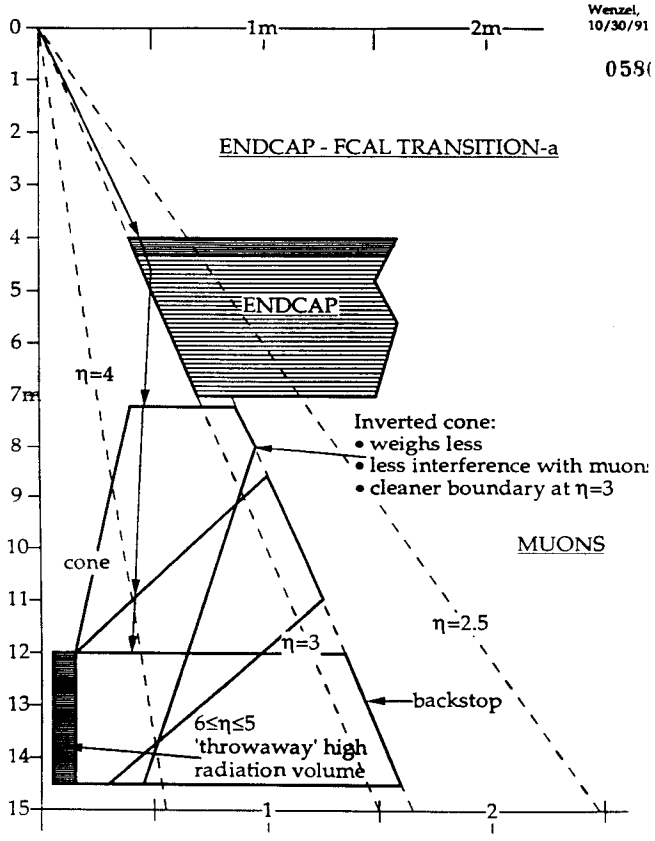

FCAL - $\Delta\phi=\Delta\eta=\Delta\rho/\rho=\Delta z/z=\pi/32$ - integrated cone Wenzel, 5/10/91

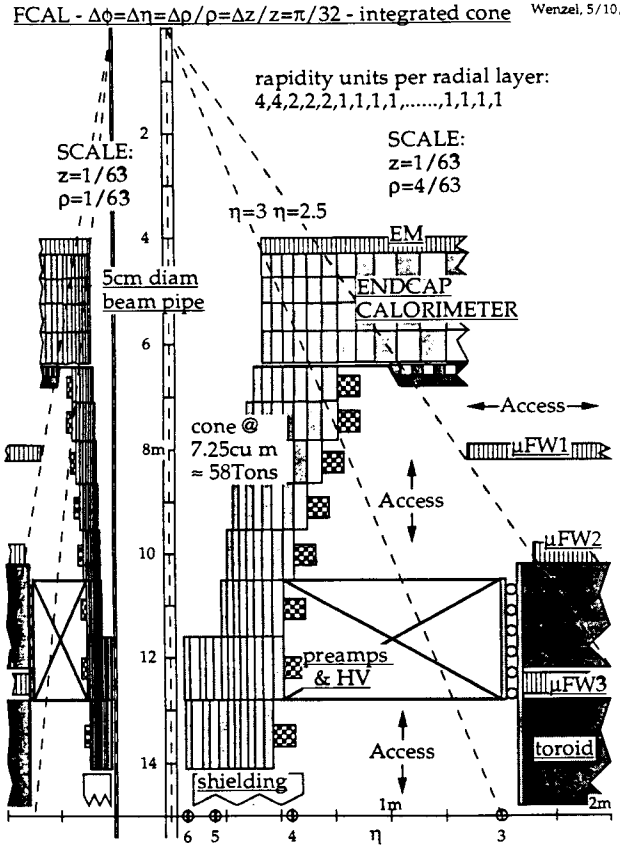

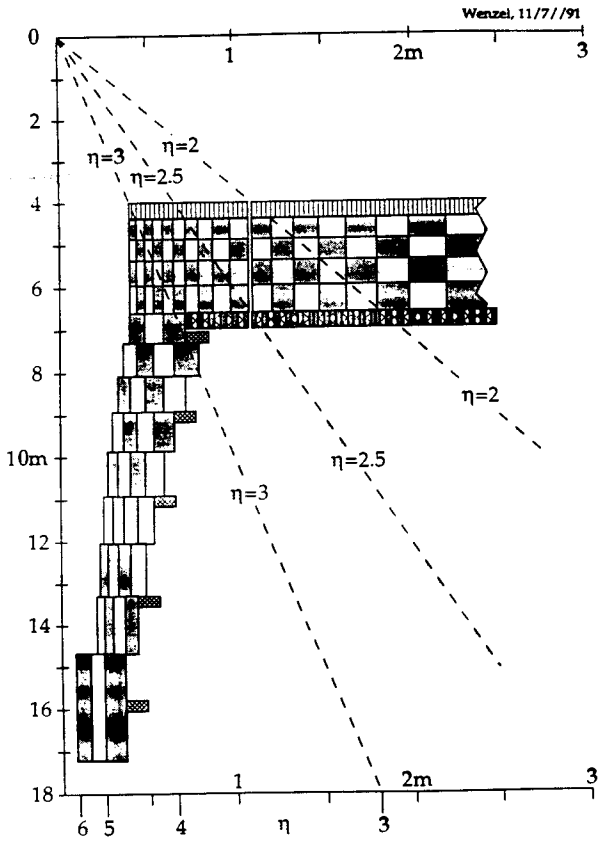

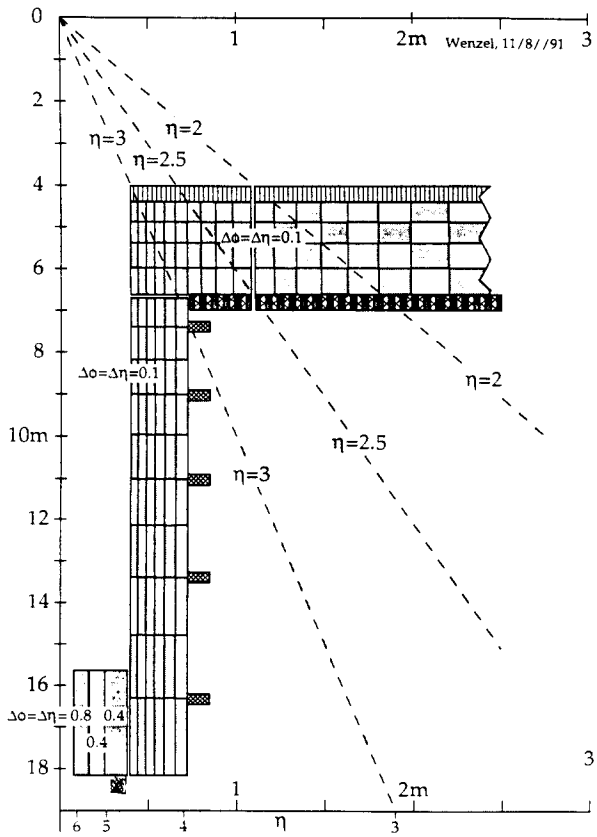

9. R&D Plans **Frisken et al.**

• Short term needs---> February 92

High Pressure Gas. **$78.76K**

build 4 protoype modules
perform mechanical, electrical testing
continue radiation damage testing

Warm Liquid Ionization **$18K**

assemble hadron swimming pool prototypes irradiate same (intense Co60), measure degredation of lifetimes, repurify, refill, remeasure lifetimes.

Liquid Scintillator Spaghetti **$35K**

Study (Co60) radiation damage to liquids, glass, liquids in glass, and liquids in glass in absorber. Finish current test beam program, make detailed camparison with Geant simulations. Extend Pb casting technology to 2-3 meter long modules.

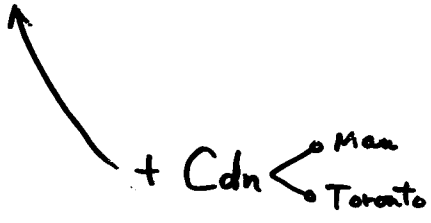

• Longer term-----> end of FY92

High Pressure Gas. $50K

Finish enough modules for a 40*40*300 cm**3 em/hadronic prototype array. (Operating funds to test this array have ~~been applied~~ for to TNRLC).

Warm Liquid Ionization $150K

Design and construct and fill a large FCal prototype, tailored to the new FCal specifications. Beam test costs are unknown (because of test site uncertainty) and not included.

Liquid Scintillator Spaghetti $50K

Engineer and build a large hadronic prototype. Study the light collection problem, More extensive investigation of liquid fibers (rad damage, attenuation, etc).

Frisken@SSCL, 11/11/91

Summary of FCal PERFORMANCE REQUIREMENTS

• Radiation Survival Strategy (strongly eta dependent):

recycling and disposal of sampling medium and (eventually) absorber to be designed in to cope with potential lifetime doses up to 10's of Gigarads.

• Rate/Speed/Pileup:

keep back, so lat seg = shower size

signal duration = shower decay time

rise time << 16ns

• Eta coverage (fiducial range = detector range - 1 lambda)

Detector range at startup: 2.5 < eta < 6.0

At high Luminosity (later): 2.5 < eta < 4.5

• Energy resolution

<10% at 1TeV

Watch the tails

Frisken@SSCL, 11/11/91

• Eta/phi segmentation

+deta*dphi=0.2*0.2 at eta=3.0, relaxing to 0.4*0.4 at eta=5.0

+dphi=0.2 (0.4) means 32 (16) phi bins.

• Depth, compartments in depth.

+ Default position is 10 lambda (2.5 meters in Z), with (EM) HAC1 and HAC2 segments.

Impact of EM Calorimeter Thickness on Resolution

C. Hearty(LBL)

Impact of EM Calorimeter Thickness on Resolution

Christopher Hearty
LBL

SDC Collaboration Meeting, SSCL
Nov. 15, 1991

Leakage from EM calorimeter worsens resolution.

Size of effect depends on
- EM calorimeter thickness
- design of first hadronic section (HAC1)

Details of EM section are less important.

Study with EGS, 10--400 GeV e-

==========

Why not have a very thick EM section?

- π conversions ==> poorer e/π separation (recover with EM2/EM1 ratio?)
- extra cost

How thin can EM section be for a desired precision?

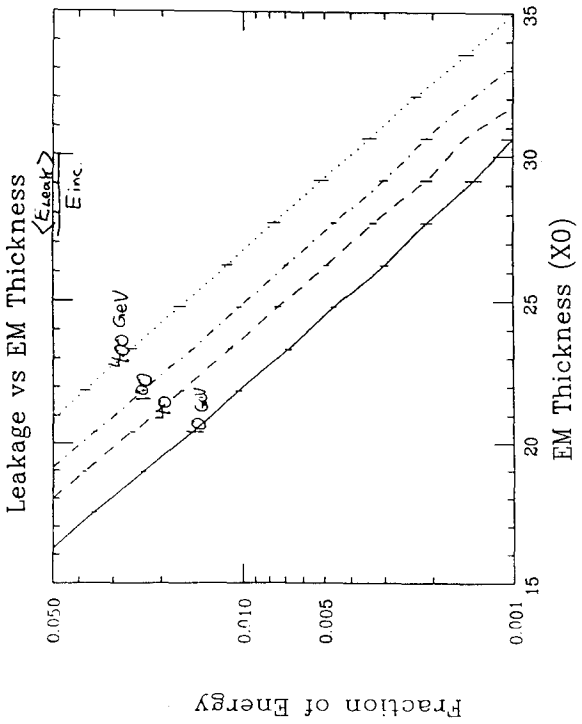

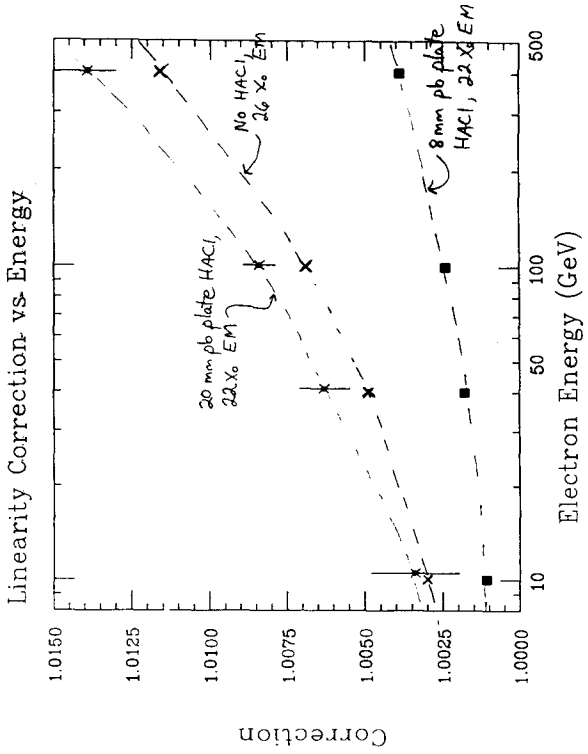

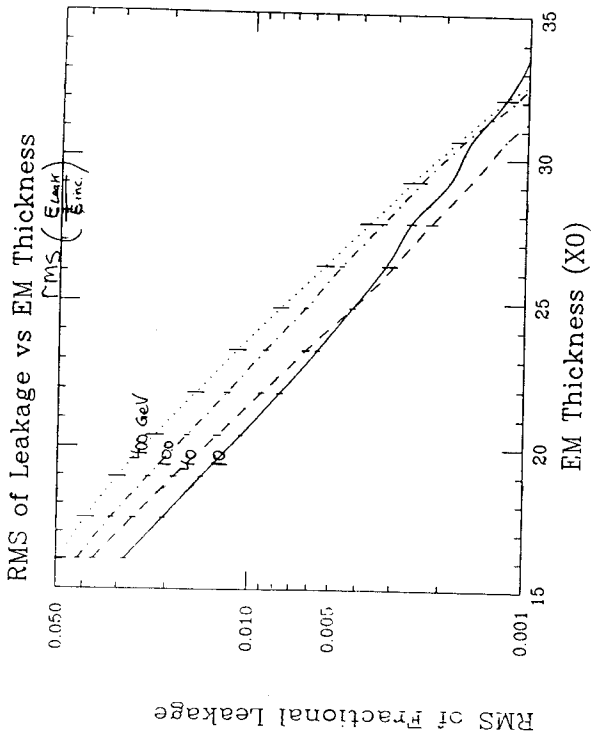

EGS Model

- 70 layers of 4mm lead + 4mm LAr (51 X0 total)
- EM section is first 22-48 layers (16-35 X0), HAC1 is the rest.
- five HAC1 variations considered:
  - no HAC1
  - 8, 16, 20 or 32mm lead sampling (use every nth LAr gap, weight energy with value n, for n = 2, 4, 5, or 8)

Weighting EM2 or HAC1 differently does not improve resolution significantly.

Application to SDC

Three calorimeters under consideration:

LAr: 26 X0 EM, 14mm pb sampling HAC1

Scintillator Model A:
barrel: 1 inch Fe HAC1 (~8mm pb)
endcap: 2 inch Fe HAC1 (~16mm pb)

Scintillator Model B:
barrel: 20mm pb HAC1
endcap: 32mm pb HAC1

Scintillator EM sections are 22X0 in all cases.

LAr HAC1 noise ≈560 MeV in 0.1 by 0.1 cell
==> do not use HAC1 to measure e- energy.

HAC1 of scintillator calorimeter ≈ noiseless.

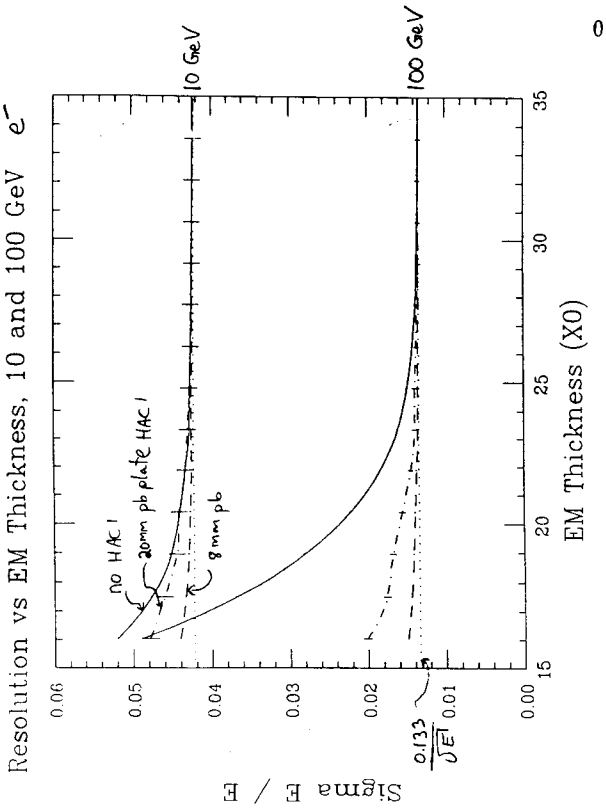

Degradation of Resolution

$\alpha \equiv \sigma_E / E_{inc}$

$\alpha_0 \equiv \sigma_E / E_{inc}$ for 51X0 EM section

$\Delta\alpha \equiv \sqrt{\alpha^{**}2 - \alpha_0^{**}2}$ quadratic increase in resolution

If HAC1 is not used, $\Delta\alpha \approx \text{rms}(E_{leak}) / E_{inc}$

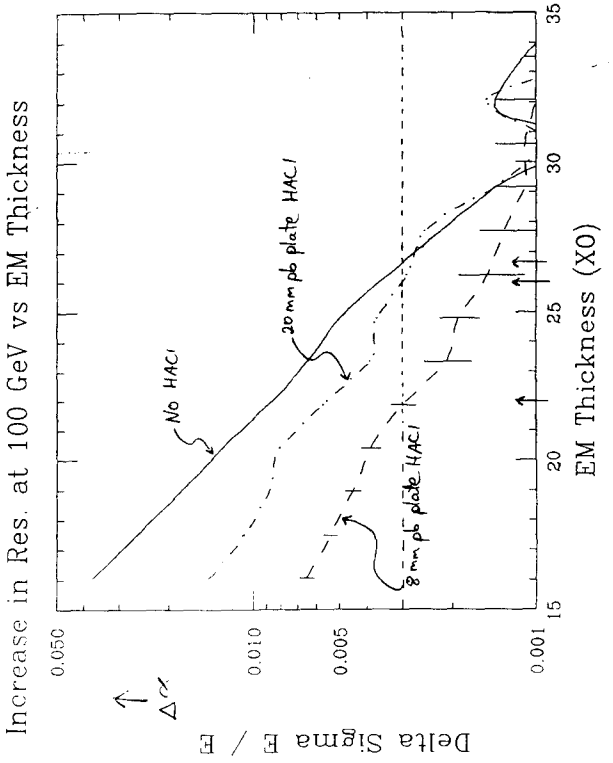

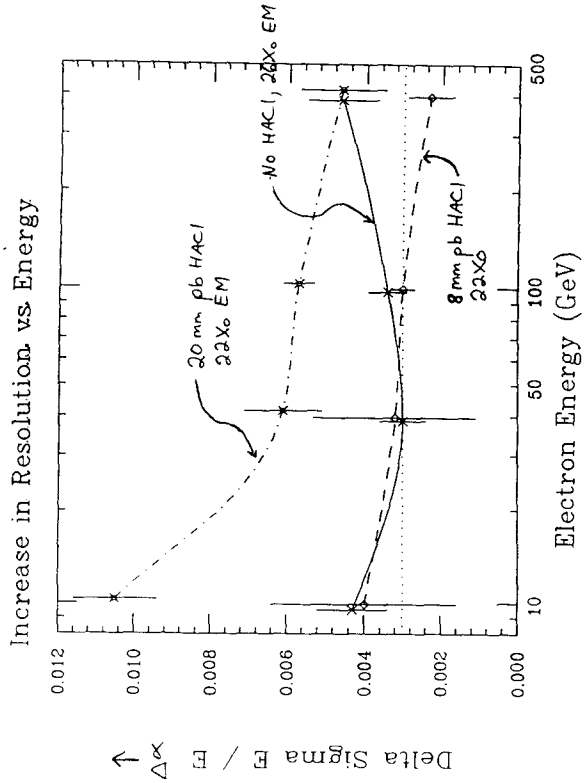

Boxes enclose three proposed SDC barrel calorimeter cases

Table 1. Increase in resolution (σ_E/E) as a function of EM calorimeter thickness, for various incident electron energies and five different HAD1 sections.

HAD1 Config	E (GeV)	EM Thickness (X_0) 20.4	21.9	23.3	24.8	26.2	LAr 27.7	29.2	30.6
No HAD1	10	.0117 ± .0012	.0088 ± .0011	.0081 ± .0010	.0053 ± .0009	.0043 ± .0009	.0038 ± .0007	.0034 ± .0006	.0028 ± .0006
	40	.0120 ± .0008	.0094 ± .0008	.0067 ± .0007	.0046 ± .0008	.0030 ± .0006	.0021 ± .0006	.0017 ± .0006	.0010 ± .0011
	100	.0130 ± .0005	.0089 ± .0004	.0065 ± .0004	.0050 ± .0005	.0034 ± .0005	.0022 ± .0004	.0014 ± .0004	.0007 ± .0016
	400	.0205 ± .0910	.0139 ± .0000	.0094 ± .0008	.0071 ± .0007	.0046 ± .0009	.0031 ± .0008	.0019 ± .0010	.0005 ± .0008
Model A barrel	10	.0052 ± .0015	.0040 ± .0024	.0032 ± .0018	.0031 ± .0010	.0019 ± .0015	.0018 ± .0009	.0010 ± .0021	.0010 ± .0015
8 mm	40	.0048 ± .0008	.0032 ± .0021	.0022 ± .0010	.0013 ± .0010	.0001 ± .0010	.0001 ± .0010	.0001 ± .0010	.0001 ± .0010
	100	.0039 ± .0003	.0030 ± .0003	.0021 ± .0004	.0019 ± .0003	.0016 ± .0004	.0013 ± .0003	.0011 ± .0003	.0011 ± .0003
	400	.0027 ± .0008	.0022 ± .0008	.0018 ± .0007	.0011 ± .0008	.0011 ± .0006	.0001 ± .0010	.0007 ± .0010	.0003 ± .0004
	10	.0090 ± .0016	.0068 ± .0013	.0064 ± .0015	.0071 ± .0011	.0041 ± .0014	.0031 ± .0010	.0022 ± .0010	.0001 ± .0004
16 mm	40	.0071 ± .0009	.0054 ± .0009	.0041 ± .0011	.0036 ± .0009	.0019 ± .0010	.0013 ± .0014	.0014 ± .0008	.0010 ± .0006
	100	.0071 ± .0003	.0049 ± .0005	.0044 ± .0004	.0025 ± .0004	.0029 ± .0003	.0012 ± .0008	.0023 ± .0003	.0007 ± .0010
	400	.0061 ± .0007	.0046 ± .0008	.0022 ± .0009	.0029 ± .0008	.0001 ± .0072	.0010 ± .0006	.0000 ± .0008	.0004 ± .0004
	10	.0121 ± .0011	.0105 ± .0011	.0071 ± .0011	.0085 ± .0013	.0070 ± .0009	.0040 ± .0013	.0024 ± .0009	.0001 ± .0006
20 mm	40	.0086 ± .0009	.0061 ± .0010	.0055 ± .0008	.0049 ± .0007	.0028 ± .0007	.0032 ± .0006	.0023 ± .0005	.0017 ± .0007
Model B barrel	100	.0081 ± .0004	.0057 ± .0004	.0039 ± .0004	.0037 ± .0004	.0029 ± .0005	.0025 ± .0003	.0014 ± .0006	.0009 ± .0006
	400	.0060 ± .0008	.0046 ± .0011	.0041 ± .0008	.0029 ± .0007	.0001 ± .0011	.0001 ± .0010	.0014 ± .0007	.0012 ± .0007
	10	.0152 ± .0015	.0117 ± .0014	.0075 ± .0011	.0056 ± .0009	.0079 ± .0010	.0049 ± .0007	.0013 ± .0006	.0065 ± .0006
32 mm	40	.0100 ± .0009	.0089 ± .0010	.0060 ± .0008	.0043 ± .0008	.0038 ± .0007	.0029 ± .0006	.0017 ± .0010	.0007 ± .0008
	100	.0095 ± .0004	.0074 ± .0004	.0058 ± .0004	.0038 ± .0005	.0038 ± .0004	.0027 ± .0005	.0027 ± .0003	.0011 ± .0010
	400	.0114 ± .0007	.0084 ± .0008	.0054 ± .0008	.0042 ± .0009	.0027 ± .0007	.0013 ± .0008	.0001 ± .0016	.0011 ± .0004

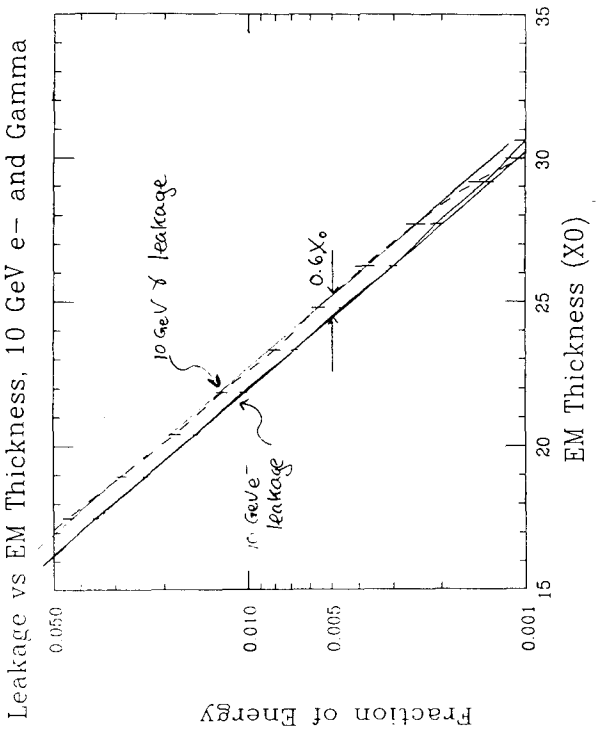

Conclusions

- nonlinearity due to leakage is small and correctable

- Thickness (X0) required for increase in resolution to be less than:

Case		$\Delta\alpha$=0.003	$\Delta\alpha$=0.005
LAr (barrel & endcap) (HAC1 not used)		28	26
Model A	barrel (≈8mm pb)	22	20
	endcap (≈16mm pb)	25	22
Model B	barrel (20mm pb)	26	23
	endcap (32mm pb)	28	24

Table is applicable to more than just SDC.

- Photons require slightly thicker EM calorimeter.

ELECTRONICS

(PARTIAL)

WEDNESDAY, NOVEMBER 13

Options for Electronic Location Inside and Outside the SDC	C. Bebek(LBL)
Detector Layouts with Various Electronic Layouts and Placement	T. Thurston(SSCL)

THURSDAY, NOVEMBER 14

Silicon Strip Front End Electronics	H. Sadrozinski(UC/SC)
Muon Front End Analog Electronics (See paper under MUON SYSTEM)	J. Oliver(Harvard)
1st and 2nd Level Muon Triggers Based on the Jet Chamber System (See paper under MUON SYSTEM)	H. Sakamoto(KEK)

FRIDAY, NOVEMBER 15

Data Acquisition Status Report and Discussion of Sub-Detector Crates	E. Barsotti(FNAL)
SDC Second Level Trigger Using ASP	J. Brisson(CEN Saclay)
Report on Location of Electronics Inside or Outside Muon Steel	Electronics Working Group
Technical Assessment of the Electronics for the Central Tracking Options	Electronics Working Group

LPBautz:12/13/91

Options for Electronic Location Inside and Outside the SDC

C. Bebek(LBL)

0605

Why are we here?

Tech. Board meets Saturday to decide access space.

Issue drivers: management's view

- #1 ΦM/m radius
- # 2M/m length
- we own a gallery

Options

	ΔR
• Calor. mounted crates	1.6 m
• Crates in racks inside	1.2/1.5m straw/sci.fi
• Crates in racks outside	1.1 m
• No crates	1.3 m

Note: minimum ΔR is determined by calor support structure

0606

Calor. mounted crates

Institutionalized

- Front end design work has assumed this in many ways

Problems

- Access to PMTs & FE cards
- Safety
- VLPC population explosion

0607

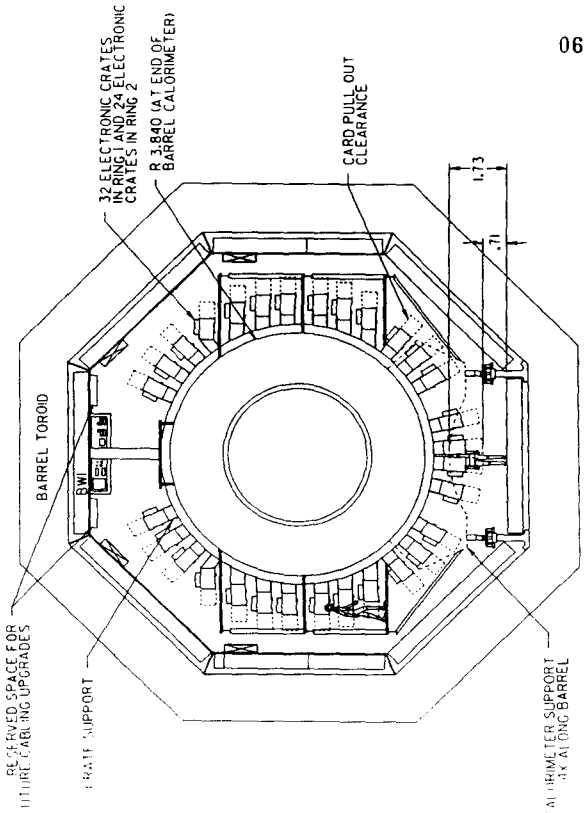

0608

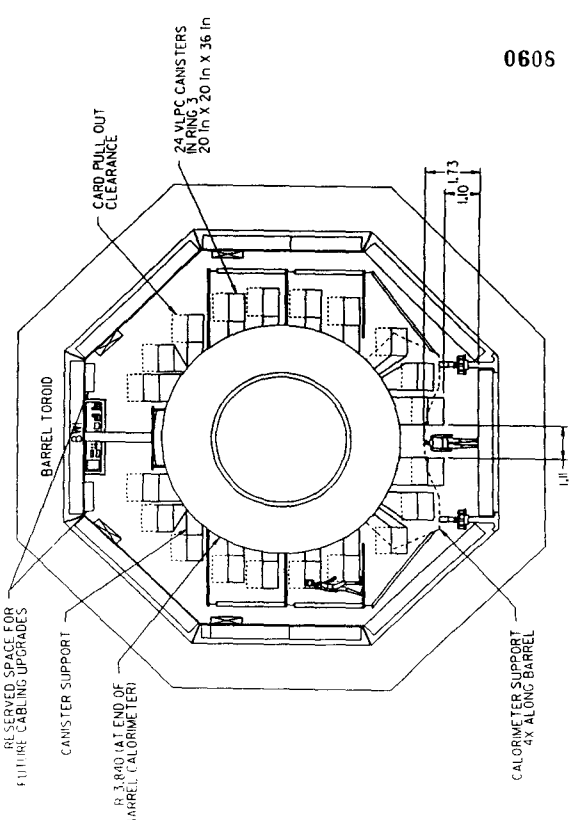

Crates in racks inside

0609

Insight was to use a common space for PMT access and FE card extraction

Pluses

- access (personel)
- safety
- cluster utilities (AC, H_2O...)
- PMT maintainance (VLPCs)
- FE card/crate/ps removal

Minuses

- cable costs – longer cables (7-10m)
- different signal technology

VLPC	50mV single ended
FADC	low level single ended (?)
SCA	1mV to 5V analog
Stevens	need a way station for power distribution

0610

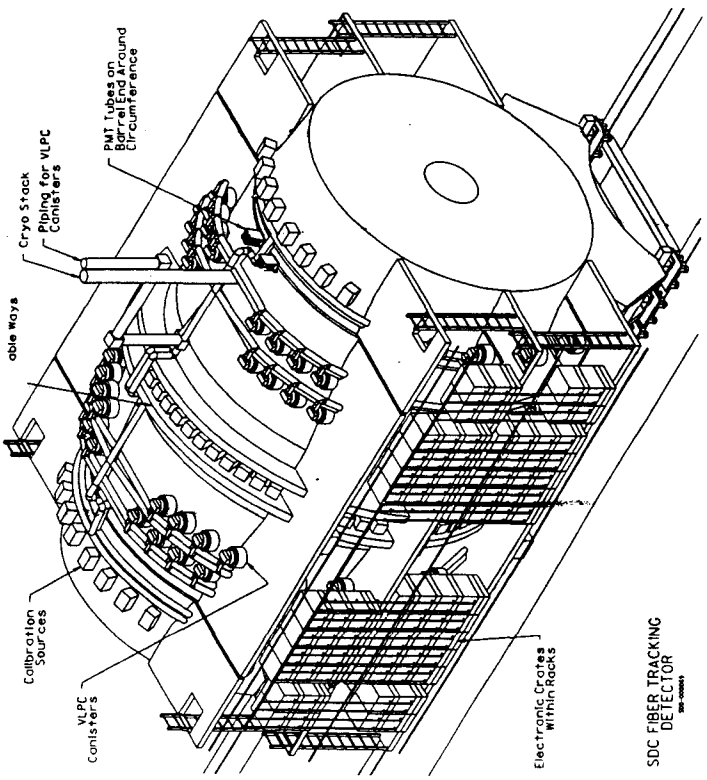

0611

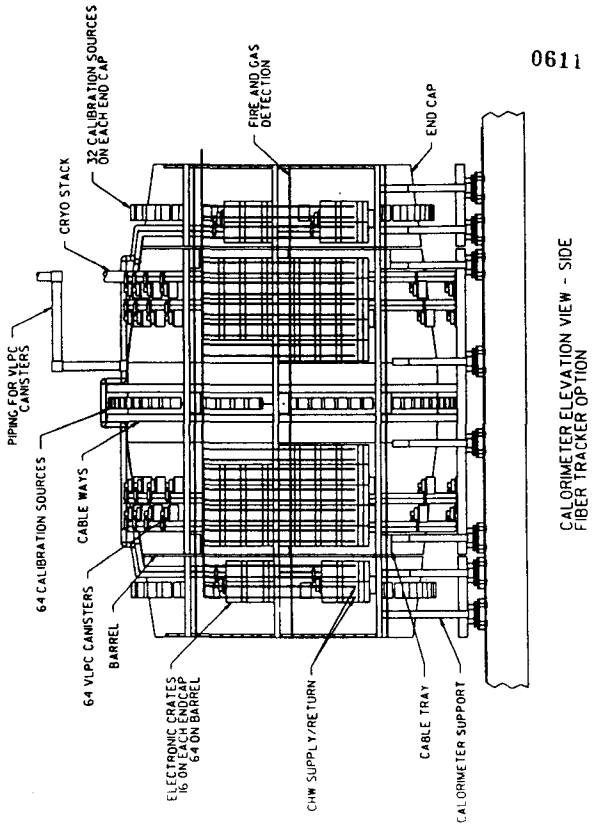

0612

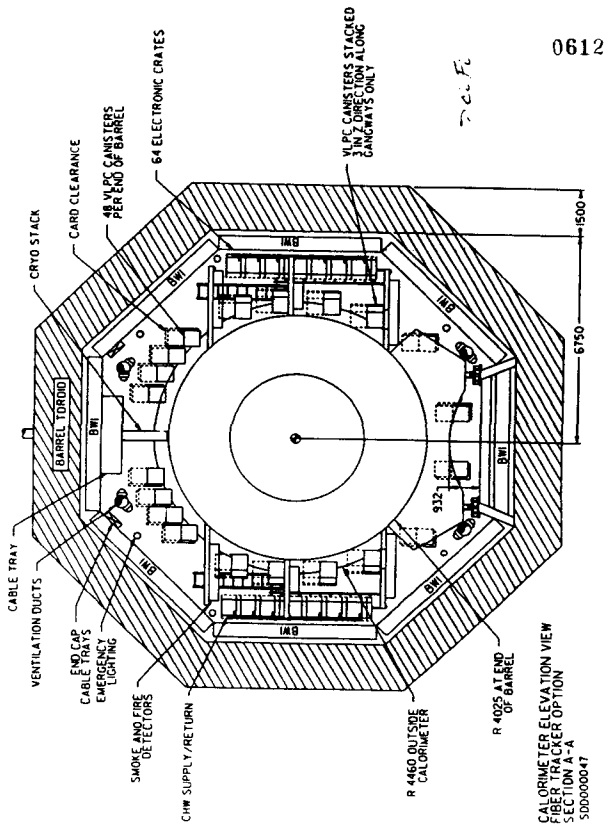

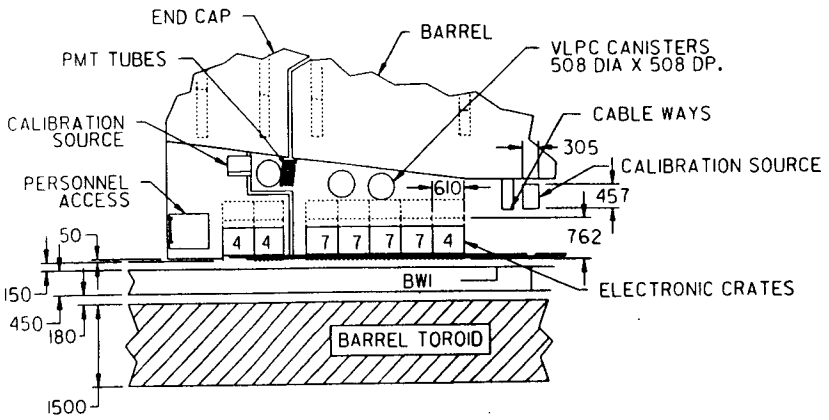

CALORIMETER - DETAIL B
FIBER TRACKER OPTION

SDD000064

0615

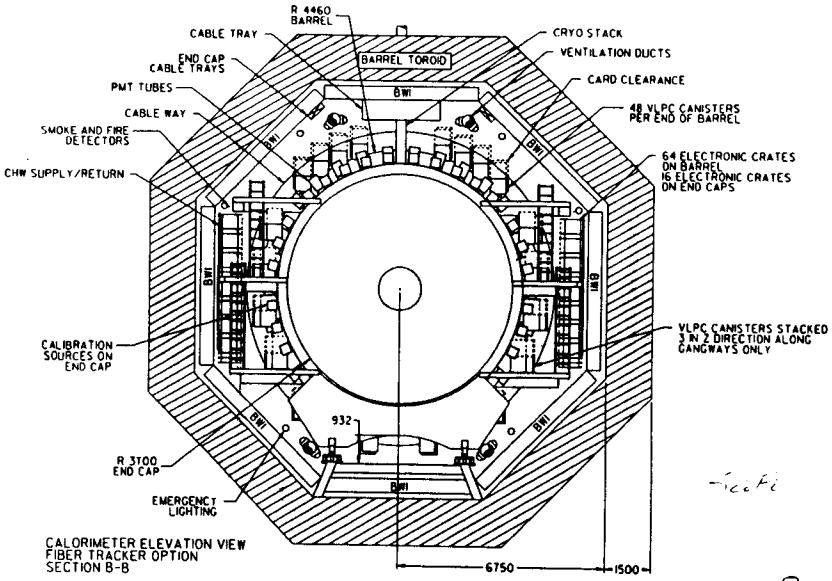

CALORIMETER ELEVATION VIEW
FIBER TRACKER OPTION
SECTION B-B

SDD000063

0613

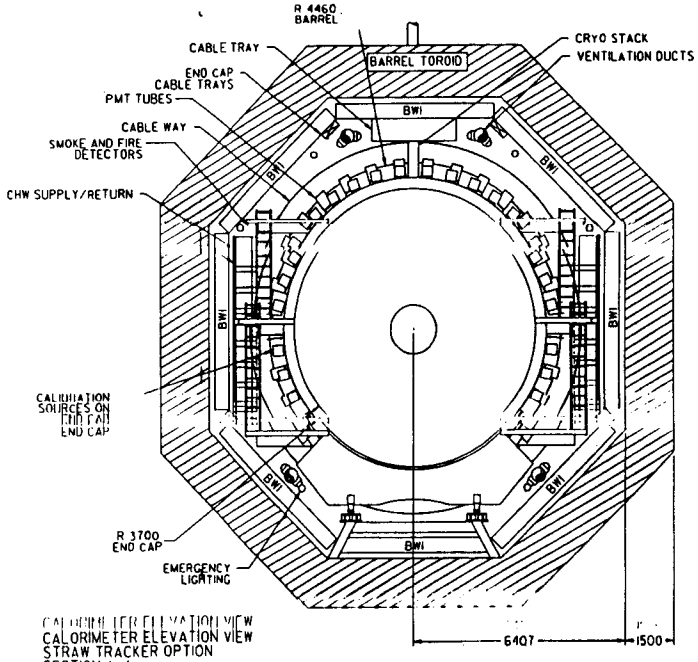

CALORIMETER ELEVATION VIEW
STRAW TRACKER OPTION
SECTION A-A

SDDDD0067

0616

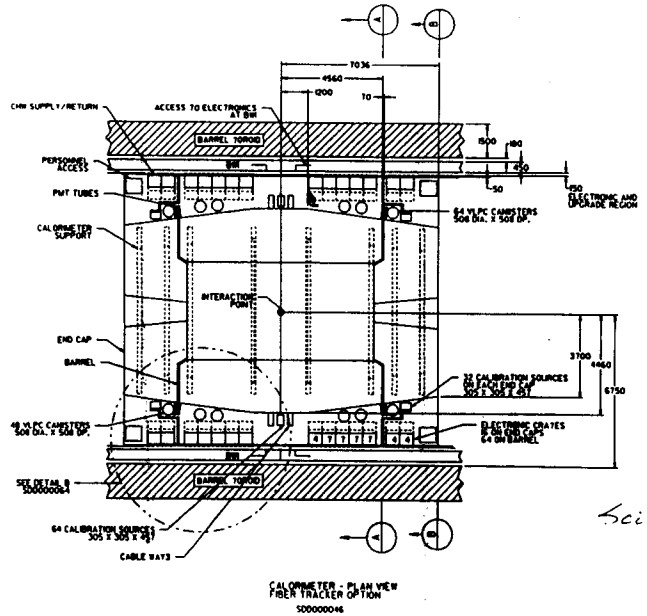

CALORIMETER - PLAN VIEW
FIBER TRACKER OPTION

SDD000046

0614

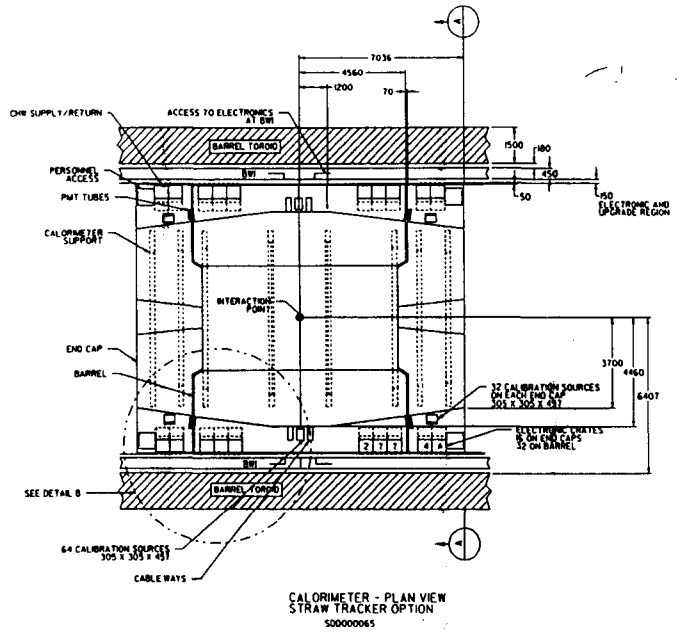

CALORIMETER - PLAN VIEW
STRAW TRACKER OPTION
SDD000065

0617

Cables in racks outside

Possible destinations are IW3 and gallery

Pluses

- same as "inside"
- room better access

Minuses

- same as "inside" but worse
- holes in muon iron for cables
- axial
- gyrostack
- cable lengths
- 30m to IW3
- 40m to gallery via gyrostack

Observation

Increased cable costs can offset some or all of muon iron savings

0619

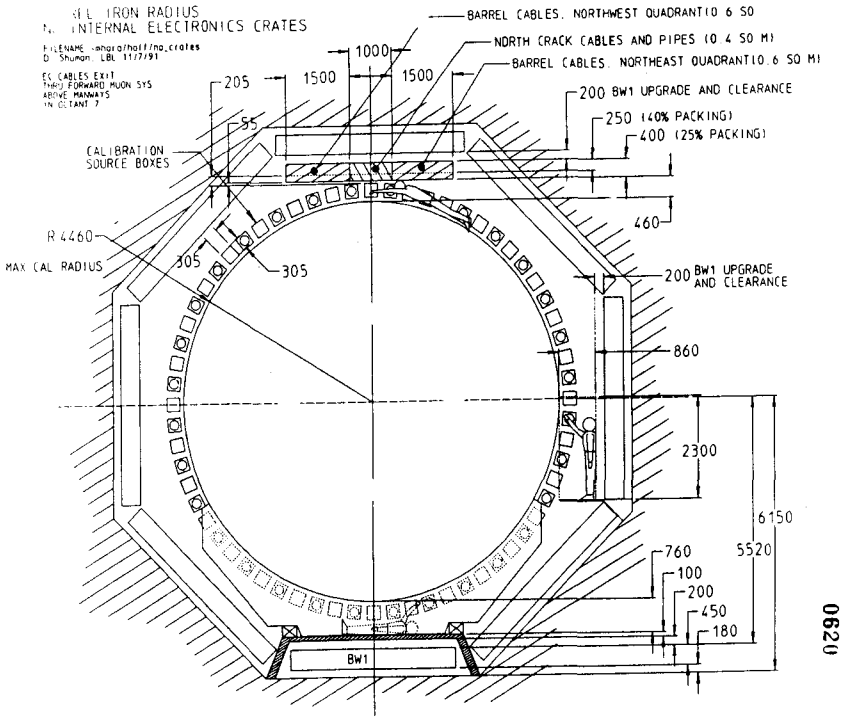

0620

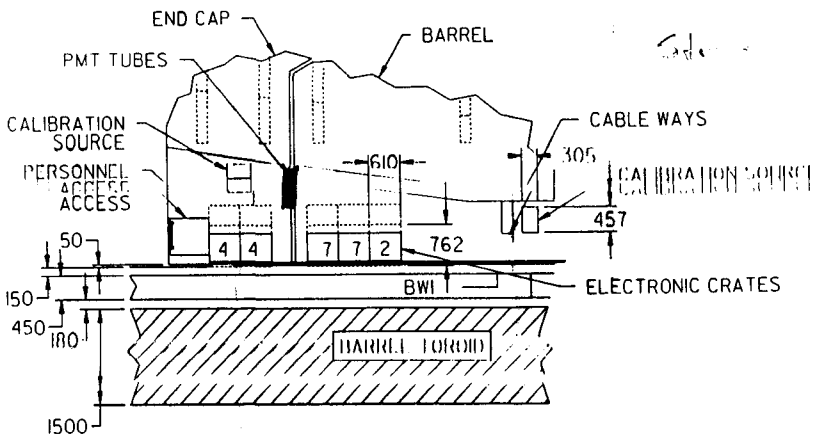

CALORIMETER - DETAIL B
STRAW TRACKER OPTION
SDD000066

0618

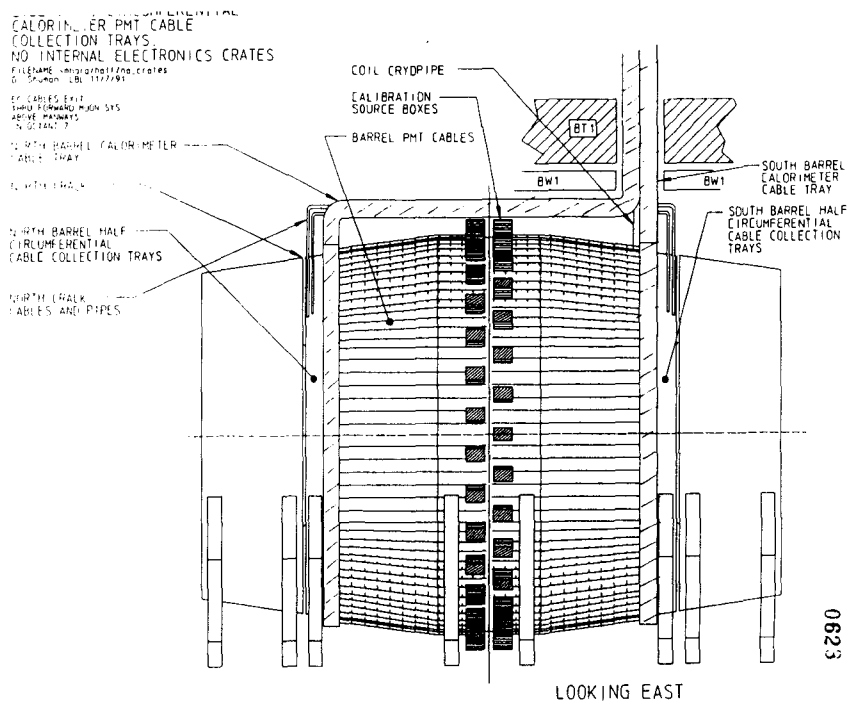

0623

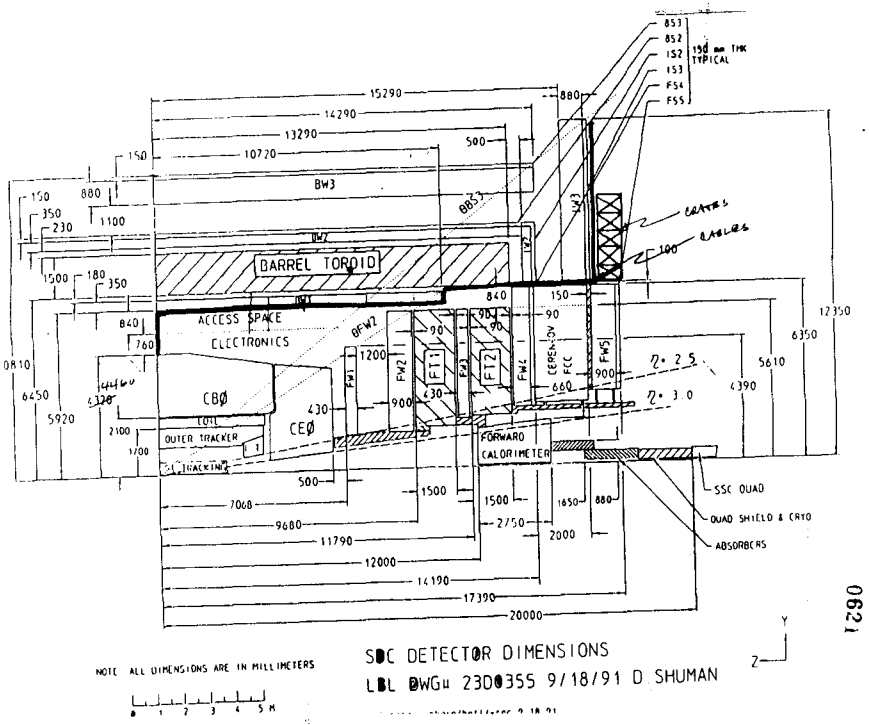

0621

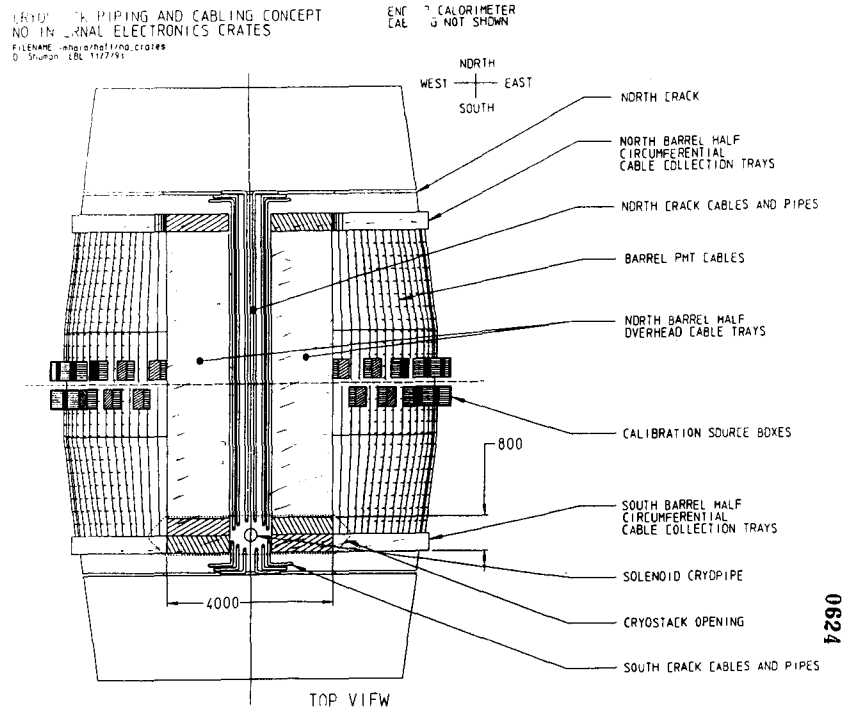

0624

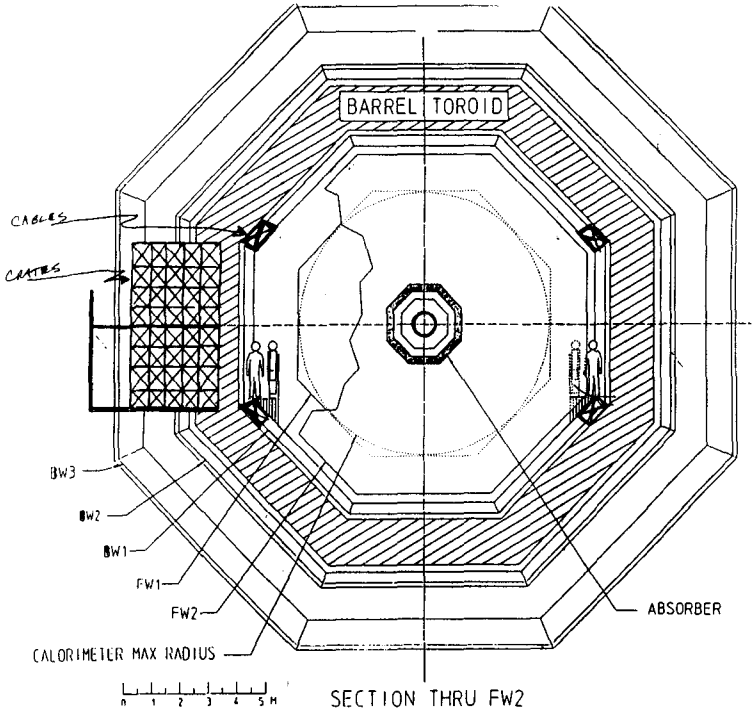

0622

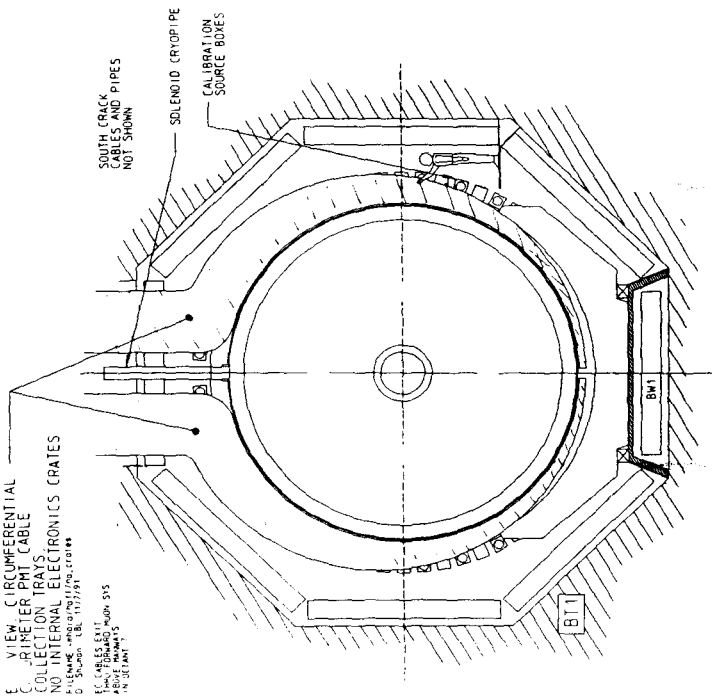

Summary

	$M to IW3	$M to gallery	σ (m²) small cable	σ (m²) large cable
Straw[1]	0.21	0.28	0.04	-
Straw[2]	0.28	0.37	0.11	0.44
SciFi	1.00	1.30	0.50	2.00
Cal FADC	2.50	3.30	0.80	3.20
Cal SCA	2.80	3.60	0.40	1.40
SM FADC[3]	0.13	0.16	0.04	0.16
SM FADC[4]	8.00	10.60	2.60	10.20
SM SCA	4.50	6.00	0.70	2.30

[1] One cable for 200 detector elements.
[2] One cable for 50 detector elements.
[3] One cable for 64 detector elements.
[4] One cable for each detector element.

Crates as tiles

De-institutionalize crate based FEs

Planar electronics

Calor example

- Natural unit is PMT cluster shadowed by HAC2
- Radially mount PMTs on parent board w/ HV, FE, DAQ, trigger, and timing
- Small networks for DAQ & timing OR point-to-point.

Pluses

- Eliminate Cu cable plant
- Maintain locality & use less space

Minuses

- Fine grain distribution of:
  - timing
  - DAQ
  - slow control
  - power
  - cooling

Detector Layouts with Various Electronic Layouts and Placement

T. Thurston(SSCL)

Detector Layouts With Various Electronic Layouts and Placements

Option 1: Distributed Electronics Around Barrel

Option 2a: Fiber Tracker Option with Electronics Inside Detector Volume offset to the side in racks

Option 2b: Fiber Tracker Option with Electronics Inside Detector Volume offset to the side in racks

Option 3: All Electronics Outside of Detector Volume

Distributed Electronics Around Calorimeter Barrel

SDC Integration — SSCL Mechanical Integration
Dimensions of Detector — 11/13/91
(Distributed Electronics)
Tables are based on LBL drawing #23D0375, 9/30/91, SDC Detector Dimensions
Fixed Values are in bold type. Computed values are in plain type.

Forward Assy Z Dimensions			**Barrel / Intermediate Z Demensions**			
Description	Delta Z	Boundry Z	Description	Delta Z	Boundry Z	Remarks
Interaction Point	**0**		Interaction Point		0	
		0				
Calorim Length	**6,560**					
		6560				
Electron Space	**500**					
		7060				
FW1	**430**					
		7490				
Clearr	**1,200**					
		8690				
FW2	**900**					
		9590				
Clear & FT1 Coil	**90**					
		9680				
FT1 Steel	**1,500**					
		11180				
Clear & FT1 Coil	**90**		BW1		10,625	Some Octants Are Short
		11270				
FW3	**430**		BW2 & BS2		13,790	
		11700				
Clear & FT2 Coil	**90**		BW3 & BS3		14,290	
		11790				
FT2 Steel	**1,500**		BT1	**13,290**		Z of FT2
		13290			13,290	
Clear & FT2 Coil	**90**		Space	**500**		
		13380			13,790	
FW4	**660**		IW2	**350**		
		14040			14,140	
FS4	**150**		IS2	**150**		
		14190			14,290	
FCC (Cerenkov)	**2,000**		Entry Access	**1,000**		
		16190			15,290	
FW5 Support	**150**		IW3	**880**		
		16340			16,170	
FW5	**900**		IS3	**150**		
		17240			16,320	
FS5	**150**					
		17390				

SDC Integration — SSCL Mechanical Integration
Dimensions of Detector — 11/13/91
(Distributed Electronics)
Tables are based on LBL drawing #23D0375, 9/30/91, SDC Detector Dimensions
Fixed Values are in bold type. Computed values are in plain type.

Barrel R Dimensions			**Forward System R Dimensions**		
Description	Delta R	Boundry R	Description	Boundry R	R is Calculated As A Function Of:
Interaction Point	**0**				
		0	***Inside Radius of:***		
Tracker	**1,675**		FW1	1,248	ETA = 3.0, Z of FW1, +550
		1,675	FW2	1,485	ETA = 2.5, Z of FW2, -100
Space	**25**		FT1	1,748	ETA = 2.5, Z of FT1, -100
		1,700	FW3	1,834	ETA = 2.5, Z of FW3, -100
Cryostat	**350**		FT2	2,097	ETA = 2.5, Z of FT2, -100
		2,050	FW4 & FS4	2,221	ETA = 2.5, Z of FW4, -100
Space	**50**		FCC	2,576	ETA = 2.5, Z of FCC, -100
		2,100	FW5 & FS5	2,749	ETA = 2.5, Z of FW5, -100
Poly Moderator	**0**		IW2 & IS2	6,950	I.R. OF BT1
		2,100	IW3 & IS3	6,950	I.R. OF BT1
Calorim Barrel	**2,220**				
		4,320			
Elec./Service Acc.	**2,000**		***Outside Radius of:***		
		6,320	FW1	4,772	Theta FW2, Z of FW1, Rnd'd
BW1 Upgrade	**0**		FW2	6,110	BT1 - 840
		6,320	FT1	6,110	BT1 - 840
BW1	**450**		FW3	6,110	BT1 - 840
		6,770	FT2	6,110	BT1 - 840
BW1 Rail Space	**180**		FW4 & FS4	6,850	IW2 - 100
		6,950	FCC	6,850	IW2 - 100
BT1	**1,500**		FW5 & FS5	6,850	IW2 - 100
		8,450	IW2 & IS2	9,180	O.R. of BS2
BW2 Rail Space	**230**		IW3 & IS3	12,920	Theta BS3, Z of IS3, Rnd'd
		8,680			
BW2	**350**				
		9,030			
BS2	**150**				
		9,180			
Truss	**1,100**				
		10,280			
BW3	**880**				
		11,160	ANGLE w/r I.P.	DEGREE	TANGENT
BS3	**150**		Eta = 3.0	5.700	0.099822
		11,310	Eta = 2.5	9.385	0.165284
			Theta FW2	32.502	0.637122
			Theta BS3	38.360	0.791462

0633

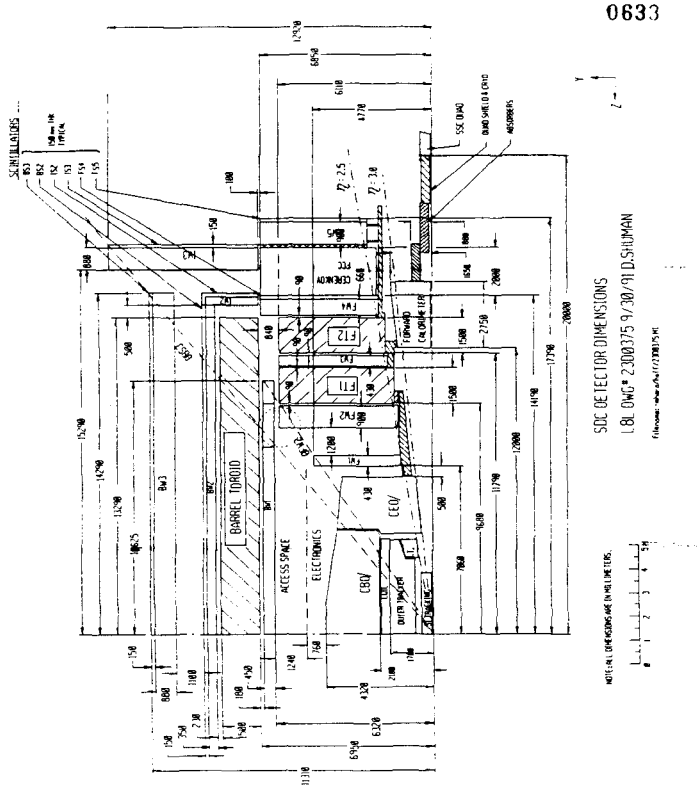

0634

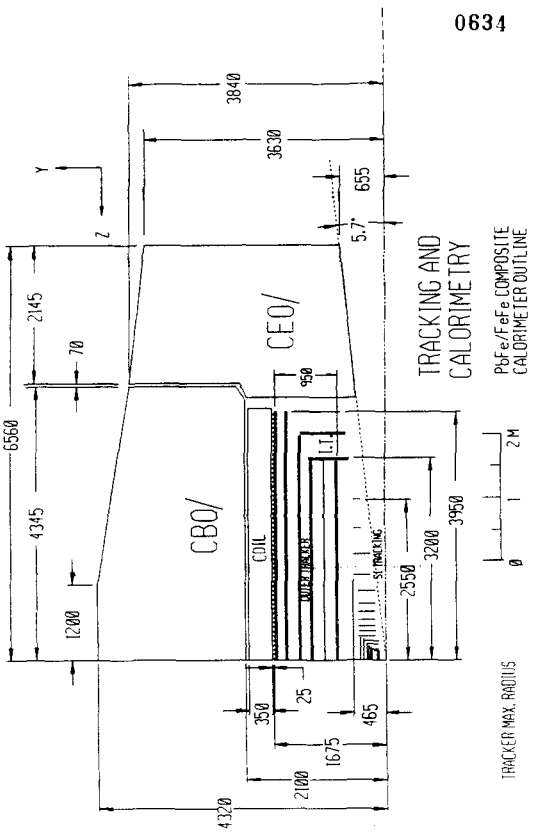

0635

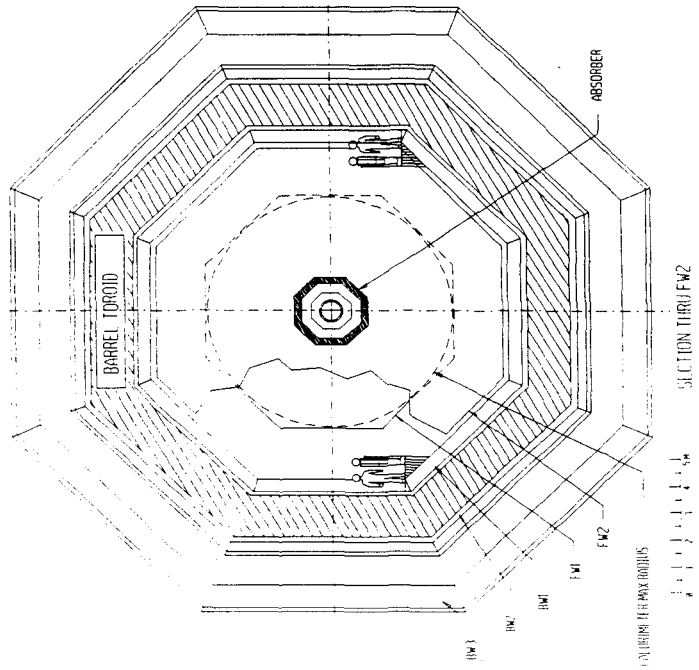

0636

Fiber Tracker Option
with
Electronics in Racks
Inside
Detector Volume

0640

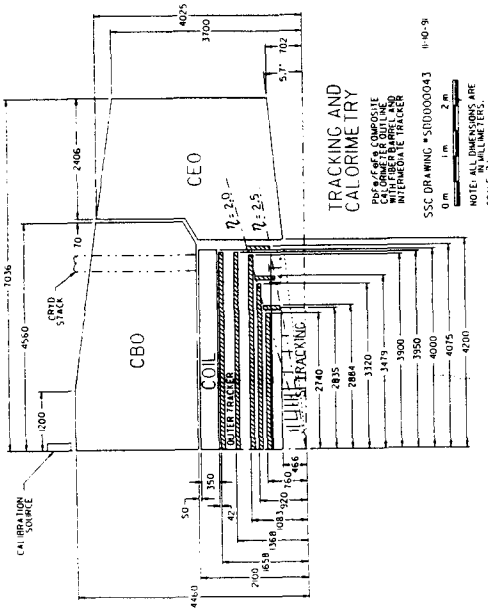

0639

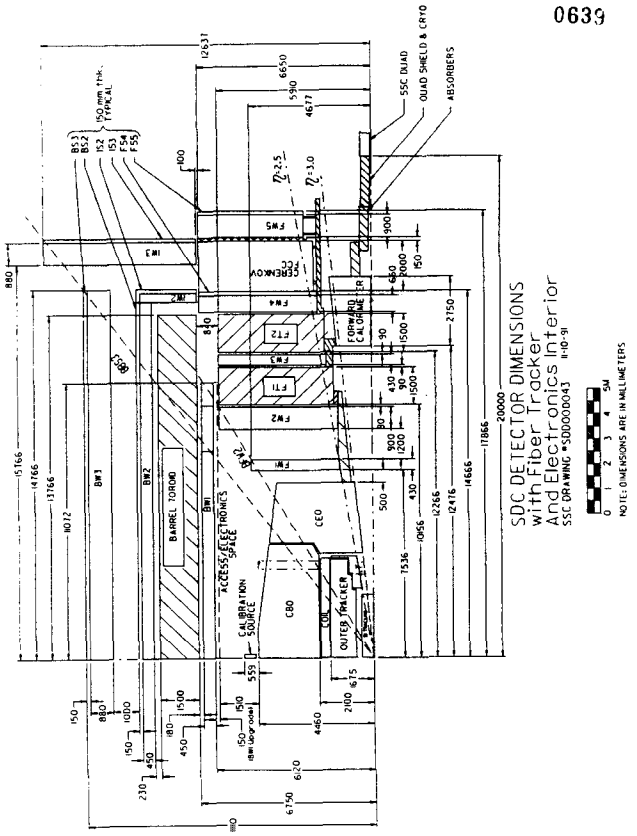

0638

SDC Integration					SSCL Mechanical Integration
Dimensions of Detector					Revised 11/10/91
(Fiber Tracker Option & Electronics Inside Detector Volume)					
Tables are based on SDD000043, 11/10/91, SDC Detector Dimensions					
Fixed Values are in bold type. Computed values are in plain type.					
Barrel R Dimensions			**Forward System R Dimensions**		
Description	Delta	Boundry	Description	Boundry	R Is Calculated As
	R	R		R	A Function Of:
Interaction Point	**0**				
		0	***Inside Radius of:***		
Tracker	**1,675**		FW1	1,295	ETA = 3.0, Z of FW1, +550
		1,675	FW2	1,564	ETA = 2.5, Z of FW2, -100
Space	**25**		FT1	1,827	ETA = 2.5, Z of FT1, -100
		1,700	FW3	1,912	ETA = 2.5, Z of FW3, -100
Cryostat	**350**		FT2	2,175	ETA = 2.5, Z of FT2, -100
		2,050	FW4 & FS4	2,299	ETA = 2.5, Z of FW4, -100
Space	**50**		FCC	2,655	ETA = 2.5, Z of FCC, -100
		2,100	FW5 & FS5	2,828	ETA = 2.5, Z of FW5, -100
Poly Moderator	**0**		IW2 & IS2	6,750	I.R. OF BT1
		2,100	IW3 & IS3	6,750	I.R. OF BT1
Calorim Barrel	**2,360**				
		4,460			
Elec./Service Acc.	**1,510**		***Outside Radius of:***		
		5,970	FW1	4,677	Theta FW2, Z of FW1, Rnd'd
BW1 Upgrade	**150**		FW2	5,910	BT1 - 840
		6,120	FT1	5,910	BT1 - 840
BW1	**450**		FW3	5,910	BT1 - 840
		6,570	FT2	5,910	BT1 - 840
BW1 Rail Space	**180**		FW4 & FS4	6,650	IW2 - 100
		6,750	FCC	6,650	IW2 - 100
BT1	**1,500**		FW5 & FS5	6,650	IW2 - 100
		8,250	IW2 & IS2	9,080	O.R. of BS2
BW2 Rail Space	**230**		IW3 & IS3	12,637	Theta BS3, Z of IS3, Rnd'd
		8,480			
BW2	**450**				
		8,930			
BS2	**150**				
		9,080			
Truss	**1,000**				
		10,080			
BW3	**880**				
		10,960	ANGLE w/r I.P.	DEGREE	TANGENT
BS3	**150**		Eta = 3.0	5.700	0.099822
		11,110	Eta = 2.5	9.385	0.165284
			Theta FW2	30.418	0.587125
			Theta BS3	36.95e	0.752404

0637

SDC Integration					SSCL Mechanical Integration	
Dimensions of Detector					Revised 11/10/91	
(Fiber Tracker Option & Electronics Inside Detector Volume)						
Tables are based on SDD000043, 11/10/91, SDC Detector Dimensions						
Fixed Values are in bold type. Computed values are in plain type.						
Forward Assy Z Dimensions			**Barrel / Intermediate Z Demensions**			
Description	Delta	Boundry	Description	Delta	Boundry	Remarks
	Z	Z		Z	Z	
Interaction Point	**0**		Interaction Point		0	
		0				
Calorim Length	**7,036**					
		7036				
Electron. Space	**500**					
		7536				
FW1	**430**					
		7966				
Clear	**1,200**					
		9166				
FW2	**900**					
		10066				
Clear & FT1 Coil	**90**					
		10156				
FT1 Steel	**1,500**					
		11656				
Clear & FT1 Coil	**90**		BW1		11,072	Some Octants Are Short
		11746				
FW3	**430**		BW2 & BS2		14,266	
		12176				
Clear & FT2 Coil	**90**		BW3 & BS3		14,766	
		12266				
FT2 Steel	**1,500**		BT1	**13,766**		Z of FT2
		13766			13,766	
Clear & FT2 Coil	**90**		Space	**500**		
		13856			14,266	
FW4	**660**		IW2	**350**		
		14516			14,616	
FS4	**150**		IS2	**150**		
		14666			14,766	
FCC (Cerenkov)	**2,000**		Entry Access	**1,000**		
		16666			15,766	
FW5 Support	**150**		IW3	**880**		
		16816			16,646	
FW5	**900**		IS3	**150**		
		17716			16,796	
FS5	**150**					
		17866				

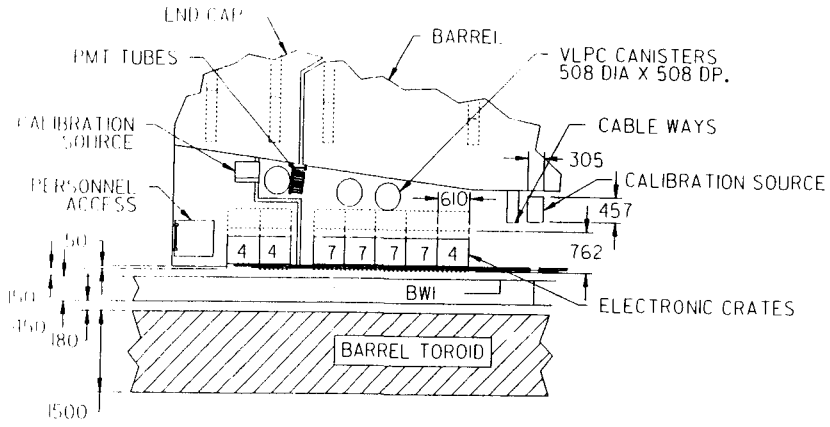

CALORIMETER - DETAIL B
FIBER TRACKER OPTION

SDD000064

0643

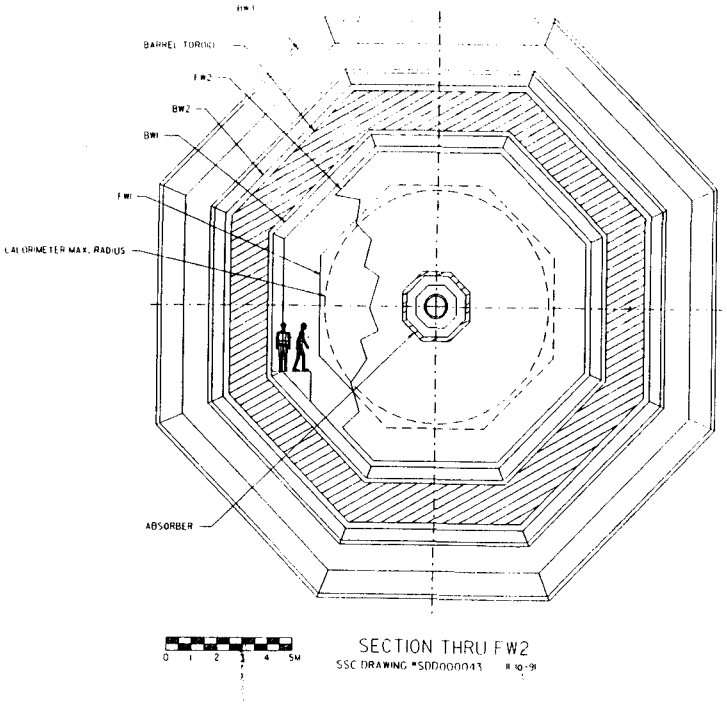

SECTION THRU FW2

SSC DRAWING #SDD000043 REV-91

0641

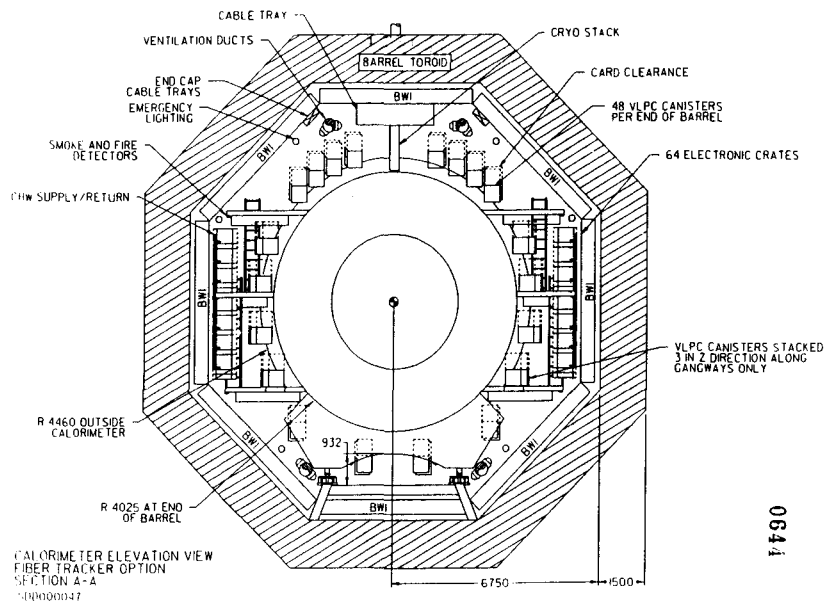

CALORIMETER ELEVATION VIEW
FIBER TRACKER OPTION
SECTION A-A

SDD000047

0644

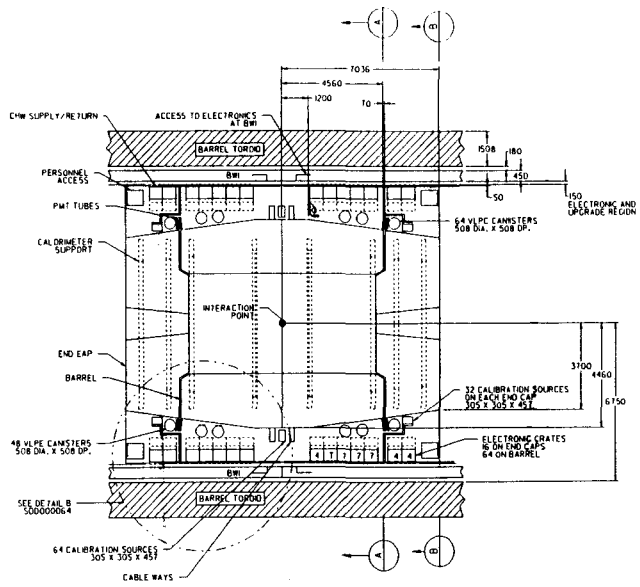

CALORIMETER - PLAN VIEW
FIBER TRACKER OPTION

SDD000046

0642

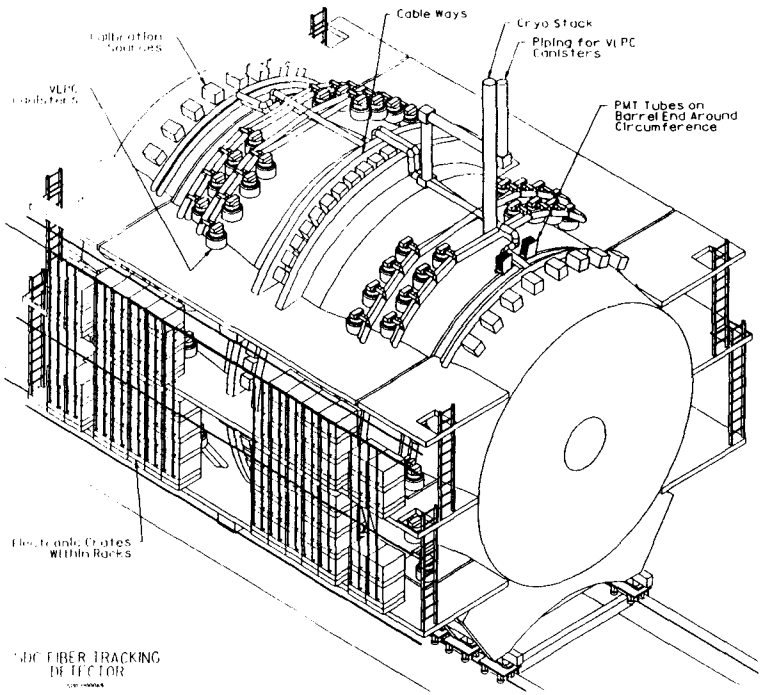

SDC FIBER TRACKING DETECTOR

0647

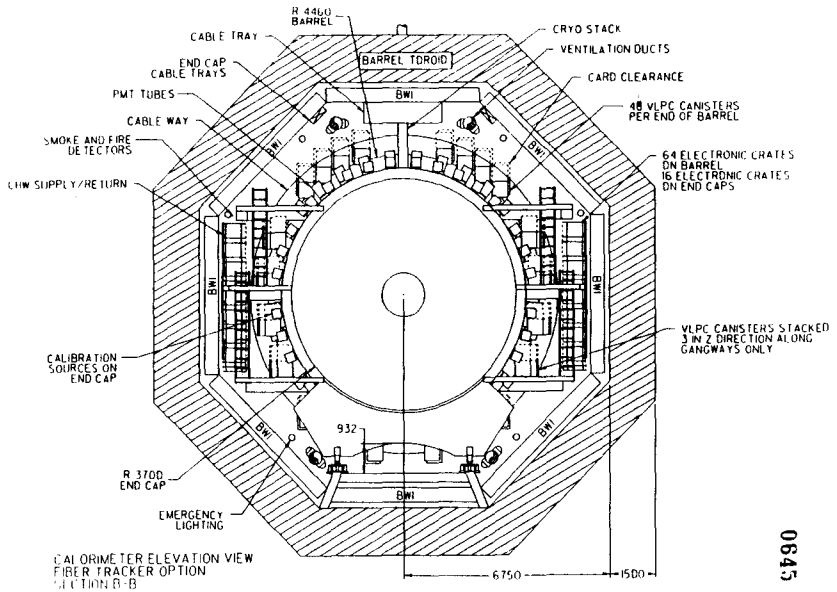

CALORIMETER ELEVATION VIEW
FIBER TRACKER OPTION
SECTION B-B

SDD0000065

0645

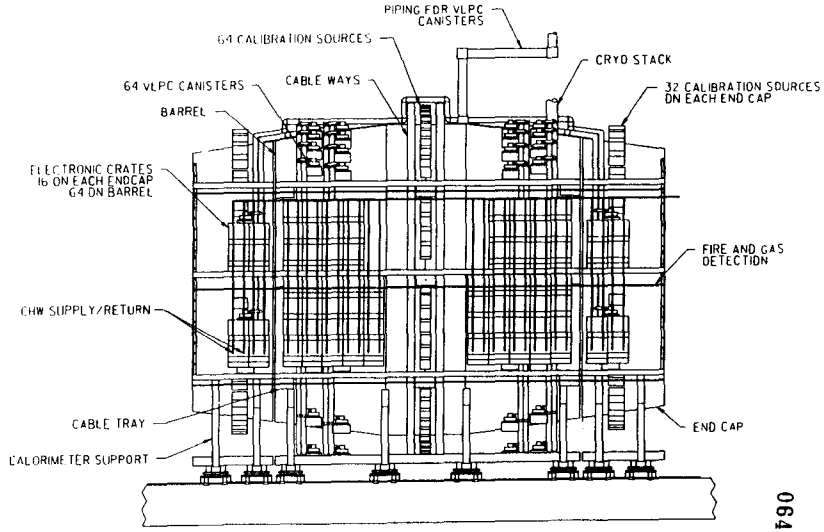

CALORIMETER ELEVATION VIEW - SIDE
FIBER TRACKER OPTION

SDD0000068

0648

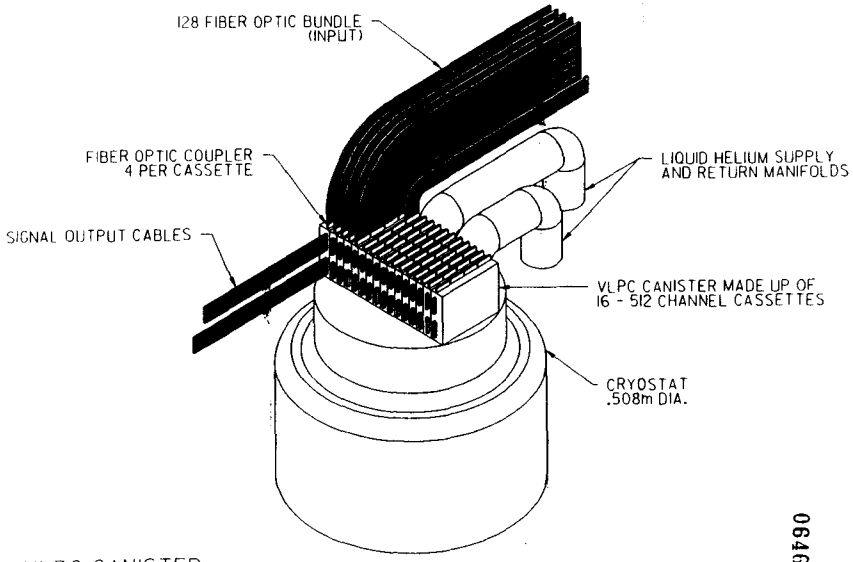

VLPC CANISTER
8,192 CHANNELS

SDD 0000070

0646

Straw Tracker Option
with
Electronics in Racks
Inside
Detector Volume

SDC Integration					SSCL Mechanical Integration
Dimensions of Detector					Revised 11/10/91
(Straw Tracker Option & Electronics Inside Detector Volume)					
Tables are based on strawlayout, 11/10/91, SDC Detector Dimensions					
Fixed Values are in bold type. Computed values are in plain type.					
Forward Assy Z Dimensions			**Barrel / Intermediate Z Demensions**		
Description	Delta Z	Boundry Z	Description	Delta Z	Boundry Z	Remarks
Interaction Point	**0**	0	Interaction Point		0	
Calorim Length	**7,036**	**7036**				
Electron. Space	**500**	**7536**				
FW1	**430**	**7966**				
Clear	**1,200**	9166				
FW2	**900**	10066				
Clear & FT1 Coil	**90**	10156				
FT1 Steel	**1,500**	11656				
Clear & FT1 Coil	**90**	11746	BW1		11,072	Some Octants Are Short
FW3	**430**	12176	BW2 & BS2		14,266	
Clear & FT2 Coil	**90**	12266	BW3 & BS3		14,766	
FT2 Steel	**1,500**	13766	BT1	13,766	13,766	Z of FT2
Clear & FT2 Coil	**90**	13856	Space	**500**	14,266	
FW4	**660**	14516	IW2	**350**	14,616	
FS4	**150**	14666	IS2	**150**	14,766	
FCC (Cerenkov)	**2,000**	16666	Entry Access	**1,000**	15,766	
FW5 Support	**150**	16816	IW3	**880**	16,646	
FW5	**900**	17716	IS3	**150**	16,796	
FS5	**150**	17866				

SDC Integration						SSCL Mechanical Integration
Dimensions of Detector						Revised 11/10/91
(Straw Tracker Option & Electronics Inside Detector Volume)						
Tables are based on strawlayout, 11/10/91, SDC Detector Dimensions						
Fixed Values are in bold type. Computed values are in plain type.						
Barrel R Dimensions			**Forward System R Dimensions**			
Description	Delta R	Boundry R	Description	Boundry R	R Is Calculated As A Function Of:	
Interaction Point	**0**	0	***Inside Radius of:***			
Tracker	**1,675**	1,875	FW1	1,295	ETA = 3.0, Z of FW1, +550	
Space	**25**	1,700	FW2	1,564	ETA = 2.5, Z of FW2, -100	
Cryostat	**350**	2,050	FT1	1,827	ETA = 2.5, Z of FT1, -100	
Space	**50**	2,100	FW3	1,912	ETA = 2.5, Z of FW3, -100	
Poly Moderator	**0**	2,100	FT2	2,175	ETA = 2.5, Z of FT2, -100	
Calorim Barrel	**2,360**	4,460	FW4 & FS4	2,299	ETA = 2.5, Z of FW4, -100	
Elec./Service Acc.	**1,167**	5,627	FCC	2,655	ETA = 2.5, Z of FCC, -100	
BW1 Upgrade	**150**	5,777	FW5 & FS5	2,828	ETA = 2.5, Z of FW5, -100	
BW1	**450**	6,227	IW2 & IS2	6,407	I.R. OF BT1	
BW1 Rail Space	**100**	6,407	IW3 & IS3	6,407	I.R. OF BT1	
BT1	**1,500**	7,907	***Outside Radius of:***			
BW2 Rail Space	**230**	8,137	FW1	4,406	Theta FW2, Z of FW1, Rnd'd	
BW2	**450**	8,587	FW2	5,567	BT1 - 840	
BS2	**150**	8,737	FT1	5,567	BT1 - 840	
Truss	**1,000**	9,737	FW3	5,567	BT1 - 840	
BW3	**880**	10,617	FT2	5,567	BT1 - 840	
BS3	**150**	10,767	FW4 & FS4	6,307	IW2 - 100	
			FCC	6,307	IW2 - 100	
			FW5 & FS5	6,307	IW2 - 100	
			IW2 & IS2	8,737	O.R. of BS2	
			IW3 & IS3	12,247	Theta BS3, Z of IS3, Rnd'd	
			ANGLE w/r I.P.	**DEGREE**	**TANGENT**	
			Eta = 3.0	5.700	0.099822	
			Eta = 2.5	9.385	0.165284	
			Theta FW2	28.945	0.55305	
			Theta BS3	36.099	0.729175	

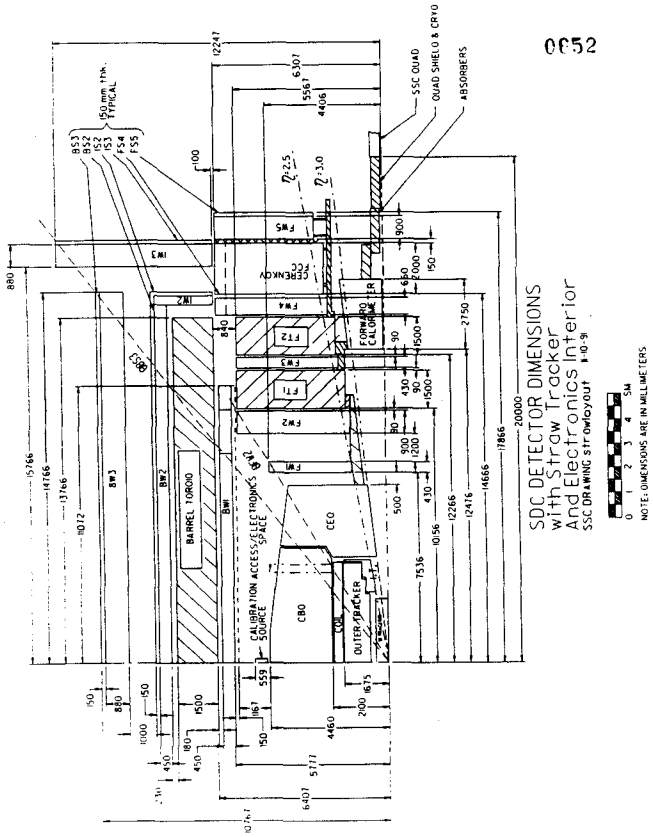

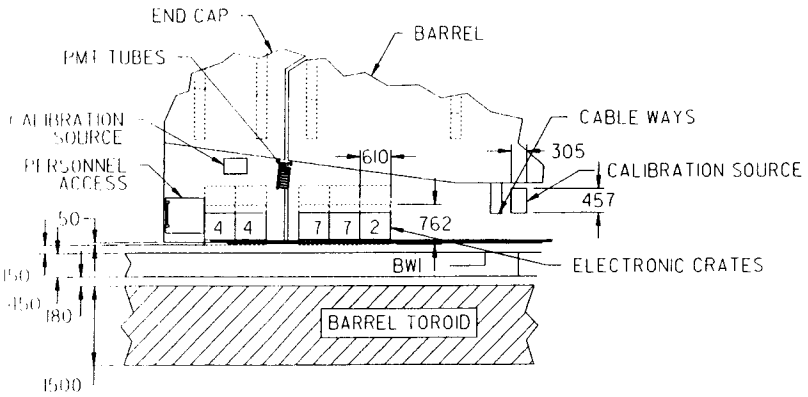

CALORIMETER - DETAIL B
STRAW TRACKER OPTION

SDD000066

0655

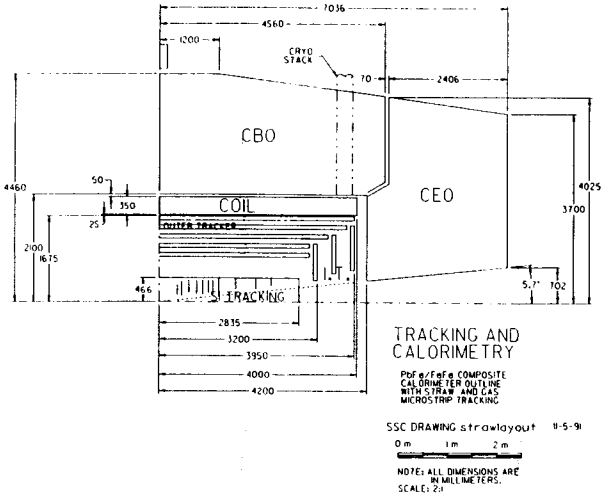

0653

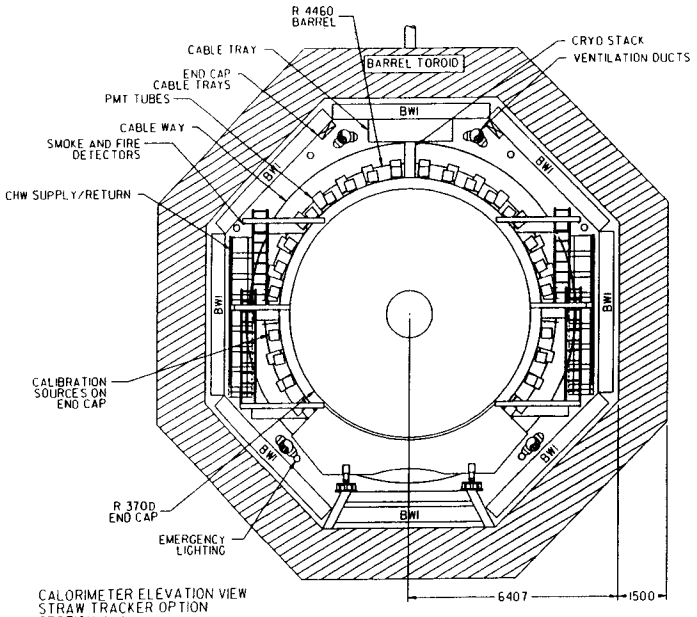

CALORIMETER ELEVATION VIEW
STRAW TRACKER OPTION
SECTION A-A

SDD000067

0656

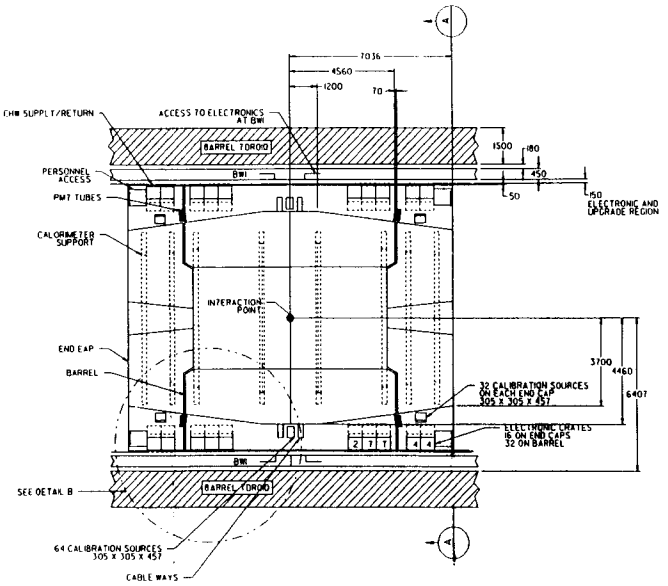

CALORIMETER - PLAN VIEW
STRAW TRACKER OPTION

SDD000065

0654

0657

All Electronic Crates Exterior of Detector Volume

0658

SDC Integration					SSCL Mechanical Integration
Dimensions of Detector					11/13/91
Electronics Outside Detector Volume					
Tables are based on LBL Drawings, SDC Detector Dimensions					
Fixed Values are in bold type. Computed values are in plain type.					
Forward Assy Z Dimensions			**Barrel / Intermediate Z Demensions**		
Description	Delta Z	Boundry Z	Description	Delta Z	Boundry Z	Remarks
Interaction Point	0		Interaction Point		0	
		0				
Calorim Length	7,036					
		7036				
Electron. Space	500					
		7536				
FW1	430					
		7966				
Clear	1,200					
		9166				
FW2	900					
		10066				
Clear & FT1 Coil	90					
		10156				
FT1 Steel	1,500					
		11656				
Clear & FT1 Coil	90		BW1		11,072	Some Octants Are Short
		11746				
FW3	430		BW2 & BS2		14,266	
		12176				
Clear & FT2 Coil	90		BW3 & BS3		14,766	
		12266				
FT2 Steel	1,500		BT1	13,766		Z of FT2
		13766			13,766	
Clear & FT2 Coil	90		Space	500		
		13856			14,266	
FW4	660		IW2	350		
		14516			14,616	
FS4	150		IS2	150		
		14666			14,766	
FCC (Cerenkov)	2,000		Entry Access	1,000		
		16666			15,766	
FW5 Support	150		IW3	880		
		16816			16,646	
FW5	900		IS3	150		
		17716			16,796	
FS5	150					
		17866				

Page 1

0659

SDC Integration					SSCL Mechanical Integration
Dimensions of Detector					11/13/91
Electronics Outside Detector Volume					
Tables are based on LBL Drawings, SDC Detector Dimensions					
Fixed Values are in bold type. Computed values are in plain type.					
Barrel R Dimensions			**Forward System R Dimensions**		
Description	Delta R	Boundry R	Description	Boundry R	R Is Calculated As A Function Of:
Interaction Point	0				
		0	***Inside Radius of:***		
Tracker	1,675		FW1	1,295	ETA = 3.0, Z of FW1, +550
		1,675	FW2	1,564	ETA = 2.5, Z of FW2, -100
Space	25		FT1	1,827	ETA = 2.5, Z of FT1, -100
		1,700	FW3	1,912	ETA = 2.5, Z of FW3, -100
Cryostat	350		FT2	2,175	ETA = 2.5, Z of FT2, -100
		2,050	FW4 & FS4	2,299	ETA = 2.5, Z of FW4, -100
Space	50		FCC	2,655	ETA = 2.5, Z of FCC, -100
		2,100	FW5 & FS5	2,828	ETA = 2.5, Z of FW5, -100
Poly Moderator	0		IW2 & IS2	6,150	I.R. OF BT1
		2,100	IW3 & IS3	6,150	I.R. OF BT1
Calorim Barrel	2,360				
		4,460			
Elec./Service Acc	910		***Outside Radius of:***		
		5,370	FW1	4,202	Theta FW2, Z of FW1, Rnd'd
BW1 Upgrade	150		FW2	5,310	BT1 - 840
		5,520	FT1	5,310	BT1 - 840
BW1	450		FW3	5,310	BT1 - 840
		5,970	FT2	5,310	BT1 - 840
BW1 Rail Space	180		FW4 & FS4	6,050	IW2 - 100
		6,150	FCC	6,050	IW2 - 100
BT1	1,500		FW5 & FS5	6,050	IW2 - 100
		7,650	IW2 & IS2	8,480	O.R. of BS2
BW2 Rail Space	230		IW3 & IS3	11,955	Theta BS3, Z of IS3, Rnd'd
		7,880			
BW2	450				
		8,330			
BS2	150				
		8,480			
Truss	1,000				
		9,480			
BW3	880				
		10,360	ANGLE w/r I.P.	DEGREE	TANGENT
BS3	150		Eta = 3.0	5.700	0.099822
		10,510	Eta = 2.5	9.385	0.165284
			Theta FW2	27.812	0.527518
			Theta BS3	35.442	0.71177

Page 2

0660

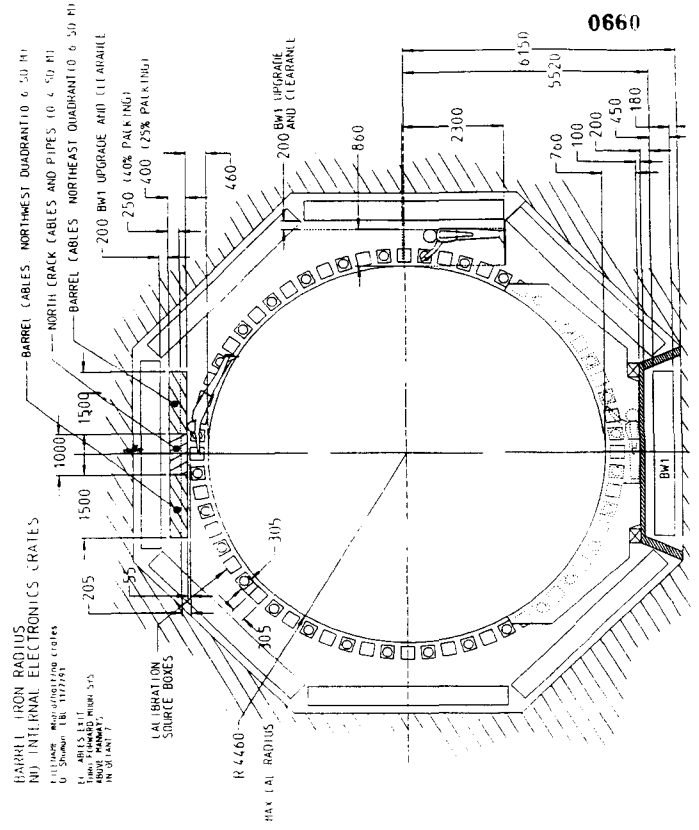

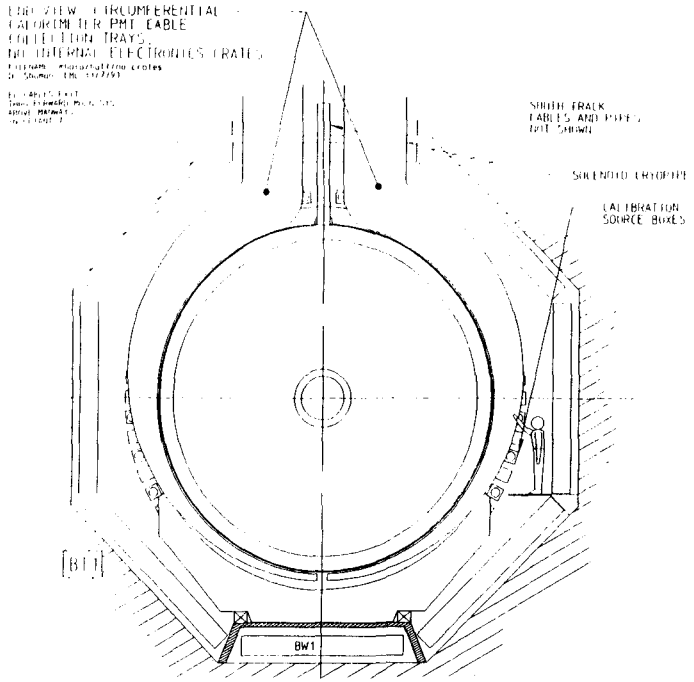

0663

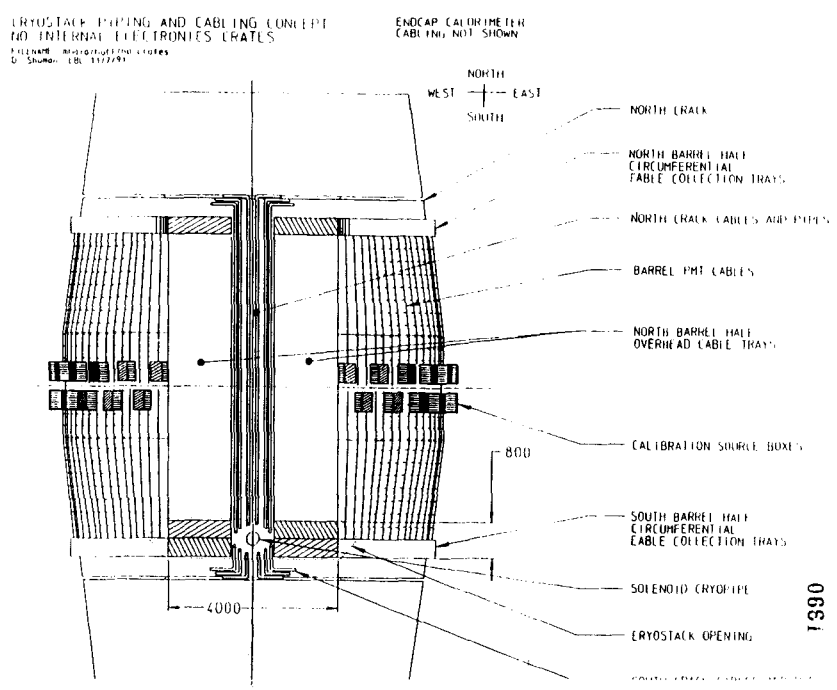

1390

Electronics Access Space Cable Plant Parameters

Barrel Section - half quadrant:

Calorimeter/Shower max Electronics Options:

Option 1 - analog calorimenter electronics with shower max (LBL design):

Cabling between calorimeter surface and the electronics racks:

- Requires 8 electronics crate spaces in the rack

- Calorimeter electronics:
  - 2240 calorimeter channels, 2240 PMTs, 224 mother boards (10 PMTs each)
    - 224 - 2" x .04" ribbon cables (data)
    - 224 - 2" x .04" ribbon cables (control, calibration and logic power)
    - 224 - 1/4" OD shielded-twisted pair (STP) cables (PMT voltage)
- Shower max electronics:
  - 4480 shower max channels, 448 multi-anode PMTs, 448 mother boards (1 PMT each)
    - 448 - 2" x .04" ribbon cables (combined function)
    - 448 - 1/4" OD STP cables (PMT voltage)

- Totals:
  - 896 - 2" x .04" ribbon cables - 71.68 sq. in.
  - 672 - 1/4" OD STP cables - 32.97 sq. in.
  - 104.65 sq. in. or .73 sq. ft.

0664

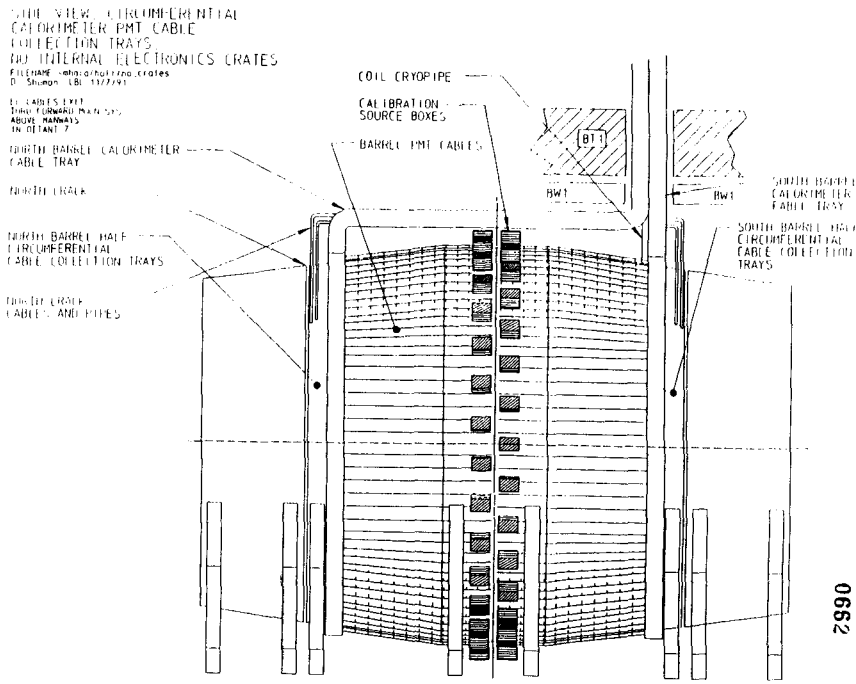

2990

Cabling between electronics racks and outside detector:

- Calorimeter electronics:
  - 8 - .5" OD multi-strand fiber optic cables (trigger and DAQ)
  - 8 - .75" OD five conductor, #10 wire cables (AC power)
- Shower max electronics:
  - 8 - .5" OD multi-strand fiber optic cables (trigger and DAQ)

- Totals:
  - 16 - .5" OD multi-strand fiber optic cables - 3.14 sq. in.
  - 8 - .75" OD five conductor, #10 wire cables - 3.53 sq. in.
  - 6.67 sq. in. or .05 sq. ft.

Cabling between electronics racks and outside detector:

- Calorimeter electronics:
  - 8 - .5" OD multi-strand fiber optic cables (trigger and DAQ)
  - 8 - .75" OD five conductor, #10 wire cables (AC power)
- Shower max electronics:
  - 8 - .5" OD multi-strand fiber optic cables (trigger and DAQ)

- Totals:
  - 16 - .5" OD multi-strand fiber optic cables - 3.14 sq. in.
  - 8 - .75" OD five conductor, #10 wire cables - 3.53 sq. in.
  - 6.67 sq. in. or .05 sq. ft.

Central Tracker Electronics Options:

Option 1 - straw tube tracker electronics:

Cabling between calorimeter surface and electronics racks:

- Option 1A - If paired with the LBL calorimeter electronics design, straw tube electronics are contained in the same crates as the calorimeter/shower max electronics - no additional crates required
- Option 1B - If paired with the FNAL calorimeter electronics design, 1 additional electronics crate is required to house the straw tube electronics

- Straw tube tracker electronics (same for options 1A and B):
  - 16384 straw tube tracker channels, 64 modules, 64 DCC boards
    - 64 - 2" x .04" ribbon cables (data, trigger and control)
    - 64 - 3/16" OD mini-coax cables (module high voltage)

- Totals:
  - 64 - 2" x .04" ribbon cables - 5.12 sq. in.
  - 64 - 3/16" OD mini-coax cables - 1.77 sq. in.
  - 6.89 sq. in. or .05 sq. ft.

Option 2 - digital calorimenter electronics with shower max (FNAL design):

Cabling between calorimeter surface and electronics racks:

- Requires 8 electronics crate spaces in the racks

- Calorimeter electronics;
  - 2240 channels, 2240 PMTs, direct wiring from PMT bases, no mother boards
    - 2240 - 1.2" x .04" ribbon cables (combined function)
- Shower max electronics:
  - 4480 channels, 448 multi-anode PMTs, 448 mother boards (1 PMT each)
    - 448 - 2" x .04" ribbon cables (combined function)
    - 448 - 1/4" OD STP cables (PMT voltage)

- Totals:
  - 2440- 1.2" x .04" ribbon cables - 117.12 sq. in.
  - 448 - 2" x .04" ribbon cables - 35.84 sq. in.
  - 448 - 1/4" OD STP cables - 21.98 sq. in.
  - 174.94 sq. in. or 1.21 sq. ft.

Option 2 - sci-fi central tracker (4 layer tracker) electronics:

Cabling between calorimeter surface and the electronics racks:

- Requires 3 electronics crate spaces in the racks

- Sci-fi tracker electronics:
  - 39000 sci-fi tracker channels, 3 VLPCs
    - 1182 - 1.3" x .04" ribbon cables (combined function)
- Totals:
  - 1182 - 1.3" x .04" ribbon cables - 61.46 sq. in. or .43 sq. ft.

Cabling between electronics racks and outside detector:

- Sci-fi tracker electronics:
  - 6 - .5" OD multi-strand fiber optic cables - (combined function)
  - 3 - .75" OD five conductor, #10 wire cables (AC power)

- Totals:
  - 6 - .5" OD multi-strand fiber optic cables - 1.18 sq. in.
  - 3 - .75" OD five conductor, #10 wire cables - 1.32 sq. in.
  - 2.5 sq. in. or .02 sq. ft.

Intermediate Tracker Electronics Options:

Option 1 - sci-fi tracker electronics:

Cabling between calorimeter surface and the electronics racks:

- These electronics will be housed in the same crates as those used for the central sci-fi tracker electronics

- Sci-fi tracker electronics:
  - 13750 sci-fi tracker channels, uses same VLPS as central sci-fi tracker
    - 418 - 1.3" x .04" ribbon cables (combined function)

- Totals:
  - 418 - 1.3" x .04" ribbon cables - 33.44 sq. in. or .23 sq. ft.

Cabling between electronics racks and outside the detector:

- These electronics will share the fiber optic cables used by the central sci-fi tracker, no additional cabling required

Cabling between electronics racks and outside detector:

- Straw tube tracker electronics:
  - Option 1A:
    - 8 - .5" OD multi-strand fiber optic cables (combined function)
    - 8 - .125" OD RG-58 coax cables (straw tube high voltage)

  - Totals:
    - 8 - .5" OD multi-strand fiber optic cables - 1.57 sq. in.
    - 8 - .125" OD RG-58 coax cables - .1 sq. in.
    - 1.67 sq. in. or .01 sq. ft.

  - Option 1B:
    - 1 - .5" OD multi-strand fiber optic cable (combined function)
    - 8 - .125" OD RG-58 coax cables (straw tube high voltage)
    - 1 - .75" OD five conductor, #10 wire cable (AC power)

  - Totals:
    - 1 - .5" OD multi-strand fiber optic cable - .2 sq. in.
    - 8 - .125" OD RG-58 coax cables - .1 sq. in.
    - 1 - .75" OD five conductor, #10 wire cable - .4 sq. in.
    - .7 sq. in or .005 sq. ft.

Return-path: <baumbaugh@fnal.bitnet>
Received: from FNAL by lbl.Bitnet via BITNET ;
Thu, 31 Oct 91 14:54:40 PST
Received: From FNAL(BAUMBAUG) by LBL with Jnet id 2557
for OBERSTEIN@LBL; Thu, 31 Oct 1991 14:54 PST
Message-Id: <9110311454440.2160016c98ca3.LBL.Gov>
Date: Thu, 31 Oct 1991 16:53 CST
From: <BAUMBAUGH@FNAL>
Subject: RE: Tracking System Review - 11/12/91
To: oberstein@lbl.Bitnet"
Original_To: Bitnet%"oberstein@lbl.Bitnet"
Original_cc: BAUMBAUGH,UNDHEP::ROCHTT

Gene:

On the issue of channel counts I now have the following information:

Intermediate tracker 55K per end for a total of 110,000

4 layer Barrel would have a total of 312,000 (247,000 in trigger layers) for a total count barrel and intermediate of 422,000, I guess that this would be called the partially staged system although I am not sure if the simulation people will agree to the staging.

5 layer Barrel would have a total of 507,000 (345,000 in trigger layers) for a total count barrel and intermediate of 617,000. This would be the fully implimented system, no staging left. (although there is the possibility of adding U and V layers to one layer which would add 41,000 channels to the total)

I will be sending the additional WBS info as soon as I have it together.

Alan Baumbaugh

Cabling between electronics racks and outside detector:

- Calorimeter electronics:
  - 4 - 5" OD multi-strand fiber optic cables (trigger and DAQ)
  - 4 - .75" OD five conductor, #10 wire cables (AC power)
- Shower max electronics:
  - 4 - .5" OD multi-strand fiber optic cables (trigger and DAQ)

- Totals:
  - 8 - .5" OD multi-strand fiber optic cables - 1.57 sq. in.
  - 4 - .75" OD five conductor, #10 wire cables - 1.77 sq. in.
  - 3.34 sq. in. or .02 sq. ft.

Option 2 - digital calorimenter electronics with shower max (FNAL design):

Cabling between calorimeter surface and electronics racks:

- Requires 4 electronics crate spaces in the racks

- Calorimeter electronics:
  - 1600 channels, 1600 PMTs, direct wiring from PMT bases, no mother boards
    - 1600 - 1.2" x .04" ribbon cables (combined function)
- Shower max electronics:
  - 1792 channels, 112 multi-anode PMTs, 112 mother boards (1 PMT each)
    - 112 - 2" x .04" ribbon cables (combined function)
    - 112- 1/4" OD STP cables (PMT voltage)

- Totals:
  - 1600- 1.2" x .04" ribbon cables - 76.8 sq. in.
  - 112 - 2" x .04" ribbon cables - 8.96 sq. in.
  - 112 - 1/4" OD STP cables - 5.5 sq. in.
  - 91.26 sq. in. or .63 sq. ft.

Option 2 - gas microstrip tracker:

Not much is known about the design of this tracker option at the present time. From the information that we have, the electronics configuration will be similar to that of the silicon tracker; i.e., the front-end electronics will be located on the micro-strips and will be cabled directly to the surface via fiber optic cables. Our best guess is that there will be approximately 8000 fibers connecting the tracker to electronics racks in the counting room. This would be equivalent to about 900 multi-strand fiber optic cables, .5" OD each.

End-cap Section - quadrant:

Calorimeter/Shower max Electronics Options:

Option 1 - analog calorimenter electronics with shower max (LBL design):

Cabling between calorimeter surface and the electronics racks:

- Requires 4 electronics crate spaces in the rack

- Calorimeter electronics:
  - 1600 calorimeter channels, 1600 PMTs, 160 mother boards (10 PMTs each)
    - 160 - 2" x .04" ribbon cables (data)
    - 160 - 2" x .04" ribbon cables (control, calibration and logic power)
    - 160 - 1/4" OD shielded-twisted pair (STP) cables (PMT voltage)
- Shower max electronics:
  - 1792 shower max channels, 112 multi-anode PMTs, 112 mother boards (1 PMT each)
    - 112 - 2" x .04" ribbon cables (combined function)
    - 112 - 1/4" OD STP cables (PMT voltage)

- Totals:
  - 432 - 2" x .04" ribbon cables - 34.56 sq. in.
  - 272 - 1/4" OD STP cables - 13.43 sq. in.
  - 47.99 sq. in. or .33 sq. ft.

Cabling between electronics racks and outside detector:

- Calorimeter electronics:
  - 4 - .5" OD multi-strand fiber optic cables (trigger and DAQ)
  - 4 - .75" OD five conductor, #10 wire cables (AC power)
- Shower max electronics:
  - 4 - .5" OD multi-strand fiber optic cables (trigger and DAQ)

- Totals:
  - 8 - .5" OD multi-strand fiber optic cables - 1.57 sq. in.
  - 4 - .75" OD five conductor, #10 wire cables - 1.77 sq. in.
  - 3.34 sq. in. or .02 sq. ft.

Silicon Strip Front End Electronics

H. Sadrozinski(UC/SC)

SDC SILICON ELECTRONICS

- FRONTEND : AMP & COMP
  (CMOS : g_m, NOISE)
  BIPOLAR : RAD HARDNESS
  BIJFET : 1 mW / CHANNEL
- DIGITAL DATA STORAGE
  CMOS : DATA DRIVEN
- INTEGRATION
- DATA TRANSMISSION
- PRICES OF CHIPS

HARTMUT SADROZINSKI

FRONT END :

- DOUBLE SIDED, 12 CM LONG DETECTORS
  RAD HARDNESS OK.
  MINIMIZE CAPACITANCE < 1.2 pF/cm
- RADIATION DAMAGE
  (CMOS)
  BIPOLAR, JFET TEKTRONIX SHPi
- LAY OUT : CHANNEL WIDTH
- PROOF OF PRINCIPLE : 1 mW /CHANNEL
  BIJET, BICMOS
- NEXT : BIPOLAR WITH ACTIVE LOADS
  pnp : H. SPIELER et al LBL
  JFET : W. DABROWSKI, N. SPENCER } UCSC

RADIATION DAMAGE CMOS - BIPOLAR

- BASELINE : 2 CHIP DESIGN
  ANALOG : BIPOLAR
  DIGITAL : CMOS
- CMOS UTMC (1 MeV γ ^{60}Co SOURCE UC SANTA CRU
  UP TO 5 Mrad
  NOISE, g_m at LOW drain currents
  (IEEE POSTER (SCIPP 91-24) # 4H4)
- BIPOLAR TEKTRONIX SHPi
  (650 MeV p at LAMPF, ~20% INCREASE OVER MIN. ION.)
  UP TO $1.1 \cdot 10^{14}$ P/cm^2
  BOTH IONIZING & DISPLACING

H. SADROZINSKI
SCIPP

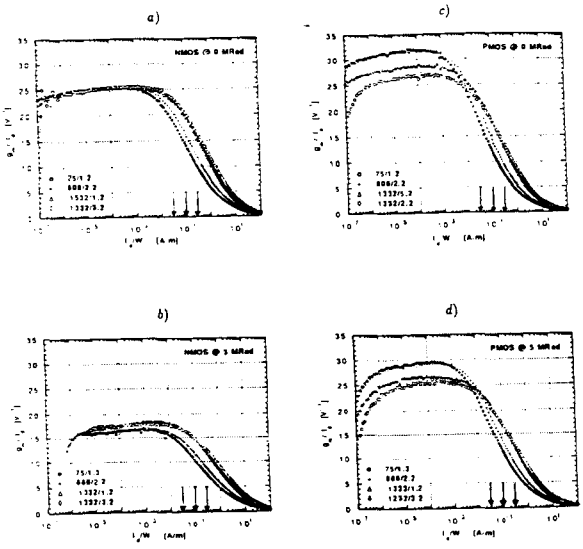

Fig. 2. Transconductance scaled by the drain-source current g_m/I_D as function of the current density I_D/W for the transistors measured: a) NMOS pre-rad, b) NMOS post-rad (5 MRad), c) PMOS pre-rad, d) PMOS post-rad (5 MRad). The arrows indicate the current settings of the noise measurements.

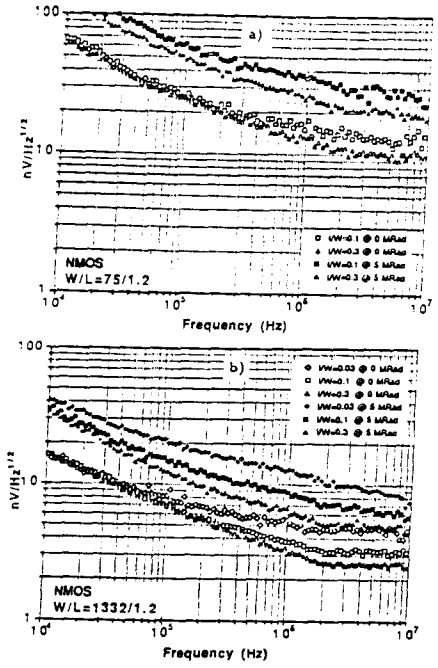

Fig. 3. Spectral noise voltage v_n in $nV/\sqrt{Hz}$ for the three current densities I_D/W = 0.03, 0.1, 0.3 pre- and post-rad (5 MRad) separately for the transistors measured. a) NMOS W/L = 75/1.2. b) NMOS W/L = 1332/1.2.

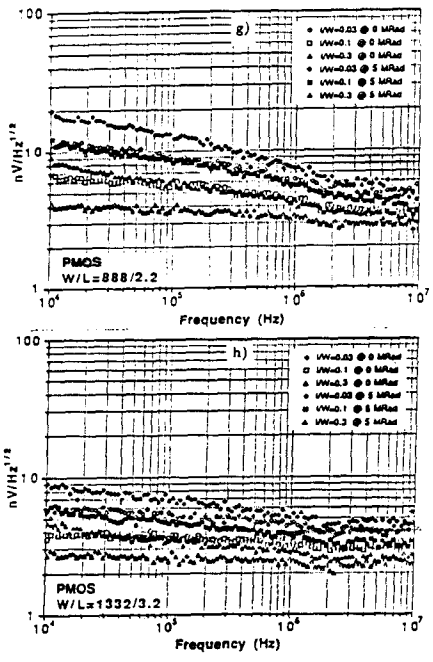

Fig. 3. continued g) PMOS W/L = 888/2.2, h) PMOS W/L = 1332/3.2.

Table 1. Threshold Voltages $|V_{GS}|$

Geometry	0.00 MRad	0.25 MRad	0.50 MRad	1.00 MRad	2.00 MRad	5.00 MRad
NMOS 75/1.2	0.79	0.69	0.66	0.60	0.59	0.59
NMOS 1332/1.2	0.72	0.60	0.69	0.58	0.67	0.62
NMOS 888/2.2	0.79	0.73	0.68	0.64	0.62	0.65
NMOS 1332/3.2	0.73	0.55	0.66	0.56	0.60	0.55
PMOS 75/1.2	0.62	0.70	0.70	0.71	0.72	0.76
PMOS 1332/1.2	0.65	0.77	0.81	0.78	0.84	0.80
PMOS 888/2.2	0.80	0.87	0.89	0.90	0.92	0.95
PMOS 1332/3.2	0.78	0.88	0.90	0.88	0.93	0.93

Table 2. Noise Coefficient $\gamma_n = \frac{v_n^2 g_m}{4kT}$

	75/1.2 NMOS	75/1.2 PMOS	1332/1.2 NMOS	1332/1.2 PMOS	888/2.2 NMOS	888/2.2 PMOS	1332/3.2 NMOS	1332/3.2 PMOS
Ids/W=0.03								
Pre Rad	*	*	0.91	0.81	0.64	0.58	0.66	0.50
Post Rad	*	*	2.17	0.84	1.00	0.58	1.50	0.69
Ids/W=0.10								
Pre Rad	1.10	0.70	1.20	1.10	0.80	0.80	0.80	0.60
Post Rad	3.80	1.10	3.40	1.60	1.30	0.90	1.70	0.70
Ids/W=0.30								
Pre Rad	1.40	1.30	2.00	1.70	1.10	1.00	1.10	0.77
Post Rad	5.00	2.90	4.80	2.70	1.90	1.40	1.20	0.81

RADIATION HARDNESS OF BIPOLAR

INTERESTING DEVICES:

- npn TRANSISTORS
- pnp TRANSISTORS
- JFET's
- DIODES
- RESISTORS

IMPORTANT CONSIDERATIONS:

- BIAS DURING IRRADIATION
- MEASURE AT LOW CURRENTS
- CHANNEL HAS 30 μm PITCH

NPN TRANSISTORS (TEKTRONIX SHP)

GEOMETRIES: 2x (min), 8x, 32x

a) CURRENT GAIN h_{FE} AS FUNCTION OF COLLECTOR CURRENT I_C SCALES WITH GEOMETRY

b) REDUCTION IN CURRENT GAIN IN 1.1×10^{14} n/cm²

92 → 40	(100μA)	88 → 35
91 → 35	(50μA)	86 → 29
88 → 23	(10μA)	82 → 20

FOR 2X (minimum geom.) ($R_B \approx 300$) ⬆ 8x ($R_B \approx 80$)

c) POST RAD, CURRENT GAIN h_{FE} AS FUNCTION OF COLLECTOR CURRENT SCALES WITH GEOMET

****** GRAPHICS PLOT ******

CH4N8 HFE-IC

HFE ( ) SHP: TEKTRONIX N8

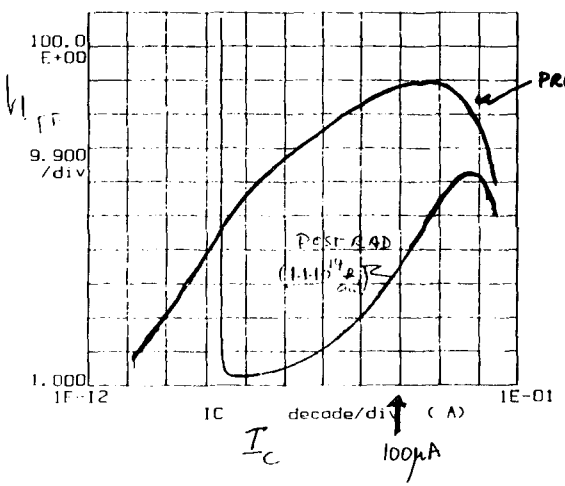

h_{FE}

I_C

Variable1:
IE -Ch1
Log sweep
Start -5.000pA
Step -30.00mA
Step LOG50

Constants:
VB -Ch2 .8500V
VC -Ch3 .8500V
VSUB -Vs1 -10.000V

I_C	PRE	POST
100μA	88	35
10μA	82	20

HFE ( ) = IC/IB

****** GRAPHICS PLOT ******

CH4N32 HFE-IC

HFE ( ) SHP: TEKTRONIX N32

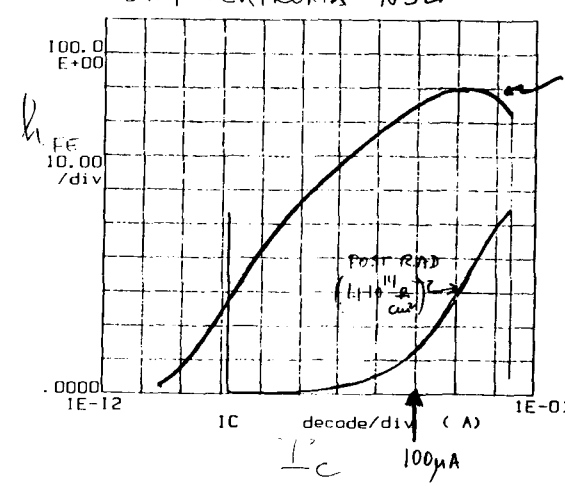

h_{FE}

I_C

Variable1:
IE -Ch1
Log sweep
Start -5.000pA
Stop -30.00mA
Step LOG50

Constants:
VB -Ch2 .8500V
VC -Ch3 .8500V
VSUB -Vs1 -10.000V

I_C	PRE	POST
100μA	85	13
10μA	77	4

HFE ( ) = IC/IB

****** GRAPHICS PLOT ******

CH4N2 HFE-IC

HFE ( ) SHP: TEKTRONIX N2

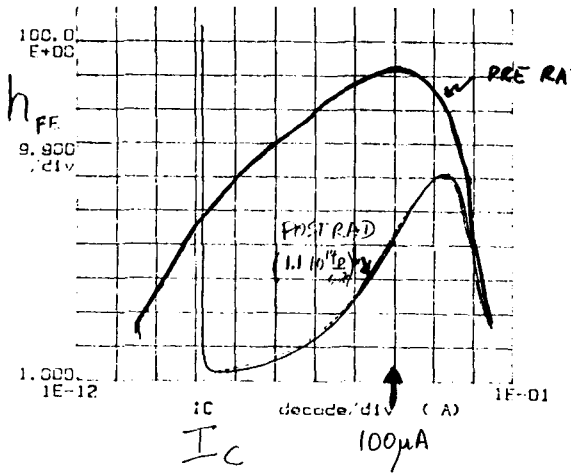

h_{FE}

I_C

Variable1:
IE -Ch1
Log sweep
Start -5.000pA
Step -30.00mA
Step LOG50

Constants:
VB -Ch2 .8500V
VC -Ch3 .8500V
VSUB -Vs1 -10.000V

I_C	PRE	POST
100μA	92	40
10μA	88	23
1μA	80	12

HFE ( ) = IC/IB

PNP TRANSISTORS (LATERAL)

CURRENT GAIN β CHANGES DURING IRRADIATION:

	$I_c = 25\mu A$	$50\mu A$	$100\mu A$	$200\mu A$
PRE RAD	45-50	40-50	35-45	27-30
$1 \cdot 10^{13}$ P/cm^2	26	26	25	28
$3 \cdot 10^{13}$ P/cm^2	12	12	12	11
$1.1 \cdot 10^{14}$ P/cm^2	5	5	5	5

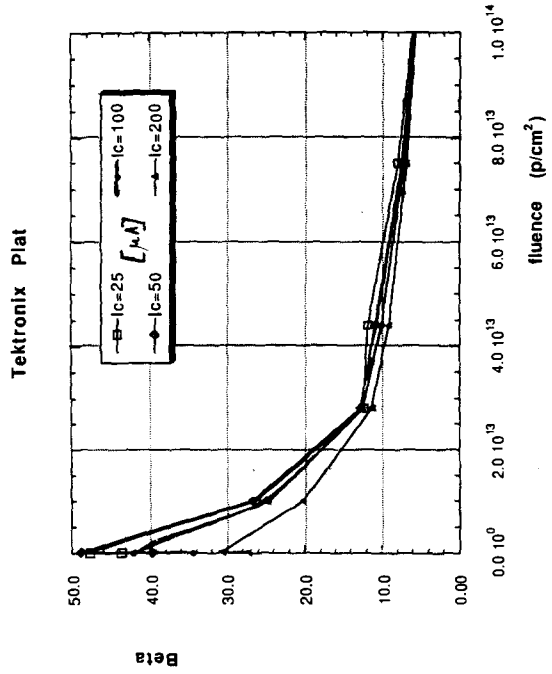

JFET's (P CHANNEL)

THE PINCHOFF VOLTAGE CHANGES:

$\Delta V_{P.O.} = 120\,mV$ in $1.1 \cdot 10^{14}$ P/cm^2

AFTER CORRECTING FOR THIS CHANGE IN VOLTAGE, THE I-V CHARACTERISTIC AND THE OUTPUT RESISTANCE ARE IDENTICAL

VERY GOOD MATCHING.

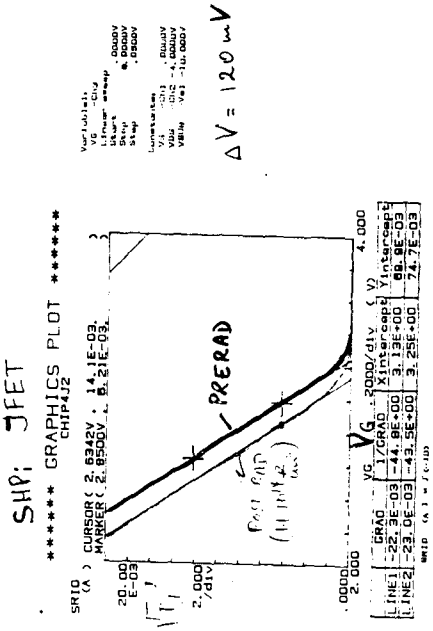

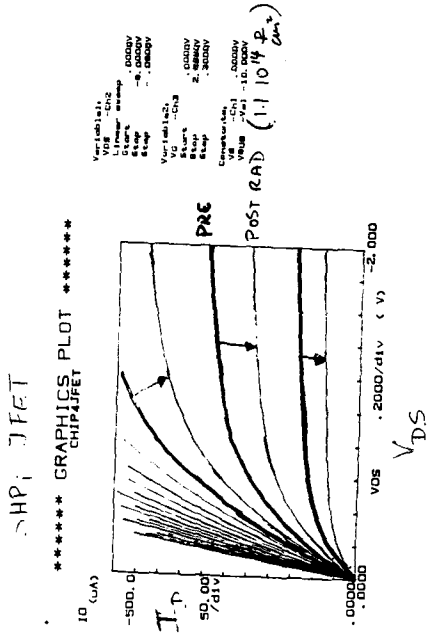

SHP; JFET VOLTAGE CORRECTED

****** GRAPHICS PLOT ****** POST RAD (1.1 10^{14} $\frac{p}{cm^2}$)

CHIP4JFET

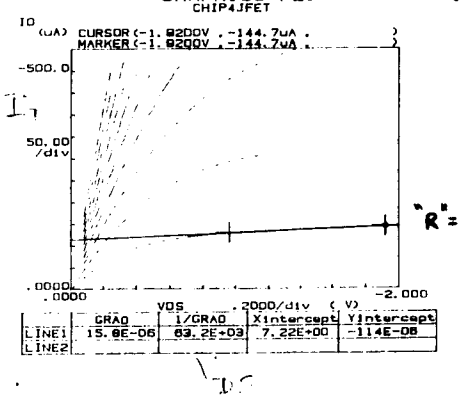

"R" = 63 kΩ at 150 μA

	GRAD	1/GRAD	Xintercept	Yintercept
LINE1	15.8E-06	63.2E+03	7.22E+00	-114E-08
LINE2				

V_{DS}

0697

SHP; JFET - VOLTAGE CORRECTED POST RAD -

****** GRAPHICS PLOT ******

CHIP4JFET

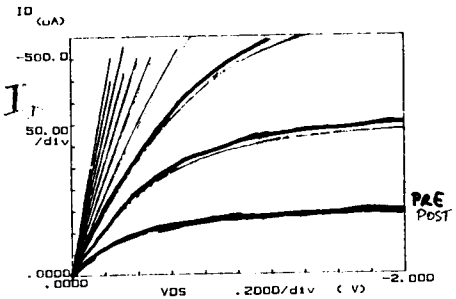

PRE
POST RAD (1.1 10^{14} $\frac{p}{cm^2}$)

V_{DS}

0695

SHP; JFET MATCHING

****** GRAPHICS PLOT ******

CHIP4J2

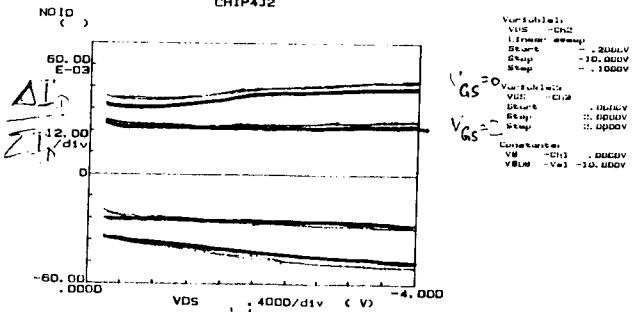

$V_{GS}=0$

$V_{GS}=$

$\frac{\Delta I_D}{\Sigma I_D}$

V_{DS}

0696

SHP; JFET

****** GRAPHICS PLOT ******

CHIP4JFET

PRE RAD

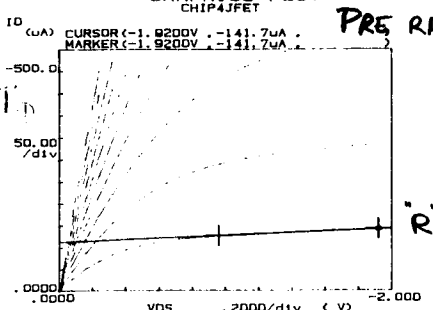

"R" = 64 kΩ at 150 μA

	GRAD	1/GRAD	Xintercept	Yintercept
LINE1	15.5E-06	64.4E+03	7.21E+00	-112E-08
LINE2				

V_{DS}

0694

DIODES

LOW LEAKAGE CURRENTS AT ~1V
REVERSE BIAS PRE AND POST RAD

RESISTORS (STILL UNDER INVESTIGATION)

250 Ω, 1kΩ, 4 kΩ

Ω METER CHECK AFTER IRRADIATION:
STABLE TO FEW % IN $1.1 \cdot 10^{14}$ P/cm²

NEED TO INVESIGATE INFLUENCE OF
EPITAXY BIAS ON RESISTANCE.

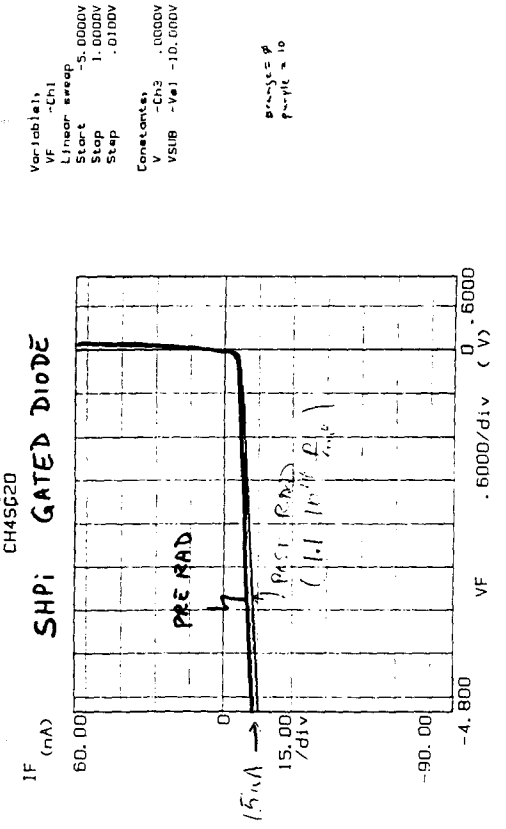

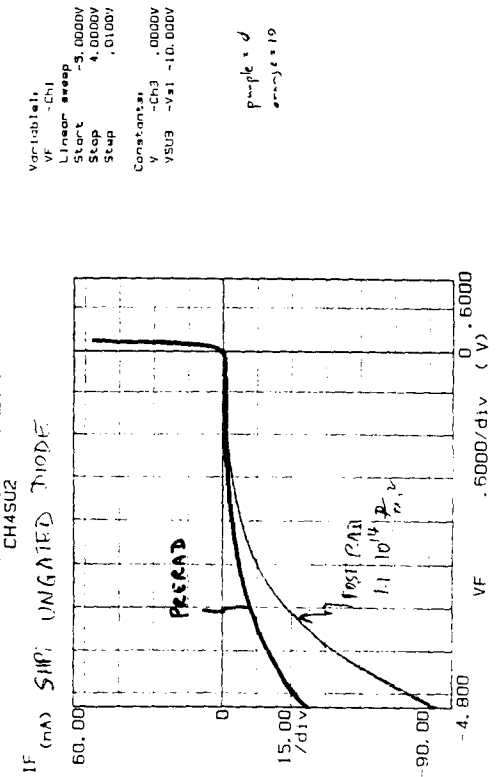

WIDTH OF CHANNEL:

ASSUME 128 CHANNEL CHIP : 6.4 mm
50 μm CHANNEL

SPACE FOR BONDING BETWEEN CHIPS — 1.4 mm
5.0 mm

SET BACK OF BOND PADS — 0.25 mm

BOND PADS — 0.60 mm

SPACE FOR BIAS CONTROL — 0.15 mm

SPACE LEFT FOR 128 CHANNELS 4.00 mm

4.0 mm / 128 = 31.25 μm

DESIGN FOR 30 μm.

LENGTH:
PRESENTLY: 72 μm PITCH, 3.5 mm active
0.72 PADS

ASSUME WITH 30 μm PITCH,
NEED MAX LENGTH 8.64 mm ?

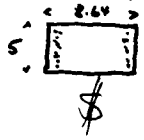

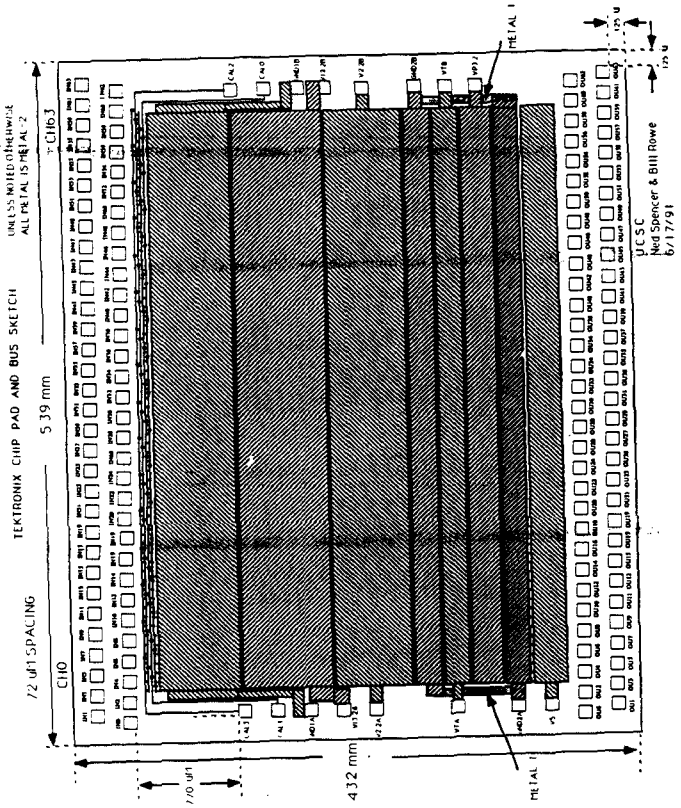

1 mW/CHANNEL AMP - COMP

(W. DABROWSKI , KRAKOW - UCSC)

FAST : 20 ns RISE TIME

: 100 ns DEAD TIME

NOISE : 1900 e^- (BIJFET)

1500 e^- (BICMOS)

TIME WALK: 15 ns (2 - 8 fc)

- min ion = 4 fc

THRESHOLD = 1 fc -

64 CHANNELS : ORBIT VIA MOSIS

SCIPP 91-31

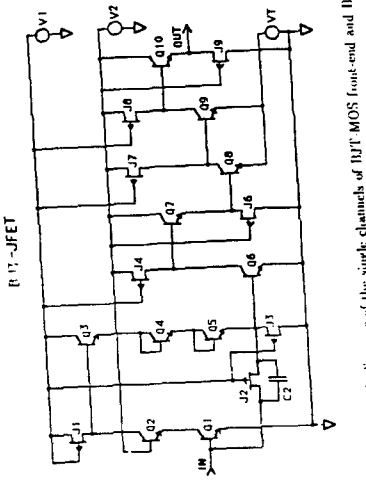

Fig. 2. Circuit diagrams of the single channels of BJT-MOS front-end and BJT-JFET front-end.

Qx : MODIFIED MINIMUM GEOMETRY n p n

Jy : JFET

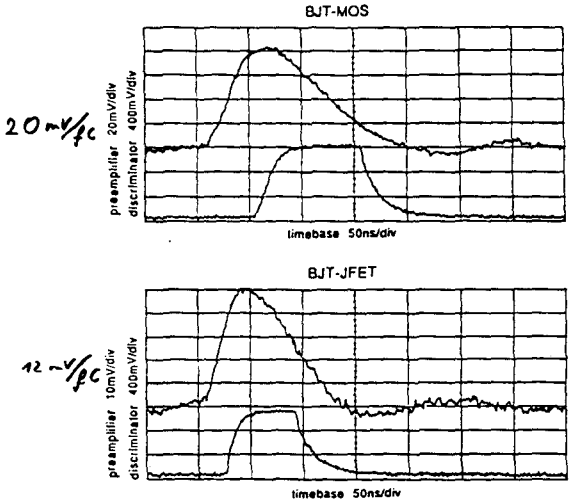

WALK

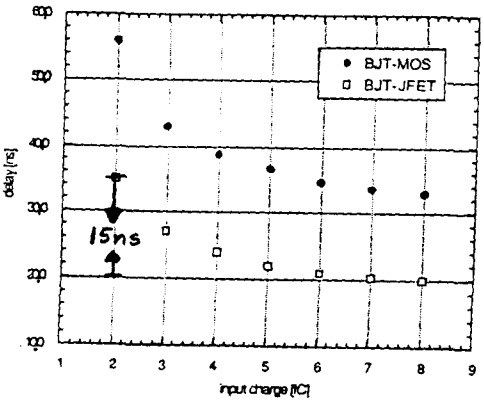

THRESHOLD = 1 fC

NOISE HITS RATE

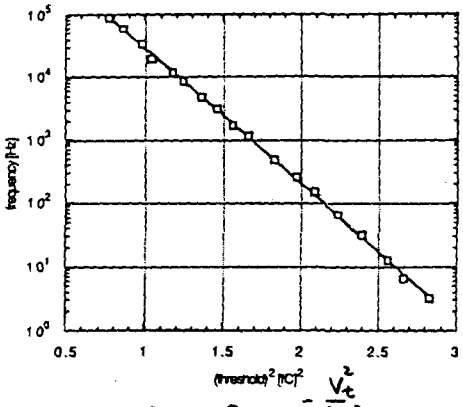

RICE: $f_{nt} = f_{no} e^{-\frac{V_t^2}{2\sigma^2}}$

MEASURE: $f_{no} = 4$ MHz $\sigma = 0.32$ fC (2000e

EXPECT: $f_{no} = \frac{0.14}{\tau_{PEAK}} = \frac{0.14}{35ns} \approx 4$ MHz $\sigma = 1500e$

DIGITAL DATA STORAGE : CMOS

4 μsec LVL1 LATENCY

→ CLOCK DRIVEN ARCHITECTURE

OUT

DATA DRIVEN DESIGN:

KANEX SHANKAR - RAL-

TEST CHIP FOR UTMC 1.2 μm

FULL CHIP FOR

- BASIC IDEA:

  EACH CHANNEL HAS n STORAGE LOCATIONS FOR VALID TIME STAMP

  - n = 4, 6 -

- MOST LIKELY WILL BUILD 2 CHIPS:

  n=6 FOR INNER LAYERS "HI OCC"

  n=4 FOR OUTER LAYERS "LO OCC"

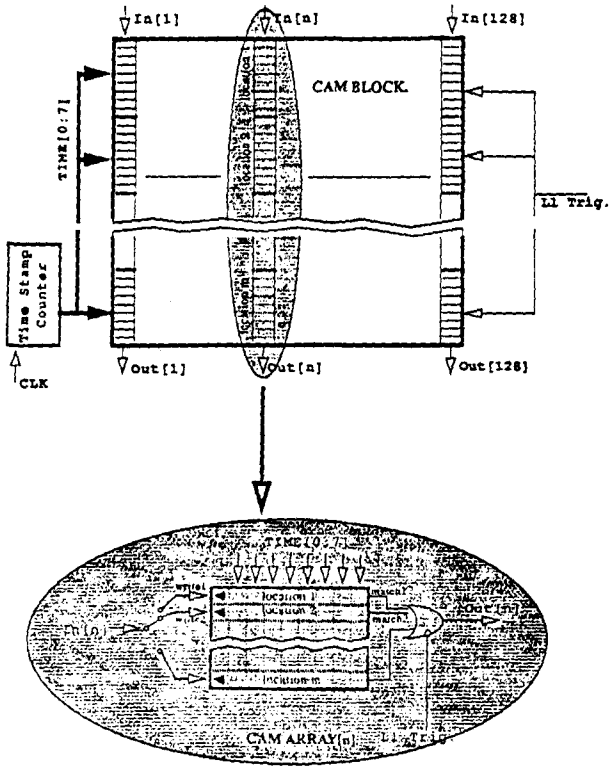

Fig 1.1a Outline of The Data Driven Readout.

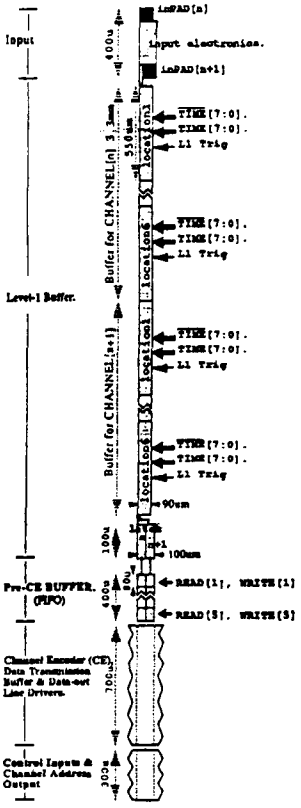

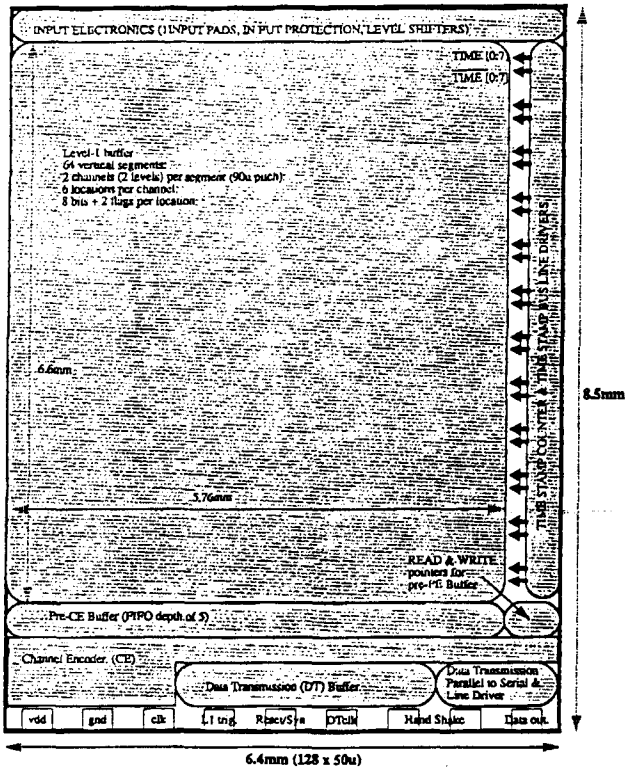

Fig 2.1(a) floor plan of the data driven architecture.

4.1 Efficiency of the data driven scheme.

Tables 4.1(a) and 4.1(b) shows the efficiency of the data driven scheme against the depth of the level-1 buffer. Table 4.1(a) is for the case of level-1 latency equal to 128 beam crossings and Table 4.1(b) is for the case of level-1 latency equal to 256 beam crossing.

The figures for the efficiency is obtained using the Verilog behavioral description simulator. In this simulation the functions of a channel are described using a behavioral description language and the input to this channel is generated using random events generator with a occupancy of 1%. The values for the efficiency is obtained by running this simulation over 2e06 clock cycles (beam crossings).

Efficiency = (No. of events recorded / No. of total events) x 100

1% OCCUPANCY = 10X DESIGN AT MINIMUM R

Level-1 latency = 128

No. of location per channel.	Data recording efficiency.
1	44%
2	74%
3	90%
4	96.8%

Table 4.1(a) Efficiency of the data driven architecture @ T1=128

Level-1 latency = 256 ≈ 4μsec

No. of location per channel.	Data recording efficiency. 1% occ	0.5% occ	0.2% occ
1	28%	68.3	90.6
2	52%	86.0	98.5
3	72%	95.7	99.8
4	85%	98.8	99.97
5	92.6%	99.6	
6	97%	99.77	

ESTIMATE – HPISC-

Table 4.1(b) Efficiency of the data driven architecture @ T1=256

4.2 Summary on the Merits of both architecture.

The tables 4.2(a) and 4.2(b) gives the summary on the merits of both architectures. Table 4.2(a) is for the case level-1 latency equal to 128 and table 4.2(b) for the case level-1 latency equal to 256.

level-1 latency = 128

Architecture	Power dissipation	length	efficiency
data driven	197uW	6.3mm	96.8%
clock driven	330uW	12.22mm	99.99%

Table 4.2(b) Summary on the Merits of the Architecture @ T1=128

level-1 latency = 256

Architecture	Power dissipation	length	efficiency
data driven	260uW	8.5mm	97%
clock driven	520uW	22.5mm	99.99%

Table 4.2(b) Summary on the Merits of the Architecture @ T1=256

ABM with kapton

0717

INTEGRATION (LBL - LANL)

INTEGRATE:

- MECHANICAL STRUCTURE
- COOLING RING
- DETECTOR
- FRONT END CHIPS
- DIGITAL DATA STORAGE CHIPS
- DATA COLLECTION CHIPS (?)
- POWER BUSSES
- DATA BUSSES
- CONTROL BUSSES

RIGID TO 5 μm
W/O PICK-UP
W/O X-TALK

0715

Schematic of module assembly with cables

0713

0716

DATA TRANSMISSION

LBL : LOW MASS CABLES
(NEEDED FOR POWER, CONTROLS)

OXFORD: OPTICAL FIBRES
(ONE PER CHIP 50K
ONE PER DETECTOR SIDE 10K)

MAX PARALLEL ARCHITECTURE:
LVL 2 TRIGGER
NO DATA COLLECTION CHIP?
FAULT IMMUNITY

CONTROLS ? NEED CONTROL BROADCAST CHIP?

Data storage chip (CMOS), highest speed ~ 63 MHz of machine.

Choice - Many low speed (63 MHz) links using LED's and fibers.

or

Multiplexing with smaller number of high speed links. Use lasers or optical modulators plus fibers.

For low speed case:
Fiber/Chip ⇒ 50,000 fibers.
Fiber/Detector ⇒ 5,000 fibers.

ESTIMATES ON CHIP COSTS

(128 CHANNELS, 50μm PITCH DETECT

① CMOS (RAD-HARD)
WRITTEN QUOTES (100K) FROM UTMC FOR 2 CHIPS:

"SMALL" $5.51 \times 3.0\ mm^2 = 0.165\ cm^2$ $ 10.97
"LARGE" $5.51 \times 6.0\ mm^2 = 0.33\ cm^2$ $ 17.79

→ PRICE/CHIP $P = \left(2.35 + 46.79 \frac{\text{AREA}}{cm^2}\right)$ $

DDS CHIP 5.5 x 6.3 (n=4) P = 18.56 $/CHIP
5.5 x 8.5 (n=6) P = 24.26 $/CHIP

② BIPOLAR
EXPECT QUOTE FROM TEKTRONIX } "SMALL", "BIG"
ASKED IKEDA FOR QUOTE FROM NTT/LAT } FOR 50,000 QUANTITY

FOR NOW, USE TEKTRONIX PRICE $ 2150/4" WAF

SMALL CHIP: $5.0 \times 3.6 = 0.18\ cm^2$ → 436 CHIPS/WAFE
YIELD Y1 = 30% → P = $16/CHIP
YIELD Y2 = 15% → P = $32/CHIP

LARGE CHIP $5.0 \times 8.6 = 0.43\ cm^2$ 182 CHIPS/WAFER
YIELD Y1 = 30% → P = $40/CHIP
YIELD Y2 = 15% → P = $80/CHIPS

Muon Front End Analog Electronics

J. Oliver(Harvard)

(See paper under MUON SYSTEM)

1st and 2nd Level Muon Triggers Based on the Jet Chamber System

H. Sakamoto(KEK)

(See paper under MUON SYSTEM)

Data Acquisition Status Report and Discussion of Sub-Detector Crates

E. Barsotti(FNAL)

Data Acquisition Status Report

and

Discussion of Sub-Detector Crates

Ed Barsotti

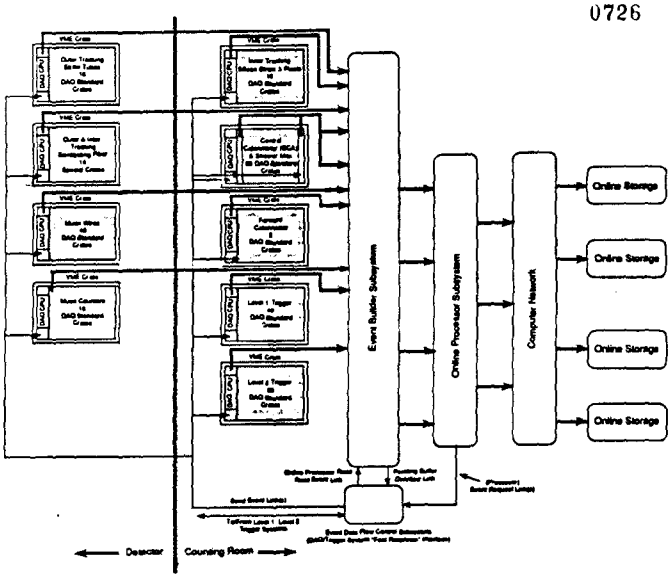

Update

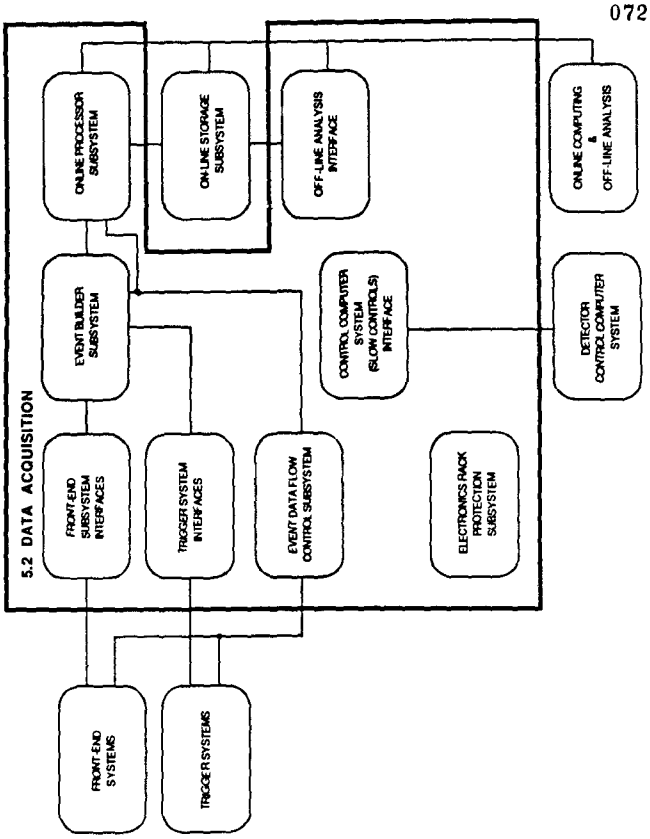

SDC Data Acquisition
WBS Item Quantities & Descriptions

WBS Item	Quantity	Description
Project Management		Staff & administrative people to technically manage the development, production, installation & commissioning of the data acquisition system
Infrastructure		CASE & CAE workstations, networking equipment & software, logic state analysers, oscilliscopes, etc. needed for development, production, installation & commisioning of the data acquisition system (one half of required infrastructure; other half assumed to be owned by collaborators already)
DAQ Control/Monitoring Network	1	A network interconnecting DAQ subsystems and DAQ CPUs to both the Online Computer network and the overall detector Slow Controls network Each front-end and trigger system connected to this network is electrically isolated from one another by network bridges, etc.
DAQ Standard Crates, Supplies, Etc.	~400	Commercially-available crates, power supplies, backplanes, etc. with SDC DAQ standard methods for powering the crates, housing auxiliary cards, redundancy (if required), etc.
DAQ Standard Event Data Readout & DAQ Control/Monitoring Network Interface	~400 ~400 ???	This WBS item consists of several parts: · Standard SDC DAQ CPU modules · Event Data Readout & DAQ Control/Monitoring Network interface (logic on a 6U to 9U module adapter module (assumes VMEbus), on an auxiliary card to a DAQ CPU or on a front-end or trigger system module which interfaces these systems to the SDC DAQ system in a standard way) · DAQ Control/Monitoring Network interface to remote components (serial links which originate at DAQ readout crates and which interconnect the DAQ Control/Monitoring Network to 'on-detector' components not housed in Standard DAQ crates with DAQ CPUs (includes repeaters))

Event Builder Subsystem	1	This WBS item consists of three parts: - Data Balancing & Input Queueing Logic (Receives event data from the near 400 event data fragment sources (DAQ CPUs, buffer modules), multiplexes the data sources into a smaller number of relatively evenly distributed data sets and transmits these data sets in packets to the switching network) - Switching Network (Builds events in parallel by switching packets of event fragment data on serial links in a barrel shift mode; capable of one Gigabyte per second typical and ten Gigabytes per second maximum throughput) - Interface to the Online Processor Subsystem (Interfaces the output links of the Switching Network to the Online Processor Subsystem)
Event Data Flow Control Subsystem	1	Interfaces the DAQ Event Builder & Online Processor Subsystems to the Level 2 Trigger System and is responsible for the control of the flow of event data from standard event data interfaces (DAQ CPUs, etc.) through the Event Builder Subsystem and to the Online Processor Subsystem. Also responsible for providing trigger disable signals to the Level 2 Trigger System from the Event Builder and Online Processor Subsystems and receiving Level 2 accept information from the Level 2 Trigger System
Online Processor Subsystem	1	A commercially-available array of processors totalling 100K MIPS of processing power
DAQ Control Computing		Software for the following purposes: - Runtime user interface - Control, monitoring & downloading user interface - Applications software for supporting the use of memories & intelligent processors - Applications software for supporting "slow" (non-event) data acquisition - Applications software for supporting unusual occurences - Applications software for supporting the control & monitoring of adjustable devices
DAQ Offline Analysis Interface	1	Commercially-available network hardware & software for interfacing the Online Processor Subsystem to the offline analysis computer system

DAQ Sub Detector Crates	One to a few crates per each front-end and trigger system used to accept that system's event data fragment sources (from DAQ CPUs, buffer modules), multiplex the event data and transmit the data both to the Event Builder Subsystem during normal data taking and to a workstation for local processing (for calibrations, etc.) If these crates are necessary, the multiplexing (data balancing) and input queueing of the Event Builder Subsystem will be done in these crates and the outputs from these crates will be transmitted directly to the Event Builder Subsystem's Switching Network over fiber. If these crates are not used, the output of the Event Builder Subsystem's Input Queueing Logic is locally transmitted over copper to the Switching Network.

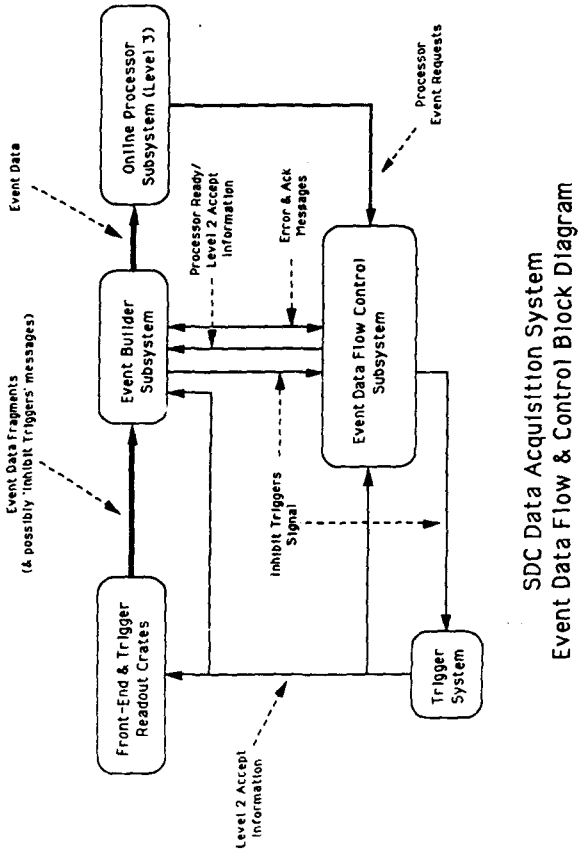

SDC Data Acquisition System
Event Data Flow & Control Block Diagram

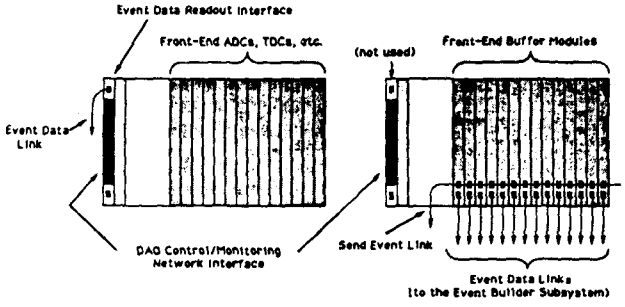

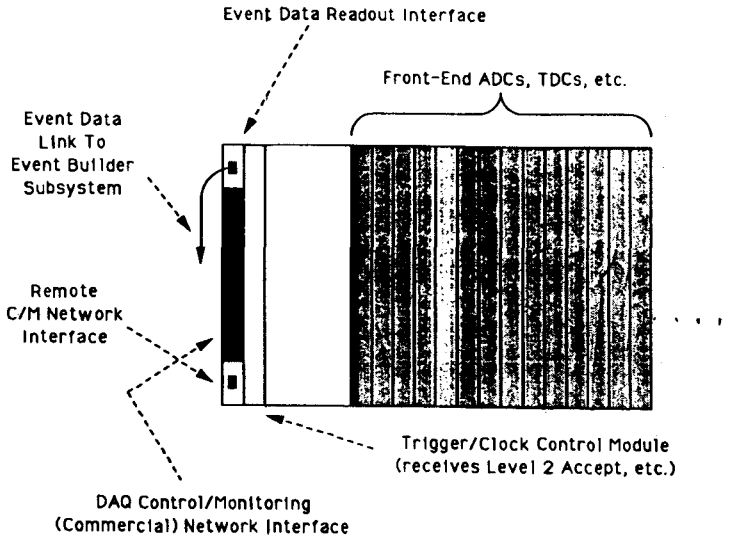

SDC Standard DAQ Crate
(with commercial crate & backplane (& no Buffer Modules))

0733

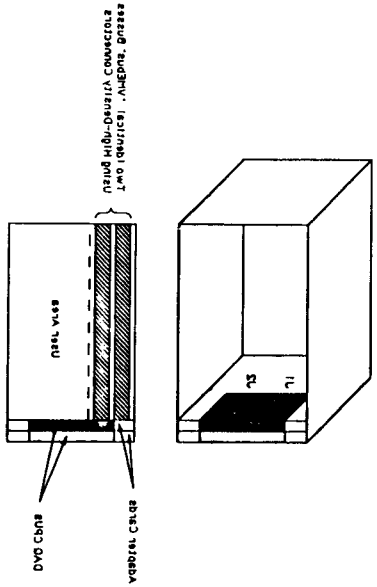

0735

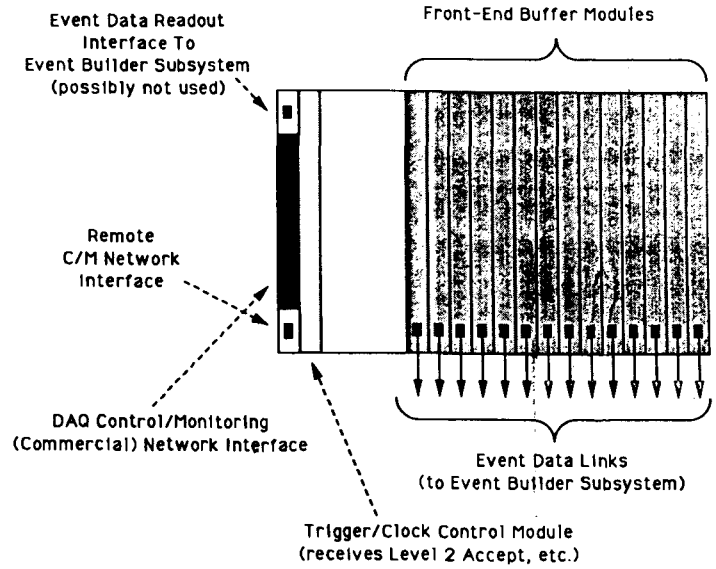

SDC Standard DAQ Crate
(with commercial crate & backplane (& Buffer Modules))

0734

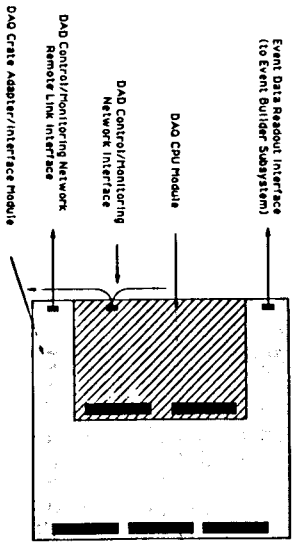

0736

0737

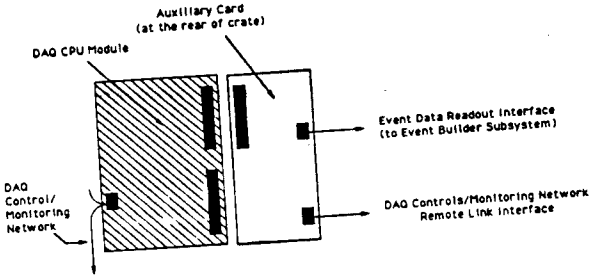

0738

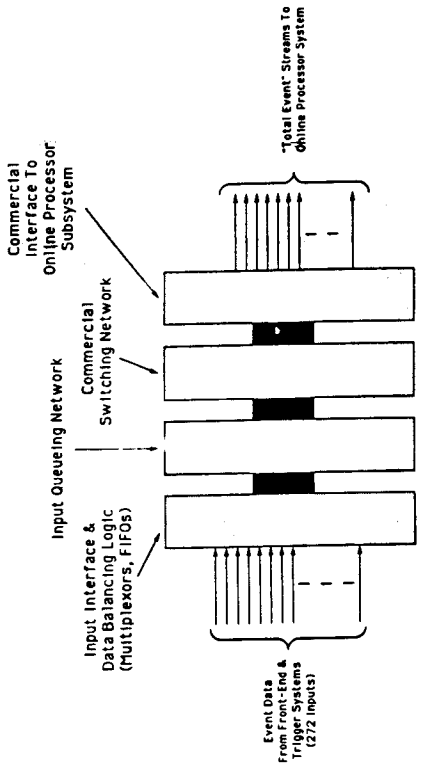

0739

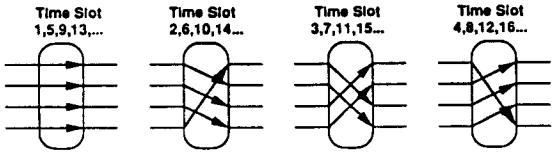

0740

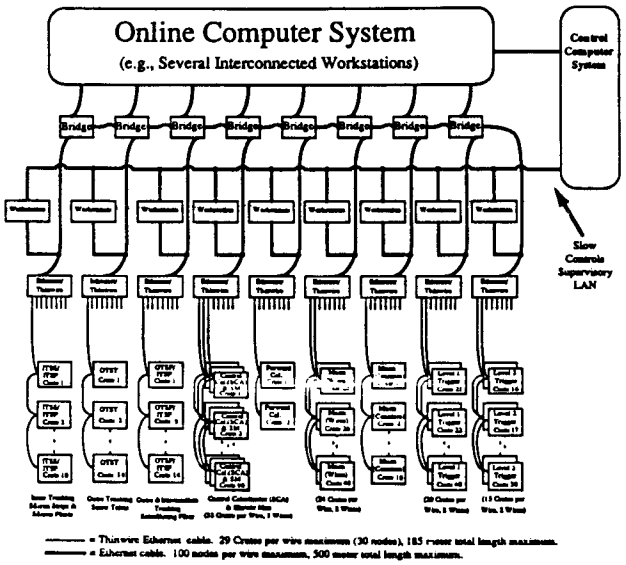

Commissioning & Maintaining
The SDC Data Acquisition System

Commissioning includes installation, integration & testing. Maintaining includes error detection & correction quickly & easily.

Requirements:

1. Independent (stand-alone) commissioning of a single front-end system or trigger system
2. Calibrations & various other tests
3. Monitoring & control of a front-end system or trigger system
4. Data sampling during run
5. Etc.

Subsystem crates or local data nodes, if implemented, are called Sub-Detector crates in the following:

Arguments Against Sub-Detector Crates:

1. All requirements are met without them.
2. Additional costs & complexity are incurred.
   a. Extra crates, modules, supplies, etc. (some front-end systems may require more than one Sub-Detector Crate)
   b. Interruption of fiber cables & fewer but costlier higher-speed fiber cables
   c. Data balancing into Event Builder Subsystem only by front-end (or trigger) system

SDC Data Acquisition System
(Without Sub-Detector Crates)

Event Builder Subsystem Implementations

With No Sub-Detector Crates

With Sub-Detector Crates

SDC Data Acquisition System
(With Sub-Detector Crates)

SDC Data Acquisition System
Current Status Of CDR, Technical Proposal & Costing Tasks
November 14, 1991

Tasks	Status
Conceptual Design Report	- 9/4/91 draft reviewed by SDC DAQ group - 9/24/91 draft distributed and reviewed at ORNL SDC Collaboration meeting - Next draft 75% completed; being restructured more into Technical Proposal format
Technical Proposal DAQ Section	- Initial outline revised and being sent to Fred Kirsten - Will be written by Ed Barsotti & Irwin Gaines - Writing just started - Backup material must be written up into a single document; some not attained yet
Descoped Costing	- Excel spreadsheet M&S 95% complete; manpower component 15% complete but not yet incorporated into spreadsheet - MacProject 20% completed

Miscellaneous Tasks	Status
Switch-Based Data Acquisition System Prototype Project Report	- Project completed successfully in April, 1991 - Results report 80% complete; to be distributed at the February, 1992 SDC Collaboration meeting as a SSC Technical Note
Event Builder Subsystem Detailed Implementation Proposal	- 20% completed - Being written using either a commercial switching network or one built by the collaboration

SDC Data Acquisition
Descoped Costing Summary
(November 14, 1991)

M&S	Estimated Cost
- Infrastructure	$865.0K
- DAQ Control/Monitoring Network	70.0K
- Crates, Power Supplies, Etc.	40.0K
- Event Data Readout & Control/Monitoring Network Interfaces	
- DAQ CPU Modules	1510.0K
- Crate Adapter/Interface Modules	120.0K
- Event Data Links	137.0K
- (Other Items)	15.0K
- Event Builder Subsytem & Links To The Online Processor Subsystem	1100.0K
- Event Data Flow Control Subsytem	11.0K
- Online Processor Subsystem	6640.0K
- DAQ Offline Analysis Interface	250.0K
- Electronics Rack Protection Subsystem	1782.0K
M&S Total	**12540.0K**

Manpower	Estimated Cost
Manpower Estimated Total	**12460.0K**
Overall Totals	**25000.0K**

+++DRAFT+++

SDC Data Acquisition System
Technical Proposal Outline
(11/14/91)

8.9 Data Acquisition and Slow Control

8.9.1 Data Acquisition System Overview

8.9.2 Data Acquisition System Requirements
- 8.9.2.1 Data flow and event collection requirements
- 8.9.2.2 Data monitoring requirements
- 8.9.2.3 Slow control requirements
- 8.9.2.4 Partitioning and stand-alone operation requirements
- 8.9.2.5 ...abilities requirements

8.9.3 Relationship of Data Acquisition to other Subsystems
- 8.9.3.1 Relationship to front-end system
- 8.9.3.2 Relationship to trigger system
- 8.9.3.3 Relationship to slow controls system
- 8.9.3.4 Relationship to On-line computing system
- 8.9.3.5 Relationship to level 3 processor system

8.9.4 Data Acquisition System Architecture
- 8.9.4.1 Logical block diagram
- 8.9.4.2 Physical block diagram and layout
- 8.9.4.3 Data flow paths
- 8.9.4.4 Control paths and slow control system
- 8.9.4.5 Partitioning and stand alone operation
- 8.9.4.6 Major DAQ components and channel counts
  - a) Event data read-out modules
  - b) Subsystem crate
  - c) Event builder subsystem
  - d) Event data flow control
  - e) On-line processor subsystem
  - f) Control computing interface
  - g) Rack protection subsystem
  - h) Software systems

8.9.5 Additional DAQ Component Details
- 8.9.5.1 Front-end & trigger system event data readout & control/monitoring interface
  - a) Crates, backplanes and power supplies
  - b) DAQ CPU modules
  - c) DAQ event data readout bus slave interface
  - d) DAQ crate adapter/interface module
  - e) Event data links
  - f) DAQ control/monitoring network
  - g) Remote DAQ control/monitoring network interface, links & repeaters
- 8.9.5.2 Event builder subsystem
  - a) Input interface & data balancing/input queueing network
  - b) switching network
  - c) Interface to online processor subsystem
- 8.9.5.3 Event data flow control subsystem
  - a) Interface to trigger subsystem
  - b) Interface to other DAQ subsystems
  - c) Event data flow and trigger inhibiting
- 8.9.5.4 Online processor subsystem
  - a) Processing and software development environment
  - b) Interface to other DAQ subsystems
- 8.9.5.5 Software systems
  - a) Run control
  - b) Runtime user interface
  - c) Control and monitoring interface
- 8.9.5.6 Stand-alone DAQ systems

8.9.6 Commissioning the Data Acquisition System (Installation, Integration & Testing)

8.9.7 Status, Ongoing and Future R&D, Milestones & Critical Path Items

SDC DAQ Milestones

Completion of DAQ requirements	Nov, 91
Completion of DAQ system design, incl. technical choices	1993
Completion of DAQ component design	1994
Portable DAQ for use in test beams/labs	1994
Prototypes of all DAQ components	1995
Delivery of partial DAQ systems for subsystems	Jan, 97
Muon subsystem	?
Calorimeter subsystem	?
Tracking subsystem	?
Installation of complete DAQ system	Jan, 99
Certification of full, working DAQ system	July, 99

SDC Second Level Trigger Using ASP

J. Brisson(CEN Saclay)

Second Level Trigger

==> ***Tightly coupled to Data Acquisition*** <==

Quick decision to refine the selection of triggered events

- Better granularity than level 1
- Better energy resolution : Digital
- Multi-detector correlation
- Topological decisions
- In the 5/50μs range

==> ***Needs flexible algorithms*** <==

R & D for new architectures ==> ***Parallelism***

Proposed solution ==> ***ASP : Associative String Processor***

0753

SDC Second Level Trigger using ASP

November 1991

J. C. BRISSON - O. GACHELIN - P. LEDU - B. THOORIS

D.A.P.N.I.A.

CEN SACLAY

91191 Gif sur Yvette CEDEX France

0751

VASP-64 : String of associative processors

→ ***two basic concepts (Prof LEA) :***

- Suppress memory access → One processor for each data word
- Suppress addressing → Associative access to multiple data

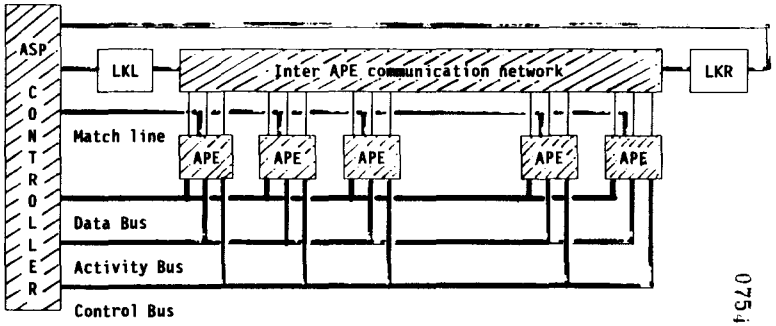

0754

* 64 bits data register * * 64 processors on each chip * * 2K Machine working

Event selection at SDC

==> ***At least one event for each beam crossing*** <==

One event ==> ***several Mega-bytes of data.***

==> ***Needs for an efficient selection of good candidates*** <==

First level Trigger :

- → reduction of event rate by a factor of 1000

Second level Trigger :

- → further reduction of event rate by a factor between 50 and 100

Third level Trigger :

- → final selection → processors farm (RISC)

0752

ASPEN Architecture

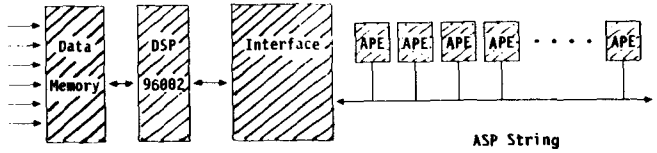

★ ***Model***

- μP pushes requests for execution
  - → of one single instruction
  - → or a linear sequence of (prestored) instructions
- μP handles :
  - → control flow
  - → serial field addressing
- μP has memory mapped access to ASP vector

0757

ASP's Embedded in DAQ as Trigger Processor

ASP distributed on front end acquisition boards

- Data channels connected to ASP string
- Logical machine distributed over many boards
- ASP controller on board (DSP ?)
- Correlation network (Transputers ?)

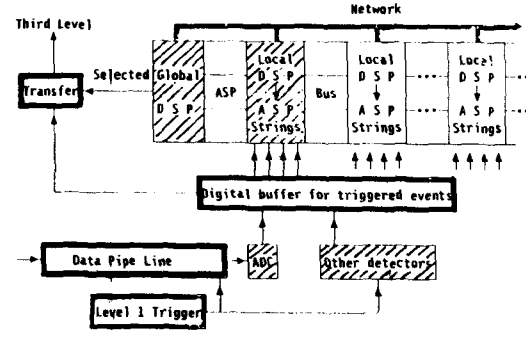

0755

DSP/ASP Interface

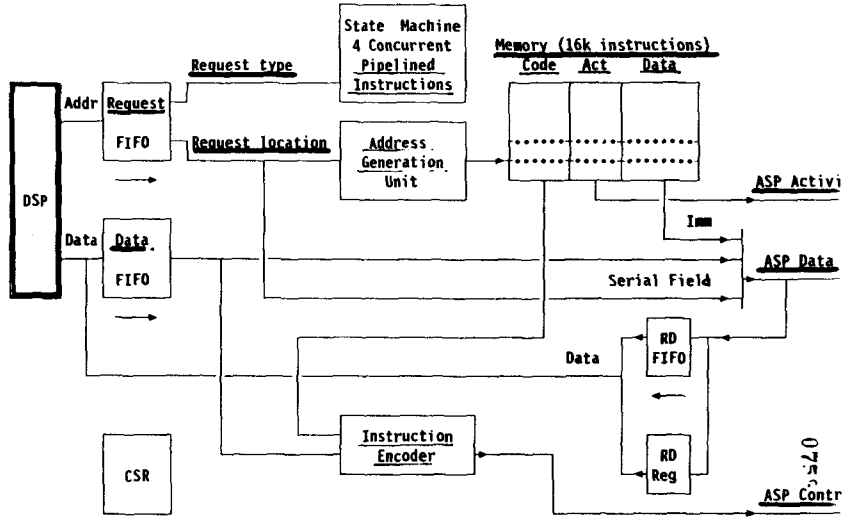

ASPEN (ASP Embedded Node)

★ ***Hardware : Fast microprocessor (DSP 32 bits, floating point) → ASP String***

- ASP string controller
- interface to other trigger elements
- detector interface
- use as scalar processor
- prototype ready in February 92 (1K)

★ ***Software : Program written in C language***

- DSP program control :
  - microprocessor activity
  - ASP activity
  - rendez-vous
- ASP primitive procedures embedded in source DSP program sequence
  - Compiler builds an ASP "data list" of instructions
  - Compiler replace initial ASP code by a "move" to ASP interface
- Dynamic interpretation at run time

0756

Second level trigger project for SDC

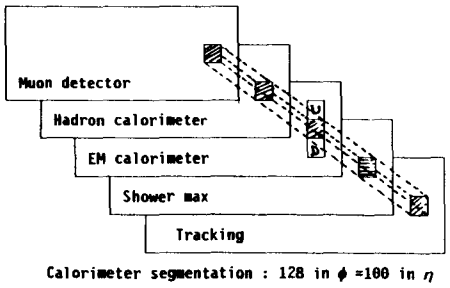

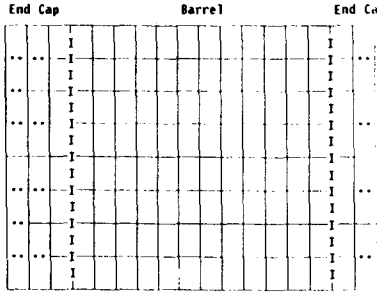

Data in APE register : 2 APE for each projected pixel

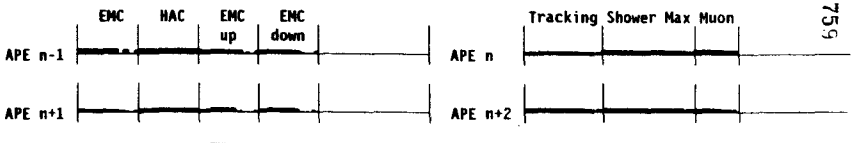

0759

Results of Simulations

Timing evaluation performed on VASP-64 Simulator

Does not depend on the number of towers

Isolated Electrons:

- First threshold = 1 μs to find electron candidate
- Second threshold = 1 μs to separate from hadron
- Third threshold on neighbors and electrons counting = 2 μs
  - Total = 4 μs

0760

Report on Location of Electronics Inside or Outside Muon Steel

Electronics Working Group

TO: Gil Gilchriese and Tim Thurston

FROM: SDC Electronics Working Group

DATE: November 15, 1991

RE: **LOCATION OF ELECTRONICS INSIDE OR OUTSIDE MUON STEEL**

The Electronics Working Group considered four possible locations for electronics currently being located between the calorimeter and the muon systems:

1) Location outside the muon system

2) Location in rack-mounted crates along the vertical walls of BW1

3) Location in crates mounted on the back of the calorimeter

4) Revised layout of electronics on the back of the calorimeter, possibly in more compact crates or without crates

Some of the issues in locating the electronics are:

Electronics Performance
Reliability
Ease of Maintenance
Ease of Design
Cost

Conclusions of the discussion are summarized below without full elaboration of the issues.

GENERAL CONCLUSIONS

The following general conclusions were drawn:

1) VLPC cryostats must be located in close proximity to the endcap-barrel crack to minimize attenuation of signals to the VLPCs. This conclusion could change as the attenuation length of clear fiber waveguides becomes better understood; however, it is unlikely that the fibers could be extended more than a few meters.

2) Calorimeter calibration source pigs must be located on the calorimeter.

3) Power distribution for chamber-mounted straw tube electronics must be located near the endcap-barrel crack to minimize length of leads.

4) For SCA-based calorimeter and shower max readout, preamplifiers and shaping amplifiers must be physically coupled to photodetectors to minimize electronic pickup prior to signal amplification.

5) For flash digitizer-based calorimeter and shower max readout, current splitters, integrators, and flash digitizers must be physically coupled to photodetectors to minimize electronic pickup prior to signal integration and digitization.

6) VLPC, straw tube, and all calorimeter readout systems should be located as close as feasible to signal sources to optimize cable length in order to minimize:

a) signal dispersion in cables
b) signal ground return paths and ground loops
c) required signal swings
d) power dissipation in cable drivers
e) crosstalk to other signals
f) signal feedback to analog input of electronics
g) cross section of cables
h) cost of cables for a given cross section

7) All electronics, including photomultipliers, must be accessible for repair.

LOCATION OUTSIDE THE MUON SYSTEM

With respect to location of electronics outside the muon system, it was concluded that:

1) There is no compelling cost advantage to an outside location. Cost savings due to reduction in size of the muon system are approximately offset by additional cable costs. (Please see report of Chris Bebek.) Cable drivers, supplemental engineering to handle cable dispersion, and supplemental cable installation costs would likely more than offset any residual muon system savings.

2) Electronics performance with the required cable runs is uncertain.

3) The large aggregate cross-sectional area of the cable plant would introduce additional dead space in the muon system.

4) Access to and delivery of services to electronics outside the muon system would not be significantly improved compared to rack-mounted electronics within the muon system.

The group strongly agreed that the electronics should not be located outside the muon system and that the inner radius of the muon radius should be chosen to be adequate for electronics located between the calorimeter and the muon system.

LOCATION IN RACKS VS. ON BACK OF CALORIMETER

With respect to location of electronics in racks within the muon system as compared to location of electronics on the calorimeter, it was concluded that:

1) The required inner radius of the muon system, and hence the cost of the muon system, is essentially the same for electronics located in crates in either location. (Please see report of Tim Thurston.)

2) Electronics performance may be compromised by the longer cables required by the rack-mounted location. In addition, it may be compromised in the rack location by the fact that the electronics ground is less well tied to the ground of the upstream electronics and of the detector. The particular issues here are signal dispersion, electronic pickup, and ground loops.

3) The rack-based system affords more convenient access to the electronics; however, access to electronics in crates on the calorimeter is adequate. Electronics can be designed to be sufficiently reliable for location on the calorimeter. Requirements for reliability are not as severe for electronics on the back of the calorimeter as for the silicon tracker and straw tube electronics which has similar functionality and is embedded deep within the detector. Routine servicing of electronics will be by card replacement.

4) Access to most, but not all, photomultipliers is better if electronics is rack-mounted. An adequate plan for access to photomultipliers has not yet been developed for the case of electronics on the calorimeter.

5) Access to electronics on the back of the calorimeter, and to photomultipliers, will be different for layout of electronics for different choices of tracking detector and calorimeter readout technologies. For instance, the case of a straw tube tracker and readout of the calorimeter by switched capacitor arrays (SCA's) may require the least physical space among the current scenarios; whereas, the case of a scintillating fiber tracker and readout of the calorimeter by digital photomultiplier bases may require the most. Access to photomultipliers may be adequate in some scenarios but not in others.

The group concluded that locating the electronics on the back of the calorimeter is preferable to rack-mounting next to the muon system and that an electronics layout which affords adequate photomultiplier access should be developed for each of the different combinations of tracking technology and calorimeter readout, rather than only for a worst case scenario. The group recognized the need for substantial cooperation with the integration group in order to develop appropriate layouts. Finally, the group recommends that provision be maintained for the rack-mounted location as a backup in case no appropriate layout is possible for the combination of tracking and calorimeter readout technologies finally adopted.

ALTERNATIVE PACKAGING SCHEMES

With respect to development of electronics to be mounted on the calorimeter without crates or in more compact crates, the group recommends that alternative packaging schemes be considered as well as layout of crate-based electronics for possible scenarios as suggested above, but that consideration of crate-based layouts on the back of the calorimeter be given priority. As well as improving access to photomultipliers, re-packaging may reduce or eliminate cables and connections, with consequent performance and possible reliability gains, at the cost of increased engineering effort.

RECOMMENDATIONS

In summary, the Electronics Working Group recommends that:

1) The inner radius of the muon system should be chosen so as to allow location of electronics in crates on the back of the calorimeter or optionally in racks adjacent to the vertical BW1 muon chambers.

2) Layout schemes which locate electronics on the back of the calorimeter with adequate access to photomultipliers should be developed for presentation in the technical proposal.

Technical Assessment of the Electronics for the Central Tracking Options

Electronics Working Group

TECHNICAL ASSESSMENT OF THE ELECTRONICS FOR THE CENTRAL TRACKING OPTIONS.

FIBER TRACKING SYSTEM

The success of the fiber tracking system depends on the development of a VLPC which meets the criteria:

Quantum efficiency >80%
Reduced infrared sensitivity
Contact resistance <200Ω
Small bias variation
Reduced sensitivity to latchup

The progress to date in the development of this device by Rockwell has been impressive, but there does not yet exist a device that meets all of the criteria. The proponents of the fiber tracking system expressed their optimism that such a device will be made before the year's end.

One important characteristic of the device that has not been shown is the ability to produce a pulse that can be amplified and shaped with the required risetime and pulse slewing. The direct output of the VLPC has not been prasanted.

A new custom circuit will have to be designed to amplify, shape, and discriminate the signals from the VLPC. This appears from the specification to be a straight forward adaptation of the straw tube ASD. There are questions about what modifications to the amplifier design will have to be made to alleviate the latch-up problem. Wa would like to have more information on the equivalent circuit parameters for the VLPC and custom cable in the cryostat.

The mounting of the ASD's on a P.C. board and the mounting of the P.C. board on the cassette part of tha cryostat seem to be straight forward. However two significant issues are (1) how the electronics is to be cooled (120 to 160 watts per cryostat) given the high packing density, and (2) whether the outputs of the ASD can be single-ended over a ground plane as currently proposed. It is possible that single-anded outputs will not work and that differential outputs will be required. In this case the cable plant from the cryostat, to the crata, which is already large and dense, will double in size.

The digital electronics for the trigger and data buffer appear do-able. The number of iterations needed to make the full custom integrated circuits work has probably been underestimated. While the boards as designed can probably be mada, the cabling plant will be a nightmare. The space required for the crates, cryostat, and the cables aggravate the already difficult problem of laying out the area around the calorimeter. Much of tha complexity of the system particularly the cabling and interconnection has been driven by the requirement to do tracking reconstruction using all superlayers with uniform efficiency in the trigger, at the beam crossing rate. It has not yet been demonstrated that this is necessary to meet the triggering goals.

Finally, since Rockwell is the sole supplier of this device one can not choose fibers for the outer tracker until a suitable contract with guaranteed price and delivery has been negotiated and signed.

STRAW TUBE TRACKING ELECTRONICS

Most of the electronics for the straw tube tracker will be mounted on a board at the end of the straw tubes. The ASD circuit for straw tube readout is straight forward and there are at least two vendors for this chip. An 8 channel chip is in fabrication now.

The time measurement and level one storage chip, the TMC, has been shown to work, although the present version, which incorporates 4 channels per chip, has only 1 microsecond of storage. It is thought to be reasonably straightforward to extend this to 4 microseconds. The outstanding problem that has to be addressed is increasing the radiation hardness. The level 2 buffer as currently designed is a separata chip. There are advantages to combining the level 1 and level 2 storage on a single device. The details of the connection to the DAQ and to the overall trigger system have not been worked out. The risk of having a single source for the TMC is not viewed as being a problem.

The trigger chip for the straw tubes does not appear to have any problems. There are multiple sources for this device.

The major problems for the straw tube electronics are packaging all of the components, demonstrating that the digital logic can operate without too-much cross talk to the straws and preampifiers and design of a satisfactory system for cooling. Several solutions are being pursued, the amount of effort applied is commensurate with the problem, and it is likely that one or more solution will work.

CONCLUSIONS

Overall the signal processing and digital logic for both the straw and fiber systems seem reasonably straightforward (though not trivial). The difficulties of packaging, cooling, and minimizing cross talk ara greater for the straw chamber electronics than for either tha ASD or digital logic of the fiber tracker. However, given the problem of the interconnection in the fiber tracker and the uncertainty in the operation and delivery of the VLPC, the overall risk for the fiber system is larger than that of the straw tubes.

A substantial system test of both systems will be required to unambiguously address these concerns. This test should involve fully instrumenting 256 to 512 channels of the detector. For the fiber system this would correspond to at least one fully loaded cassette. For the straw tube systam this would correspond to at least one module with an attached electronics board. It is thought that it is unlikely that either system could produce this full system test prior to September 1992.

Review Committee: M. Campbell
H.H. Williams
J. Oliver
C. Bebek

MUON SYSTEM

(PARTIAL)

NOVEMBER 13-14

Design of a JET-cell Chamber System for the SDC Muon Detector	KEK Muon Chamber Group
Concept for the Intermediate Region and BW3 vs. IW3	H. Iwasaki(KEK)
1st and 2nd Level Muon Triggers Based on the Jet Chamber Design	H. Sakamoto(KEK)
Forward Muon System	A. Skuja(Maryland)
SDC Muon Simulation at University of Illinois	Errede, et al.
Muon Matching Studies	S. Errede(Illinois)
BW3 - BW2 Radial Separation Studies	J. Wiss(Illinois)
Muon System Alignment Studies	J. Wiss(Illinois)
Muon Momentum Resolution	V. Slonim(Colorado)
Preliminary Proposal for SDC Muon Scintillator System	R. Thun(Michigan)
Possibility of Constructing a First Level Muon Trigger with Adjustable Pt Threshold	V. Molchanov(Protvino)
Muon Front End Analog Electronics	J. Oliver(Harvard)
Muon System Front End Electronics - Preliminary Conceptual Design Report	J. Oliver(Harvard)
Drift Tube Development at Minnesota	K. Heller(Minnesota)
Prototypes	R. Loveless(Wisconsin)

LPBautz:12/13/91

Design of a JET-cell Chamber System for the SDC Muon Detector

KEK Muon Chamber Group

Design of a JET-cell chamber system for the SDC Muon Detector

KEK Muon Chamber Group

Y. Funahashi, Y. Higashi, H. Iwasaki, T. Kondo,
A. Maki, S. Odaka, T. Shinkawa and S. Terada

October 8, 1991

Draft prepared for the presentation to the muon cost review workshop at SSCL on October 9-10, 1991

1. Introduction

As a natural solution to fulfill the challenging requirements on overall spatial resolution of ~200μm to the muon track measurement for the SDC muon detector system, which covers ~2000 m^2 in barrel region, an innovative design of a drift chamber module based on a Jet cell structure has been proposed and worked out by the KEK muon group.

In this draft, we will present a clear illustration of the chamber system to demonstrate that the design is feasible and realistic, and also present a set of data with which we could extract the system cost as reliable as possible. The R&D is yet in a mid-way, however, and we still have many things to do to reach a satisfactory complete system design. Accordingly, the data we present here are by no means final. Therefore, we try to make the data to be in conservative side, if not precise, so that any further progress of R&D and design optimization should more likely give us a corresponding cost reduction rather than cost escalation.

2. Basic configuration of the chamber module

a) Oriented Jet cell

The cell structure is a jet cell of three sense wires in a cell with minimum set of electrodes as shown in Fig.1. The cells are gradually tilted as they go toward the edge of the barrel toroid so that any row of sense wires points at the interaction region. The cathode is made of thin rigid plates which separate individual cell. It is helpful for isolating broken wires. Relevant parameters of the cell design are summarized in Table 1. Those parameters have been modified from the original one by considering the recent results of the gas gain study using a small test chambers.

b) Two-story chamber module

Also shown in Fig 1 is a basic cell arrangement in a chamber module. The chamber module is essentially a rectangular flat box with thin aluminum structure. The module consists of two half-cell-staggered jet cell layers partitioned by a middle honeycomb plate. The benefit of this module configuration is to provide a very effective trigger scheme utilizing a mean-timer logic as well as to solve a left-right ambiguity.

3. Physical requirement

a) Module boundary and chamber width optimization

In order to minimize dead regions in the muon coverage, relatively wide modules of about 3.5 m in width for the theta layer in BW3 were originally considered. The boundary region, where the half cell staggered two layer arrangement is not perfect, becomes about 6 % of the whole barrel muon coverage in η. However, as shown in Fig 2 and also as summarized in Table 2, at least one cell of each superlayer covers the boundary and at least one superlayer, either BW2 or BW3, provides a healthy trigger at any η. Since the boundary is not very critical, we should optimize the module width by taking the various other factors into consideration such as mechanical rigidity, fabrication, transportation, handling, supermodule assembly, overall cost. In this draft we propose a somewhat narrower module width of ~2.5 m for the BW3 layer as a typical large size chamber module.

b) Layout of the chamber

Based on this new chamber width, a layout of the chamber module and a supermodule configuration were worked out in accordance with the 'Muon System Baseline Parameters (9/25/91)'. Schematic illustrations of the chamber arrangement are shown in Figs. 3 to 5. The arrangement is not exactly the same as

the one proposed by the Wisconsin group. We have four stereo layers in BW2 instead of two layers in BW3 in the Wisconsin design. The stereo layers are made of thin aluminum sheets and I-beams to form a single wire drift cell of 5 cm x 8 cm of cell size. Half cell staggered two layers are built into one single flat plate module two of which, as illustrated in Fig. 6, could serve as strong top and bottom lid of the BW2 chamber to withstand gas pressure of about 10 gr/cm^2. This kind of stereo chamber arrangement has already been used successfully for the L3 muon chamber system.

The phi chamber that we propose is also a jet chamber; essentially the same as the theta chamber, but the size is somewhat smaller so as to fit to the overall size of the supermodule.

c) Chamber size and channel count

The size of the chamber modules is listed in Table 3, separately for each superlayer. Number of sense wires were calculated for this arrangement, and are listed in Table 4. The increase of the channel count from the previous number (59k channels) is mostly due to a difference in the phi chamber arrangement. The phi chamber was placed in BW1 in the previous counts (6.0 k) and was longitudinally divided into 3 modules. In the present layout it is in BW3 and is divided into 4 modules.

4. Chamber structure and fabrication

a) Frames and middle honeycomb plate

The chamber frame structure consists of a pair of end frames, side frames, middle plates and a center support. The frame components are made of an extrusion aluminum, and the middle plate is an aluminum honeycomb plate. As illustrated in Fig 7, the frame components are tightly bolted and glued to the middle plates so as to form a rigid frame structure. In a frame assembly, the center

support should be properly aligned with respect to the end frames. To this end, as conceptually shown in Fig. 7, the center support should have some small (a few mm) adjustability with respect to the frame structure. An optimum shape of the frame cross-sections and a connection scheme to the honeycomb plate are shown in Fig. 8.

Holes to fix the feed-throughs and wire supports are precisely NC-milled on the end frames and the center support, respectively. Some details of the holes are shown in the drawings of the R&D module (Figs. 9 and 10).

Since the frame is expected to be very rigid even without having top and bottom plates, we can work on wire stringing and cathode plate assembly on an open frame structure.

b) Top and bottom lid plates

After finishing the wire stringing and cell structure assembly, the frame is closed with top and bottom plates to make a gas-tight rectangular box.
A critical requirement to the lid plates is that they should hold an inner gas pressure of ~10 gr/cm^2 with a small small deformation of a few mm or less, since they searve as a part of electrodes for the drift cell . As the chamber width becomes wide, this requirement is no more trivial. A honeycomb plate of ~4 cm thick with 1 mm thick aluminum skin can be one of choices. Thin aluminum sheets with I-beam interleaved structure or thin corrugated aluminum sheets with skins, as shown in Fig. 11, may also be a good choice. We need more study to find a cost optimum solution for the lids.

As discussed in chapter 3, like the L3 Jet chamber, we can use stereo-layer chambers for the lids of the theta chamber in BW2. With this arrangement, we can save cost and space to some extent.

c) Cathode plate arrangement

As shown in Figs. 12 and 13, cathode plates are supported with narrow insulator strips which are fixed to the side frames and the middle plates. Cathode plates and this strips form a matrix structure with sufficient rigidity. Although there may be many materials suitable for the cathode plate, we are going to try conventional 1 mm thick GFRP plates with copper clad for the R&D prototype chamber.

d) Feed-through and wire support

Plastic feed-throughs and wire supports can be made by an injection mold method. Since high voltage applied to sense and guard wires are comfortably low of ~2 kV (summarized in Table 2), conventional materials and techniques can be used. We have made several pieces of the feed-throughs and the wire supports for R&D and will make several 10 pieces to be used for the R&D prototype chamber.The design drawings are shown in Figs. 14 and 15. They are made by machining in the present R&D stage, while in a future mass production they will be made by an injection mold technique. The design will be modified so as to be optimized to the technique.

e) Wire Stringing

Similar technique used for CDF-CTC, illustrated in Fig. 16, can be used. Since the cathode plates are simple flat plate and wires are moderately thick, wire stringing must be relatively easier.

f) Middle support adjustment and position monitoring

To make a middle support adjustment easy and reliable, a LED-lens-CCD optical system, illustrated in Fig.17, will be implemented inside the chamber. Utilizing this system, we can always monitor the position of the center support in chamber fabrication, mounting and aligning on the truss and usual operation.

g) Weight of the module

Weight of the 2.5 m wide x 9 m long x 0.4 m thick module is estimated. The results are summarized in Table 5.

5. Supermodule assembly

a) Chamber module mounting

Similar truss structure as the Wisconsin system, shown in Fig. 18, can be used to mount the chambers into a supermodule. Some complication of the chamber support scheme compared with the Wisconsin chamber is that the position of the center support of the Jet chamber needs to be aligned with respect to the end frames. This can be done by pushing or pulling the center point of the side frame with a adjustable bracket which is fixed on the truss. Since the required stroke for the adjustment is a few mm only to compensate a gravitational sag of the chamber. Since the sag is estimated to be ~1mm at worst, a simple bracket might be used. The optical position measurement system in the module, discussed in chapter 4-e). must be very helpful for this adjustment.

b) Weight of the supermodule

One supermodule outside toroid consists of, as illustrated in Fig 19, three BW3 theta chambers, four BW3 phi chambers, three BW2 theta chambers and four layers of stereo chambers. Results of the weight calculations are listed in Table 6. The supermodule is indeed very light compared with the other systems.

6. Allgnment

i) Wire-to-module

Wires are accurately positioned to the end plate with precision NC-mill machining. The precision of this machining must be better than 50 μm.

ii) Wire-to-cell

Positioning of the cell walls(cathode plates) does not require good accuracy. They can be placed within ~1 mm accuracy. Since positioning of the cell walls are completely decoupled to the wire positioning, inaccuracy of the wall placement has nothing to do with the wire positioning.

iii) Chamber-to-chamber and Chamber-to-supermodule

This issue is not yet worked out seriously. We only say the following statements: The chambers are simple rectangular rigid boxes. They can be fabricated with the great precision of a few 100 μm. Laying the precision boxes each other and mounting them in a supermodule must be relatively easier.

We need to study in more detail how to fix and adjust the chambers on a truss to assemble the supermodule. One possible scenario is illustrated in Fig. 20.

7. Cost issues

Most of the basic parameters relevant to the cost estimation, such as the chamber size, cell structure, channel count etc. , have already been covered in the previous sections. Conceptual view of the module fabrication processes was also described in chapter 4, though we have to proceed more R&D to make a complete plan for an actual mass production process of the chamber.

8. Planning, scheduling and facllity lssues

Not covered in this draft. We will work on this issues, as soon as possible, with help of a company.

9. Development prototype description, schedule and status

a) Large prototype chamber

A prototype module of 3 m (width) x 8 m (length) x 0.42 m (height) has been under construction. Principal items to be studied with this prototype are i) mechanical rigidity of the module, ii) wire stringing and cathode plate furnishing,

iii) performance of the chamber, iv) mass production capability and so on. Some detailed drawings of the R&D chamber are shown in Figs. 9, 10, 20, 21 and 22.

b) Short prototype chamber

Basic chamber studies using short Jet chambers have been also going on. We have already obtained some useful data to optimize wire diameters and operating voltages as discussed in section 2-a). A short Jet chamber of the largest orientation of 30 deg. is almost ready to operate.

c) Schedule and status

The NC-mill machining of the frames and their assembly will be completed in the middle of October '91. We could start measuring mechanical properties of the R&D module by the end of October.

10. Comments and questions to WBS

In the WBS table for the jet chamber cost estimate, honeycomb plates dominate the overall chamber cost.

Now we bought a two honeycomb plates of 3m x 4 m x 4cm thick for the R&D module. The company charged us 1,200,000 yen which is about $8,600 with an exchange rate of 140 yen/dollar. This price is very close to the unit cost used in WBS, which is $329/m^2 for 40 mm thick plate. However we were told by the sales person from the honeycomb company (Showa Airplane Co. Ltd),that the price might go down significantly, say 1/2, if we order hundreds of plates. Has the WBS already taken this factor into account ?

Apart from the middle plate, we need not to use aluminum honeycomb for the top and bottom lids which we don't need great accuracy. As discussed in chapter 4-b), thin corrugated aluminum plate might be a good candidate, then the price for the lids may easily go down to 1/2 or lower.

Table 1. Parameters of the wires and the cathode plane.

	material	diameter	tension	voltage	wires/cell
sense	W	70 μm	400 g	+2.1 kV	3
potential	CuBe	140 μm	690 g	0	4
guard	CuBe	200 μm*	1.2 kg*	+2 kV*	2
cathode	—	—	—	−3.0 kV	—

*Yet to be optimized.

Table 2. Summary of the dead area for triggering in BW3, to be caused by module boundaries.*

position		dead area	
θ (deg)	η	Δθ (mrad)	Δη (×10^{-2})
80.9	0.16	8	0.8
64.3	0.46	18	2.0
51.3	0.73	15	1.9
41.7	0.97	13	1.9
total		54	6.6

*The estimation is based on the LOI geometry and our previous module design (9 modules/octant).

Table 3. Summary of the module size.

	length (m)	width (m)	height (m)
BW1 (θ)	5.4	2.5 (2.0)	0.40
BW2 (θ/s)	7.3	2.5 (2.0)	0.54
BW3 (φ)	7.5	2.15	0.40
BW3 (θ)	9.0	2.5	0.40

Table 4. Number of measurements along a muon track and summary of the channel count.

	measurements	cells	sense wires
BW1 (θ)	6	3.5 k	10.5 k
BW2 (θ)	6	4.5 k	13.5 k
BW2 (s)	4	13.9 k	13.9 k
BW3 (φ)	6	6.9 k	20.7 k
BW3 (θ)	6	4.9 k	14.7 k
total	28		73.3 k

Table 5. Summary of the module weight for the BW3 θ-chamber.

Component		weight (kg)	pieces/module
Frame	Side frame	98	2
	End frame	59	2
	Center support	32	1
	Middle plate	83	2
Frame total		512	
Top/bottom plate		83*	4
Top/bottom plate total		332*	
Cathode plate etc.		90	
total		940	

*We tentatively assume that the material is the same honeycomb plate as is used for the middle plate.

Table 6. Summary of the chamber weight in each supermodule.

	weight/module (ton)	modules	weight (ton)
BW2 (θ/s)	1.3	3	3.9
BW3 (φ)	0.72	4	2.9
BW3 (θ)	0.94	3	2.8
total			9.6

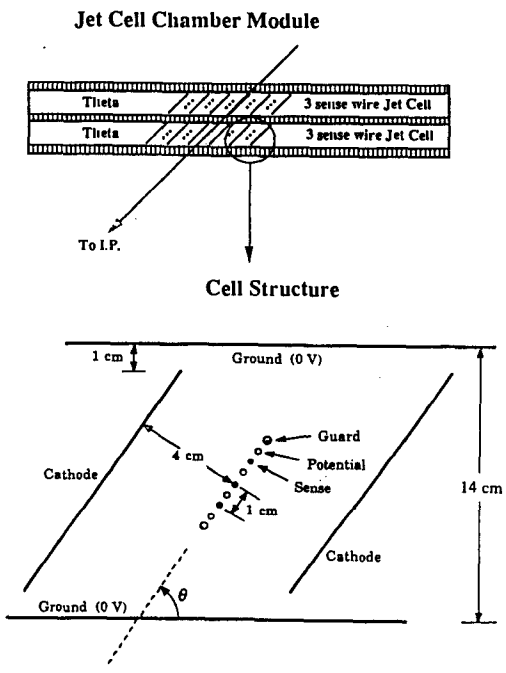

Fig. 1 Jet cell arrangement in a chamber and an oriented Jet cell

Boundaries of WC3 Theta Chamber

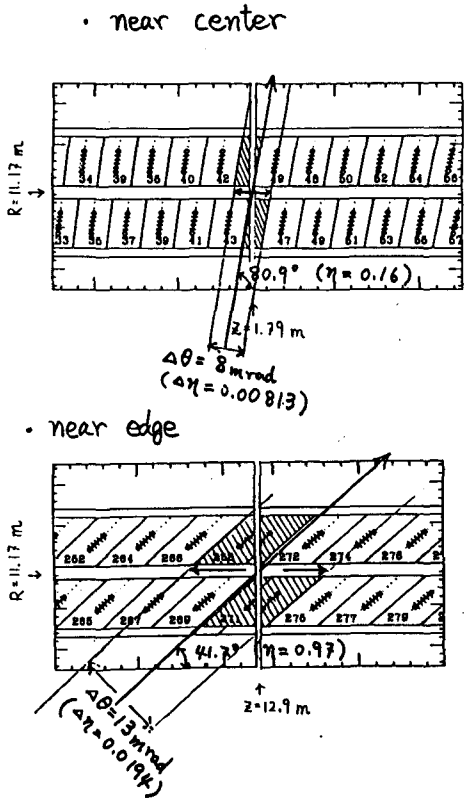

Fig. 2

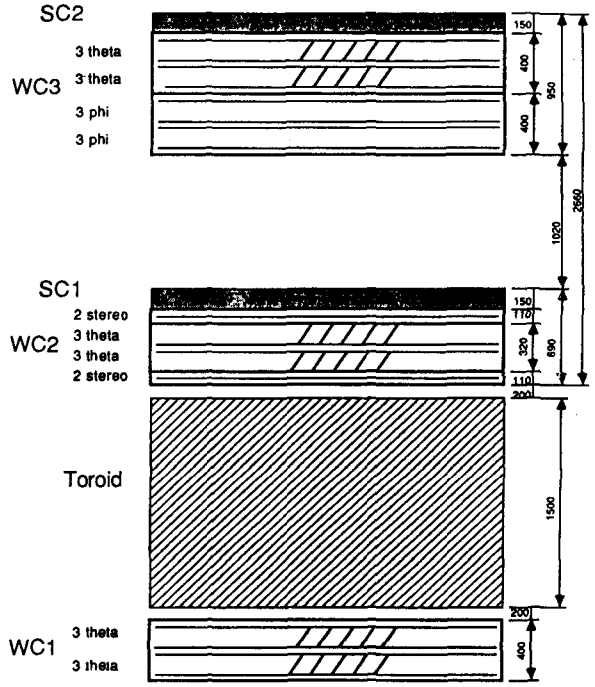

Fig. 3

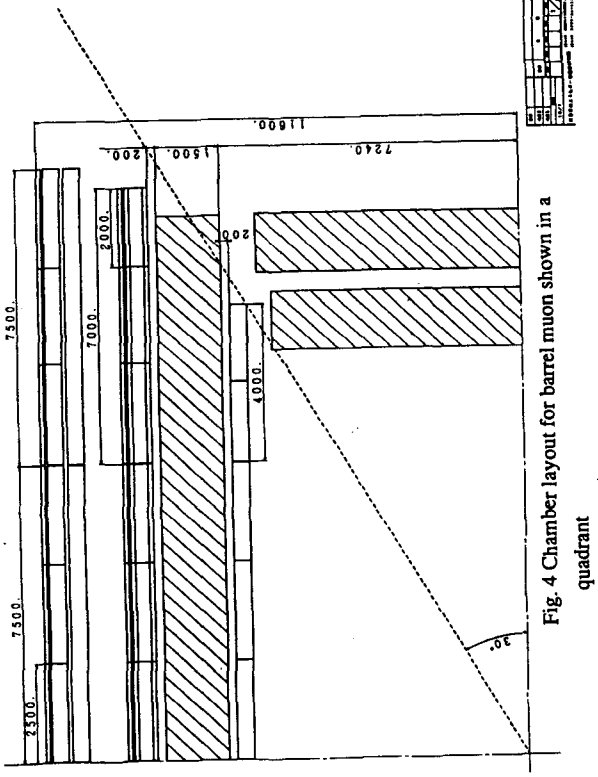

Fig. 4 Chamber layout for barrel muon shown in a quadrant

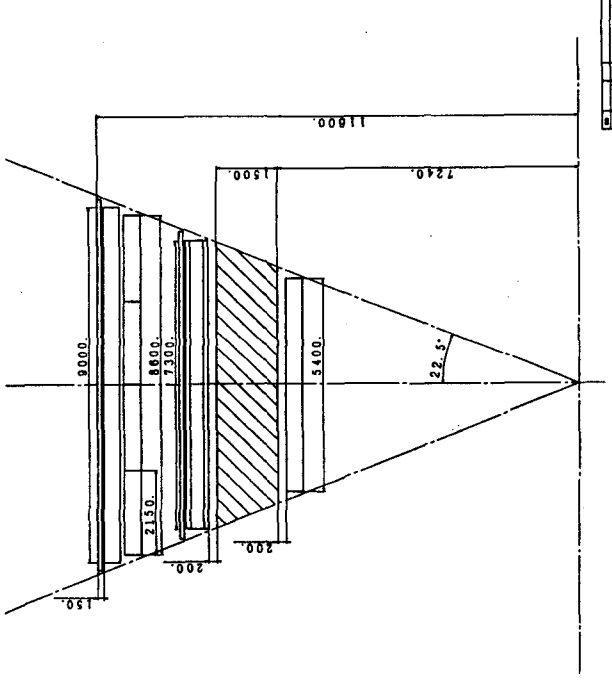

Fig. 5 Chamber layout for barrel muon shown in an octant

WC2 Jet Chamber with Stereo Layers as the Top and Bottom Plates

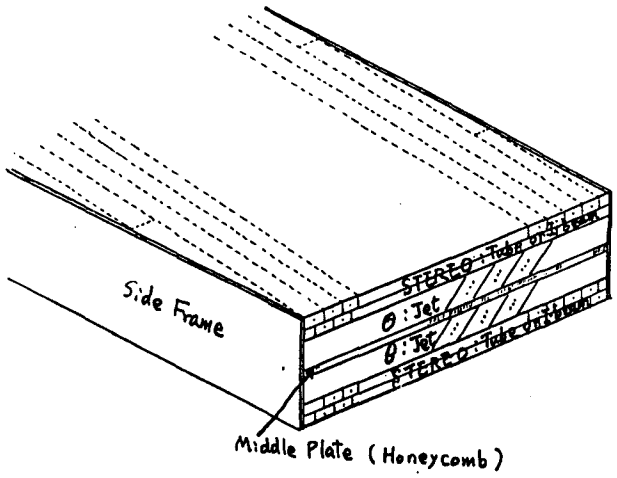

Stereo tube or I beam Chamber:
small slant angle with respect to the θ Jet Chamber
⇒ "Nothing comes out from the side"

Fig. 6

Frame structure and assembly procedure:

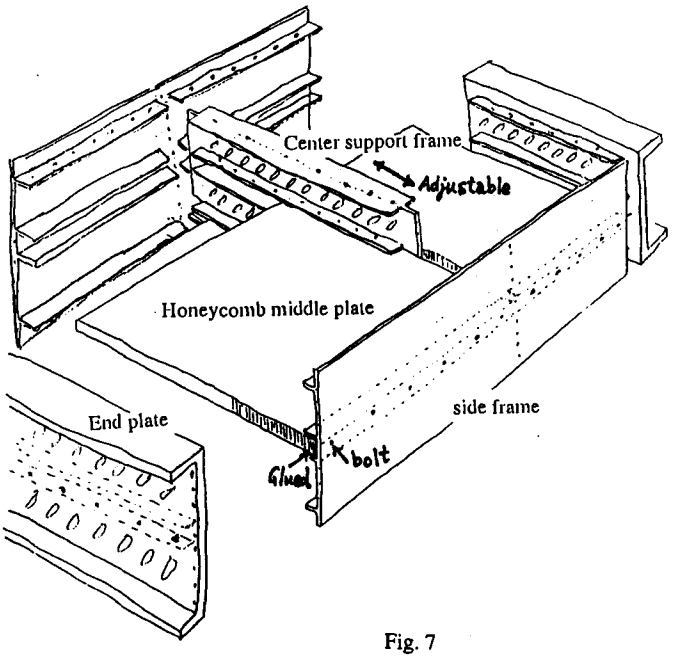

Fig. 7

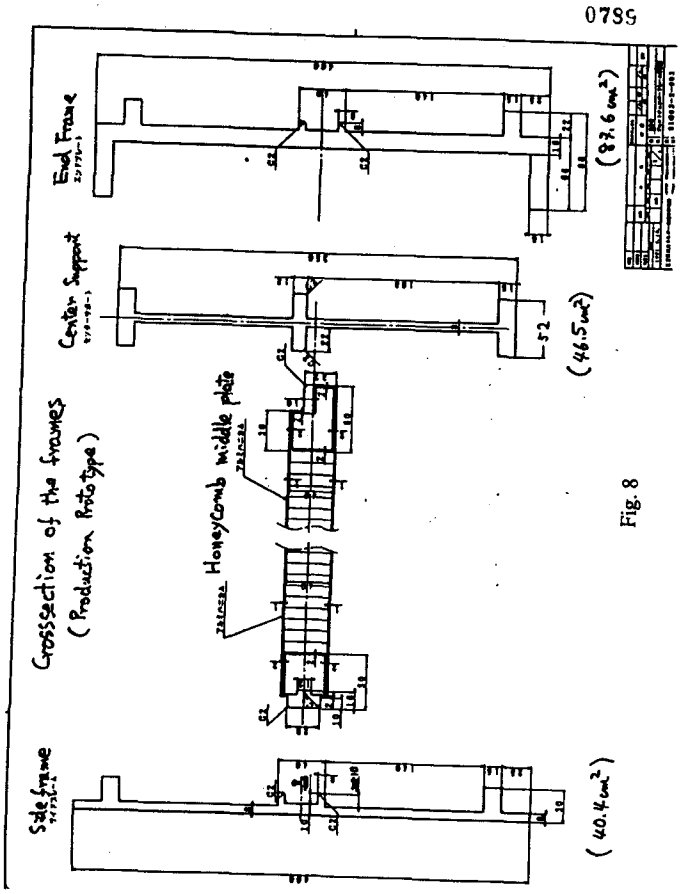

Fig. 8

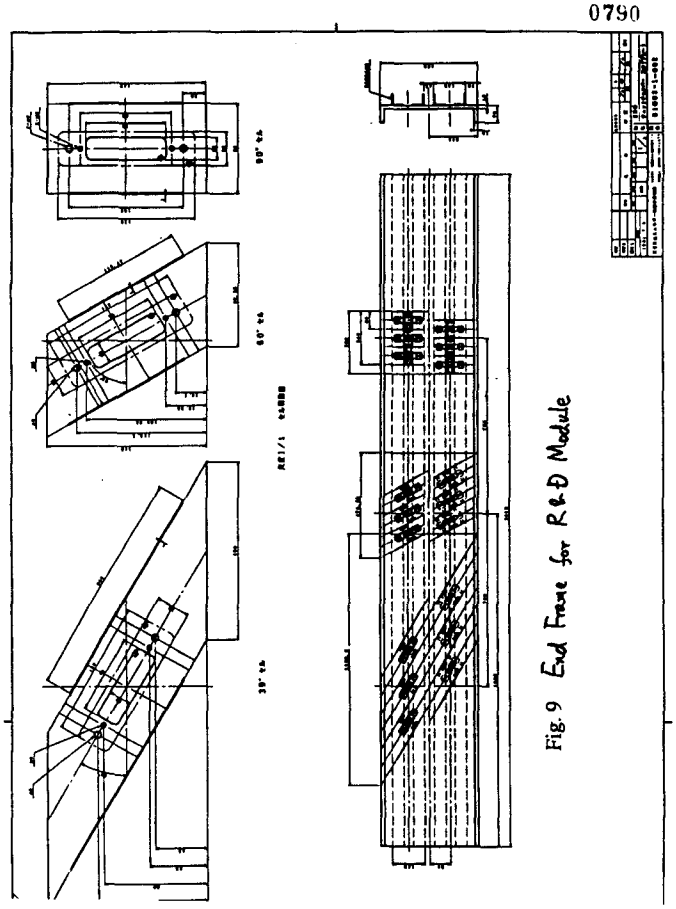

Fig. 9 End Frame for R&D Module

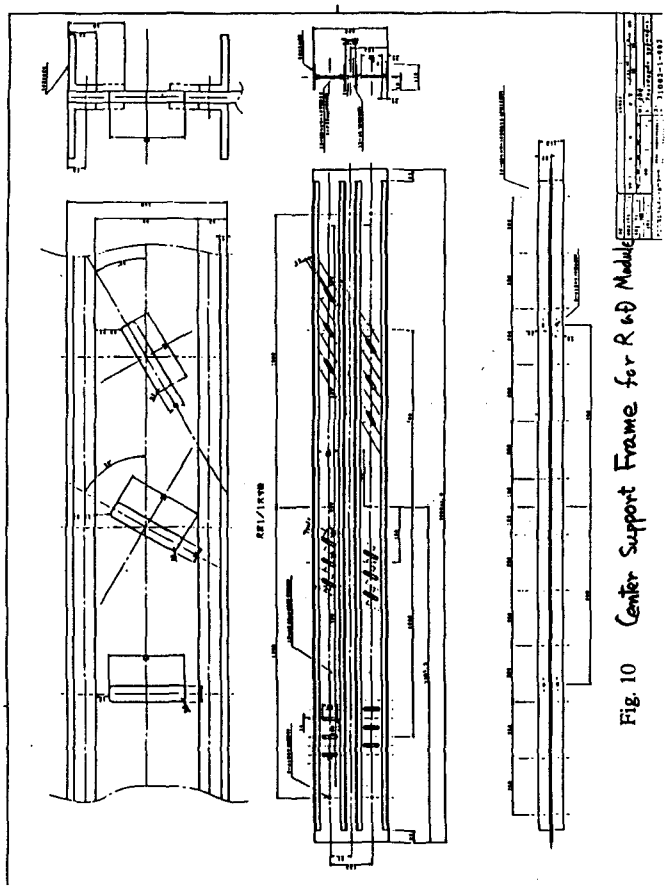

Fig. 10

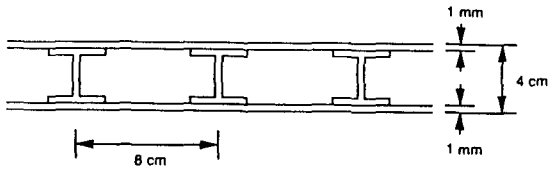

Thin sheets interleaved with I-beam.

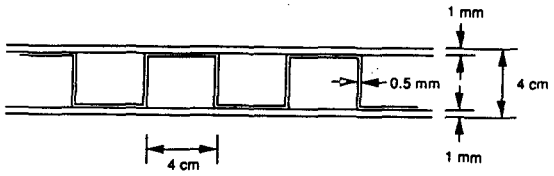

Corrugated aluminum with skins.

Fig. 11 Configurations of thin aluminum to produce a rigid plate for the top and bottom lids

Cathode Plate Arrangement
(Perspective view)

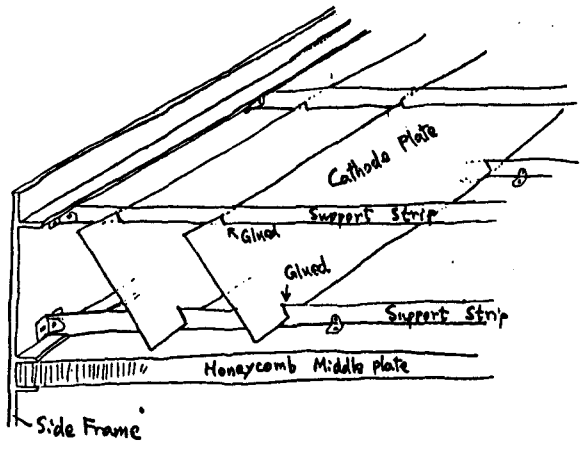

Fig. 12

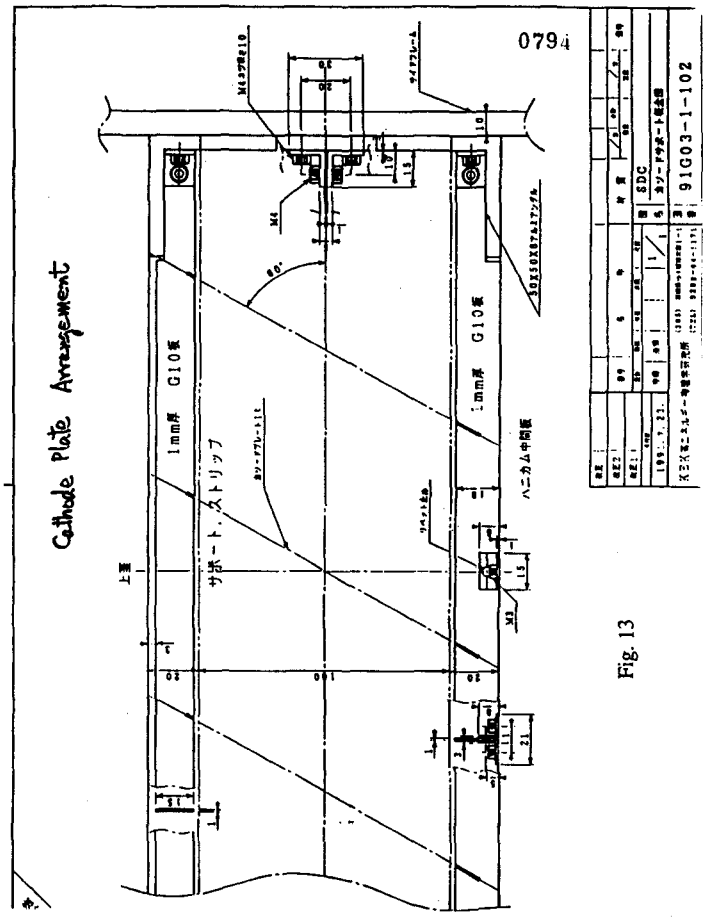

Fig. 13

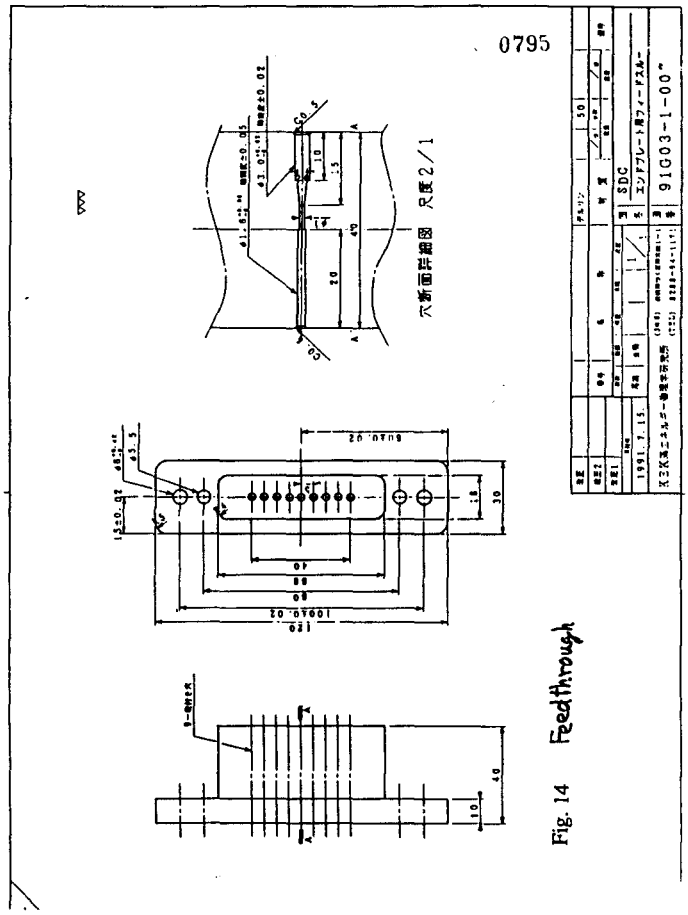

Fig. 14 Feedthrough

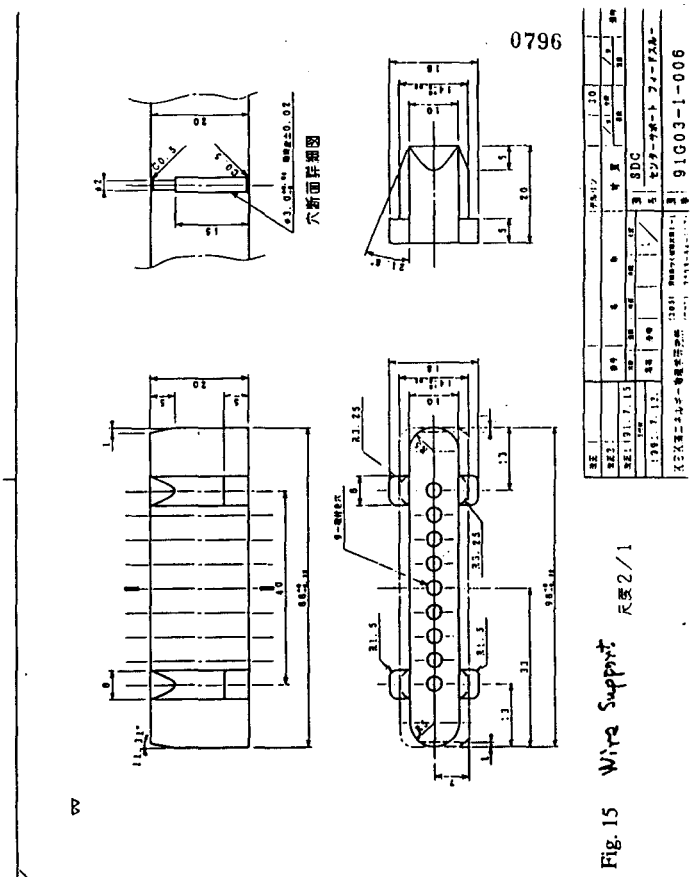

Fig. 15 Wire Support 尺度2/1

Wire Stringing Scheme

0797

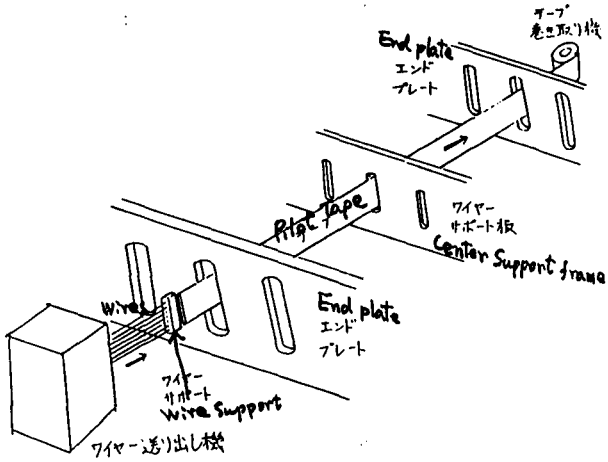

ワイヤー張り概念図 1991.5.7 尾高(S.Odaka)
(CDF-CTC方式)

Fig. 16

How to Compensate the deformations :

0795

a) Multiple spport points

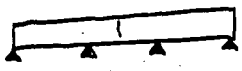

b) Adjust the frame Center

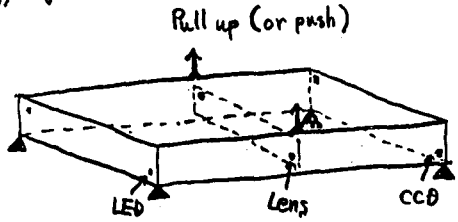

Position Measurement & Monitoring

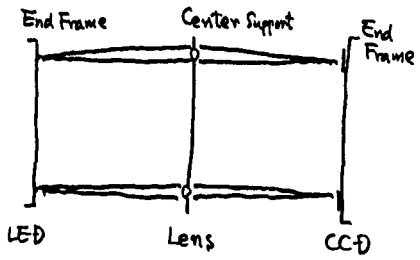

Fig. 17

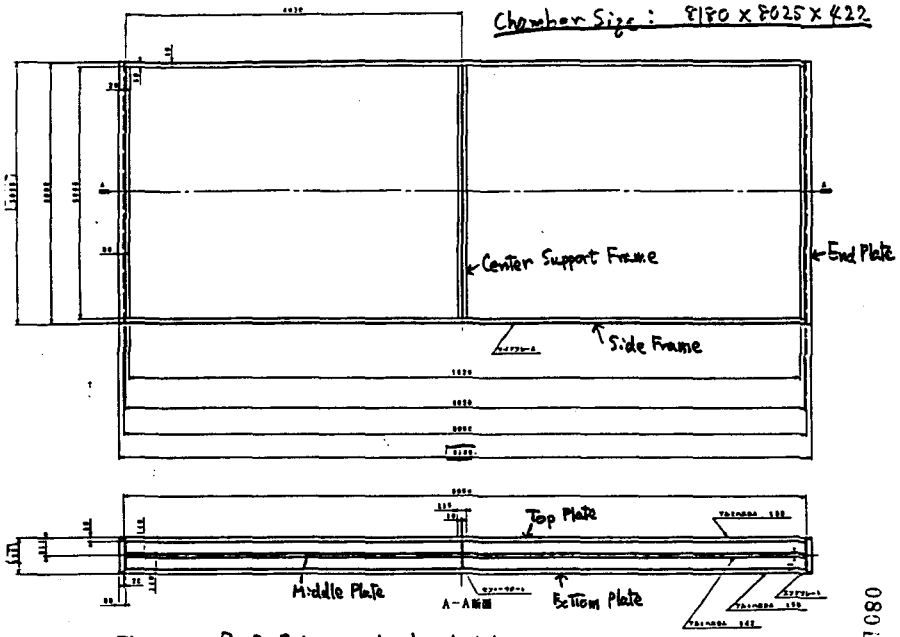

Fig. 20 R&D Prototype chamber Module

0801

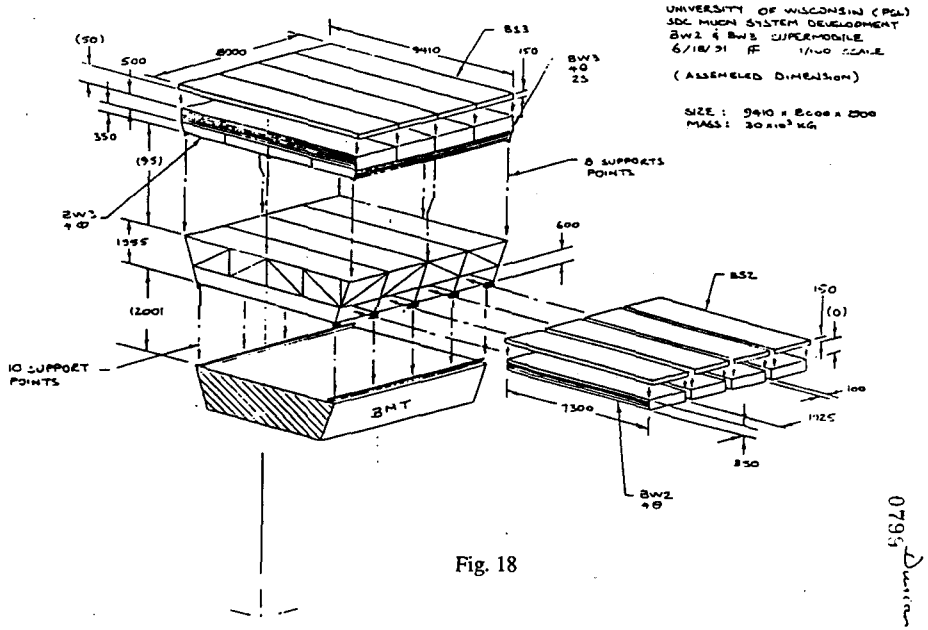

Fig. 18

0795

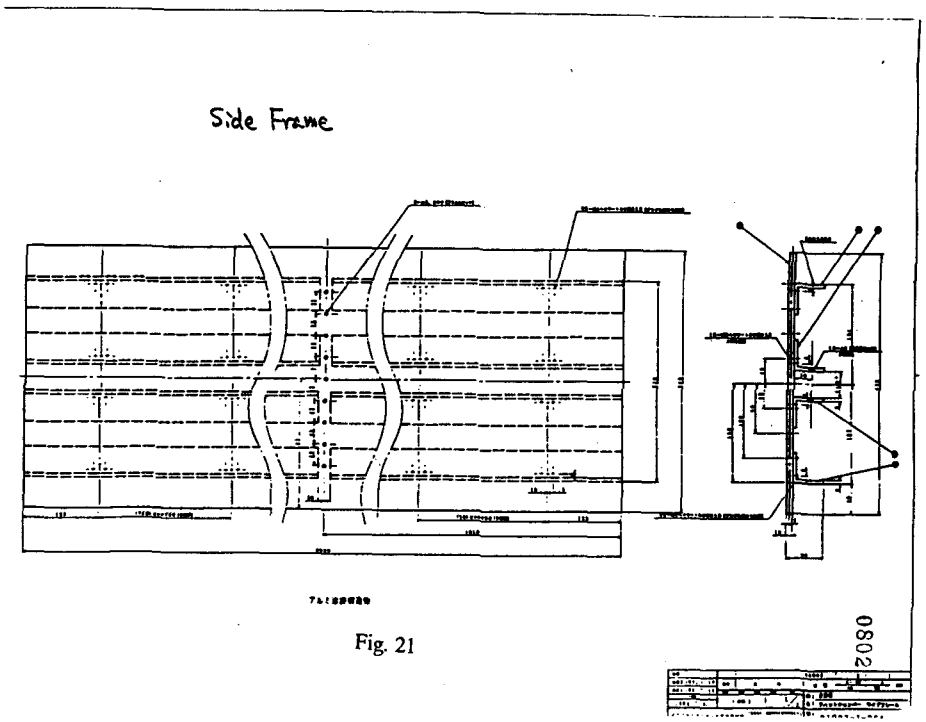

Fig. 21

0802

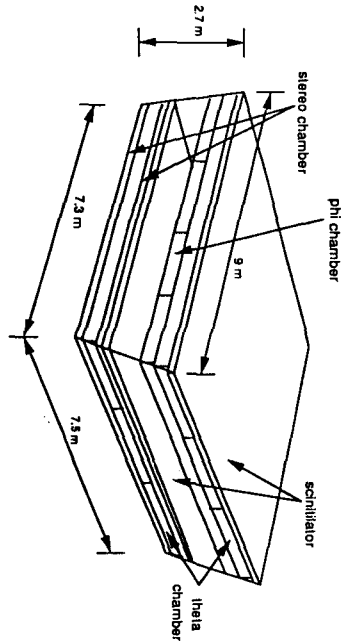

Fig. 19 Layout of the Jet chambers in a supermodule

0800

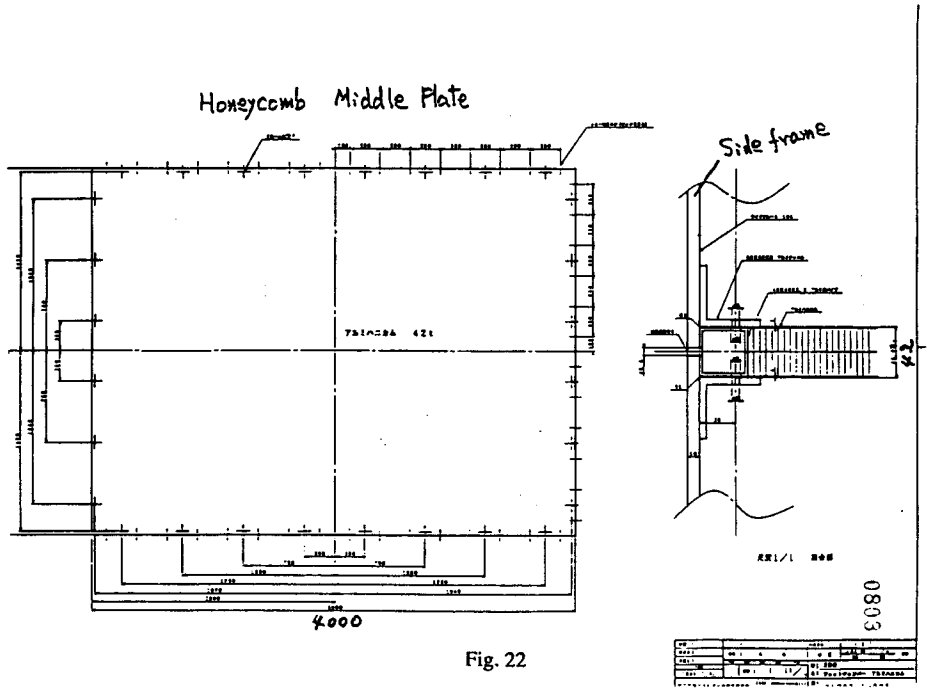

Fig. 22

Concept for the Intermediate Region and BW3 vs. IW3

H. Iwasaki(KEK)

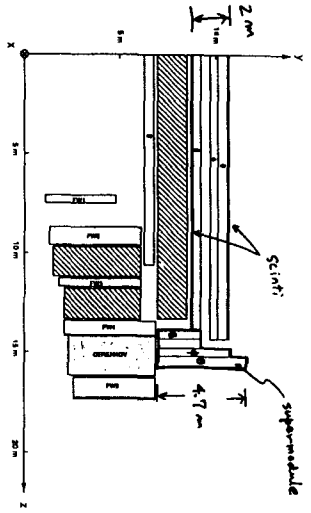

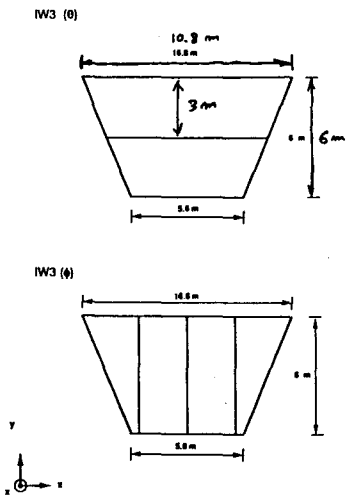

H. Iwasaki (KEK)
SDC Collab. meeting
@ SSCL
Nov. 13-16, 1991

1. Concept for the Intermediate region

2. BW3 vs IW3 $\begin{cases} \sigma_{P_t}/P_t \\ \text{Total channel} \end{cases}$

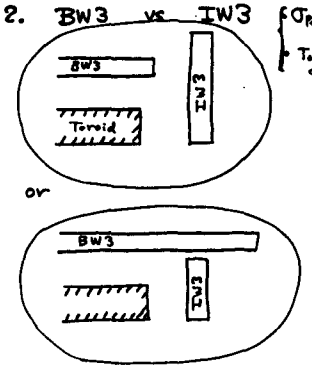

1. Concept for the Intermediate region

➡ Similar to the "Barrel"

θ-chambers

- μ-trigger (P_t discrimination)
- P_t measurement for μ-ID
- "projective geometry"

φ-chamber

- veto the cosmic rays
- φ information
- △ "projective geometry"

Stereo-chambers

- resolve ghost
- △ poor resolution can be acceptable

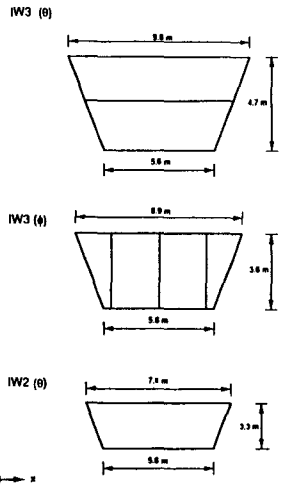

Intermediate muon chambers

superlayer	IW2	IW3	
chamber	θ	φ	θ
measurements	6	6	6
wire geometry ; parallel to / projective to	x - axis / yz - plane	y - axis / xz - plane	x - axis / yz - plane
No. of modules /oct /end	1	4	2
No. of cells /oct /end	48	217	100
Total no. of cells	450	3471	1585
No. of sense wires /oct /end	147	651	300
Total no. of sense wire	2.4 k	10.4 k	4.8 k

Total no. of sense wire in IWs = 17.6 k

17.6 k

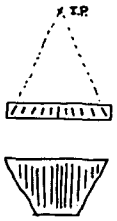

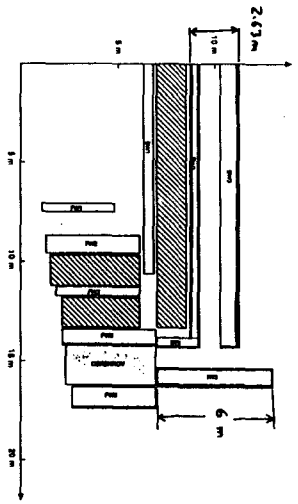

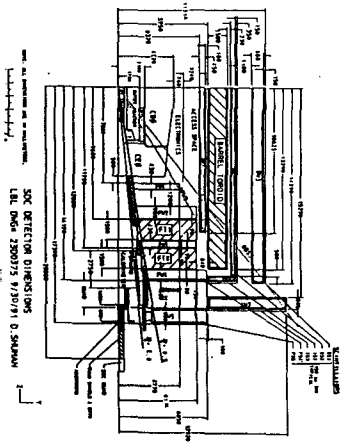

2. BW3 vs IW3

0809

Geom_1

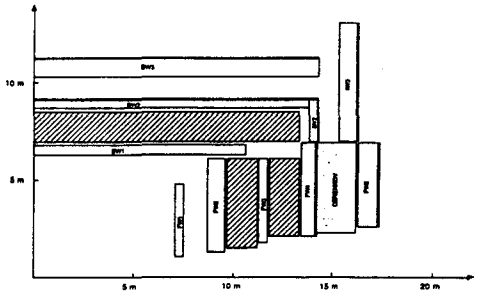

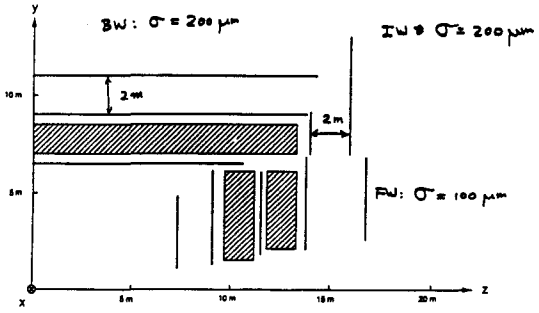

0810

Geom_1

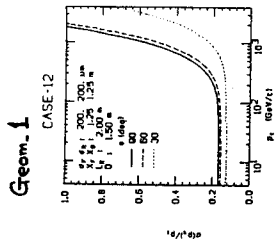

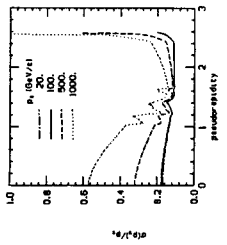

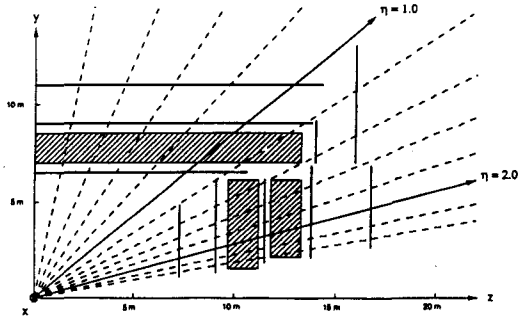

0811

Geom_2
(KEK concept)

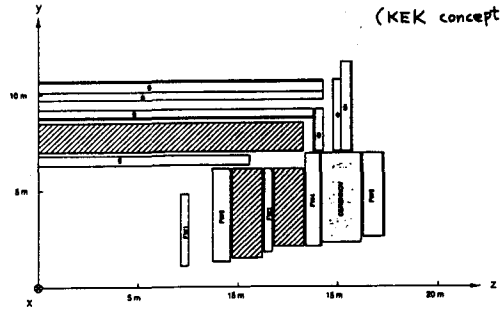

0812

Geom_1 and (σ(BW1) = 1 mm, σ(FW1,2,3) = 1 mm)

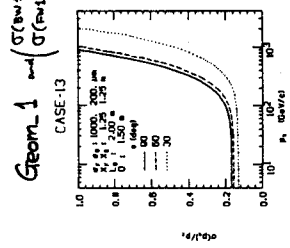

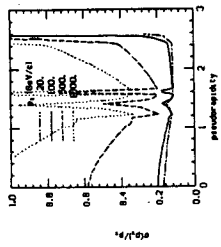

Geom_2

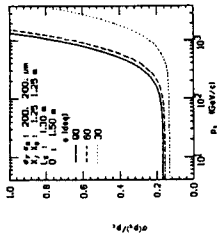

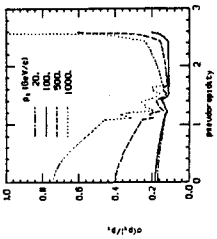

Geom_2 and (σ(BW1) = 1 mm, σ(FW1,2,3) = 1 mm)

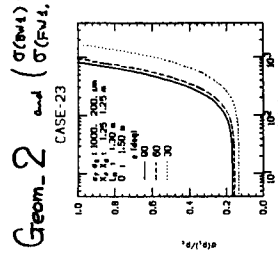

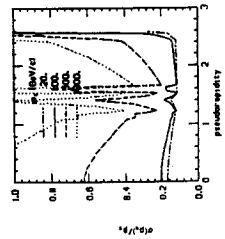

Geom_3

CASE-32

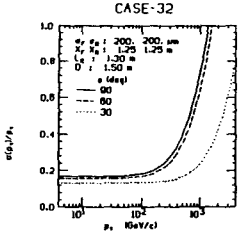

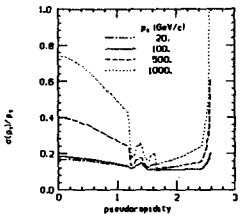

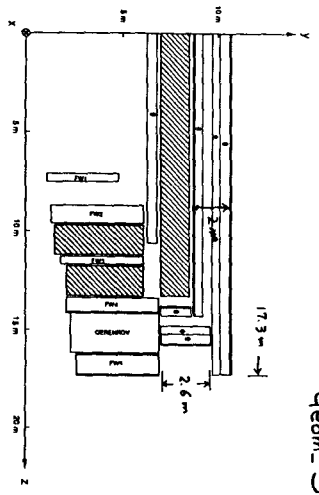

Geom_3

Total No. of sense wires

6 sense wires/superlayer

Total number of channels (except stero wires)

	Geom_1	(KEK) Geom_2	Geom_3
BW1(θ)	9.9 k	9.9 k	9.9 k
BW2(θ)	13.2 k	13.2 k	13.4 k
BW3(φ)	20.4 k	19.2 k	19.2 k
BW3(θ)	14.2 k	14.1 k	16.0 k
total(BW)	57.7 k	56.4 k	58.5 k
IW2(θ)	2.3 k	2.3 k	1.7 k
IW3(φ)	11.6 k	10.4 k	9.5 k
IW3(θ)	6.1 k	4.8 k	4.7 k
total(IW)	20.0 k	17.5 k	15.9 k
total(BW + IW)	77.7 k	73.9 k	74.4 k

(-5%)

Summary of "BW3 vs IW3"

- σ_{P_t}/P_t
  almost the same
- No. of total sense wires
  almost the same
- mechanically

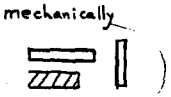

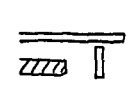

How to support IWs ? (and BW3 ?)

1st and 2nd Level Muon Triggers Based on the Jet Chamber Design

H. Sakamoto(KEK)

1st and 2nd level muon triggers based on the jet chamber system

KEK Hiroshi Sakamoto

1. Introduction

1.1 Trigger logic

How to make a trigger decision?

i) Finds a track segment in each jet cell.

ii) Connects track segments in staggered cells.

iii) Connects track segments between two superlayers.

1.2 Requirement

a) Spacial resolution of around 0.2mm (4nsec).

b) Chamber inefficiency (5/6 for example).

c) Tunable threshold momentum (10GeV/c-50GeV/c).

32ns in one cell, 8 half-cells between 2 superlayers.

1.3 Level 1 and Level 2

	Level 1	Level 2
Prg. step	~100 fixed	~10000 variable
Resolution	coarse	fine
Programming	LUT/gate array	software
Data transfer	heavy	light
	local	global

Superlayer Arrangement in the Barrel Region

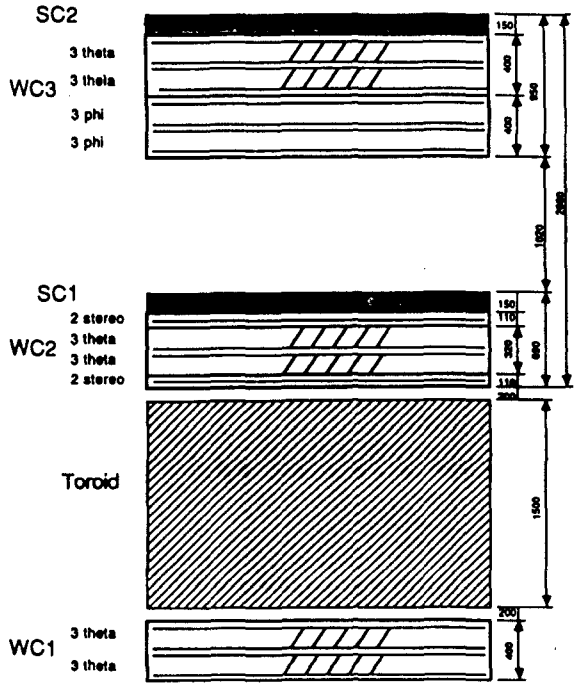

Fig. 3

2. Level 1 trigger

Hard-wired logic /Look-up table /Gate array

16nsec pipeline.

Input = Discriminator output signals

2.1 Finding a track segment in a jet cell.

3 anode signals in one jet cell. 3/3 or 2/3 coincidence.

Maximum tilt around 16nsec between two anodes.

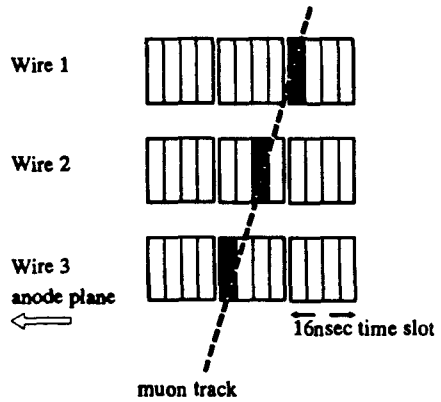

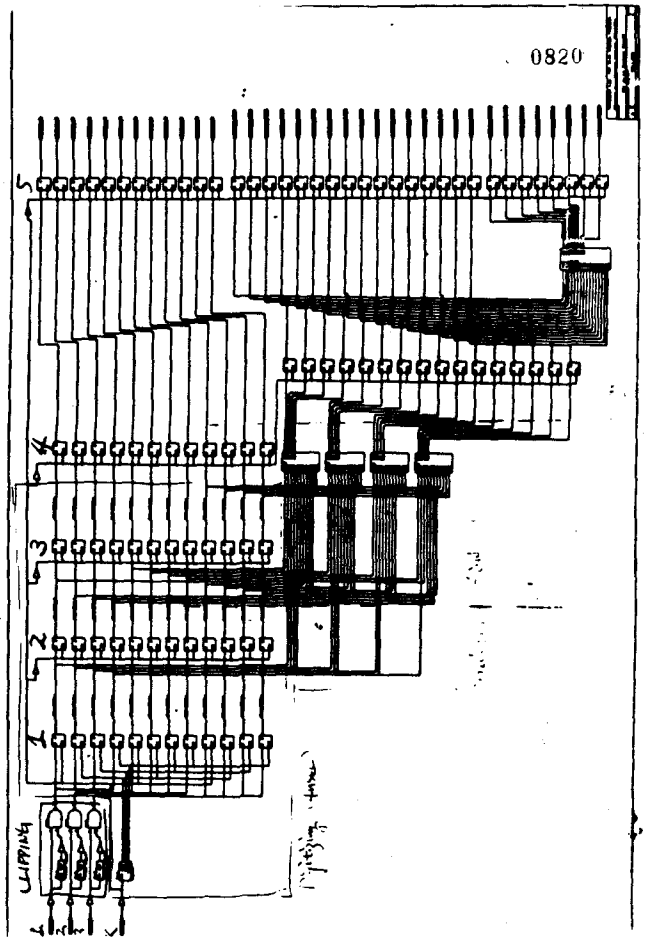

2.2 Connecting track segments in staggered half cells. 0821

Track segment information from staggered two layers.

Timing signal from the trigger scintilator.

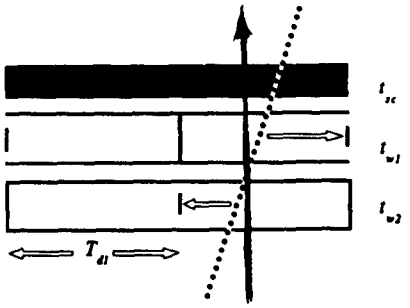

$$T_{dl} = (t_{w1} - t_{sc}) + (t_{w2} - t_{sc})$$

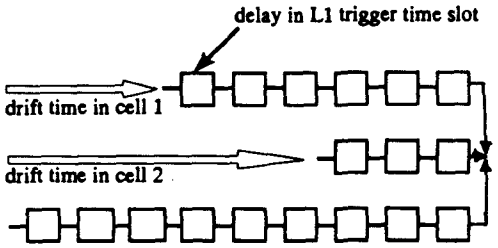

scintilator signal delay = full drift length of the cells

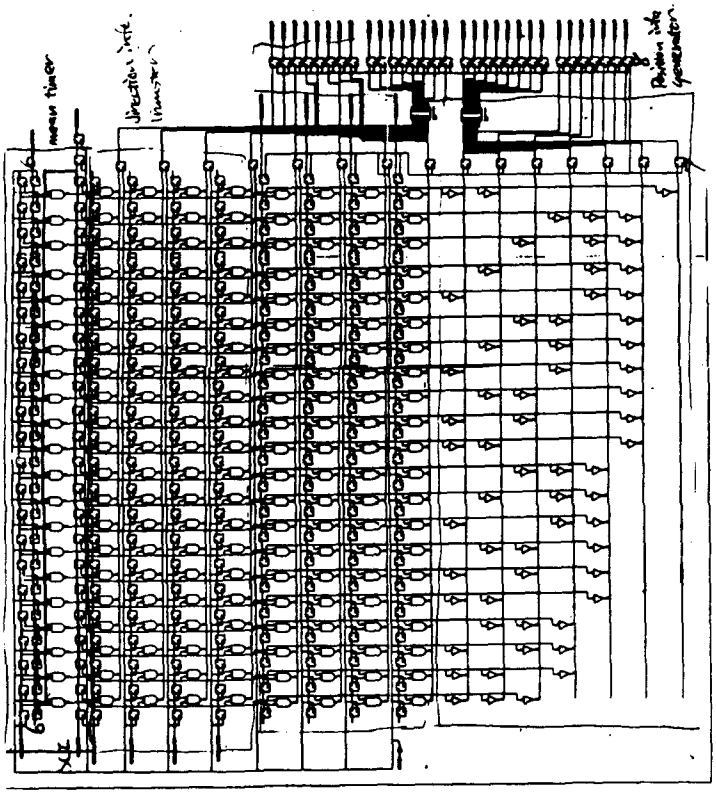

2.3 Connecting track segments between the superlayers. 0823

Extrapolates a track segment in BW2 toward BW3.

Finds segments consistent in position and direction.

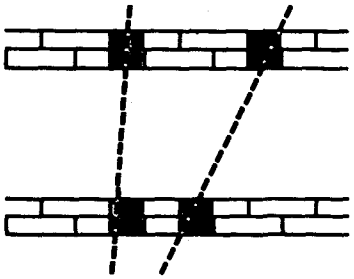

2.4 Level 1 Trigger Circuit

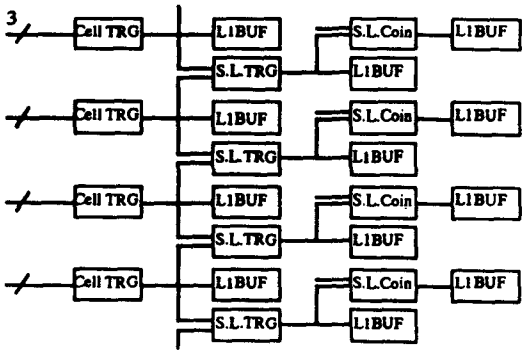

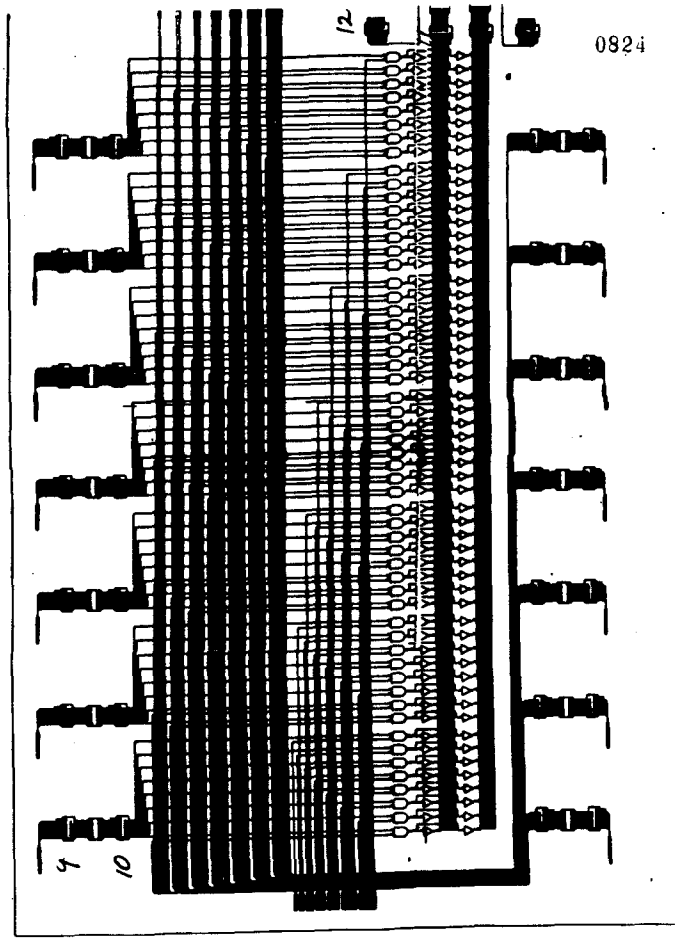

	BW1-θ	BW2-θ	BW2-s	BW3-ϕ	BW3-θ	total
sampling	6	6	4	6	6	28
cells	3500	4500	13900	6900	4900	33700
sense wires	21000	27000	55600	41400	29400	174400
TMC chips	5250	6750	13900	10350	7350	43600
TMC boards	164	211	434	323	230	1363
TMC crates	10	13	27	20	14	85
L1 cell chips	875	1125	0	1725	1225	4950
L1 superlayer chips	3500	4500	0	6900	4900	19800
L1 superlayer boards	109	141	0	216	153	619
L1 superlayer crates	7	9	0	13	10	39
L1 s.l.coin chips	0	1125	0	0	0	1125
L1 s.l.coin boards	0	281	0	0	0	281
L1 s.l.coin crates	0	18	0	0	0	18
L1 crates	17	40	27	34	24	141
L1 cost (k$)	889	2057	1412	1752	1244	7353

TMC channels/chip	4
TMC channels/board	128
TMC channels/crate	2048
ch. /L1 cell chip	4
ch. /L1 superlayer chip	1
ch. /L1 s.l. coin chip	4
ch. /L1 superlayer brd	32
ch. /L1 superlayer crt	512
ch. /L1 s.l.coin brd	16
ch. /L1 s.l.coin crt	256
board cost (k$)	3
crate cost (k$)	52
boards/crate	16
L2 crate processors	141
L2 crates/sector	16
L2 sector proc. crate	9
L2 subsystem proc.	1
Data size/crate	20
Data size/sector	181
Data size/subsystem	2896
Chamber occupancy	0.01

3. Level 2 trigger

Microprocessor/microcontroller/DSP...

100microsec maximum latency.

Input = muon TMC output (2ns resolution)

L1 muon trigger information

3.1 Level 2 trigger interface

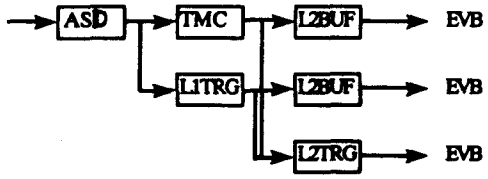

ASD	Amplifier/Shaper/Discriminator
TMC	muon chamber digitizer/level 1 buffer
L1TRG	Level 1 trigger circuit
L2BUF	Level 2 buffer
L2TRG	Level 2 trigger circuit

L2 trigger interface

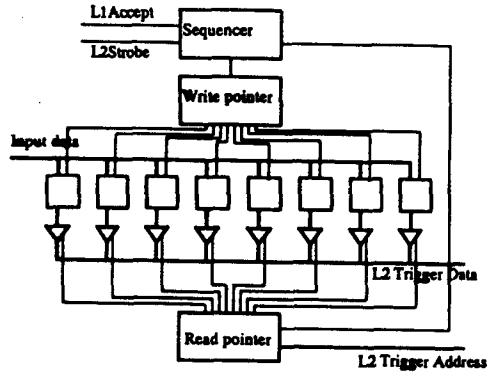

3.2 L2 trigger configuration

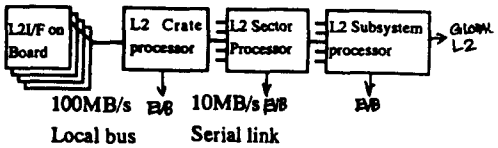

L2 Sector processor concept

0825

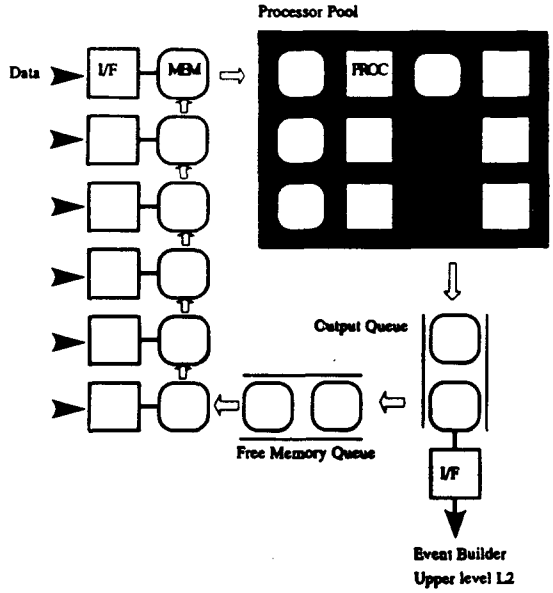

0829

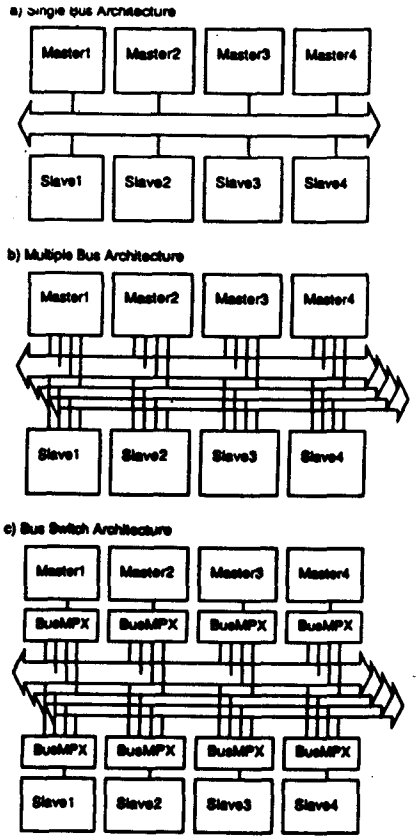

Fig I-1. Multiprocessor System Bus Architecture.

0830

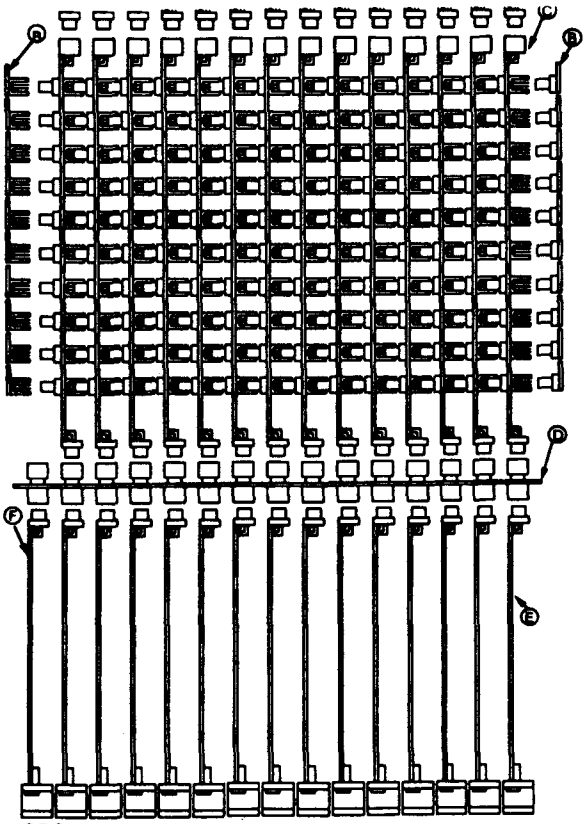

SBS system
A:D-bus terminator B:W-bus terminator C:Multiplexer PCB D:C-bus PCB
E:Normal VME/SBS module F:SBS controller (Slot #0)

Top view

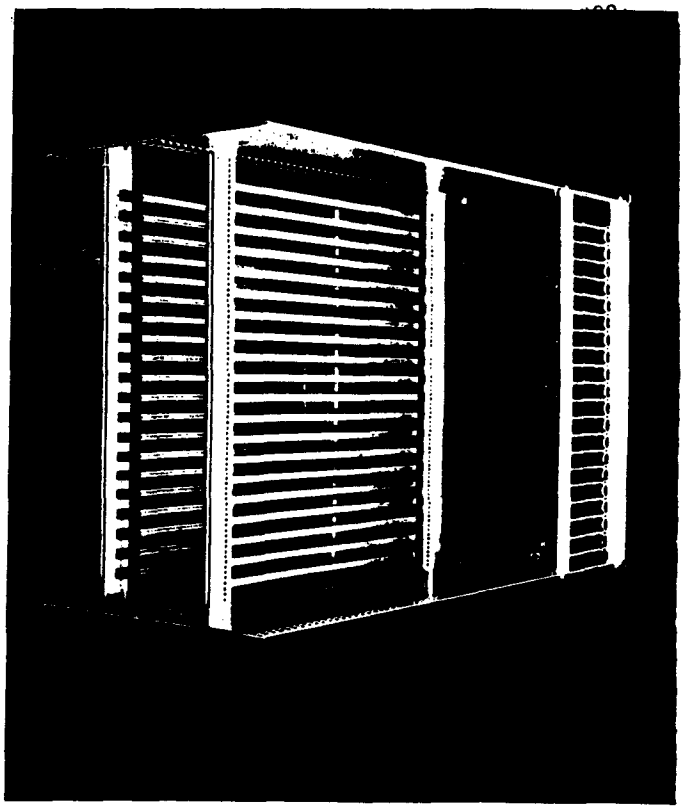

4. Summary

Conceptual design of muon L1 and L2 trigger scheme
based on the jet chamber system

* L1 estimation of pipeline trigger steps
* L2 interface to L1 buffer

Next step =
Implementation of these L1 and L2 architecture using existing technology.

* L1 prototype PCB at 30MHz
  programmable gate array / static RAM
* L2 prototype
  VME based / TRANSPUTER (T805 / T9000)
  Bus switch for L2 buffer/trigger backbone

Forward Muon System

A. Skuja(Maryland)

0834 A. Skuja

0835

Forward Muon System

Trigger 1st, 2nd and 3rd levels
Muon i.d.
Momentum determination

Requirements: 100 μm resolution / station
Adequate alignment ~ 1mm in z
~ 1mm vertical tilt
GOAL ⇒ ~ 50μm radial chamber mount

For good $\frac{\delta p}{p}$ and particle i.d. we need to KNOW p when chambers are located.
Projective trigger requires absolute space location
Simulation work required on all of this

We had a meeting on Oct 26, here at SSCL

At Maryland: Working on engineering integration (not enough people)
Chamber cell design
4×4 cm
3×6 cm cells } main construction
3×8 cm cells }
Cell beam tests at FNAL (especially if Am extended into January)

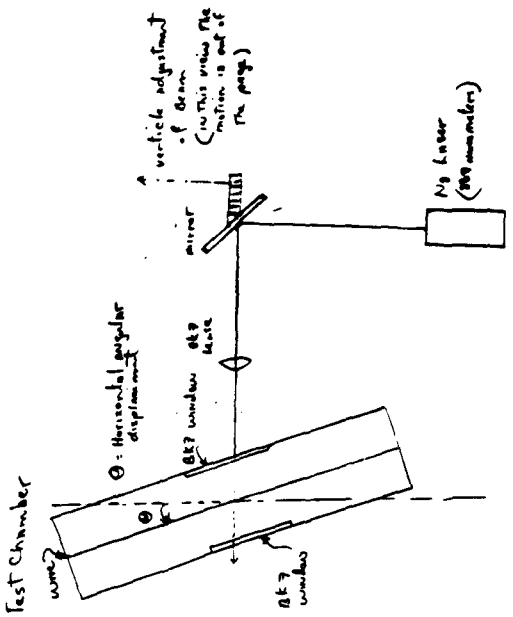

0836

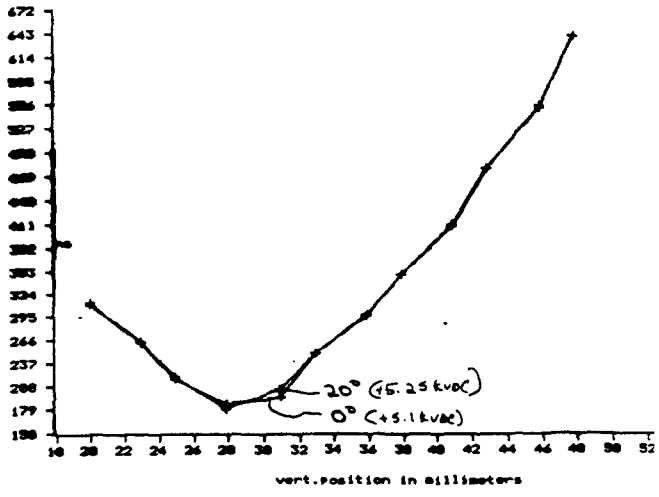

0837

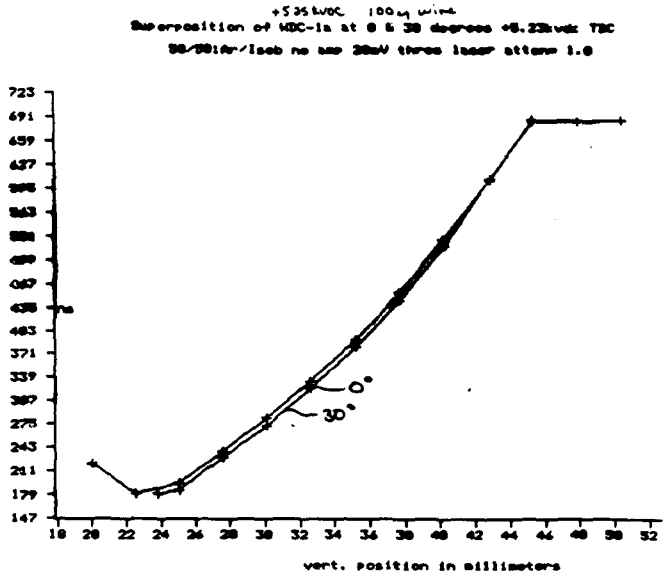

Oct 26 meeting
Participants from
- Colorado
- Maryland
- Martin Marietta
- Michigan
- Northern Illinois
- Protvino
- SSCL

Trigger Jay Chapman
Chapman/Thun note on trigger, electronic crates
(work on electronics density must be completed using this document as a basis)
⇒ Proposed TDC measures drift time relative to each beam crossing. It is thus deadtimeless and restricted only by two particle resolution in drift cells.
Occupancy not a factor in choosing drift cell size since "electronic occupancy" is about the same for large cells and small cells.
Cell geometry must be determined by chamber resolution.

Cherenkov counter work
Trigger on p not p_t (~30 GeV)

Remove "low energy" particles from trigger
This p-cut is OK at $\eta = 2.5$ but not at $\eta = 1.5$ (too high)

Testing 5" tube from Protvino at FNAL

Protvino investigations (lots of interested physicists)

Scintillator (at Michigan) 20 p.e.'s at 2.2 m for 6mm thick scintillator
May have difficulty producing enough scintillator if thicker

Photomultiplier work
Possible scintillator & photo tube arrangement

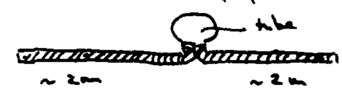

Thus can cover 4m with one tube

Test beams
Lab may not run after '91 if not outside money
If no test beams in the US until '96 then this may be a good possibility

Extrusions = 0.7mm tubes of stainless steel
Other possibilities?
Use look at support structure

Have built and installed SAMUS for DØ
(1cm tubes — too small for SDC)

Alexei Kalik calculating background rates from beam pipe and low-β shielding.
Rates very high in FWS (preliminary)

NEED more coherent organization

FORWARD MUON SIMULATION JOBS: 0840
(IN NO PARTICULAR ORDER)

① HOW WELL DO THE WIRES HAVE TO BE POSITIONED FOR THE TRIGGER? (i.e. GUESS: 0.5-1.0 mm
BEHRENDS (CENTRAL), ETREDE (?), WISS (ASK?)

② MINIMUM CELL SIZE FOR 10 GeV/c p_t CUT AFTER THE FACE OF THE DETECTOR, USING PROJECTIVE TRIGGER GUESS: >4 cm AT 25°

③ ALIGNMENT REQUIREMENT WITHIN STATIONS FOR ⊖ TRIGGER + LEVER ARM BETWEEN LAYERS " " ; REPOSITIONING ERROR
GUESS: 1.0 mm

④ ERRORS INTRODUCED INTO PROJECTIVE TRIGGER BY FIXED CELL SIZE; EFFECT OF VARYING CELL SIZE

⑤ BACKGROUNDS, ESP. NEUTRONS - IN CHAMBERS, SCINTILLATORS + ČERENKOV
KUNORI, KWIK, JOHNS

⑥ GET PARAMETRIZED SIMULATION FOR TRIGGER GROUP
WILLIS, (SULLIVAN)

⑦ EFFECT OF LARGE-ANGLE SCATTERS GUESS: NOT IN GENT

⑧ ČERENKOV TRIGGER EFFICIENCY AS A FUNCTION OF ANGLE
NAUENBERG ET AL.

⑨ LINKING SCINTILLATOR + ČERENKOV IN TRIGGER, INCL. SEGMENTATION MELCHANOV (ASK)
IDEA: USE 2-LAYER SCINT FOR p_t ROAD, AMP TO SCINT.

⑩ CAN TRIGGER BE DONE WITHOUT ČERENKOV AT OUTER EDGES?
AND IF NOT, WHAT'S THE MINIMUM p_t THRESHOLD?

⑪ EFFECT OF MULTIPLE SCATTERING ON ČERENKOV EFFICIENCY
NAUENBERG ET AL.

⑫ EFFECT OF OCTANT OVERLAPS ON TRIGGER (FAKE DIMUONS?)
ČERENKOV CAN SORT IT OUT

⑬ EFFECT OF NONLINEAR DRIFT TIME ON TRIGGER
GUESS: MAYBE OK IN 4cm CELLS; NEED FIELD SHAPING IF BIGGER

①,⑥,⑧ - NEED SOON

NEW PLAYERS: SIDORENKO, BAKKEN

0841

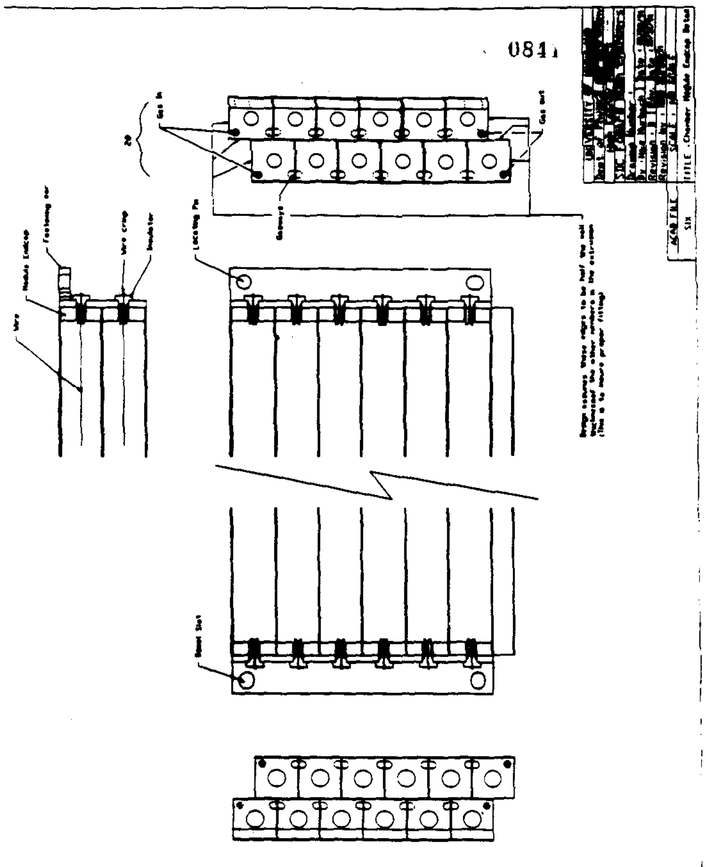

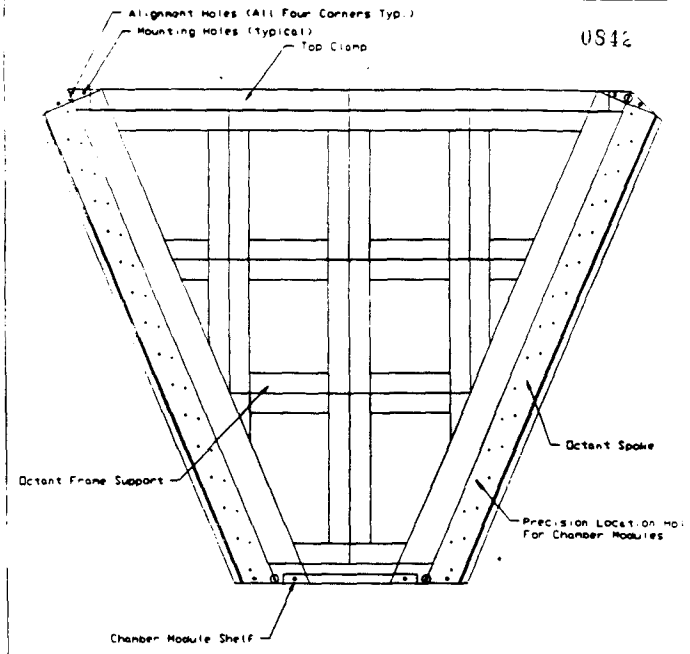

0842

OCTANT MODULE TRAPEZOIDAL FRAME (TYPICAL)

UNIVERSITY OF MARYLAND
Dept. of Physics and Astronomy
High Energy Physics
STC Forward Muon Chamber
Drawing Number
By Wes Burleson Date 10/30/87
Revision # 1 Rev. Date 10/30/87
Revision By Wes Burleson
ACAD FILE SCALE NO SCALE
SHEET2 TITLE Octant Frame

DISCRETE ATTACHED TO OCTANT SPOKE TYPICAL OF μFW1 μFW2 μFW3 AND 8μ + 8ν + 4θ PORTION OF μFW5

FIGURE 3 TOP VIEW OF OCTANT MODULE

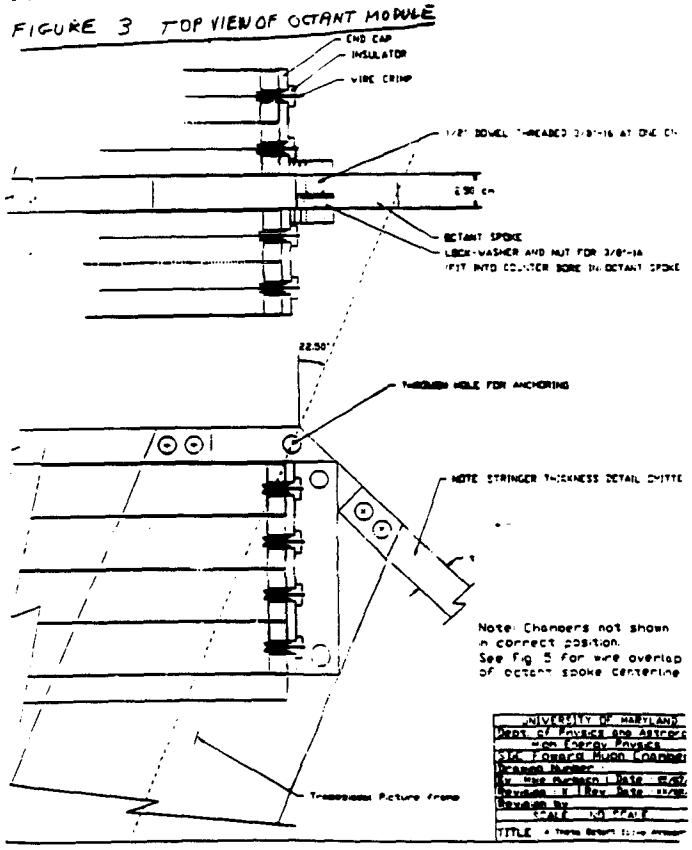

UNIVERSITY OF MARYLAND
Dept. of Physics and Astronomy
High Energy Physics
STC Forward Muon Chamber
Drawing Number
By Wes Burleson Date 10/30/87
Revision # 1 Rev. Date 10/30/87
Revision By
SCALE NO SCALE
TITLE A Three Dimensional Drift Chamber

FIGURE 6 OVERLAP OF OCTANTS

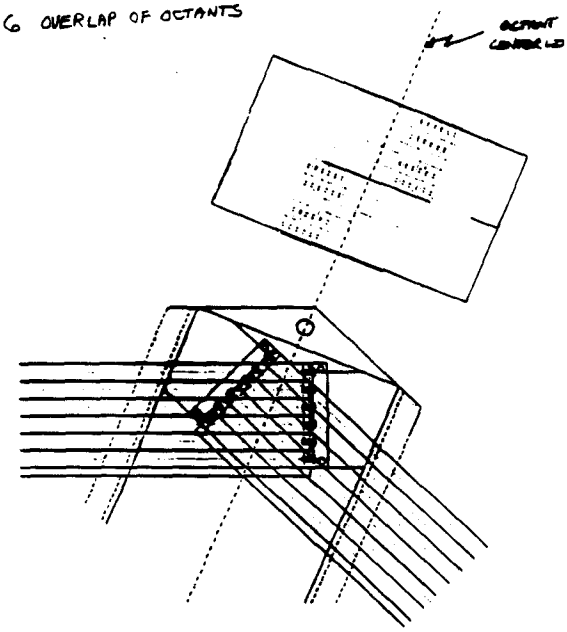

TYPICAL WIRE OVERLAP OF
THE OCTANT SPACE CENTERLINE

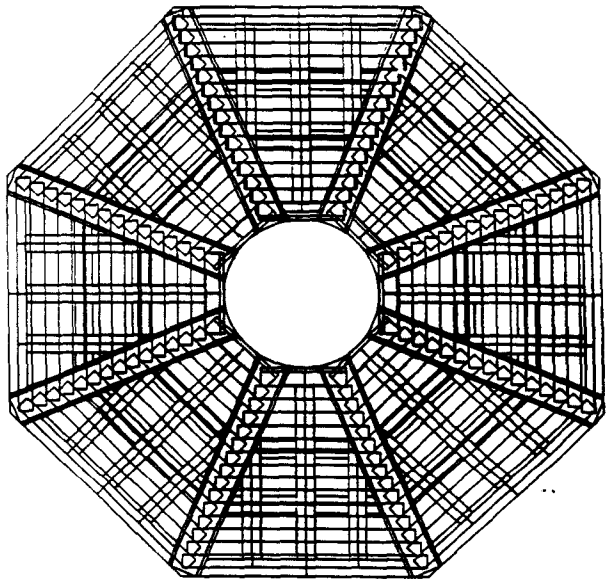

μFW1 — 4θ

OCTANTS ARE STAGGERED AND ELECTRONICS ARE LOCATED
ON FACES OPPOSITE WIRE MODULES

FIGURE 4
SUPERMODULE
TYPICAL

UNIVERSITY OF MARYLAND
Dept. of Physics and Astronomy
High Energy Physics
STC Forward Muon Chamber
Drawing Number
By Wes Burleson Date 10/30/87
Revision # 1 Rev. Date 10/30/87
Revision By
ACAD FILE SCALE NO SCALE
SHEET3 TITLE Supermodule

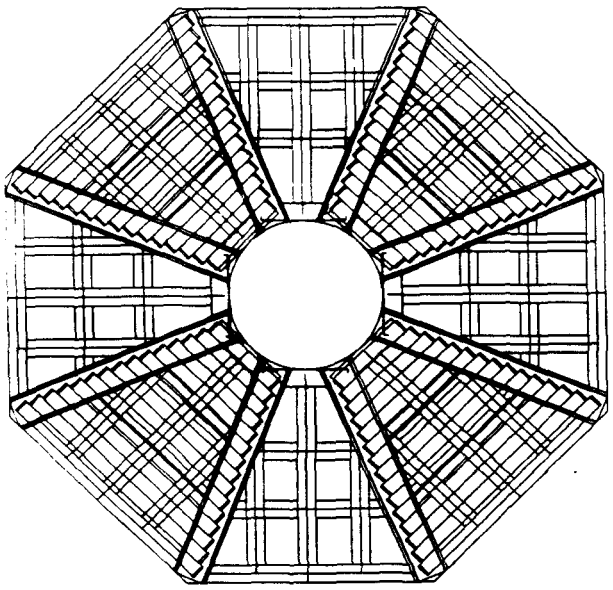

$\mu FW1 - 4\theta$

FRONT LAYER OF A SUPERMODULE

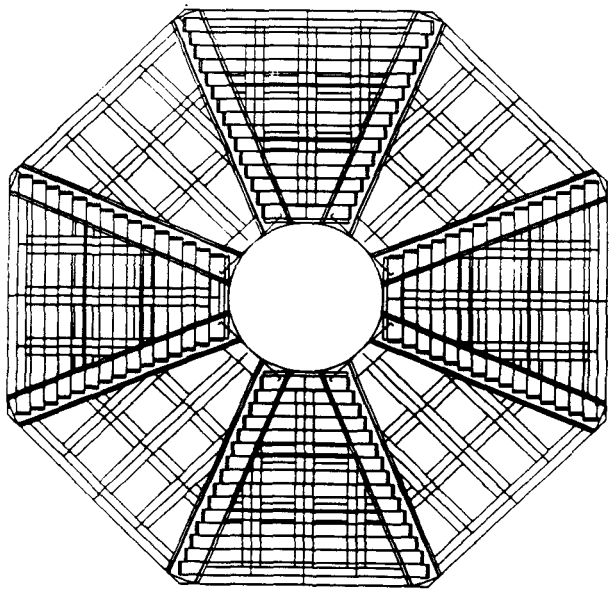

$\mu FW1 - 4\theta$

BACK LAYER OF A SUPERMODULE

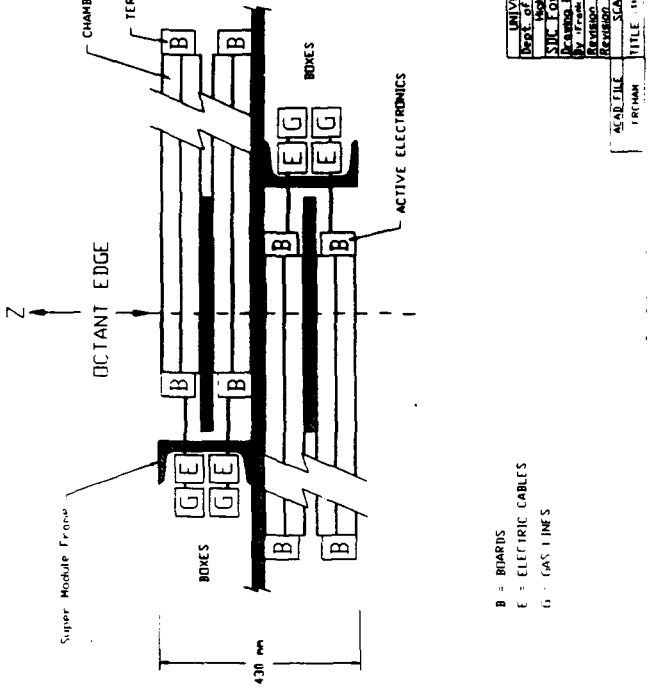

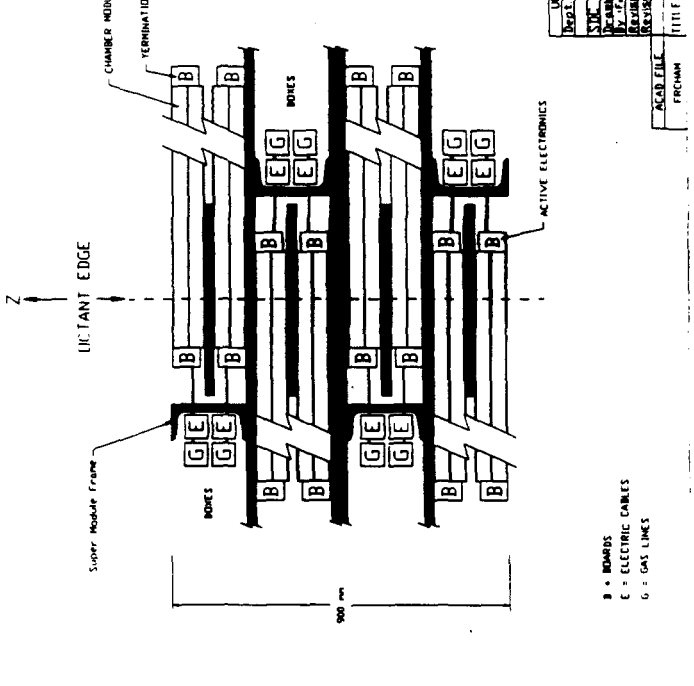

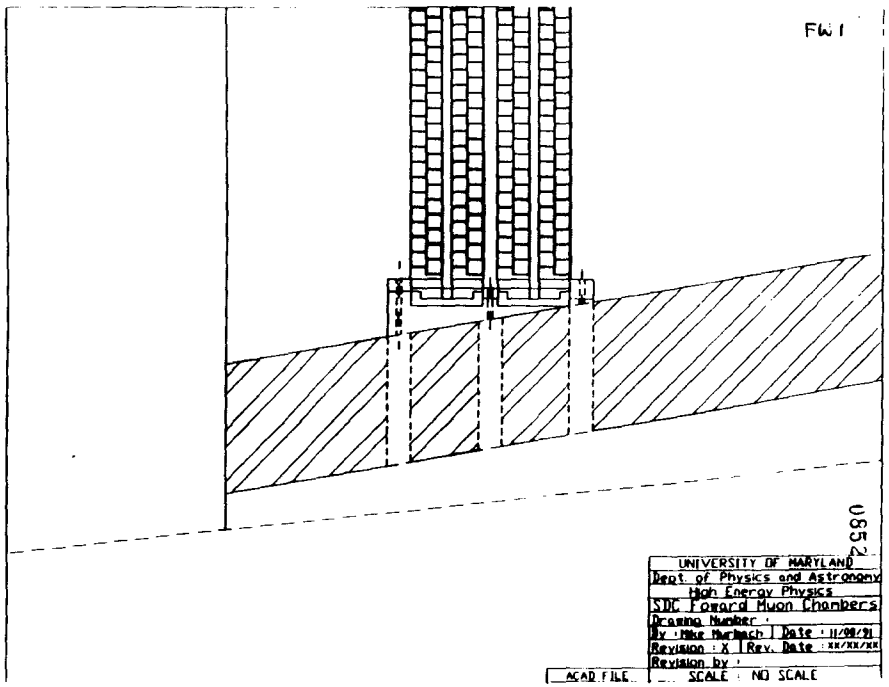
FW1
0852
UNIVERSITY OF MARYLAND
Dept. of Physics and Astronomy
High Energy Physics
SDC Forward Muon Chambers
Drawing Number :
By : Mike Marbach | Date : 11/08/91
Revision : X | Rev. Date : XX/XX/XX
Revision by :
ACAD FILE
SCALE : NO SCALE

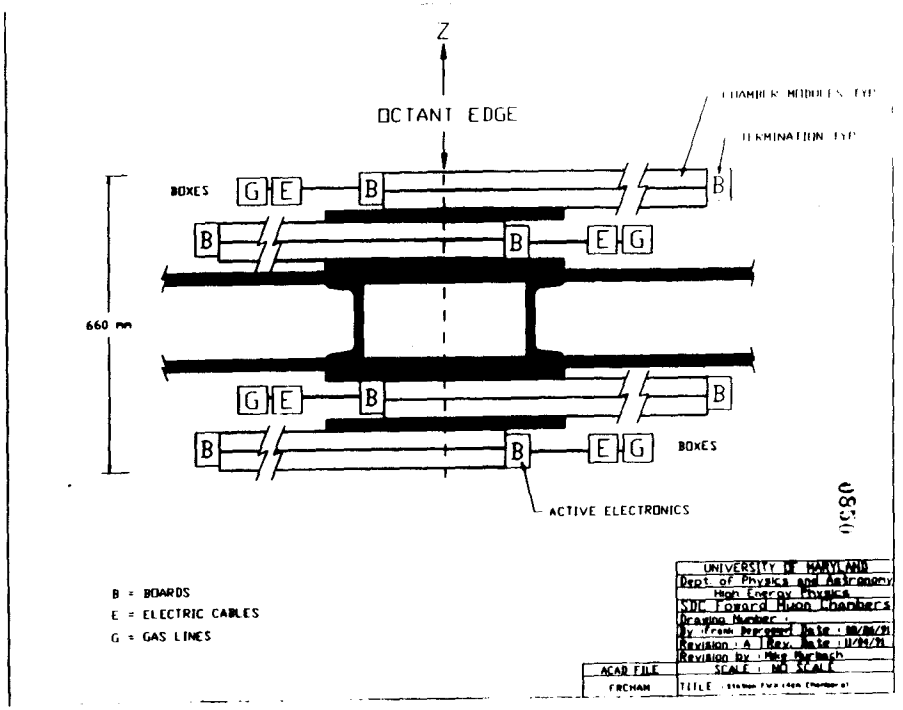
Z
OCTANT EDGE
BOXES
G E B
B
E G
660 mm
ACTIVE ELECTRONICS
0850
B = BOARDS
E = ELECTRIC CABLES
G = GAS LINES
UNIVERSITY OF MARYLAND
Dept. of Physics and Astronomy
High Energy Physics
SDC Forward Muon Chambers
Drawing Number :
By : Frank Borgonovi | Date : 08/06/91
Revision : A | Rev. Date : 11/04/91
Revision by : Mike Marbach
ACAD FILE
SCALE : NO SCALE
FNALHAM

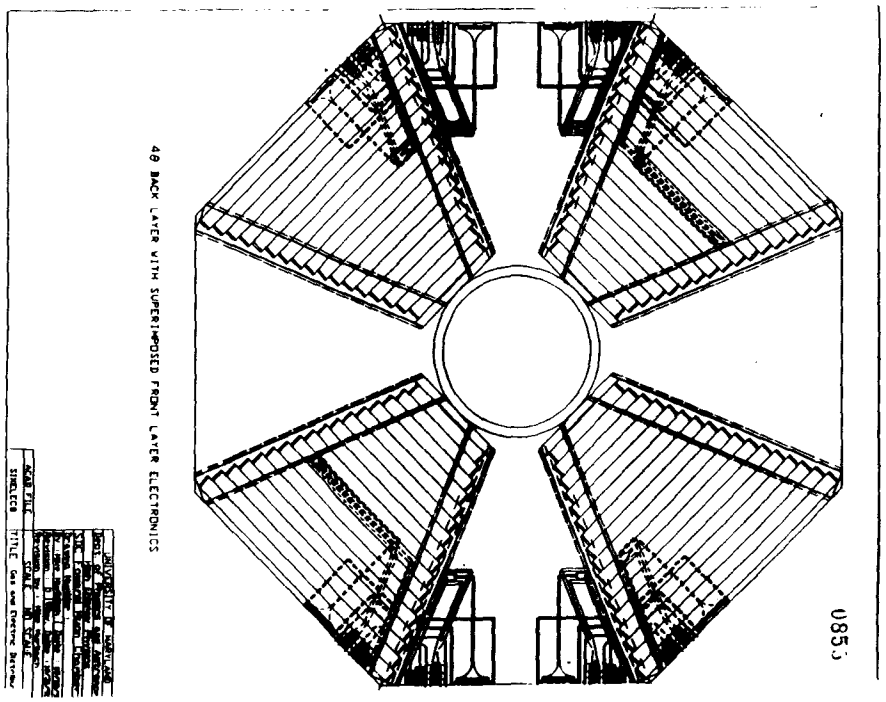
40 BACK LAYER WITH SUPERIMPOSED FRONT LAYER ELECTRONICS
0853

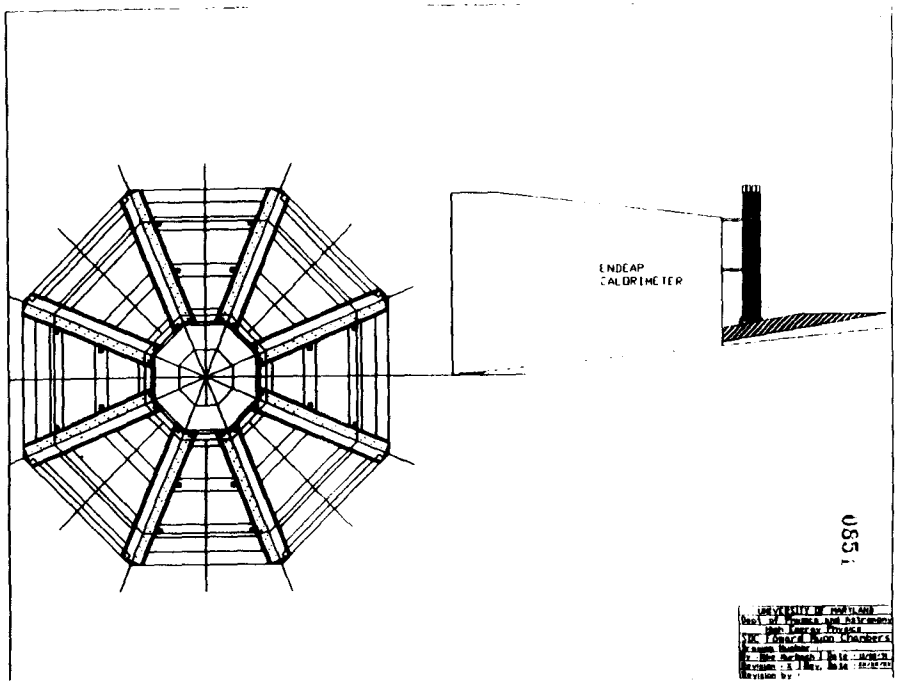
ENDCAP
CALORIMETER
0851

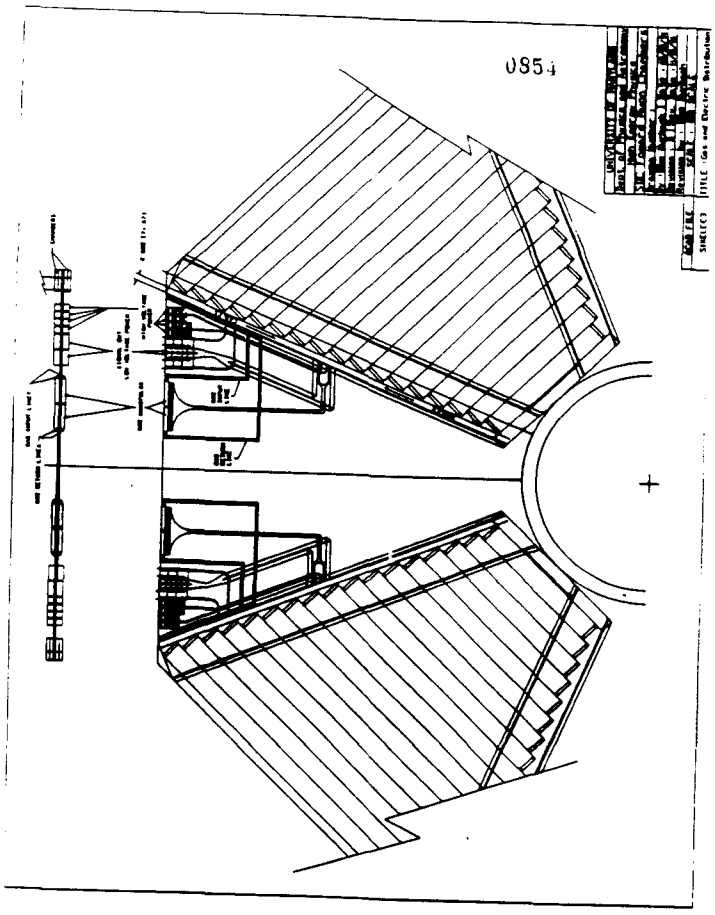

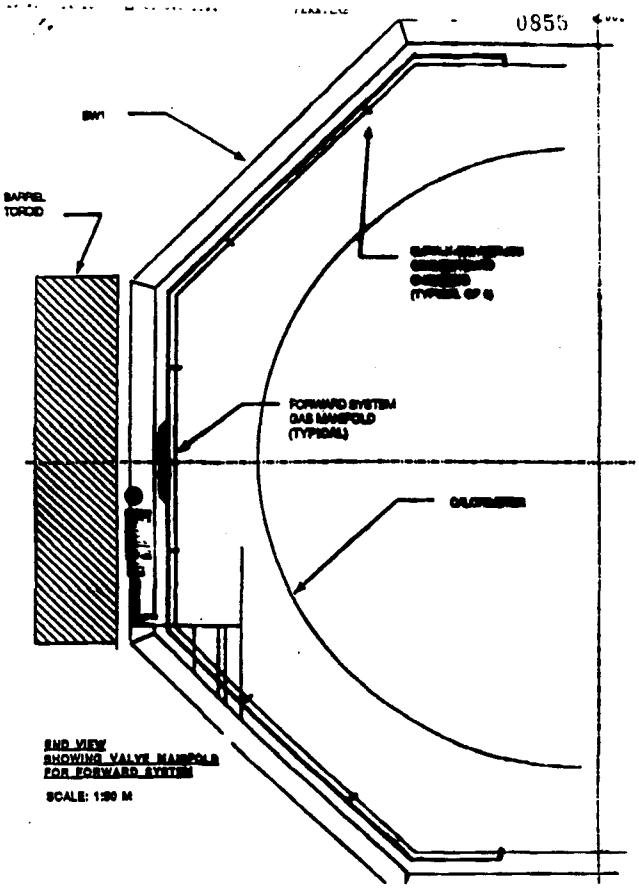

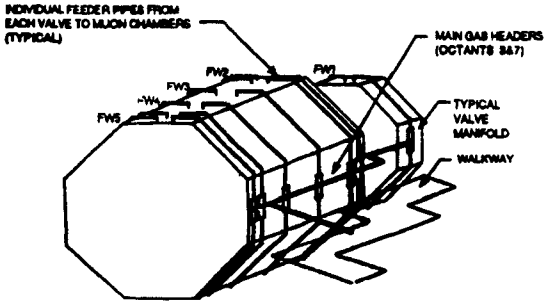

MUON GAS PIPING DISTRIBUTION
FORWARD SYSTEM

NOT TO SCALE

SDC Muon Simulation at University of Illinois

Errede, et al.

Nov 16, 1991 SDC Collab. Wrtg ~~Sept. 23, 1991~~ SSCL

SDC Muon Simulation at University of Illinois

D. Errede, S. Errede, R. Gardner, M. Haney, I. Karliner D. Miller & J. Wiss

Purpose/Goals:

- In-depth studies of relative & absolute performance characteristics of candidate muon subsystem design(s):
  - barrel & intermediate regions
  - Overall drift chamber design(s) – # layers, chamber orientation (θ, ϕ, stereo)
  - Drift chamber cell configurations, shaping fields, DCH gases, etc.
  - Projective vs. non-projective cell geometries...
- In-depth studies of relative & absolute performance characteristics of candidate muon trigger design(s):
  - barrel & intermediate regions
  - HDL Verilog & VHDL trigger simulation(s)
  - Scintillator & Cherenkov counter L1 triggers
  - Muon drift chamber L1 & L2 triggers
  - Evaluate trigger efficiencies, biases, failure modes...
  - Evaluate on-line momentum resolution
  - Evaluate trigger rates
  - DACQ pipeline studies, etc.

- Need **realistic** detailed simulation of muons in SDC
  - Event generators for input stimulus
    - Single monochromatic muons
    - Inclusive muons from $\sqrt{s} = 40\ TeV$ p-p collisions
      - prompt muons (heavy flavors, DY, W, Z^0...)
      - $\pi^{\pm}$, $K^{\pm}$ DKIF,
      - Punchthru background(s)
    - For benchmark physics processes
      - Use conventional event generators:
      - Isajet, Papageno, Herwig, CDFxxx...
  - Prompt muons & π, K, punchthru background(s)
  - Muon transport in $\vec{B}$ region(s)
  - Multiple coulomb scattering in cal & toroid(s)
  - δ–ray, QED bremm and hadronic processes
  - Detailed muon detector geometries
  - Chamber resolution effects, inefficiencies, noise
  - Chamber front-end electronics, trigger electronics
  - Propagation dispersion, drift time & time-slewing effects
  - Event pileup effects
  - etc.

L1 - Muon Trigger Simulation: Fortran + VHDL

Fortran

"fast" simulation of muon trajectories for $|\eta| < 1.1$

isolated muons: one every 10 μs

wire hits as seen at WC2

projective geometry

constant 80 mm cell-size at mid-line of WC2

1000 muons each at 10, 20, 30, 40, 50, 60, 70, 80, 90, 100, 125, 150, 175, 200, 250, 300, 400, 500 GeV/c

VHDL - hardware description language model of L1-trigger

(8 wires)*(4 layers) in a module

20 modules

all 8 octants treated as one

+/- z treated as same

trigger = layer-pair coincidence < threshold

base thresholds of 10, 15, 20, 30, 40, 50 ns

additional weighting - depending on run

10% resolution: 10ns +/- 1,2,3... ns

trigger suppression: no more than one per 1.6 μs

S. Errede, M. Haney, J. Wiss
U of I 16-Oct-91

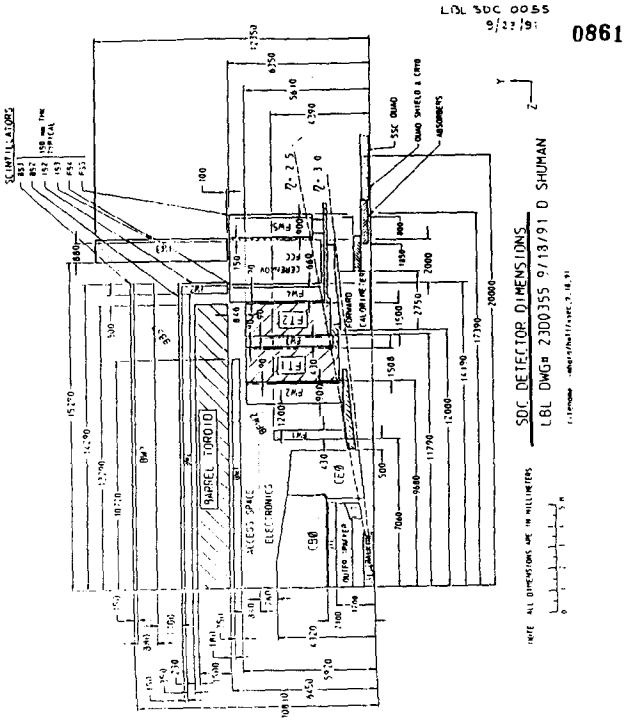

Baseline: "1.6 μs"

0862

drift time based on muon trajectory intercept with wire-plane
constant weighting of all coincidence times
significance: This is what you get "for free" from projective geometry

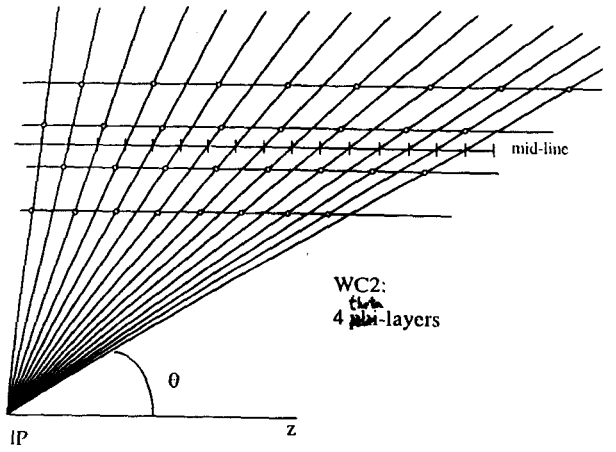

0863

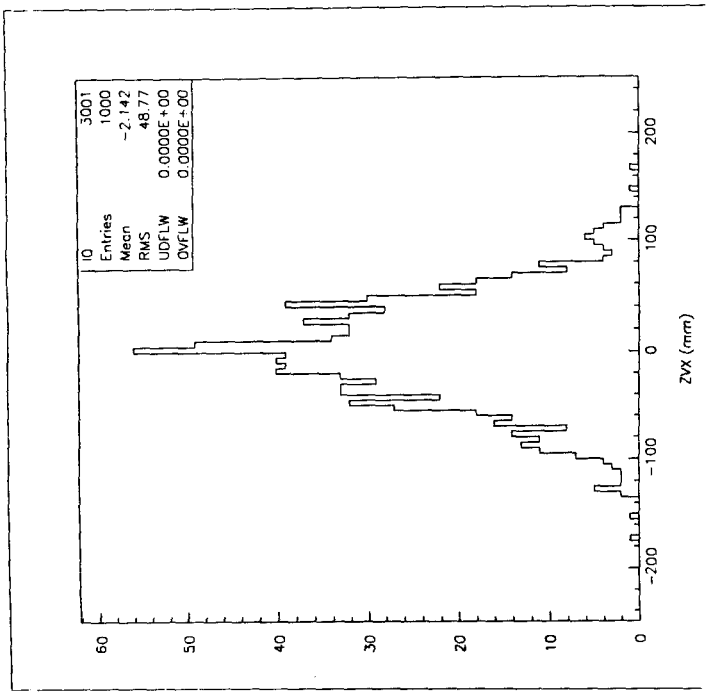

0864

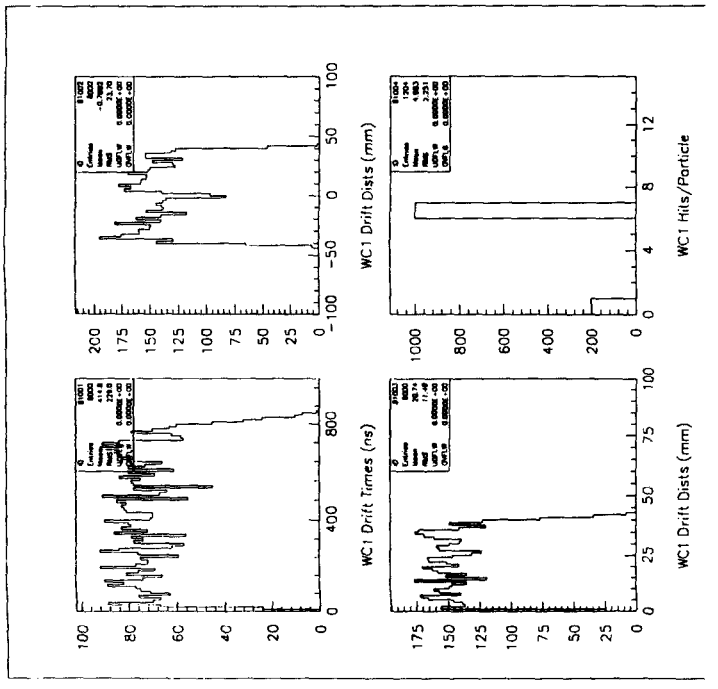

0865

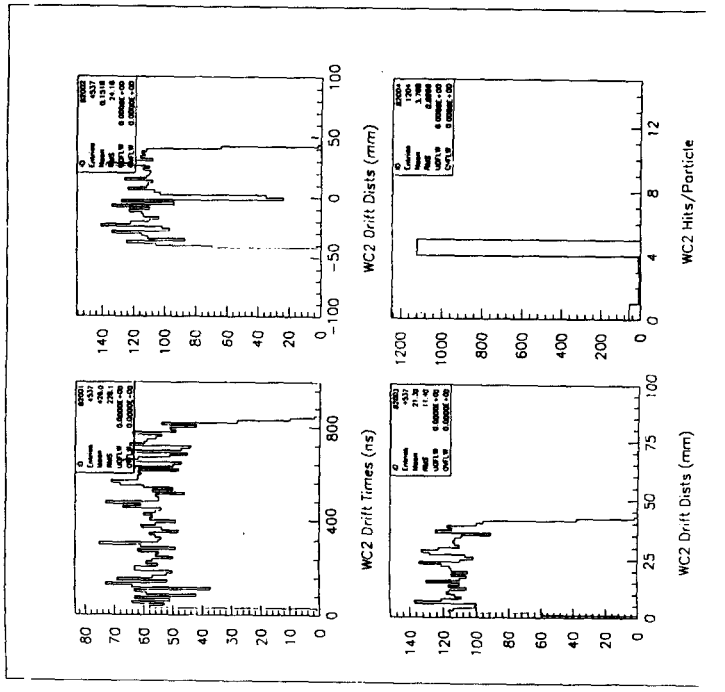

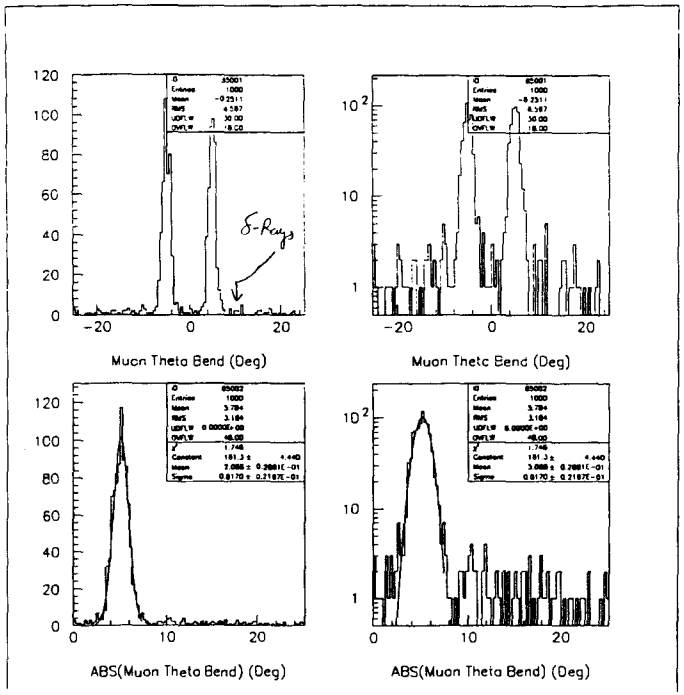

8980

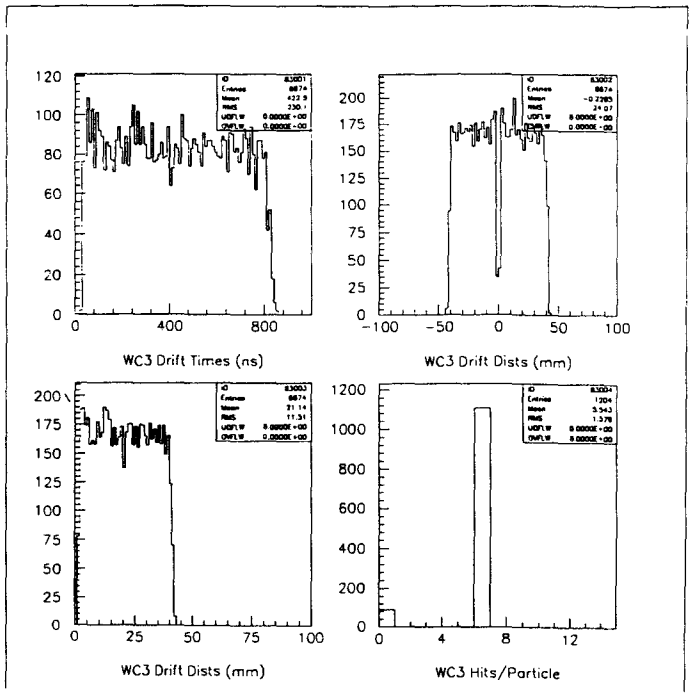

8981

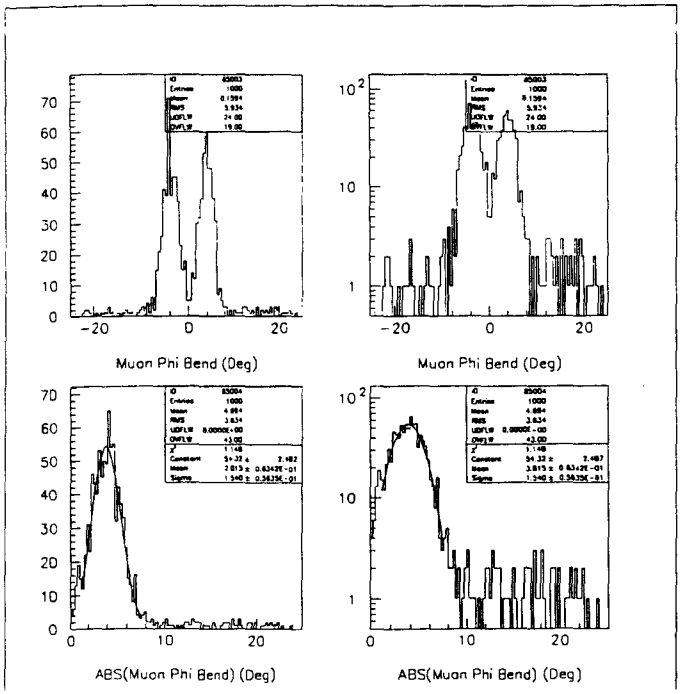

8983

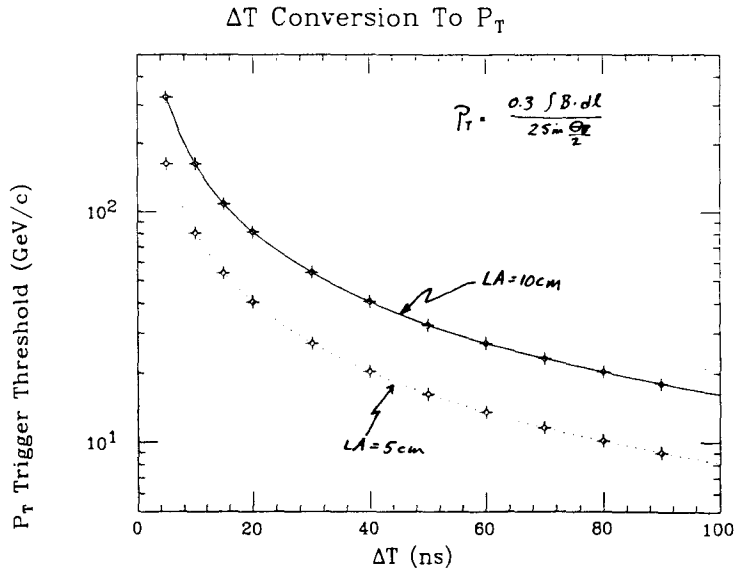

8987

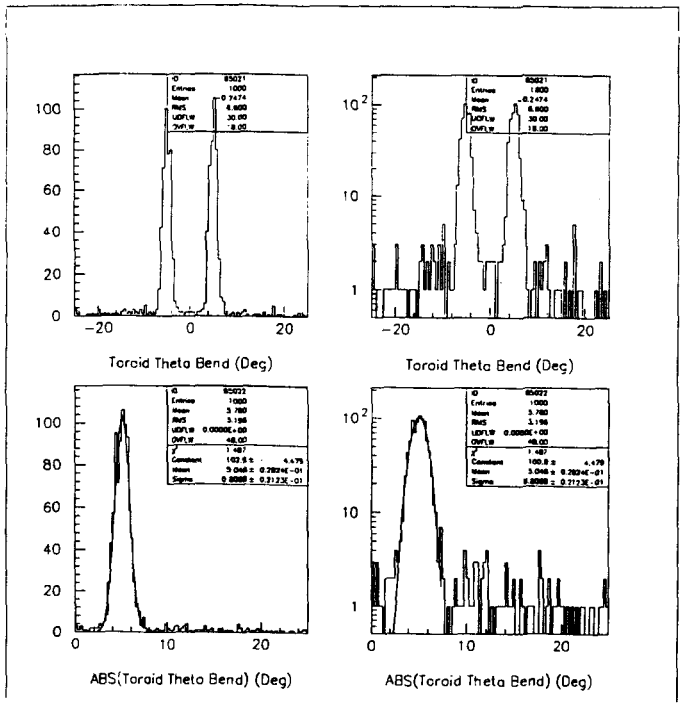

0872

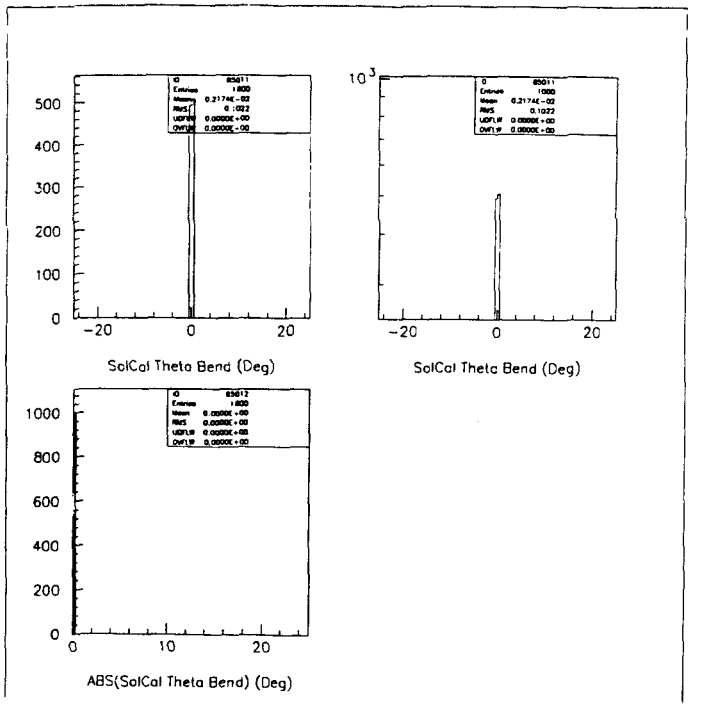

0870

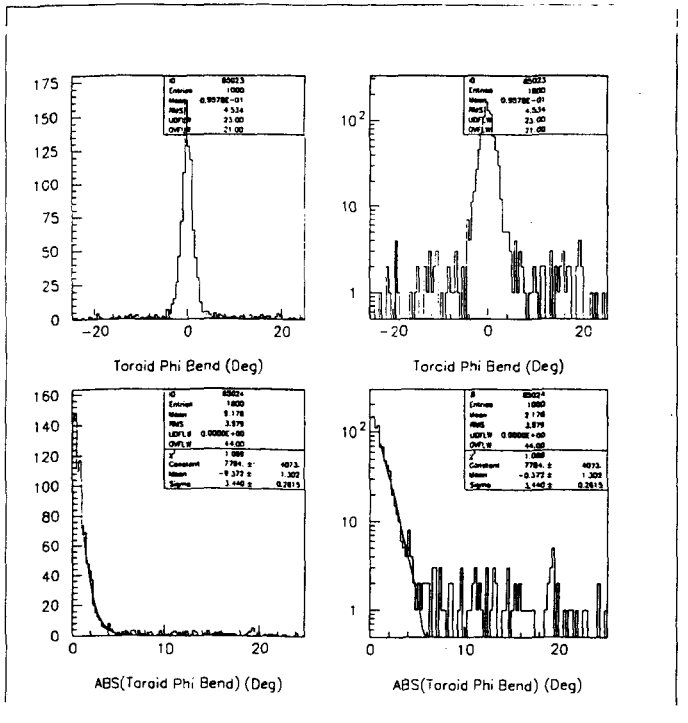

0873

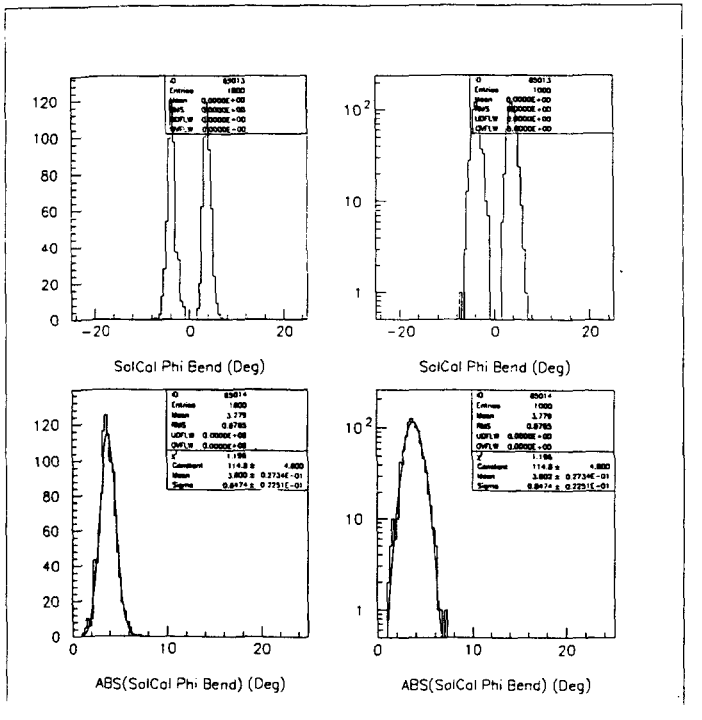

0871

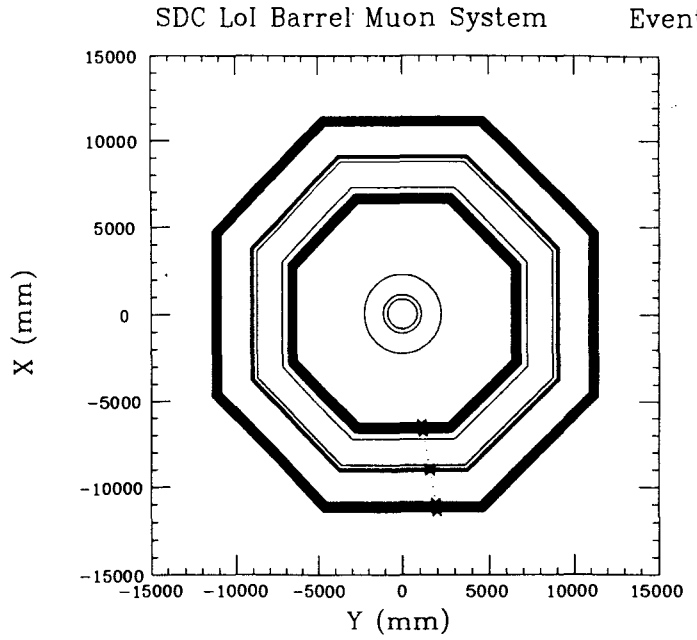

0876

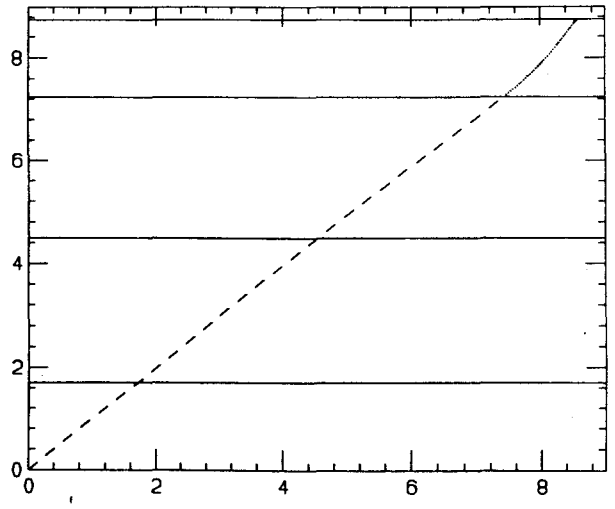

0874

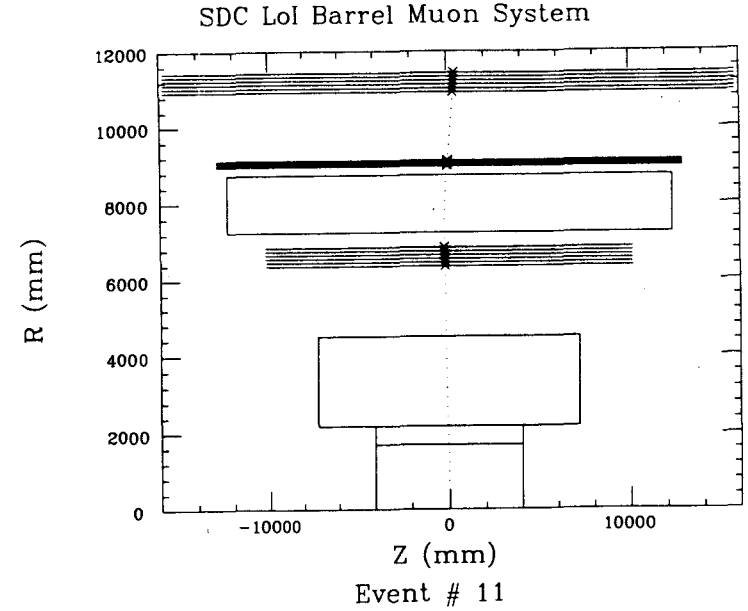

0877

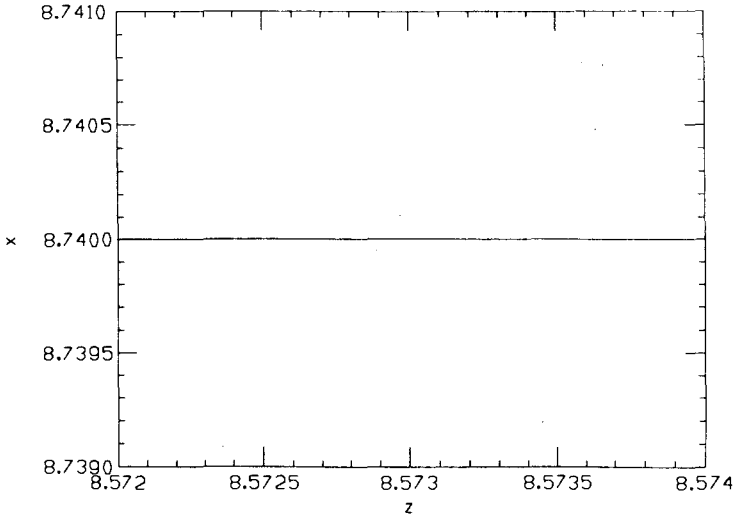

0875

VHDL Oliver Trigger

Oliver, 11-90

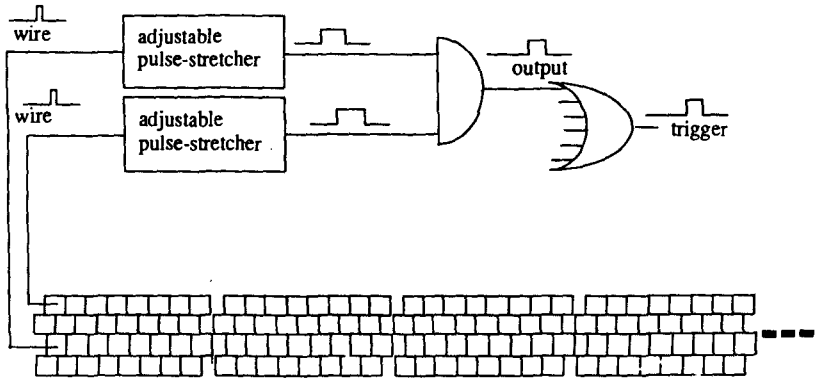

8 wires per module-layer, 4 layers (WC2), 4 modules shown...

0880

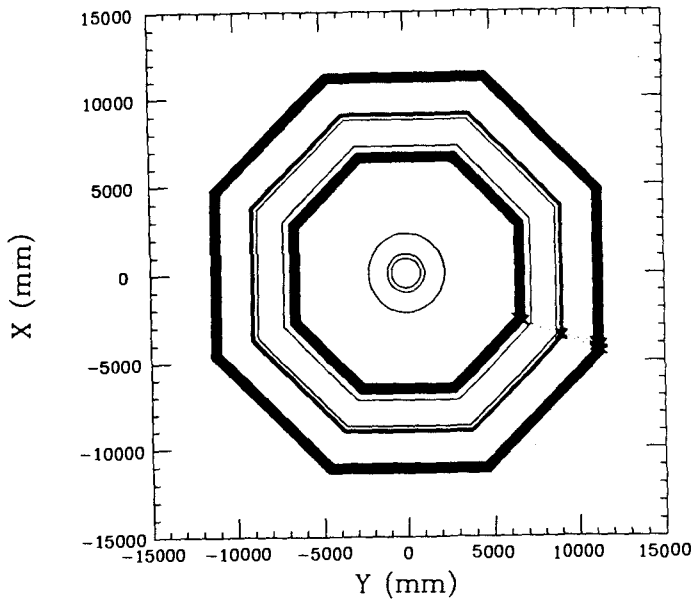

0878

Input to the Model

time (ns)	O LL S wir	E MM
10034.70117	1202000	101
10034.75391	1206000	101
10140.35547	1206020	102
10504.10059	1202020	102
10538.95605	1204019	102
10758.48242	1208020	102
10825.54199	1208000	101
10825.59473	1204000	101
20432.49023	-1202068	202
20514.68164	-1202098	201
20591.84961	-1204098	201
20627.90039	-1204068	202
20649.34570	-1208068	202
20669.01758	-1206099	201
20746.18555	-1208099	201
20823.32031	-1206069	202
30083.30078	-1202098	301
30099.93164	-1204098	301

O=Octant (+/- 1..8)
S=SuperLayer (WC1,2,3)
LL=2*layer
wir=wire_number
E=event_number
MM=muon_number

0881

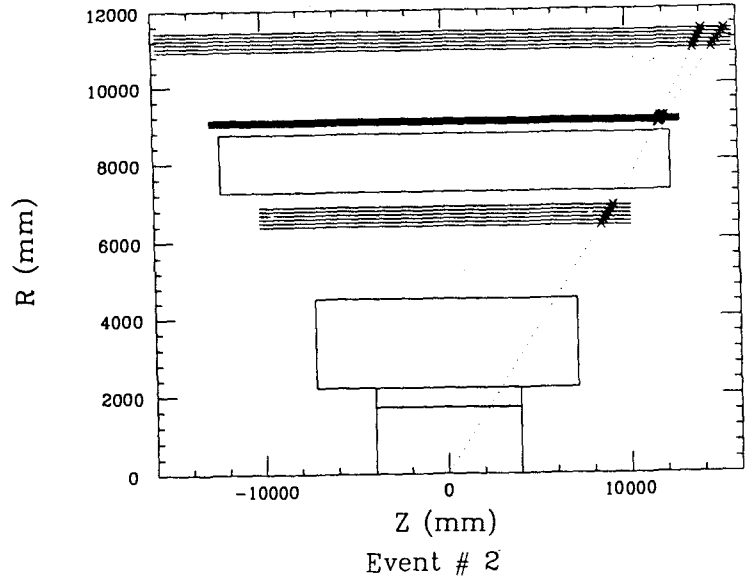

0879

0882

"Results"

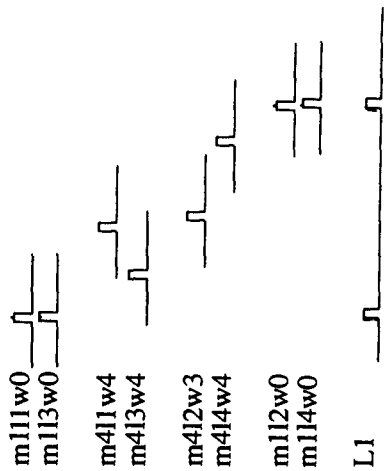

0883

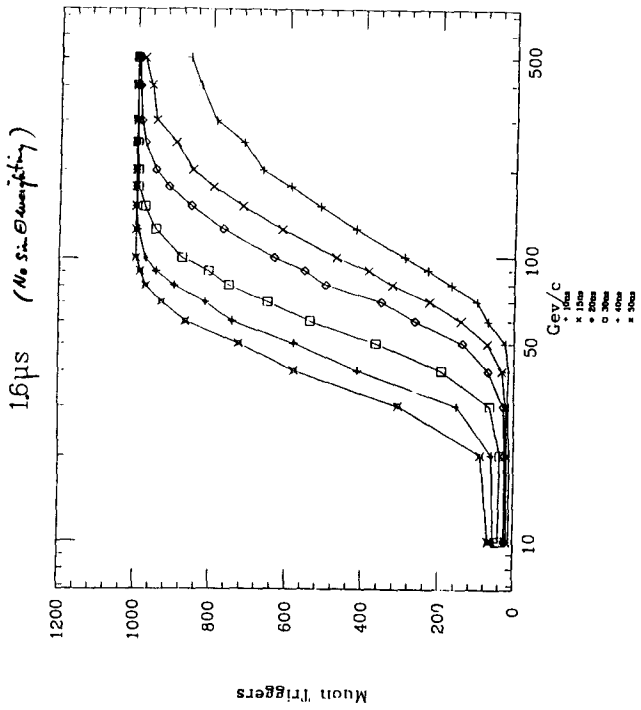

Weighted: "1/(sin*sin)"

0884

drift time based on muon trajectory intercept with wire-plane

coincidence times weighted with 1/(sin(0))**2 to account for projective geometry

significance: This is what projective geometry can do given a little tweaking of individual coincidence times

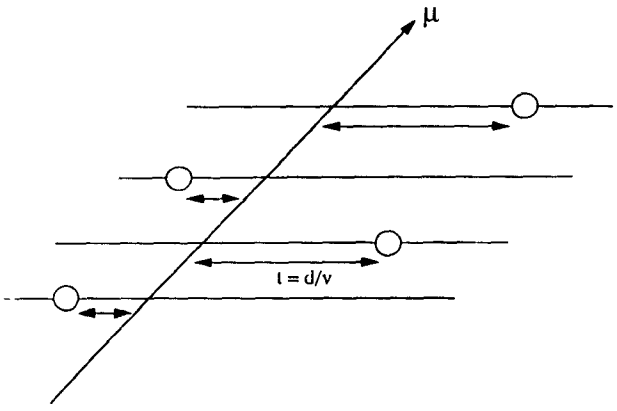

0885

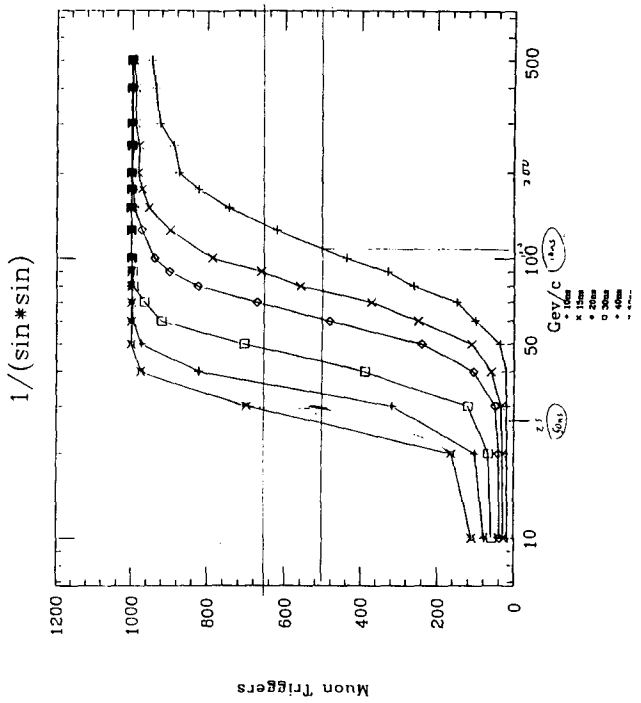

Finite IP: "Smeared/sin*sin"

drift time based on muon trajectory intercept with wire-plane

coincidence times weighted with 1/(sin(0))**2 to account for projective geometry

Interaction point "smeared" with gaussian distribution

σ = 5 cm in z

[redacted]

significance: This is what happens if the IP is not a singularity

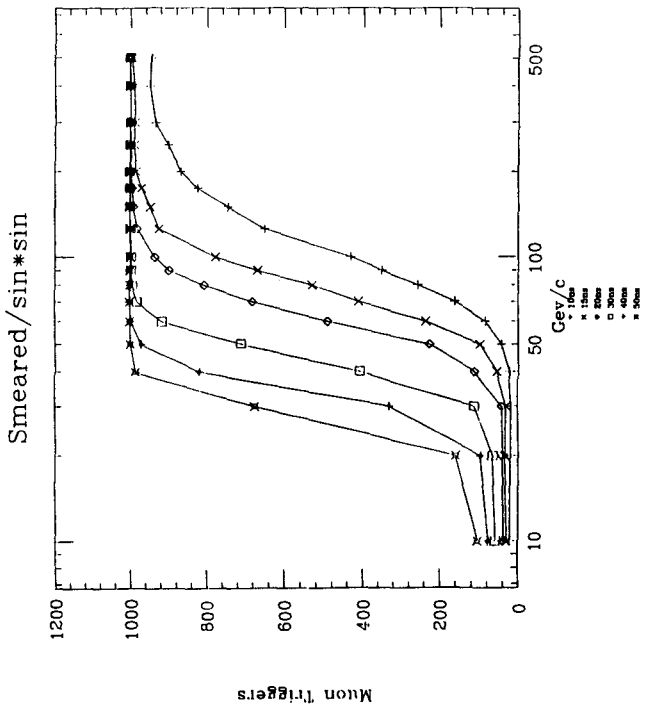

Closest Approach: "Impact/(sin*[redacted])"

drift time based on closest approach of muon trajectory to wire

coincidence times weighted with 1/(sin(θ))[redacted] to account for projective geometry ("[redacted]")

significance: This is what you get if the drift cell aspect ratio is closer to 1 than you thought (maybe)

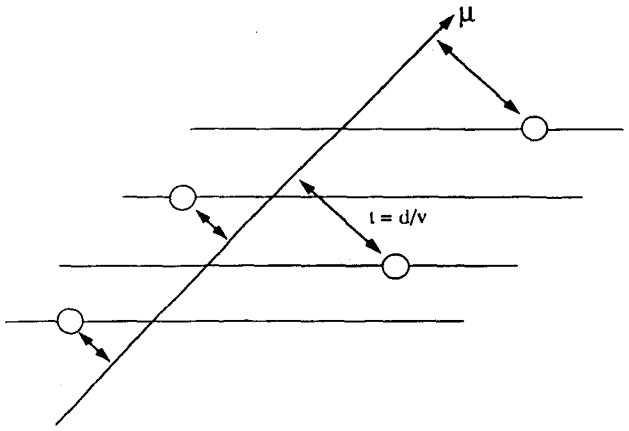

What's next:

- [redacted]
- use "generate" to represent more modules
- write CDF-type trigger model
- write Chapman-racetrack model for coincidence detection
- get other trigger ideas and write models
- compare triggers
- get better input data! [redacted]
  - projective geometry from fast muon simulation (S. Errede)
  - interface to SDC-SHELL software development project (I. Karliner)
- [redacted]

Table 3- Isajet V6.43 SSC $B\overline{B} \rightarrow$ 1 μ Simulation Results

# Events	$P_\perp(B)$ Limits	σ (mb)	$\int \mathcal{L}\, dt$ (mb^{-1})
10000	10- 50 GeV/c	0.6033E-02	0.1658E+07
10000	50-100 GeV/c	0.5710E-04	0.1751E+09
10000	100-200 GeV/c	0.5223E-05	0.1914E+10
10000	200-300 GeV/c	0.3309E-06	0.3022E+11
10000	300-400 GeV/c	0.5503E-07	0.1817E+12
5000	400-500 GeV/c	0.1412E-07	0.3539E+12

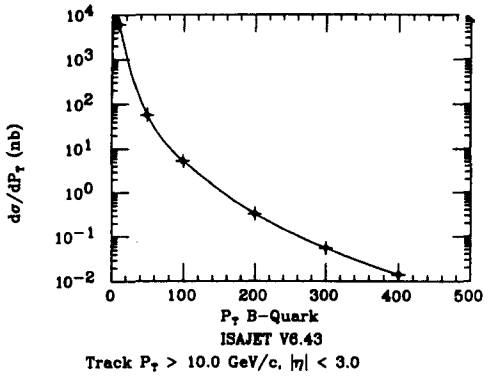

Muon Matching Studies

S. Errede(Illinois)

Steve Errede
Rob Gardner
Jim Wiss

November 11, 1991

Muon Matching Studies

This note summarizes the results of studies investigating the ability to match muon tracks measured in the Central Tracker (CTD) with hits in the muon system without confusion from adjacent putative (candidate) tracks in the CTD. We began this study to investigate how the placement of ϕ and stereo planes in BW1 $\rightarrow$ BW3 and the thickness of BW1 affects the ability to match CTD tracks to the muon system. After describing the calculational technique, we present some analytic calculations of a quantity we call the confusion volume which serves as a sort of "Rayleigh criterion" as to when a candidate track has track parameters which are too close to those of a muon track to be resolved within the muon system. The (inverse) size of the confusion volume provides figure of merit when comparing possible chamber layouts for the barrel muon system. At low $P_\perp$, where multiple scattering effects predominate, it is better to place ϕ layers in BW1 and thus avoid the multiple scattering of tracks by the toroid. At very high $P_\perp$, where measurement error dominates over multiple scattering, one gets better matching resolution by moving the ϕ layers to BW3 thus allowing the extrapolated tracks to separate more in space relative to the intrinsic chamber resolution. An initially surprising conclusion is that in the low $P_\perp$ limit, layouts with two ϕ layers[1] in BW1 exhibit significantly reduced matching confusion (by a factor of ≈ 2.6) over layouts with no ϕ layers in BW1 but with ϕ layers outside of the toroid. Nearly all of this improvement is made possible by the local ϕ slope measurement provided by the two ϕ layers in BW1. This big BW1 advantage is not present in strawman layouts with only a single ϕ layer, or in arrangements with a short lever arm between the ϕ planes at moderate $P_\perp$.

In order to assess the level of confusion, and find out which $P_\perp$ regime is relevant for physics processes we have performed Monte Carlo (ISAJET) simulations

of the high $P_\perp$ $B\overline{B}$ process. These Monte Carlo studies confirm that the low $P_\perp$ (multiple coulomb scattering dominated) limit is appropriate and a factor of ≈ 2 improvement in matching confusion should indeed be realized by placing two ϕ layers in BW1 rather than placing them outside of the muon toroid.

One word of caution... the results discussed here represent a lower bound on the real confusion since we have neglected the effects of δ-rays, bremsstrahlung, etc. which undoubtedly increase confusion[2].

1. Technique

We assume that the off line matching of the muon chamber hits with a possible CTD track is performed using a χ^2 test to the extrapolated track trajectory. A track is matched if it has a minimum, acceptable confidence level to the muon chamber hits where the confidence level is chosen so that the vast majority (*eg* 98 %) of real CTD muons are successfully matched (*eg*, $CL > 0.02$). Confusion results when an adjacent track has sufficiently similar track parameters that its extrapolation satisfies the muon confidence level cut.

It is fairly easy to "simulate" such a matching criteria by calculating the expectation value of the χ^2 for a given putative track to the hits of a given muon track in terms of the difference between the muon track and putative track parameters. We can then approximate the matching criteria by declaring confusion if $< \chi^2 > < \chi^2\ (\mathrm{CL} = 0.02)$. The matching χ^2 is computed as follows:

Let the relevant track parameters be denoted as $t_\alpha^{(\mu)}$ for the muon and $t_\alpha^{(p)}$ for the putative track. In our studies possible track parameters include the azimuth (ϕ), polar angle (θ), and curvature (Q/P). We define a *transport matrix* $T_{i\alpha}$ which multiplies the α'th track parameter to predict the i'th hit in the muon system (where we call this hit w_i). In our approach we assume that the i'th hit is due to the muon and follows the muon trajectory $T_{i\alpha}t_\alpha^{(\mu)}$ but suffers fluctuations δw_i due to multiple scattering and measurement error. The matching χ^2 will be constructed from the CTD putative track trajectory and the inverse coordinate

covariance matrix $C_{ij}^{(p)\,-1}$ of the putative track. We assume that this inverse coordinate covariance matrix can be computed for the putative track using the momentum as measured by the CTD and the known measurement errors of the muon system. We further assume that the CTD track parameter errors are negligible and ignore issues of left/right ambiguity and δ - ray effects. With these simplifications, the matching χ^2 is given by:

$$\chi^2 = \left(T_{i\alpha}t_\alpha^{(p)} - T_{i\alpha}t_\alpha^{(\mu)} - \delta w_i\right)\ C_{ij}^{(p)\,-1}\ \left(T_{j\beta}t_\beta^{(p)} - T_{j\beta}t_\beta^{(\mu)} - \delta w_j\right)$$

Taking the expectation value and autocorrelating we get:

$$< \chi^2 >= \Delta t^t\ H^{(p)}\ \Delta t + Tr\ C^{(\mu)}\ C^{(p)\,-1} \qquad (1)$$

where:

1. Δt^t is the transpose of the vector describing the difference between the muon and putative track track parameters.
2. $H^{(p)}$ is the fit matrix for the putative track. The inverse of the fit matrix is the putative track parameter error matrix. The components are $H_{\alpha\beta}^{(p)} = C_{ij}^{(p)\,-1}\ T_{i\alpha}T_{j\beta}$
3. $C^{(\mu)}$ and $C^{(p)}$ are the coordinate covariance matrices for the muon and putative tracks including measurement and multiple scattering effects.

The second term of Eqn.(1) has a straightforward physical interpretation. If the covariance matrix of the putative track is the same as that of the muon which caused the hits, the second term will be the trace of the unit matrix which is just the the number of muon system coordinates or the number of degrees of freedom in the χ^2 matching test. If, in addition, $\Delta t = 0$, one would obtain the familiar result: $< \chi^2 >= N_{\mathrm{dof}}$. If, on the other hand, the putative track is much better measured than the muon (*eg* resolution is mcs dominated and the putative track has a much higher momentum than the muon), the second term will insure

$< \chi^2 > \gg N_{\mathrm{dof}}$ even if $\Delta t = 0$. In this hypothetical case, even though putative track extrapolates the same as the muon, the spread in the hits around the track is much larger than expected given the putative track momentum and thus the match will typically be unacceptable.

2. "Analytic" Results

In this section we compare the matching confusion characteristics of various possible muon chamber layouts which differ in the number and placement of ϕ layers in BW1 $\rightarrow$ BW3. Each layout places two (projective) θ layers[3] in each of the stations BW1 $\rightarrow$ BW3. Each layer is assumed to offer a spacial resolution of 250 μm. The positions and thicknesses of the BW1 $\rightarrow$ BW3 chamber stations are those suggested by the integration group[4], **except** we use a 60 cm thick BW1 rather than the 35 cm allowed in integration group layout. The below tables summarize the assumed geometry and various layouts used in these studies.

Table 1 : Radial Geometry

	R_{in}	R_{out}
Calorimeter[5]	2.1 m	4.32 m
BW1	5.67	6.27
Toroid	6.45	7.95
BW2	8.18	8.53
BW3	9.78	10.66

Table 2 : Layout Description[1,3]

Layout	BW1	BW2	BW3
1	2ϕ , 2θ	2θ	2θ
2	2θ	2ϕ , 2θ	2θ
3	2θ	2θ	2ϕ , 2θ
4	2ϕ , 2θ	2ϕ , 2θ	2ϕ , 2θ

We next compare the level of matching confusion for the 4 possible layouts. A convenient comparison measure of matching confusion is the volume of the space of parameter differences which gives a χ^2 change of 1 unit. By Equation 1, the $\chi^2 = 1$ boundary will form an ellipsoid in $\Delta 1/P$, $\Delta\phi$, and $\Delta\theta$. The volume of this ellipsoid will be proportional to the reciprocal square root of the product of the eigenvalues of the $H^{(p)}$ matrix[6]. In principle one can match a putative track to muon hits using just the ϕ layers ($\Delta\phi$), or just θ layers ($\Delta 1/P\ \Delta\theta$), or all layers ($\Delta 1/P\ \Delta\phi\ \Delta\theta$).

Figure 1a compares the $\Delta\phi$ confusion volume for putative tracks at $\eta = 0$ as a function of $P_\perp$ for Layout 1 (ϕ layers in BW1: solid curve) , Layout 2 (ϕ layers in BW2 : dash) , Layout 3 (ϕ layers in BW3 : dot), and Layout 4 (ϕ layers in all BW : dash dot). We actually plot $P_\perp \times \Delta\phi$ since $\Delta\phi \propto 1/P_\perp$ at low $P_\perp$ where mcs effects dominate measurement error. The η dependence of the $P_\perp \times \Delta\phi$ is proportional to $1/\sqrt{sin\ \theta}$ at low $P_\perp$. A useful summary of Figure 1a and the foregoing is that the effective ϕ resolution in the low $P_\perp < 20\ GeV$ limit is:

$$\sigma_\phi = \left(\begin{array}{l} \frac{31\ mrad-GeV}{P_\perp \sqrt{sin\ \theta}} \quad (2\phi \text{ in BW1 }) \\ \frac{80\ mrad-GeV}{P_\perp \sqrt{sin\ \theta}} \quad (2\phi \text{ in BW2/3}) \end{array} \right)$$

At low $P_\perp$, cases where ϕ layers are placed in BW1 (Layouts 1 and 4) have about 2.6 times less confusion than cases where BW1 contains no ϕ layers (Layouts 2 and 3). Our Monte Carlo studies of $B\overline{B}$ production (discussed in Section 3) show that low $P_\perp$ is the most relevant limit. We note that the confusion volume for Layout 2 is exactly the same as the volume for Layout 3. If one must put the ϕ layers outside the toroid, the radius choice for the outer ϕ layers makes no difference at low $P_\perp$.

We note the double plateau structure of the volume versus $P_\perp$ curve (Figure 1a) which is most pronounced for Layout 1 (solid curve). The double plateau structure is crucial to the case for placing ϕ layers in BW1. Figure 1b hints at the explanation for this effect by showing the effects of removing one of the two

ϕ layers in Layout 1 (lower curves) or in Layout 3 (upper curves). The solid curves have two ϕ layers: while the dashed curves have only one. Apparently the lower $P_\perp$ plateau uses information from both ϕ layers, while the higher $P_\perp$ plateau effectively uses information from just one layer. A ϕ match can be made using both the ϕ intercept (which can be measured with just one layer) and the ϕ slope (which requires two ϕ layers). Figure 1a,b suggests that the slope information provided by two ϕ layers in BW1 is vastly superior in discriminating among matches at low $P_\perp$ but owing to the short lever arm $\approx$ 30 cm between the two planes, the slope information rapidly deteriorates with increasing $P_\perp$ as measurement information begins to dominate over mcs. Reduction in the ϕ lever arm below 30 cm creates an even more rapid deterioration in the slope information. For example if the radial separation between the two ϕ layers is reduced to 10 cm, a 52% degradation in ϕ matching resolution will occur relative to the 30 cm case even at $P_\perp$ as low as 25 GeV.

Figure 1c shows the matching confusion volume $P_\perp \times (\Delta P_\perp\ \Delta\phi\ \Delta\theta)$ as a function of $P_\perp$ of the putative track at $\eta = 0$ for the 4 layouts. The same solid, dash, dot, dash dot code is used in Figure 1c as 1a. Again in the low $P_\perp$ limit, layouts 1 and 4 which feature two ϕ layers in BW1, have about a factor of 2.6 times less confusion than layers 2 and 3 which have no ϕ layers in BW1. A factor of $sin\ \theta\ P^2$ was included in the calculation of the $(\Delta P_\perp\ \Delta\phi\ \Delta\theta)$ volume to convert from $\Delta 1/P$ to $\Delta P_\perp$. To facilitate comparisons we include an additional factor of $P_\perp$ since again the volume $(\Delta P_\perp\ \Delta\phi\ \Delta\theta) \propto 1/P_\perp$ in the low $P_\perp$ limit where resolution is mcs dominated. The η dependence of the $P_\perp \times (\Delta P_\perp\ \Delta\phi\ \Delta\theta)$ is proportional to $\sqrt{sin\ \theta}$ at low $P_\perp$.

Finally we consider the effects of an station to station misalignment on our matching confusion studies. We assume that all the layers within a BW1 $\rightarrow$ BW3 station are well aligned with respect to each other, however each station is miss aligned with an rms error (in $R\ \phi$) of $\sigma = 1mm$ with respect to the CTD. Figure 1d is a plot of $P_\perp \times \Delta\phi$ versus $P_\perp$ at $\eta = 0$ for the 4 layouts (using the same solid , dashed , dot , dash dot code as in Figure 1a) under the misalignment assumption.

In the low $P_\perp$ region the misalignment has no effect. We believe this is because the matching information comes from the ϕ slope rather than the intercept and the slope measurement is unaffected by station to station misalignment.

3. Monte Carlo Studies

The latest version of ISAJET (V6.43) was used to generate $B\overline{B}$ pair TWO-JET events for $\sqrt{s} = 40$ TeV p-p collisions. The B-meson/baryon in each ISAJET event was FORCE1 semi-muonically decayed to allowed B-decay modes as specified in the latest DECAY.DAT table. ISAJET runs varying the B-quark Pt interval were made. Information for charged, stable particles with $P_\perp > 10.0$ GeV/c and $|\eta| < 3.0$ were written to a separate file for input to the confusion analysis program(s). Table 3 (below) summarizes the results of these MC runs. Figure 2 shows the $B\overline{B} \rightarrow 1\mu$ cross section $\times$ semi-muonic branching ratio versus $P_\perp(B)$.

Table 3- Isajet V6.43 SSC $B\overline{B} \rightarrow$ 1 μ Simulation Results

# Events	$P_\perp(B)$ Limits	σ (mb)	$\int \mathcal{L}\ dt\ (mb^{-1})$
10000	10- 50 GeV/c	0.6033E-02	0.1658E+07
10000	50-100 GeV/c	0.5710E-04	0.1751E+09
10000	100-200 GeV/c	0.5223E-05	0.1914E+10
10000	200-300 GeV/c	0.3309E-06	0.3022E+11
10000	300-400 GeV/c	0.5503E-07	0.1817E+12
5000	400-500 GeV/c	0.1412E-07	0.3539E+12

For all charged, stable particles generated/event, require:
a.) $P_\perp(trk) > 10.0$ GeV/c
b.) $|\eta(trk)| < 3.0$

Analysis of the $400 < P_\perp(B) < 500$ GeV/c data set is presented first, followed by results for the remaining $P_\perp(B)$ intervals. In Figure 3, distributions for the accepted event multiplicity, the muon $P_\perp$, and the muon η are shown which characterize the event sample. Only muons satisfying $|\eta| < 1.5$ were subjected to the matching analysis.

For computing expediency, tracks falling within ± 100 mrad (in both $\Delta\phi$ and $\Delta\theta$) of the muon candidate were considered putative tracks for the confusion test. **Computation of muon and putative track confusion is restricted to tracks within the fiducial cone.**[7] Typical values for the number of of tracks close enough to the muon to fall into the putative track category ranged between 0 and 15, as illustrated in Figure 3d. To gauge the level of confusion, putative track parameters were used to compute the expectation value of the matching χ^2 described above. If a putative track was found to have a confidence level greater than 2% then the associated muon was declared confused.

The results of the confusion analysis on the $400 < P_\perp(B) < 500$ GeV/c run confirm the analytic results regarding placement of ϕ layers. We consider first matching tests performed using information from the ϕ layers only. The four geometry layouts of Table 2 and an additional three layouts, which are identical to layouts 1-3 except that each ϕ chamber consists of only one left-right unambiguous layer, are used as test configurations. A histogram of the number of tracks which are confused is shown for layout 1 in Figure 4a. The points in Figure 4b give the average number of confused tracks corresponding to the each of the layout schemes. The case of a single ϕ layer placed in BW1 is layout 5, a single ϕ layer in BW2 is layout 6, and a single ϕ layer in BW3 is layout 7. The increase in confusion that results when the ϕ layers are moved from BW1 to BW2 is about a factor of 2.2, consistent with the analytic result given the average momentum of putative tracks is 25 GeV/c. Note also that placement of the ϕ layers in either BW2 or BW3 makes little difference in the average number of confused tracks for this $P_\perp$ region. When only one ϕ layer per BW station is used (the last three bins of Figure 4b) the confusion is 15% to 90% worse than the corresponding deployment with two ϕ layers.

Similarly, when matching is performed using information from all layers ($\Delta Q/P\ \Delta\phi\ \Delta\theta$) the average number of confused tracks is consistent with analytic calculations. Figures 4c,d give the number of confused putative tracks and the average number of confused putative tracks for each of the layouts. Confusion rates for layouts 2 and 3, which have no ϕ layers in BW1, are found to be a factor of 2.4 greater than those having ϕ layers in BW1.

The dependence of the confusion on the $P_\perp$ and η of the muon is shown in

Figures 5a,b for $(\Delta\phi)$ matching using layout 2. (The results for layout 1 are similar but with reduced statistics). The η dependence reflects the reduced resolving power of $(\Delta\phi)$-only measurements for tracks traversing greater lengths of material. For $(\Delta Q/P\ \Delta\phi\ \Delta\theta)$ matching the corresponding dependencies are shown in Figures 5c,d. Curvature matching improves with large $P_\perp$ and η resulting in a flat η dependence.

In Figure 6 the results of the confusion analysis of the remaining ISAJET Monte Carlo runs are shown. Each row in the figure corresponds to one of the data sets (the $10 < P_\perp(B) < 50$ GeV/c and $50 < P_\perp(B) < 100$ GeV/c samples have been combined) and gives the number of tracks falling within the fiducial cone as well as the average number of confused tracks using the two matching criteria. Note that the number of confused tracks inside the fiducial cone is a strong function of $P_\perp(B)$. For either full matching or $(\Delta\phi)$ matching, the average confusion tends to increase with $P_\perp(B)$. Events in the highest $P_\perp(B)$ sample have confusion rates which are a factor of 4 to 7 times that of the lowest $P_\perp(B)$ sample when $(\Delta\phi)$ matching is used. When full matching is employed the corresponding confusion growth is typically a factor of 3 for most geometry configurations. Figures 7,8 give the confusion dependence on $P_\perp(B)$ according to layout scheme employed for both matching criteria.

We repeated the analysis for a sample of decays $T\overline{T} \rightarrow \mu X$ generated with a top quark mass of 130 GeV. The average number of confused tracks in the fiducial cone were found to differ only by a few percent from the $B\overline{B}$ samples when full matching was used; however the number of tracks within the fiducial cone is much smaller than in the $B\overline{B}$ samples.

4. Summary

We have presented studies on the ability to match putative tracks from the CTD to hits in the muon system. We have concentrated on how the placement of ϕ layers in the three chamber stations affects the level of confusion. These results have potential applications to both the offline analyses such as B physics, inclusive muon studies, as well as in the 3rd level trigger. In the interests of expediency, we have simplified the problem by ignoring the effects of δ-rays, left/right ambiguity, muon showering etc. and hence our absolute estimates of

confusion are really lower bounds; we hope the comparisons of confusion between different layout scenarios are valid.

Our central conclusion is that the placement of two ϕ layers in BW1 significantly ($\times 2.6$) reduces matching confusion in the low $P_\perp$ limit compared to layouts without ϕ layers in BW1. At sufficiently high $P_\perp$ (for the putative track), the station choice and number of ϕ layers becomes irrelevant to the muon - CTD matching issue. Beyond $P_\perp = 10 TeV$, ϕ layers in BW3 is actually preferable to ϕ layers in BW1. If two ϕ layers are placed in BW1, shortening the lever arm between the two ϕ layers will significantly reduce the range of $P_\perp$ with excellent ϕ matching resolution. These conclusions follow from resolution calculations, and are confirmed in high $P_\perp$ $B\overline{B}$ simulations.

In addition, analysis of the ISAJET simulations showed that reduction in confusion levels acheived by placement of ϕ layers in BW1 with adequate lever arm were significant over a large $P_\perp(B)$ momentum range. Typically the average confusion level for putative tracks is 0.1% to 0.5% when ϕ layers are placed in BW1 and full matching is employed. If only ϕ matching is used putative and muon tracks are confused 20% to 50% of the time on average. The confusion levels were also found to exhibit reasonable behavior as a function of $\eta(\mu)$; the confusion grows with $|\eta(\mu)|$ when only ϕ information was used while becoming essentially independent of $|\eta(\mu)|$ with full matching.

Footnotes

[1] We model this as two independent ϕ measurements separated by an $\approx 30cm$ lever arm. In reality four physical ϕ layers might be used because of drift time and ambiguity considerations.

[2] We hope that comparisons between one possible layout and another are still valid, however!

[3] One θ layer is placed close to the inside radius of each BW package and the other is placed on the outside radius. The ϕ layers are sandwiched in between the two θ layers with a maximum possible spacing between them.

[4] Dated 9/23/91 , distributed at the October ORNL SDC meeting

[5] We model the calorimeter (for scattering purposes) as a 2.22 meter thick slab of iron.

[6] Or the reciprocal square root of the $H^{(p)}$ determinant.

[7] The effect of the cone definition on putative track selection is $\approx 5\%$ underestimation of the absolute confusion level over a large $P_\perp(B)$ region.

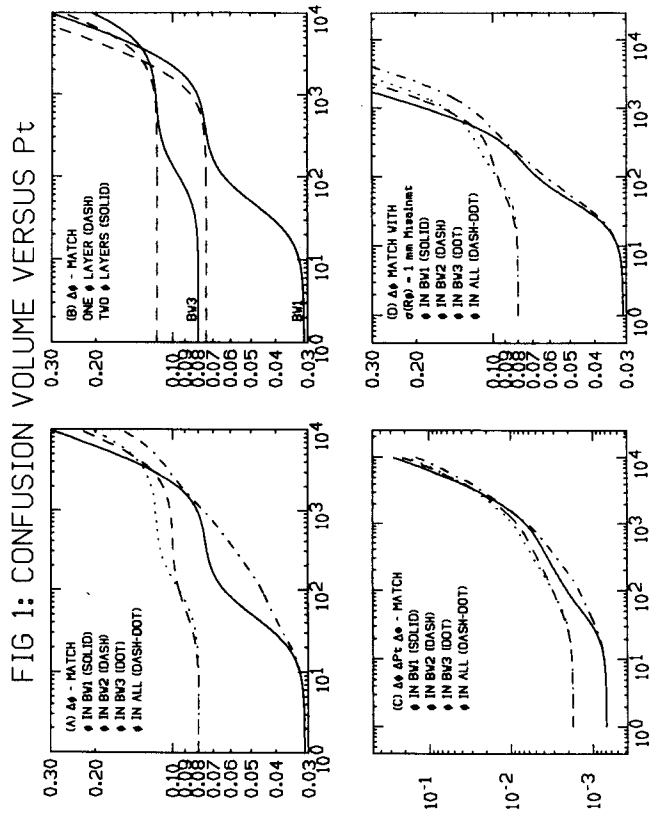

FIG 1: CONFUSION VOLUME VERSUS Pt

Fig 4a: # confused ($\Delta\phi$)–match

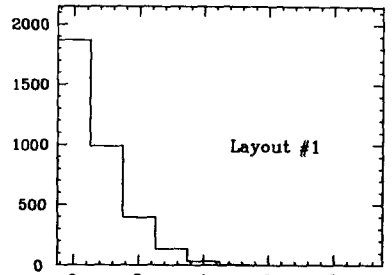

Fig 4b: ($\Delta\phi$)–match

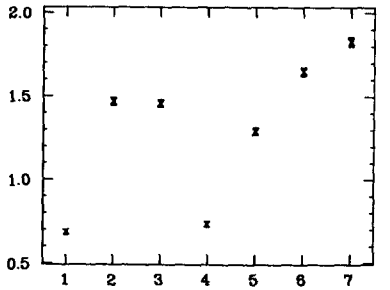

Fig 4c: # confused ($\Delta\phi$ $\Delta Q/P$ $\Delta\theta$)–match

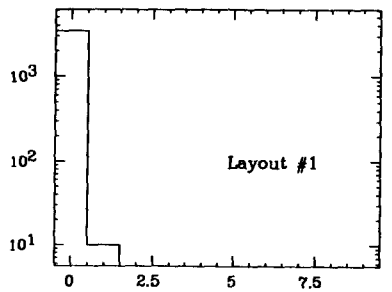

Fig 4d: ($\Delta\phi$ $\Delta Q/P$ $\Delta\theta$)–match

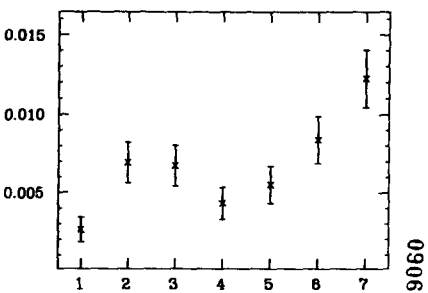

9006

Figure 2:BBbar -> 1 μ Cross Section

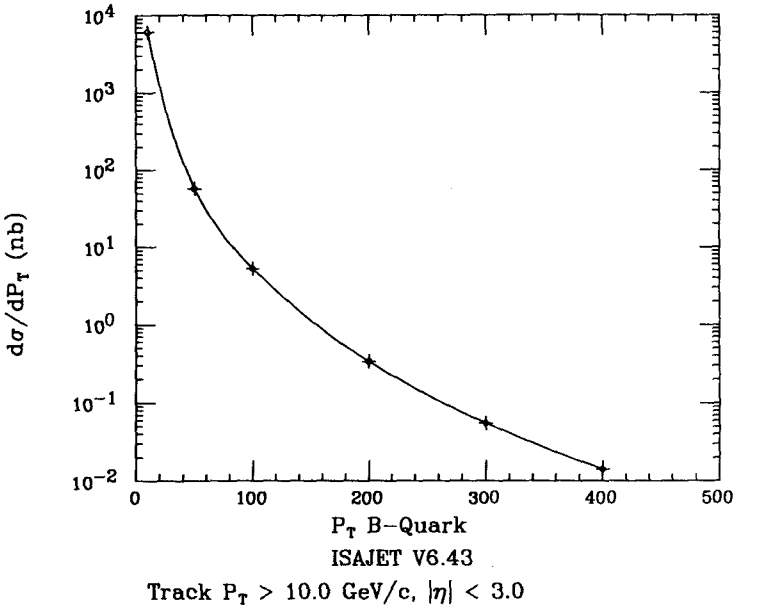

9004

(Layout #2)

Fig 5a: conf vs Pt(μ) ($\Delta\phi$)–match

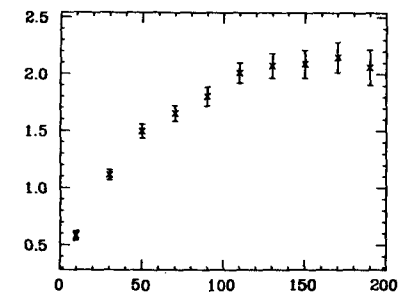

Fig 5b: conf vs η ($\Delta\phi$)–match

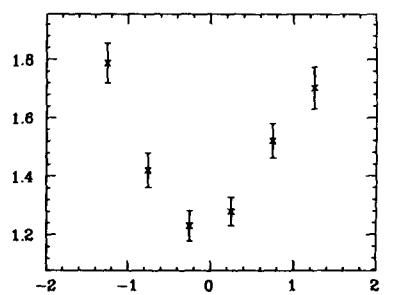

Fig 5c: conf vs Pt(μ) ($\Delta\phi$ $\Delta Q/P$ $\Delta\theta$)–match

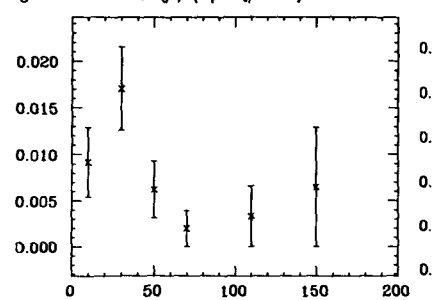

Fig 5d: conf vs η ($\Delta\phi$ $\Delta Q/P$ $\Delta\theta$)–match

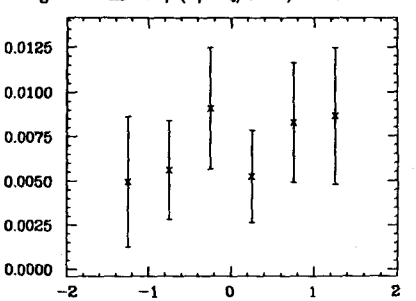

9007

Fig 3a: NTRAK

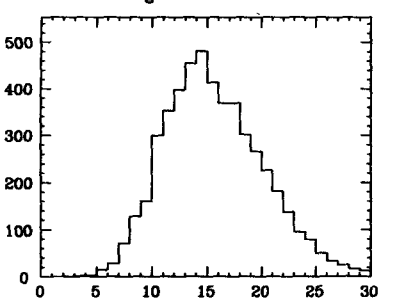

Fig 3b: $\eta(\mu)$

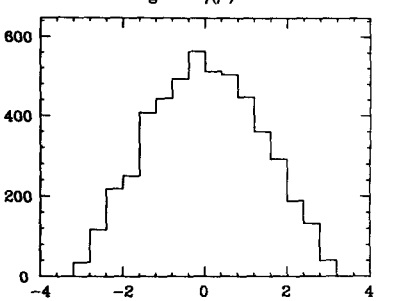

Fig 3c: Pt(μ)

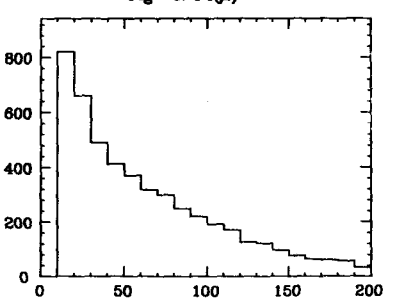

Fig 3d: NCONE ($-1.5<\eta(\mu)<1.5$)

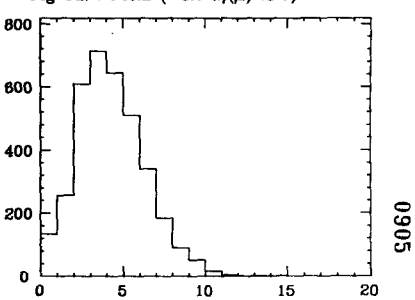

9005

Fig 8: Confusion vs B P_T

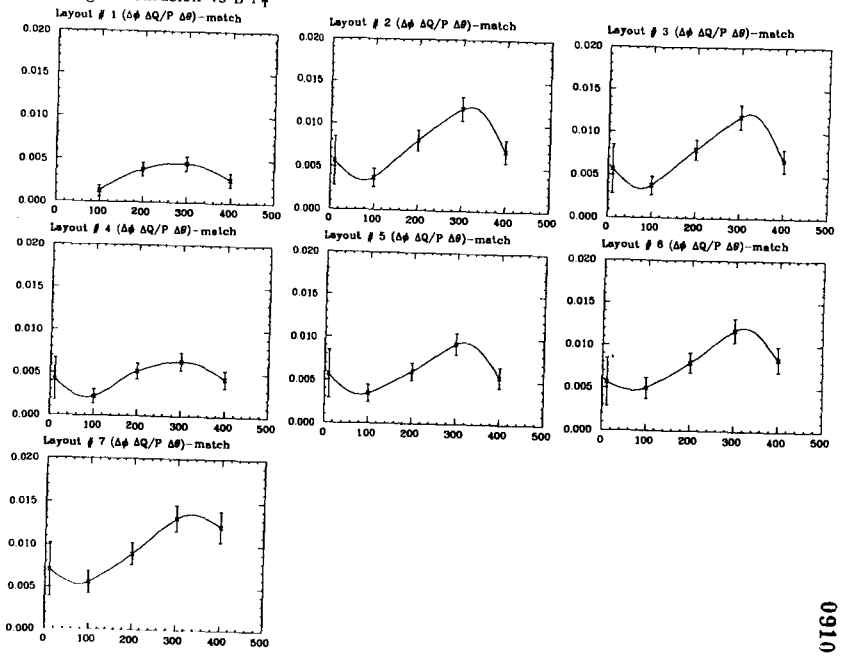

Fig 6: ISAJET BBbar -> 1 μ Events:10 < Pt(B) < 400 GeV/c

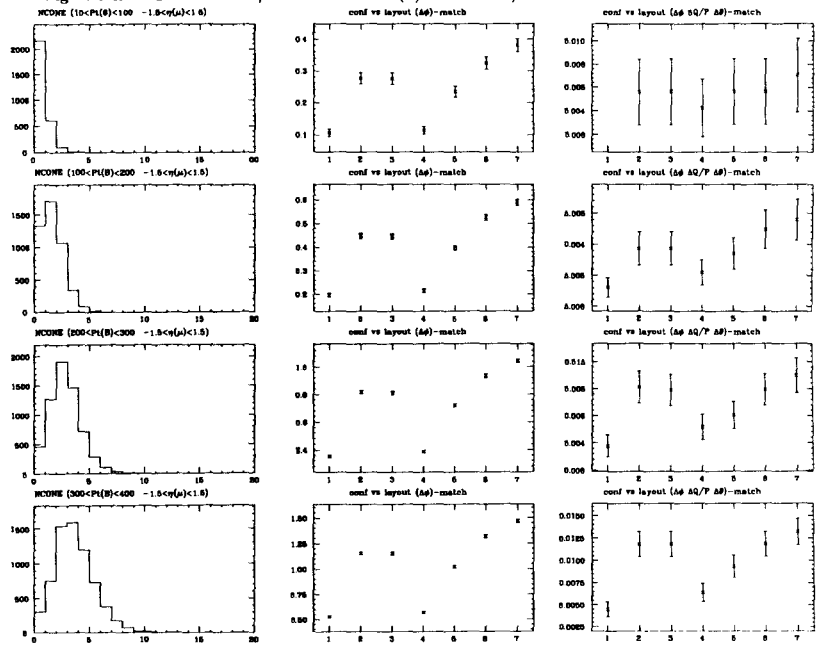

Fig 7: Confusion vs B P_T

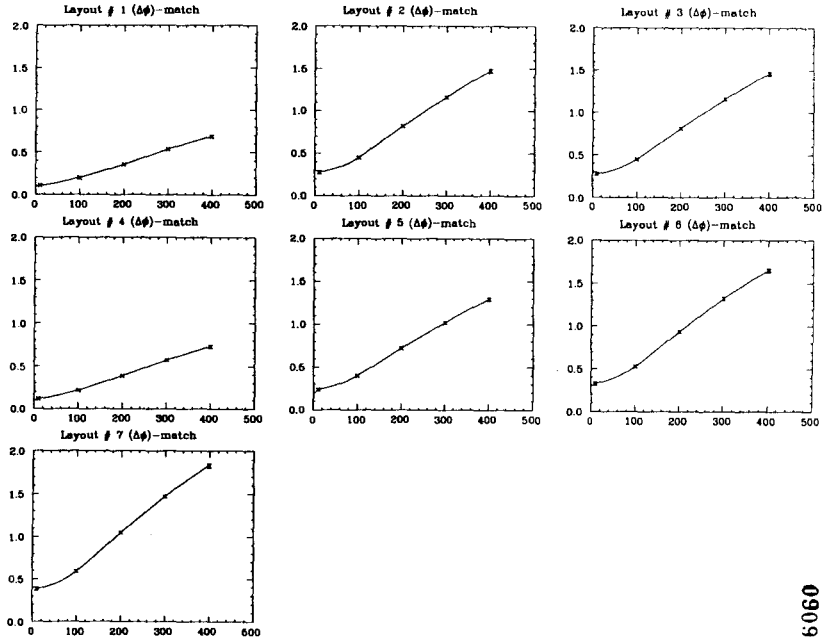

BW3 - BW2 Radial Separation Studies

J. Wiss(Illinois)

Jim Wiss

November 29, 1991

BW3 - BW2 Radial Separation Studies

This brief note summarizes some calculations on the efferts of decreasing the radial separation between the two muon chamber stations which lie on the outside of the barrel muon toroid. We concentrate on momentum resolution, muon confusion, and changes in alignment tolerances as the spacing between BW2 and BW3 is varied. All studies reported here assume the presence of two, projective θ planes in each of the three muon stations and two ϕ layers[1] placed in just BW1[2].

The below tables summarize the assumed nominal geometry[3] used in these studies:

Table 1 : Radial Geometry

	R_{in}	R_{out}
Calorimeter[4]	2.1 m	4.32 m
BW1	5.67	6.27
Toroid	6.45	7.95
BW2	8.18	8.53
BW3	9.78	10.66

This nominal geometry assumes a 1.25 meter separation[5] between BW2 and BW3. This memo studies how various performance parameters of the system depend on this separation.

1. Momentum Resolution

Figures 1 and 2 give the fractional momentum resolution ($\sigma P_t/P_t$) as a function of the BW3 - BW2 separation distance[5] at P_t of 100 , 200 , 400 , & 600 GeV. The momentum is measured using the θ planes of the muon system as a

stand alone system. This momentum resolution is relevant to both a second level (θ) trigger as well as for off line applications such as the use redundant momentum measurement in order improve muon matching and reduce punch through. Figure 1 is for $\eta = 0$ muons; Figure 2 is for $\eta = 1.5$ muons.

These figures show that increased BW2 - BW3 lever arm appears to significantly improve stand-alone momentum resolution only for muons with $P_t > 300$ GeV. The figures also illustrate the point that barrel toroid performance is better at large η than small η. At low P_t where the momentum measurement is MCS dominated, one can show that $\sigma P_t/P_t \propto 1/\sqrt{\sin\theta}$

2. Muon Matching

In an October 31 memo entitled *Muon Matching Studies* by Steve Errede, Rob Gardner, & Jim Wiss, we discuss a quantity called the *confusion volume* which serves as a sort of "Rayleigh criterion" as to when a candidate track has track parameters which are too close to those of a muon track to be resolved within the muon system. We assume that the off line matching of the muon chamber hits with a possible CTD track is performed using a χ^2 test to the extrapolated track trajectory. A track is matched if it has a minimum, acceptable confidence level to the muon chamber hits. Confusion results when an adjacent track has sufficiently similar track parameters that its extrapolation satisfies the muon confidence level cut. We define a *confusion volume* as the volume[6] of the space of parameter differences which gives a χ^2 change of 1 unit.

Figure 3 shows the matching confusion volume: $P_\perp \times (\Delta P_\perp\ \Delta\phi\ \Delta\theta)$ as a function of $P_\perp$ of the candidate track at $\eta = 0$ for the case of the nominal BW2 - BW3 spacing (solid curve) and for the case of zero separation (dashed curve) where the inner boundary of BW3 just touches the outer boundary of BW2. Below $P_t < 100$ GeV, there is essentially no difference in muon matching confusion. Even at P_t of 1 TeV, muon confusion increases by only 31 % if the BW2 - BW3 separation is reduced to zero. We note that our assumed chamber layout (ϕ layers in BW1) has been chosen to minimize matching confusion.

3. Misalignment Tolerances

Table 2 compares the maximum error normalized momentum biases ($\Delta P_t/\sigma P_t$) induced by rigid body misalignments of BW3 in fits where the barrel toroid is used as a stand alone system for $P_t = 100$ GeV and $P_t = 2$ TeV muons. A more complete description of rigid body alignment momentum biases is presented in my October 29th memo *Muon System Alignment Studies*. For pitches, rolls and transverse shifts, the maximum normalized bias occurs at the most extreme η; for z shifts the maximum bias occurs at $\eta = 0$. The alignment biases generally approximate sinusoidal distributions in ϕ. The table below gives maximum bias found after scanning over all ϕ.

Table 2 : BW3 Misalignment– Toroid Stand Alone

Max Δ/σ vrs BW3 - BW2 Separation

	100 GeV	100 GeV	2 TeV	2 TeV
	1.25 Sep	0 Sep	1.25 Sep	0 Sep
.5 mm shift x	0.15	0.24	1.02	0.97
.5 mm shift z	0.27	0.41	1.14	1.06
.1 mrad pitch	0.80	1.18	5.47	4.72
.1 mrad roll	0.12	0.18	0.83	0.71

For the case of $P_\perp = 100$ GeV muons, reducing the BW2 - BW3 sparing to zero, induces an ≈ 1.5 increase in the error normalized momentum bias due to BW2 - BW3 alignment. On the other hand a reduction of this separation may make it easier to align BW3. The $P_\perp = 100$ GeV case is probably most relevant to 2nd level triggering considerations. At $P_t = 2$ TeV, a case relevant to offline analysis, reduction of the BW2 - BW3 separation results in a slight decrease in error normalized momentum biases. I believe that this reflects the increase in the momentum error rather than a decrease in the momentum bias as one reduces BW2 - BW3 separation.

4. Conclusions

A series of studies are presented on the effects of reducing the BW3 - BW2 radial separation. For muons with P_t's up to several hundred GeV, the only deleterious effect I was able to find was an increased sensitivity ($\times 1.5$) in BW3 rigid body alignment. Beyond $P_t > 300$ GeV a noticeable degradation occurs in the fractional momentum resolution obtained using the stand-alone muon system as one reduces the BW2 - BW3 separation. Muon confusion studies show that muon confusion should be relatively insensitive to the BW2 - BW3 separation up to very large P_t. These studies assume[3] a relatively thick BW3 package of 88 cm.

Footnotes

[1] We model this as two independent ϕ measurements separated by an $\approx 30cm$ lever arm. In reality four physical ϕ layers might be used because of drift time and ambiguity considerations.

[2] One θ layer is placed close to the inside radius of each BW package and the other is placed on the outside radius. The ϕ layers are sandwiched in between the two θ layers with a maximum possible spacing between them.

[3] The nominal geometry is based on the SDC integration group document Dated 9/23/91 , distributed at the October ORNL SDC meeting, **except** we assume a 60 cm thick BW1 station rather than the 35 cm assumed in that document.

[4] We model the calorimeter (for scattering purposes) as a 2.22 meter thick slab of iron.

[5] Throughout this memo, the separation is defined as the radial distance between the outer boundary of BW2 and the inner boundary of BW3. The nominal separation is 1.25 meters.

[6] This is the volume enclosed by an ellipsoid whose principle axes depend on the fit matrix of the candidate track.

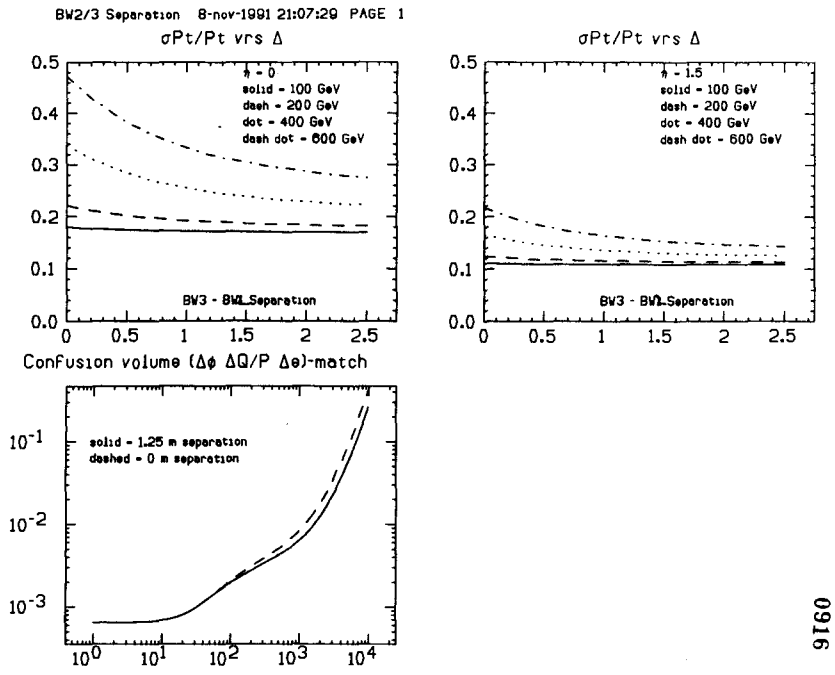
BW2/3 Separation 8-nov-1991 21:07:29 PAGE 1
σPt/Pt vrs Δ
η = 0
solid = 100 GeV
dash = 200 GeV
dot = 400 GeV
dash dot = 600 GeV
BW3 - BW2 Separation
σPt/Pt vrs Δ
η = 1.5
solid = 100 GeV
dash = 200 GeV
dot = 400 GeV
dash dot = 600 GeV
BW3 - BW2 Separation
Confusion volume (Δφ ΔQ/P Δθ)-match
solid = 1.25 m separation
dashed = 0 m separation

Muon System Alignment Studies

J. Wiss(Illinois)

Jim Wiss

October 29,1991

Muon System Alignment Studies

This note reports on studies of the effects of muon chamber misalignment on the momentum resolution and muon matching obtainable for several off line and 2nd level trigger muon scenarios. We hope such studies can serve to set alignment criteria on the components of the muon system. Presumably the off line criteria set tolerances on the ***knowledge*** of muon chamber misalignment as opposed to trigger criteria which set tolerances on the ***placement*** of muon chamber components. This memo augments the work described in the July 31, 1991 memo ***Alignment Resolution Studies of the Muon System*** by Jim Wiss. The previous memo concentrated on the question of how Gaussian distributed chamber station misalignments degrade momentum resolution. This work concentrates on the momentum biases created by rigid body chamber station misalignment. We begin by describing the technique, and then show results.

1. Technique

In a linearized fit, changes in the track parameters (t_α) are just a linear function of changes in the measured coordinates (w_i). We will call the linear transformation the ρ matrix. Systematic residuals in the coordinates created by chamber misalignment will create average biases in track parameters given by:

$$< \Delta t_\alpha >= \rho_{\alpha i} \ < \Delta w_i > \qquad 1$$

The calculation of alignment biases involves both the ρ matrix and the dependence of $< \Delta w_i >$ on the misalignment parameters. We begin with a discussion of the ρ matrix.

The $\rho_{\alpha i}$ matrix element serves as a direct measurement of the importance of the information of the i'th coordinate in determining the α'th track parameter. The ρ matrix depends on the coordinate covariance matrix assumed in performing

the fit C_{ij} as well as the transport matrix which ($T_{i\alpha}$) which relates the predicted coordinate from the track parameters ($w_i = T_{i\alpha} t_\alpha$).

$$\rho_{\alpha i} = H^{-1}_{\alpha\beta} \ C^{-1}_{ij} \ T_{j\beta} \quad \text{where} \quad H_{\alpha\beta} = C^{-1}_{ij} \ T_{i\alpha} \ T_{j\beta}$$

To get the best (minimal variance) results, the coordinate covariance matrix should reflect multiple scattering as well as measurement errors.

Figure 1 shows ρ matrix elements for the two θ and the two ϕ layers placed in BW1 as a function of P_t for muons created at $\eta = 0$. The ρ matrix is for a fit where information from the beam constraint ($\sigma = 20\mu$), silicon , CTD , and BW1 $\rightarrow$ BW3 is combined to find the track curvature. The ρ matrix depends significantly on η. We consider a muon layout with two θ planes in each of the three muon stations and two ϕ layers placed in just BW1. The rapid growth in ρ with increasing P_t for the two ϕ layers shows that they play an active role in determining momentum even at modest P_t. The growth in the ρ elements for the two θ layers is considerably more gradual. Evidently the muon toroid acts as a significant source curvature information only at large P_t.

We note that at low P_t the ρ elements for the inner and outer ϕ planes have the opposite signs. This means that the curvature fit is using the ϕ coordinate differences or essentially using the ϕ slope in BW1. Rigid body misalignment of the whole BW1 station will create nearly equal displacements in the two ϕ layers and thus a canceling momentum bias in the low P_t limit. At larger P_t, the ρ elements for the two ϕ layers have the same sign and rigid body misalignment becomes more important. Evidently in the high P_t domain the fit is concentrating on the the ϕ intercept rather than the ϕ slope. In the 1 TeV P_t domain, the θ layers become as important as the ϕ layers in BW1 in determining track curvature.

We next address the calculation of the chamber plane residuals (Δw_i) induced by rigid body misalignment error. The barrel muon system consists of a series of detector planes which can be specified by a read-out direction ($\hat{w}$), a plane

normal ($\hat{\eta}$), and an arbitrary point in the plane ($\vec{D}$). The below table gives a set of these vectors for two types of projections at radius R. The $\hat{y}$ geometry serves as a non-projective ϕ geometry for the first octant (the octant normal to $\phi = 0$). In the projective θ geometry, each plane (drift cell) is orientated such that its normal points back to the origin.

Table 1 – Detector Geometries in $\phi \approx 0$ Octant

Geometry	$\vec{D}$	$\hat{\eta}$	$\hat{w}$
$\hat{y}$	$(R \ \ 0 \ \ 0)$	$(1 \ \ 0 \ \ 0)$	$(0 \ \ 1 \ \ 0)$
projective θ	$(R \ \ 0 \ \ R/T_\theta)$	$(S_\theta \ \ 0 \ \ C_\theta)$	$(-C_\theta \ \ 0 \ \ S_\theta)$

Where $S_\theta \equiv sin\ \theta$, $C_\theta \equiv cos\ \theta$, $T_\theta \equiv tan\ \theta$

Let us imagine a track which passes through a point $\vec{M}$ and travels in a direction $\hat{p}$. The intersection ($\vec{r}$) of the track with the detector plane is given by:

$$\vec{r} = \vec{M} + \frac{t\hat{p}}{\hat{p}\cdot\hat{\eta}} \quad \text{where} \quad t = \hat{\eta}\cdot\left(\vec{D} - \vec{M}\right) \qquad 2$$

When viewed relative to a chamber station, a shift misalignment ($\vec{\Delta}$) can represented as a change in $\Delta\vec{M} = -\vec{\Delta}$ of the track origin and an angular misalignment can be a rotation ($\vec{\alpha}$) of $\hat{p} = -\vec{\alpha}\times\hat{p}$. The misalignment will create a change in coordinates given by:

$$\Delta w = -\hat{w}_i \ \frac{\partial\vec{r}_i}{\partial\vec{M}_j}\ \vec{\Delta} - \hat{w}_i \ \frac{\partial\vec{r}_i}{\partial\hat{p}_j}\ (\vec{\alpha}\times\hat{p})_j \qquad 3$$

The partial derivatives of Eqn. (2) are:

$$\frac{\partial\vec{r}_i}{\partial\vec{M}_j} = \delta_{ij} - \frac{\hat{p}_i\hat{\eta}_j}{\hat{p}\cdot\hat{\eta}} \quad ; \quad \frac{\partial\vec{r}_i}{\partial\hat{p}_j} = \frac{\ell}{\hat{p}\cdot\hat{\eta}}\left(\delta_{ij} - \frac{\hat{p}_i\hat{\eta}_j}{\hat{p}\cdot\hat{\eta}}\right) \qquad 4$$

Combining Eqn. (3) and (4) we have:

$$\Delta w = -\vec{g}\cdot\vec{\Delta} - \frac{\ell}{\hat{p}\cdot\hat{\eta}}\vec{g}\cdot\vec{\alpha}\times\hat{p} \quad \text{where} \quad \vec{g} = \hat{w} - \frac{\hat{\eta}\ \hat{p}\cdot\hat{w}}{\hat{p}\cdot\hat{\eta}} \qquad 5$$

Figure 2-4 show the residuals versus ϕ resulting from a 0.5 mm x shift (Figure

2) , a pitch rotation of 0.1 mrad about the $\hat{x}$ axis (Figure 3), and a roll of 0.1 mrad about the $\hat{z}$ axis. The solid curves are for Δw_ϕ ; the dashed curves are for Δw_θ. The figures are for muons produced at $\eta = 1.5$ (or $\theta = 25.2°$). The residuals are computed using Eqn. (5), where $\hat{p} = (\ C_\phi S_\theta \quad S_\phi S_\theta \quad C_\theta\ )$, and $\vec{D}$, $\hat{\eta}$, and $\hat{w}$ are taken from Table 1.

Several features are apparent from inspection of Figures 2-4. The residual pattern for (transverse) shifts and rotations are roughly sinusoidal with the Δw_ϕ being 90° out of phase with the Δw_θ phase. Significant discontinuities are present which reflect the octant structure of the muon chambers. The curved sections are essentially due to the same effects which create the ϕ angular factors described in my September 23, 1991 memo, *Octagonal Geometry Effects*. At $\eta = 0$, the transverse shifts create Δw_ϕ residuals but no Δw_θ residuals. The Δw_θ residuals grow from zero as η increases. This pattern is reversed for the case of transverse rotations (pitch and yaws). The approximate amplitude and phase of the various misalignments follows from simple trigonometric arguments and is summarized in Table 2.

Table 2 : Residual Envelope Functions

	MisAlign amount	Δw_ϕ	Δw_θ
Shift$_\perp$	$(\ \Delta_\perp cos\phi_s \quad \Delta_\perp sin\phi_s\ )$	$\Delta_\perp\ sin\ (\phi - \phi_s)$	$\Delta_\perp\ cos\theta\ cos(\phi - \phi_s)$
Shift$_z$	Δ_z	0	$-\Delta_z\ sin\theta$
Rot$_\perp$	$(\ o_\perp cos\phi_r \quad \alpha_\perp\ sin\phi_r\ )$	$\alpha_\perp\ R\ cos(\phi - \phi_r)/tan\ \theta$	$-\alpha_\perp\ R\ sin(\phi - \phi_r)/sin\ \theta$
Roll	α_z	$R\ o_z$	$-R\ \alpha_z\ cos\ \theta\ \ sin\ (\phi - \phi_{oct})$

$\phi - \phi_{oct}$ is the angle of the track wrt the octant normal

2. Results

In this section we develop alignment tolerances for rigid body motions of BW1 for a variety of curvature fits. We are guided by selecting misalignment tolerances which insure that P_t biases are always less than some fraction of the

P_t resolution up to some desired P_t over all ϕ and the η covered by the barrel muon system. The criteria can be computed using the calculations summarized in Tables 3 - 6. Throughout these calculations we assume a "minimal" muon chamber layout with two projective θ layers in BW1 → BW3 and two ϕ layers in BW1 only. The radial geometry is summarized below:

Table 3 : Radial Geometry

	R_{in}	R_{out}
Calorimeter	2.1 m	4.32 m
BW1	5.67	6.27
Toroid	6.45	7.95
BW2	8.18	8.53
BW3	9.78	10.66

(a) Full system fits

We begin by illustrating the effects of rigid body misalignment on BW1 in a curvature fit using the complete SDC detector (beam constraint, silicon , CTD, and muon system). Figure 5 shows the error normalized momentum bias ($\Delta P_t/\sigma P_t$) as a function of P_t for the case of $\eta = 0$, $\phi = 0$ muons for various misalignment errors (a 0.5 mm $\hat{y}$ shift , 0.5 mm $\hat{z}$ shift , a 0.1 mrad yaw , and a 0.1 mrad roll). The orientation of the shifts was chosen to give a maximum bias (for $\eta = 0$ muons) at $\phi = 0$. The magnitude of the misalignments were chosen to give a roughly $\pm 1\sigma$ bias at $P_t = 2\ TeV$, $\eta = 0$. Figure 5 shows that misalignments which primarily affect Δw_ϕ are far more important than misalignments which primarily affect Δw_θ in the domain $P_t < 200\ GeV$. The relative importance of ϕ layers rather than θ layers at low P_t is demonstrated by the strength of their respective ρ matrix elements shown in Figure 1.

Figure 6 shows the maximum $\Delta P_t/\sigma P_t$ as a function of ϕ for $P_t = 2000\ GeV$ muons for transverse and longitudinal shifts and rotations. For transverse shifts

and all rotations the maximum misalignment effect occurs the largest η (drawn for $eta = 1.5$); for $\hat{z}$ shifts the curve is drawn for $\eta = 0$ where the effect of a $\hat{z}$ shift creates maximum bias. Much of the ϕ residual structure seen in Figures 2 - 4 is recognizable in the ϕ bias structure shown in Figure 6. For $P_t = 2000\ GeV$, $\eta = 1.5$ muons, both Δw_ϕ and Δw_θ residuals play important roles and phases other than 0 and 90°'s are observed in the transverse shifts and rotations. The effects of shifts and rolls (rotations about $\hat{z}$) are well balanced; the effects of transverse rotations (pitches and yaws) is more important by a factor of ≈ 3. Much of the increased bias created by pitch and yaw relative to shifts and rolls is due to the aspect ratio of the barrel detector (it is about 2.12 times longer than its radius if it extended out to $\eta = 1.5$). The below table gives both the maximum and ϕ averaged rms values of $\Delta P_t/\sigma P_t$ for the case of $P_t = 2\ TeV$ muons. We also summarize calculations for misalignments in BW2 and BW3. Recall that in these calculations BW1 is the only muon station which contains ϕ layers.

Table 4 - Full system :B.C. , Si , CTD , & Muon System
Maximum & RMS Deviations at $P_t = 2\ TeV$

	BW1	BW1	BW2	BW2	BW3	BW3
	max	rms	max	rms	max	rms
.5 mm shift x	1.19	0.79	0.61	0.43	0.98	0.69
.5 mm shift z	0.91	0.91	0.48	0.48	0.86	0.86
.1 mrad pitch	3.60	2.34	2.59	1.82	5.20	3.65
.1 mrad roll	1.09	0.64	0.39	0.23	0.79	0.45

The momentum biases simply scale with the magnitude of the misalignments. One can simply scale the indicated misalignment in column one by the ratio of the desired error normalized tolerance to the maximum or RMS computed bias to set alignment tolerances. If we wished to limit biases to less than 1 σ over the full $\eta - \phi$ range at 2 TeV P_t, shifts will have to be kept to less than ≈ 0.5 mm , rolls will have to be kept to ≈ 0.1 mrad and pitches and yaws will have

Table 5 - High Lum Option: B.C. , Si & Muon System only
Maximum & RMS Deviations at $P_t = 2\ TeV$

	BW1	BW1	BW2	BW2	BW3	BW3
	max	rms	max	rms	max	rms
.5 mm shift x	1.03	0.61	1.09	0.77	0.61	0.43
.5 mm shift z	0.25	0.25	0.56	0.56	0.31	0.31
.1 mrad pitch	2.79	1.67	4.65	3.26	3.26	2.29
.1 mrad roll	1.22	0.90	0.70	0.41	0.49	0.28

We see from Table 5, that the shift z alignment tolerances can be relaxed to about 1 mm for the high luminosity fits. Transverse misalignment must be kept to within ≈ 0.5 mm.

(c) Muon Toroid as a Stand Alone System

By a stand along system, we mean that the muon system provides momentum measurement by measuring the θ bend through the 1.5 m toroid without any help from the beam constraint, CTD , or silicon. One can imagine the stand alone use of muon system as a second level muon trigger as well as an off line tool which provides a redundant momentum measurement of muons for the purpose of matching and punch through rejection. For triggering purposes a $P_t = 100\ GeV$ seems appropriate, for off line purposes the 2 TeV scale may be relevant. Figure 9 and 10 show error normalized biases for BW1 misalignments subject to our standard misalignments ((a 0.5 mm $\hat{y}$ shift , 0.5 mm $\hat{z}$ shift , a 0.1 mrad pitch , and a 0.1 mrad roll) for $P_t = 2\ TeV$ (Figure 9) and $P_t = 100\ GeV$ (Figure 10). Table 6 & 7 give the error normalized maximum and rms biases over the range $(0 < |\eta| < 1.5$ for misalignments in BW1 → BW3.

to be kept to $\approx 27\ \mu$rad of BW1 relative to the CTD. These tolerances mean that all corners of the barrel muon detector should be located to within ≈ 0.5 mm relative to the CTD insure good performance over the full detector up to 2 TeV. These conclusions are consistent with those reached in my earlier memo *Alignment Resolution Studies of the Muon System*.

(b) Hi Luminosity option

We next consider curvature measurement in the high luminosity limit where the CTD has too high an occupancy to be useful. In the high luminosity fit, the curvature is measured using information from the beam constraint, silicon, and muon system. Figure 7 shows the momentum bias divided by the momentum error ($\Delta P_t/\sigma P_t$) as a function of P_t for the case of $\eta = 0$, $\phi = 0$ muons for various misalignment errors (a 0.5 mm $\hat{y}$ shift , 0.5 mm $\hat{z}$ shift , a 0.1 mrad yaw , and a 0.1 mrad roll). We see that the misalignments which most affect w_θ ($\hat{z}$ shift and yaw) are about a factor of 4 less important relative to the misalignments which primarily affect w_θ. This is in contrast to the results of Figure 5 for the full muon fit and reflects the much smaller size of the sum of the θ plane ρ matrix elements in this type of fit for muons produced at $\eta = 0$.

Figure 8 shows the maximum $\Delta P_t/\sigma P_t$ as a function of ϕ for $P_t = 2000\ GeV$ muons for transverse and longitudinal shifts and rotations. For transverse shifts and all rotations the maximum misalignment effect occurs the largest η (drawn for $\eta = 1.5$). For $\hat{z}$ shifts the curve is drawn for $\eta = 0$ where the effect of a $\hat{z}$ shift creates maximum bias. Table 5 gives the maximum and (ϕ averaged) rms error normalized momentum biases for misalignments in BW1 → BW3.

Table 6 - Toroid Stand Alone
Maximum & RMS Deviations at $P_t = 2\ TeV$

	BW1	BW1	BW2	BW2	BW3	BW3
	max	rms	max	rms	max	rms
.5 mm shift x	0.81	0.57	1.83	1.29	1.02	0.72
.5 mm shift z	0.90	0.90	2.04	2.04	1.14	1.14
.1 mrad pitch	2.35	1.65	7.83	5.49	5.47	3.84
.1 mrad roll	0.36	0.21	1.18	0.68	0.83	0.48

Table 7 - Toroid Stand Alone
Maximum & RMS Deviations at $P_t = 100\ GeV$

	BW1	BW1	BW2	BW2	BW3	BW3
	max	rms	max	rms	max	rms
.5 mm shift x	0.08	0.06	0.23	0.16	0.15	0.11
.5 mm shift z	0.18	0.18	0.44	0.44	0.27	0.27
.1 mrad pitch	0.18	0.13	0.98	0.69	0.80	0.56
.1 mrad roll	0.03	0.02	0.15	0.09	0.12	0.07

The results of Table 7 indicate that the $R\theta$ misalignments of BW2 must be kept below ≈2 mm to keep $\Delta P_t < \sigma P_t$ at $P_t = 100\ GeV$. Since the second level trigger does not have the time to put in alignment corrections, this means that BW2 must really be placed in space within this ≈ 2 mm tolerance. To maintain $\Delta P_t < \sigma P_t$ at $P_t = 2\ TeV$ over the full η range will require $R\theta$ misalignments of less than 0.25 mm. This is a tolerance on the knnwledge of the BW2 position. As one would expect, the roll tolerances in this type of fit are rather loose.

(d) σ Second Level Trigger

Next we discuss studies of the alignment tolerance for a ϕ second level trigger where infnrmation from a beam constraint, the outermost two layers of the CTD

(providing an angular resolution of ≈2 mrad) is combined with information from the two ϕ layers in BW1 to measure momenta. No use is made of the toroid. The only relevant misalignment is for the ϕ planes in BW1. Figure 11 shows the error normalized biases for our standard list of misalignments (a 0.5 mm $\hat{x}$ shift , 0.5 nim $\hat{z}$ shift , a 0.1 mrad pitch , and a 0.1 mrad roll) for muons with $\eta = 1.5$ & $P_t = 100\ GeV$. The maximum and RMS normalized biases are summarized in Table 8 for $P_t = 50$, 100 & 200 GeV.

Table 8 - ϕ 2nd Level Trigger
Maximum & RMS Deviations for BW1 Motions

	50 GeV	50 GeV	100 GeV	100 GeV	200 GeV	200 GeV
	max	rms	max	rms	max	rms
.5 mm shift x	0.0644	0.0466	0.1057	0.0765	0.1663	0.1203
.5 mm shift z	0.0000	0.0000	0.0000	0.0000	0.0000	0.0000
.1 mrad pitch	0.1067	0.0739	0.2017	0.1397	0.3843	0.2661
.1 mrad roll	0.0543	0.0489	0.1026	0.0924	0.1954	0.1761

Table 8 shows that BW1 alignment tolerances must be kept to 3 mm in the Rϕ direction to keep the maximum biases to less than 1 σ for $P_t = 200\ GeV$ muons in the range $0 < \eta < 1.5$. If one is only interested in maintaining this performance up to $P_t = 100\ GeV$, the alignment tolerance can be relaxed to ≈ 5 mm. Presumably alignment corrections cannot be made at the trigger level and hence BW1 would actually have to be placed relative to the CTD within these tolerances. The tolerances required in the 2nd level ϕ trigger are presumably looser than in the 2nd level θ trigger since the CTD does much of the measurement work in the ϕ trigger.

(e) Muon Matching

Finally we address the effects of chamber misalignment on the ability to match muons with putative tracks measured in the CTD. We assume that the off

line matching of the muon chamber hits with a possible CTD track is performed using a χ^2 test to the extrapolated track trajectory. A track is matched if it has a minimum, acceptable confidence level to the muon chamber hits where the confidence level is chosen so that the vast majority (*eg* 98 %) of real CTD muons are successfully matched (*eg* , $CL > 0.02$). The χ^2 is kept as low as possible (consistent with keeping muon efficiency) to eliminate confusion resulting when an adjacent track has sufficiently similar track parameters that its extrapolation satisfies the muon confidence level cut. A study of matching confusion is presented in the memo ***Muon Matching Studies*** hy Steve Errede , Rob Gardner, and Jim Wiss.

The effects of misalignment will be to create a ϕ dependent average χ^2 increase of which is proportinnal to the square of the misalignment strength. If the $\Delta\chi^2$ were sufficiently large, real muons would fail to satisfy the matching χ^2 cut resulting in efficiency losses. To get a feel for these effects we compute the χ^2 increase due to misalignments as:

$$\Delta\chi^2 = \Delta\ w_i\ C_{ij}^{-1} \Delta w_j \quad \text{where } \Delta w_i \text{ are due to misalignment}$$

Figure 12 shows $\sqrt{\Delta\chi^2}$ as a function of ϕ for 2 TeV muons for our four standard misalignments. Table 7 & 8 summarize the maximum and RMS $\sqrt{\Delta\chi^2}$ as one scans over ϕ for the case of 2 TeV and 50 GeV muons.

Table 9 - $\sqrt{\Delta\chi^2}$
Maximum & RMS $\sqrt{\Delta\chi^2}$ at $P_t = 2\ TeV$

	BW1	BW1	BW2	BW2	BW3	BW3
	max	rms	max	rms	max	rms
.5 mm shift x	2.27	1.82	2.07	1.46	1.42	1.00
.5 mm shift z	2.55	2.55	2.33	2.33	1.71	1.71
.1 mrad pitch	6.91	5.34	8.89	6.24	7.41	5.20
.1 mrad roll	2.08	1.73	1.35	0.78	1.12	0.65

Table 10 - $\sqrt{\Delta\chi^2}$
Maximum & RMS $\sqrt{\Delta\chi^2}$ at $P_t = 50\ GeV$

	BW1	BW1	BW2	BW2	BW3	BW3
	max	rms	max	rms	max	rms
.5 mm shift x	0.30	0.22	0.65	0.46	0.54	0.38
.5 mm shift z	0.48	0.48	0.82	0.82	0.62	0.62
.1 mrad pitch	0.96	0.68	2.83	1.99	2.45	1.72
.1 mrad roll	0.17	0.12	0.43	0.25	0.37	0.21

Table 9 suggests that the alignment tolerances required to keep $\Delta\chi^2 < 1$ at 2 TeV correspond to ≈ 0.25mm position uncertainties. At 50 GeV, the matching alignment criteria can be relaxed hy roughly a factor of 3 (≈1 mm position uncertainty).

3. Conclusions

This work has concentrated on setting alignment criteria both for use in possible 2nd level triggers and off line applications including momentum resolution and matching muon tracks in highly clustered jets. We been guided by the concept that momentum biases induced by misalignment should be less than the momentum resolution over the full $\eta - \phi$ range spanned by the barrel muon detector up to some desired momentum. For off line studies we choose a maximum P_t of 2 TeV ; for triggering we typically use a maximum P_t of 100 GeV.

Although each type of misalignment has its own unique pattern of momentum biases within the context of a given curvature fit, a general picture emerges for what we hope are reasonable alignment tolerances. Generally the position tolerances for triggering purposes must be kept within $2 \rightarrow 3$ mm. To maintain performance from $0 < |\eta| < 1.5$, this implies pitch and yaw tolerances of roughly 150 μrad. These are probably tolerances on the actual transverse and longitudinal positions of the muon chamber stations relative to the CTD.

Off line analysis tolerances at P_t = 2 TeV range from roughly 0.2 → 0.5 mm. The looser tolerances are for fits which combine information from other trackers such as the CTD or silicon system. The tighter tolerance is for redundant measurement by the muon toroid as a stand alone system or for matching high P_t tracks measured in the CTD to hits in the muon system. These position tolerances imply pitch and yaw tolerances of $< 15\ \mu rad$ if one wishes to maintain performance up to $|\eta| < 1.5$.

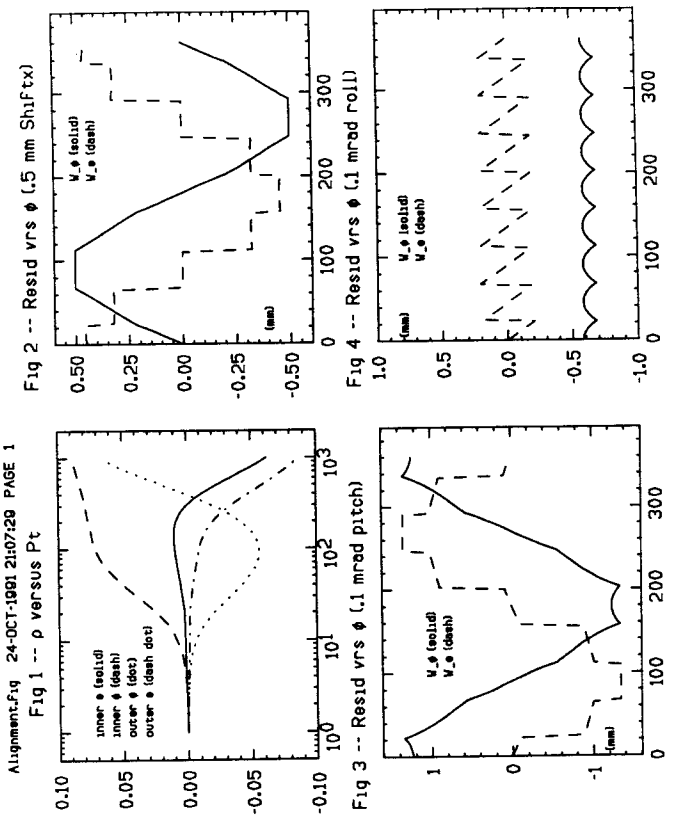

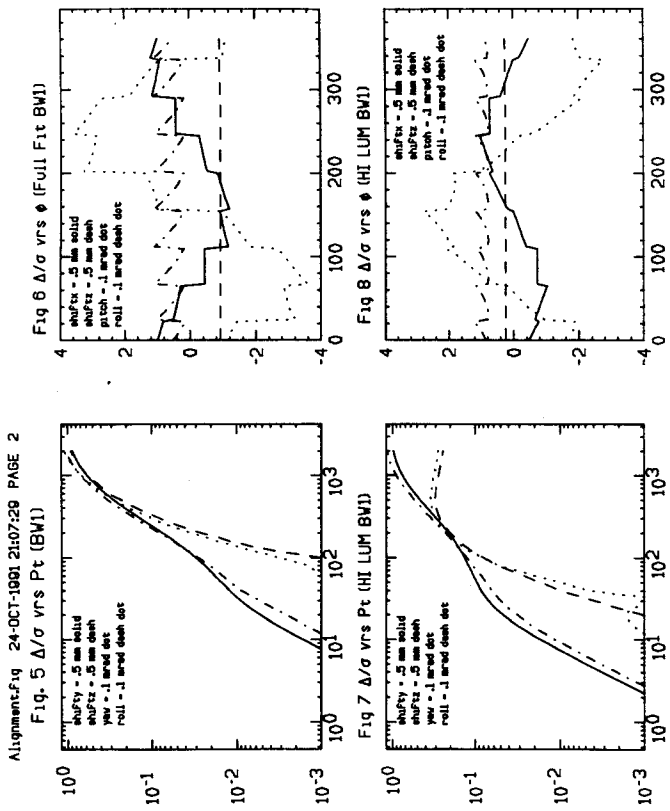

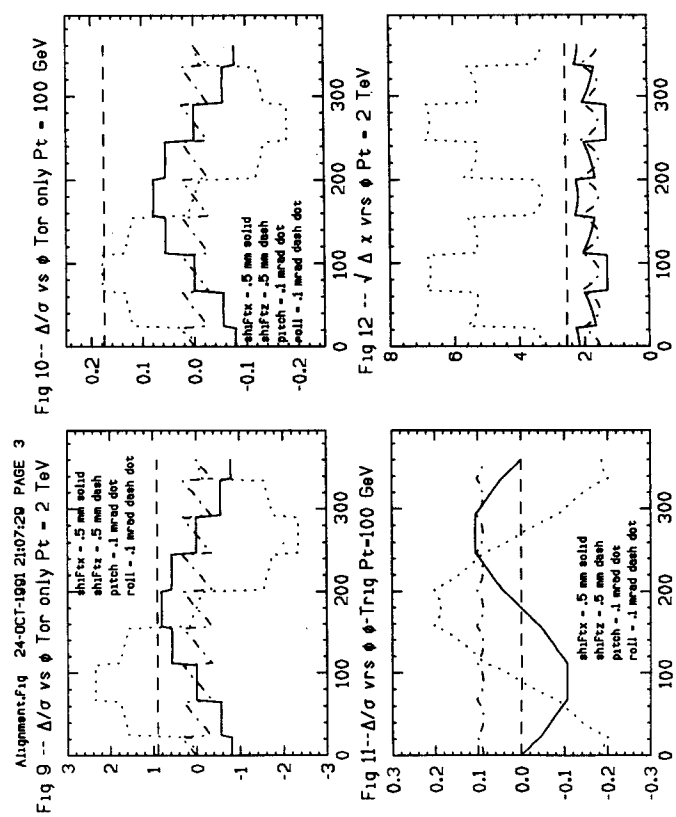

Muon Momentum Resolution

V. Slonim(Colorado)

MUON MOMENTUM RESOLUTION V. SLONIM

FIT CHARACTERISTICS

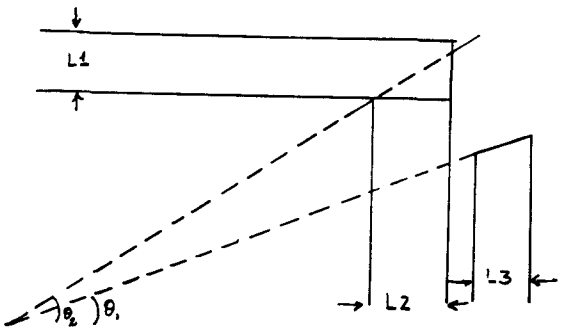

$B = 1.8\ T \quad L1 = 1.5\ m \quad L2 = L3 = 2\ m$

$$\theta_B = \frac{0.3BL}{p} \begin{cases} L = L_1/\sin\theta & \theta > \theta_2 \\ = L_2/\cos\theta & \theta_2 < \theta < \theta_1 \\ = (L_2+L_3)/\cos\theta & \theta < \theta_1 \end{cases}$$

$$\Delta\theta_{meas} = \frac{\Delta z}{D_y}\sin^2\theta \qquad \theta > \theta_2$$

$$= \frac{\Delta x}{D_x}\cos^2\theta \qquad \theta < \theta_1$$

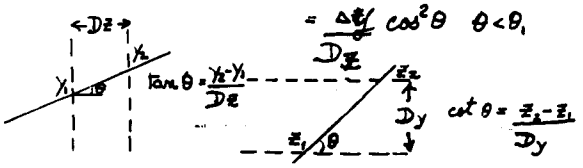

$$\Delta\theta_{mscatt} = \frac{0.015}{p}\sqrt{\frac{L}{X_0}}(\ldots\ldots)$$

$X_0 = 1.76$ cms. $\quad L = L_1/\sin\theta$ .....

$$\Delta\theta_{error} = \left\{(\Delta\theta^{BW1}_{meas})^2 + (\Delta\theta^{BW2,3}_{meas})^2 + \Delta\theta^2_{mscatt}\right\}^{1/2}$$

$$\frac{\Delta(1/p)}{(1/p)} \simeq \frac{\Delta(1/p_t)}{1/p_t} = \frac{\Delta\theta_{error}}{\theta_B}$$

$$\frac{\Delta 1/p}{1/p} = \frac{p}{0.3BL}\left\{\frac{(0.015)^2}{p^2}\frac{L}{X_0} + C_2\left[\frac{\sin^4\theta}{\cos^4\theta_1}\right]\right\}^{1/2}$$

In barrel $\theta > \theta_2$, $L = L_1/\sin\theta$

$$\frac{\Delta 1/p}{1/p} = \frac{p\sin\theta}{0.3BL_1}\left\{\frac{(0.015)^2}{p^2}\frac{L_1}{X_0\sin\theta} + C_2\sin^4\theta\right\}^{1/2}$$

$$= \frac{p_t}{0.3BL_1}\left\{\frac{(0.015)^2}{p_t^2}\frac{L_1}{X_0}\sin\theta + C_2\sin^4\theta\right\}^{1/2}$$

In intermediate Region $\theta < \theta_1$, $\quad L = (L_2+L_3)/\cos\theta$

$$\frac{\Delta 1/p}{1/p} = \frac{p\cos\theta}{0.3B(L_2+L_3)}\left\{\frac{(0.015)^2}{p^2}\frac{(L_2+L_3)}{X_0\cos\theta} + C_2\cos^4\theta\right\}^{1/2}$$

$$= \frac{p_t\cot\theta}{0.3B(L_2+L_3)}\left\{\frac{(0.015)^2}{p_t^2}\frac{(L_2+L_3)\sin^2\theta}{X_0\cos\theta} + C_2\cos^4\theta\right\}^{1/2}$$

MOMENTUM RESOLUTION FOR VARIOUS θ CHAMBERS IN BW1
BARREL REGION ONLY

$\sigma(\delta(1/P)/(1/P))\%$
Point Resolution = 200 μ

P(GeV/c)	σ % 2 θ layers Dy= 24 cms.	σ % 4 θ layers Dy=8 cms. each
25	18.9 ± 0.5	18.5 ± 0.5
50	19.2 ± 0.5	18.9 ± 0.5
100	22.4 ± 0.6	22.1 ± 0.6
200	28.2 ± 0.8	28.0 ± 0.9
500	69.2 ± 1.7	69.6 ± 1.6
1000	113.8 ± 3.2	113.8 ± 3.0

Theory:

$$\Delta\theta_{meas}(4\ layers) = \frac{3}{\sqrt{10}}\,\Delta\theta_{meas}(2\ layers)$$

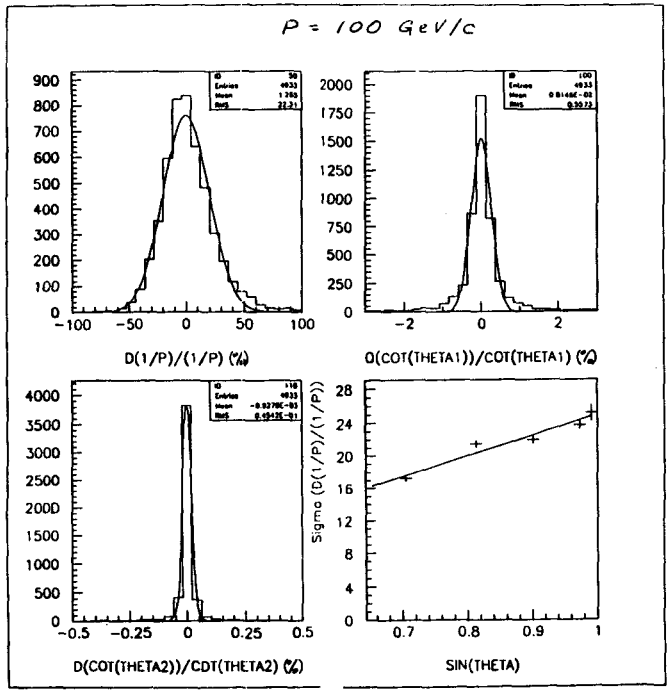

0941

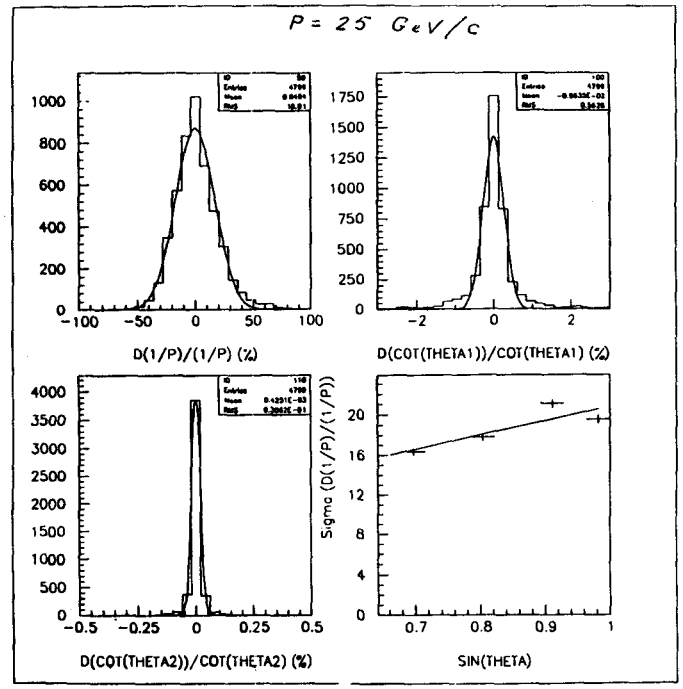

0939

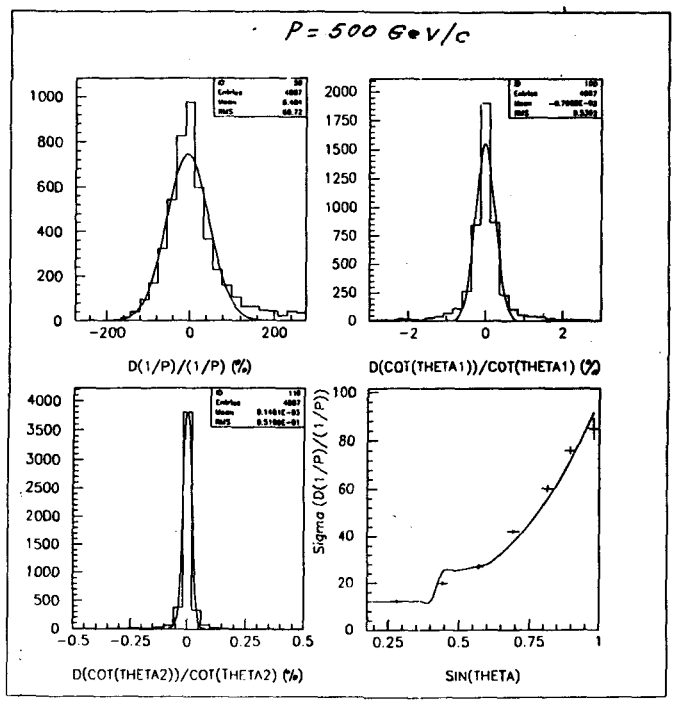

0942

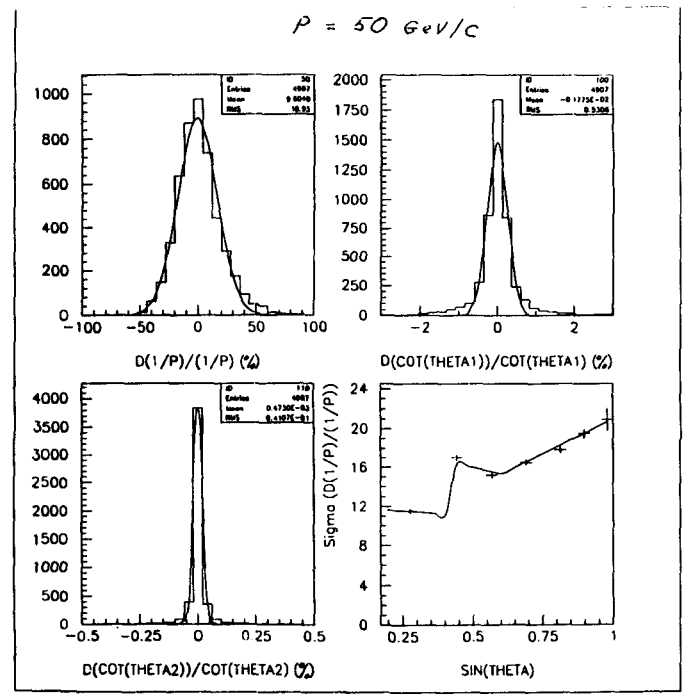

0940

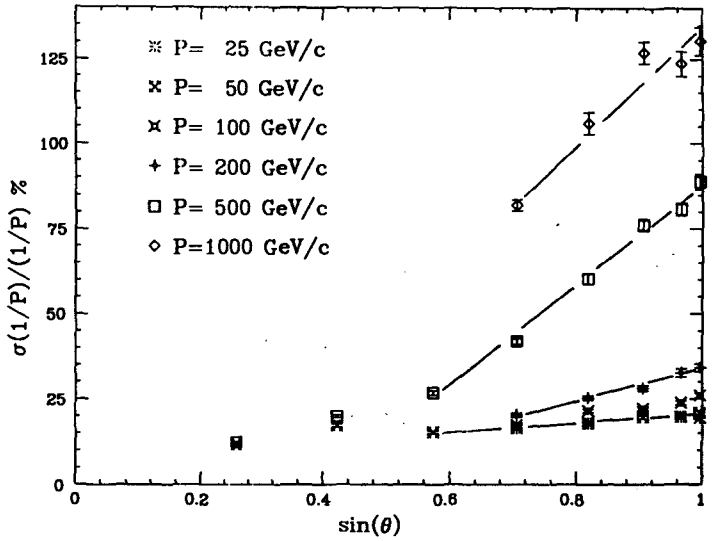

FIG. 2

0945

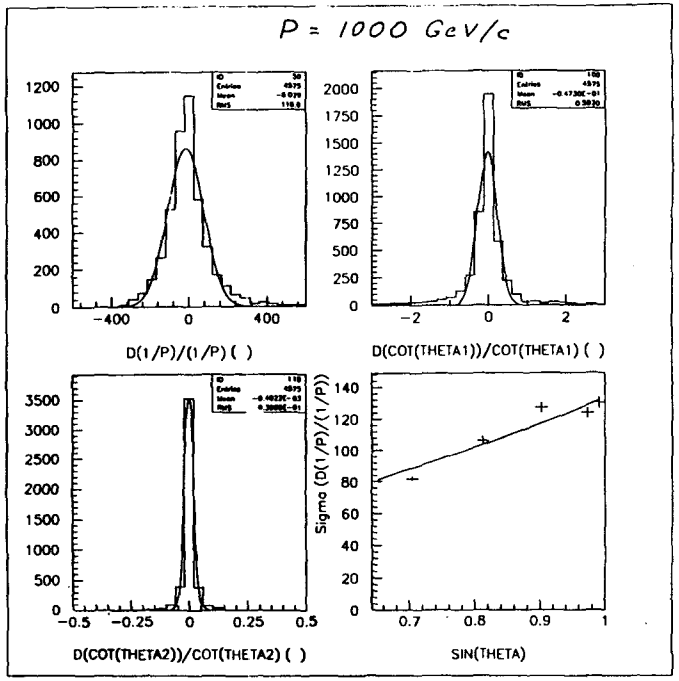

0943

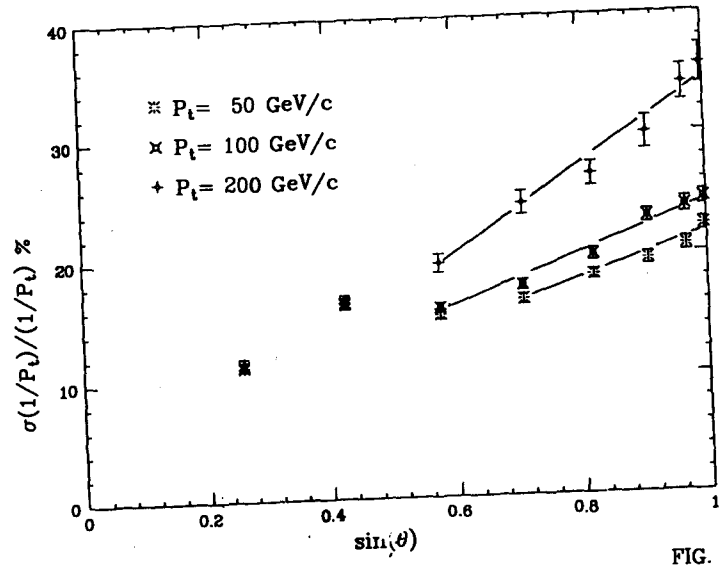

FIG. 3

0946

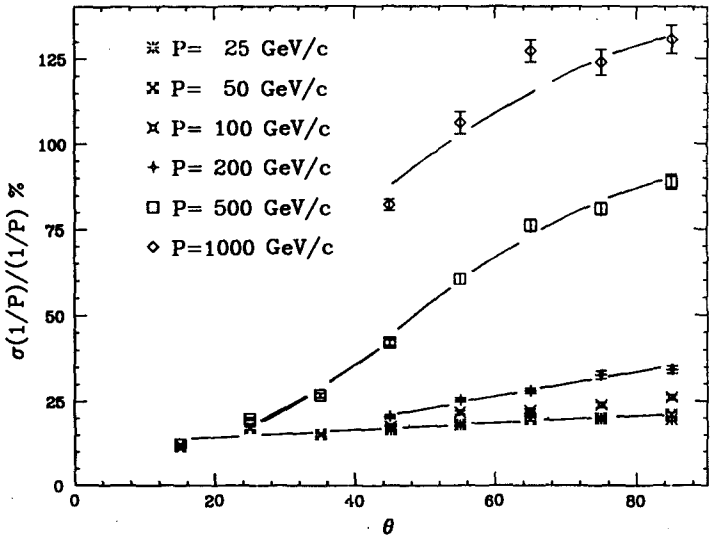

FIG. 1

0944

CONCLUSIONS

1) Resolution ~~dominated by~~ weak link is BW1

2) $\delta\theta$ (40 layers) = $\frac{3}{\sqrt{10}}$ $\delta\theta$ (20 layers)

We recommend some ϕ layers in BW1

3) Model of resolution seems to agree with data but not exactly. Tails in resolution distribution need to be explained.

4) Cerenkov test beam data and simulation agree very well with calculations.

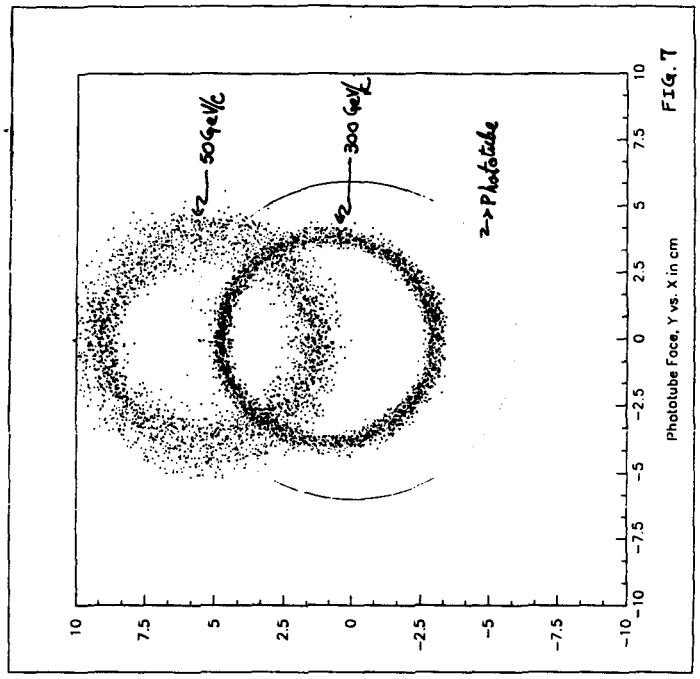

FIG. 7

Preliminary Proposal for SDC Muon Scintillator System

R. Thun(Michigan)

PRELIMINARY PROPOSAL FOR SDC MUON SCINTILLATOR SYSTEM 0950
V. Rykalin, R. Thun.....21 Oct 91

We propose two possible solutions for the configuration of the SDC muon scintillation counters. The first of these eliminates the need for elaborate light guides through the use of special phototubes with long photocathode surfaces. Such tubes have been developed at IHEP. A second, possible configuration employs standard 2" phototubes which are coupled to the scintillation counters via adiabatic, twisted-strip light guides. The dimensions of scintillators is the same in both configurations. The precise thickness has yet to be determined, but is in the range 6-10 mmm. The length of the counters depends on location and on final SDC dimensions but is approximately 1.8-2.2 m. With either readout scheme we expect to obtain 20 or more photoelectrons for all impact points. (Note: preliminary tests of light collection using waveshifting fibers or simple, tapered light guides have given poor results. Further tests are planned and will be documented elsewhere).

We have not yet studied in detail the time resolution of these counters vis-a-vis unambiguous identification of bunch crossings (which occur every 16 nsec). In the barrel, we are planning to span an octant side with four counters. In BW2 this requires counters approximately 1.8-1.9 m in length, corresponding to light transit times of about 12 nsec. In BW2 the length is about 2.2 m giving 14 nsec. These numbers are uncomfortably close to 16 nsec, and hence we propose that matched counters in BW2 and BW3 be read out from opposite ends and that their signals be processed by a mean-timing circuit. As will be seen below, for the second configuration the counters at the octant edge in one of the two layers will require 180 degrees reflectors, which have not yet been tested.

1) Configuration with long phototubes (PMKS)

The transverse layout in one of eight identical octants looks es follows in the barrel:

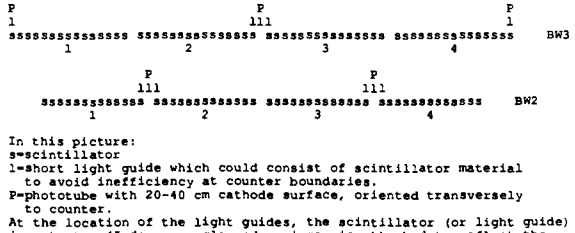

In this picture:
s=scintillator
l=short light guide which could consist of scintillator material to avoid inefficiency at counter boundaries.
P=phototube with 20-40 cm cathode surface, oriented transversely to counter.
At the location of the light guides, the scintillator (or light guide) is cut at a 45 degree angle and a mirror is attached to reflect the light through 90 degrees. This has been tested with good results.

The number of required phototubes can be reduced from 8 to 5 per set of 8 counters by sharing readouts as indicated above. For example, in BW2, counters 1 and 2 share a single phototube placed at their common boundary.

2) Configuration with twisted-strip light guides

Here the layout looks as follows: 0951

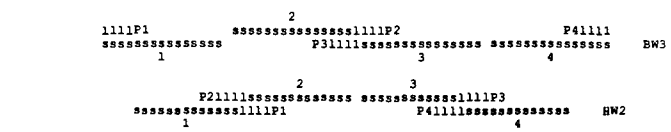

The symbols are as given above.

In this scheme, counters 1 and 4 in BW3 require 180 degree reflectors at the light-guide end. Unlike configuration (1), each counter has its own phototube.

3) General comments

Configuration (1) with the long PMKS phototubes has two major advantages over the other layout:

i) Channel count is reduced by a factor of 5/8 for a total count of about 3800 in the barrel and 1800 in the forward system (both ends combined). Where two counters are read by one phototube there is, of course, a left-right ambiguity with its attendant loss of absolute position information.

ii) The need for elaborate light guides is eliminated. This further reduces cost, and provides better mechanical stability.

However, there are some risks. The PMKS tubes have been produced only in small numbers and are not commercially available enywhere in the world. Moreover, while PMKS tubes with photocathodes up to 20 cm have been produced, counters at the ends of the barrels are 60 cm wide and require photocathodes of about 40 cm.

To achieve a uniform pt threshold independent of angle (or eta), counters in the barrel must have a width that follows a 1/sin**2(theta) pattern. We propose that this shape be approximated by a number of finite steps in width (e.g. 20, 25, 30, 35, 40, 45, 50, 55, 60 cm). One possibility is to further reduce the number of differently dimensioned scintillators by combining two narrower pieces lengthwise, for example 30 + 30 = 60 cm. The impact of this segmentation on light collection has not yet been studied in detail.

4) Proposal

The possibility has been raised that IHEP might deliver most and perhaps all of the scintillators and phototubes of the SDC muon system with some relatively modest contribution in hard currency (about 2 MS equivalent). The scintillator consists of extruded polystyrene with properties similar to Kuraray SCSN-81. The phototubes could be either conventional or of the type with the long photocathode. For the latter (PMKS), a special arrangement would have to be worked out with Soviet industry. If the USSR delivers most or all of the required scintillator and phototubes, the US and other countries would concentrate on bases, HV power supplies, preamps, trigger and readout electronics, calibration systems, and design integration. The US would become the site for final testing and assembly into the muon supermodules.

0952

A proposal wherein IHEP becomes the primary supplier of scintillator and phototubes would require:

a) A long-term, scientific commitment by IHEP to SDC.
b) An R&D plan to develop the phototubes and scintillators for counters up to 60 cm in width with a goal of detecting >20 photoelectrons/muon at all impact points. Such R&D would have to be completed by mid-1992.
c) Demonstration of long-term reliability of phototubes and scintillators.
d) Proof of industrial capability to produce special (PMKS) phototubes.
e) Funding plan (rubles and $).
f) At least one senior IHEP physicist or engineer in residence at SSCL to help coordinate design, testing and assembly of muon counters. This person would also act as a liason between SSCL and IHEP. Residency would begin in 1992 and continue through 1997. The position could be filled on a rotating basis.
g) The provision for short-term travel (<1 month) between US and IHEP for the purpose of completing R&D work and coordinating the design.
h) Agreement to design the counter system in such a way that either configuration described above (long tubes or twisted-strip light guides) could be implemented at any time during the construction phase. This condition requires a common set of scintillator and mechanical box dimensions. The purpose of this condition is to provide a sure alternative in case the long-tube option is chosen with subsequent failure to deliver such tubes.
i) An overall agreement on who does what for the complete counter system.

0953

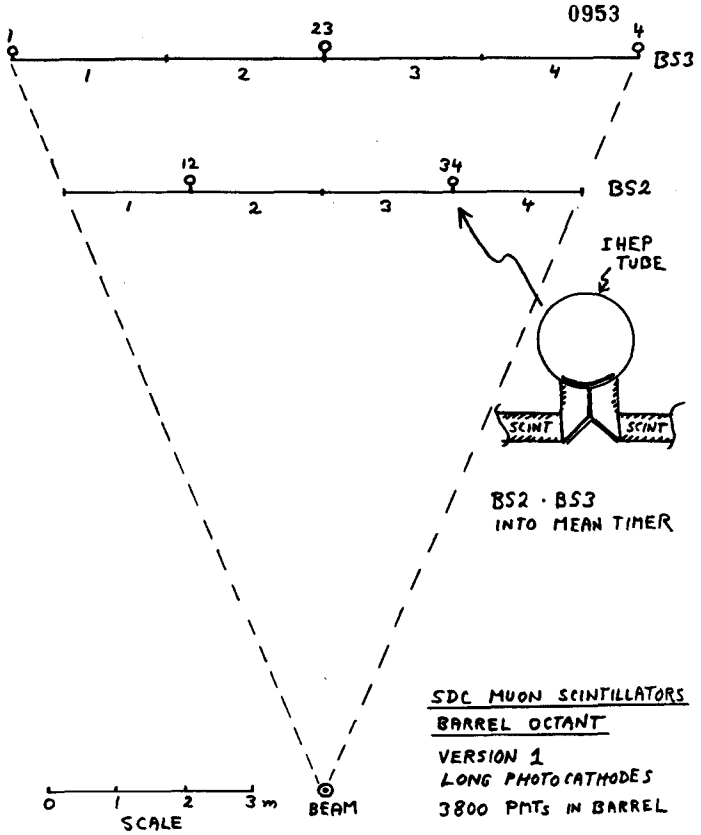

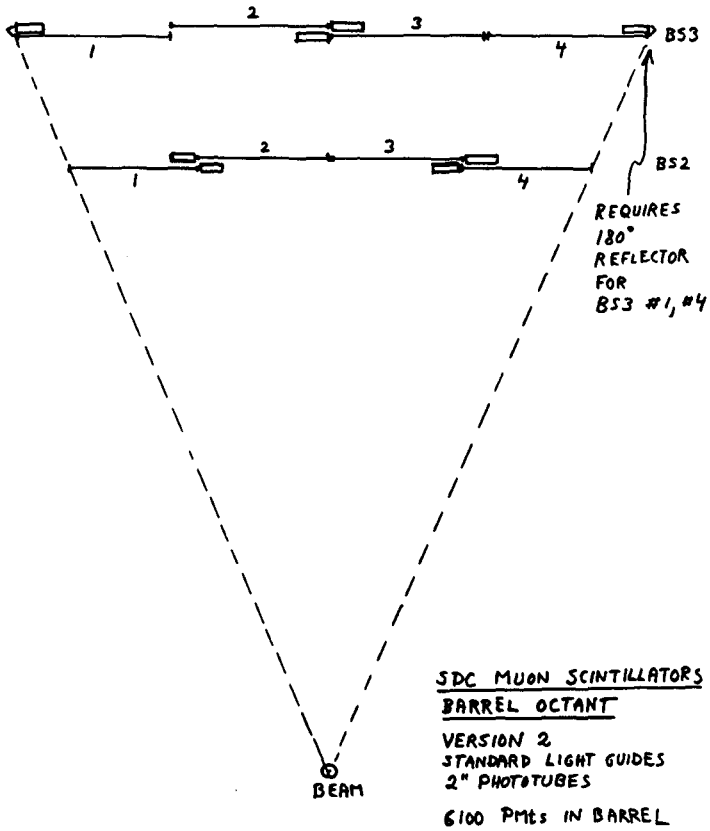

SDC MUON SCINTILLATORS

BARREL OCTANT

VERSION 2
STANDARD LIGHT GUIDES
2" PHOTOTUBES

6100 PMTs IN BARREL

12 NOV 91

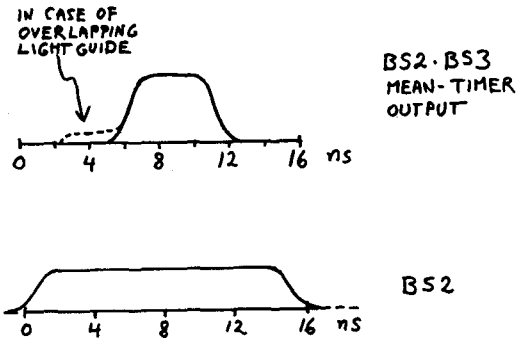

BARREL MUON TIME DISTRIBUTIONS

12 NOV 91

 12 NOV 91

SOME RESULTS ON PHOTOELECTRON YIELDS

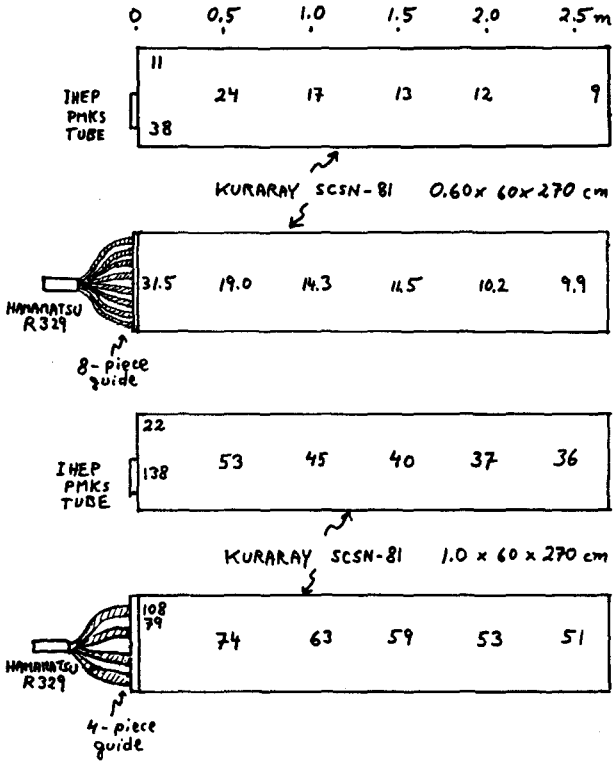

Possibility of Constructing a First Level Muon Trigger with Adjustable Pt Threshold

V. Molchanov(Protvino)

V.Molchanov
IHEP, Protvino

Possibility of constructing first level muon trigger with adjustable p_t threshold

The following is a study of the first level muon trigger in the central region, based on scintillating counters. Two trigger layers of the counters are assumed outside the barrel toroid, covering approximately $|\eta| < 1.1$ range in pseudo-rapidity. The scintillators are segmented projectively in the θ-direction, and centre of the counter in the first layer is projected onto border between two counters in the second. To form a trigger signal we require simultaneous hits in the first layer counter and at least in one of the two corresponding to it counters in the second layer.

As it was shown by R.Thun [1], width of counters should be scaled proportional to $1/\sin^2\theta$, in order to get roughly uniform p_t efficiency over η. An initial width $W_0 = 15$ cm will provide p_t cut-off in the region of 10 GeV, and more than 90% effeiency for muons with $p_t > 20$ GeV. That model assumes individual size for each counter, so total number of different sizes in one layer would be about 60, there width increasing with $|\eta|$ from 15 cm to 45 cm.

From technological point of view, however, it is more convenient to assemble counters with desired width from scintillator strips of standard sizes. Natural step is to fix few "base" sizes, and form counters with necessary dimensions from these base ones. Let us start with base width of 7.5 cm. In that case we can approximate any necessary width with accuracy $7.5/2 = 3.75$ cm. So when we need counter with width less than 18.75 cm we will combine two 7.5 cm scintillator strips into one counter, for counters with width in the range 18.75–26.25 cm we will use three 7.5 cm strips, and so on. Result of such a procedure is some additional non-uniformity of the trigger efficiency over η. But that non-uniformity is rather small (see Fig. 1), and average over η efficiency curve almost coincides with ideal one. Calculations were done with a program, similar to that of described in [1].

In such a scheme it is possible to read-out each 7.5 cm strip of scintillator. If one is going to do this with conventional photomultipliers (PM), then number of PM's will be increased substantially. Cheap multianode PM's are available in the USSR, they are tested recently at the University of Michigan. Making use of these PM's would enable one to read-out each scintillator strip without increase in PMs' number.

Individual scintillator read-out makes trigger system rather flexible: one may change muon p_t threshold simply by changing the trigger logic. Scheme,

described two paragraphs earlier, can be straitforwardly implemented by logical OR of necessary number of scintillator strips into one counter. But other logical schemes are also possible. As an example, let us consider following option:

- For the counters in the region $|\eta| < 0.75$ we form trigger signal when there are hits in first layer counter and in one of the two corresponding to it counters in the second layer.
- For the counters in the region $|\eta| > 0.75$ we form trigger signal when there are hits in first layer counter and in one of the four corresponding to it counters in the second layer.

Average (over η) trigger efficiency for such an option is shown in Fig. 2. According to estimates, trigger rate for such option will drop by a factor of 4.4. That could be useful for the operation under high luminosity, or if due to some reasons it is desirable to slow down input rate for the second level trigger.

In order get accustomed to the idea, calculations were done also for the 5 cm base size. Results are shown in Flg. 3, 4 respectively. In Fig. 4 hardest possible muon p_t threshold for 5 cm wide scintillator strips is also shown. It is worth to mention the possibility of setting intermediate threshold values. Dashed curve correspond to the following option:

- For the counters in the region $|\eta| < 0.6$ we form trigger signal when there are hits in first layer counter and in one of the four corresponding to it counters in the second layer.
- For the counters in the region $0.6 < |\eta| < 0.9$ we form trigger signal when there are hits in first layer counter and in one of the six corresponding to it counters in the second layer.
- For the counters in the region $|\eta| > 0.9$ we form trigger signal when there are hits in first layer counter and in one of the eight corresponding to it counters in the second layer.

Expected reduction of the first level trigger rate is 2.4.

References

[1] R.Thun, SDC note, SDC-90-00077.

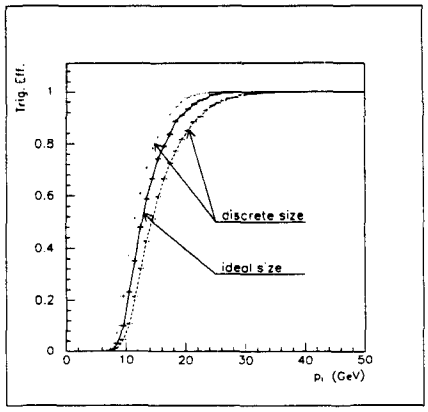

Figure 1: Variations of the muon trigger efficiency due to discrete width of counters: $W = n \times 7.5$ cm

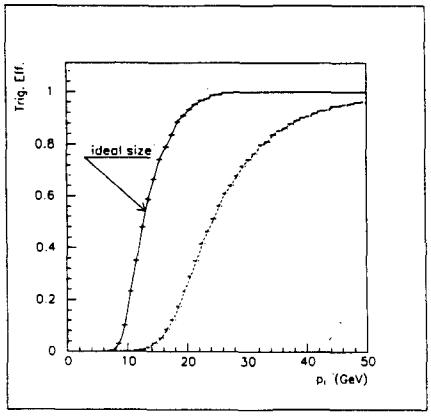

Figure 2: Possible trigger threshold on the muon p_t for the option with 7.5 cm wide scintillator stripe

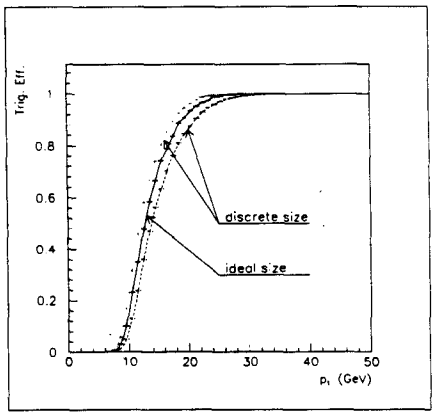

Figure 3: Variations of the muon trigger efficiency due to discrete width of counters: $W = n \times 5$ cm

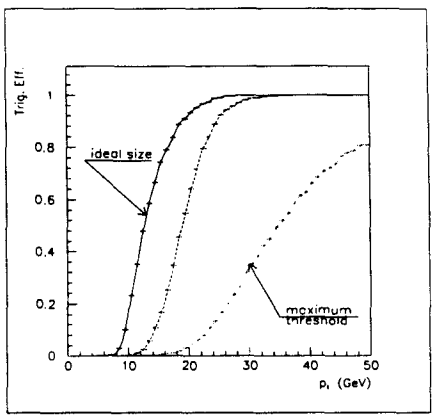

Figure 4: Possible trigger threshold on the muon p_t for the option with 5 cm wide scintillator stripe. Dashed curve correspond to described in the text option

Muon Front End Analog Electronics

J. Oliver(Harvard)

Muon Front End Analog Electronics

11-15-91
J. Oliver

0965

FUNCTION

1. Send amplified, shaped & discriminated signals to regional L-1/Readout crate.
2. Receive signals from L1 crate for test pulse
3. Distribute high voltage to chambers

PHASE-I

16 channel board for chamber testing, contains

1. Penn single channel monolythic preamps – differential transimpedance ampl.
2. Hybrid pole/zero tail cancellation (from E665)
3. LeCroy MVL407 quad discriminator (ECL)
4. Test pulse circuitry using ECL chips
5. $P_D \approx 500 mw/_{ch}$ total

0966

PHASE-II

Objective – provide same function at lower power consumption, lower cost/channel, smaller physical size.

Components

1. Monolythic amp/shaper/disc chip (Penn-Tektronics)
2. Low power CMOS for cable driver to L1 crate
3. Low power CMOS for test pulse circuits.

0967

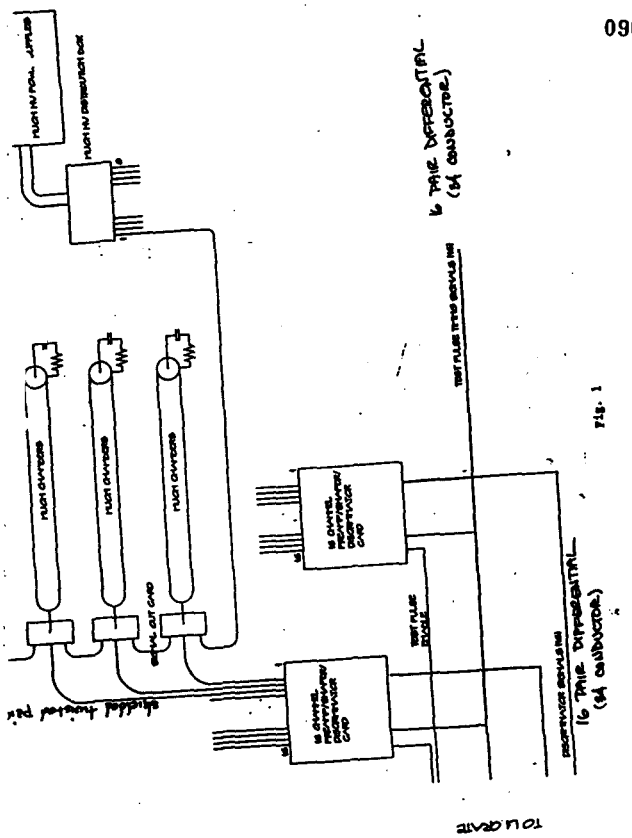

0968

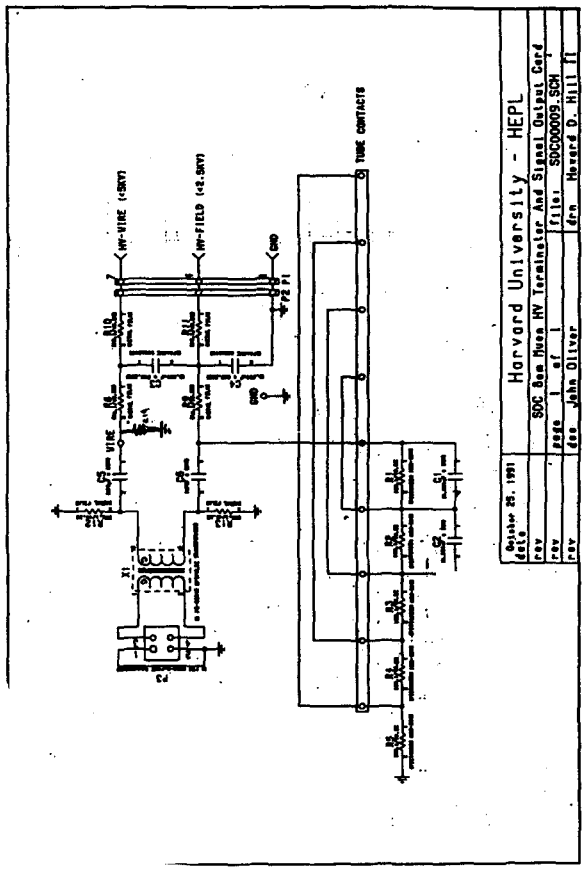

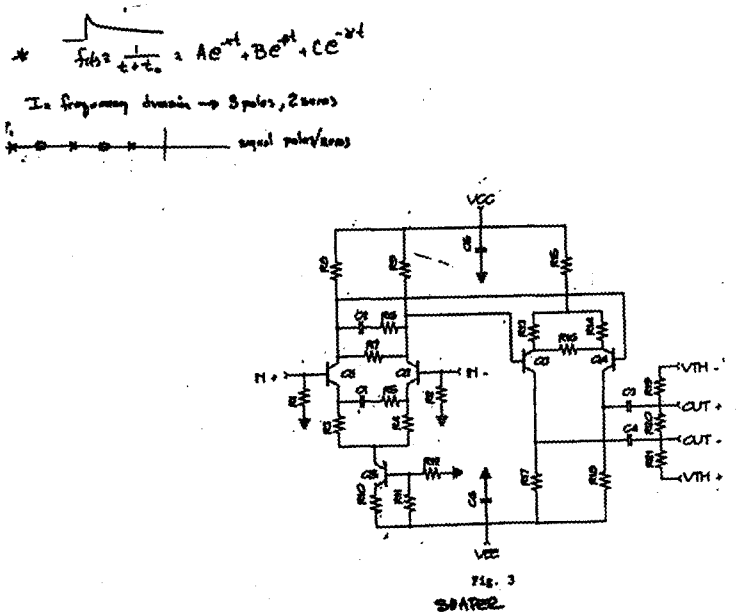

Fig. 3

SHAPER

0972

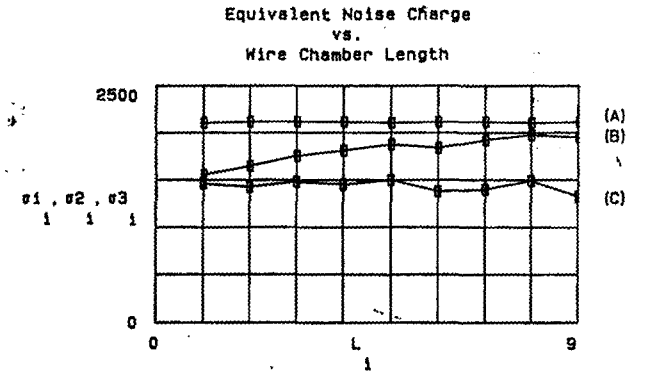

Fig. 2

0970

0971

0969

0973

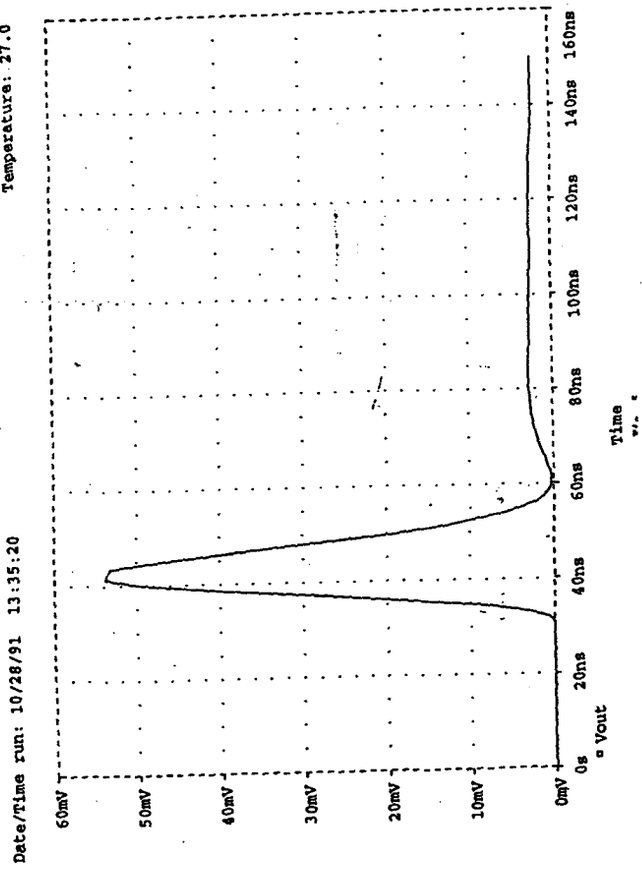

0974

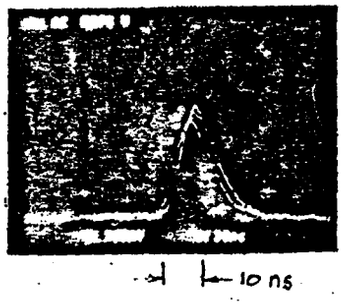

Fig. 6

Shaped pulses from E665 jet chamber due to Ruthenium source.

0975

PRELIMINARY MEASUREMENTS ON [illegible]

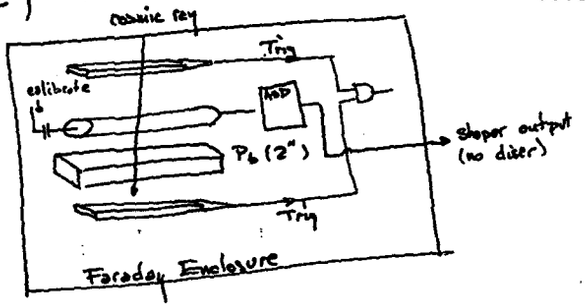

1. Look at cosmic ray pulses
   (a) pulse shape & width
   (b) effect of shaper
   (c) estimate pulse pair resolution

2. Observe:
   (a) shielding difficulty - external rf
   (b) stability i.e. feedback (output to input)
   (c) equivalent noise charge
   (d) Determine feasible cable length/type from chamber to Asd card.

0976

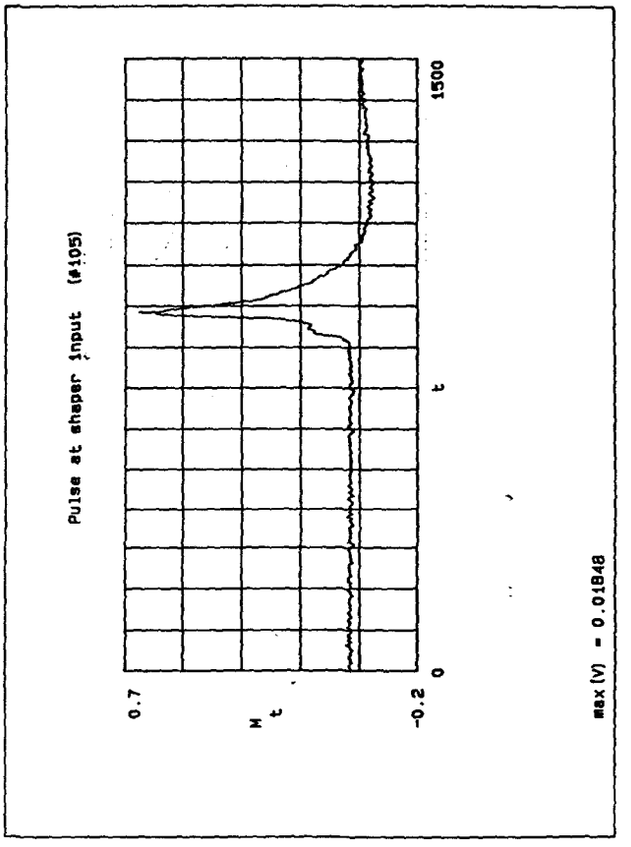

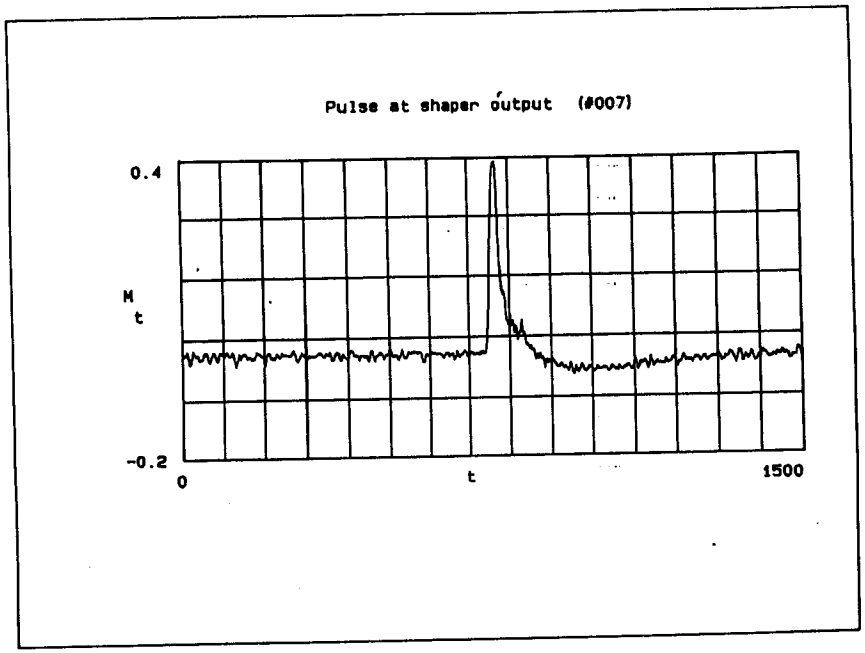

0979

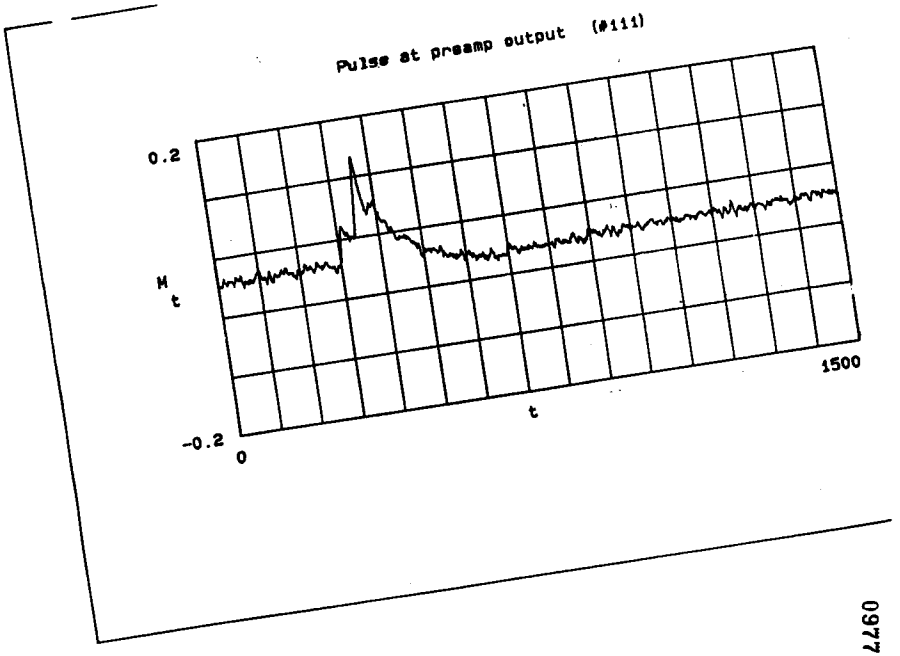

0977

f2

13-Nov-91
10:59:52

Harvard Univ, High Energy Physics Lab

LeCroy

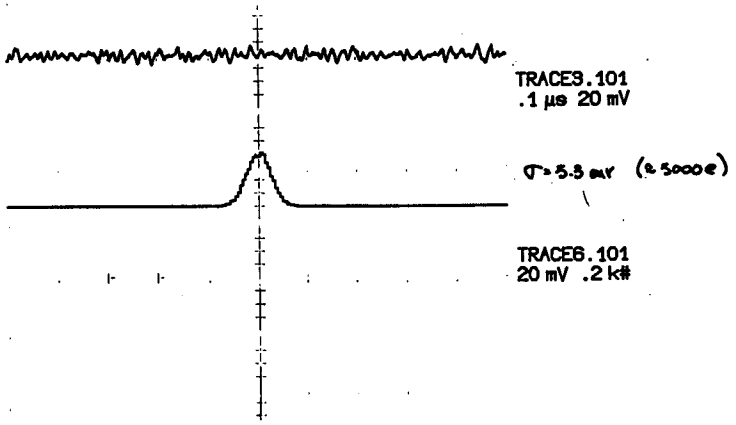

0980

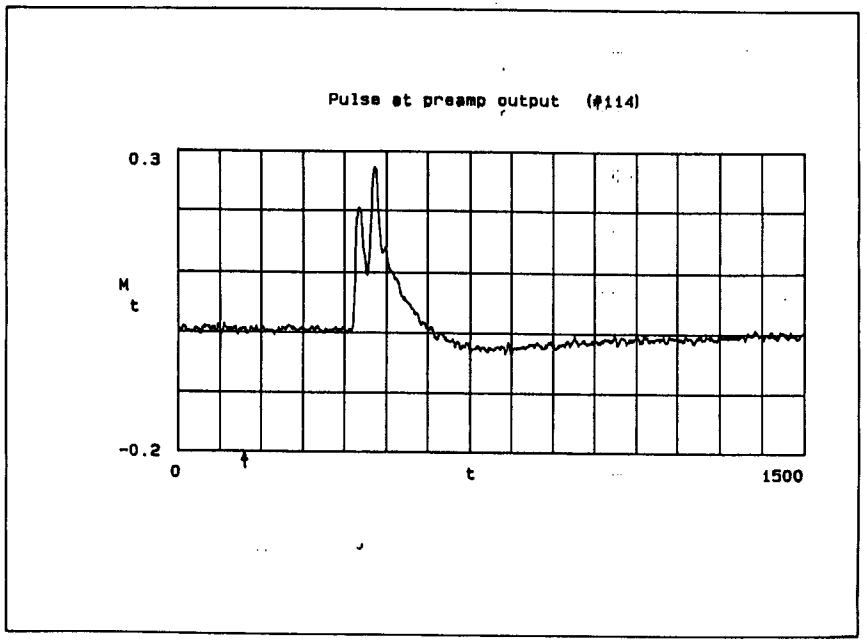

0978

FRIDAY ENCLOSURE CLOSED

Amp/shaper bandwidth

Date/Time run: 10/30/91 12:53:30 Temperature: 27.0

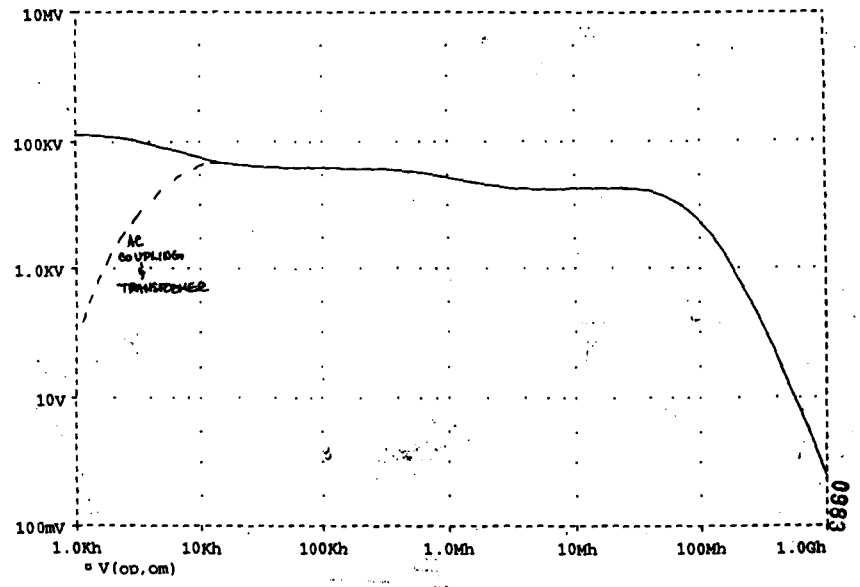

12-Nov-91
11:00:33

Harvard Univ, High Energy Physics Lab

LeCroy

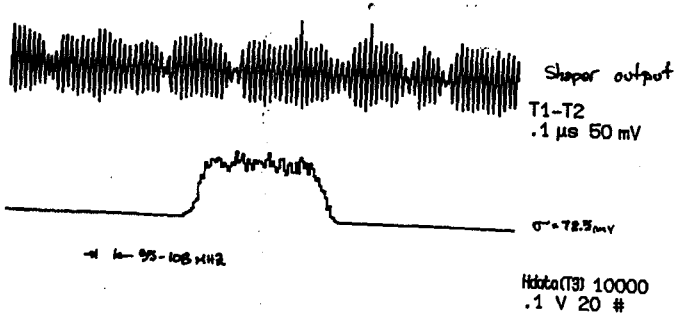

FARADAY ENCLOSURE OPENED

0991

13-Nov-91
12:47:17

Harvard Univ, High Energy Physics Lab

Cable length 18"

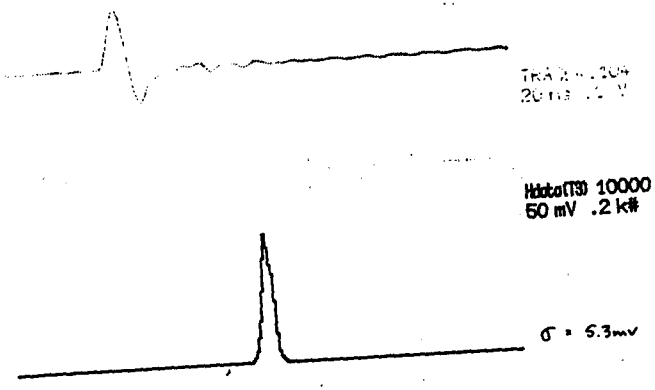

0994

13-Nov-91
11:15:31

Harvard Univ, High Energy Physics Lab

LeCroy

CHAMBER ENDS ENCLOSED

0992

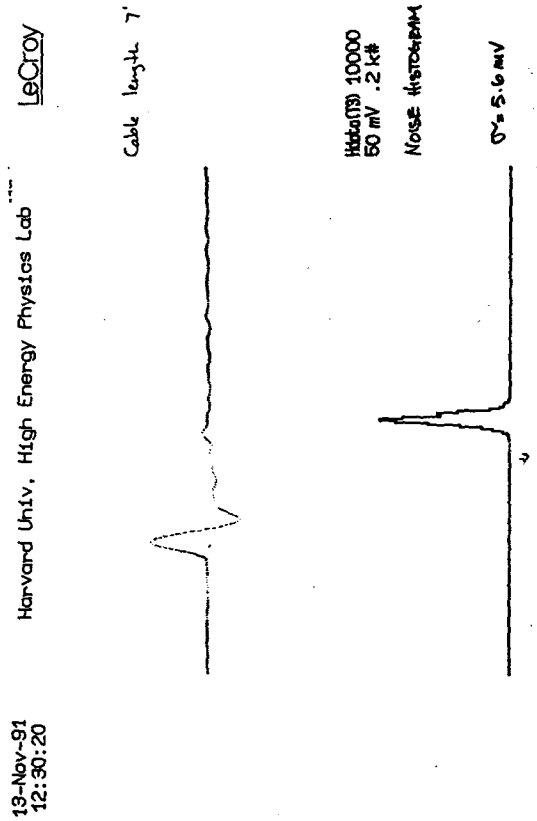

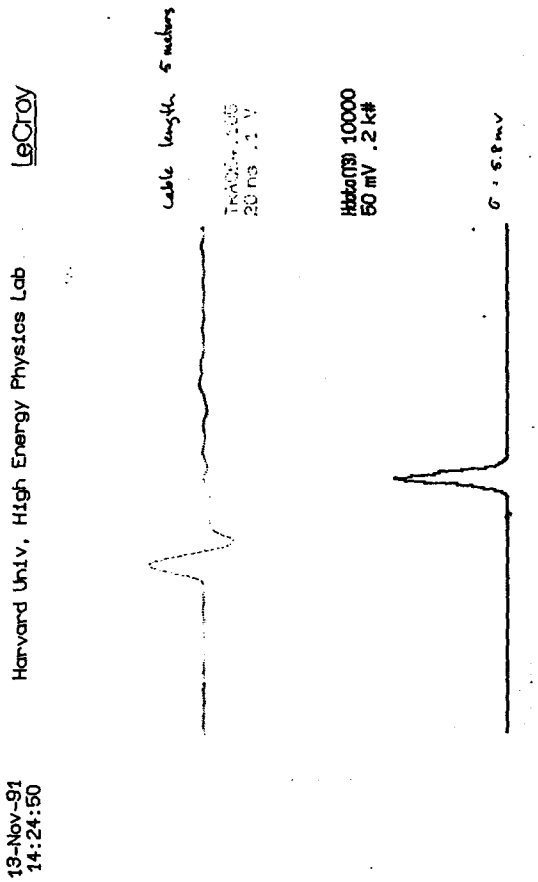

Preliminary Conclusions

1. RF SHIELDING IS A NECESSITY FOR ALL EXPOSED ELECTRODES, CABLING, ELECTRONICS
2. MEASURED EQUIVALENT NOISE CHARGE ~ 5000 e (0.8 fc)
3. USE OF LONG SIGNAL CABLE FROM CHAMBER TO ELECTRONICS APPEARS FEASABLE WITH PROPER IMPEDANCE MATCHING.
   — CABLES TESTED TO 5 METERS
4. ENC IS (ALMOST) INDEPENDENT OF CABLE LENGTH AS EXPECTED FOR TERMINATED CHAMBER

Test Pulses

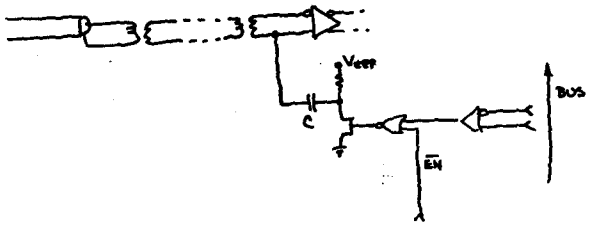

Requirements

1. INJECT SMALL CHARGE ≥ 10^3 of fc
   eg. 10 fc = 100mv × 100ff
2. AVOID ANY STRAY SINGLE ENDED VOLTAGE SWINGS
   eg. 1 VOLT × 10ff = 10 fc !
3. LOW POWER
4. TIGHT CHANNEL TO CHANNEL TIMING DIFFERENCE TOLERANCE TO TEST L1 TRIGGER IN PROJECTIVE PAIRS.

⇒ CMOS IMPLEMENTATION SATISFIES 1.–4. IN STRAIGHTFORWARD DESIGN (LIKELY 2μ)

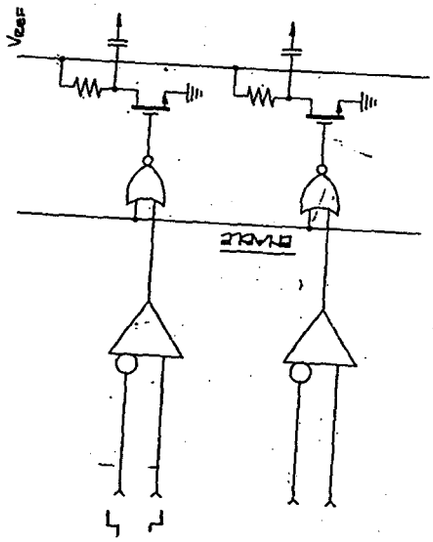

TEST PULSE INJECTION
Fig. 7

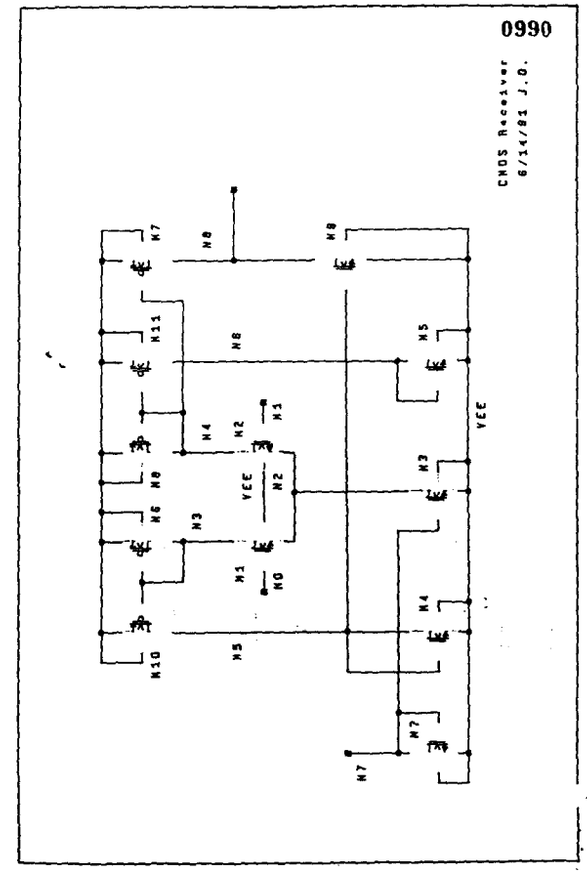

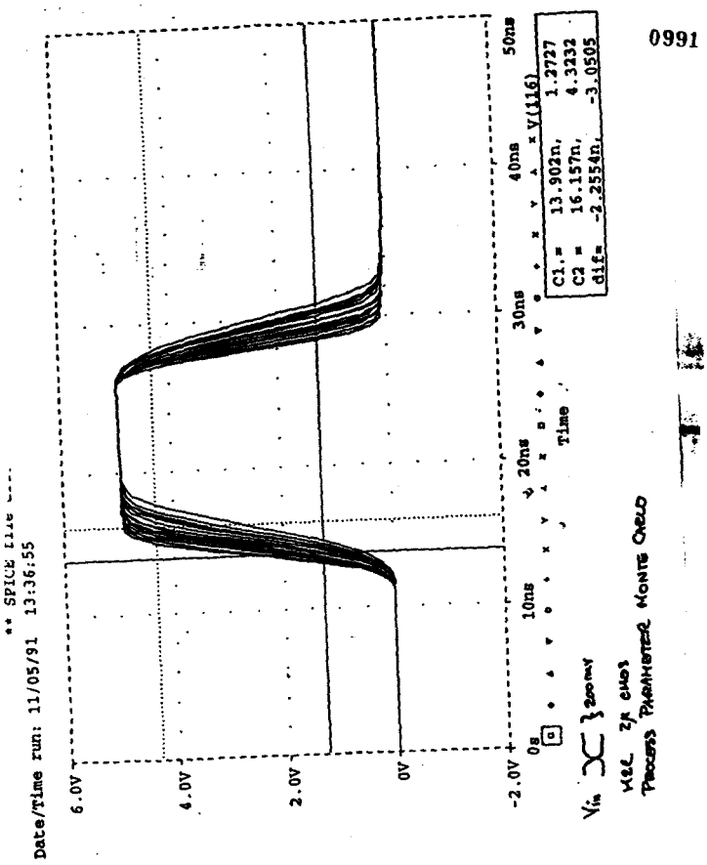

3LG DRIVER

REQUIREMENTS

1. DISCRIMINATOR MUST DRIVE TERMINATED TWISTED PAIR CABLE WITH ACCEPTABLE VOLTAGE SWING eg. 0.8V ECL (OR LESS?)
2. DRIVING WITH DISCR. BIPOLAR OUTPUT STAGE IMPLIES LARGE STANDING CURRENT & LARGE POWER DISSIPATION (≥ ORDER 100 MW/CH)
3. HIGH DATA RATE IS NOT A REQUIREMENT I.E. SIGNALS ARE LOW DUTY CYCLE
4. LOW POWER.

#3. IMPLIES AC COUPLING (AND OR AC TERMINATION) IS SUFFICIENT I.E. SUPPLY DRIVING CURRENT ONLY DURING PULSE (LOW DUTY CYCLE)

⇒ CMOS IMPLEMENTATION CAN SATISFY REQUIREMENTS IN MODEST TECHNOLOGY (eg. 2μ)

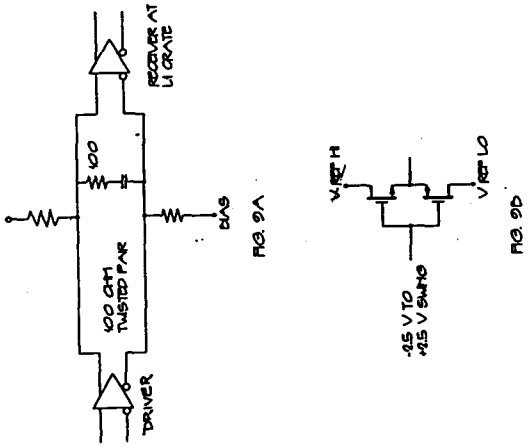

OPTICAL ALLIGNMENT ELECTRONICS
(HARVARD, DRAPER LABORATORY)

PURPOSE

TO MONITOR DEFLECTIONS IN MUON SUPER TOWERS OVER 9 METER SPAN

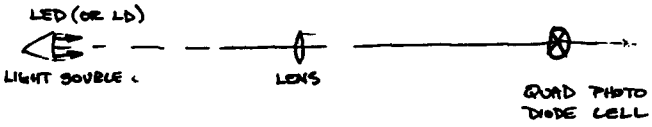

OBJECTIVE

1. TO DETECT LENS MOTION IN 2 DIRECTIONS
2. SOME IMMUNITY TO AMBIENT LIGHT (LEAKS)

BASIC SCHEME

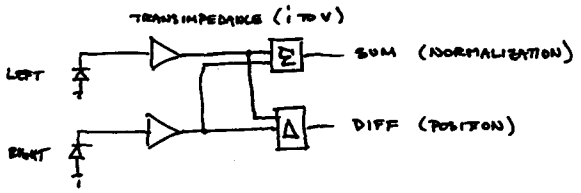

⇒ NOT IMMUNE TO AMBIENT LIGHT (PARTICULARLY 60HZ)

⇒ SYNCHRONOUS DETECTION

1. CHOP THE LIGHT SOURCE (~500HZ)
2. ADD TWO SAMPLE/HOLD CIRCUITS & DIFFERENCE AMP.

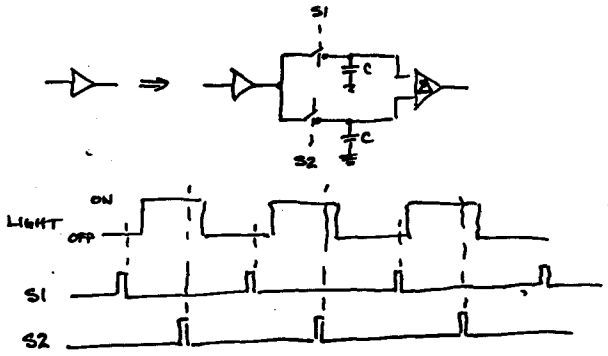

IMPLEMENTATION (8 QUAD CELL CHANNELS)

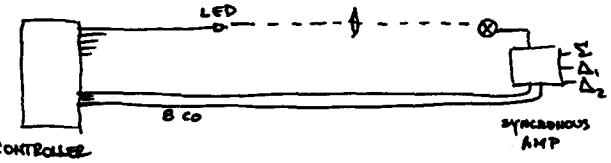

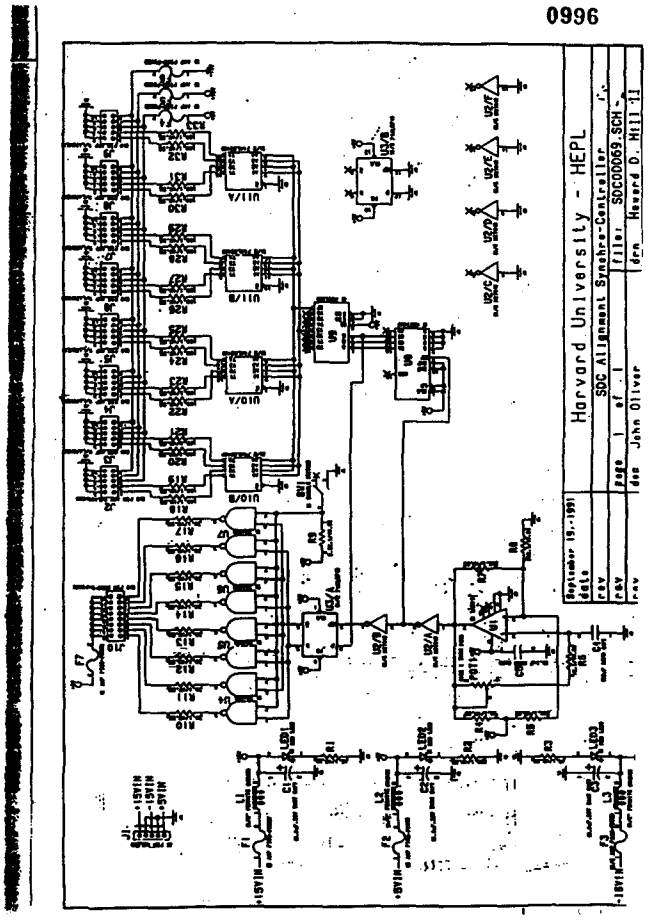

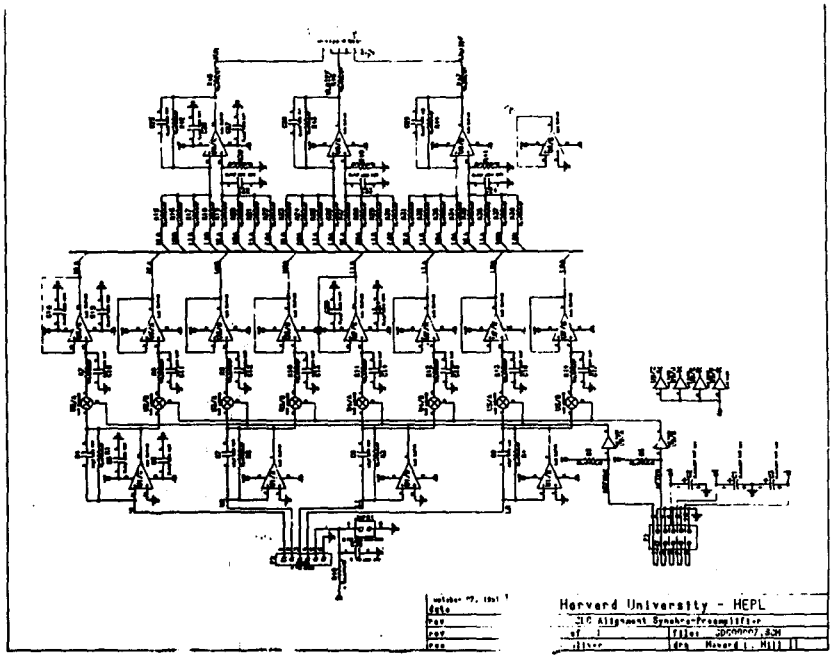

0997

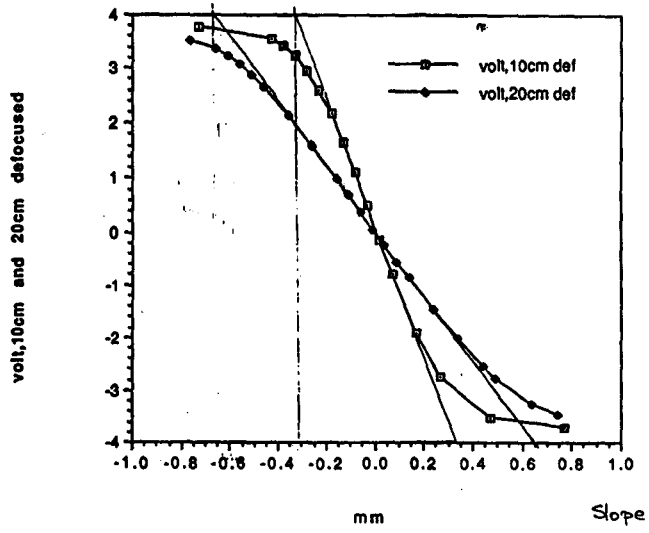

9660

Slope ≈ 5–10 mV/μ

noise ≈ 1 ~ 2 mV

Muon System Front End Electronics Preliminary Conceptual Design Report

J. Oliver(Harvard)

Muon System Front End Electronics
Preliminary Conceptual Design Report

John Oliver

Nov. 12, 1991

The SDC muon system will provide muon coverage over more than 2500 square meters of the detector and and over many depth segmentations in both the theta and phi directions. The individual chamber lengths vary from approximately 5 to 9 meters. As of this writing, there are four distinct chamber designs under consideration for this function. One of these designs, or a combination of features from several, will ultimately be chosen for SDC. The total channel count varies considerably for the different chamber designs and is anticipated to be in the range of 40,000 to 138,000 electronic channels. The front end electronics discussed in this report is confined to that required to bias the chambers, amplify and shape signals, inject test pulses into the chambers, and send discriminated outputs to the regional front end crates for readout and trigger generation. The electronics is sufficiently general that the various chamber designs can be accomodated.

The electronics for this function is being developed in two phases. The first phase utilizes single channel monolythic preamplifiers, single channel hybrid circuits for pole-zero tail cancellation, and commercially available quad discriminator chips. These will be combined on a sixteen channel board and will be utilized for the initial phases of chamber performance testing.

A multiple channel chip containing preamp, pole-zero tail shaper, and discriminator is under development at University of Pennsylvania, primarily for use in the straw tube central tracker. It is anticipated that this chip will serve the function of muon amp/shaper/disc (ASD). A similar device is being developed at KEK. The second phase of muon front end electronics will be the testing of such monolythic ASD devices with muon chambers, the selection of a suitable device and the incorporation of a monolythic multichannel ASD into the front end muon board.

Two CMOS integrated circuits will be developed for the front end muon board. The first will be a device for injecting test pulse charges into the muon chambers while maintaining channel to channel timing accuracy required for in-situ testing of the L1-trigger. The second is a low power differential cable driver to buffer the signals from discriminator chips to drive twisted pair cable to the regional L1-trigger/readout crates. These devices will be described in detail later in this report.

This report will describe the overall architecture of the front end electronics, the specific features of the electronics used for phase-I testing, and the features of monolythic ASDs for phase-II.

Front End Electronics Configuration

Figure 1. shows the configuration of the front end electronics. The following specific description is based on the Boston muon chamber design with field shaping electrodes, however

only minor modification is required for the other chamber designs. A small printed circuit board which contains a high voltage resistive divider for field shaping, bypass capacitors, and a pulse transformer is mounted to the front of each tube. High voltage is distributed from commercial bulk supplies through local distribution boxes, to the chamber end cards. It is anticipated that 96 tubes will be fed by a single commercial hv output. An RC terminator is attached to the far end of each tube. Signals from the tube are coupled via pulse transformer into shielded twisted pair cable to the ASD card. Testing will determine acceptable cable length for the interconnection. Longer cable lengths are desirable for mechanical reasons and for accessability to the electronics but suffer from increased noise and susceptability to pickup of external signals.

Generation of Level-1 trigger is based on time difference measurements between signal in towers which project to the interaction point. These signals, generated in the L1 crates, must be tested by injection of accurately timed pulses into the chamber preamplifiers. A seperate twisted pair cable for each channel for this purpose is possible but would represent a substantial cable plant. Instead, we propose to distribute a 16 twisted pair Timing Bus, originating from a board in the L1 crate, to many front end board to carry accurately timed test signals. A single ENable line is distributed to each front end board. On receipt of a pulse on the Timing Bus, charge is injected into the corresponding muon chamber on boards which have been enabled. Charge is injected by capacitor discharge through an FET. A sixteen channel wide CMOS circuit will be constructed which contains the necessary line receivers, logic, and FETs.

Chamber Signals, Noise, and Pulse Shaping

Chamber signals are produced by gas amplification and have the familiar long tails due to positive ion drift. In particular, a single electron drifting to the sense wire produces a current in the wire with the functional shape

$$i(t) = \text{constant} / (t + t_0)$$

where t0 is a constant typically in the range 1 to 3 ns. In order to maintain high chamber resolution we will need to trigger the discriminator on a small number of primary charges hitting the wire. The required thresholds are expected to be in the range 3 to 10 primary electrons. Gas gain depends on voltage applied to the sense wire and to it's diameter. Wire diameter varies significantly between the present chamber design groups and results in a large uncertainty in the expected value of gas gain. Current estimates are between 10^4 and several times 10^5 depending on chamber design. Most of the charge in the pulse resides in the tail and does not contribute to the signal delivered to the discriminator. The efficiency is determined by SPICE simulations and is on the order of 20%. That is, only 20% of the gas gain is usable in delivering a signal to the discriminator, or equivalently, the ballistic deficit is 80%. Combining these numbers gives a desired threshold setting at the discriminator input of between 1fc and over 50fc referred to a delta function charge injection. A

reasonable level will probably lie in the range of 3 to 10 fc.

The lower limit of threshold setting is determined by system noise. This falls into two broad categories; inherent electronic and thermal noise, and noise induced by pickup in the exposed electrodes and cable interconnections.

The inherent noise is reasonably easily analyzed by SPICE simulations and results from preamplifier input voltage noise (transistor base resistance thermal noise and collector shot noise), thermal noise in the chamber wire resistance, and thermal noise in the chamber terminating resistor. The Penn preamplifier has been described in the literature and in the Straw Tracker Conceptual Design Report and will not be described here. A SPICE model of this device was supplied by Penn. and used for these simulations.

The chamber is modelled as a lossy transmission line of characteristic impedance 360 ohms with a wire resistance of 30 ohms per meter, corresponding to a 50 μ tungsten wire. For simulation purposes, the lossy line is approximated by a lumped parameter line with each lump corresponding to 10 cm of wire. The results of noise simulations are shown in Fig. 2. The three traces correspond to the equivalent noise charge for a lossless unterminated line, a lossy unterminated line, and a lossy line which has a termination. For a nine meter chamber a termination is required to avoid unwanted signal reflections.Its contribution to noise is not significant compared to the thermal noise generated by the sense wire resistance. The upper curve of 2100 electrons indicates that to be at 3-sigma above the noise, the minimum threshold level at the discriminator is at least 1 femptocoulomb.

To achieve the 1 fc one would have to place the preamplifier directly on the wire output and use substantial shielding to prevent pickup of external noise. In practice some cabling is required between wire and preamp and we anticipate that pickup in the cable will require raising the threshold to several fc. Tests will be performed to determine acceptable cabling length, quality, and interconnections. We anticipate that some form of shielded twisted pair will be acceptable.

Shaping techniques to handle the long tails produced in wire chambers have been described by Boie et. al [1]. The general procedure is to approximate the tail shape by the sum of three exponential functions. In the frequency domain, this is equivalent to a function with three poles and two zeros. The shaper is then tailored to have poles and zeros in the location of the unwanted zeros and poles of the input pulse. The cancellation leaves only the highest frequency pole of the input pulse and results in a narrow signal whose width is of order 25ns. The shaper we have employed in the phase-I boards is a hybrid circuit shown in Fig. 3 originally designed and produced for the E665 muon scattering experiment at Fermilab[2].

Figures 4. and 5. are the results of SPICE simulations and represent the waveforms at the input and output of the shaper respectively, due to a chamber signals with the characteristic long tail. Fig. 6 shows and oscilloscope trace of the shaped signals from the E665 jet chamber produced by a Ruthenium source. The horizontal scale is 10ns showing agreement with the SPICE model.

Test Pulse Injection Circuit

Fig. 7 shows the required logic for injecting test pulses as previously described. In order to operate at low power and to insure small channel to channel timing variations, we propose to implement this function in a 16 channel CMOS chip. The line receiver will operate from low input swing differential signals to minimize RFI generation. Initial simulations of the receiver shown in Fig. 8 indicate that a 2 micron standard CMOS process is adequate for this function. The power dissipation for this circuit will be in the range 3-5 mw/channel. We plan to utilize the foundry services of Mass. Microelectronics Center (M2C) which has a low cost 2 μ CMOS process available to member Massachusetts universities, as well as to national laboratories.

Transmission of timing signals takes place over a 34 conductor twist and flat cable which will be terminated on the last card in a bus. The signals on the bus will be differential with a nominal swing of 0.8 volts in the middle of the power supply rails. Timing signals will be ac coupled so that de level is not important. Thus the drivers which are located in the L1 crates could in principle be ECL but will more likely be low power CMOS drivers

Discriminator Output Cable Driver.

The monolythic amp/shaper/disc under development is expected to operate at significantly lower power levels than a discrete design; approximately 10mw for the preamp, 7mw for the shaper, and 15mw for an output stage at low power operation. Such an output stage cannot drive a differential sign of adequate size into a terminated twisted pair cable as required to send signals to the L1 crates. We propose to construct a CMOS cable driver for this purpose. For the muon system, one can take advantage of the low data rate and use a cable which has an ac coupled termination at the receiving end i.e. at the L1 crate. This is shown in Fig. 9a and implies essentially zero standby power. A cable driver whose output stage is shown in Fig. 9b is being considered. The output transistors are of sufficient size to drive an adequate signal into the cable but require no standby power.

The discriminator output cable will be 34 conductor twist and flat and carry 16 differential signals. The nominal swing will be 0.8v. The use of signal swings which are smaller than the ECL standard have been suggested and discussed as a means to reduce emission of rf interference generated by fast edges in long cable runs. We propose to set the signal levels by an external reference voltage (e.g. diode drops) so that output cables can be driven at lower voltage swing if desired.

Power Dissipation

(1) High Voltage

(a) For field shaping designs this is approximated by
2.5kV x 10μA = 25mW / channel
(b) Sense wire bias
(5kv)^2 / 1 Gohm ~ 25mW

Total = 50mW / channel

(2) Phase-I front end design

(a) Preamp 20mW
(b) Shaper 200mW
(c) Discr. 200mW
(d) Misc 80mW

Total = 500mW / channel

(3) Phase-II with monolythic ASD chip

(a) ASD chip 35mw
(b) Test pulse
chip 5mW
(c) Cable driver
chip assuming ac cable
termination 5mW
(d) Overhead 10mW

Total = 55mW / channel

Packaging and Cooling

Front end ASD cards will be uniformly distributed throughout the muon detector. This precludes the use of water cooling and imposes low power dissipation on the front ends. Ambient air flow is therefore required to remove this heat.

The packaging and cabling questions which need to be addressed are driven mainly by the requirement of shielding the front end boards from external rf pickup. These issues can only be resolved by measurements on prototype muon chambers, and will certainly vary among the four proposed chamber designs. These efforts are under way as of this writing.

References

(1) "Signal Shaping and Tail Cancellation for Gas Proportional Detectors at High Counting Rates" R.A. Boie, A. T. Hrihoso, & P. Rehak, Nuclear Instruments and Methods 192(1982) 365-374

(2) "A Low Noise Drift Chamber Readout System for Experiment E665" J. Oliver, B.Baller - E665 Report

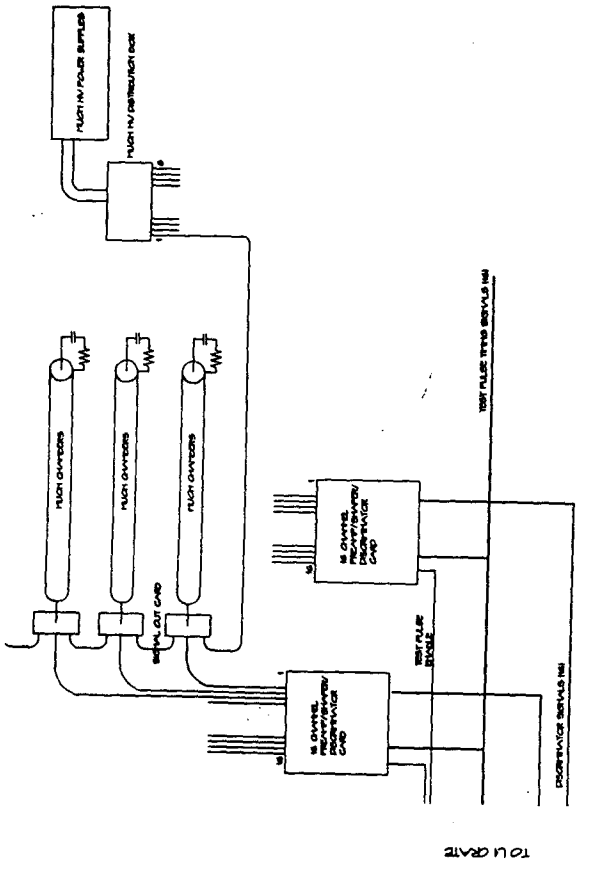

Fig. 1

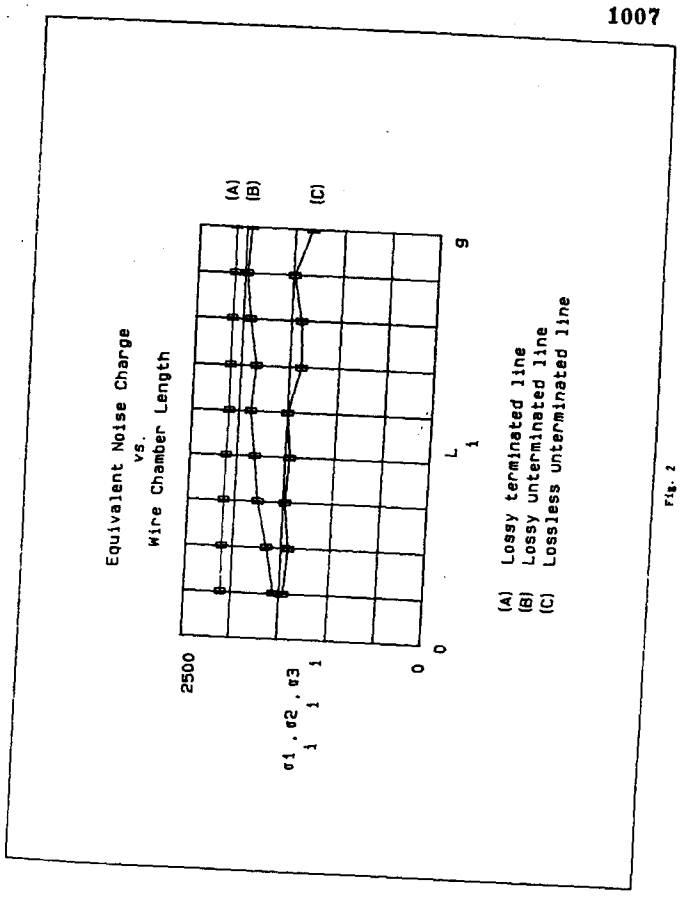

Fig. 2

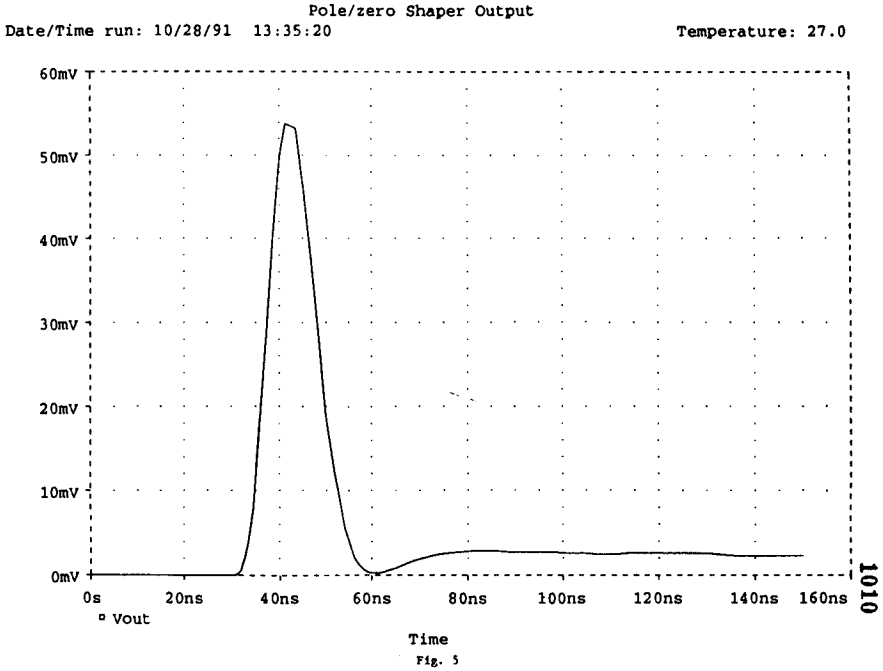

Fig. 5

1010

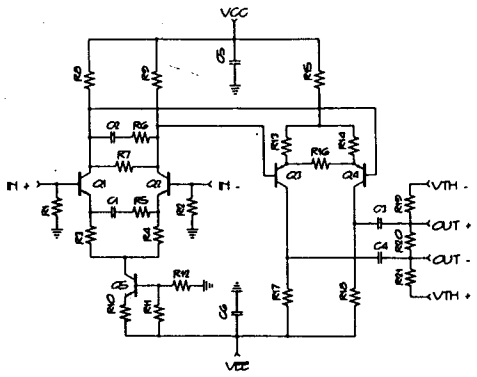

Fig. 3

1008

Shaped pulses from E665 jet chamber due to Ruthenium source.

Fig. 6

1011

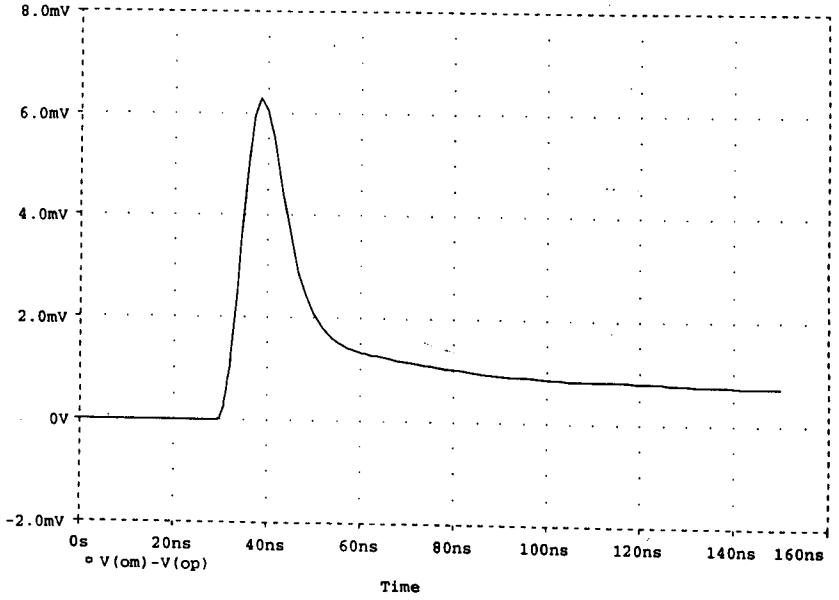

Fig. 4

1009

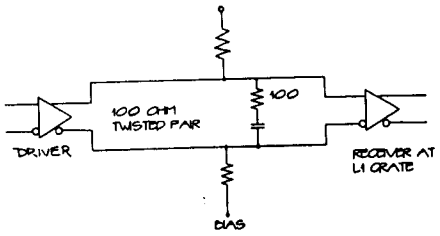

FIG. 9A

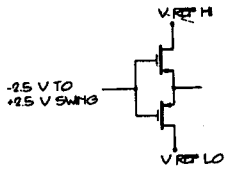

FIG. 9D

1014

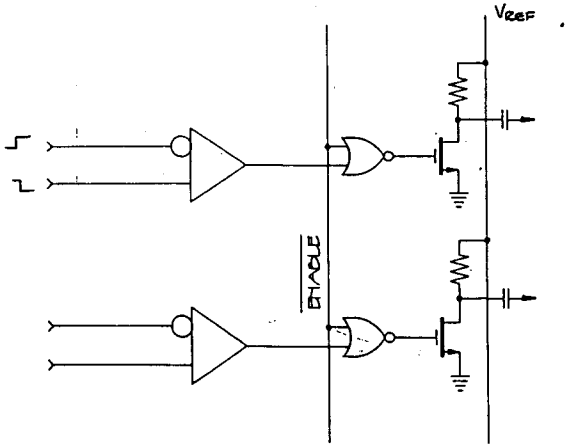

TEST PULSE INJECTION

Fig. 7

1012

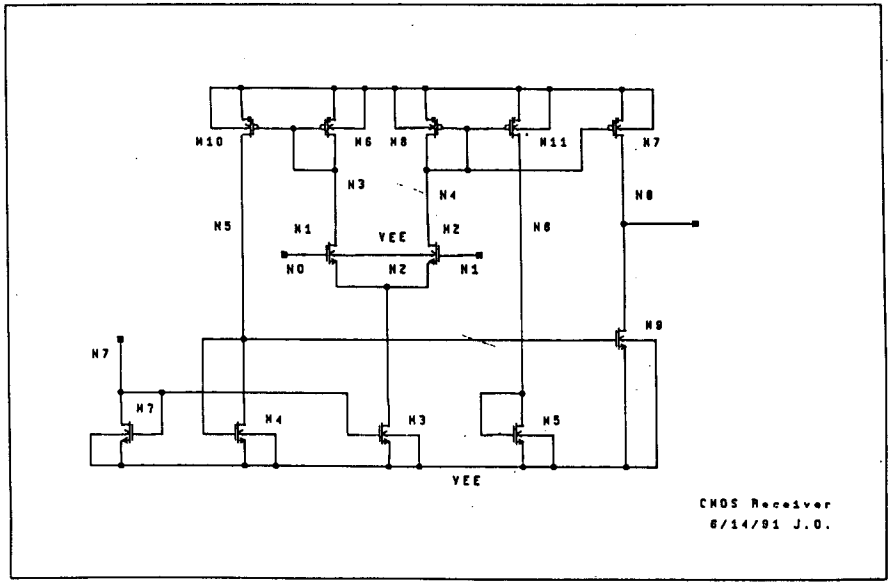

Fig. 8

1013

Drift Tube Development at Minnesota

K. Heller(Minnesota)

K. Heller

1016

Drift Tube Development at Minnesota

The idea is to make electrode structures by extruding plastics with different resistivities into one tube. It should result in very economical drift tubes.

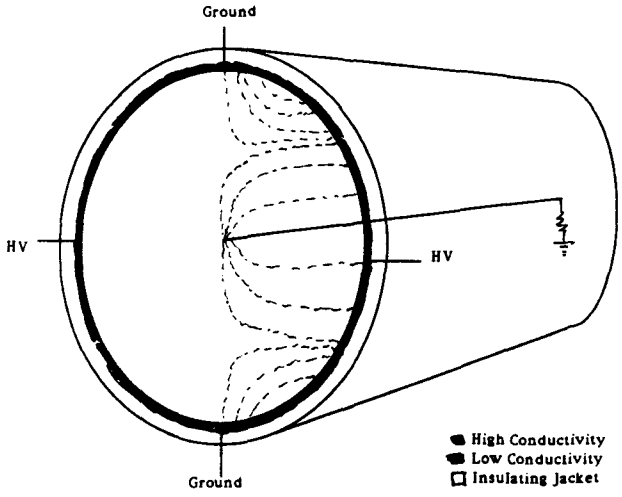

1017

Endcap Design

The current idea is to use the plasticity of the tube for a gas seal- shrink a plastic slug by cooling it in liquid nitrogen, then let it expand into the tube and seal against the walls.

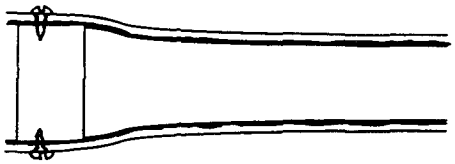

Connections are made to the strips by putting screws through the strips into the endcap. This also immobilizes the endcap.

1018

REALITY

1) The mold exists and works.
2) First round of extrusions is done. Nice mold test, but there is a problem.
3) CR test stand works in MPLS.
4) Beam test scheduled at FNAL.

Many unresolved problems

~~[redacted]~~?

Aging?

Ripples on tubes?

Roll?

Straightness?

Module construction?

Alignment?

Prototypes

R. Loveless(Wisconsin)

R, LOVELESS
15 NOV 91

Prototypes

1020

- develop production techniques:
  - stringing h/w → 14mm "poker" & snake
    - designing 8mm "poker" for smaller, more accurate endgaps
  - forming jigs for 9m extrusions
  - measure wire positions in actual prototype
  - measure endplate hole locations → milling Technique
    - ⇒ must keep plates cool
      - for 16-cell plate $\sigma \sim 5$ microns
      - machined at PSL on CNC mill
      - meas. at physics shop with vertical probe
- 16-cell prototype 1m long (sealed tube version)
  - assembled without glue → no problems
  - wire positions meas. with holes in extrusions
  - try out electronics mounting
- 32-cell prototype 9m long
  - trouble with ends of extrusions: during acid bath company bent ends → must cut off
    - ⇒ need clear specs for manufacture!
- 16-cell prototype 1m long (new design)
  - fewer pieces → more accurate wire placement

1021

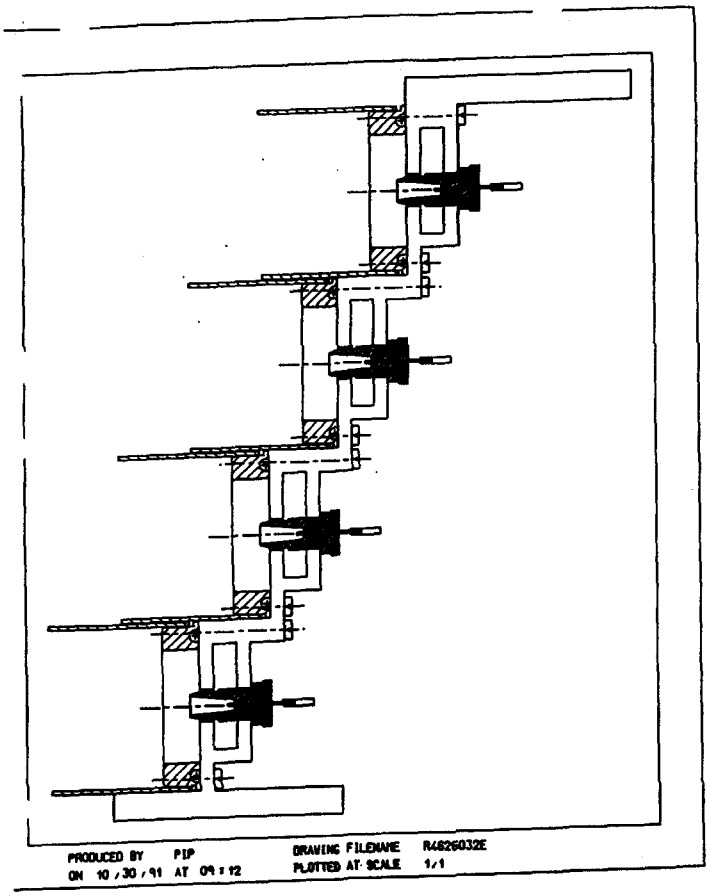

1022

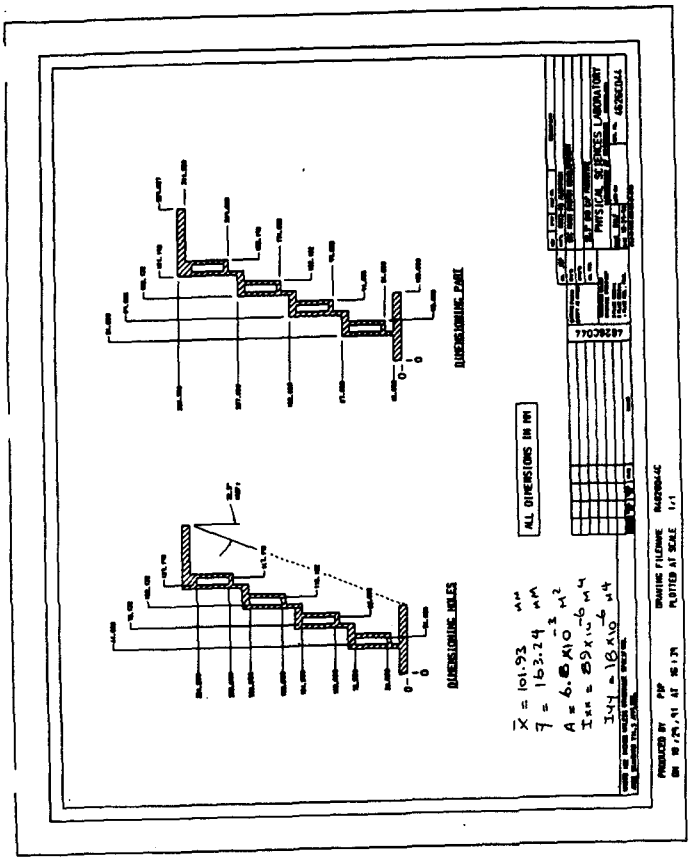

1023

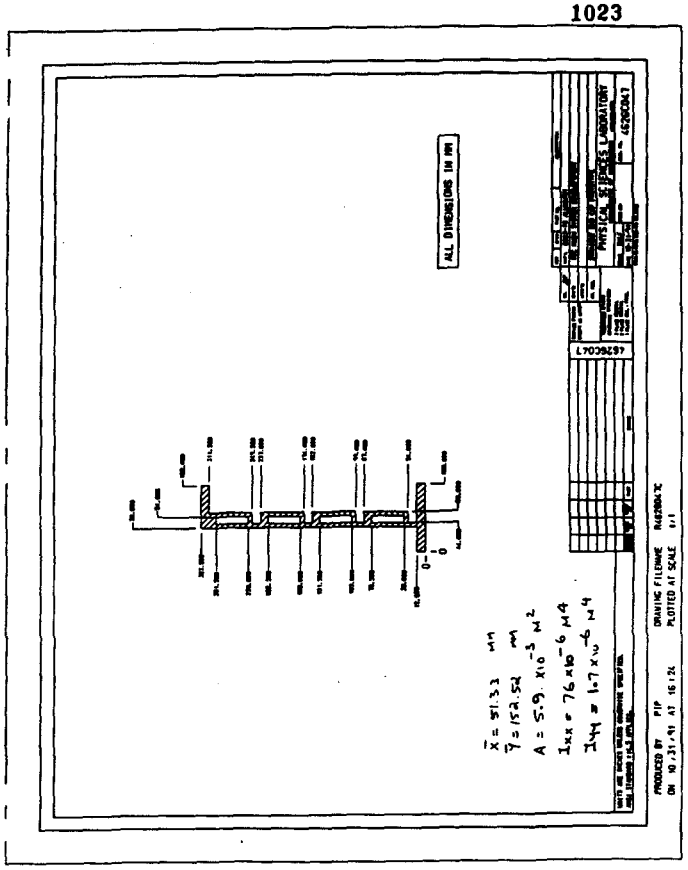

1024

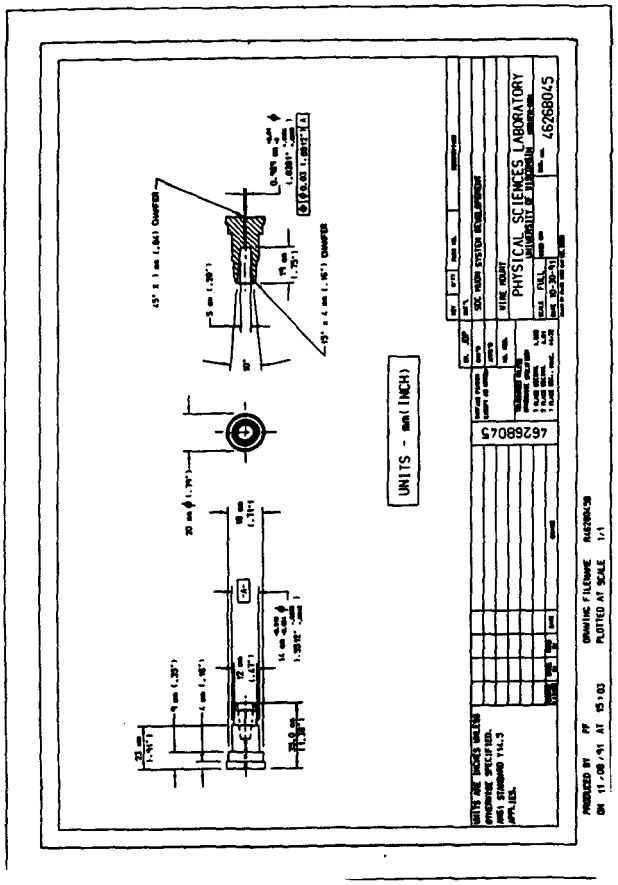

1025

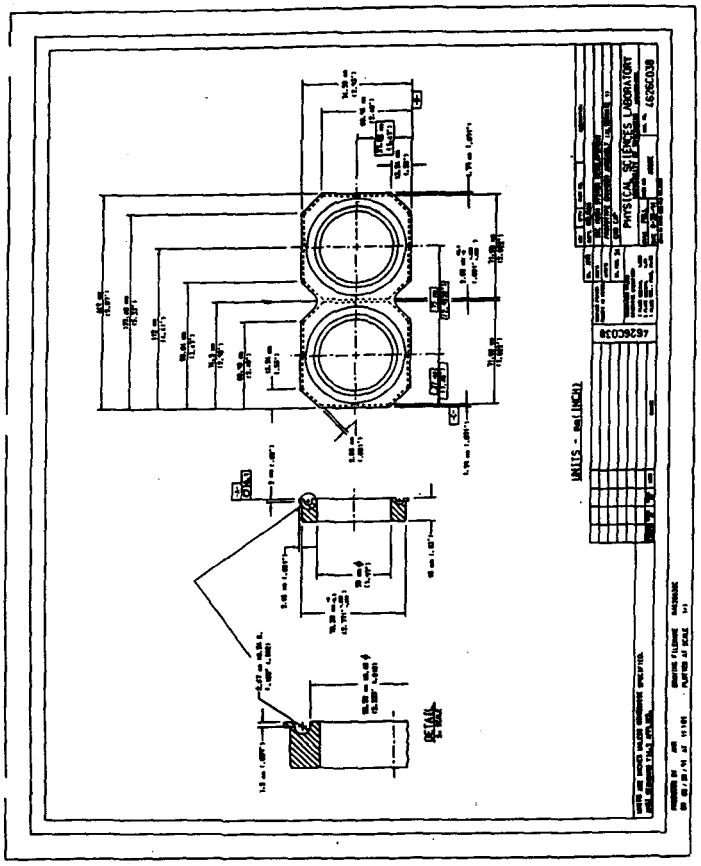

1026

Engineering studies

- wire location meas.

  meas. y positions for 16-cell prototype (double-plug endcap)
  use barrel focus telescope: points reproducible to 5-10 μ
  difficult to change focus

- thermal meas.

  "typical" 16-cell section (100 mm long)
  insulate with 2" fiberglass: bottom & sides (top open)
  electric heaters on bottom for Q input (easy to measure)
  temp. meas. at 4 points from bottom to top

  ⇒ ~ 17 watts/m² gives 1°C difference

  ⇒ 1mm curl in 9m extrusion

1027

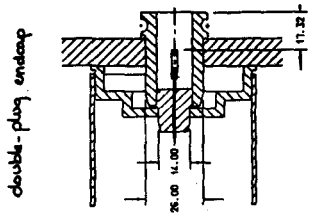

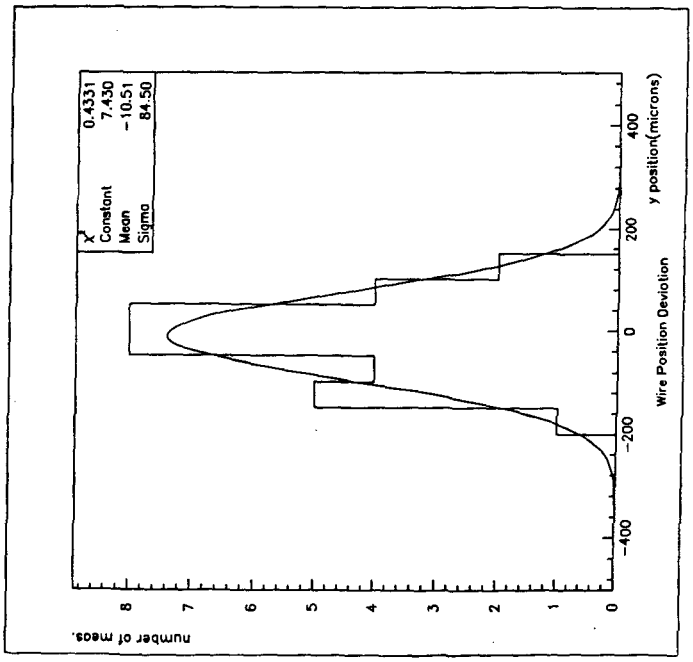

1028

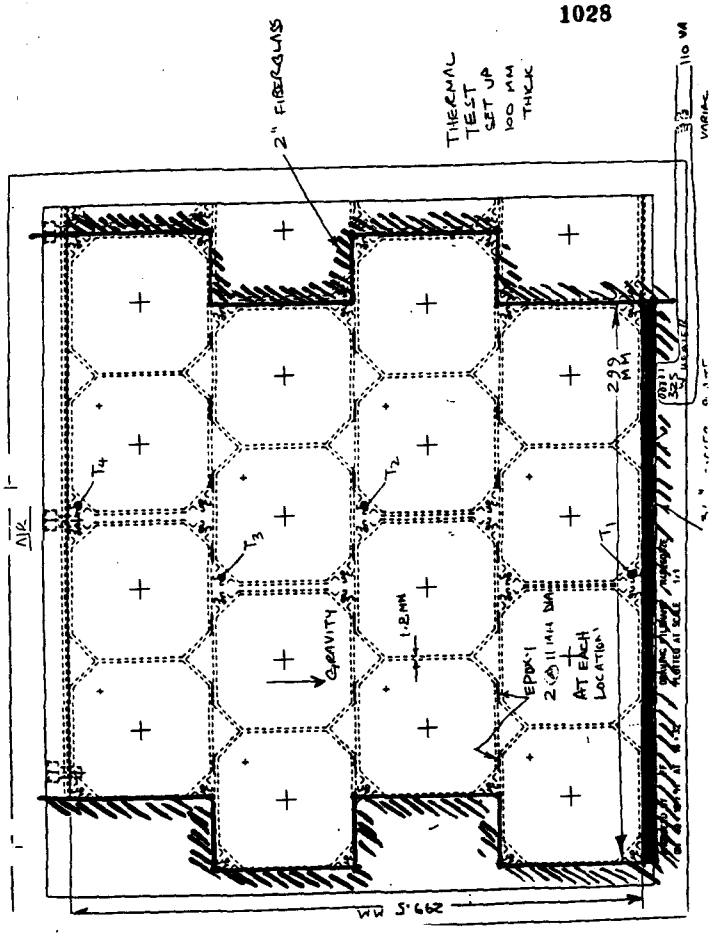

1029

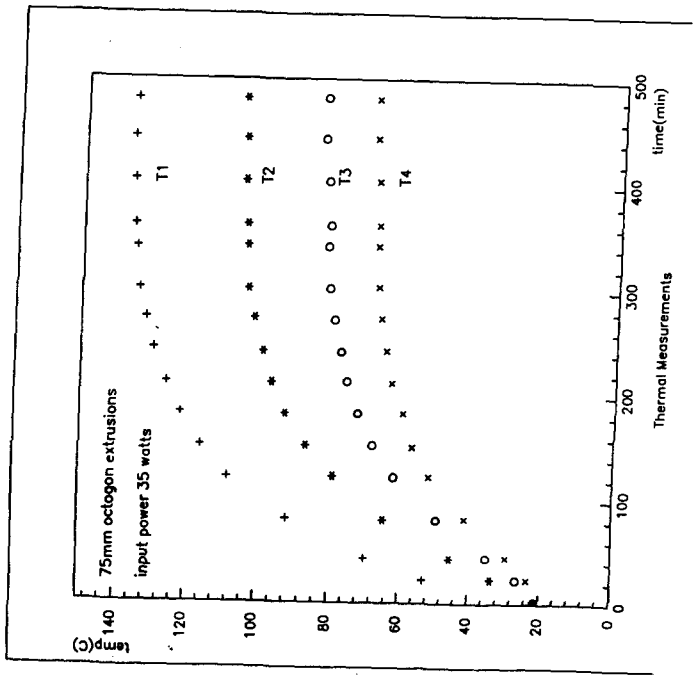

1030

Electronics mounting

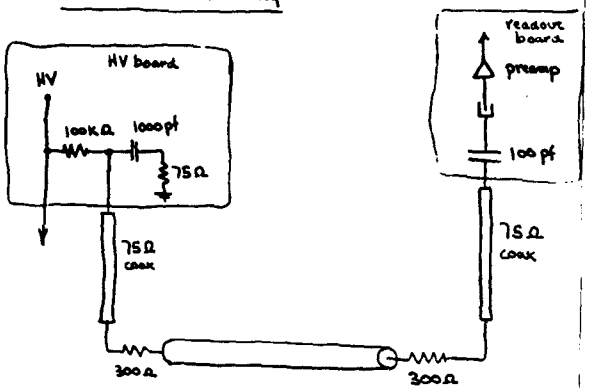

chamber impedance ~ 400Ω

chamber cap ~ 70pf

- boards mounted "on top" of chamber
  - most components accessible
  - could be on opposite ends of chamber
  - both HV & signal carried by coax from board
  - to crimp tubes ⇒ easy to install
  - spring-loaded caps mount on crimp tubes

TRACKING

(PARTIAL)

WEDNESDAY, NOVEMBER 13

Silicon Tracking Conceptual Design Report	A. Seiden(UC/SC)
Modular Straw Outer Tracking System Conceptual Design Report	H. Ogren(Indiana)
Conceptual Design Scintillating Fiber Outer Tracking	D. Koltick(Purdue)
Conceptual Design Report for the Straw-Fiber Tracking System for the SDC	S. Reucroft (Northeastern)
Progress towards the Conceptual Design Report for the SDC Intermediate-Angle Tracking Detector	A. Sill(Rochester)

THURSDAY, NOVEMBER 14

Pattern Recognition in Silicon and Straw Tracking System	B. Hubbard(UC/SC)
Pattern Recognition in a Silicon and Scintillating Fiber SDC Tracking System	D. Adams(Rice)

LPBautz:12/12/91

Silicon Tracking Conceptual Design Report

A. Seiden(UC/SC)

Silicon Tracking
Conceptual Design Report

DRAFT

Table 1. Summary of Requirements for Tracking System

(1) $|\eta|$ coverage out to $|\eta| \leq 2.5$, implying $H^0 \to 4$ charged lepton geometrical efficiency $\geq 60\%$ for $m_H \geq 200$ GeV.

(2) Reconstruction efficiency $\geq 90\%$ (for $|\eta| < 2.5$) for $H^0 \to 4$ charged leptons, for each lepton having $P_\perp \geq 5$ GeV, at design luminosity (exclusive of lepton identification and trigger cuts), but assuming twice the occupancy calculated by Monte Carlo for $pp \to X$. Number of false tracks of $P_\perp \geq 5$ GeV ≤ 0.1 per event of this class.

(3) Reconstruction efficiency for same as in (2) $\geq 75\%$ at 10 x design luminosity.

(4) Reconstructed (as opposed to parametric) vertex constrained momentum resolution of $\sigma_{P_\perp/P_\perp^2} < 20\%(100\%)$ (TeV^{-1}) for $|\eta| \leq (\geq)1.8$ for $H^0 \to 4$ charged leptons.

(5) Efficiency contribution from tracking to lepton identification of $\geq 85\%$ for electrons with $P_\perp \geq 10$ GeV and $\geq 95\%$ for muons with $P_\perp \geq 10$ GeV.

(6) Position resolution at the calorimeter of ≤ 2.5 mm in $r-\phi$ or z (want error $\lesssim \sigma/2$ of calorimeter position accuracy).

(7) No special position resolution requirements at the muon system. Achievable numbers ≤ 1 cm.

(8) B single tagging efficiency $\geq 50\%$ for 125 GeV $\leq m_{top} \leq 250$ GeV, with $\leq 10\%$ impurity.

(9) First level trigger with momentum resolution $\sigma_{P_\perp/P_\perp^2} \leq 10$ (TeV^{-1}) – implies a 10% error for a 18 GeV lepton.

(10) Second-level trigger with momentum resolution $\sigma_{P_\perp/P_\perp^2} = 2.5$ (TeV^{-1}). Gives a 10% error for a 40 GeV lepton for triggering on $Z \to e^+e^-$, $W \to e\nu$ – needed for calorimeter calibration.

(11) Discovery potential – hard to quantify. In general want maximum capabilities from detector. Based on history highest priority (other than isolated lepton of Higgs case above) would be reconstruction and impact parameter measurement of leptons within jets up to the largest jet $P_\perp$ possible (at least ≥ 500 GeV). Desired reconstruction efficiency $\geq 50\%$.

(12) Measurement of jet fragmentation at modest luminosity for QCD studies and for modelling backgrounds from jets.

(13) Survivability at standard $\mathcal{L}$ for ≥ 10 years.

(14) Allows a natural path for upgrading to a system with survivability of ≥ 10 years at 10x standard $\mathcal{L}$ with emphasis (e.g. momentum resolution, pattern recognition, isolated track efficiency) to be decided based on what is learned during initial running.

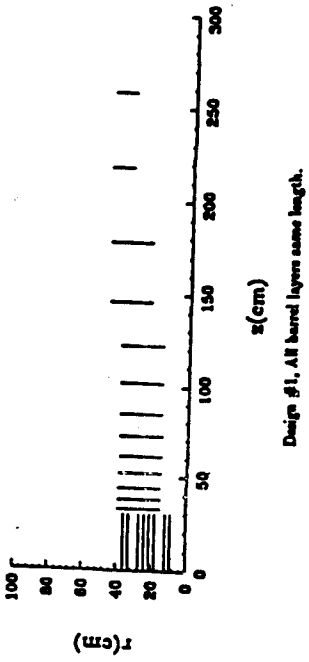

~ 17 m² of detectors.
6 x 10⁶ channels.

Design #1 (All Square) Y.Unno 1991/11/1

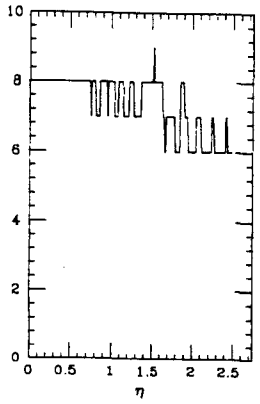

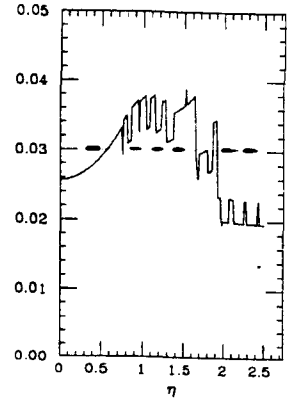

Detectors – Material	
$\eta = 0$	2.6 %
$\langle\eta\rangle$	2.9 %

Goal, •SI_NEW including beam pipe and enclosu.

$\eta = 0$	6%
$\langle\eta\rangle$	6.5%

Strip Configuration

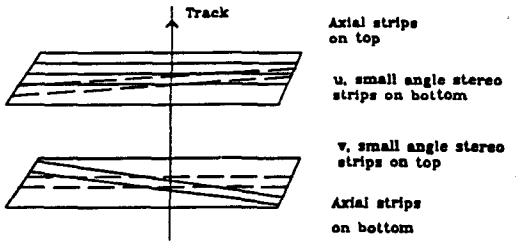

Fig. 3. Orientation of double-sided strips on radially adjacent detector pairs.

Extrapolation of Tracks from Silicon

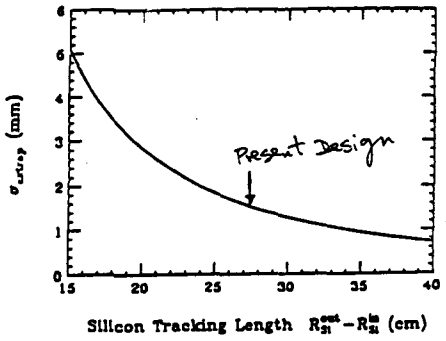

Fig. 6. Position error at 1.6 m radius vs. silicon tracking length.

Impact Parameter Error

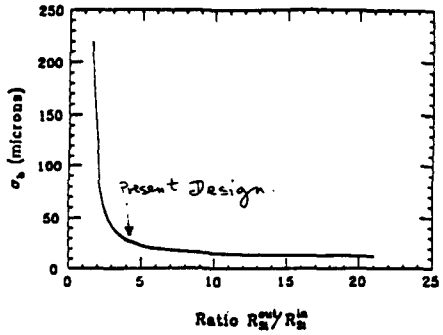

Fig. 4. Impact parameter error vs. detector geometry for high momentum.

Silicon Only.

Vertexing: e^- (data points) μ^- (histogram)

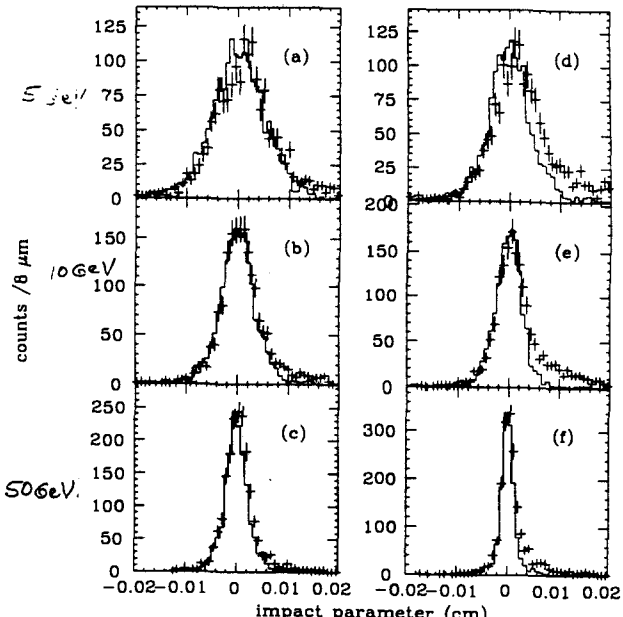

E/p cut: Efficiency ~ 95%
for cut at 1.5.

Compares to 92.5% for
CDF for cut at 1.5.

Tracking Efficiency
400 GeV Higgs Events
at 10^{33}

All Tracks with $P_\perp > 1$ GeV

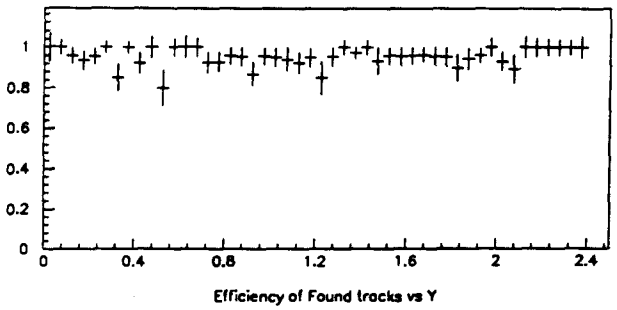

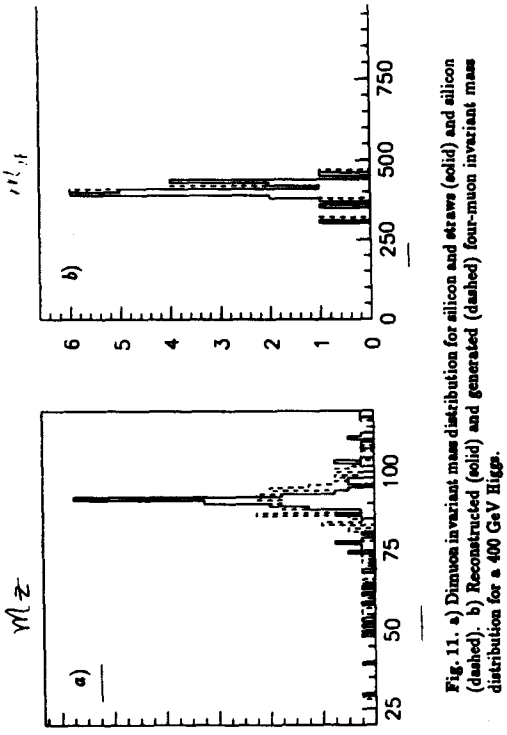

Fig. 11. a) Dimuon invariant mass distribution for silicon and straws (solid) and silicon (dashed). b) Reconstructed (solid) and generated (dashed) four-muon invariant mass distribution for a 400 GeV Higgs.

Silicon Detectors: Radiation Effects

1.—Leakage current generation. Not too serious if detectors run at 0^0C and fast amplifiers used. Expect for 0^0C, after a fluence of 10^{14} particles/cm^2, a leakage current of .5 μamp for a strip of dimensions 12 cm length $\times$ 50 μm pitch $\times$ 300 μm thickness. Gives 350 e$^-$ shot noise contribution for 20 nsec rise-time electronics. Small compared to typical signal which is 25,000 e$^-$.

2.—Changes in doping concentration (fixed electric charges in the silicon), necessitating changes in detector voltage for full depletion and efficient charge collection. Describe by:

$N = No\, e^{-C\Phi} - \beta\Phi$.

No = Initial donor concentration.

C – Characterizes donor removal.

β – Characterizes acceptor creation.

Φ – Fluence.

3.—Trapping of drifting charges by defects:
—Not a large effect for $\Phi \lesssim 10^{14}$ particles/cm^2.

Need more quantitative understanding for
$5 \times 10^{13}/\text{cm}^2 \leq \Phi \leq 5 \times 10^{14}/\text{cm}^2$.

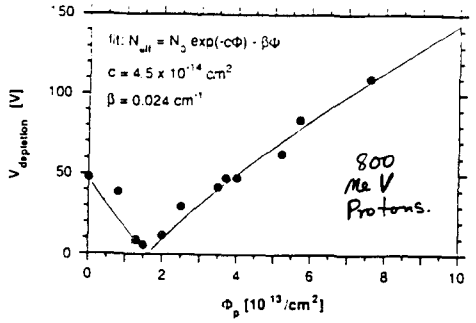

Depletion voltage versus proton fluence for SI detectors. Type inversion occurs at $\Phi = 1.5 \cdot 10^{13}$/cm^2. The line is the best fit according to equations (1) and (2).

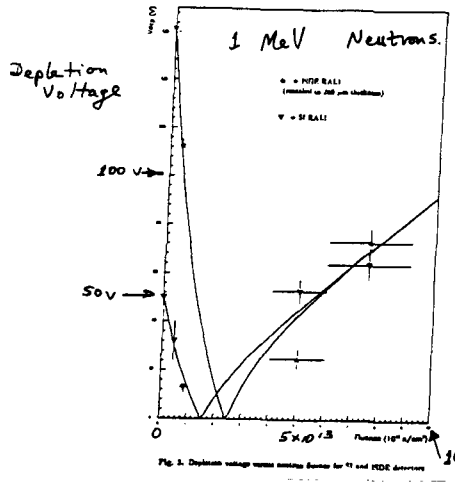

Data: Gribelline et al.

Data of: G. Hall and S. Sotthibandhu Imperial College

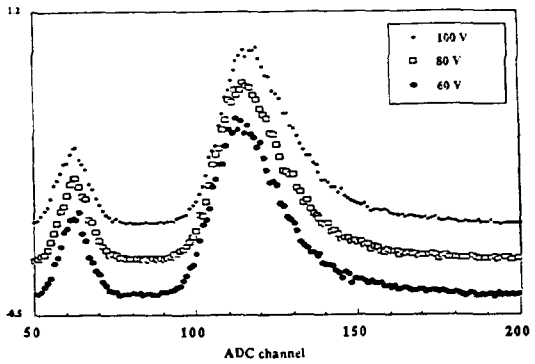

Charge Collected Using ADC with 40 nsec gate.

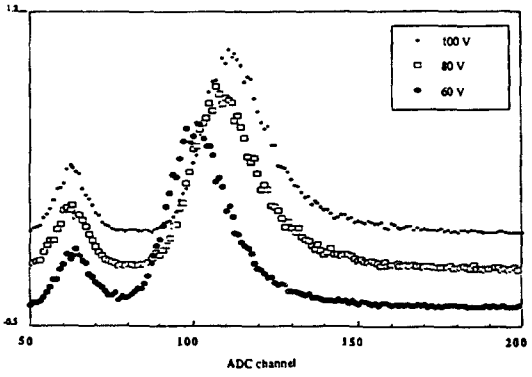

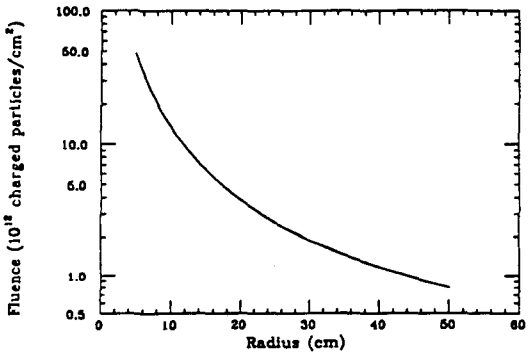

Fig. 12. Charged particle fluence vs. radius for one year at Standard Luminosity.

Table 6. Yearly Fluence Versus Radius

Radius (cm)	Fluence Particles/cm^2)	Number of Years to Reach 10^{14}/cm^2
10	11×10^{12}	9
15	5.9×10^{12}	17
20	3.3×10^{12}	30
25	2.2×10^{12}	45
45	$.95 \times 10^{12}$	105

← Includes factor of 2 safety margin.

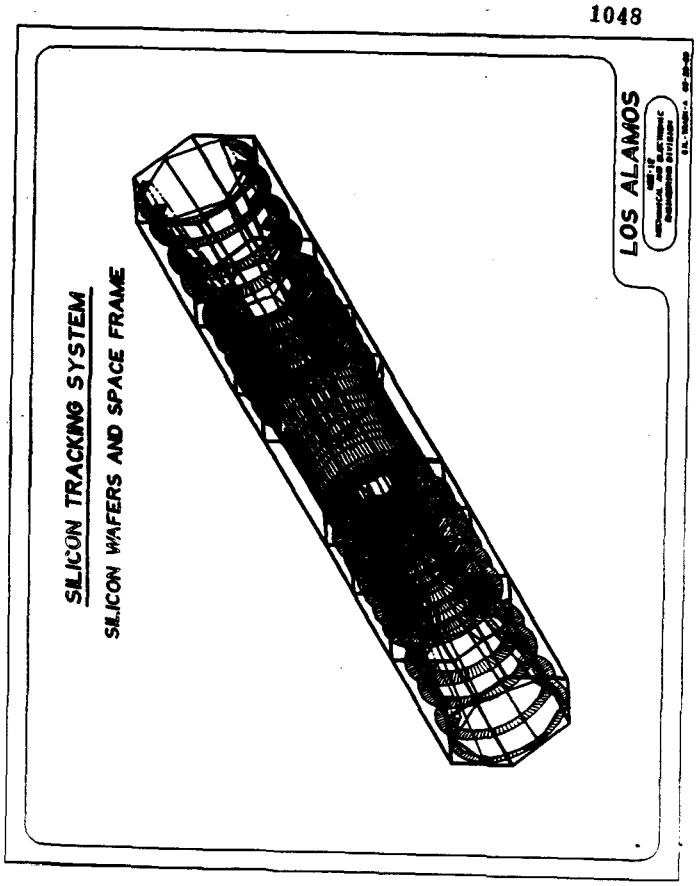

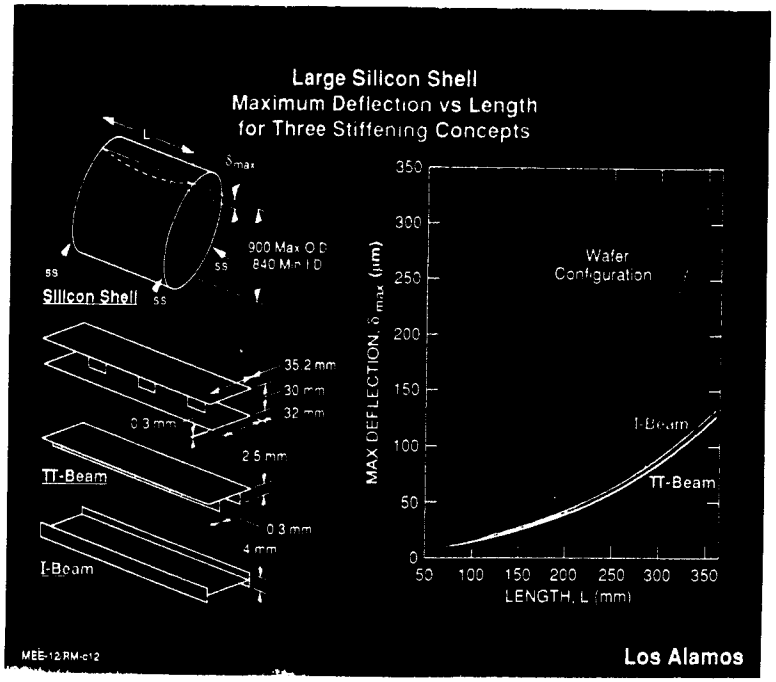

1051

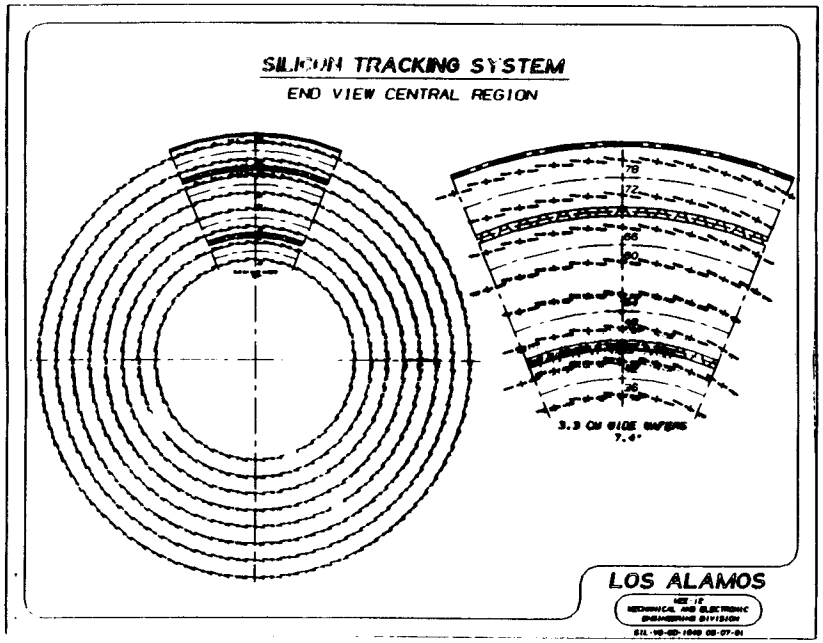

1049

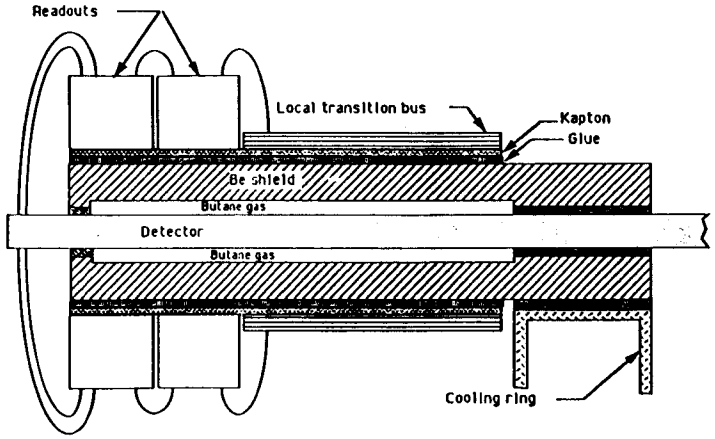

1052

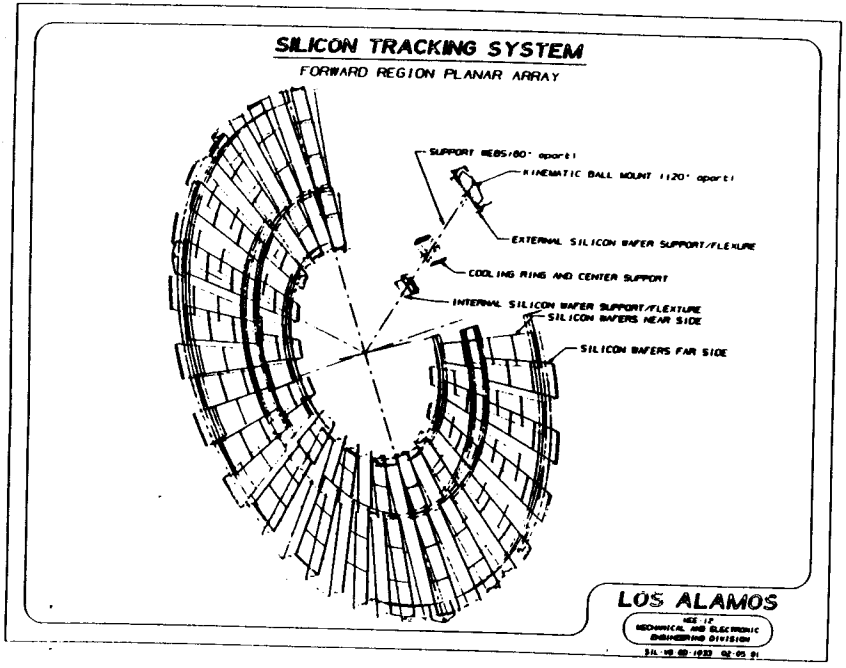

1050

1053

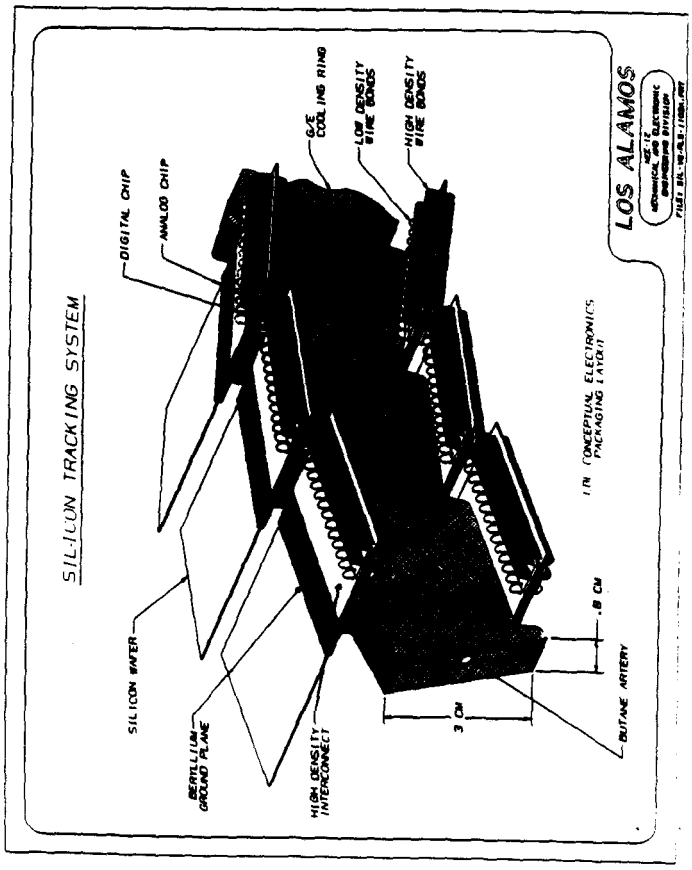

1054

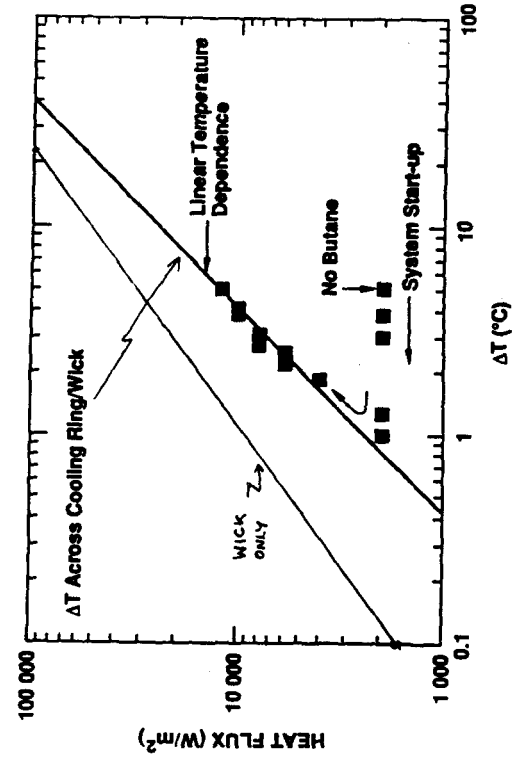

Figure 3-12. Contoured polystyrene-wick cold boundary test heat flux results expressed as a function of temperature change.

1055

1056

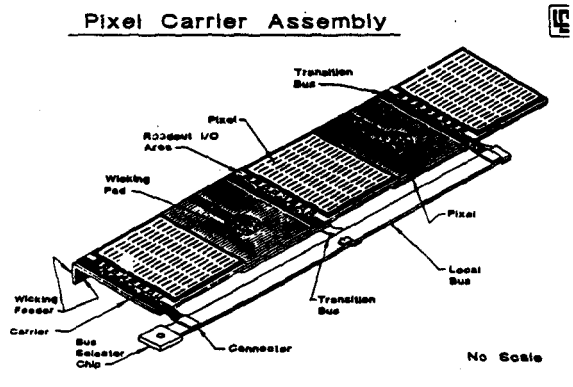

The pixel/carrier subassembly illustrating the evaporative cooling concept.

Table 13. Total Power of BJT Front Ends. Strip Capacitance= 1.2 pF/cm; CR-RC Shaping Time τ = 20 ns. Shunt Resistance R_s = 200 kΩ; Leakage Current= 60 nA/cm. Preamplifier. Supply Voltage= 3.5 V; Current in Output Buffer= 10 μA. Total Noise = 1.1 × Noise of Input Transistor Alone.

Q_n [el]	Preamplifier Current [μA] vs. Strip Length				Power per Channel [mW] vs. L_{strip} (P_{fix} = 0.5 mW)			
	6cm	8cm	12cm	18cm	6cm	8cm	12cm	18cm
DC Current Gain of Input Transistor B = 100								
1000	46	134			0.70	1.00		
1100	34	66			0.65	0.77		
1200	27	49	171		0.63	0.71	1.13	
1300	22	39	102		0.61	0.67	0.89	
1400	18	32	78		0.60	0.65	0.81	
1500	16	27	63		0.59	0.63	0.76	1.18
DC Current Gain of Input Transistor B = 30								
1000								
1100								
1200	34				0.65			
1300	25	56			0.62	0.73		
1400	20	38			0.60	0.67		
1500	17	30			0.59	0.64		

Full System

choose longest strip length where we can get 20-to-1 signal to noise: 12 cm.

Table 15. Efficiency of the data-driven architecture

No. of locations per channel	Data recording efficiency
Level-1 Latency = 128	
1	44%
2	74%
3	90%
4	96.8%
Level-1 Latency = 256	
1	28%
2	52%
3	72%
4	85%
5	92.6%
6	97%

Inner me layer a $\bar{\epsilon} = 10^{-3}$.

Table 16. Summary of the Merits of the Architecture

Architecture	Power dissipation	Length	Efficiency
Level-1 latency = 128			
data-driven	197 μW	6.30 mm	96.80%
clock-driven	330 μW	12.22 mm	99.99%
Level-1 latency = 256			
data-driven	256 μW	8.50 mm	97.00%
clock-driven	520 μW	22.50 mm	99.99%

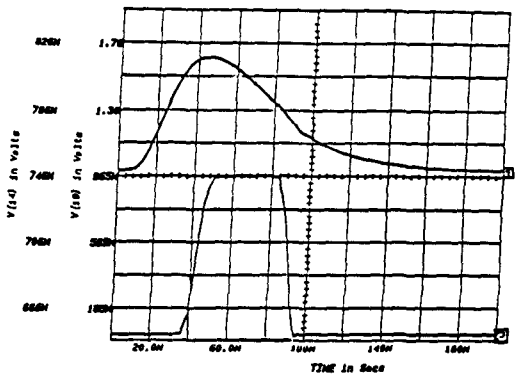

Simulated output waveforms of BJT-JFET circuit for a minimum ionizing particle and detector capacitance of 10 pF; 1-V(14) preamplifier output, 2-V(19) discriminator output.

Front end + Discriminator. .88 milliwatts.

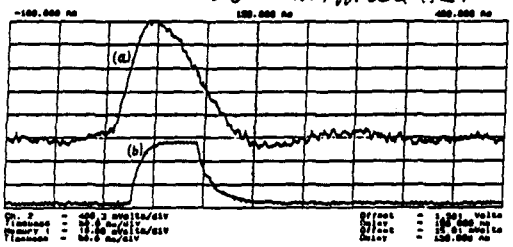

Records of the output signals from the BJT-JFET circuit for input charge of 4 fC and input capacitance of 10 pF; (a) preamplifier output, (b) discriminator output.

Data storage chip (CMOS), highest speed ~ 63 MHz of machine.

Choice - Many low speed (63 MHz) links using LED's and fibers.

or

Multiplexing with smaller number of high speed links. Use lasers or optical modulators plus fibers.

For low speed case:

Fiber/Chip ⇒ 50,000 fibers.

Fiber/Detector ⇒ 5,000 fibers.

MAJOR ITEM COST (After R & D)

VQ - Vendor quote
EE - Engr est
C - Catalogue

ITEM	UNIT COST	UNIT	NUMBER	TOTAL, K	BOE
Barrel detector	$750	each	3600	$2,700	VQ
Frwd detector	$1,500	each	3384	$5,076	VQ
Barrel readout	$36	each	18000	$642	VQ
Frwd readout	$36	each	30456	$1,086	VQ
Modules	$107	each	3492	$374	VQ/EE
Data cable	$15	each	9462	$146	EE
Bus selector chip	$10	each	5862	$59	EE
Optical trans:rec	$500	set	1238	$619	C
Optical fiber	$160	run	1238	$198	EE
Enclosure	$633 k	each	1	$633	EE
Space frame	$599 k	each	1	$599	VQ
Ctrl cooling ring	$30 k	each	16	$480	EE
Ctrl support cyl	$108.3 k	each	2	$217	EE
Ctrl mount	$0.7 k	each	72	$50	EE
Ctrl coolant dist	$0.7 k	each	16	$107	EE
Ctrl align/assy/test	$11.4 k	each	12	$137	EE
Disc cooling ring	$15.7 k	each	44	$691	EE
Disc support ring	$4.2 k	each	24	$101	EE
Disc mount	$1.5 k	each	144	$216	EE
Disc coolant dist.	$1.5 k	each	44	$66	EE
Disc align/assy/test	$31.2 k	each	24	$749	EE
Power cable/bus	$177 k	each	1	$177	EE
Int. optical sys	$300 k	system	1	$300	EE
Slow control	$40 k	system	1	$40	EE
Heat rejection sys	$595 k	system	1	$595	EE/C
Gas system	$35 k	system	1	$35	EE
			TOTAL	$16,092	

Total w/o contingency = $32,428 k
Total with contingency = $42,615 k

Modular Straw Outer Tracking System Conceptual Design Report

H. Ogren(Indiana)

SDC

MODULAR STRAW

OUTER TRACKING SYSTEM

CONCEPTUAL DESIGN REPORT

B. Adrian, D. Alexander, B. Corliss, F. Ellis, E. Erdos, W. T. Ford, D. Johnson, M. Lohner, P. Rankin, G. Schultz and J. G. Smith
University of Colorado

R. Foster, G. Hanson, F. Luehring, B. Marvin, H. Ogren, D. R. Rust and E. Wente
Indiana University

Y. Arai
KEK

J. W. Chapman, A. Dann and J. Mann
University of Michigan

J. Mayhall, T. Ryan and J. Sheffer
Oak Ridge National Laboratory

H. M. Newcomer, R. Van Berg and H. H. Williams
University of Pennsylvania

R. L. Swensrud and D. T. Hackworth
Westinghouse Science and Technology Center

Modular Straw

Outer Tracking System

Conceptual Design Report

Tracker requirements

The charged particle tracker has an important role in almost all of the physics questions we wish to address with SDC.

The list of requirements is daunting, but we believe that a straw outer-tracking system and a silicon inner tracker can satisfy them.

1) Eta coverage < 2.5
2) Reconstruction efficiency > 90%, with p_t>5 GeV at design luminosity with false tracks l<0.1 for p_t>5 GeV/c
3) Reconstruction efficiency >75% at 10 x design L
4) dp/p_t^2< 20%TeV^{-1} for eta < 1.8
5) Effficiency for electron ID >85%
   Eff for muon id> 95% for PT>10 GeV.
6) Position resolution at the calorimeter< 1mm
7) Position resolution wrt Muon 100 microns in transverse, 1000 microns in z.
8) Jet charge multiplicity measurement with in 15% for jets up to 1 Tev.
9) B single tagging efficiency >50% for 125<M_t<250 GeV
10) First Level trigger with dp/pT,10Tev^{-1} implies a 10% res for 10 GeV leptons
11) Second level trigger with s/pt^2<5 Tev^{-1} which gives 20% resolution for 20 GeV Lepton
12) Discovery potential
13) Measurement of jet fragmentation
14) survivability for L- 10^{33} for>10 years
15) Natural upgrade path.

FIVE SUPERLAYER STRAW TRACKER

The straw tracker we have designed is the minimal wire system that satisfies the following very important requirements for the outer tracker:

1) High P_t track segment trigger Level 1, Level 2 trigger

2) It can meet the momentum resolution requirements with the silicon system.

3) Pattern recognition capabilities for segment linking to the silicon system.

4) Z coordinate measurement for improved invarient mass resolution

Two outer axial layers can be used for the Level 1 trigger.

Two stereo layers for the Z measurements and pattern recognition.

Inner axial layer for linking to Silicon system.

1066

Superlayer	Mean Radius (m)	Straws/Layer	Modules	Layers/Superlayer	z_{max} (m)	Stereo Angle (°)
1	0.7096	1060	80	6	2.00	0
2	1.0670	1590	120	6	3.20	+3
3	1.3510	2014	152	8 (trigger)	3.90	0
4	1.4877	2226	168	6	3.95	-3
5	1.6315	2438	184	8 (trigger)	3.95	0

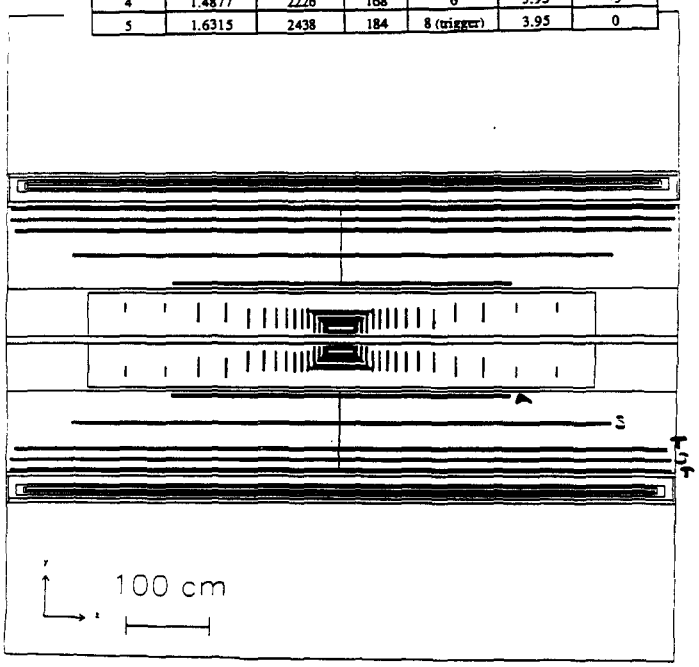

1067

SIMULATION

This is system is being studied by a combined Silicon - Straw Monte Carlo as part of SDCSIM.

The complete tracking detector has been modeled, the material in all systems is real, the straw tracker responses are correctly modeled, and loopers from all previous events are handled correctly.

The study of the combined system is just now beginning. Future studies will help guide us to the optimal layout.

1068

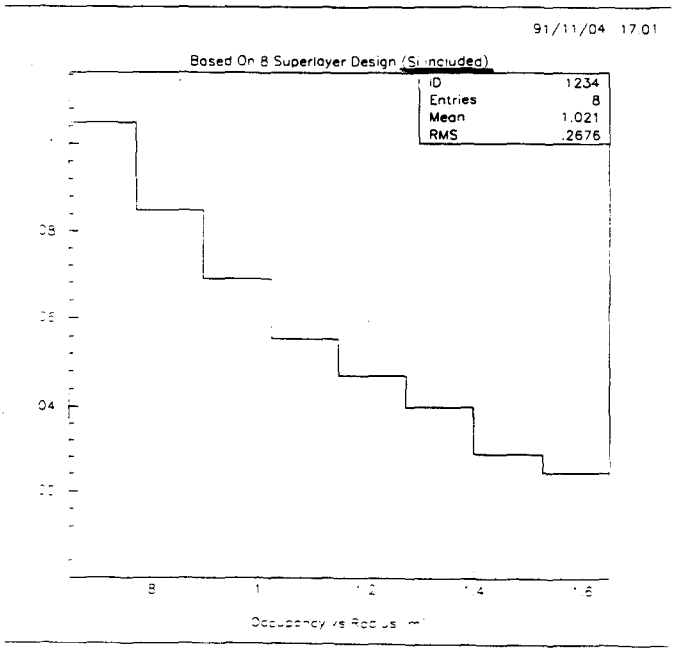

1069

1) LOCATING CLUSTERS - SEGMENTS
2) LINKING SEGMENTS INTO TRACKS - STRAW + S.' 'ROAD' algorithm
3) FITTING TRACKS

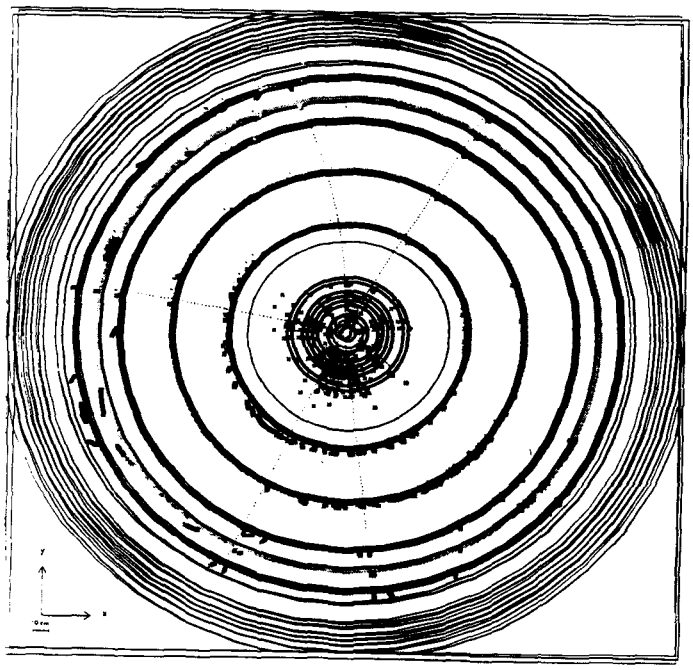

1070

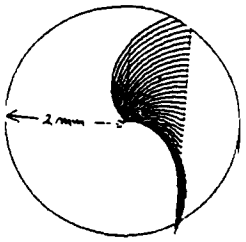

STRAW DRIFT TUBE

4 mm Diameter straw

37 μ metalized Kapton

25 μ Dia. Au-W wire

CF4-Isobutane (20%)

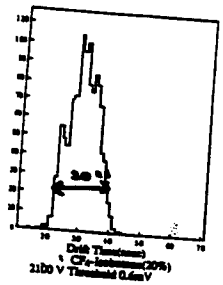

Drift time- 29 ns at 2T.

1071

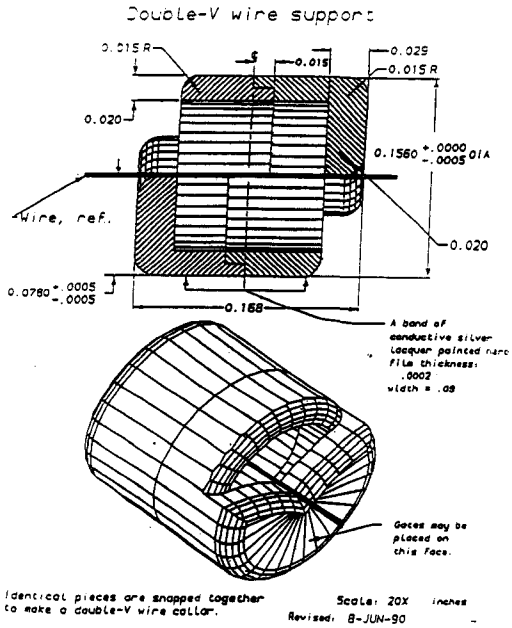

ALSO, NEW DESIGN

AT

CHARPAK

Fig. III.2. A detailed drawing of the double-V wire support.

1072

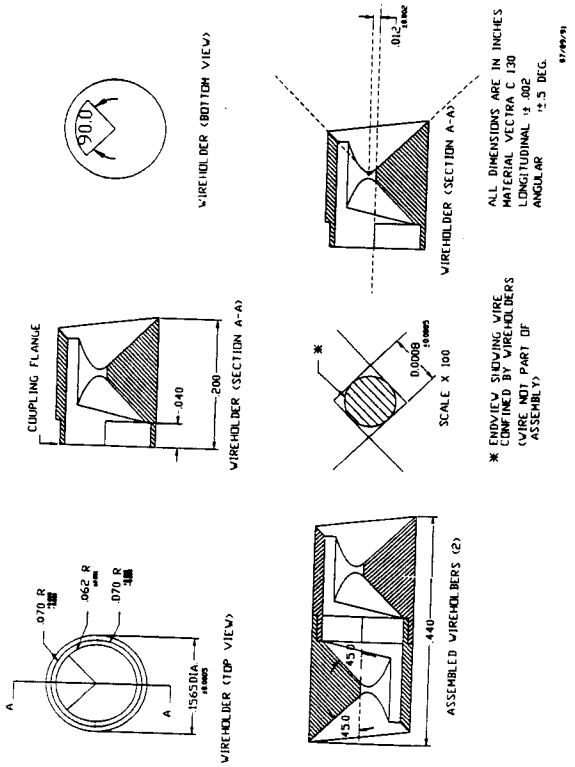

Wire support (D. Alexander)

1073

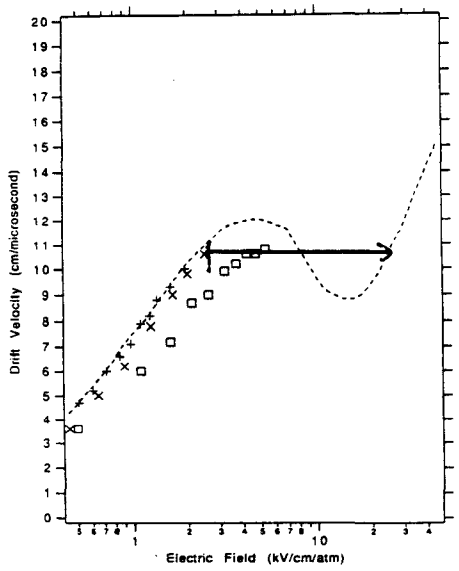

Fig. III.4. Measurements of the drift velocity in CF_4-isobutane 80:20 as a function of electric field strength. The squares are from R. Openshaw *et al.*, the + are from T. Yamashita, *et al.* and the × are from J. Va'vra, *et al.* See the references. The curve is drawn through the points of Va'vra and continued according to the shape of the pure CF_4 and CF_4 - CH_4 mixture curves.

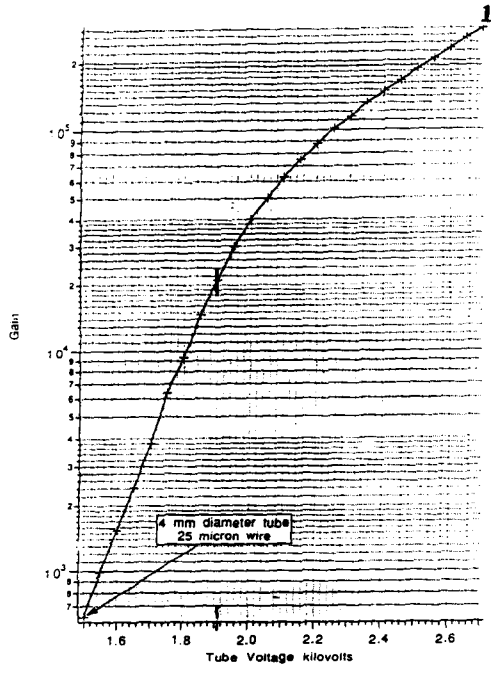

Fig. III.3. The gain curve of a 4 mm straw drift tube with CF_4 -isobutane 80:20 gas. The absolute calibration of the curve is accurate to about 15% but the shape of the curve reflects the true dependence of the gain on voltage.

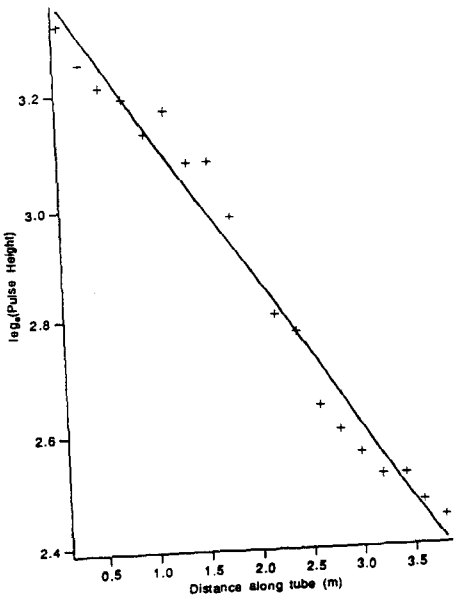

Fig. III.1. The pulse height of signals from an Fe^{55} source in a 2 m unterminated 4 mm straw tube. Both the direct signals and the reflected signals are plotted. The error on each point is about ±15% reading error. The attenuation length is 3.8 m.

Expect 35 mm with Cu cathodes
And 20μ W?

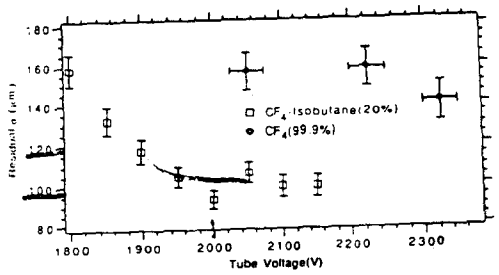

Fig. 15. Wire resolution for CF4 gas mixtures

have also measure the efficiency of these gas mixtures as a function of voltage. These
surements, shown in Fig. 16, will depend rather importantly on the noise immunity of the
tronics and the resulting threshold level, so they should only be taken as an indication of the
al size for this particular gas.

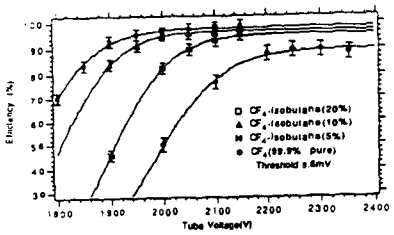

Fig. 16 Cosmic ray efficiencies for CF_4 mixtures

Table III.1. Occupancy and Current Draw.

Superlayer	Radius(m)	Length(m)	Occupancy	I(Ch. Part) na/cm	I(Total) na/cm
1	.708	2.00	0.105	1.9	2.1
2	1.04	3.20	0.07	0.8	1.0
3	1.35	3.90	0.04	0.37	0.6
4	1.48	3.95	0.03	0.27	0.5
5	1.61	3.95	0.02	0.18	0.4

Since there seems to be very little concern about deterioration of the anode surface, attention has been focused on the survivability of the cathode. It soon appeared after irradiating the prototype tubes with aluminum coating that there was a problem of damage to the cathode. The symptom was that after a certain amount of radiation the chamber would start to break down at the normal operating voltage. There have been some observations of breakdowns occurring in chambers with aluminum cathodes operating in fairly large radiation fluxes.[22] After this problem was recognized, some studies were done to try to understand and ameliorate it.

The breakdowns which were observed depended on three conditions: a sufficiently high gas gain, a sufficiently large accumulated dose and the presence of a sufficiently large radiation flux. An increase in the dose over time finally resulted in a decrease in the values of radiation flux or gain that could be sustained without breakdown. Even in this state, however, the gain could be raised well above the operating point if the radiation source was weakened sufficiently. Another factor was the level of water contamination in the gas. If the water contamination was increased, the gain could be raised as long as the other factors remained constant.

studies cathode damage
Burrows

OVERVIEW OF MODULES

Mechanical properties of straws

a) **Straws are not strong**

They must be supported.
They cannot support wire tension.

b) **Straws are not round**

Use internal wire supports for close packed alignment

c) **Straws are not straight**

Align straws in module

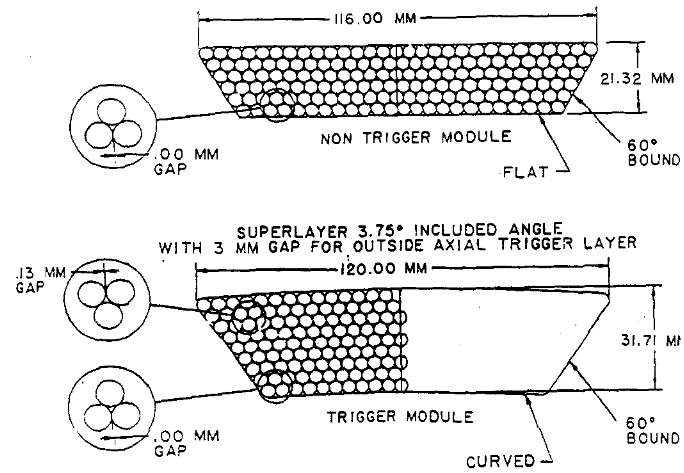

Fig. IV.2. The basic module design is shown here schematically. The two basic designs are shown; a 6 layer module for non-trigger layers and stereo layers, and a 9 layer trigger module that has all straws on a radial line. The present design will probably use an 8 layer trigger module.

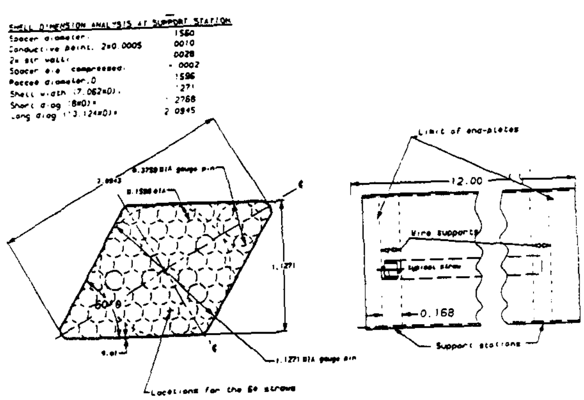

Fig. IV.3. A 64 straw test module with a length of 30 cm.

Six modules have been built
DU, Colorado, Michigan, Penn, Wisc

[illegible]

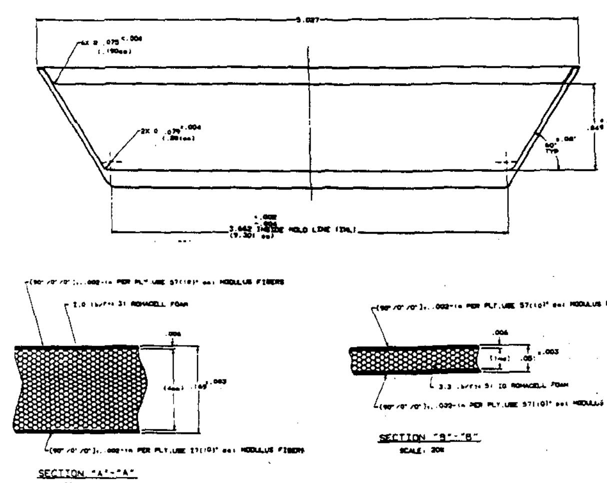

[illegible]

Fig. IV.4. The cross section details for the full size prototype module, showing the Rohacell foam sandwich construction. A detail of foam construction is shown in the insert.

Assembly considerations.

For a five layer straw system there could be
130,000
straws to assemble.

2.5meters-4 meters in length

- Modules allow us to assemble, units of about 200 straws.
- Each module can be pretested, calibrated, and measured prior to installation
- Module can be replaced and repaired.
- Work can be done in parallel.
- Final assembly and alignment of about 80 -184 modules per

PARALLEL ASSEMBLY

- Use several assembly sites
- This could be done at several University sites.
- Require about 300 modules produced, tested and calibrated at three sites in a a two year

Alignment precision requirements

$$\sigma^2_{\text{superlayer}} = (\sigma^2_{\text{intrinsic}}+\sigma^2_{\text{wire place}})/6 + \sigma^2_{\text{module intrinsic}}+\sigma^2_{\text{module place}}$$

σ intrinsic= 100 microns

σ wire placement= 30 microns

σ module intrinsic= 50 microns

σ module placement= 50 microns

Super layer resolution= 82 microns

Alignment of straws in a module

- require an error < 50 microns Straw-to-straw.

measurements with clamping of wire supports for precision close packing are within tolerances (30 microns)

- Intrinsic module straightness is being tested with first 1 meter module. (< 50 microns).
- 4 meter module. Mold in production measurements in December.

Fig. 1 Eight Layer array convention

Fig. IV.5. The deviation of the theoretical close packed fit in x position (a) and y position (b) for an 8 layer trapezoid.

Fig. IV.6. The verucal displacement of the inside shell corner as measured in the first prototype one meter shell.

Test and calibration of each module

- check gas tightness
- test module with HV
- x ray for wire positon ⇐
- cosmic ray tests
- Determine best fit to close packed geometry at each 80 cm point.

Assembly of straws in modules

- Carbon composite shell
- straws and wire supports
- endplates
- wires
- Prototype of 64 straws

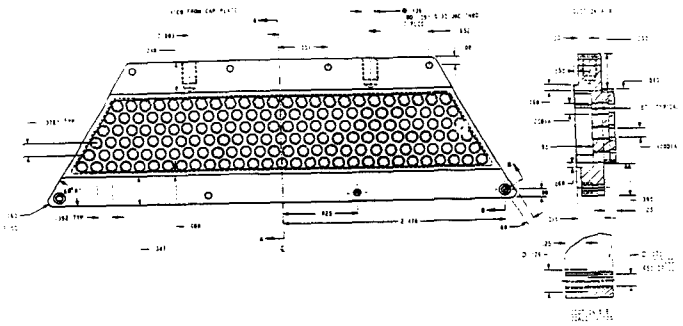

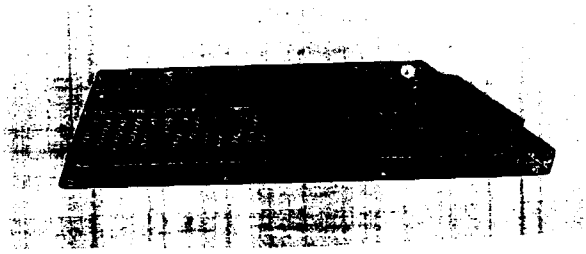

Fig. IV.7 a) Details of the end of a module. The end of the straws stops short of the end plate. The End plate holds the wire tension clips, provides the gas manifold, and hold the cap plate which carries the electronics. b) An isometric view of the end tension plate that is bonded to the shell.

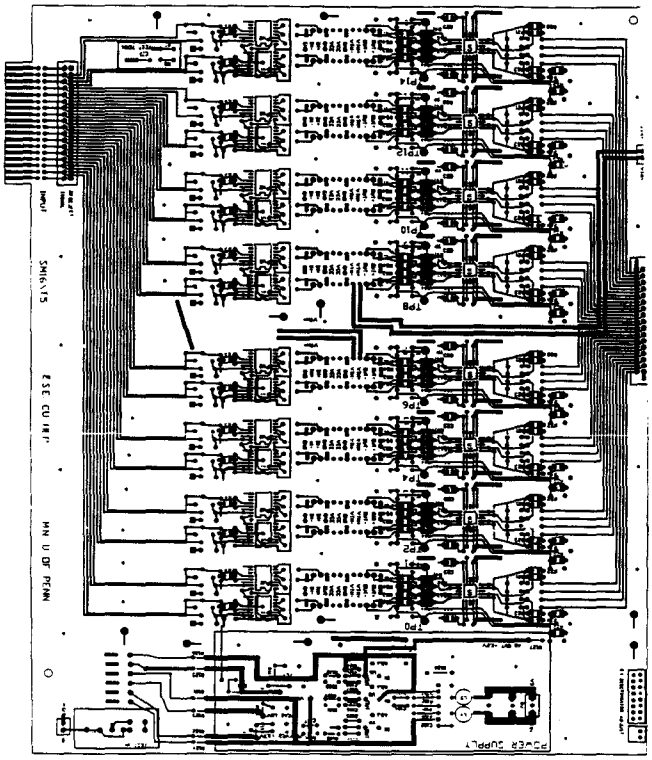

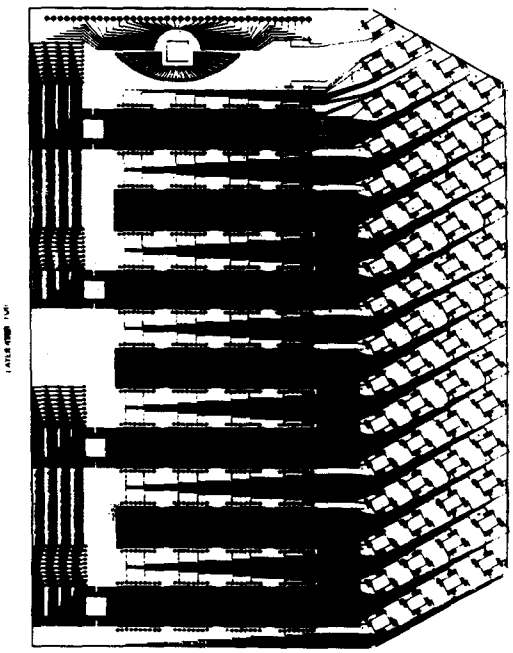

1094

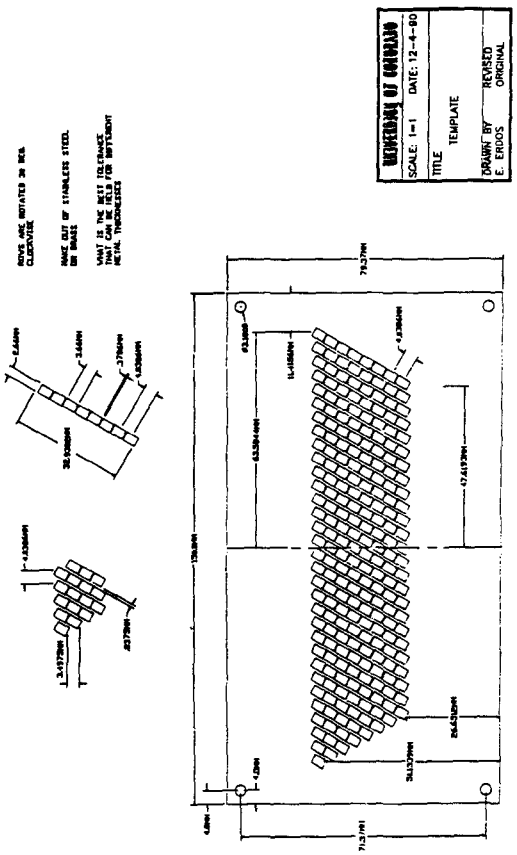

1095

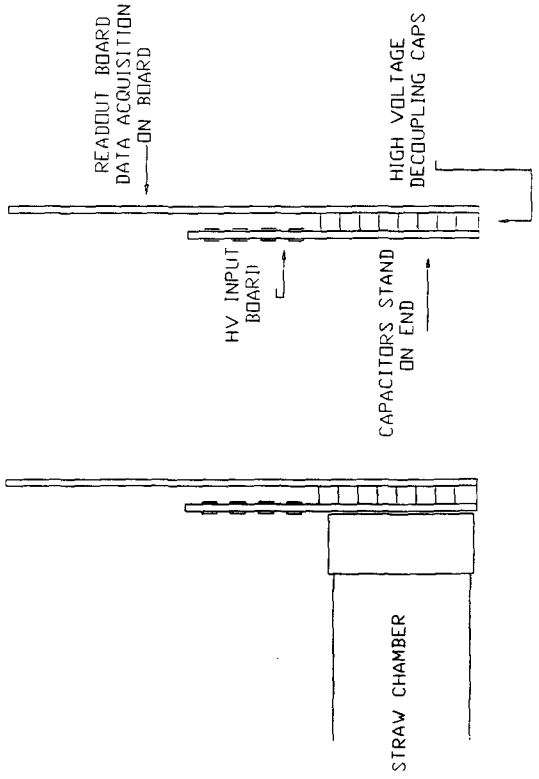

HV supply & decoupling scheme

1096

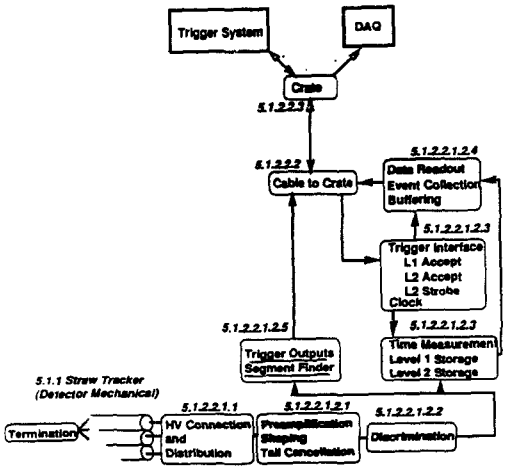

Fig. V.3. Block diagram of the straw readout system with WBS numbers indicated. Note that this particular WBS numbering scheme is outdated and incomplete.

1097

4.3.8.1 STRAW TUBE R&D

	Milestone and goals	Date
→	Design of endplate for detachable readout board	10/91
→	Evaluation of first preamp/shaper/discriminator prototype	12/91
→	Completion of full-scale prototype ~~multi-straw element~~ module	1/92
	Develop HV distribution with failure confinement (e.g. fuses); establish cable and utilities plant requirements	2/92
	Complete construction of second prototype multi-straw element	4/92
→	Prototype support structure assembly of full-scale sector/superlayer	10/92
	Auto assembly and manufacturing design	10/92
→	Complete evaluation of efficiency, resolution, and attenuation of full-scale multi-straw element with prototype of full electronics (preamp/shaper/discriminator/TVC or TMC)	12/92
	Construction of full-scale sector/superlayer	5/93
	Test beam studies	93-94

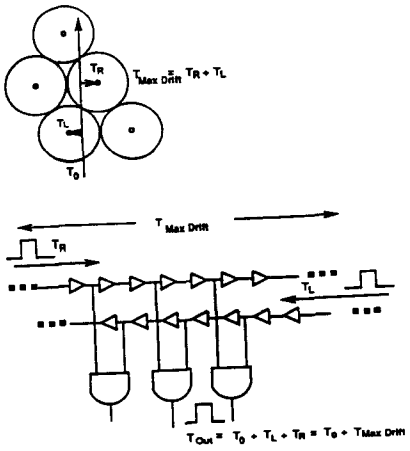

Fig. V.8. Mean time method of segment finding.

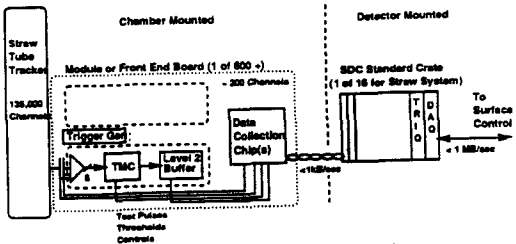

Fig. V.9. Control path to the straw electronics.

One of Eight Patterns

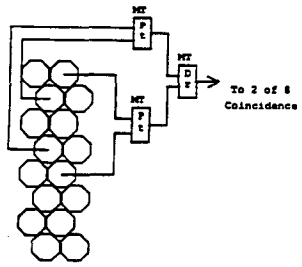

Fig. V.22. A representative mean timer connection for an 8 tube superlayer. The connection shows two mean timers each requiring hits to be consistent with a preset momentum lower limit and output pulses averaged in time to a common radial position. The third mean timer averages these output pulses to arrive at a final pulse whose timing is fixed relative to the particle passage time plus the signal propagation time from its z position to the end of the straws. The pattern shown is one of 8 used in a two-fold coincidence to produce a stiff track trigger.

Mean Timer Trigger (8 Tubes) at Design Luminosity 1100

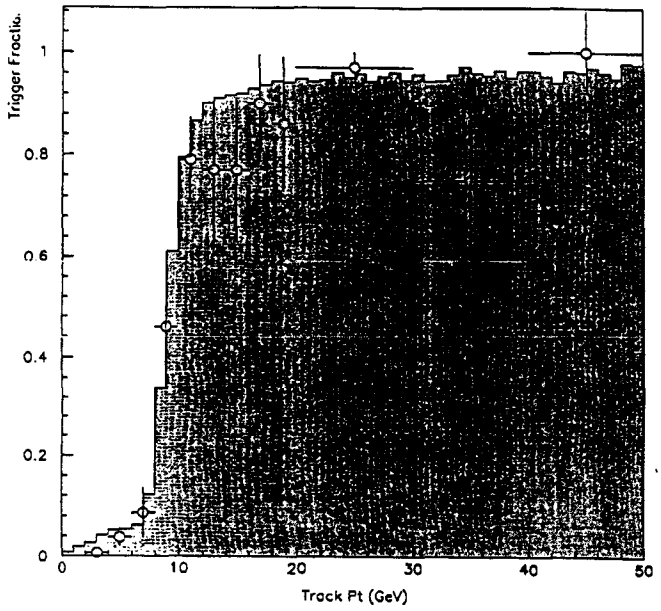

FIG. 3 The efficiency as a function of P_t for a digital mean timer based trigger operating on signals from an 8 tube deep superlayer of packed straw cells. The points are from a GEANT simulation of Higgs → ZZ events at 10^{33} luminosity and the shaded histogram is for a fast parameterized simulation tuned to match the GEANT points.

be effected) and the stiff track momentum resolution requirements (approximately 10% or

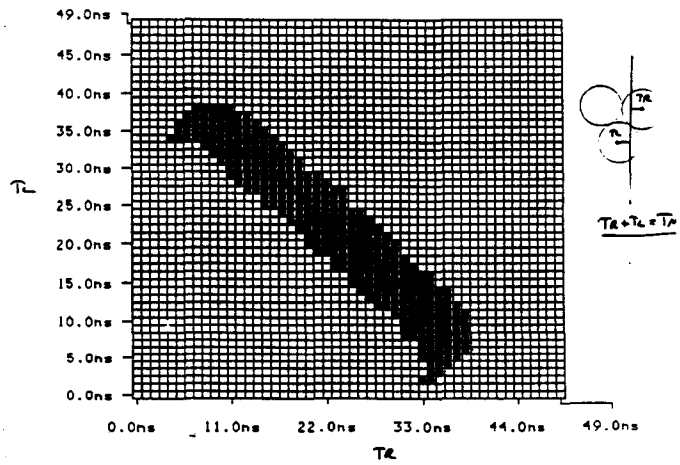

Fig. V.24. A test plot of the p_T cut portion of the mean timer IC. The axes are the times of the aligned wire inputs and the plotted points are those values of the axis coordinates for which an output was generated at a predetermined value. A falling 45° is expected for correct averaging of the input times. The cutoff of the line at large coordinate differences is due to the time difference restriction (momentum cut).

SPACE F. .AME

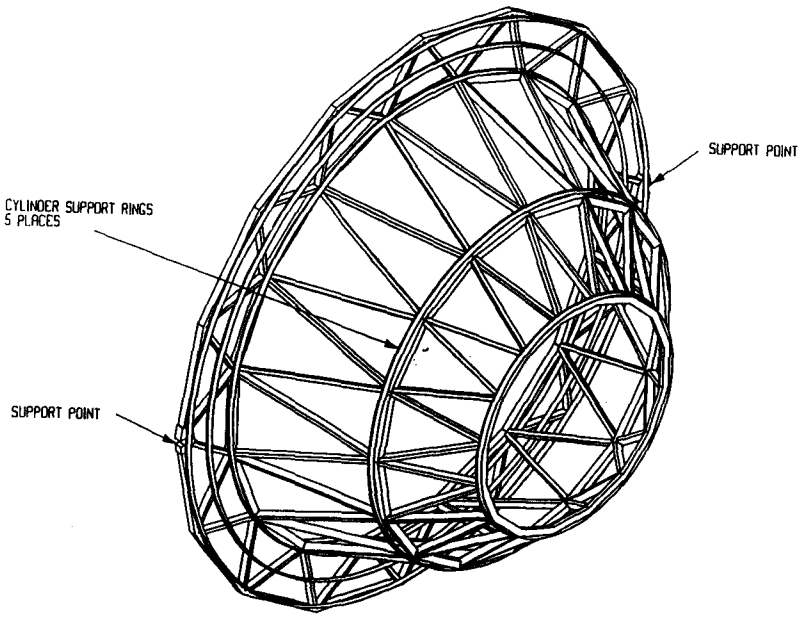

1104

MODULAR STRAW TRACKER CDR

1.1 SUPPORT STRUCTURE OVERVIEW

THE REVISED MODULAR STRAW TRACKER GEOMETRY

1) Five Superlayers of Straw Modules
2) Two Trigger, Two Stereo, and One Axial Layer

Westinghouse
Science & Technology Center

1102

MODULAR STRAW TRACKER CDR

2.2 SUPPORT CYLINDERS

THE DESIGN USES:

1) Composite Cylinders of Graphite Lamina With Foam Core On Which The Detectors Are Mounted
2) Cylinders use Commercially Available Technology (Hercules, Inc.)
3) Need At Least Two 0.009 Inch 6 Ply Layups with 5 Millimeter (.234 Inch Thick Rohacell 31IG Core
4) Meets Radiation Length Requirements
5) Advocate Graphite Bolts For Cylinder Spaceframe Interface which Are Commercially Available (K-Karb from Kaiser Aerotech)

Westinghouse
Science & Technology Center

1105

MODULAR STRAW TRACKER CDR

2.1 SPACEFRAMES

THE DESIGN USES:

1) Simple Spaceframe Which Utilizes Commercially Available Technology (Kaiser Aerotech)
   - o High Stiffness Graphite Fiber Struts
   - o Molded Graphite Joints
2) Assembled and Machined to Form a Precision Cylinder Interface
3) Kaiser Issued Written Estimate on Spaceframe Costs (11-04-91)

Westinghouse
Science & Technology Center

1103

SPACE FRAMES WITH CYLINDERS, RINGS AND MODULES

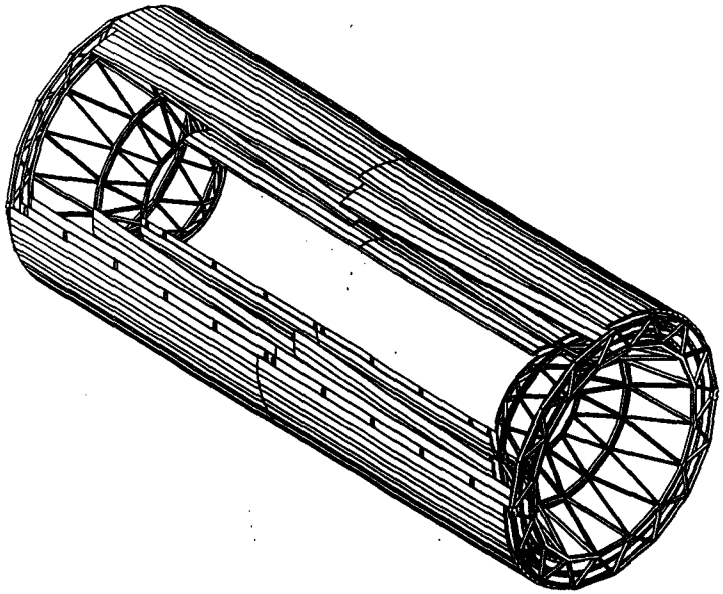

SUPPORT CYLINDER DIMENSIONS

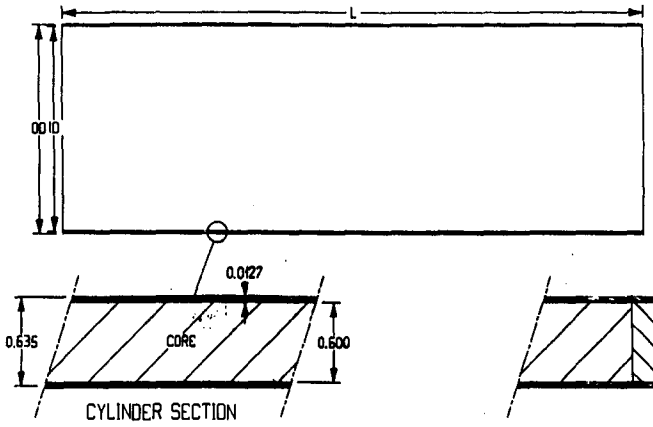

CYL	ID	OD	L
1	132.15	133.42	570
2	204.12	205.39	650
3	260.22	264.49	790
4	288.27	289.54	800
5	316.32	317.59	800

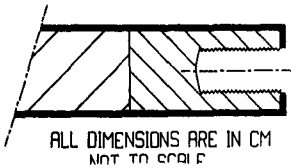

MODULAR STRAW TRACKER CDR

2.2 SUPPORT CYLINDERS (continued)

THE MANUFACTURING PROCESS USES:

1) B Staged Graphite Tape Layups with Rohacell Core
2) Steel Mandrels For Each Cylinder
3) Custom Machine Tool to Apply Tape
   - o Concept Drawing Is Made
   - o Specification Is Written
   - o Quotations Are Being Solicited

Viewgraph 12
RLS
11.06.91

Westinghouse
Science & Technology Center

SPACE FRAMES WITH CYLINDERS AND SHIM RINGS

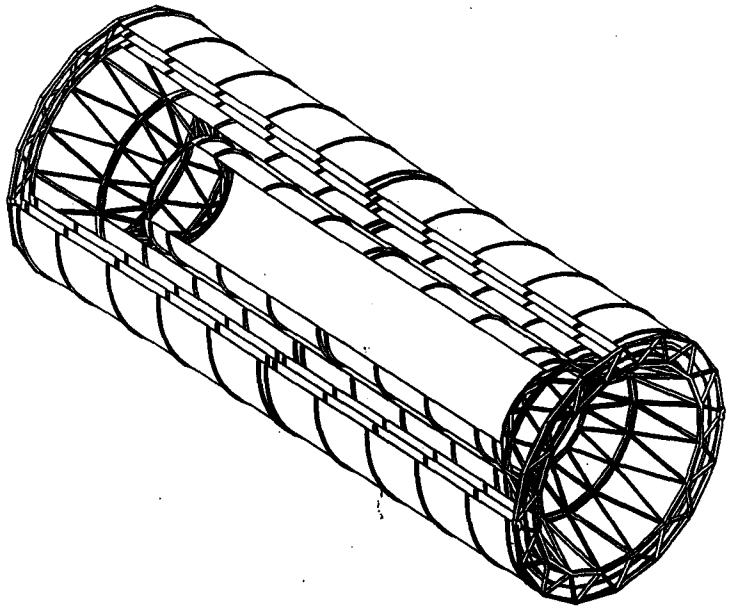

SYSTEM FOR MACHINING SHIM RINGS

1112

1110

CYLINDER SECTIONS WITH SHIM RINGS

1113

SUPPORT CYLINDER WITH SHIM RINGS

1111

WESTINGHOUSE STC

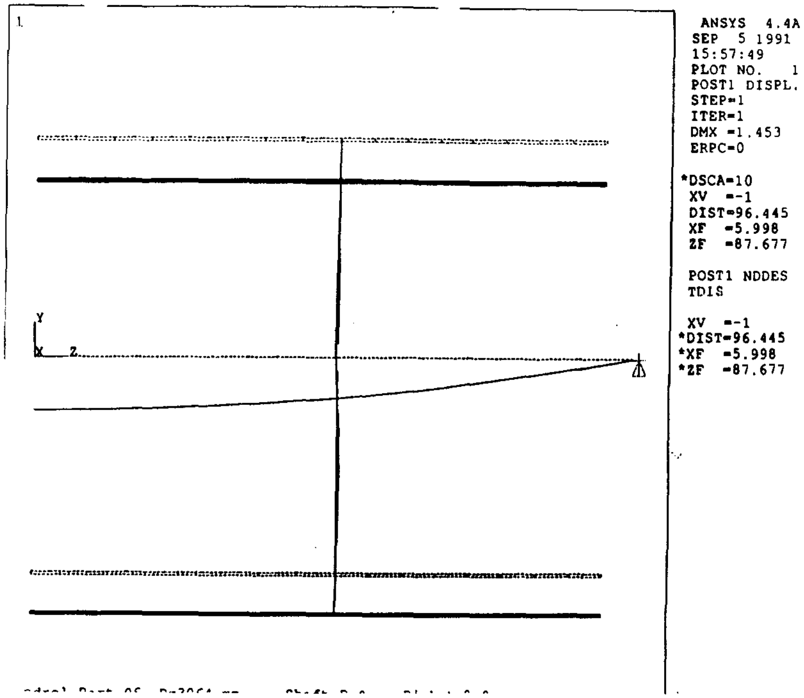

1116

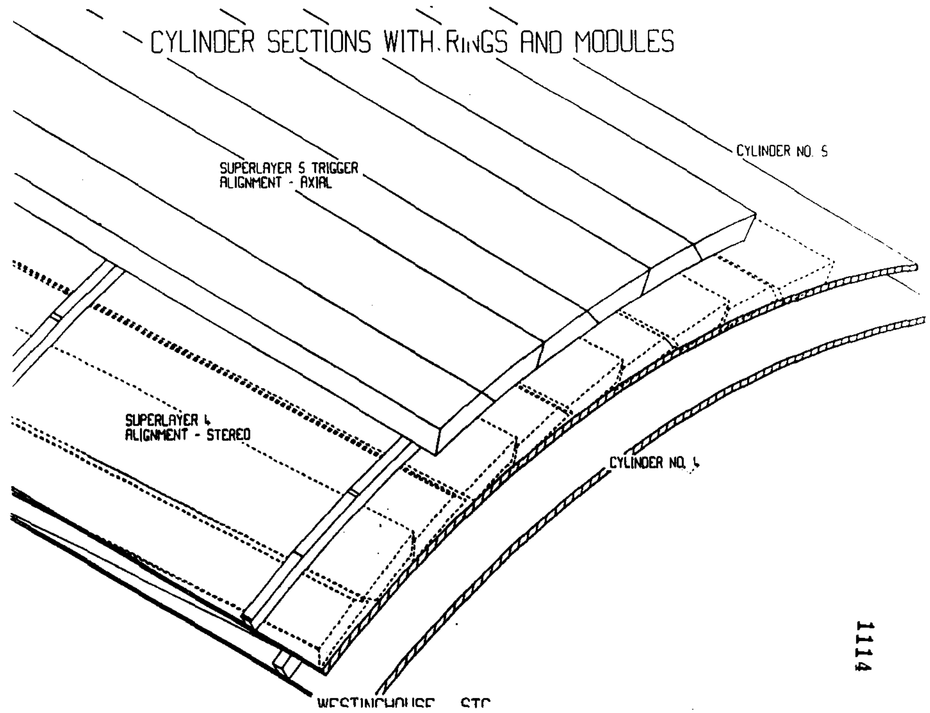

1114

CENTRAL AND FORWARD TRACKING SUBSYSTEM

7

MANDREL STRESSES & DISPLACEMENTS FROM FINITE ELEMENT ANALYSIS

Shaft Dia in.	Dsk Tk in.	Disk Nom. kips-in.	Disk Slope	Disk σ_θ ksi	Disk σ_r ksi	Place	Displacement Inches: Cyl End	Disk	Cyl Midpt	Local Max.	Local Min.
8.0	1.0	179.	0.0188	74.5	83.7	T/B	2.32452	2.32413	2.32464	2.3259	2.3226
						Side	2.32446	2.32441	2.32463		
						Shaft		2.32377			
8.9	2.9	642.	9.0092	67.9	75.1	T/B	1.61647	1.61856	1.61710	1.6196	1.6137
						Side	1.61642	1.81872	1.61715		
						Shaft		1.61634			
10.	1.0	93.	0.0091	34.1	38.2	T/B	1.11005	1.10961	1.11911	1.1107	1.088
						Side	1.11901	1.10988	1.11009		
						Shaft		1.10928			
10.	2.9	494.	0.0062	41.4	46.5	T/B	0.89374	0.89371	0.89422	9.8968	0.8916
						Side	0.89369	0.89388	9.89425		
						Shaft		0.88352			
12.0	1.9	63.	0.9051	17.8	18.8	T/B	0.60024	0.59978	0.60027	0.8005	8.5994
						Side	0.60020	0.69005	0.60024		
						Shaft		0.59948			

Viewgraph 22
RLS

Westinghouse Science & Technology Center

1117

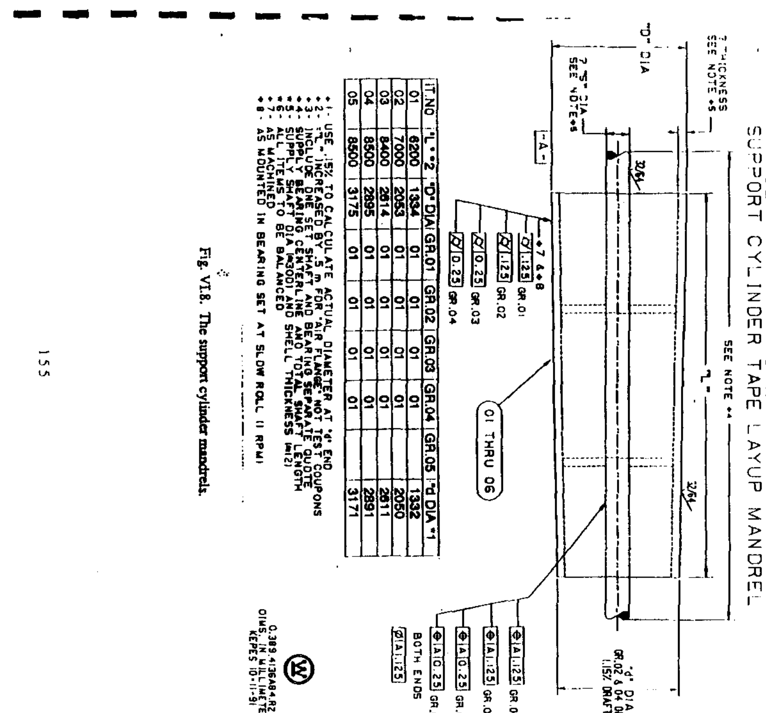

Fig. VI.8. The support cylinder mandrels.

155

1115

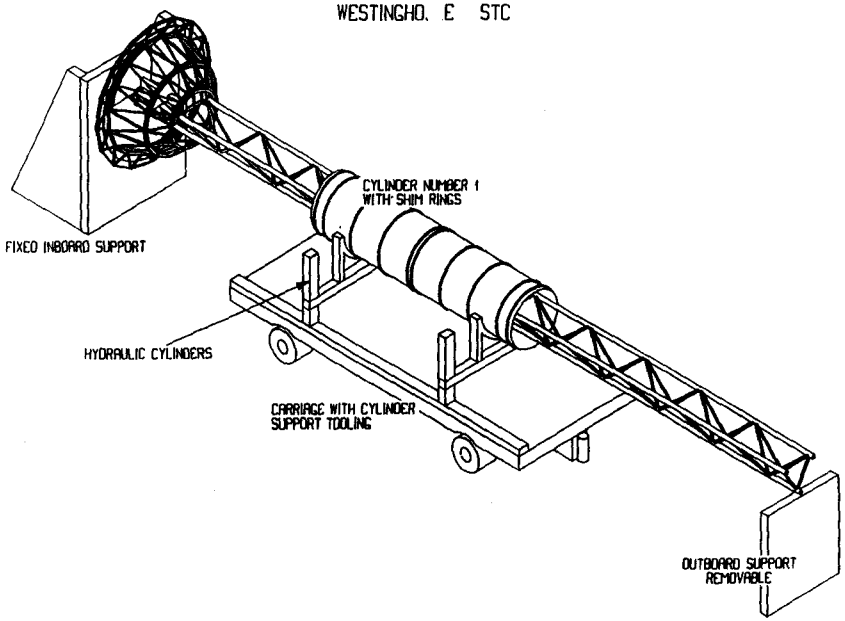

1120

FIGURE V.3.B INSTALLING SUPPORT CYLINDER 1

MODULAR STRAW TRACKER CDR

4. SPACEFRAME TO CYLINDER ASSEMBLY

THE ASSEMBLY PROCESS USES:

4.1 Cantilever Beam Main Assembly Tool With Two Movable End Supports

4.2 Spaceframe and Cylinder Components are Simply Shuttled into Position Assembly

4.3 Modules can be Placed on Each Support Cylinder Before or after Assembly to the Spaceframes Quality Assurance

4.4 Conventional Optical Laser Alignment System to Locate and Confirm Locations of Modules In Assembly

Viewgraph 19
RLS
11.09.95

Westinghouse
Science & Technology Center

1118

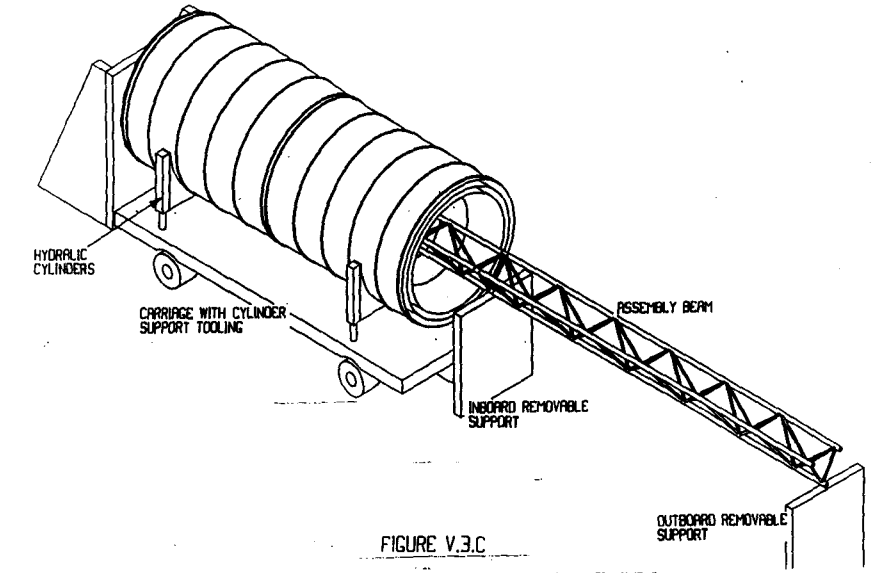

1121

FIGURE V.3.C

ASSEMBLING CYLINDER 5 TO THE SPACE FRAME

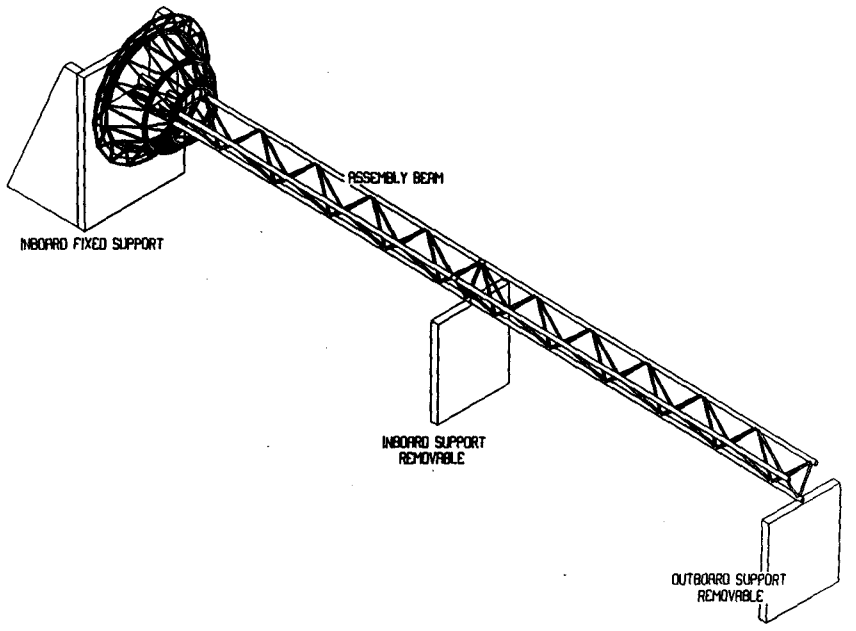

1119

FIGURE V.3.D SPACE FRAME ON ASSEMBLY FIXTURE

SPACE FRAME

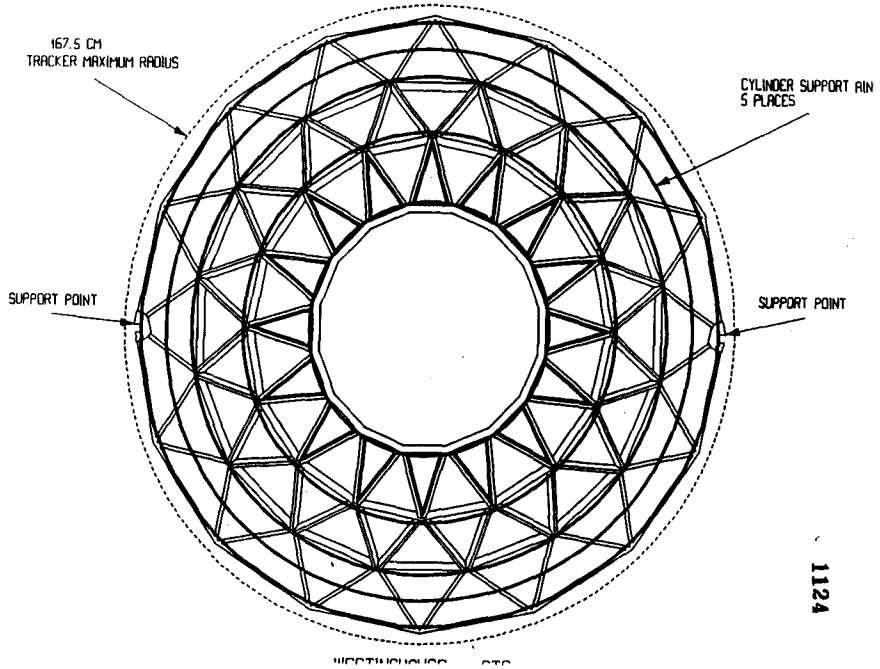

1124

WESTINGHOUSE STC

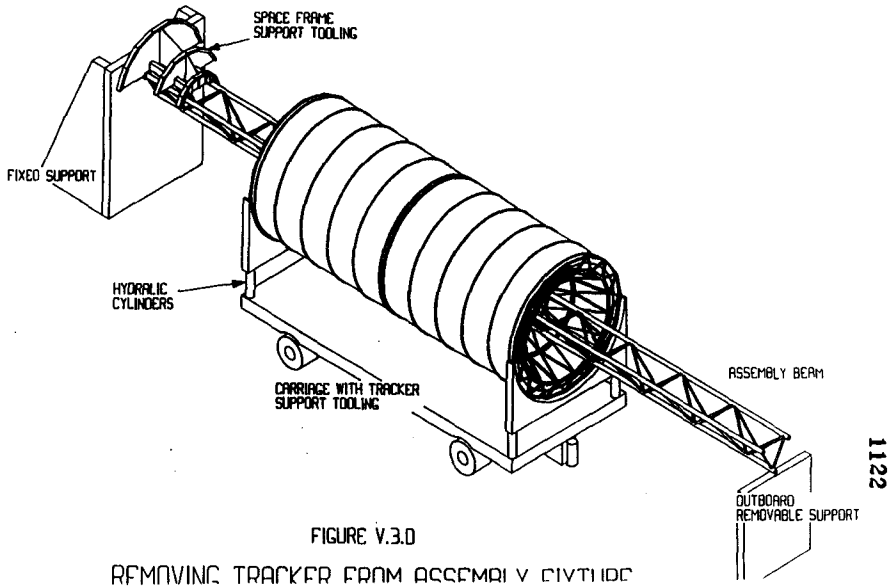

1122

FIGURE V.3.0

REMOVING TRACKER FROM ASSEMBLY CYLINDER

MODULAR STRAW TRACKER CDR

2.5 MODULE ATTACHMENTS

THE DESIGN USES:

1) **Mechanical Attachments Selected to Attach Modules Directly to Shim Rings**
2) **Uses Precision Machined Higher Density 300 WF Rohacell Block Inserts as a Load Bearing Interface**
3) **Locations are Machined Directly into Shim Rings**
4) **Replacement of Modules After Assembly is Feasible**
5) **Attachment Process is Being Worked on- Needs More Engineering**

1125

Viewgraph 18
RLS
11.99.91

Westinghouse
Science & Technology Center

SPACE FRAMES WITH CYLINDERS AND SHIM RINGS

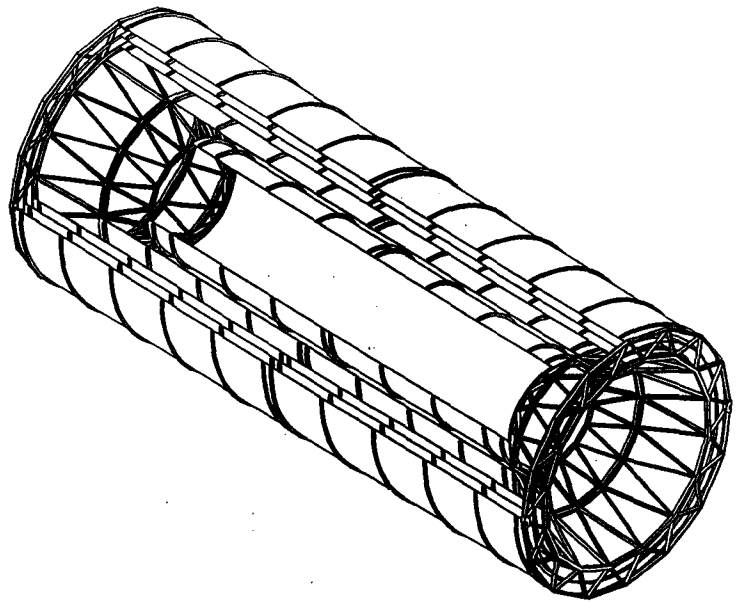

1123

SPACE FRAMES WITH CYLINDERS, RINGS AND MODULES

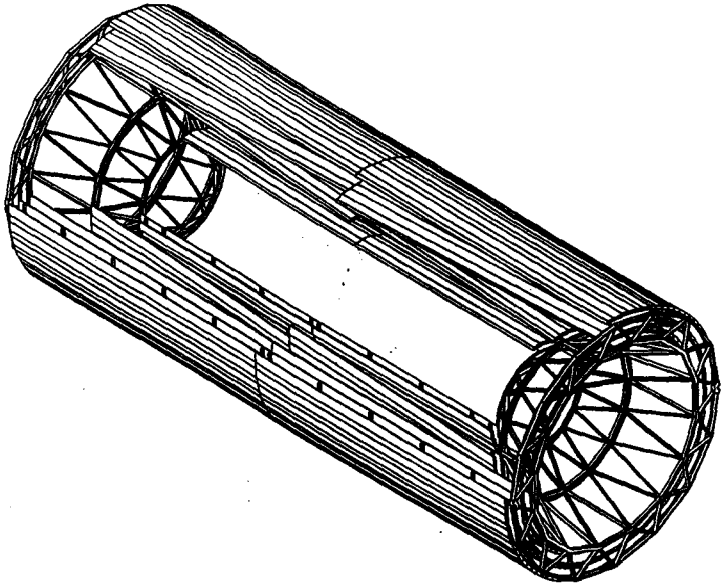

1128

MODULE POSITIONING

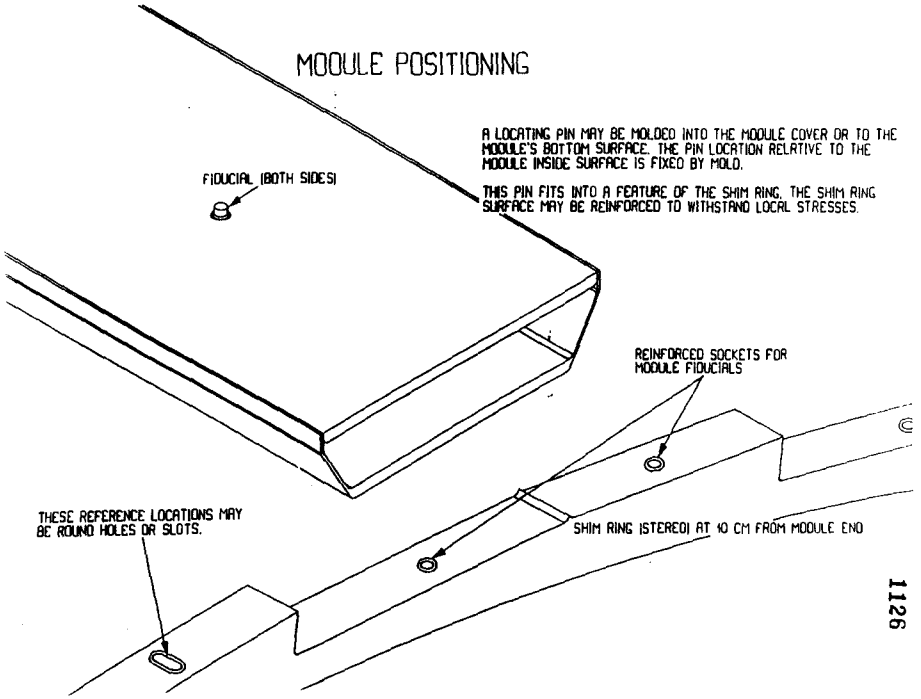

1126

CENTRAL TRACKER KINEMATIC MOUNTS

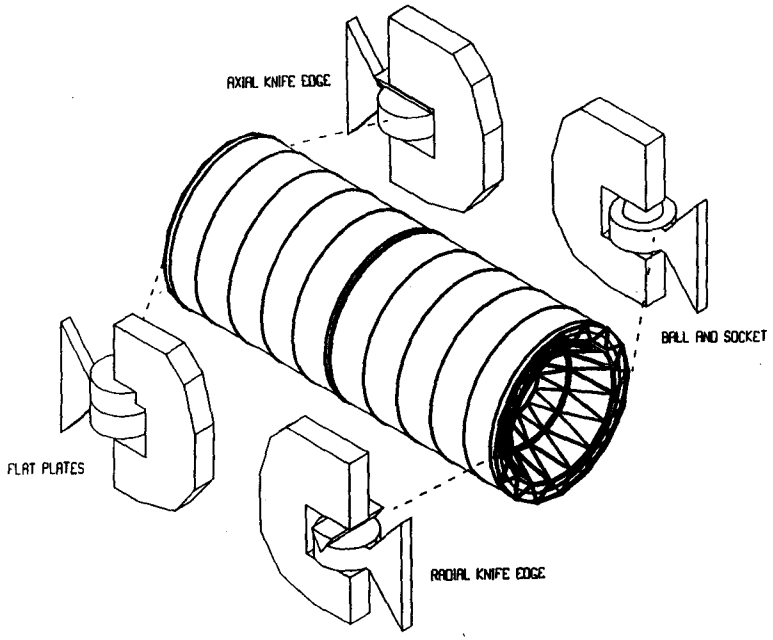

1129

MODULE ATTACHMENT

MECHANICAL ATTACHMENT

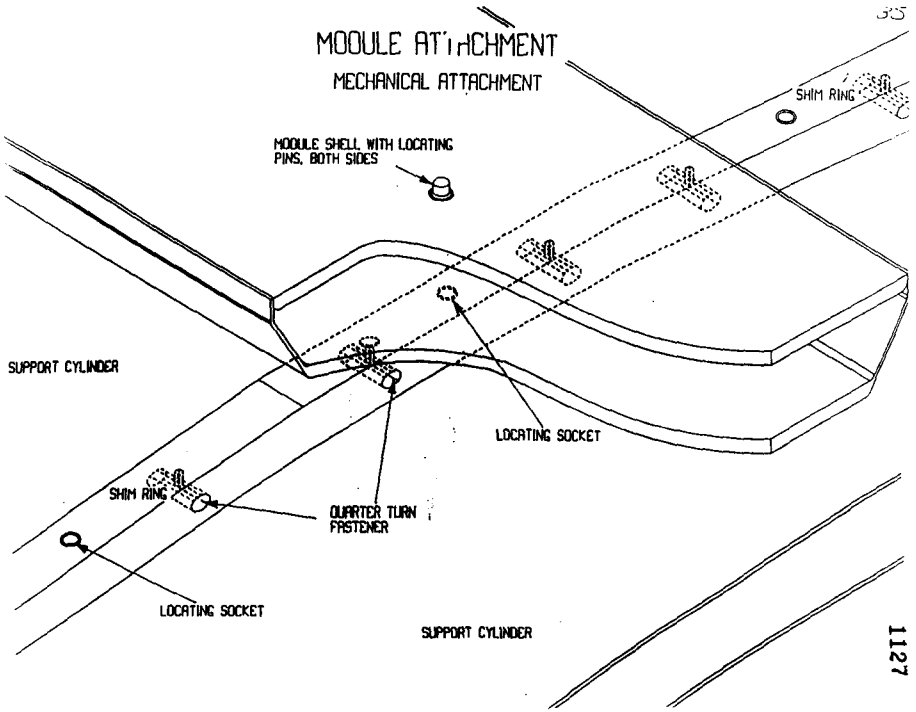

1127

COMPOSITE TABLES

TABLE VI.1.D
SUBJECT: COMPOSITE VARIATION ESTIMATE, [0 +/-60]SYM
MATERIAL: (P75/ERL 1939-3) ASSUMPTION: LOW STRAIN APPLICATION

Modulus	Low Material				High Material				Mean Material
Wrap Angles	[0 +/-55]		[0 +/-65]		[0 +/-55]		[0 +/-65]		[0 +/-60]
Moisture****	0%	0.2%	0%	0.2%	0%	0.2%	0%	0.2%	0%	0.2%
Column Number	1	2	3	4	5	6	7	8	9	10
EX, MSI	11.900	11.800	11.700	11.600	16.900	16.800	16.600	16.500	14.700	14.600
EY, MSI	9.020	8.970	14.600	14.588	12.800	12.700	20.800	20.700	14.700	14.600
EZ, MSI	0.924	0.900	0.897	0.874	1.060	1.030	1.030	1.000	0.982	0.957
GXY, MSI	5.170	5.140	3.628	3.590	7.320	7.270	5.100	5.060	5.570	5.530
GYZ, MSI	0.421	0.421	0.444	0.423	0.513	0.513	0.546	0.546	0.498	0.498
GXZ, MSI	0.446	0.446	0.423	0.409	0.548	0.548	0.515	0.515	0.499	0.499
MUXY	0.451	0.451	0.211	0.211	0.461	0.461	0.216	0.216	0.318	0.318
MUYX	0.342	0.342	0.263	0.263	0.348	0.349	0.271	0.271	0.318	0.318
MUYZ	0.201	0.201	0.221	0.221	0.266	0.266	0.328	0.328	0.232	0.231
MUZY	0.021	0.020	0.014	0.013	0.022	0.022	0.016	0.016	0.016	0.015
MUXZ	0.163	0.163	0.241	0.241	0.249	0.249	0.326	0.326	0.232	0.231
MUZX	0.013	0.012	0.018	0.018	0.016	0.015	0.020	0.020	0.016	0.015
ALPHA-X*	-0.182	-0.189	0.149	0.135	-0.337	-0.343	-0.100	-0.111	-0.155	-0.164
ALPHA-Y	0.234	0.219	-0.115	-0.123	-0.039	-0.051	-0.286	-0.296	-0.155	-0.164
ALPHA-Z	22.980	22.900	22.900	22.900	20.000	20.100	20.100	20.100	20.50	20.600

CME*** E-6/% Moisture Absorbed — 118.000
CME** E-6/% Relative Humidity — 0.397

* E-6/oF **Calculated (118E-6*0.195/55)
*** For P75/ 954-3 , 0.195% Moisture Absorpted @ 55% R.H.@RmTemp/Fiberite
**** Moisture - Hygrothermal Effect Estimate

Viewgraph 3
RLS
10 31 91

Westinghouse
Science & Technology Center

1132

MATERIAL AVAILABLE

MATERIAL		Elastic Modulus E-Msi	Density ρ (lb/in³)	CTE α ppm/F	Tensile Ultimate Strength Ksi	Compressive Strength Ksi	Volume Change 50% Humidity Percent	Effective Radiation Length l-cm
MATERIAL CANDIDATES								
Graphite & Resin**	X(Zero)	14.70	0.0600	-0.16	49.7	22.7	0.006***	25.7
	Y(90 Deg)	14.70			73.0	33.8		
	Shear	5.57			20.0			
Carbon-Carbon**		16.00	0.0600	-0.11	48.0	48.0	0.0	18.8
Al-MMC sub f*		53.07	0.0987	0.60	100.0	40.0	0.0	11.8
Al-MMC sub p****		15.07	0.1000	5.00	75.8	75.0	0.0	9.0
Rohacell 31 Ig		0.005	0.0012	2.05	0.142	0.057	0.2	936.6
51 WF		0.011	0.0010	1.83	0.232	0.116	0.2	576.4
300 WF		0.052	0.0109	?	1.450	2.320	0.2	99.9
REFERENCE MATERIALS								
Aluminum		10.40	0.1012	12.90	75.0	40.9	0.0	8.9
Beryllium		42.05	0.0665	6.44	40.0	27.0	0.0	35.4
Copper		16.00	0.3210	9.39	10.0	10.0	0.0	0.0

*Graphite Fiber (P-120) MMC-Metal Matrix Composite, uni-directional properties
**[0 +/-60]sym Composite Properties
***CME of 0.397 in/in/%R.H.@R.T.
****Particle Reinforced MMC-Metal Matrix Composite, machinable, brazable

Viewgraph 1
RLS
11.09.91

Westinghouse
Science & Technology Center

1130

MODULAR STRAW TRACKER CDR

6. SUPPORT STRUCTURE ANALYSIS
6.1 THE FINITE ELEMENT MODEL

THE MODEL USED:

1. **Spaceframe Beam and Cylinder Layered Shell Elements Used**
2. **Quarter Model Symmetry Used**

Viewgraph 20
RLS
11.09.91

Westinghouse
Science & Technology Center

1133

COMPOSITE TABLES

TABLE VI.1.C
SUBJECT: NEAT RESIN PROPERTIES
DATA IS SOURCE SUPPLIED

Resin	ERL-1962	ERL-1939-3	HX 1553	954 - 3	934	3501-6	R500
Source	Amoco	Amoco	Hexcel	Fiberite	Fiberite	Hercules	3M
TYPE	Epoxy	?	Epoxy Cyanate	Cyanate Ester	Epoxy	Epoxy	Epoxy
Tensile Stress, Ksi	10	11	12	9.4	7.10	10	8.3
Tensile Modulus, Ksi	0.540	0.480		0.44	0.6	0.643	0.507
Tensile Strain, %	2.1	3		2.5	1	1.7	1.9
Water Absorption, %	3.4	2	2	0.95	4.6	1.2	1.56
Conditions	a	a		b	b	c	d
Density, lbm/in³	0.046	0.045	0.046	0.043	0.047	0.046	0.045
CTE, in/in/F	3.6e-05		3.58e-05			2.43e-05	
Cure Temperature	350	350	350	350	350		350

CONDITIONS
a. 2 weeks soak @ 160°F
b. 48 hrs @ boil
c. 24 hrs @ boil
d. 100% RH/88°C to equilibrium

Viewgraph 2
RLS
10.31.91

Westinghouse
Science & Technology Center

1131

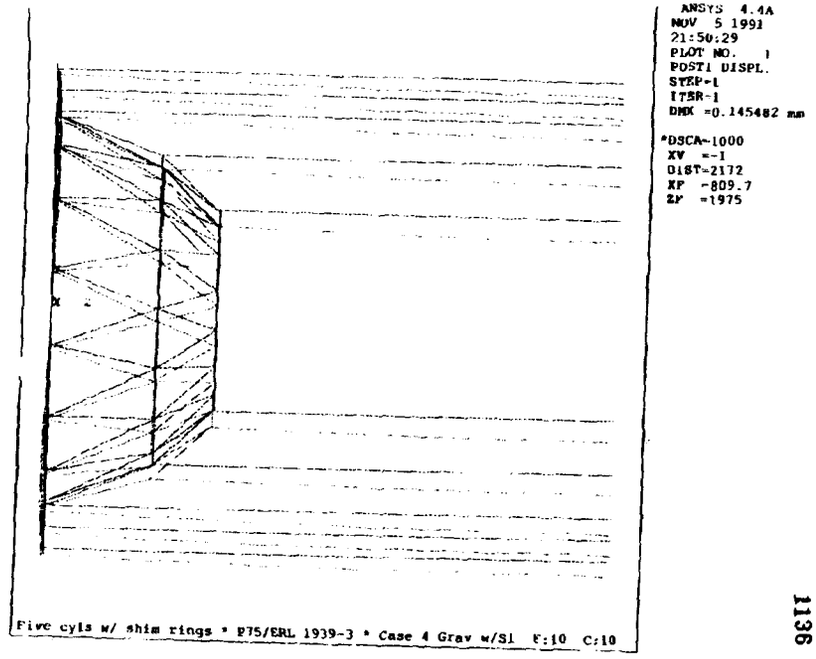

1136

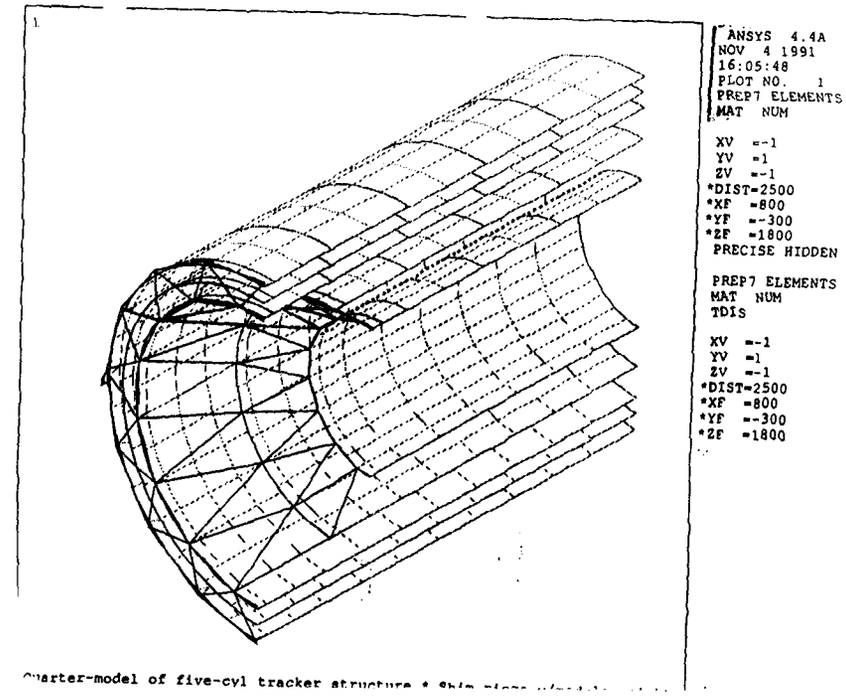

Quarter-model of five-cyl tracker structure * shim rings

1134

TRACKER SUPPORT CYLINDERS CENTERLINE DEFLECTIONS (microns)

Case 4 -- Silicon Weight Included

Cylinder No. Radius (m)	Frame-End Deflection	Midpoint Deflection	Relative Sag
5 1.5848	24	79	55
4 1.4445	31	102	71
3 1.3043	27	122	96
2 1.0238	87.5	137.5	50
1 0.6639	108	145	39

1137

MODULAR STRAW TRACKER CDR

6. SUPPORT STRUCTURE ANALYSIS CONTINUED

6.2 THE MATERIAL VARIATION SENSITIVITY ANALYSIS

THE ANALYSIS PROCESS USED:

1. Property Matrix of Highest and Lowest Values
   - o Modulus, CTE, and CME
   - o One G Gravity
   - o Thermal Delta of 30 Degrees Fahrenheit.

DEFLECTIONS CAN BE REDUCED BY:

1. Spaceframe and Cylinder Act Like Springs in Series
   - o Spaceframe Tube Wall Thickness can be Increased

THE RESULTS ARE:

1. Deflections and Loads or Forces are Small
2. Gravity Produces Largest Deflections
3. Axial Thermal Miss Match of Cylinders Produce Largest Loads.

Viewgraph 27
RLS
11/09/91

Westinghouse Science & Technology Center

1135

ANALYSIS TABLES

TABLE VI.4.B
SUBJECT: SENSITIVITY ANALYSIS
MATERIAL PROPERTIES AND LOAD CASE DEFINITION
RESULTS FROM FEA ANALYSIS (REVISED 11-11-91)

Case #	Type	Material Properties • Spaceframe		• Cylinders		Deflections Microns Radial	Deflections Microns Axial	Forces Lb./in. Radial	Forces Lb./in. A-A
	Gravity								
1	Vertical	5	High-Modulus	5	High-Modulus	98.7	N/A	N/A	+/-2.6
2	Vertical	4	Low-Modulus	4	Low-Modulus	131.8	N/A	N/A	+/-2.6
3	Vertical	10	Mean-Modulus	10	Mean-Modulus	116.5	N/A	N/A	+/-2.6
4	With Silicon	10	Mean-Modulus	10	Mean-Modulus	145.5	N/A	N/A	+/-3.2
	Thermal								
5	Radial	3	High-CTE	8	Low-CTE	-15.8	+15.3	-0.1	-0.4
6	Axial	3	High-CTE	6	Low-CTE	+7.6	+42.2	0.0	-0.7
7	Radial	6	Low-CTE	1	High-CTE	-15.9	+24.3	+0.1	+0.2
8	Axial	6	Low-CTE	3	High-CTE	-16.7	-20.2	0.0	+0.6
11	Axial	3	High-CTE	3	High-1,2,3,5	-8.1	+15.2	0.0	+2.0
				6	Low-4 ONLY				
	Humidity								
9	50%	10	Mean-Modulus	10	Mean-Modulus	+32.1	-79.1	0.0	+0.0
10	25%	10	Mean-Modulus	10	Mean-Modulus	+16.0	-39.0	0.0	+0.0

• Column Number From Table Number VI.1.D titled" Composite Variation" Refers to the Set of Material Properties Used in the Particular Case #

Viewgraph 1
RL1
10.31.91

Westinghouse Science & Technology Center

Module Alignment on support cylinder.

- Alignment points are at 80 cm wire support points
- Placement precision of 50 microns required

This will require more engineering, but it doesn't look impossible

- Module straightness of 50 microns required.

This will require detailed study of 4 meter module, measurements on 1 meter module are encouraging.

Finite element analysis will determine whether the system is stable within the required tolerances of:

Rotational stability 10-5 radians

displacement centroids 15 microns

Material in modules

The material in the tracker is mainly at smaller radii.

Effects of material:

- **Electron/ photon ID problems due to electon bremsstrahlung**
- **Electron trigger inefficiency due to electron bremsstrahlung.**
- **photons conversions confuse track finding and cause higher trigger rates**

Detail of material in the straw tracker

straws and supports (double v's) = 0.32 % radiation length
shell =0.23%
cylinder =0.25%

total 0.8%
(0.77% UV,0.84% trig)

(Material considerations)

Module endplates

A) Electronics end:

Plan on about 2% of a radiation length for normal incidence. Expect that PC boards will add about another 3-5 % (with capacitors-8%)

B) Z=0 end, no electronics

- The goal is to keep the dead space to about 1 cm at the end of each module.
- Dead area is only about 1/400 of tracker
- Total material in the last 1 cm of each module will cause 0.02 photon conversions each crossing.
- **Compare this to 0.4 photon conversions in the 6 layer straw system each crossing. Therefore the end effect is very small.**

RESULTS SUMMARY

TABLE NUMBER 1
SUMMARY TABLE OF RADIATION LENGTH CALCULATIONS

TABLE #	SUPPORT CYLINDER GRAPHITE TK/LAYER INCHES	SUPPORT CYLINDER FOAM TYPE	SUPPORT CYLINDER FOAM TK INCHES	SHIM RING EFFECTS	MODULES GRAPHITE TK/LAYER INCHES	MODULES FOAM TYPE	MODULES FOAM TK INCHES	MODULE EDGE EFFECTS	PERCENT RADITION LEN/LAYR CM
2	0.0045	31IG	1	NO	0.006	51WF	0.14	NO	0.87
2	0.0045	51WF	1	NO	0.006	51WF	0.14	NO	1.04
4	0.0045	31IG	1	NO	0.0045	51WF	0.14	NO	0.93
5	0.0045	31IG	1	NO	0.0045	31IG	0.14	NO	0.88
6	0.0045	31IG	0.59	NO	0.0045	51WF	0.14	NO	0.83
7	0.0045	31IG	0.59	NO	0.0045	31IG	0.14	NO	0.78
3	0.006	31IG	0.23	NO	0.0045	31IG	0.14	NO	0.71
12	0.006	31IG	0.47	NO	0.0045	31IG	0.14	NO	0.77
11	0.009	31IG	0.23	NO	0.0045	31IG	0.14	NO	0.77
8	0.009	31IG	0.23	NO	0.0045	31IG	0.14	YES	0.79
9	0.009	31IG	0.23	YES	0.0045	31IG	0.14	YES	0.80
9 (SAME AS ABOVE EXCEPT EDA = 1.63)									2.11
10 (SPACEFRAME END DISK SPREAD RADIATION LENGTH CALCULATION)									0.21
0.21 RAD LG IS EQUIVALANT TO 0.007 Inch Thick Aluminum Sheet)									
0.021 Inch Thick Graphite Sheet)									

Page 8

TABLE NUMBER 10
CENTRAL TRACKER
SUMMARY RADIATION LENGTH
SPACEFRAME EFFECTS
(Hollow Graphite Struts Form the Spaceframe End Disks)
(Silicon Carbide Joints Connect the Struts)
(Thin Graphite Rings Attach the Cylinders to the Spaceframe)
Table Number 10A
SURFACE AREA CALCULATIONS
(For Thickness and Rad Lg Calc See Table 5A Above)

SUPERLAYCOMPONENT NUMBER	QUANITY #	AZIMUTHAL WIDTH INCHES	RADIAL LENGTH INCHES	DISK AREA TOTAL SQ IN	COMPONE TOTAL SQ IN	PERCENT COMPONE COVERS
5 TO 4 STRUTS	16	0.79	5.51	2126.96	69.82	3.273
JOINTS	16	1.57	1.57	2126.96	39.58	1.866
RINGS	1	N/A	0.59	2126.96	236.12	11.105
4 TO 3 STRUTS	16	0.79	5.51	1906.10	69.82	3.596
JOINTS	16	1.57	1.57	1906.10	39.58	2.049
RINGS	1	N/A	0.59	1906.10	217.96	11.242
3 TO 2 STRUTS	16	0.79	11.02	3299.55	139.53	4.229
JOINTS	16	1.57	1.57	3299.55	39.58	1.200
RINGS	1	N/A	0.59	3299.55	197.21	5.977
2 TO 1 STRUTS	16	0.79	14.17	3120.35	179.01	5.737
JOINTS	16	1.57	1.57	3120.35	39.58	1.272
RINGS	1	N/A	0.59	3120.35	196.51	6.299
AVERAGE PERCENT OF AREA STRUT COVERS						4.81
AVERAGE PERCENT OF AREA JOINT COVERS						1.711
AVERAGE PERCENT OF AREA RING(CYLINDER END) COVERS						6.58

Table Number 10B
EFFECTIVE OR SPREAD RAD LG CALCULATIONS
(For Thickness and Rad Lg Calc See Table 5A Above)
(For Area Calc See Table 10A Above)

ITEM	LOCAL RAD LG	PERCENT AREA COVERED	SPREAD RAD LG
Strut	1.3444	4.81	0.0647
Joint	0.3965	1.711	0.0068
Ring	0.972	6.58	0.061
Average Per End Or Equal To			0.21

0.007 Inch Thick Aluminum Sheet
0.021 Inch Thick Graphite Sheet

Page 19

COST and SCHEDULE

Cost: 32M + 17M electronics

Schedule:Ready at end of 1998

TABLE NUMBER 2 — 11-06-91
FUNCTIONAL COST BREAKDOWN FOR MODULAR STRAW CENTRAL TRACKER

		K$ w/cont	K$ wo/cont
A1	SHELLS		
	DESIGN	322	241
	PROCURE	2511	1874
	FABRICATE	526	393
	TOOLING	1079	863
B1	CYLINDERS		
	DESIGN	226	184
	PROCURE	5474	4450
	FABRICATE	85	69
	TOOLING	2602	1923
	ALIGNMENT	312	254
C1	STRAWS		
	DESIGN	185	161
	PROCURE	1912	1670
	FABRICATE	598	519
	TOOLING	525	423
D1	SUPPORT STRUCTURE		
	DESIGN	178	267
	PROCURE	2809	2108
	FABRICATE	340	267
	TOOLING	70	55
E1	ASMB MODULES		
	DESIGN	774	680
	PROCURE	104	89
	FABRICATE	1504	1315
	TOOLING	792	635
E2	FACILITIES MODULES		
	DESIGN	21	17
	PROCURE	384	315
	FABRICATE	839	688
	TOOLING	0	8
F1	INSTALL MODULES		
	DESIGN	151	120
	PROCURE	11	10
	FABRICATE	497	395
	TOOLING	136	112
G1	ASSEMBLE STRUCTURE	173	142
	DESIGN	59	45
	PROCURE	278	228
	FABRICATE	691	540
	TOOLING		
G2	FACILITIES STRUCTURE	78	71
	DESIGN	59	54
	PROCURE	0	0
	FABRICATE	0	0
	TOOLING		
H1	SHIP AND TEST	23	16
	DESIGN	25	18
	PROCURE	19	13
	FABRICATE	1224	967
	TOOLING		
I1	INSTALLATION	133	90
	DESIGN	703	475
	PROCURE	42	28
	FABRICATE	794	597
	TOOLING		
J1	PROGRAM MANAGEMENT	2306	1994
	DESIGN	981	795
	PROCURE	441	371
	FABRICATE	0	0
	TOOLING		
K1	R & D EFFORTS	85	68
	DESIGN	88	68
	PROCURE	201	156
	FABRICATE	0	0
	TOOLING		
L1	DRIFT GAS SYSTEM	14	12
	DESIGN	372	312
	PROCURE	811	688
	FABRICATE	0	0
	TOOLING	34	28
TOTAL			

193

TABLE NUMBER 1 11-08-81

DATA SHEET FOR FUNCTIONAL COST BREAKDOWN FOR MODULAR STRAW TRACKER

TITLE	DOS	OD	EN	ENM	EA	EAM	DR	DRM	TE	TEM	LA	LAM	EXP	KS MINOR	KS MAJOR	EDIAS	EDIA+CS	MFAIS	MFAL+CS	IMATS	IMAS+CS	BASES	BAS+CS
TRIGGER STRAW TOTALS			131	0	0	0	60	0	0	140	0	0	0	202	394	79091	92176	210153	240003	875500	774445	971544	1116726
TRIGGER SHELL TOTALS			124	0	80	0	126	0	0	000	0	0	0	114	005	110284	150474	177020	230200	953750	1270025	1249842	1674790
TRIGGER ASSEMBLY TOTALS			20	0	300	0	20	0	0	2200	0	0	0	40	0	141020	102140	002250	700125	40000	39185	453070	981456
AXIAL & STEREO STRAWS TOTAL			110	0	42	0	45	0	0	1937	0	0	0	170	350	00010	02000	302000	340274	004367	1137197	1377846	1570472
AXIAL & STEREO SHELLS TOTAL			96	6	150	0	90	0	0	730	0	0	9	70	050	122250	163023	214912	207002	820000	1232800	1257164	1404603
AXIAL & STEREO ASSEMBLIES TOTAL			350	0	1140	0	20	0	0	2231	[illegible]	0	0	46	0	530350	611653	853222	742731	30007	44481	1231440	1400766
CYLINDERS			100	80	26	0	302	30	50	50	0	0	0	0	4450	163778	220044	09210	63120	4450000	54..00	4702900	5784073
SHIM RINGS			20	54	50	0	30	5	00	191	0	0	0	6	0	39309	40019	102147	120002	0000	0920	149516	165403
SPACEFRAME			8	10	20	0	16	1	10	45	0	0	0	0	1000	13430	16520	22039	20092	1000000	2337000	1530277	2381621
ASSEMBLY & MACHINING			134	110	1	0	50	25	00	206	0	0	0	5	0	70349	00101	140165	161224	5000	5750	223544	257074
MODULE INSTALATION			175	123	1	0	120	30	200	020	0	0	0	10	0	120000	150023	394001	407303	10000	10900	374601	650002
MOUNTS			07	05	7	0	00	21	0	71	0	0	0	135	5	60302	67520	40400	69033	173000	160000	233070	290065
FINAL ASSEMBLY			93	40	5	0	100	35	37	100	0	0	0	40	0	93100	03302	00230	110474	40000	52000	101400	252059
STRAW TOOLING			224	24	24	24	400	52	0	10	0	0	0	20	120	241004	200010	42100	52315	140000	173000	423252	524830
SHELL TOOLING			203	52	64	30	420	50	42	76	0	0	0	353	135	207703	350003	67220	100071	400000	611040	002000	1078007
MODULE ASSEMBLY TOOLING			00	30	5	20	190	17	00	46	0	0	0	02	300	74003	93103	00030	07013	400000	011040	034631	751834
MANDRELS			40	15	5	0	5	0	25	0	0	0	5	50	1500	21090	20400	14215	16332	1501000	2122060	1590905	2171790
TAPING MACHINE			34	11	12	0	45	0	23	23	0	0	0	90	201	30100	45143	20453	20000	271000	357720	325052	429061
SUPPORT STRONGBACK			12	0	2	0	74	4	2	4	0	0	0	35	0	13902	10701	1004	2212	25000	20000	40000	40714
SUPPORT ALIGN TOOL			20	5	5	7	0	0	30	23	0	0	0	90	170	14533	12440	22302	20076	103000	231000	220025	275000
MACHINING STATION			30	12	12	0	40	0	74	24	0	0	0	10	207	30000	40203	21400	22517	307000	392000	384594	460600
S/L ASMB TOOLING			10	0	1	0	20	4	6	0	0	0	0	45	50	15076	20325	1300	9004	95000	121000	112179	130062
FINAL ASMB TOOLING			15	0	0	30	3	0	0	0	0	0	0	37	6	7000	10000	9750	12400	37000	47360	54040	99830
TRANSPORT TOOLING			30	0	3	0	60	0	10	0	0	0	6	30	100	34305	43010	5043	2481 0	135000	172000	173150	224193
ERECTION TOOLING			45	0	2	0	90	11	10	0	0	0	0	45	100	50049	07200	0405	0070 0	145000	107000	202140	263767
TEST EQUIPMENT			72	22	0	30	0	0	0	56	0	0	6	02	379	33102	42003	30046	00373 0	437000	570400	508741	669730
TRACKER UTILITIES			309	0	10	7	465	56	10	505	0	0	6	237	0	304024	303002	102533	230257	237000	297760	724159	911717
TESTING FUNCTION			70	5	0	0	20	3	0	330	0	0	6	0	75	10400	24004	101302	132000	25000	162000	184878	259853
FINAL ALIGNMENT WORK			17	5	2	4	24	4	10	10	0	0	3	15	0	10707	22030	13001	10220.1	10000	25020	47364	66734
TRACKER TRANSPORTATION SYSTEM TOT			15	9	0	0	20	3	0	0	0	0	0	40	0	13415	10054	975	1443	10000	11800	24390	36097
ERECTION SSCL			61	41	0	0	33	10	5	00	0	0	0	0	0	50040	54304	40001	00047 4	0	0	00737	124231
DRIFT GAS SYSTEM			104	10	50	0	20	10	5	55	0	0	0	115	300	00000	933006	20305	41001 4	475000	703000	583174	477889
MODULE FACILITIES			0	250	0	0	10	378	0	750	0	0	0	40	275	11040	14100	007600	011390	515000	371700	1614548	1157147
SUPPORT FACILITIES			15	750	0	0	20	379	0	750	0	0	6	0	315	17045	20702	007925	030200	315000	384300	1018964	1244361
COST & SCHEDULE			154	0	0	0	0	0	0	0	0	0	54	0	0	70004	20003	0	0	34000	39400	124994	137488
TECHNICAL MGR			2300	300	075	0	630	0	6	0	0	0	325	0	0	2E+06	2E+06	230500	255055	325000	360750	2104925	2336466
R & D EFFORTS			400	0	0	0	000	0	400	0	0	0	40	00	350	144400	500004	140160	105011	070000	020460	1054566	1302020
INSTALLATION & TEST			87	110	2	5	71	32	89	206	0	25	87.5	0	0	93032	04795	150024	201396	67500	00325	282356	374510
																						27713700	34366170

1146

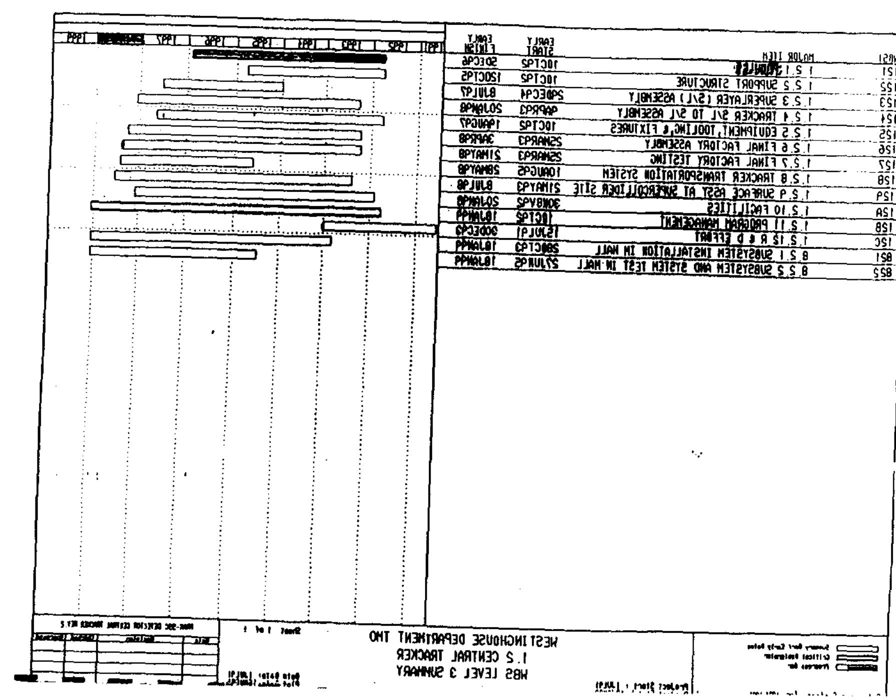

1147

Conceptual Design Scintillating Fiber Outer Tracking

D. Koltick(Purdue)

Conceptual Design
Scintillating Fiber Outer Tracking

Fiber Tracking Group (FTG)

B.Abbot[k], D.Adams[l], M.Adams[c], E.Anderson[m], T.Armstrong[i], M.Atac[a,b], A.Baumbaugh[b], B.Baumbaugh[g], M.Binkley[b], F.Bird[n], J.Bishop[g], N.Biswas[g], A.D.Bross[b], C.Buchanan[a], N.Cason[g], R.Chaney[o], D.Chrisman[a], D.Cline[a], C. Collins[n], M.Corcoran[i], R.Davies[k], J.Elias[b], G. Eppley[i], E.Fenyves[o], D.Finley[b], G.W.Foster[b], R. Fox[n], H.Goldberg[c], H.Hammack[o], A.Haran[i], S.Heppelmann[i], K.Hess[n], J. Hylen[b], J.Jaques[g], J.Kauffmani, R.Kehoe[g], C.Kelley[c], M. Kelly[g], V.Kenney[g], R.Kephart[b], D.Koltick[k], J.Kolonko[a], K.Kondo[p], J.Kubic[a], I.Leedom[f], R.A.Lewis[i], R.Leitch[h], C.Lirakis[f], J.LoSecco[g], B.Lowery[o], J.Marchant[g], R.McCutcheon[m], R.McIlwain[k], S.Margulies[c], H.Mendez[c], F.Mierc[d], H.Miettenen[i], R.Moore[i], R.J.Mountains[g], R.Nelson[b], B.Obi[i], T.Okusawa[f], J.Orgeron[o], H.Paik[d], J.Park[a], J.Passaneau[i], K.Pennington[n], M.Petroff[m], J. Piles[n], A.Pla-Dalmau[b], S.Reucroft[f], C.Rivetta[b], R.Ruchti[g], R.Scalise[i], J.Schmitz[k], W.Shephard[g], E.Shibata[k], J.Skeens[i], G.A.Smith[i], J.Solomon[c], K.Takikawa[p], T.Thurston[n], S.Tkaczyk[b], W.Toothacker[i], Balamurali V[g], D.Vandergriff[h], K.Vasavada[d], R.Wagner[b], J.Warchol[g], M.Wayne[g], J.Whitmore[i], and T.Yasuda[f]

University of California at Los Angeles[a]
Fermi National Accelerator Laboratory[b]
University of Illinois at Chicago[c]
Indiana University - Purdue University at Indianapolis[d]
Massachusetts College of Pharmacy and Allied Health Sciences[e]
Northeastern University[f]
University of Notre Dame[g]
Oak Ridge National Laboratory[h]
Pennsylvania State University[i]
Philadelphia College of Pharmacy and Science[j]
Purdue University[k]
Rice University[l]
Rockwell International Science Center[m]
Superconducting Super Collider Laboratory[n]
University of Texas at Dallas[o]
Tsukuba University[p]

Draft Presented to the SDC Collaboration
Tracking Review Committee
November 12, 1991

Compiled and Edited by
D.Adams, A.Baumbaugh, F.Bird, R.Chaney, C.Collins, W.Gall, K.Hess, D.Koltick, R.Leitch, A.Odone and R.Ruchti

D. Koltick
Nov. 13. 1991

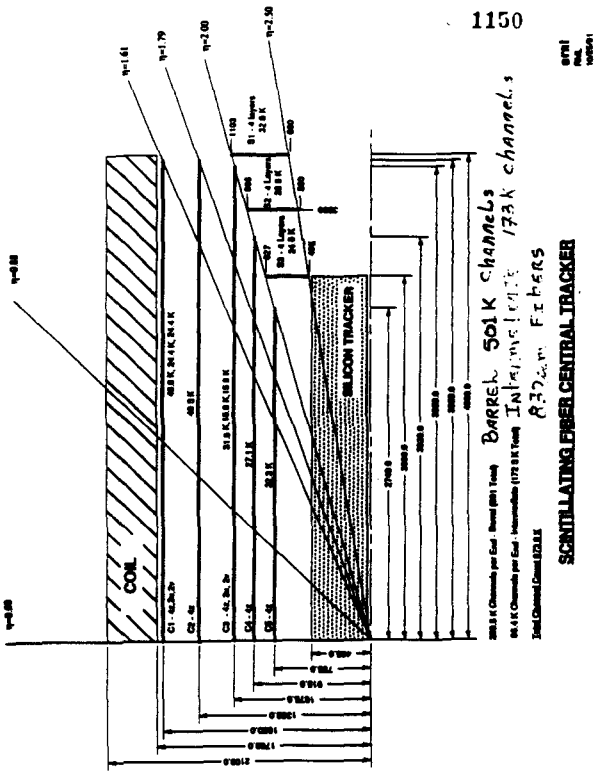

Figure 3.6-1. Acceptance in the fiber tracker vs Higgs mass for three muons from

Goals of The Fiber Tracker

- (1) to provide a first level trigger for $|\eta| < 2.5$ with sharp p_T threshold and with the capability of resolving individual beam crossings;
- (2) to provide pattern recognition capability and momentum resolution which complements and extends the capabilities of the inner silicon tracking system;
- (3) to provide three dimensional linkage with outer detection systems including the shower maximum detector, muon detectors, and calorimetry;
- and (4) to provide a tracking and track-triggering system which will operate to the highest luminosity expected at the SSC.

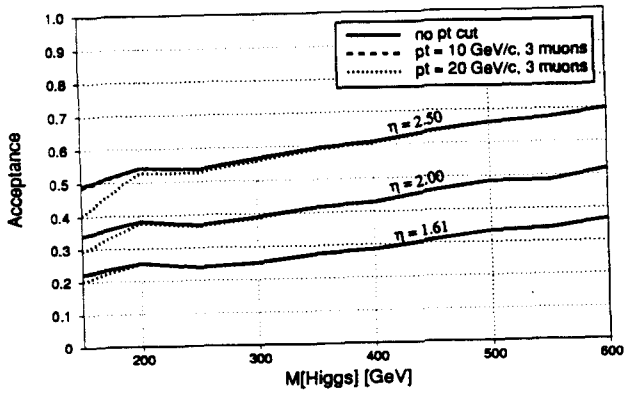

Higgs → 4 $\ell^{\pm}$

Figure 3.6-1. Acceptance in the fiber tracker vs Higgs mass for three muons from Higgs decay in the four muon channel.

BARREL

super layer	radius (cm)	Occupancy L = 0	10^{33}	10^{34}	
C1	165	0.0028	0.0045	0.020	
C2	135	0.0055	0.0085	0.036	
C3	107	0.0097	0.0159	0.07	
C4	91	0.0122	0.0216	0.11	INNER Most
C5	75	0.0166	0.0295	0.15	

Table 3-1. Occupancies in the barrel superlayers for 300 GeV Higgs decaying to four leptons at luminosities of zero, 10^{33} and $10^{34}cm^{-2}s^{-1}$. The fiber diameter is 0.83 mm.

INTER MEDIATE

super layer	z (cm)	Occupancy L = 0	10^{33}	10^{34}	
S1	400	0.0038	0.0068	0.034	
S2	350	0.0041	0.0084	0.047	
S3	300	0.0038	0.0093	0.059	INNER Most

Table 3-2. Occupancies in the disk superlayers for 300 GeV Higgs decaying to four leptons at luminosities of zero, 10^{33} and $10^{34}cm^{-2}s^{-1}$. The occupancies are based on "spiral" layers in which the fibers run from inner to outer radius remaining close-

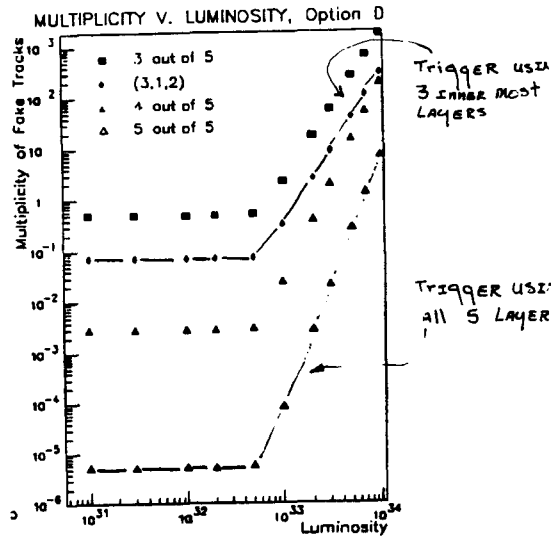

Figure 3.8-1. Trigger accidental rates (per crossing) [3-5] for various combinations of barrel superlayers. The open diamonds correspond the the three-layer case C345 discussed in the text and the open triangles are the full five-layer system.

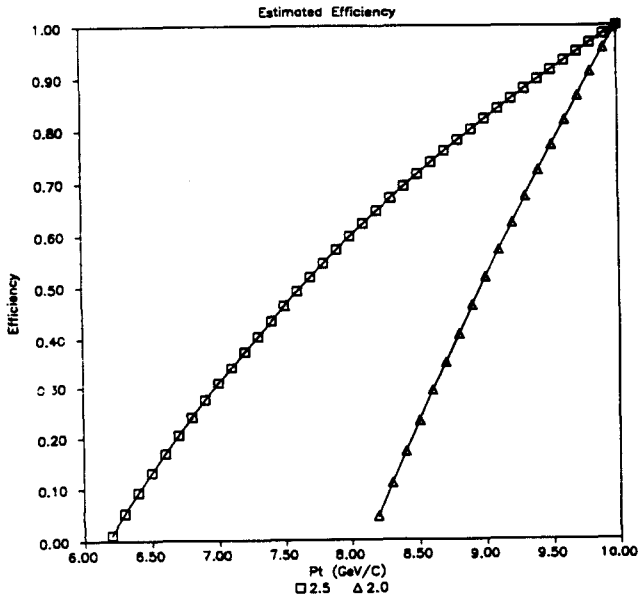

Figure 4.2-9. Estimated trigger efficiency in the forward region for $|\eta| = 2.5$ ($C_{R\phi} = 0.62$) and $|\eta| = 2.0$ ($C_{R\phi} = 0.23$) for the wedge tracker.

11. Cost and Schedule

The costing and scheduling for the Scintillating Fiber Tracking system can be broken into two parts: the barrel outer tracker and the intermediate tracker. The cost of the barrel system has been estimated to be $30.7M independent of the intermediate system tracker. The intermediate outer tracker has been costed assuming that the barrel tracker is being constructed. With this assumption, the incremental cost of the intermediate tracker is estimated at $7.8M. The costs are shown in table 11-1 below.

Table 11-1 The Total Costs of the System

	Cost	Average Contingency	Cost with Contingency	Comment
Barrel Tracker	$30.7M	0.37	$42.0M	Independent
Intermediate Outer Tracker	$7.8M	0.39	$10.8M	Dependent on Barrel

The cost estimates are based on the guidelines set forth by SDC management. Over the past 2 years each aspect of the tracker's construction has been studied and refined. The manpower, material, tooling, facilities and construction sequence has been reviewed and costed. The result of this effort is the Work Breakdown Structure (WBS) and the manpower loaded schedule. Each component required for the fabrication and assembly of the fiber tracker is identified in the Work Breakdown Structure (WBS). The cost estimate is prepared by generating time and material estimates for each item identified in the WBS.

The schedule is prepared in a similar manner. The WBS elements are assigned a duration and logic sequence in the program schedule. Eventually, the cost will be contained in the program schedule by assigning resources to each WBS item. Both the cost and schedule have been compiled and are shown at the end of this section. The WBS is a difficult document to study even for those having prepared them. We have therefore prepared a dictionary that explains the meaning of each line item in the WBS and what model was used to develop the costs, materials and manpower necessary to construct the fiber tracker.

While the dictionary will need updating as new information becomes available, it is essentially a step by step guide on how to build the scintillating fiber tracker. As new technicians, engineers and physicists enter the group, they can quickly learn how to

Major Barrel Costs

	Estimated Cost (Millions)	Cost and Contingency (Millions)
Scintillating Fiber	$4.3	$5.86
Support Structure	1.9	2.5
Assembly	1.3	1.7
Tooling	4.7	6.2
Utilities	0.4	0.5
Photon Transducer	12.8	18.7
Shipping/Assembly	.8	1.0
Tests/Installation	1.0	1.4
Facilities	0.5	0.6
Management/7 years	3.1	3.8
Total costs	$30.7	$42.0

Costing Equations

$\$14.5M + \$51 \cdot n + \$0.175M \times N + \$0.525M \times \sum R^2$

M = Millions of Dollars

n = # of Channels

N = # of Super Layers

R = Radius in Meters of a Superlayer

- Tends to be a little high -

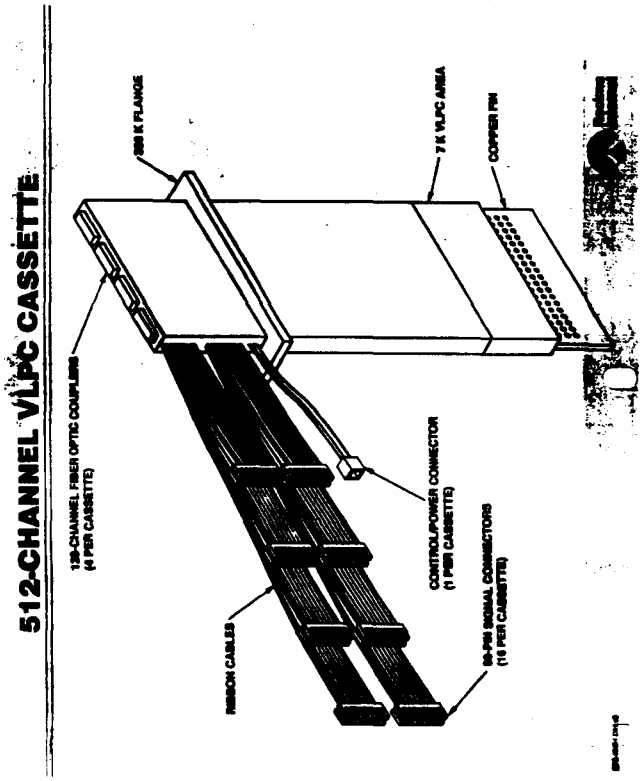

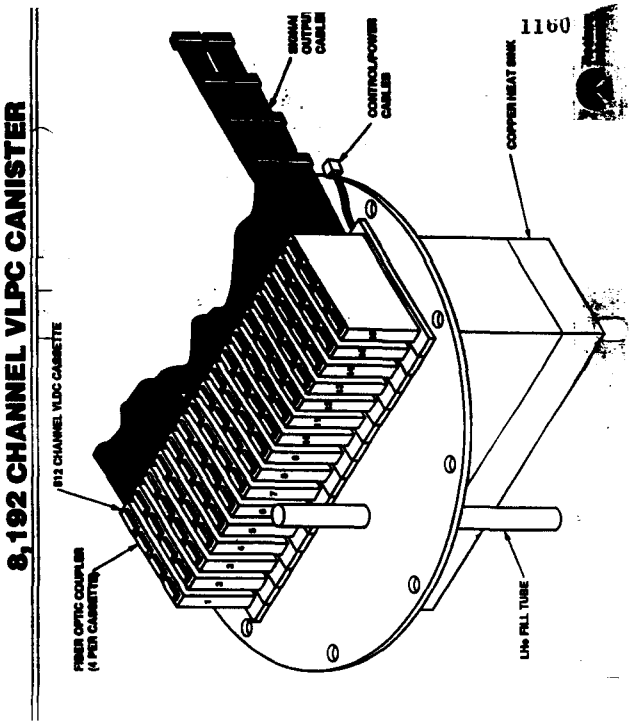

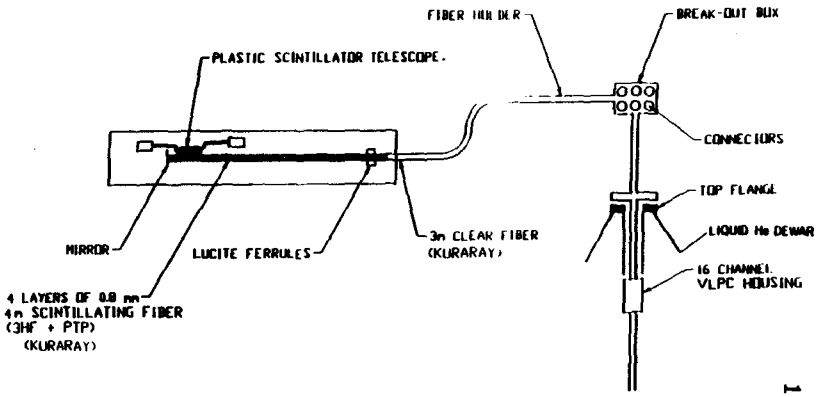

8,192 CHANNEL VLPC CRYOSTAT

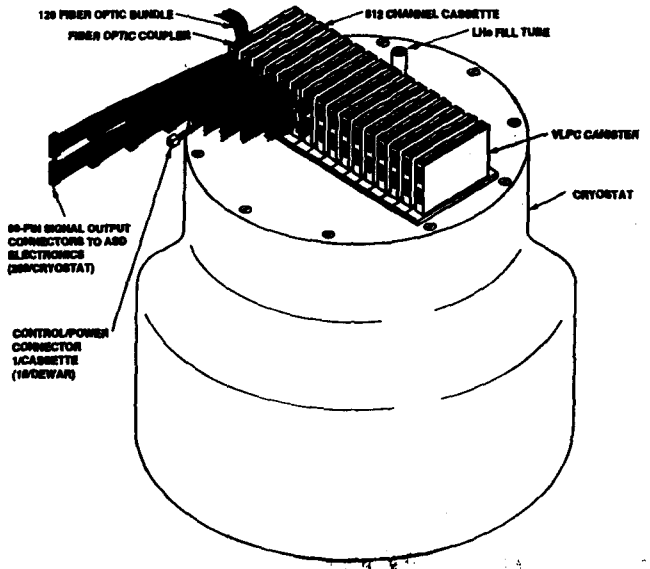

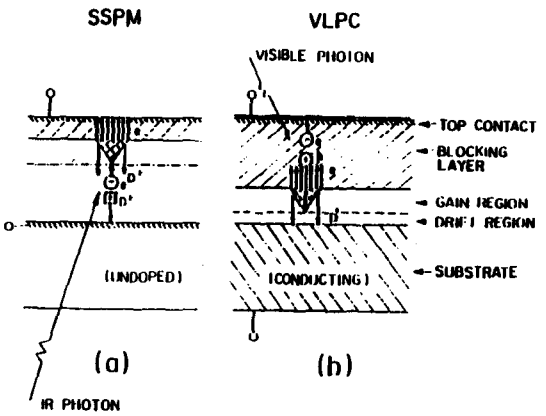

Fig. 1a and b - Operation principles of the SSPM and VLPC are indicated.

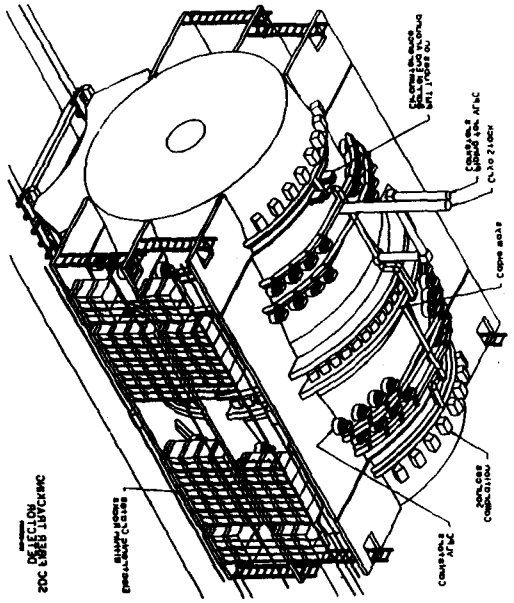

1165

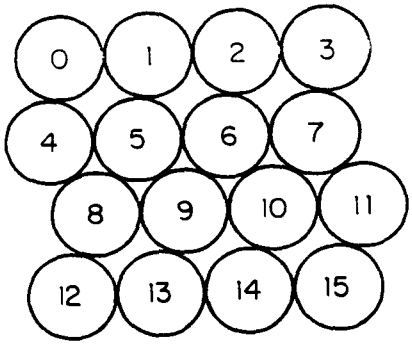

1166

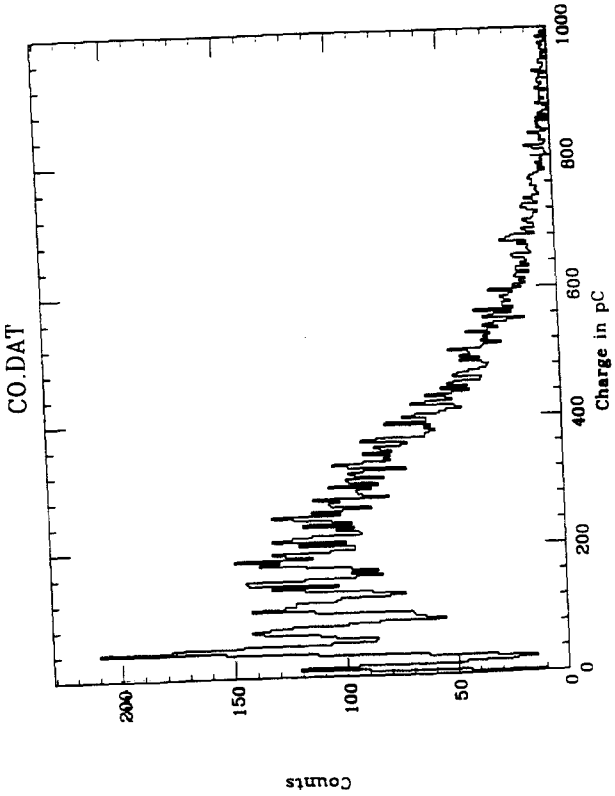

1167

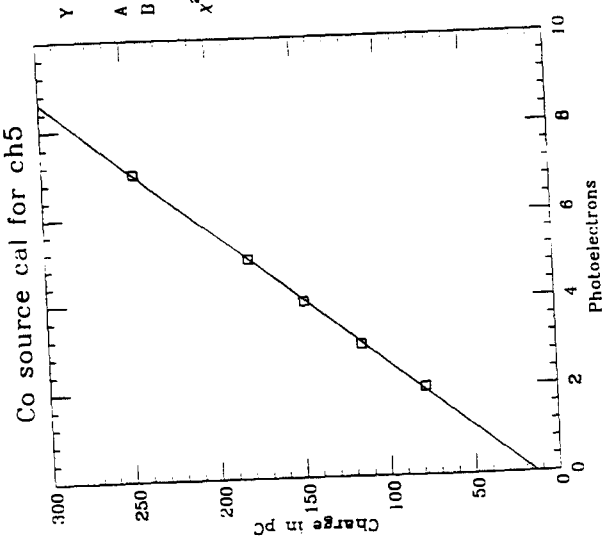

1163

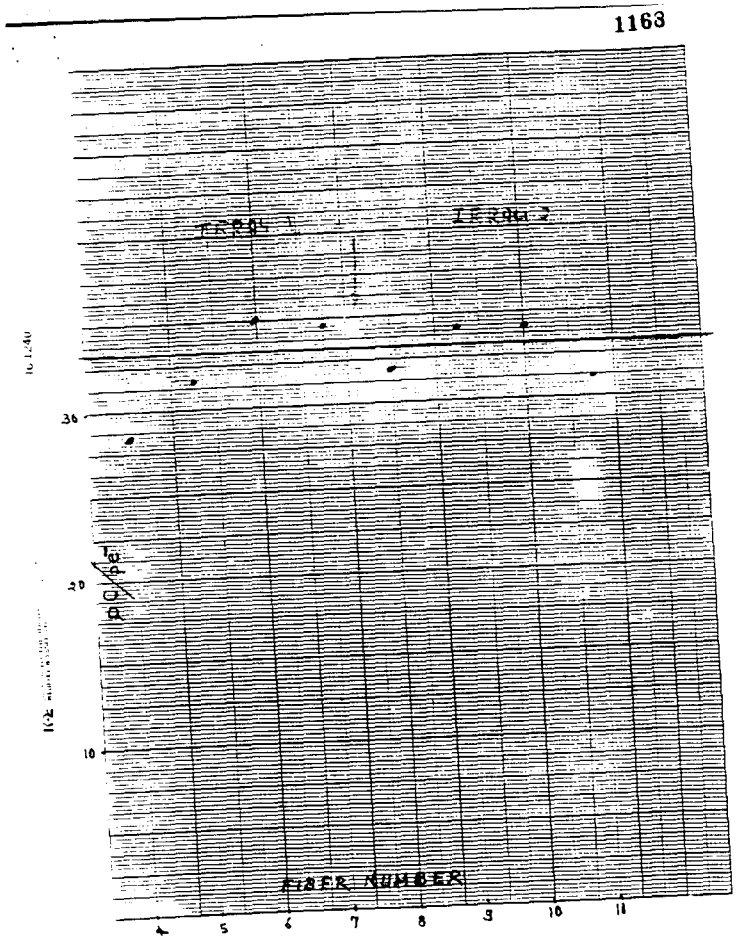

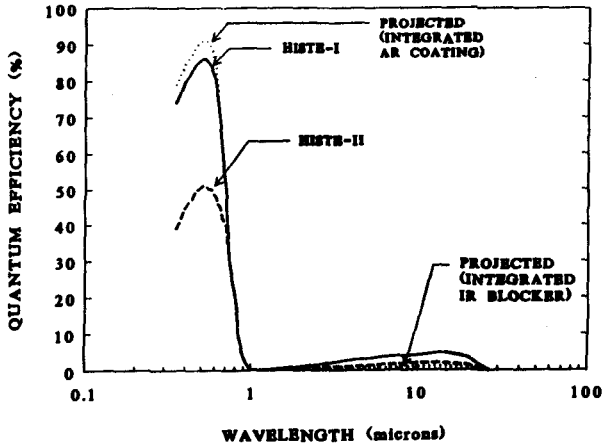

1171

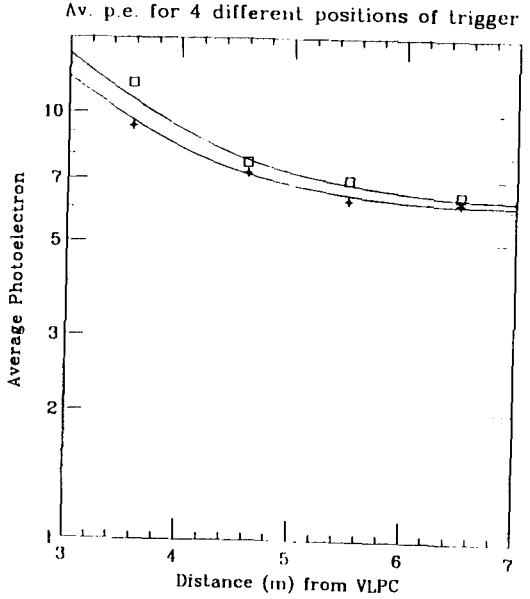

1163

M. ATAC

PRELIMINARY ROUGH DEVELOPMENT AND PRODUCTION ESTIMATED AVERAGE COSTS PER PIXEL

	QUANTITY (PIXELS)		
	1.5E5	6.0E5	1.2E6
NON-RECURING	1.5M $10	$7	$4
RECURING	$16	$16	$15
TOTAL	$26	$23	$19
TOTAL PROGRAM	$4.2M	$13.8M	$22.8M

Presented @ CFNL 1990 MEETING

1172

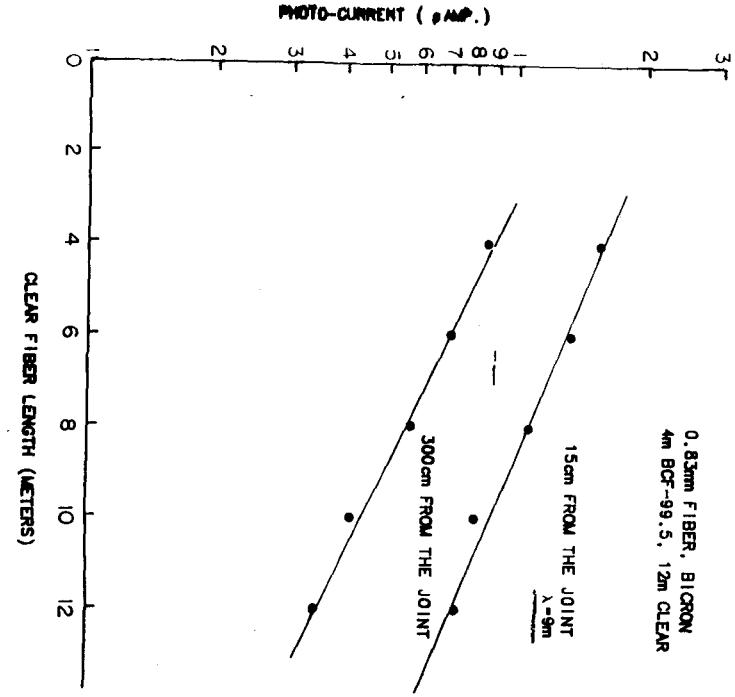

1170

M Atac & A. Brau

10.0 Risk Assessment

10.1 VLPCs - Cost/Availability

The cost estimates prepared by Rockwell International over the past six months show that a production build of between 600,000 and 800,000 VLPC pixels in canister/cryostats will be of the order of $20 to $23 per pixel. This estimate is based on the very early VLPC packaging concepts, and will change as the design matures. The drive to increase VLPC integration should result in a cost per pixel reduction, as recurring assembly and testing costs are spread over more channels. The quoted price per pixel includes all required non-recurring engineering, as well as recurring fabrication costs. A better estimation will be available at the conclusion of the current conceptual design effort at Rockwell.

A very preliminary assessment of risk is shown in Table 10-1. It also is based on the earliest VLPC packaging concept. It assumes the use of a cold pre-amplifier, which is being phased out in the current design. The expected continued development of VLPC technology over the next several years should mitigate even the moderate risk in VLPC development and production.

From Rockwell Per -DC - CDR
December 12, 1991

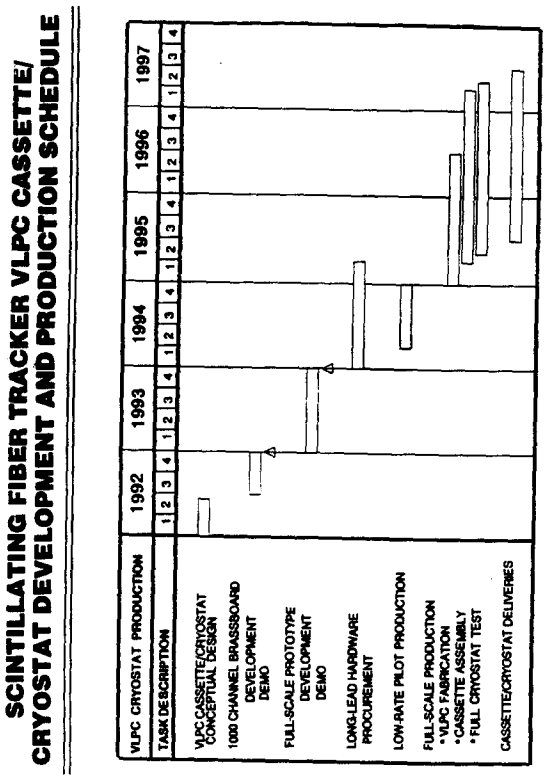

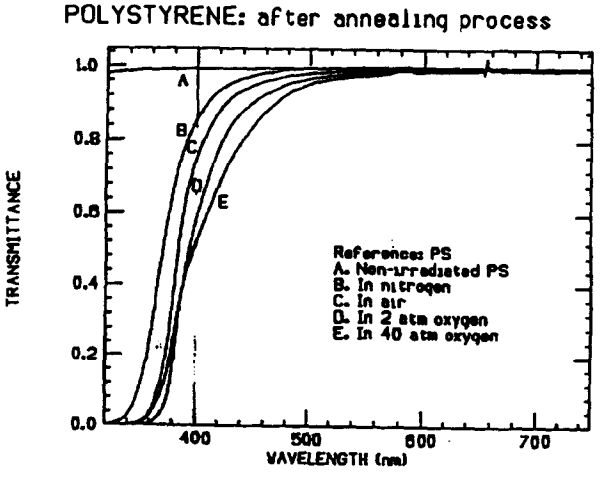

Figure 5.3-2. Irradiation and annealing of polystyrene in various atmosphere.

Table 5.3-1. Light yield in various scintillators before and after a 10Mrad dose from a ^{60}Co Source (normalized).

SCINTILLATOR[a]	λ^b (nm)	Light yield Before	After	After 13 d[c]	After 53 d[c]	Ratio[d]
MOPOM	420	0.78	0.04	0.42	0.48	0.62
MOPOM+0.01%BBQ	470	0.96	0.13	0.63	0.71	0.76
MOPOM+0.02%BBQ	470	0.96	0.16	0.69	0.76	0.79
MOPOM+0.01%K27	500	0.95	0.27	0.76	0.83	0.87
MOPOM+0.02%K27	500	0.95	0.27	0.76	0.84	0.88
O415A	415	0.92	0.49	0.78	0.88	0.96
O415A+0.01%BBQ	470	1.01	0.42	0.86	0.97	0.96
O415A+0.02%BBQ	470	1.02	0.54	0.88	0.90	0.97
O415A+0.01%K27	500	0.97	0.57	0.87	0.90	0.88
O415A+0.02%K27	500	0.90	0.53	0.88	0.90	0.99
O408	410	0.88	0.48	0.78	0.83	0.94
O408+0.02%BBQ	470	1.02	0.54	0.87	0.90	0.97
O408+0.02%K27	500	0.97	0.57	0.89	0.96	1.01
DAT	375	0.73	0.16	0.48	0.47	0.64
DAT+0.01%DMPOPOP	430	0.86	0.51	0.76	0.78	0.87
→ DAT+0.01%BBF	530	0.88	0.60	0.83	0.89	0.91
pT	380	0.84	0.51	0.61	0.62	0.80
LIKE NE 110 pT+0.01%DMPOPOP	430	0.86	0.61	0.71		

[a]Fluor concentrations are by weight, the concentrations of primaries are 1% (1.25% for DAT and pT). [b]Wavelength of peak emission. [c]First 10 days in oxygen and the rest in the air. [d]After 53 d/Before.

1177

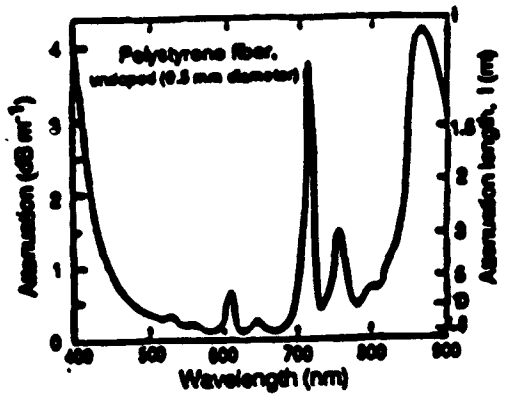

1178

DYES- CONTINUE REFINEMENT OF
PS-PTP-3HF (OPTIMIZE COMPOSITION)
(VARIANTS OF 3HF)

EXAMINE
PS-PTP- BENZOTHIAZOLES

WAVEGUIDES - CLADDING MATERIAL
n_{clad} 1.49 → 1.40
PRIMARY DYE (PTP) IN CLADDING
CLADDING THICKNESS

EXTRAMURAL COATINGS - TiO_2 (DIFFUSE REFLECTOR)
Al (SPECULAR REFLECTOR)

BEAM TESTS - T839
RAD. DAMAGE TEST? - T851

1179

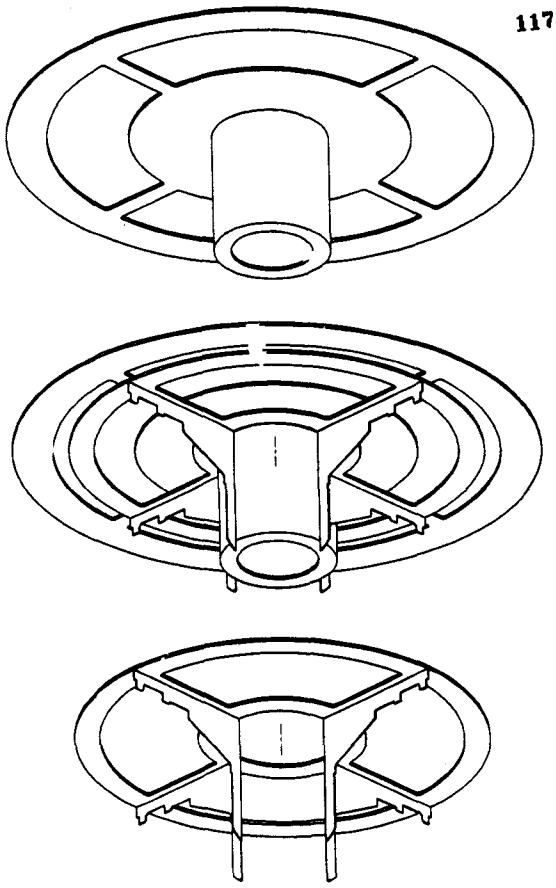

1180

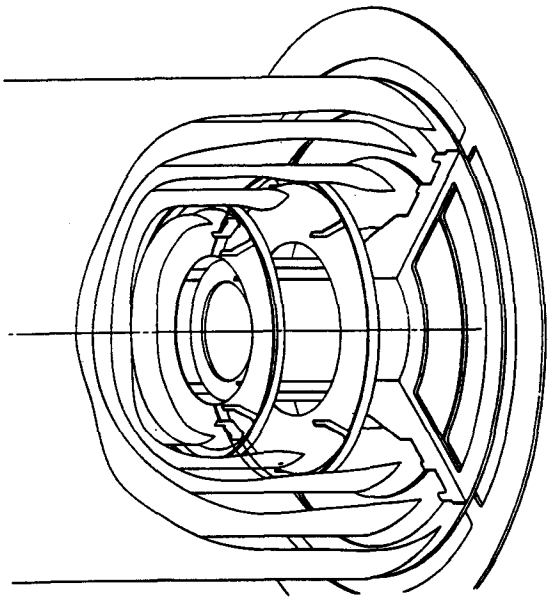

Figure 4.3-6 A cut-away view of the support structure. The intermediate tracker and barrel cylinders are held accurately in place by 4 thin support panels. The panel support is then connected to the main outer support ring which also supports the silicon tracker.

1181

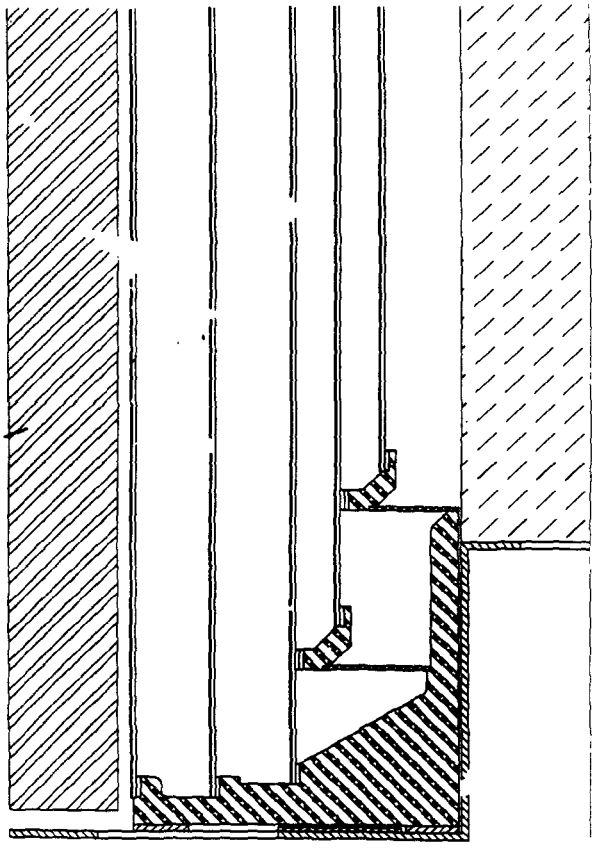

1182

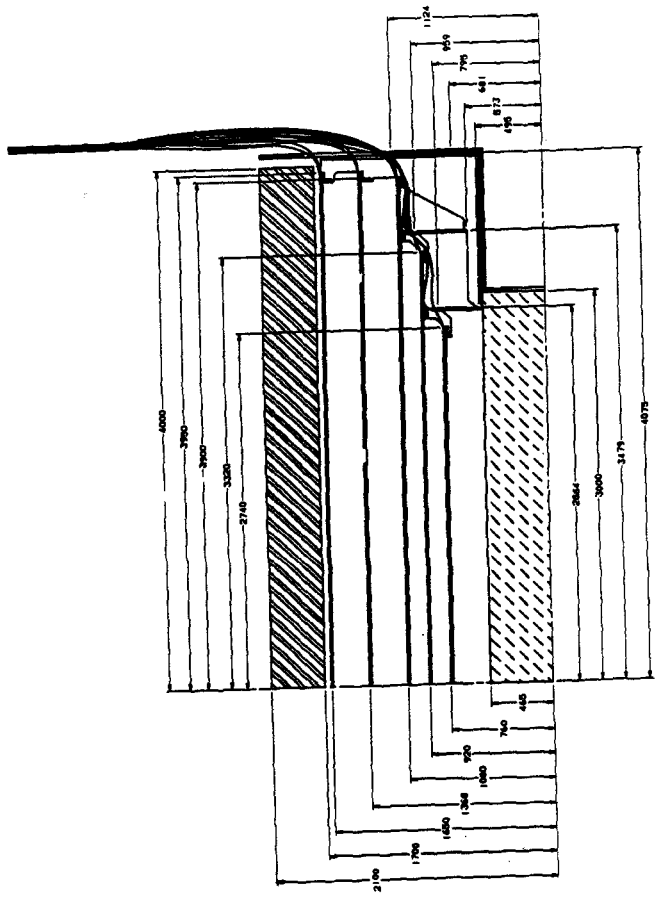

1183

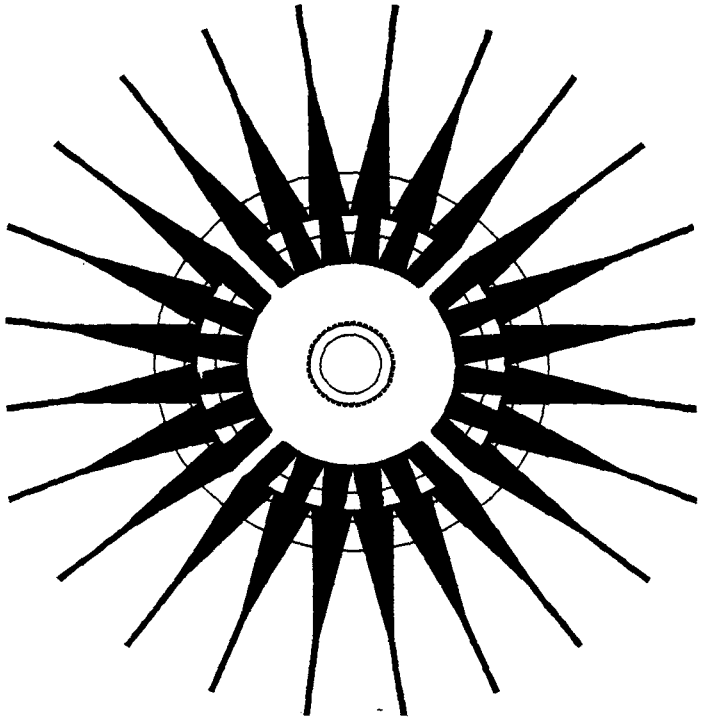

1184

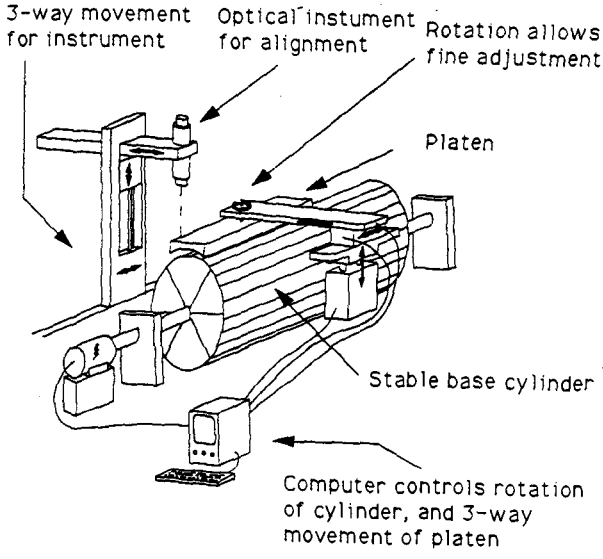

Fiber ribbon placement

Attaching the ribbons will require a large, stable, computer controlled arm for placement. The cylinder is indexed. An optical instrument is used to check the alignment.

1185

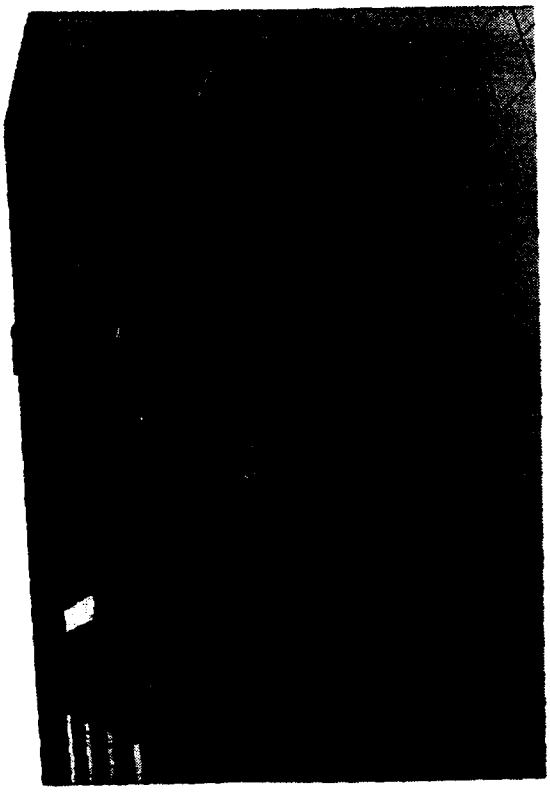

FIG. 3.1-4. Layout of the straw-fiber tracker assembly plan.

1186

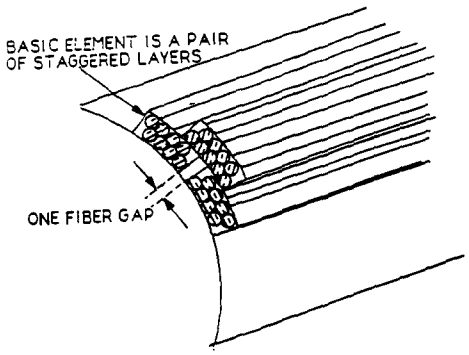

Figure 4.1-2 Axially mounted superlayer

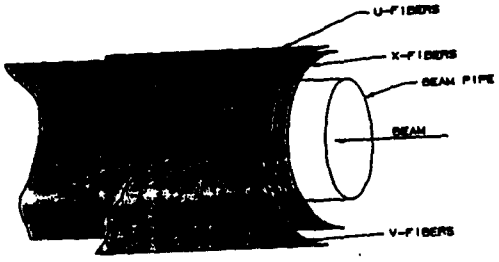

Figure 4.1-3 Stereo mounted superlayer

1187

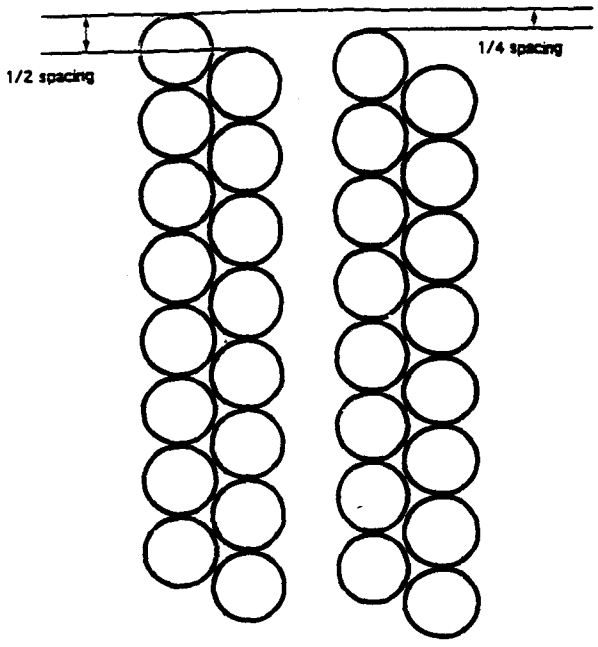

Figure 5.5-1. Schematic of a superlayer of fibers, composed of two double-layer ribbons offset by 1/4 spacing. Fibers are 830μm diameter on 850μm center-to-center spacing (pitch).

1188

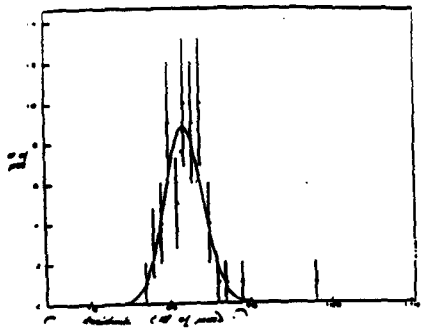

Figure 5.5-2 Registry of a ribbon of 770μm diameter fibers positioned at 820μm pitch. Mean is indeed at 820μm with σ=25μm.

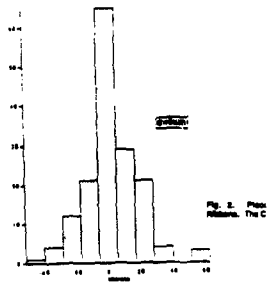

Figure 5.5-3. Registry of a fiber ribbon fabricated at Purdue. Residual is plotted for 830μm fibers at 870μm pitch.

Major Intermediate Tracker Costs

	Estimated Cost (Millions)	Cost and Contingency (Millions)
Scintillating Fiber	$0.9	$1.1
Support Structure	0.5	0.6
Assembly	0.5	0.7
Tooling	0.8	1.0
Utilities	-	-
Photon Transducer	4.2	6.1
Shipping/Assembly	-	-
Tests/Installation	0.2	0.2
Facilities	0.2	0.2
Management/7 years	0.7	0.8
Total costs	**$7.8**	**$10.8**

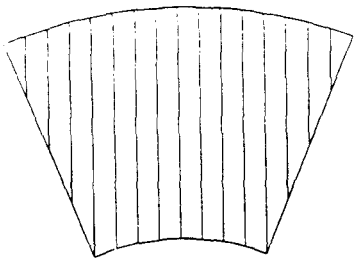

Fig. 4.2-3. Disks are formed from fiber wedges which are constructed from ribbons of parallel fibers. Sublayers can be formed using two of these disks to provide both r and φ information.

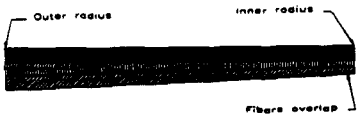

Fig. 4.2-4. Fibers are placed so that they overlap each other at the inner radius and fan out to be flat at outer radius. These wedges are then placed next to each other and repeated to form a disk.

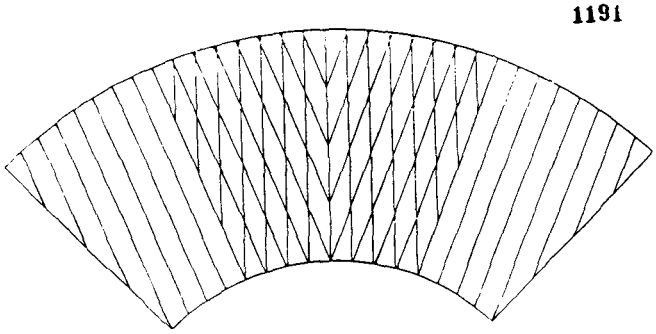

Fig. 4.2-5. Combination of two of the wedged ribbon fiber disks to show how an r and φ measurement can be obtained by locating the diamond shaped region containing the track.

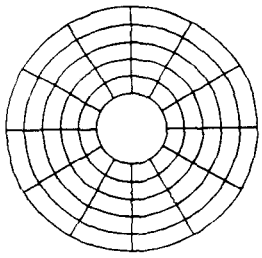

Fig. 4.2-6. Layout of the scintillating tile plates used in conjunction with the radial fiber system to obtain an r measurement.

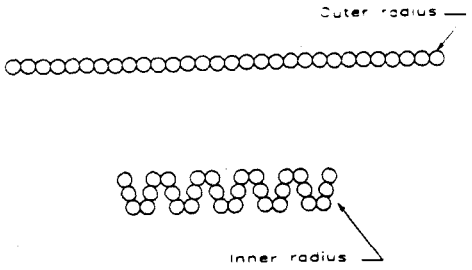

Fig. 4.2-7. End on view of a radial fiber wedge, at inner and outer radius. Notice that ribbons can be constructed from these smaller (three fiber) wedges. This fact should lead to an easier construction.

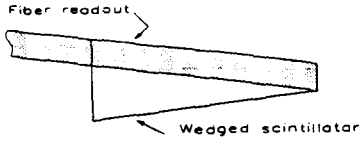

Fig. 4.2-8. Variation on the radial fiber wedge using wedged scintillator with scintillating fiber readout. This approach has the advantage that it is easy to construct, but may have problems in getting light out the readout fiber.

SCINTILLATING FIBER TRACKER MILESTONES

Procure Facilities	10/92
Begin Tooling Fabrication	10/92
Begin Scintillating Fiber Production	10/92
Begin Clear Fiber Production	10/92
Begin Stable Base Cylinder Fabrication	10/92
Begin Support Structure Fabrication	09/93
Begin Production of VLPC's	01/94
Complete Stable Base Cylinder	01/94
Complete Fabrication of Support Structure	03/94
Complete Fiber Ribbon Production	12/94
VLPC's Ready for Delivery	03/96
Complete Trigger ASIC Checkout	03/96
Superlayer Assembly Complete	04/96
Complete Fabrication of Intermediate Tracker	01/97
Final Assembly	04/97
Final Testing	10/97
Ship to Site	01/98
Begin Installation	06/98

- Excellent position resolution. Multilayer structures of 830μm diameter fibers an provide resolution on the order of or better than 100μm .
- Fine granularity resulting in low occupancies and excellent two-track separation.
- Intrinsically fast response allowing single-crossing time resolution.
- Insensitivity to magnetic fields and to RF noise.
- Simple electronics: a binary (yes/no) readout is used.
- No power dissipation or electronics in the tracking volume.
- Flexible fibers and fiber ribbons providing a simple implementation of stereo in the barrel layers.
- Good resistance to radiation damage.

Conceptual Design Report for the Straw-Fiber Tracking System for the SDC

S. Reucroft(Northeastern)

Conceptual Design Report

for the

Straw-Fiber Tracking System for SDC

- **Rationale**
- **Design Considerations**
- **Physics Performance Simulation**
- **Trigger Capability**
- **Integration Issues**
- **Cost and Schedule**
- **Summary**

13 November 1991

Contributors*

A.T. Goshaw, S. Oh, W. Robertson, M. Yin
Duke University

V. Hagopian, E. Hernandez, K. Hu, K. Johnson
Florida State University

Y. Arai, H. Ikeda
KEK

J. Dainton
Liverpool University

J. Chapman, A. Dunn, J. Mann
University of Michigan

G. Alverson, A. Grimes, M. Glaubman,
I. Leedom, S. Reucroft, T. Yasuda
Northeastern University

G. Alley, H. Brashear, C.L. Brilton, Jr., M. Emory
T. Gabriel, R.M. Leitch, T. Ryan, D. Vandergriff
Oak Ridge National Laboratory

W.L. Dunn, M. van Haaren, F. O'Foghludha, A.M. Yacout
Quantum Research Services, Inc.

M. Edwards
Rutherford Appleton Laboratory

M. Corden, M. Mermikides, D. Xiao
Supercomputer Computations Research Institute

W. Fraszer, R. Henderson, R. Openshaw, M. Salomon
TRIUMF

M. Newcomer, R. van Berg, H.H. Williams
University of Pennsylvania

Contacts: A.T. Goshaw and S. Reucroft

* We acknowledge the efforts of the following: S. Majewski, C. Zorn, *CEBAF*; S. Blake, T.S. Elleman, J. Paulos, *North Carolina State University*; H. Dautet, R. McIntyre, *EG&G, Canada*; C. Hurlbut, *Bicron*; F. Amirani, *Mitsui*; T. Shimizu, *Kurary*.

SFTS Concept ; on CDR (11/8/91).

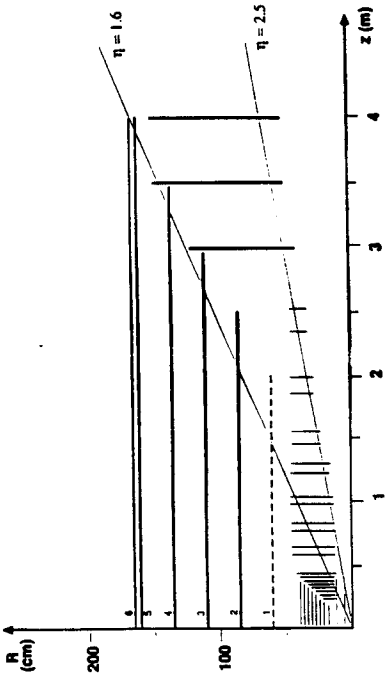

FIG. 1.1. Profile of one-quarter of the straw-fiber tracking system including one possible silicon and intermediate tracker architecture. Superlayer 1 consists of 2u 1-mm fibers separated by 4 cm from 2z 2u 2v 1-mm fibers; superlayers 2 and 3 consist of 6z 4-mm straws; superlayers 4 and 5 consist of 6z 4-mm straws; and superlayer 6 consists of 2u 2v 1.5-mm fibers. Superlayers 3-6 form the initial tracker; superlayer 6 is a staging option.

RATIONALE

- Straw tubes and scintillating fibers have different intrinsic merits
- SFTS is a natural arrangement that optimizes the use of both techniques
- Straws for precision where occupancy is low (large R)
- Fibers for stereo where most crucial (larger R)
- Fibers for full tracking (precision and stereo) at low R
- Several benefits (simplicity, performance *vs* cost, trigger, etc.)
- Both long straw tubes and long fibers work well enough for this concept

Stringing Sense Wire in Assembled Straw Tubes

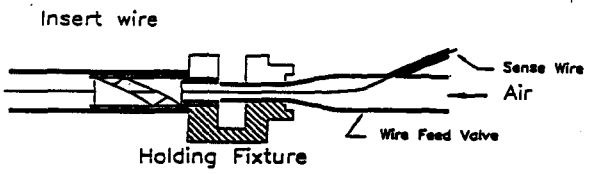

7 Meter Long straw Tubes with 8 wire supports.

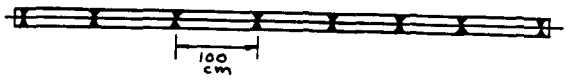

HYBRID (Duke)

Measurement of attenuation length in a 7 meter long straw tube

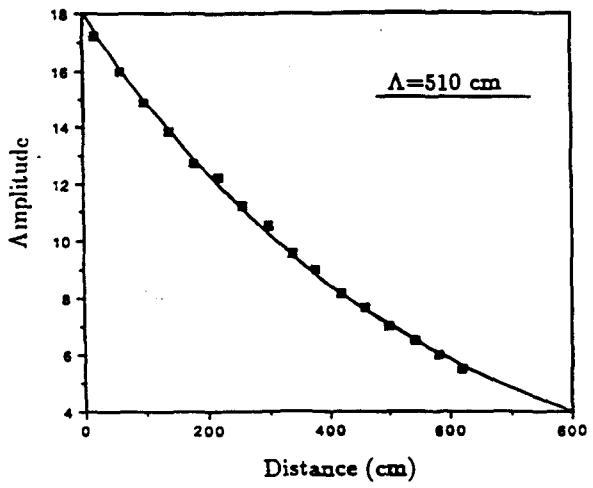

HYBRID (Duke)

Measurement of the resolution of straw tube drift cells in a 2.7m long superlayer with simulated SSC background rates.

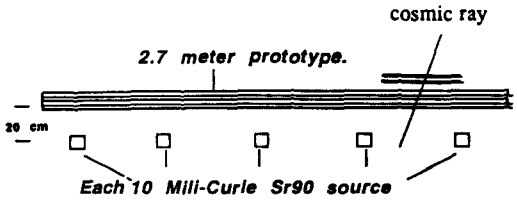

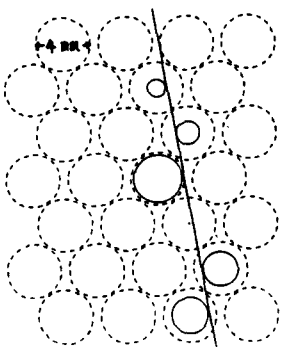

singles rate 1-2 MHz

current draw ~ 5 μA/wire

gain ~ 10^5

HYBRID
(Duke)

High rate test of straw tube position resolution.

- ⟹ σ = 120 μm / straw tube
- ⟹ $\sigma/\sqrt{8}$ = 42 μm / 8 deep superlayer

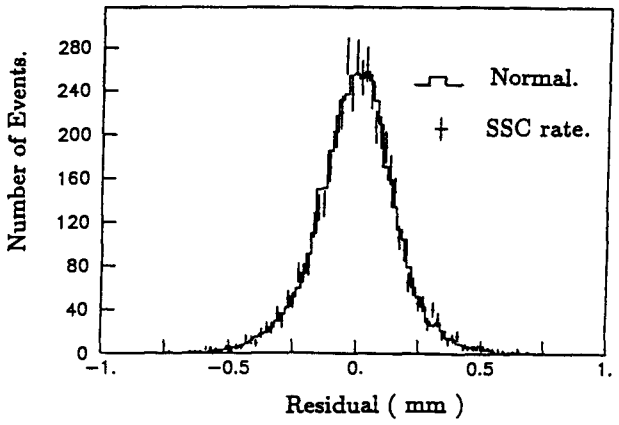

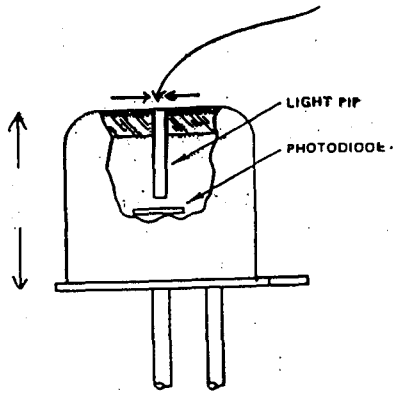

Cross-section of C30921S package.

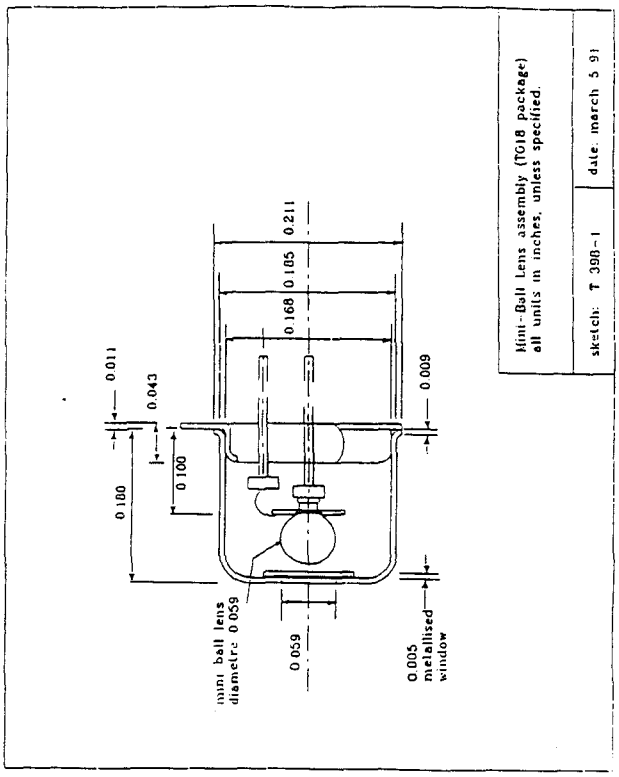

Avalanche Photodiode (500 μm ; EG&G)

Beam G2 Fiber

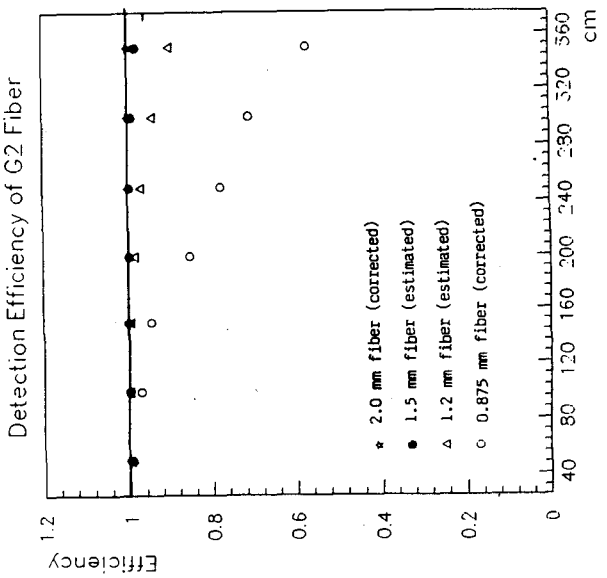

Pertinent Results

- 7-m long straws have been constructed and shown to work[●] (L_{att} ~ 5 m)
- 2.7-m long superlayer has been constructed and operated for ~ 1.5 years with cosmic ray trigger in multi-source simulated SSC rate (radius of 70 cm and L = 10^{33} cm^{-2}-s^{-1})

  Signals indistinguishable from low rate
- 4-m long, 1.5-mm diameter G2 fiber and APD[●] gives tracking efficiency > 97%

  (and we can do better: fiber; VLPC[●])
- Ribbons manufactured with < 50 μm precision
- Similar functional fiber-ribbon system in L3

● Caveats Straw HV/gain/electronics
APD dead time
VLPC not available

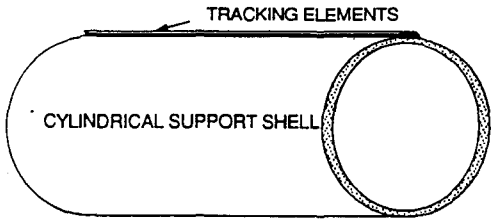

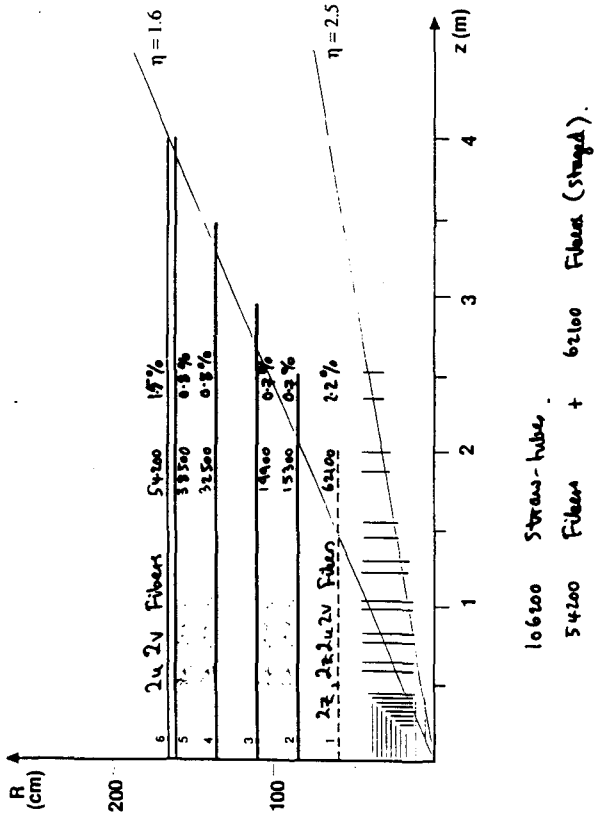

SFTS

DESIGN

S/L NO.	DIA "A"	DIM "B"
2	170	500
3	220	600
4	270	700
5	320	800

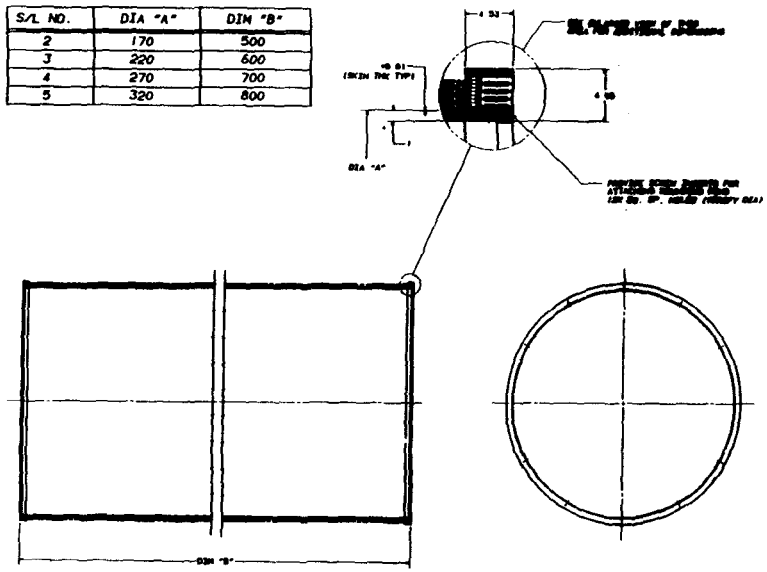

FIG. 2.10. SUPERLAYER CONFIGURATION (STRAWS)

ALL DIMENSIONS IN CENTIMETERS

1214

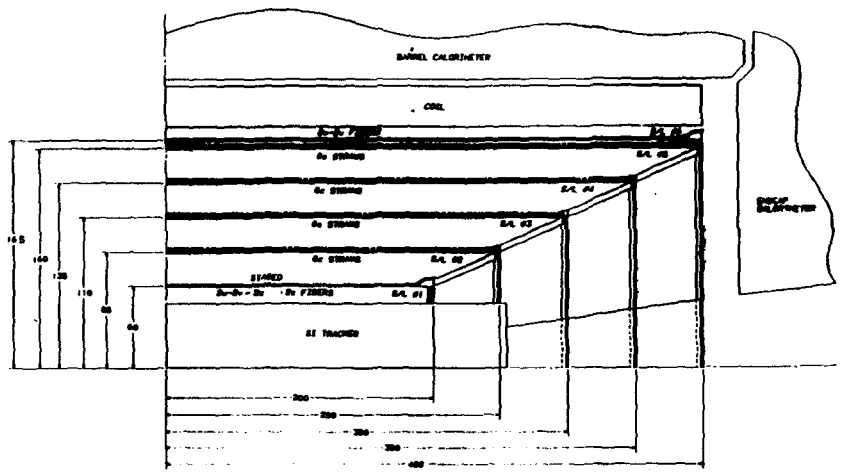

FIG. 2.1. STRAW-FIBER TRACKING SYSTEM (SFTS)

ALL DIMENSIONS IN CENTIMETERS

1212

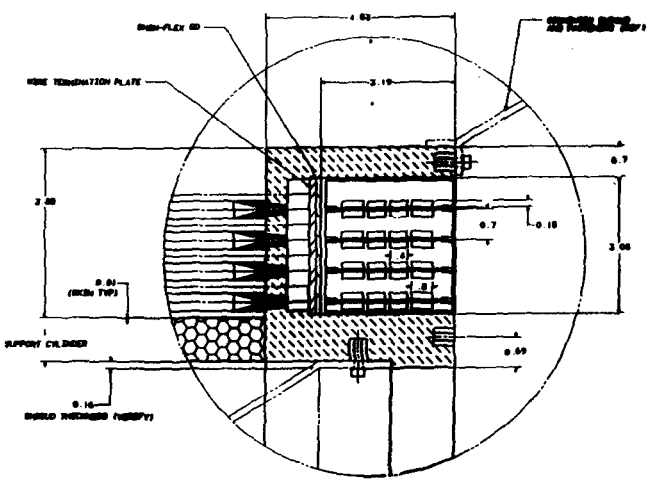

FIG. 2.20. SUPER / LAYER ENLARGED VIEW CYLINDER ENDS

1215

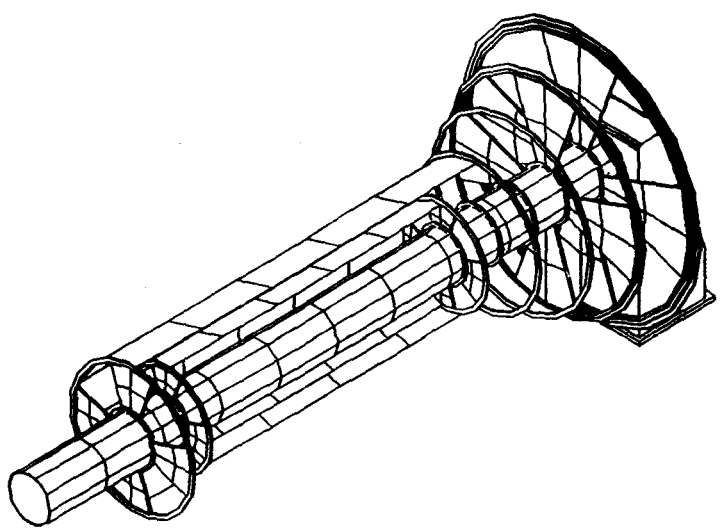

FIG. 2.8. ISOMETRIC VIEW OF CANTILEVERED SHAFT & RETAINING CLAMPS

1213

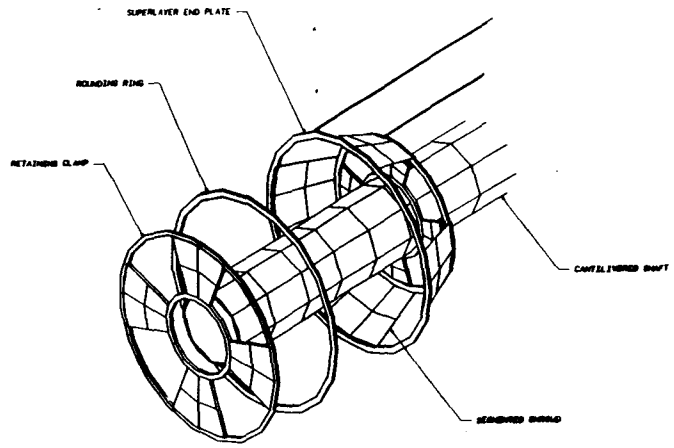

FIG. 2.13. PARTIAL EXPLODED VIEW

S/L NO.	DIA "A"	DIM "B"
1	120	400
6	330	800

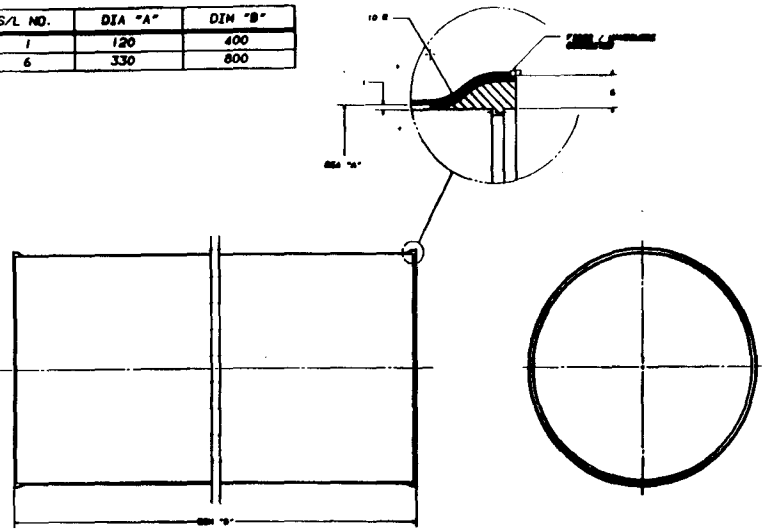

FIG. 2.11. SUPERLAYER CONFIGURATION (FIBER)

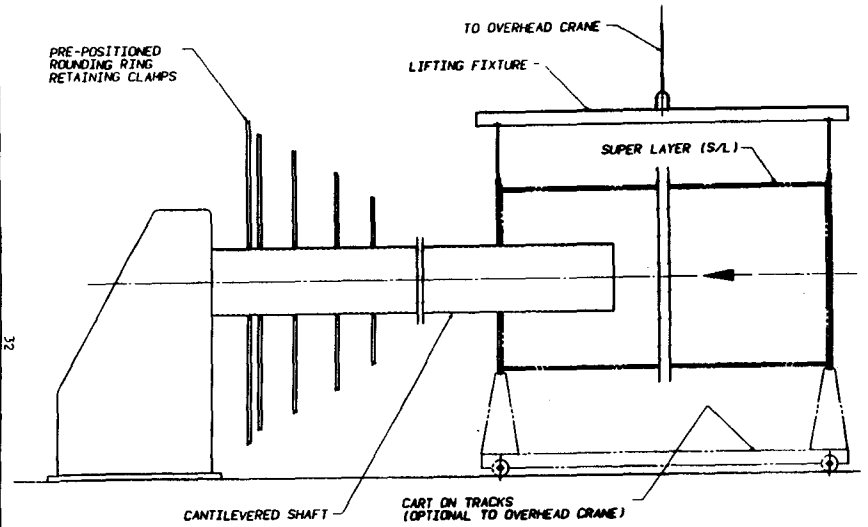

FIG. 2.15. INNER / OUTER CTC ASSEMBLY PROPOSAL
OVERALL CONCEPT

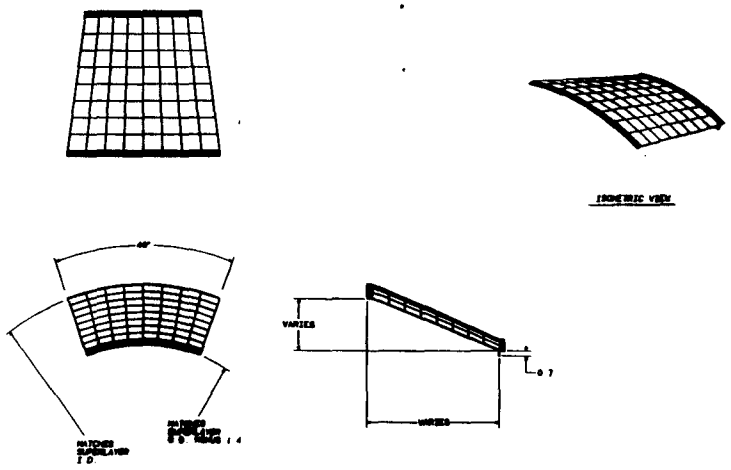

FIG. 2.12. SEGMENTED SHROUD DIMENSIONS
ALL DIMENSIONS ARE IN CENTIMETERS
CLEARANCE HOLES FOR ATTACHING TO SUPERLAYERS ARE NOT SHOWN

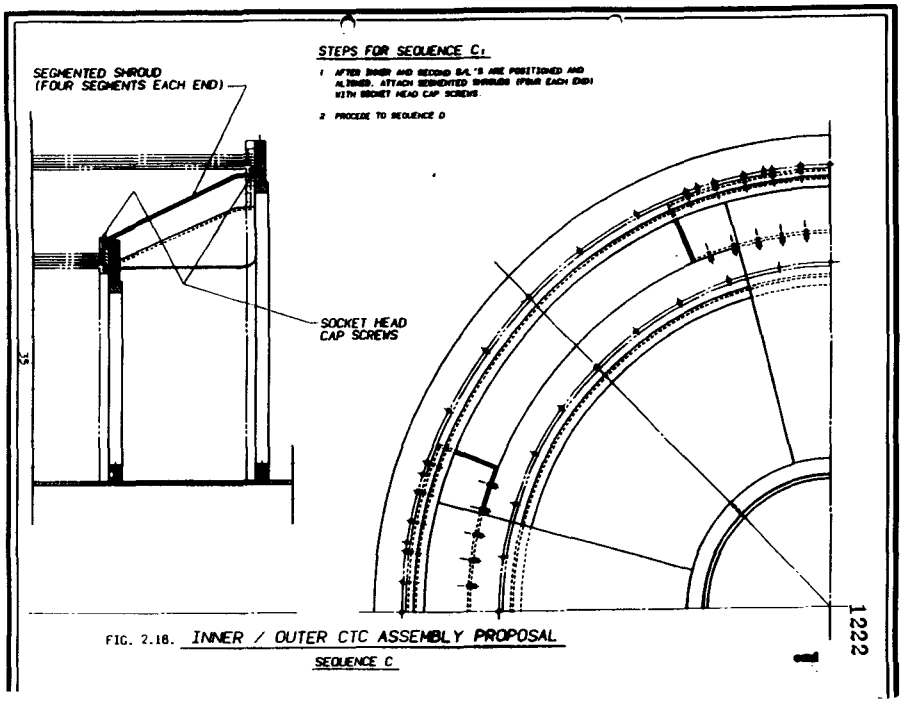

FIG. 2.18. INNER / OUTER CTC ASSEMBLY PROPOSAL
SEQUENCE C

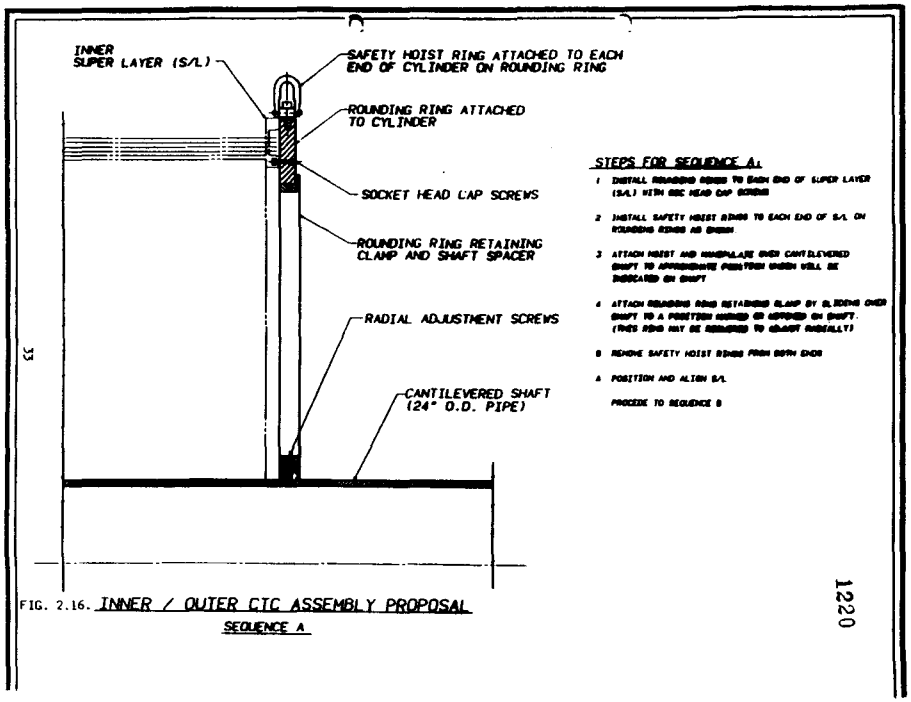

FIG. 2.16. INNER / OUTER CTC ASSEMBLY PROPOSAL
SEQUENCE A

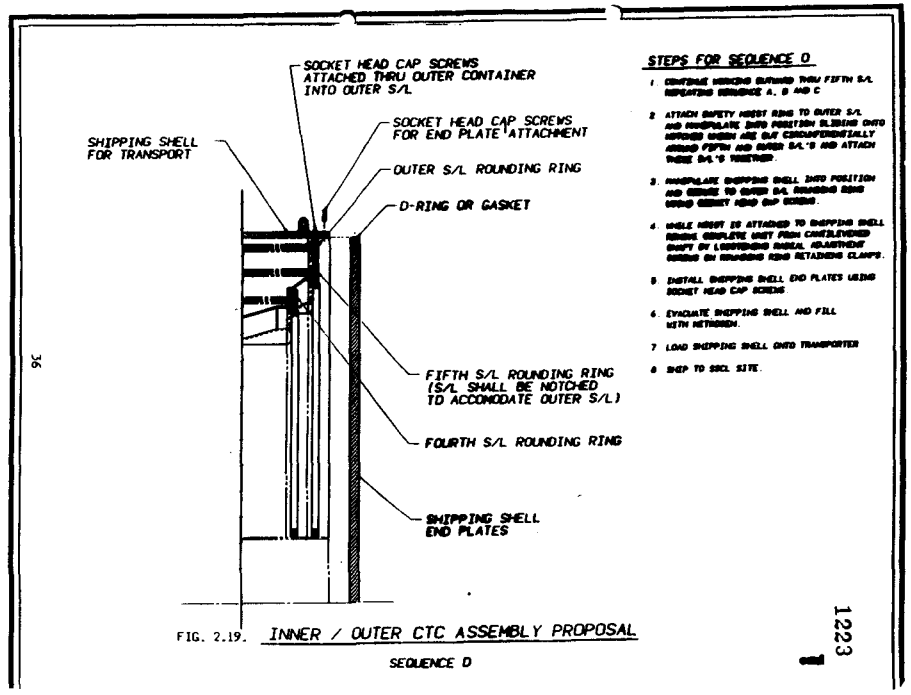

FIG. 2.19. INNER / OUTER CTC ASSEMBLY PROPOSAL
SEQUENCE D

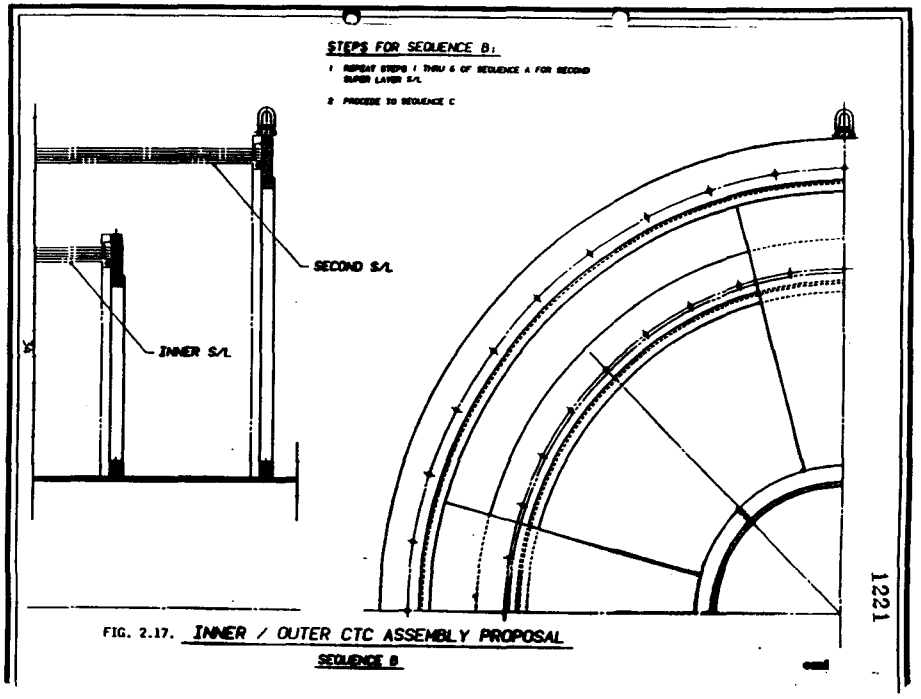

FIG. 2.17. INNER / OUTER CTC ASSEMBLY PROPOSAL
SEQUENCE B

1224

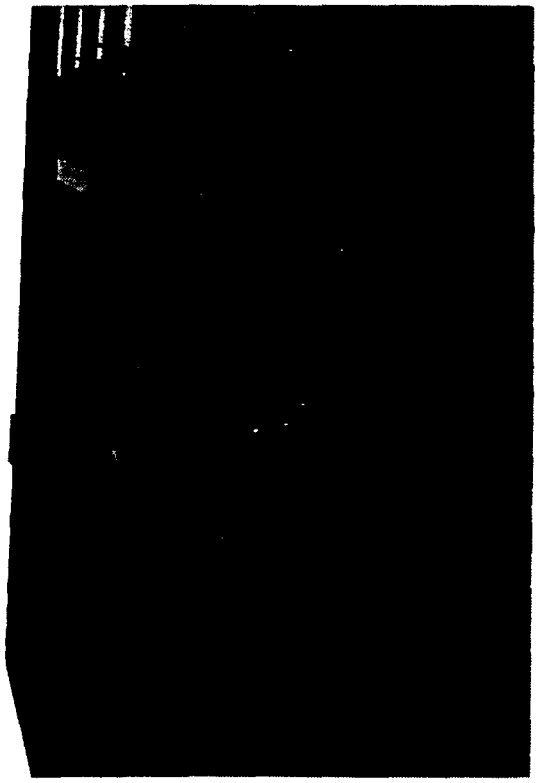

FIG. 2.14. Layout of the straw-fiber tracker assembly area.

Outer Assembly Concept Video.

1225

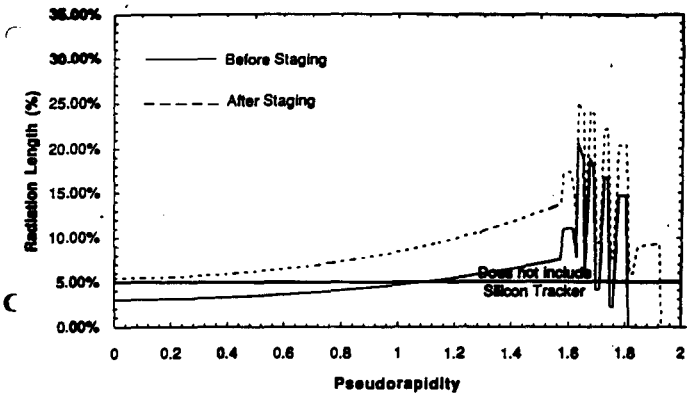

1226

PHYSICS

1227

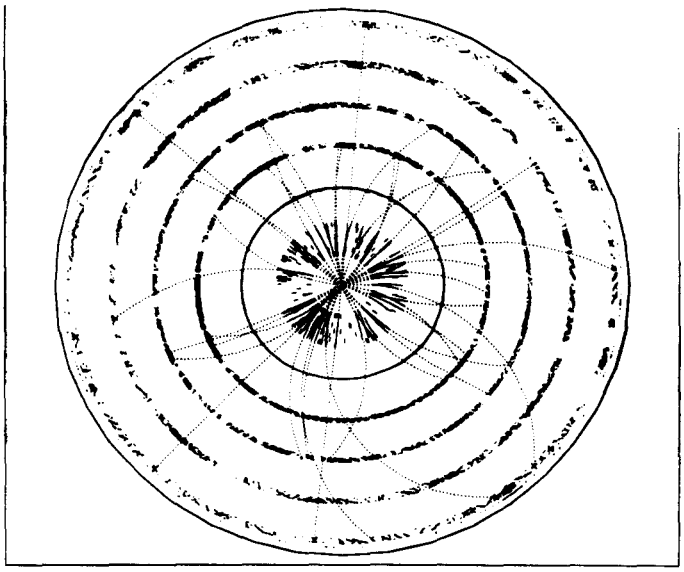

$H \rightarrow Z^0 Z^0 \rightarrow$ 4 leptons.

1228

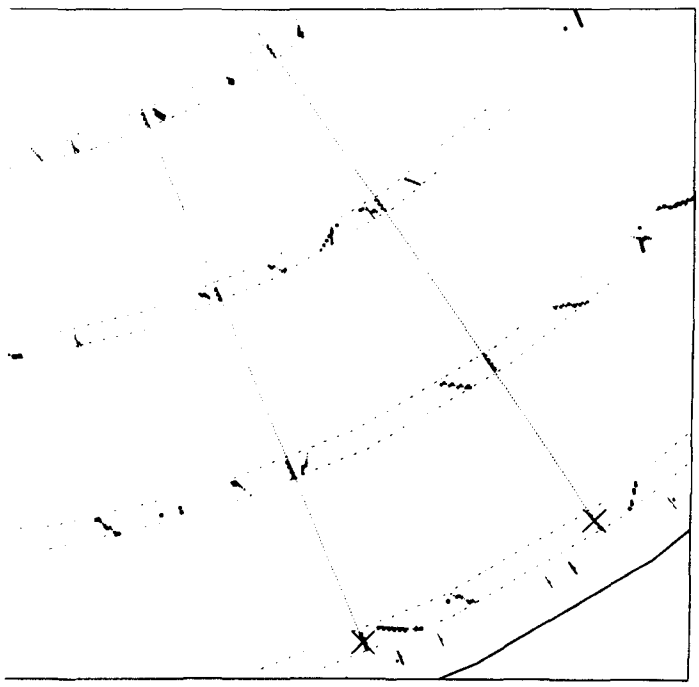

1229

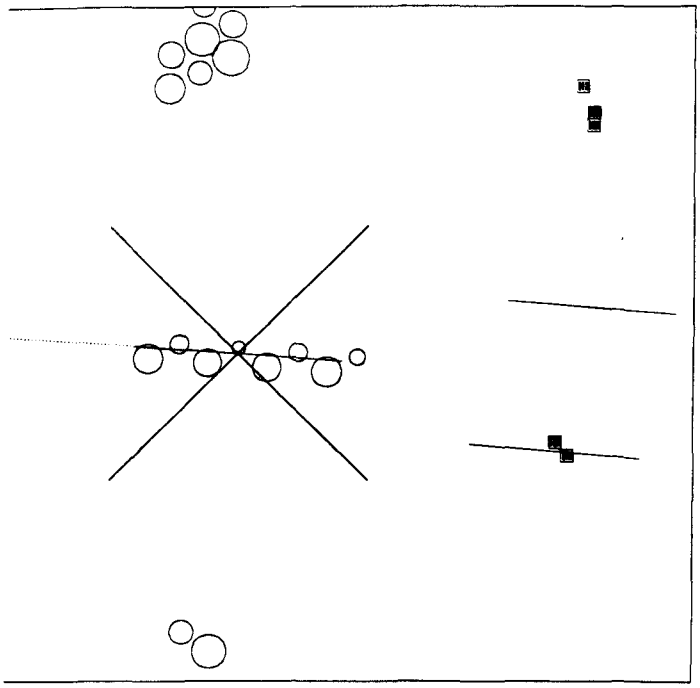

1230

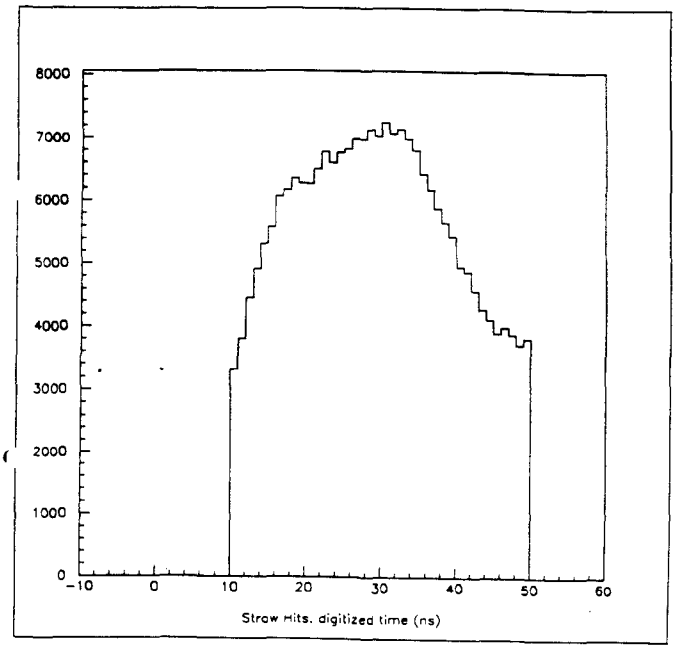

FIG. 3.1. Typical straw tube drift time spectrum, for 40 ns gate width.

1231

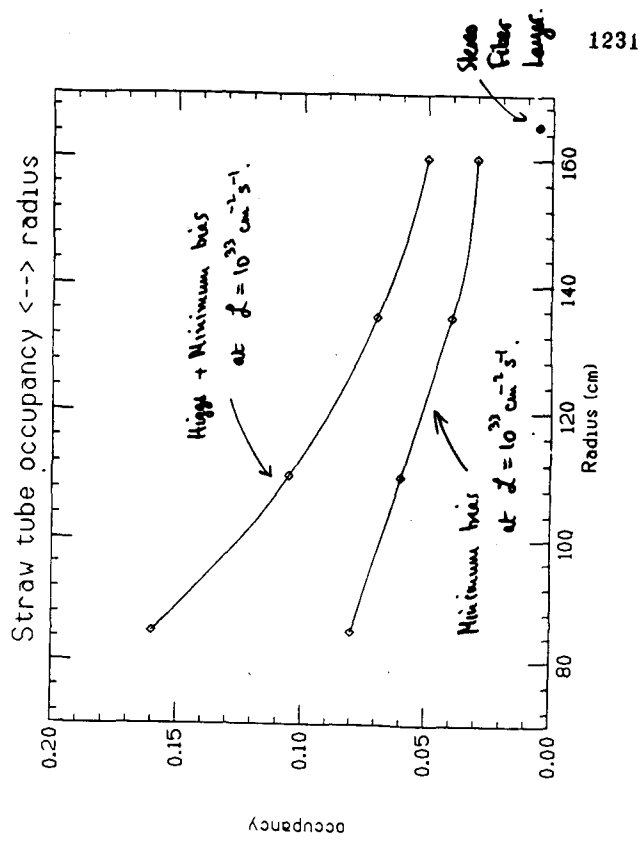

1232

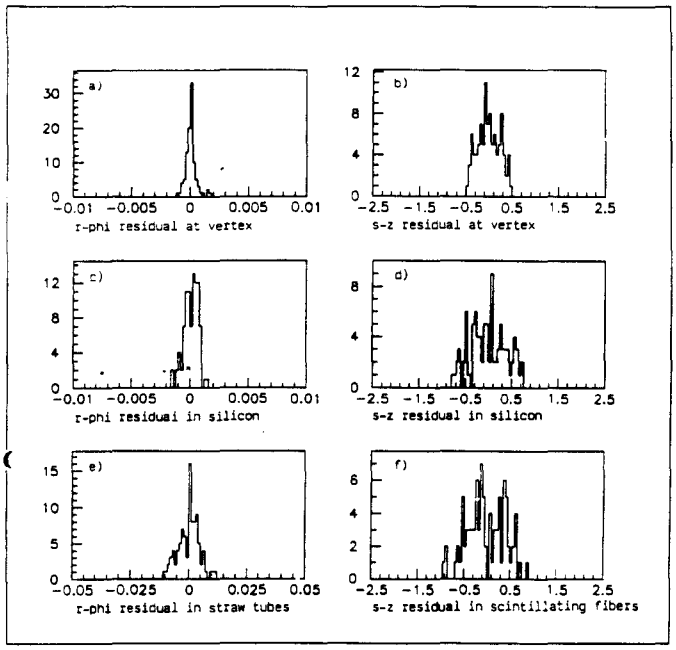

FIG. 3.3. Track fit residuals for high P_t tracks.

50

1233

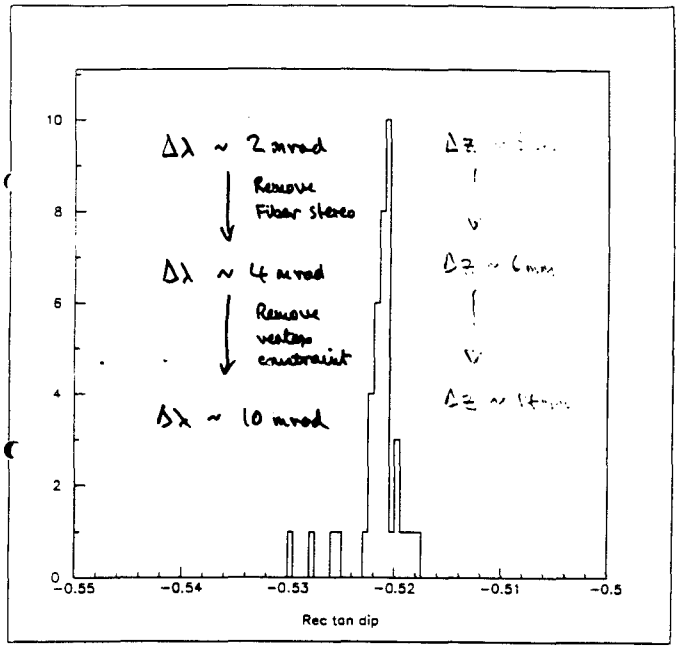

FIG. 3.4. Reconstructed tangent of dip angle for single high P_t tracks.

51

1234

$\Xi^0 \to \mu^+\mu^-$

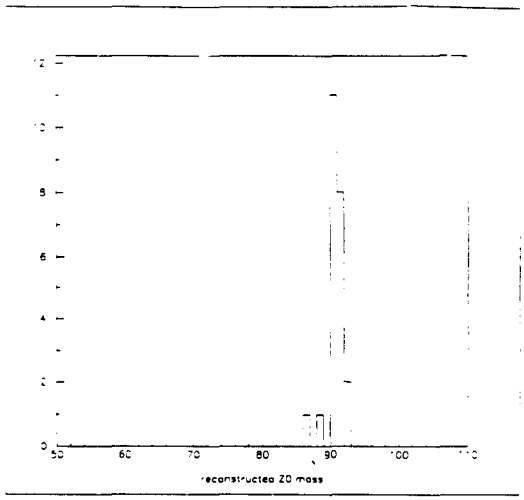

1235

$\Xi^0 \to e^+e^- + \Xi^0 \to \mu^+\mu^-$

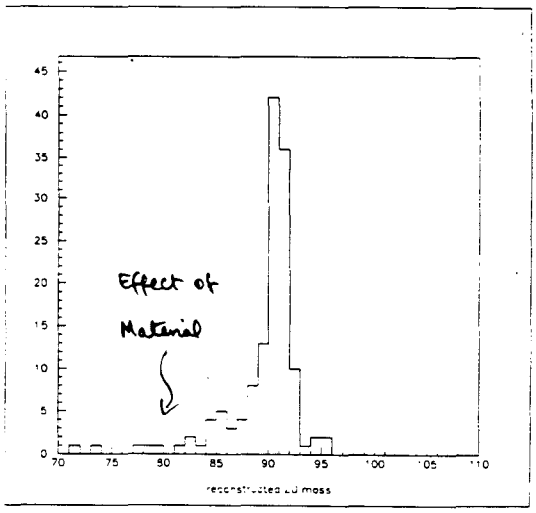

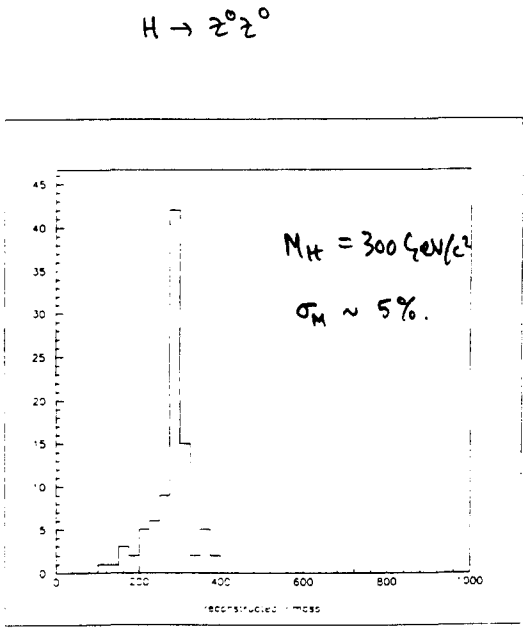

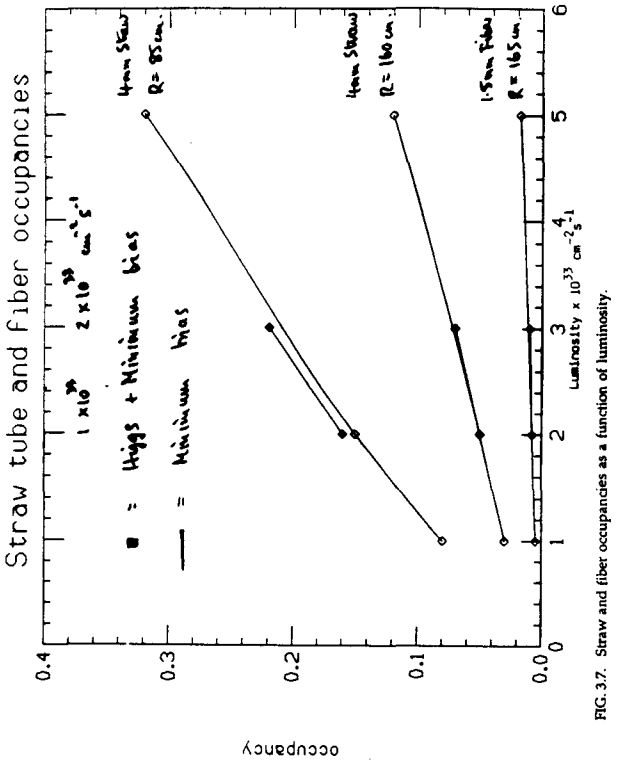

FIG. 3.7. Straw and fiber occupancies as a function of luminosity.

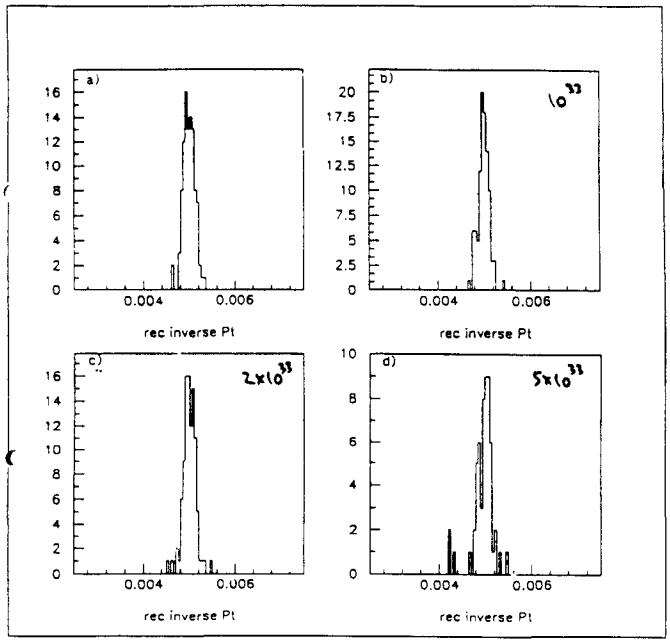

FIG. 3.9. Reconstructed transverse momentum distribution at luminosities of a) 0, b) 10^{33}, c) 2×10^{33} and d) 5×10^{33}.

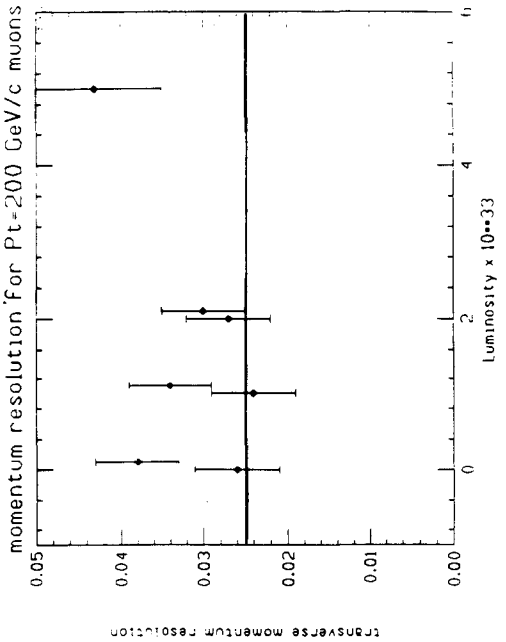

1240

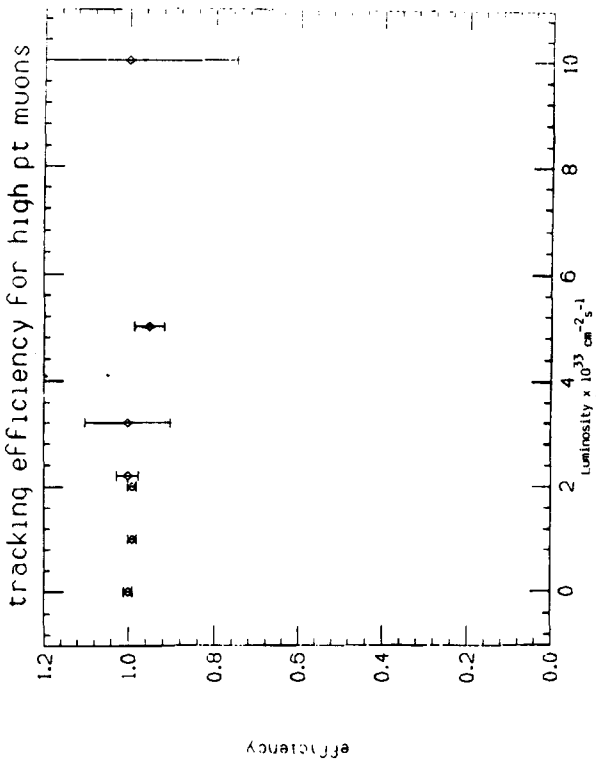

FIG. 3.8. High P_t track finding efficiency as a function of luminosity.

1241

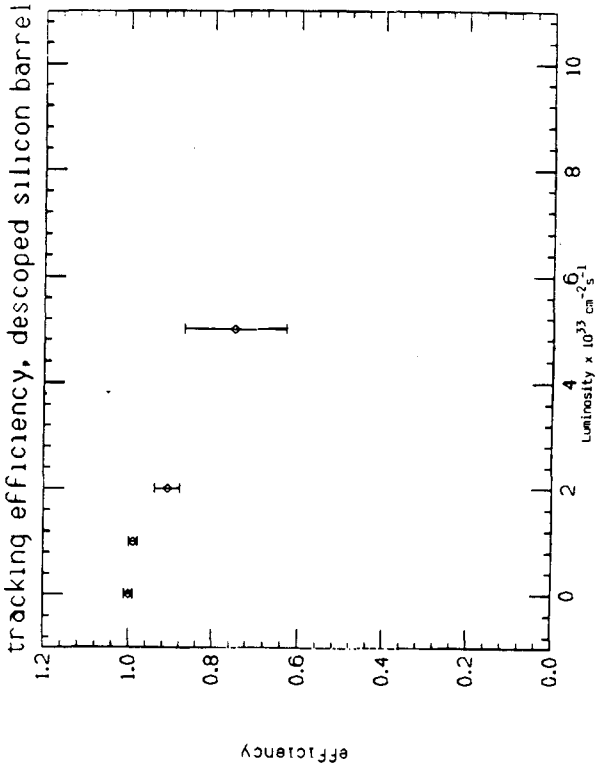

FIG. 3.10. High P_t track finding efficiency as a function of luminosity for a descoped inner silicon tracker.

1242

TABLE 9.3

Physics performance

Item	Comments
1. Simulation procedure	Operating within SDC shell. Inner and outer tracker simulation advanced. Intermediate tracker not yet included. Staged portion of outer tracker not yet included.
2. Reconstruction procedure	Uses 32 r-ϕ points plus outer r-ϕ-z vector at R = 160 cm. Staged layer will give additional r-ϕ-z vector at R = 60 cm.
3. Reconstruction efficiency versus luminosity	>99% at 10^{33} $cm^{-2}s^{-1}$ ← >95% at 5×10^{33} $cm^{-2}s^{-1}$
4. Single track resolution	~50 μm per straw tube superlayer
5. Two track resolution	~750 μm for outer fibers ~500 μm for inner fibers
6. Momentum resolution versus luminosity ($\sigma P_t/P_t^2$)	0.13 TeV^{-1} at 10^{33} $cm^{-2}s^{-1}$ ← 0.23 TeV^{-1} at 5×10^{33} $cm^{-2}s^{-1}$
7. Position resolution at calorimeter Position resolution at muon system	~3 mm in z ± 5° stereo. ← ≈1 mm ± 15° stereo. Not yet evaluated
8. Mass resolution of 300 GeV/c $H^0 \rightarrow 4$ leptons	~17 GeV/c^2
9. High luminosity performance	Initial SFTS (superlayers 2-6) acceptable up to luminosity ~ 5×10^{33} $cm^{-2}s^{-1}$. Staging (superlayers 1-6) needed for higher luminosity.

1243

TRIGGER

• Single Superlayer Stiff Track Trigger

One of 8 possible combinations

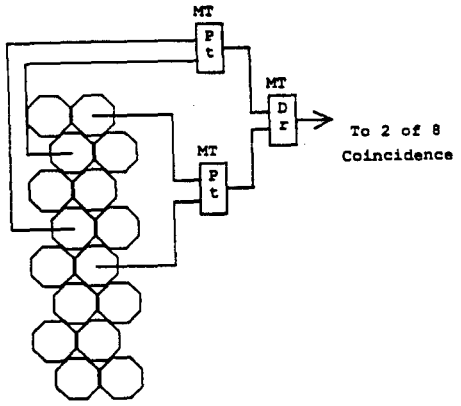

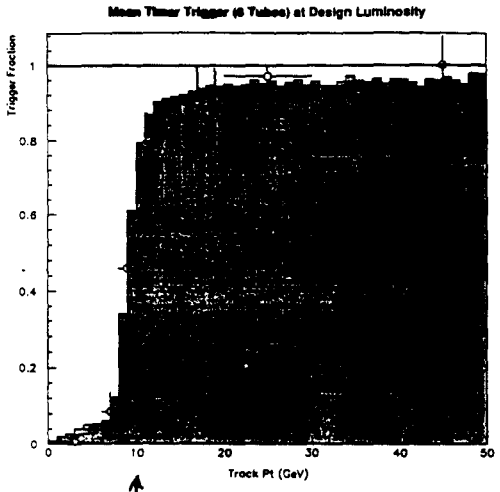

10 GeV/c threshold
(tunable).

- **Design exists based on 8-straw-tube superlayers (Jay Chapman)**
- **Single superlayer stiff track trigger**
- **Trigger superlayers located at large R**
- **Preferred solution uses 3 superlayers (2 stiff tracks out of 3)**
- **Unique feature of SFTS**

INTEGRATION

1248

- Support for silicon system provided
- Space for silicon utilities provided
- SFTS can accommodate any proposed ITD design
- 1-m access for straw electronics (move back ITD)
- Few fiber channels (54k) and possible use of APD's simplifies electronics access requirements
- APD's must be outside calorimeter because of fast neutron sensitivity

1249

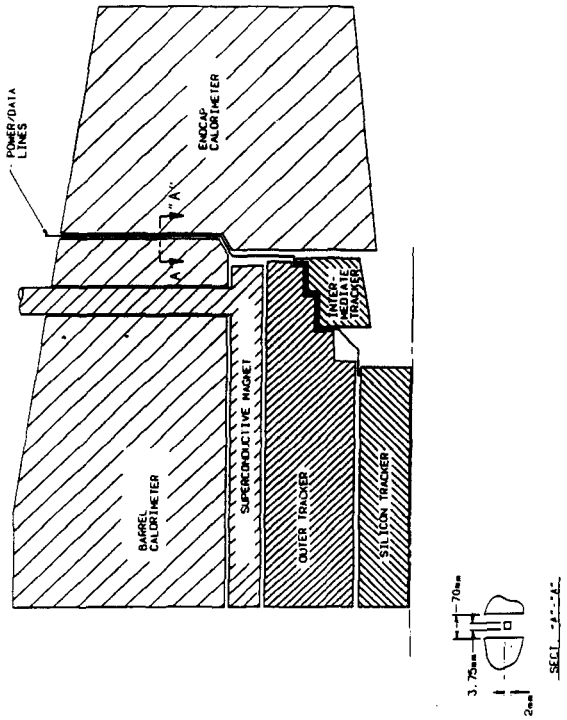

FIG 5.1 SILICON TRACKER POWER/DATA LINE ROUTING

1250

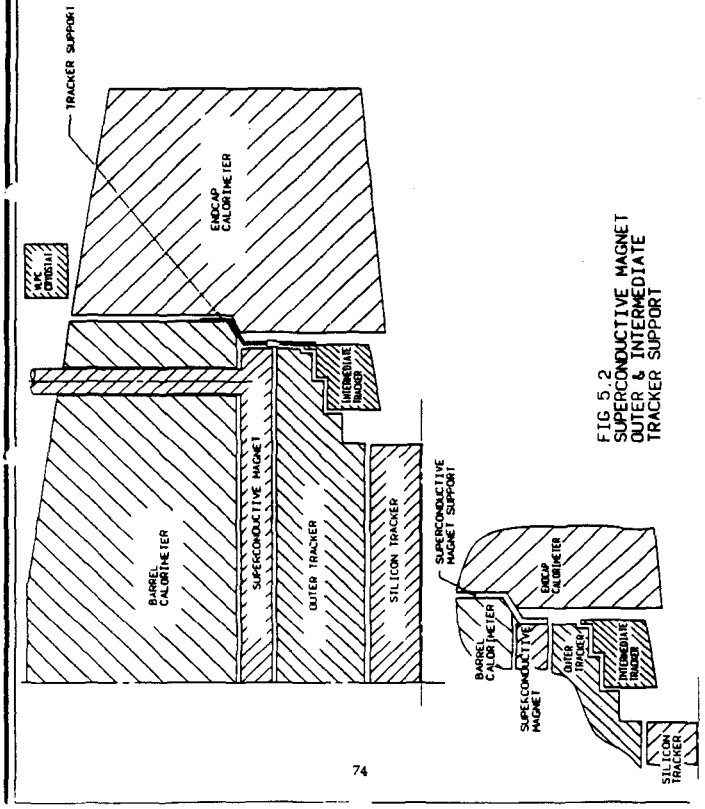

FIG 5.2
SUPERCONDUCTIVE MAGNET
OUTER & INTERMEDIATE
TRACKER SUPPORT

1251

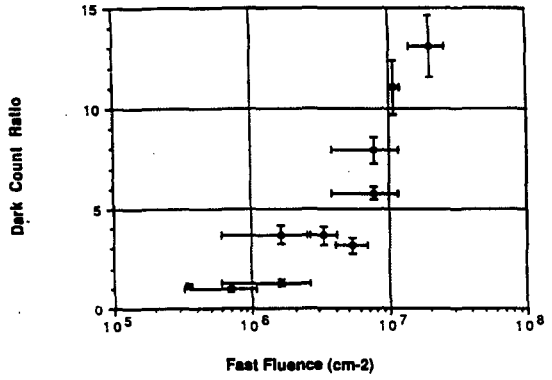

COST AND SCHEDULE

TABLE 9.4

Cost

Item	Comments
1. Number of straw-tube channels	106,200
2. Number of fiber channels	54,200
3. Number of support cylinders	5
4. Total cost plus contingency including all electronics	$38.5M
5. Total cost plus contingency without straw tube electronics	$28.7M
6. Total cost plus contingency without fiber electronics	$24.3M
7. Average contingency	29%
8. Number of staged fiber channels	62,100

Yesterday, in a cost review meeting (Dave Etherton et al.)
We added:
$2.5M for R&D
$7.5M for electronics (mainly NRE)
To yield:
Base $37.7M; base + contingency $48.9M (~30%)

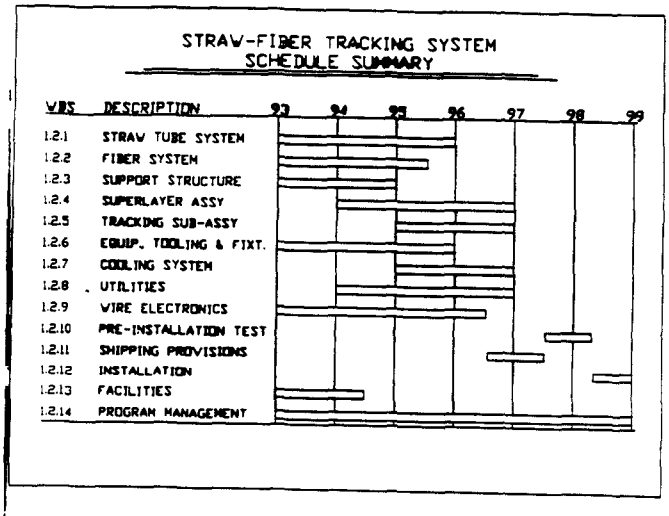

FIG. 8.I. Schedule summary for the straw-fiber tracking system.

- **Schedule feasible because of engineering simplicity**
  - **e.g., unified repetitive support structure**
  - **superlayers composed of ribbons or single straws**
- **Detailed schedule analysis performed for earlier (more complex) SFTS**
- **No critical path items that jeopardize the schedule**
  - **e.g., only 53 ribbons, technology in place**
  - **SMD fiber readout = SFTS readout**
- **Assembly task has been analyzed in detail (ORNL video)**
- **SFTS can be constructed and installed by mid 1998**

SUMMARY

- Straw-fiber tracker benefits from advantages of competing techniques
  - with NO COST PENALTY
  - and no schedule difficulty
- Advanced SIMPLE design
  - same support for all detector elements
  - all straws axial ⇒ uniform construction
  - fiber superlayers for stereo purchased as ribbons; no impossible precision or alignment constraints
  - Fiber readout same as SMD (not truly an extra technology)
- Provides 4 r-ϕ vectors and 28 r-ϕ points

  Outer vector (using superlayers 5 and 6) independent of pattern recognition
- Inner fiber superlayer a natural upgrade to high luminosity
- Optimal straw tube trigger architecture
- Appropriate physics performance

Progress towards the Conceptual Design Report for the SDC Intermediate-Angle Tracking Detector

A. Sill(Rochester)

Progress Towards the Conceptual Design Report for the SDC Intermediate-Angle Tracking Detector

SDC ITD Group

(Liverpool, Rutherford Appleton Labs, Bristol, Oxford, Carleton, Montreal, Rochester, Texas A&M, Purdue)

M. Edwards, Editor

Editorial Committee:
Gerald Oakham, Carleton
Alan Sill, Rochester
Eugene Barasch, Texas A&M
Mike Edwards, RAL

SDC - 91 -
DRAFT
November 8, 1991

Intermediate-Angle Tracking Detector Conceptual Design Report

SDC ITD Group (M. Edwards, Editor)

Outline of ITD CDR:

SECTION	TITLE
1	Introduction
2	Physics Requirements and Performance
2.1	Summary of Physics Goals
2.1.1	Need for Tracking Coverage to High Pseudorapidity
2.1.2	Summary of Basic Physics Processes
2.1.3	Tracking Requirements
2.2	Performance Considerations for the ITD
2.2.1	Momentum Resolution
2.2.2	Trigger
2.5	Material in the Tracking Volume
2.6	Pattern Recognition
2.6.1	Track Finding and Trigger
2.6.2	Track Fitting
2.7	Particle Identification
2.7.1	Electron ID and track linking to the Calorimetor
2.7.2	E/pi ID and track linking to the Silicon
2.7.3	Muon ID and track linking to the Muon System
3	Design
3.1	Layout
3.2	Mechanical Support and Engineering
3.3	Tile Elements
3.4	Cables and Data Transmission
4	Electronics and Readout
4.1	Front end electronics
4.2	Trigger electronics
4.3	Read-out electronics
5	Research, Development, and Engineering Plans
5.1	R&D programme, including test beams
5.2	Engineering plan
6	Cost and schedule
7	Risk assessment
8	Safety

Reasons for the ITD:

1) Provide a Level-1 and Level-2 Trigger
2) Improve Pattern Recognition
3) Track Matching to Silicon, Calorimeter, and Muon Systems
4) Improve Momentum and Invariant Mass Resolution
5) Reduces Length Needed for, and Occupancy of, Elements of the Outer Barrel Tracker
6) Reduces Amount of Material Between Silicon Tracker and the Calorimeter
7) Assists in Separating Particles in Closely Spaced Jets

Advantages of Gas Microstrips:

8) Devices can be Made Intrinsically Rad-hard and should be Able to Withstand High Luminosity
9) Fully Projective Layouts Possible in both Eta and Phi
10) Pseudo-rapidity Binning can be Matched to Needs of the Trigger
11) Tile-oriented Device ==> Modularity, Ease of Construction, Failure Modes Contained
12) Technology for Readout Similar to (some parts possibly the same as) that for Silicon

- **Factors to be considered :**

  technical feasibility,
  performance,
  engineering feasibility
  cost,
  triggering capability,
  impact on electronics system,
  cable plant,
  material budget,
  upgrade potential,
  high luminosity operation ,
  risk,

CHARGE TO COMMITTEE

Technical Feasibility:

This field is in its infancy. However, gas microstrip devices of similar design have already been used in a high-energy physics experiment and in medical applications (imaging of X-rays) at high rates and with good results (see following transparencies).

The devices work! The problem at this point is to understand the reasons that they do work, the extent to which they do or do not continue to operate as a function of rate, technical design (substrate, voltage settings and gas composition etc.), operating conditions, time, and so on.

Much of what is known about the operation of gas microstrips comes from the laboratory and from a relatively small number of test beams and sources. Although there is now a large and steadily increasing number of people throughout the world who have built these devices, many have been mostly repeating the initial successes (and in some cases failures!) of early workers in the field.

It is a fair statement to make, in all likelihood, that there are technical issues to investigate in detail before we can make a design for the ITD that is based on sound demonstrations in the laboratory that microstrips can handle the rates and other conditions for operation at the SSC.

Having said that, it is also true and should be pointed out that the rate of progress (increase in capability and also information) has been and continues to be high, and there is every reason to be confident that these detectors can be made to work in a manner that is consistent with SDC goals.

Institutions working on gas microstrip detectors worldwide:

Place	Substrate	Working device?	Who
CERN	Plastic	No? (not yet)	Sauli
INFN, Italy	glass	Yes	Bellazini
NIKHEF, Netherlands	glass	Yes	Udo
*RAL	glass (4% Na)	Yes	Bateman, Connolly, Edwards
*Texas A&M	Silicon (knife edge), plastic	(almost?)	McIntyre, Bouclier, Bunsch
*KEK	~~Silicon~~ plastic (knife edge), multilayer plastic/Al sandwich	(almost?)	Maki, Higashi
*Rochester	plastic	No (substrate)	Sill
*Carleton	glass, plastic	No (mask design)	Dixit, Oakham, Eichenbaum
*Liverpool	Silicon ± silicon readout	Not yet	Bingi
Tokyo Inst. Tech.	Silicon	No?	... ?

(* = SDC institutional member)

A lot of progress has been made in a short amount of time - we need to pay attention! Summaries follow...

Characteristics of Gas Microstrip Devices:

Fine (~10μm) anodes and (~100μm) cathodes on a resistive but highly insulative substrate (K-glass, Si) with typically ~200 μm spacing between anode traces (≡ "pitch").

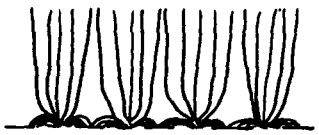

Field lines bring drift electrons from particles incident at ⊥ to plane in to the anodes, which are instrumented like gas proportional chambers or silicon microstrip devices. Operation at typically a few hundred volts.

Knife edge option

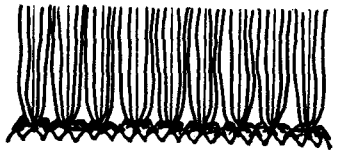

allows closer spacing of the anodes and cathodes (~25μm ⇒ 50μm pitch); gives higher rate capability & finer segmentation, due to low field region in the valleys between anodes & cathodes.

1267

Micro-Lithographed Gas Avalanche Detectors:

Microstrip detectors produced by precise lithographic methods followed by etching of metallization layer on a resistive substrate.

Processing steps similar in methods and detail to those used in semiconductor industry, but LARGER FEATURE SPACING. Anode size typically 10 um, distance between traces of order 50-100 um. Allows considerably easier (cheaper) processing and construction.

Depends on gas avalanche for signal creation -- no use of semiconductor band gap properties needed, therefore intrinsically radiation hard.

1263

Advantages of this design

Trigger in the int. ϕ region is $d\phi/dz$, with a $1/\tan\lambda$ correction. Microstrip devices can be oriented to provide the fine ϕ resolution & segmentation this implies in hardware, ensuring a fast, natural trigger processing capability.

These devices depend on gas avalanches to provide the first level of amplification, instead of semiconductor band gap properties so can intrinsically be made rad-hard and provide a high rate capability when used with the fine anode-cathode spacings and intrinsically resistive substrates just described.

Keystoned cathodes and $\tan\lambda$ binning can be used to provide projective towers for trigger processing features and track fitting geometries that are natural and suited to the problem at hand.

Finally, occupancies are low even at 10^{34} cm^{-2}s^{-1} in the SDC geometry.

1263

Performance:

Considerations in this regard can be broken into two categories: 1) performance of the detector components themselves on the microstrip-tile level, and 2) performance of an outer ITD that is based on the use of such components.

The second issue above can further be broken into the questions of

a) the magnetic field region available in which to do the job of the intermediate tracking, and

b) superlayer and tile layout and distribution options which make the most of the magnetic field and space that is available.

With regard to detector performance on the microstrip level, we can say that so far the device looks to be achievable. However, basic issues in terms of performance such as risetime of the signal (needed to tag the crossing in the time available for a level-1 trigger), minimum-ionizing efficiency, and so forth need to be investigated within the context of the 20 cm x 15 cm ("A4" size) devices that will be required to accomplish the tile pattern desired.

This program is a very strong goal of the ITD group and is our highest priority item, with milestones as early as 1992. (We should point out that since the intermediate tracking system is the last component of the tracking system to be installed before closing of the endcaps, there is extra time built into the schedule which we can and do plan to use to continue to improve on tile/detector development.)

1270

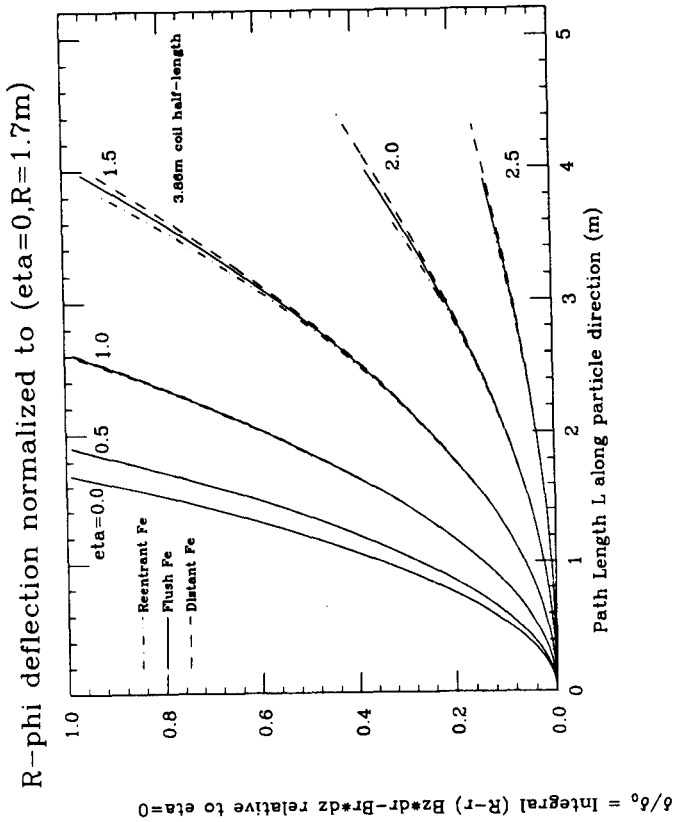

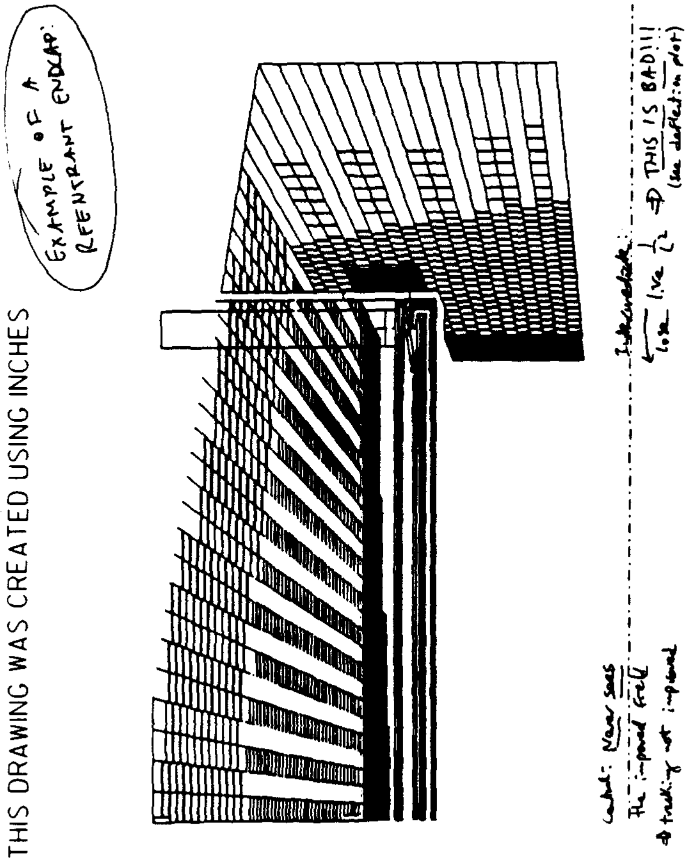

(SUMMARY OF MUCH LONGER TALK IN THE TRACKING SESSION AND AT THE INTERMEDIATE-ANGLE TRACKING DETECTOR WORKSHOP AT RAL IN ENGLAND OCT 25-27, 1991):

QUESTIONS TO BE ASKED & ANSWERED:

→ ① ARE REENTRANT ENDCAPS GOOD OR BAD FROM THE POINT OF VIEW OF THE TRACKER:

Answer: BAD, DEFINITELY. (SEE TRANSPARENCY)
Reason – they shorten the Intermediate-angle tracking region and thus reduce sagitta & deflection (proportional to z^2_{max}), and at least for the iron-loaded calorimeter being proposed, non-uniformities in the flush (or even "distant ≡ the opposite of reentrant) endcap case are small & do not introduce unworkable problems.

→ ② WHAT IS THE LAYOUT OF THE I.T.D. and HOW DO CABLES GET OUT OF THE TRACKER AT THE END REGIONS?

Answer: Considerable thought went into the design of an I.T.D. / Barrel tracking transition interface at the RAL meeting, resulting in a "shadow-the-corner" solution to provide ~20 cm x 1 m space at the ends which allows the large no. of cables in the tracker to exit.

This solution is only possible with the use of a disk-based tracker, and implies a breakpoint between barrels and the ITD at approximately 1.4 in η.

Overview of requirements

SDC Tracking workshop – Feb. 1991 at Oak Ridge: Summary talk by M. Strovink – optimum cell size for good occupancy in the intermediate angle region is a few 10's of mm²
⇒ a few x10⁶ channels

→ O($ 10/channel) ⇒ CHEAP

+ SDC budget ($ 21 M for ...)

↓ Trigger needs
Fine ϕ segmentation, level 1 trigger capability, high rates ⇒ FAST

↓
Geometry considerations of the intermediate angle region ⇒ SIMPLE PROJECTIVE STRUCTURES

Microstrip gas detectors emerge as the only option that can satisfy all these requirements simultaneously.

GENERIC INTERMEDIATE TRACKER

For order-of-magnitude arguments, invent generic tracker:

$\Delta\eta = 0.75$ (one end)

$0.6 < r < 1.4$ m

2 ends × 4 superlayers × 8 layers

⇒ 320 m² of detector layer

OCCUPANCY

$$N \equiv \frac{\text{total \# of elements in intermediate tracker (both ends)}}{\text{\# of crossings integrated}}$$

take $\left.\frac{d(\text{tracks})}{d\eta}\right|_{\text{min bias}} \approx 20$ allowing for loopers, δ rays etc.

then occupancy @ 10^{33} is

$$\boxed{\theta_{33} \cong \frac{1500}{N}}$$

⇒ to get 0.5% @ 10^{33}, 5% @ 10^{34} } need ~ N = 300K elements

⇒ max. detector element is ~ 10 cm²

1275

H.J. Trk

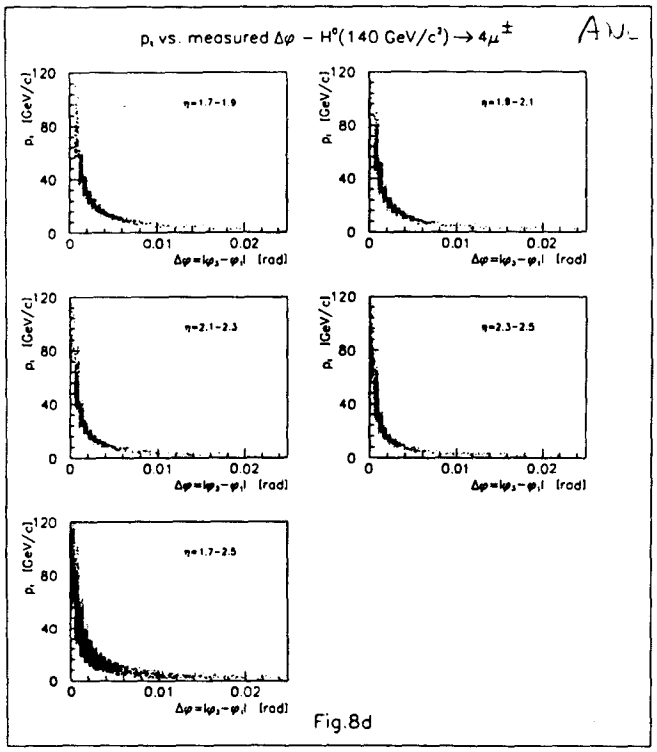

Fig.8d

HJ Trk – ANL

1276

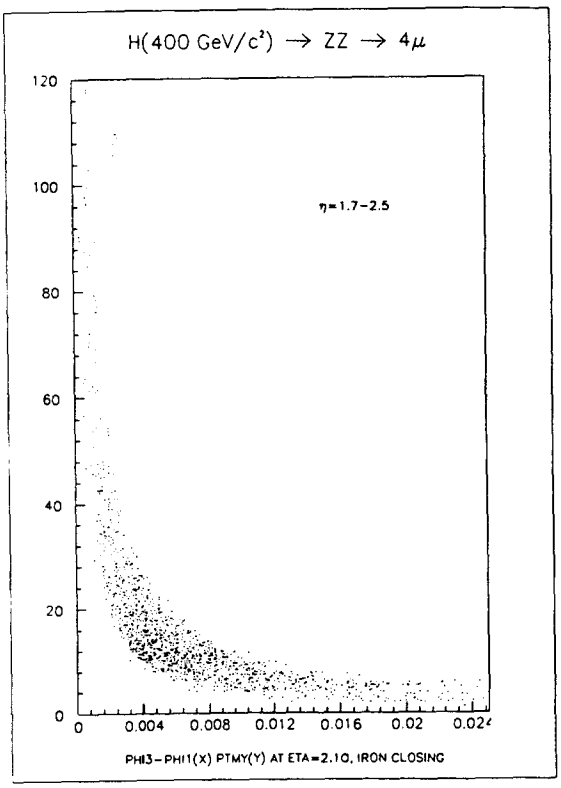

TRIGGER DESIGN:

1271 J. Matthews 1/10/91

1) NEED TO KNOW $P_{\perp\,MAX}^{THRESHOLD}$ AS THIS SETS Δz_{MAX}.

(SciFi) AS $\Delta\phi = \left(\frac{0.3}{P_\perp \tan\lambda}\right)\Delta z$

$\therefore \Delta z \geq \Delta\phi_{min}\left(\frac{P_\perp \tan\lambda}{0.3}\right)\left(\frac{m}{GeV}\right)$

$\sim \left(\frac{1.5\times10^{-3}\,rad}{5.0\times10^{-2}\,m}\right)\left(P_{\perp\,MAX}^{THRESHOLD} = \frac{6^\dagger}{0.3}\right)$

$\Delta z \simeq 0.06\; P_{\perp\,MAX}^{THRESHOLD}\left(\frac{m}{GeV}\right)$

2) NEED ≥ 3 2-LAYER TRIGGER SUPERLAYERS TO ACHIEVE LOW FAKE TRIGGER RATES.

† ASSUMES $\eta \leq 2.5$; FOR $\eta = 3$ $\tan\lambda \sim 10$.

3) NEED TO IMPLIMENT ~ 4 "$\tan\lambda$ BINS" TO COVER THE RANGE: 1273

$\left\{\begin{matrix}\tan\lambda \sim .2\\ \eta \sim 1.5\end{matrix}\right\} \Longleftrightarrow \left\{\begin{matrix}\tan\lambda \sim .6\\ \eta \sim 2.5\end{matrix}\right\}$

(THIS INCREASES TO ~ 6 IF $\eta_{MAX} \sim 3$)

4) RATHER THAN HAVING A SINGLE $P_\perp^{THRESHOLD}$, THE TRIGGER SHOULD BE DIVIDED INTO A NUMBER OF $P_\perp^{THRESHOLD}$ INTERVALS IN ORDER TO MINIMIZE $\Delta\phi_{MAX}$ (ie WANT $\Delta\phi_{MAX} \sim \Delta\phi_{MIN}$).

Performance cont'd:

For the intermediate-angle system with the solenoid magnet lengths being contemplated (on the order of 4 or so meters L/2), regardless of the technology chosen to instrument this region there are fundamental limits to the amount of bending (and hence to the momentum resolution that can be achieved). These issues have been studied and their effect spelled out in detail (see transparencies) se that the best possible choice can be made in this regard.

Simulation has also been done to spell out and study the performance of a microstrip tracker within this magnetic field (see transparencies). The basic conclusion is that the amount of bending for a 10-Gev pT particle between adjacent superlayers of a 3-superlayer system varies from 16 strips to 3 at the lowest and highest pseudo-rapidities being contemplated presently.

The sharpness of the trigger threshold for a 10-GeV pT cut is thus acceptable (i.e., very close to the design requirements document value of 10 inverse TeV sigma_pT / pT**2) for most of the pseudo-rapidity region. It softens slightly in the highest pseudo-rapidity bin (eta of 2.6 to 2.8, roughly) and is still reasonably sharp; but the majority of the accidental "fake trigger" rate comes from this bin and should be further studied.

Perhaps a 4-active-superlayer system could be used to reduce the combinatoric noise in this bin at level 1; but a more fundamental advance could be achieved once and for all by simply making the tracking half-length longer. You win like z_max**2 and hence at a half-length of perhaps 4.5 meters would allow a fundamental and permanent improvement. These performance restrictions can only be worse for a larger-pitch (e.g. fiber) ITD system.

More details need to be studied.

Steve Maxfield

ITD

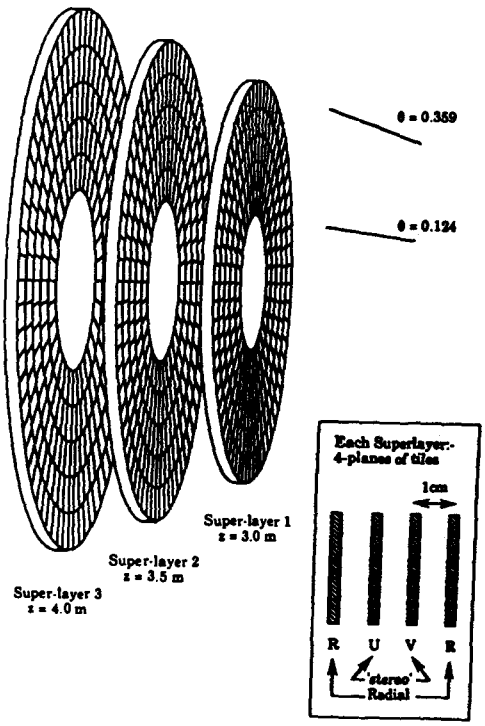

Steve Maxfield 2.

R-TILES at Z = ±4.0 m, ±4.03m.

Ring 1	0.500 - 0.700 m	32 tiles	10752 strips
Ring 2	0.700 - 0.900 m	40 tiles	12600 strips
Ring 3	0.900 - 1.100 m	48 tiles	18144 strips
Ring 4	1.100 - 1.300 m	56 tiles	18816 strips
Ring 5	1.300 - 1.500 m	64 tiles	21504 strips

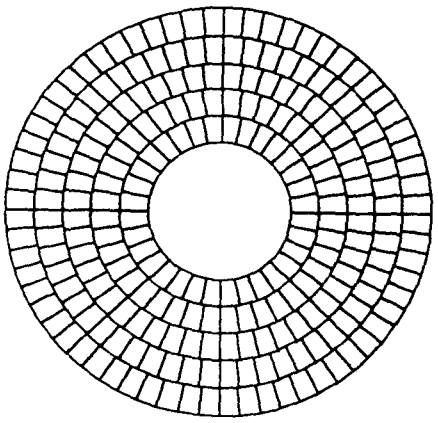

OCCUPANCY

Number of hits/event/plane. ~150

'Event' means the composite consisting of 6 bunch-crossings worth of minimum bias events + 1 Higgs event →

Mean number of hits / plane / bunch-crossing:

	~20
Maximum	~33

Define occupancy as: $\frac{\text{\# hits/plane(}ring\text{)/crossing}}{\text{\# }\mu\text{strips/plane(}ring\text{)}}$

Ring	Mean occupancy(%)	Max occupancy(%)
1	.047	.078
2	.035	.059
3	.02	.036
4	.018	.031
5	.014	.023
Mean	*.029*	*.049*

Low occupancy ⇒ low probability of 'masking' of hits by events from other bunch-crossings

ITD TRIGGER

1283

- Exploit projective geometry:
- Tracks are straight lines in ϕ vs. z and approximate straight lines in r vs. z.
  $\Rightarrow$ tracks stay in one ring.
  The slope in ϕ measures Pt
- Form trigger using one R-layer (these measure ϕ) from superlayers 1 and 2:-
- For each hit in superlayer 1, look for hits in superlayer 2 within $\pm\Delta I$ strip (in the same ring).

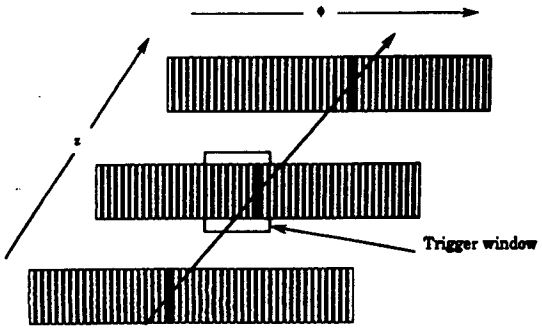

1284

TRIGGER SETTINGS FOR Pt 10GeV/c:-			
	ΔI	$\delta\phi_{track}$	$\delta\Phi_{ring}$
Ring 1	3	0.0020251680	0.0005843735
Ring 2	5	0.0026926502	0.0004986654
Ring 3	10	0.0033730555	0.0003462954
Ring 4	12	0.0040405833	0.0003339277
Ring 5	16	0.0047267745	0.0002921868

Size of trigger 'window' (±)

angle between μ-strips

Change in ϕ between superlayers for track with Pt=10GeV/c

1285

Broadening of trigger edge
– finite resolution in $\Delta\phi$
$\Delta p \sim \frac{1}{p_t}$

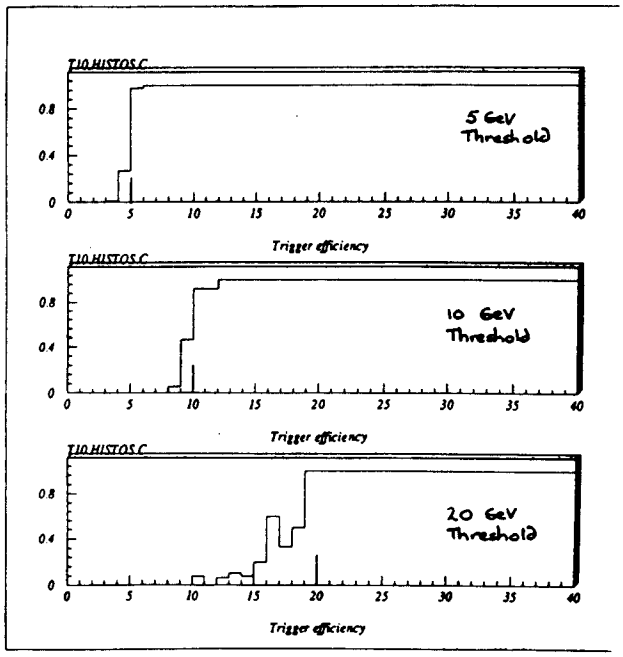

1286

Engineering Feasibility:

Under investigation at both the CRPP and Rutherford Labs. Structure based on cones and disks using composites (carbon fiber/NOMEX/Rohacell/carbon fiber supported from the ends of the coil or from the endcaps) being investigated. These structures need not be solid and could be perforated to reduce material in the tracking volume and weight.

Must maintain tolerance with respect to the silicon and also the barrel -- but structure should separate from barrel to allow access for maintenance, etc.

Tolerance needs are strong but not impossible:

- -- 10 to 20 microns in r-phi
- -- 200 microns in r
- -- z tolerance not evaluated yet

Mounting methods for tiles to the disk structures:

- -- shingled tiles vs. tiles on opposite sides of the disk
- -- dowel pins versus keys to locate tiles to support

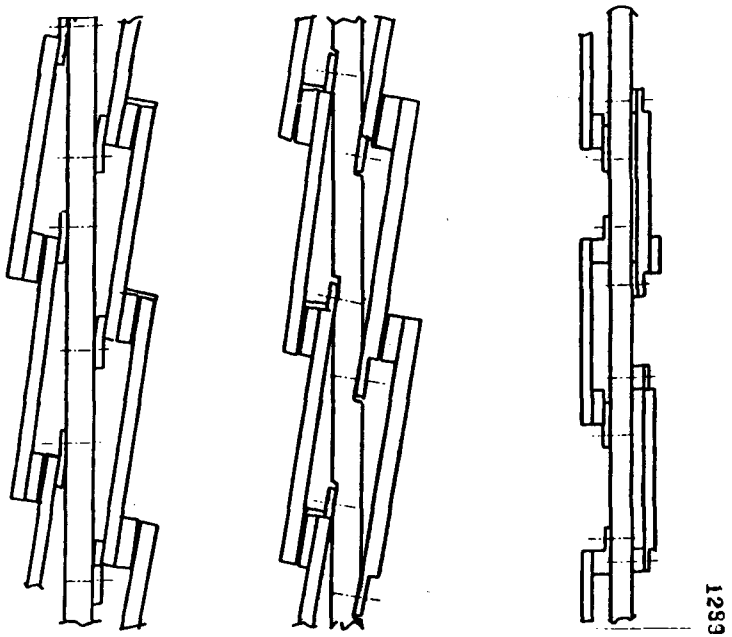

1289

8-O H 15:38:12

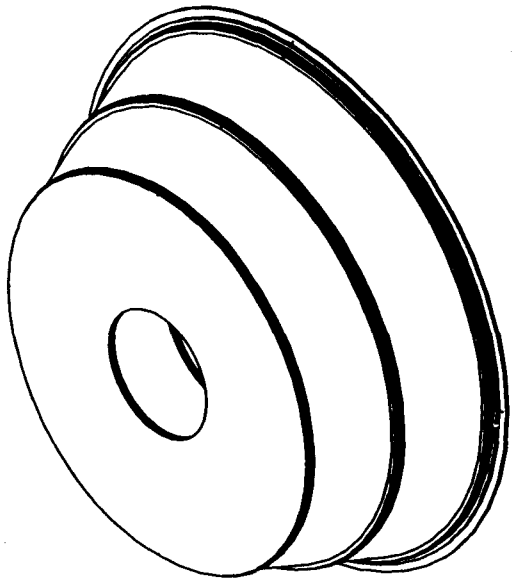

1290

ASSY_WITH_OUTER_CONE

CRPP, OTTAWA

22 SEPT 9

4 PIECES

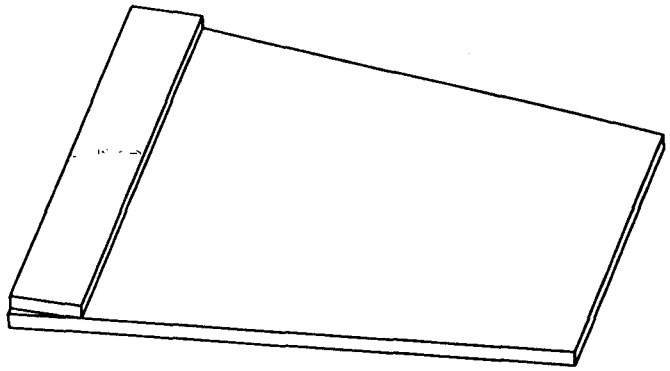

1287

TILE_WITH_ELECTRONICS

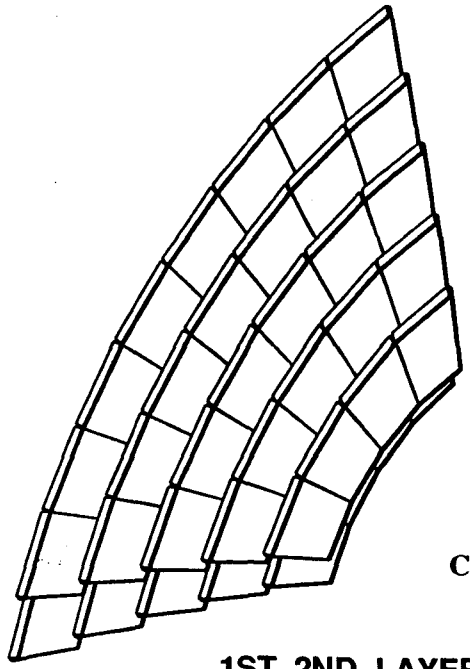

1288

CRPP, Ottawa, Canada

Sept 23, 1991

1ST_2ND_LAYER_1ST_SUPLAYER

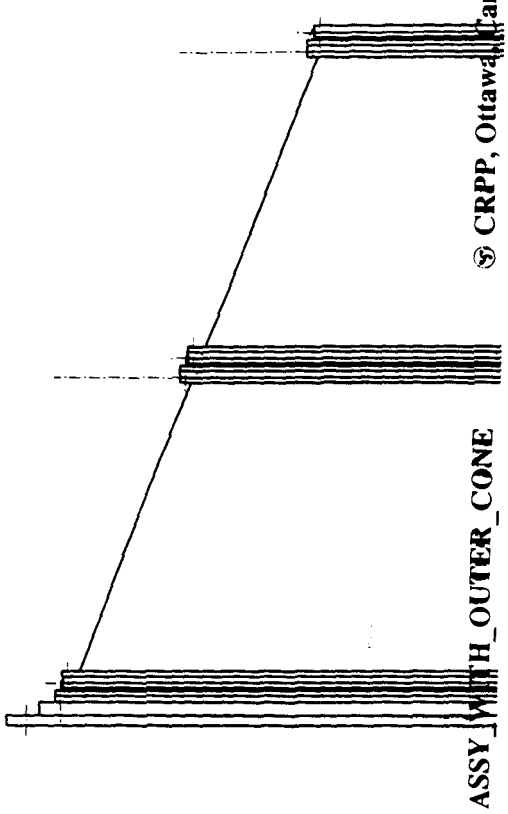

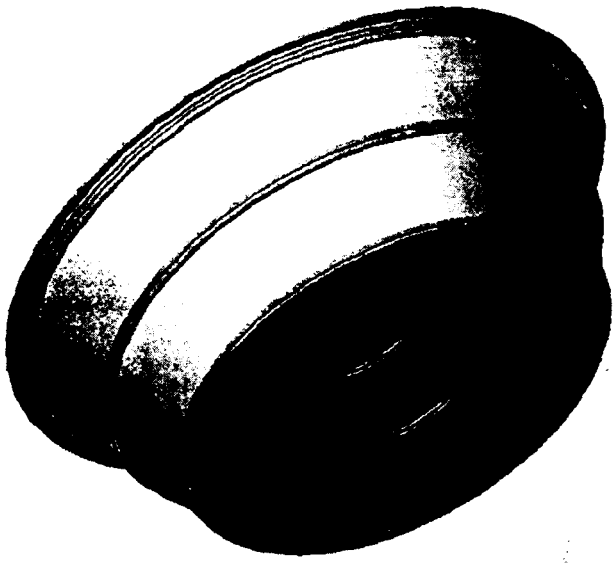

Cost:

Detailed presentation made earlier to this committee. The point to be made here is that we have assigned a very large contingency (80%) to a very conservative number for the cost of production of the most uncertain portion of this budget, namely the production and assembly of the basic detector tiles.

Further experience in the lab will help to improve the sharpness with which we know this basic number. For now, the cost to produce, metallize, lithograph, and etch an A4-size substrate is taken to be roughly $600 BEFORE encapsulation and gas sealing, a number that is comparable to the silicon wafer cost for a much more complicated (though smaller) tile element.

Costing of ITD

6th November 91
G. Oakham
version 3.2

This is the latest version that will be presented at Dallas.

The following labour rates have been used

Technical labour = 75K/year
Engineer labour = 110K/year

	COST K$	CONT K$
TOTAL costs of micro-strip chamber modules	7714	4394
TOTAL FE electronics	1020	420
TOTAL Mech Engineering	2625	980
TOTAL detector design	750	210
TOTAL miscellaneous	1840	490
TOTAL COST	13949	6494

TOTAL COST WITH CONTINGENCY = $20.443 M

not costed

External electronics
Trigger electronics $ 1.6M + M.R.E

Trigger:

This is the key to this device, and indeed to the performance of the entire outer tracker. It is also an area in which microstrips should excel.

The basic design freedom which allows production of a good first-level trigger in this device is the ability to divide naturally into radial (or pseudorapidity) bins, and to arrange the anodes to fall on constant phi lines.

This provides a structure which can be made fully projective in both eta and phi, consequently allowing a very simple first-level trigger based on comparison of strip numbers in adjacent superlayers.

Common to all of the design layouts that we are now pursuing is the concept that an infinite-momentum track at any given value of pseudo-rapidity would cross the SAME STRIP NUMBER in the SAME PSEUDORAPIDITY BIN, in some cases even with the same tile in phi, at EACH of the superlayers that it encounters. The momentum-dependent width of the trigger road is thus defined in terms of strips that are crossed. This is the best (but not the only) way we can imagine doing a fast trigger at level 1.

Time to collect charge

Track at the center of cathode
400 μ pitch chamber with Ar-Ethane 80/20

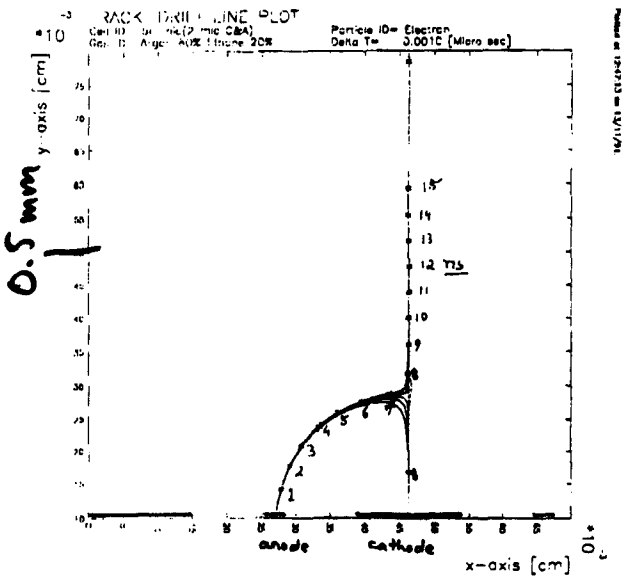

Wes Smith.
Section 2 – Trigger 3.

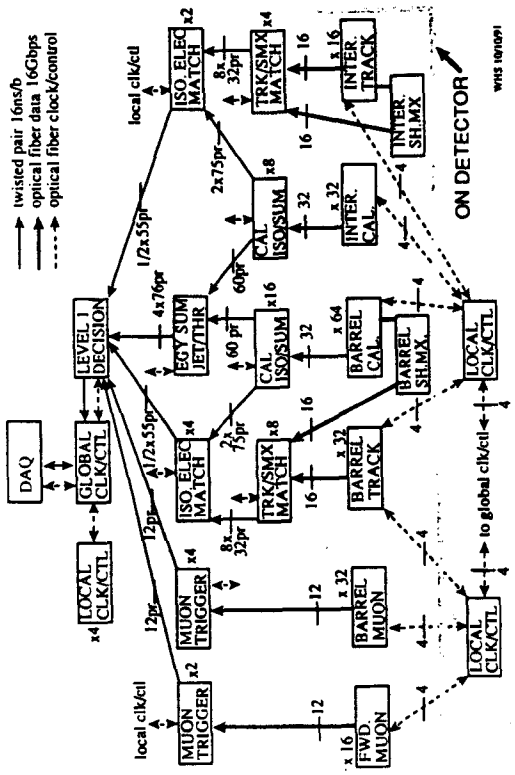

Figure 1. Level 1 Trigger Structure

L-1 HARDWARE IMPLEMENTATION (STEVE'S ALGOR.

Z – Φ LINES USING 3 PLANES

- MINIMAL

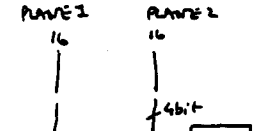

ASSUMPTIONS
- FULL PREC.
- OFF-DETECTOR
- FINITE COST
- PENUT-SIZED CHIPS
SMALL I/O/PUT

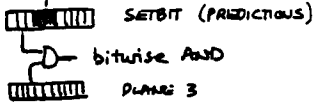

DATA TRANSMISSION

5×10^5 CHANNELS
0·2% OCCUP..
~10 bits/hit
} → ~ 10^4 bits/crossing

=> ~ 1 Tbit/s

→ 2000 500 MHz fibres
15000 63 MHz fibres

500 MHz link => ~ $250 } ~ 2 MHz/$ — MADDISON
63 MHz link => ~ $ 20
↳ UK costing!

[POWER ?]

$500K - saturated at 0·2% occup.

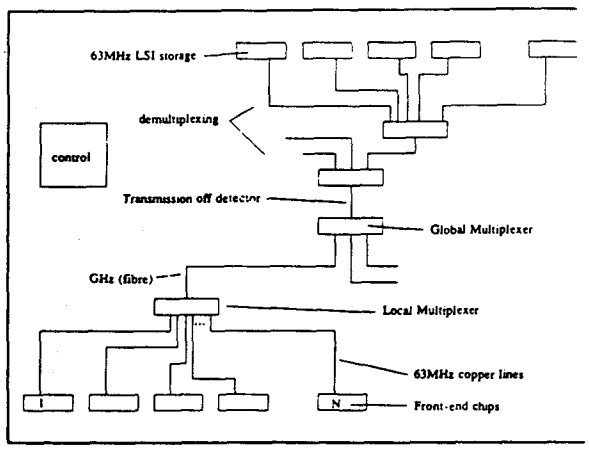

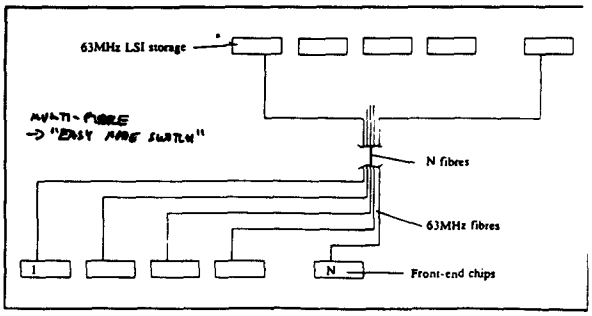

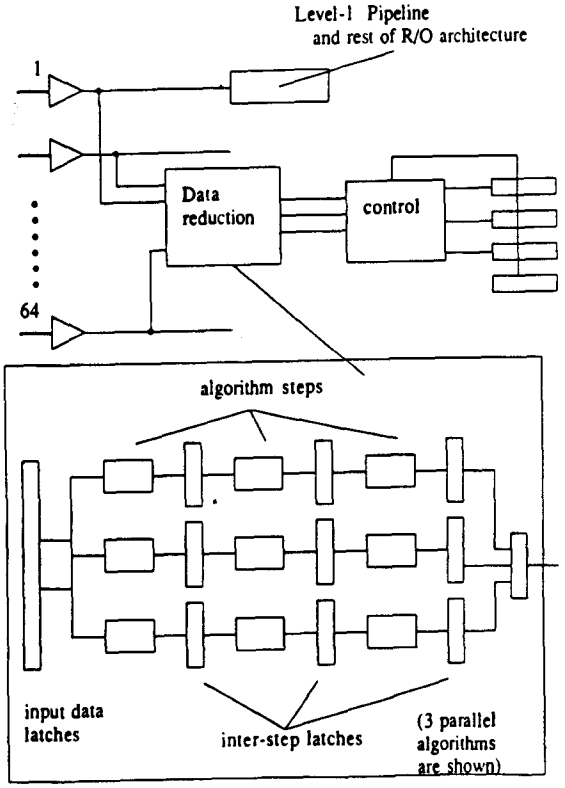

COST

1) FIE – assume part of FIE R/O chip

silicon system chip designed
few (4) hundred gates
→ small perturbation on chip
0

2) Fibre optics
32k @ $20 → ~ 700K

3) 12K channels/FB board → ~ 900K
(~300 boards. incl. control)

~ $1.6M + NRE
for "absolutely minimal" system

Electronics:

No response in detail yet. Electronics remain to be developed but are expected to be similar to silicon, especially in terms of detector readout.

Front-end electronics will see signals that are similar in size to those for silicon microstrips, but with lower signal-to-noise and perhaps a different rise time. Signals drift in over 2 to 3 beam crossings due to the drift time in the gas.

Power dissipation in the electronics is an issue from the point of view of cooling, but even at a few tens of milliwatts per channel in power load, the total comes to only on the order of 30 kW per end. It is expected this can be removed if necessary by recirculatin coolant rings to service the preamp locations only.

Texas A&M has designed a front-end electronics package (soon to go to the ASIC stage) which will have as its goal 100 microwatts of power, which would drastically reduce the amount of cooling needed.

Cabling expected to be on optical fibers, conceptually (and in fact, perhaps in detail) identical to 1/3 of those needed to read out the silicon.

While trigger and readout have received an initial look, more work is needed throughout these categories to assess differences in detail and to minimize risk.

Cable Plant:

Readout by fiber optic cable to external systems, both for microstrip data and also by trigger roads (independently) for the first-level trigger. In addition to data cables, also require high voltage, gas, and cooling lines to be run.

Data cable volume expected to be small. No estimate yet for high voltage and the rest; but this looks to be possible.

Material Budget:

This is an issue that relates to the layout and transition between barrel and disk elements in the outer tracker.

Material clearly favors a low eta breakpoint. Below 45 degrees from the beam line -- i.e. above pseudo-rapidity = 0.86, material burden for a superlayer laid out in the form of a disk is less than that for an equivalent superlayer that is a barrel. In addition, the pseudo-rapidity bite of a "lump" of electronics, fibers, or cables will be less at lower eta than for the case fo the same physical size lump at high pseudo-rapidity.

All these issues tend to favor a low eta breakpoint. However cost, risk, and other considerations tend to push the transition between barrels and disks out further in pseudorapidity. This issue needs to be reopened and studied in detail.

Pseudo-rapidity breakpoints which "shadow the corner" with disks could allow space for cables to exit the tracking volume at its ends, if that were to prove to be necessary. If not, then the considerations which enter into the decision as to the breakpoint between barrels and disks are material, cost, functionality, performance, and risk.

Various layouts are being and will continue to be investigated in order to find the solution (or solutions) which best meets all of the above requirements and needs.

LOI w/ radial wire ITI

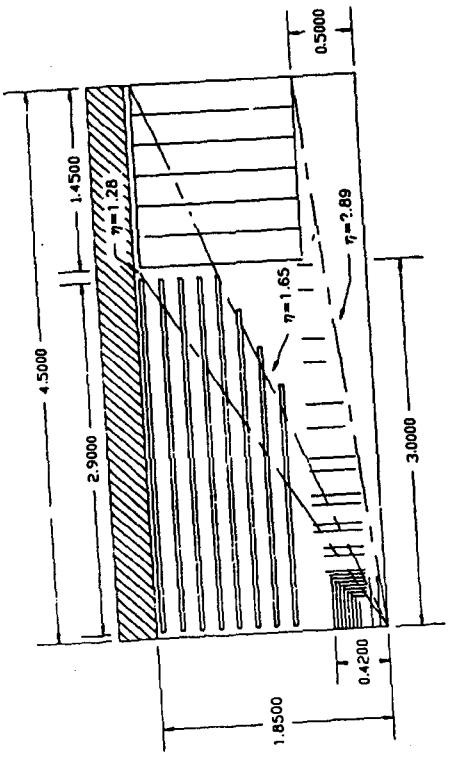

Fig. 1. Conceptual design for a pixel, silicon strip, and wire chamber tracking system for a solenoidal detector.

One ITD layout, 3 superlayers
1.6 < η < 2.5

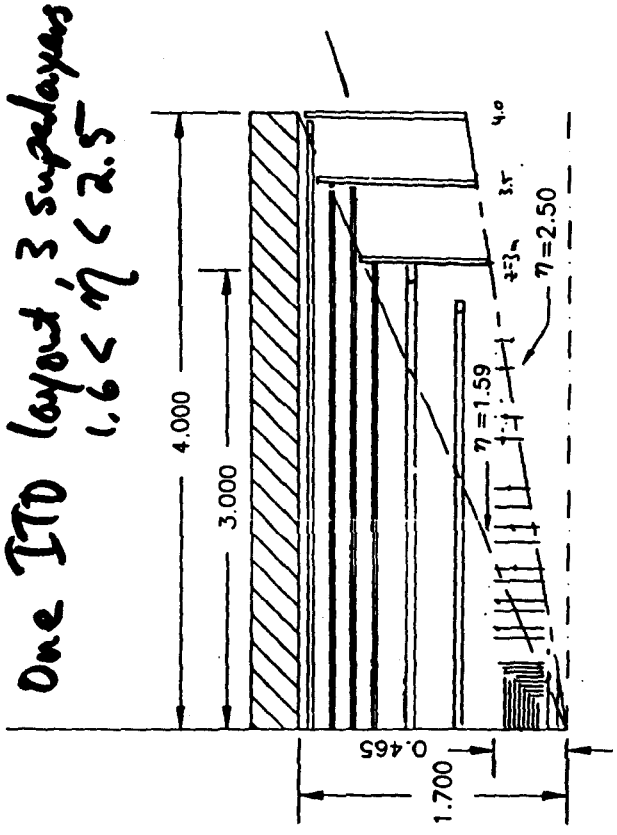

(LBL meeting example)

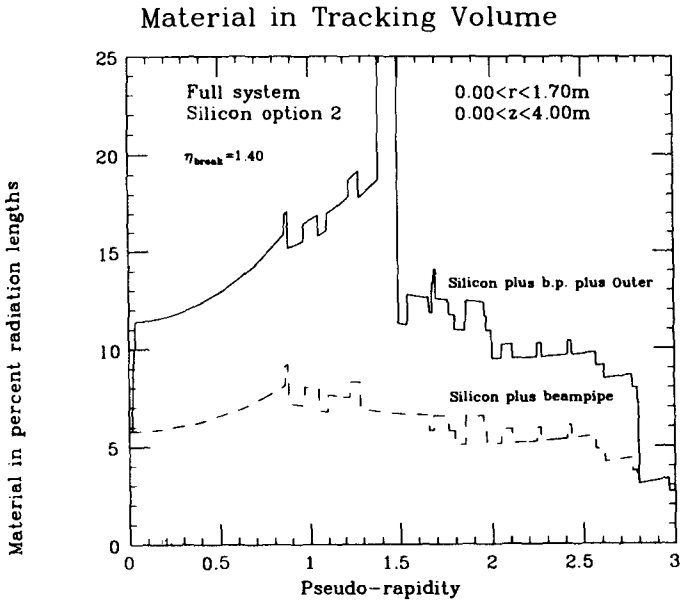

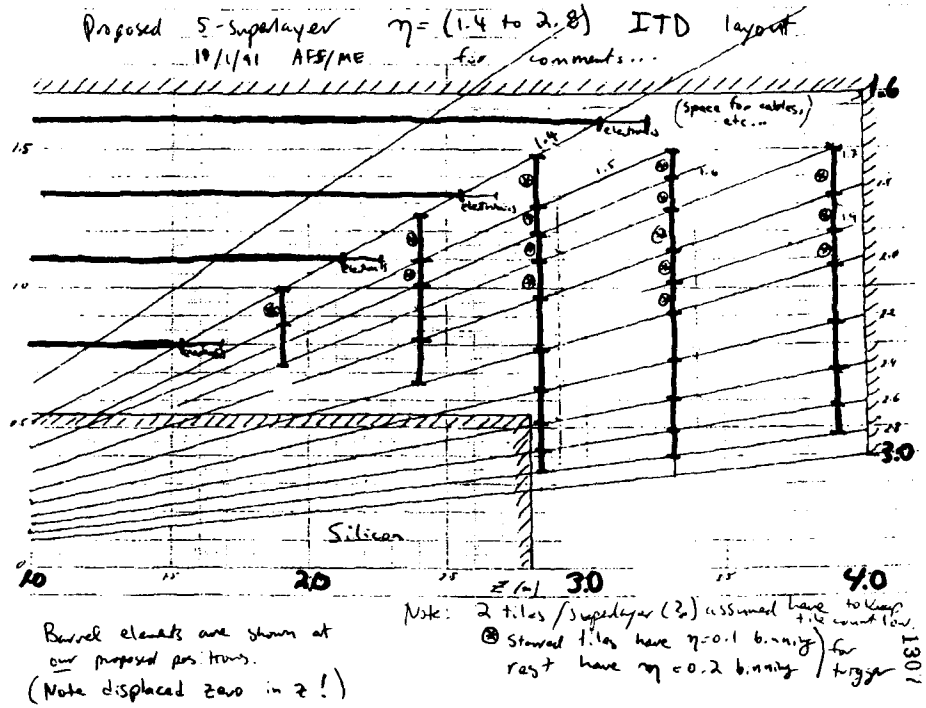

Upgrade Potential:

The gas-microstrip ITD should be able to survive comfortably up to the highest luminosity expected to be delivered. Trigger combinatoric rates for accidental backgrounds at the high-pseudorapidity ends of the detector favor a long tracking volume, so that enough bending is available to prevent this from becoming an issue as the luminosity goes up.

In the far future, microstrip developments to meter-scale devices in length could allow a natural upgrade path for the barrel tracker at the highest luminosities.

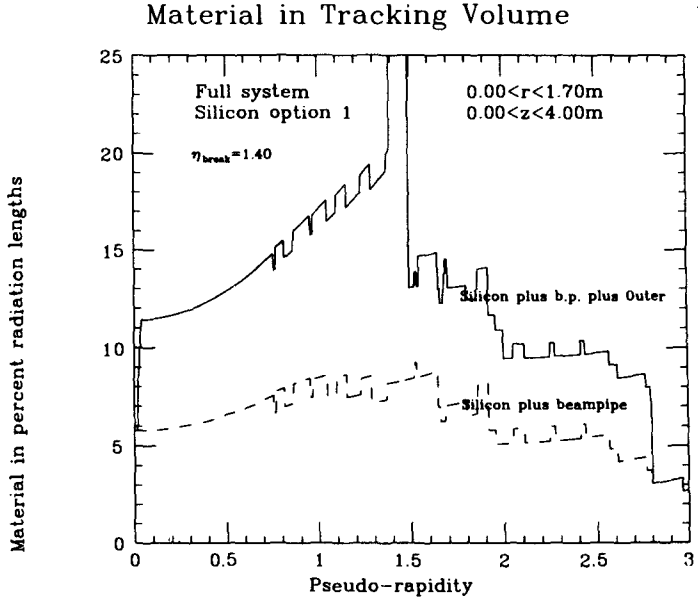

Pattern Recognition in Silicon and Straw Tracking System

B. Hubbard(UC/SC)

Pattern Recognition in Silicon + Straw Tracking System

Brad Hubbard
Kathy O'Shaughnessy
Bill Lockman
} UC Santa Cruz

Plan:

- Intro: Algorithm described
- Single track resolutions
- Study of $H \to 4\mu$ events

Tracking system simulated:

8 layer "descoped" silicon (9-36 cm radius) "ST"
5 superlayer straws (70-160 cm) "WR"

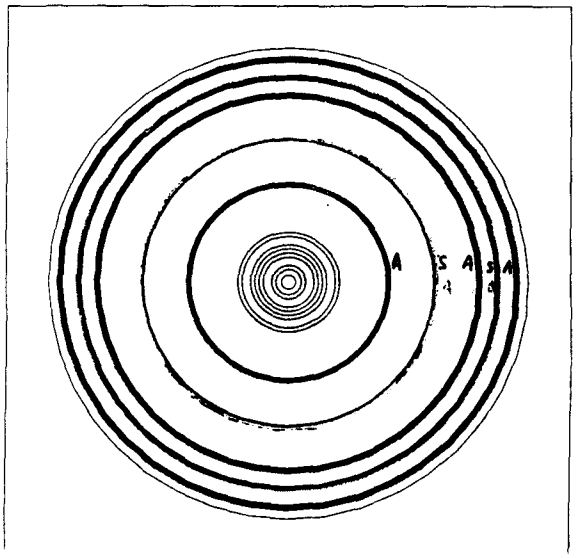

2 Silicon configurations:

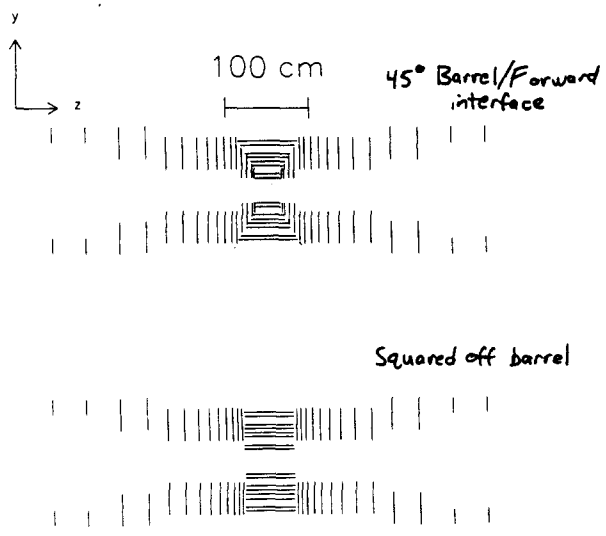

Silicon Tracker Simulation

- Realistic, flexible description of detector geometry
- Support structure not simulated in detail
- Additional material at each layer, amounting to (default) 6.8 χ° at normal incidence ~ 20% over present estimate
- Small Angle stereo, double sided detectors
- Simple hit modelling, "digital" system

Not included at present:

- noise, time walk, threshold variations
- dead time, dead channels
- diffusion or induced charge sharing
- magnetic field effects
- alignment

TS Track Reconstruction

- Tracks found with segment clustering in silicon.
- Road Technique used to add segments from outer system
- Fit with multiple scattering (in silicon)

- "Vector segments" composed of axial/stereo hit pairs from 2 adjacent layers (total 4)
- Calculate parameters · extrapolated to beam:

  Barrel: $(K_{(curvature)}, \phi_0)$ $(z_0, S = \tan\lambda)$

  Forward: ( ) ( )
- Cluster segments separately in 2×2 sub spaces:

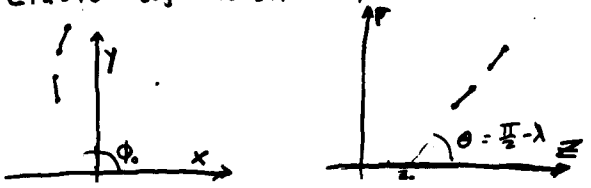

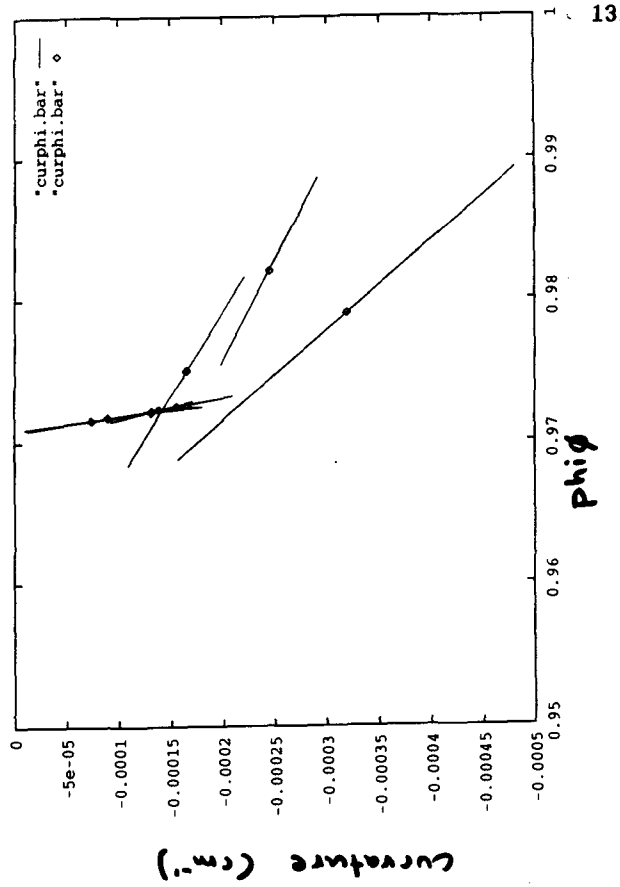

TS fitting

TF/FIT TS ON

- modified to fit TRCT banks with ST + WR data from any algorithm
- improved "road" algorithm

Iterative helix fit including multiple scattering.
Tracks are fit in 4 passes: (require 8 hits* to start

A.) Initial assigned points. Start with initial trajectory, iterate up to 4 times or until χ^2 ceases to improve.

optional:

B.) If $\chi^2 > 50$, drop hit with largest residual. Re-iterate and drop up to 8 hits.

C.) Add unused hits along road defined by track trajectory (discuss further next slide)

D.) For primary track candidates ($\frac{b_0}{\sigma_{b_0}} < 3$) add 10μ beam constraint in r-φ.

---

hit: silicon axial digi, stereo digi, or WR segment. A coordinate from PX or SF would count as 2 hits.

Road algorithm

- alternative to global segment linking approach

Especially important for:

→ • where geometry changes: Si barrel/forward interface
Si forward/outer barrel

→ stereo superlayers in WR

Now, add fewer hits at a time, refitting, repeat until no more hits remain to be added. Several stages:

1. Add Si hits within track CLASS = 1
2. Add Si hits inwards, one layer at a time CLASS = 2
3. Add Si hits outwards, one layer at a time Class = 3
4.
5. Add outer system hits, (axial WR segments) one layer at a time. CLASS=5
6. Add outer system stereo segments, one layer at a time Class = 6

1320

Road technique: Pick up hits within road defined by track parameters.

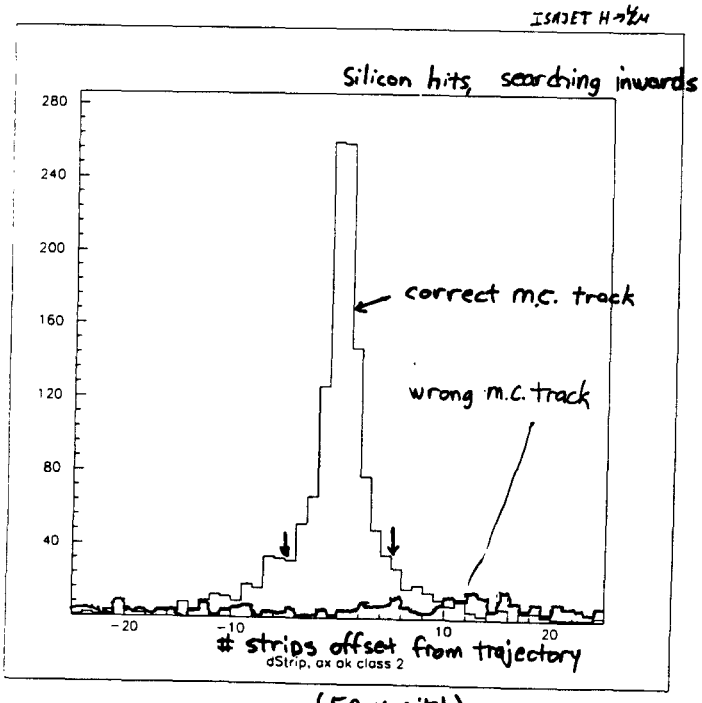

(50 μ pitch)

1321

Road Technique:

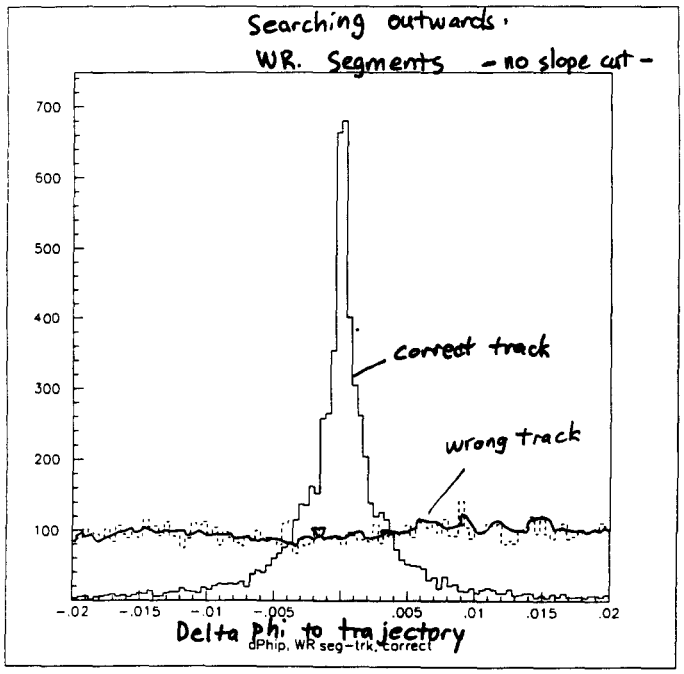

1322

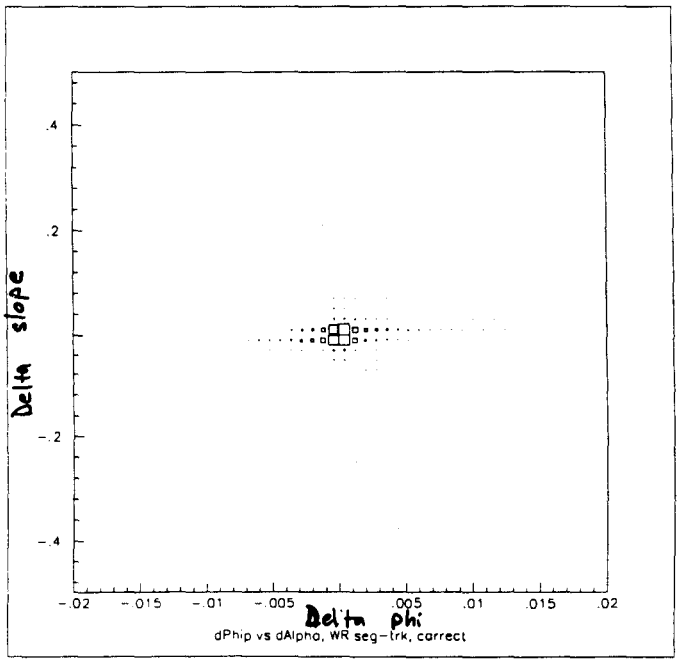

1323

Single track resolutions

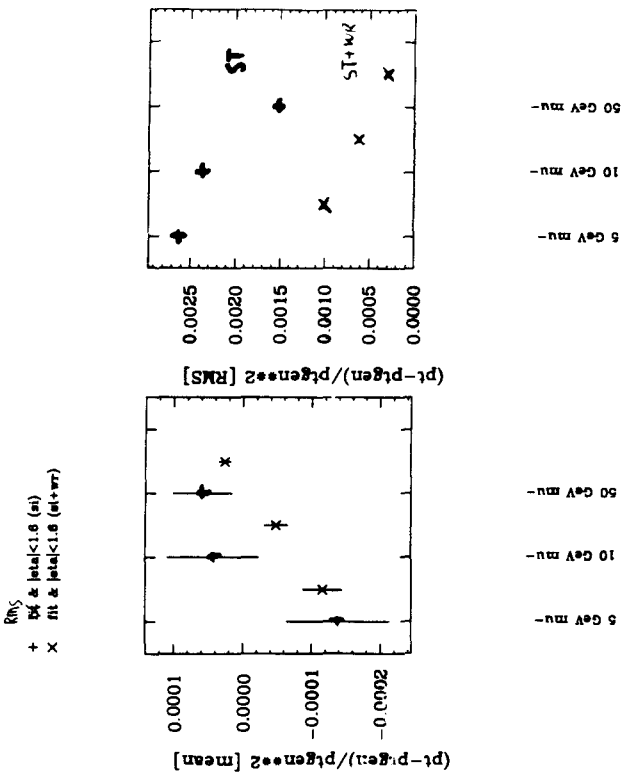

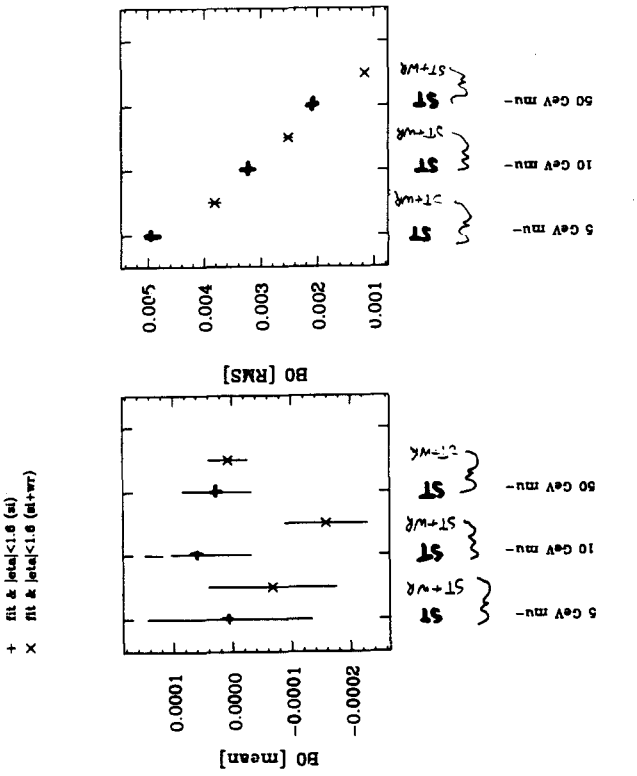

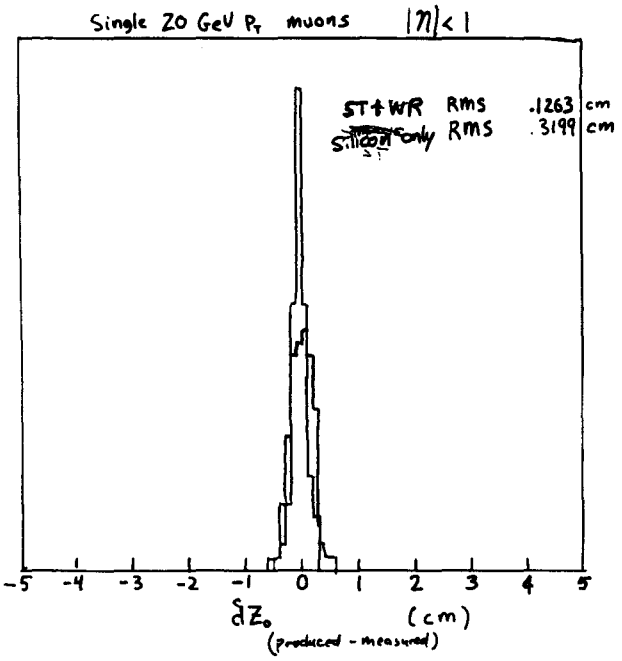

Higgs Study, (in progress):

- efficiency for single isolated leptons vs. luminosity
- mass resolution
- higgs reconstruction efficiency

Compare: different geometries
stereo angles

Event Generation

- Isajet : $H \rightarrow 4\mu$, $M_H = 400\ GeV/c^2$
  $\rightarrow ZeZ\mu$, $M_H = 300\ GeV/c^2$
- Pythia : minimum bias, $\langle N_{bg} \rangle = 1.6$ for nominal luminosity
  simulate crossings $-4 \cdots +2$
- SE Higgs filter, require 4 leptons with $|\eta| < 2.5$
- Drop HEPP MC. banks for pythia bg events
- Beam $\sigma_x = \sigma_y = 10\mu$, $\sigma_z = 5cm$
- WR + ST detectors, coil material not simulated (?)
- Hits generated for $-100\,ns < t < 100\,ns$ (?)
  (± 15 ns window for silicon,
- Default GEANT options, except:
  - Moliere scattering (not Gaussian)

Reconstruction parameters

- Fit candidate track with ≥ 3 wafers hit
- Accept track if ≥ 8 silicon hits (stereo + axial)
  or ≥ 6 silicon hits + ≥ 1 WR segm

Track flagged as "fake" if > 2 wrong hits

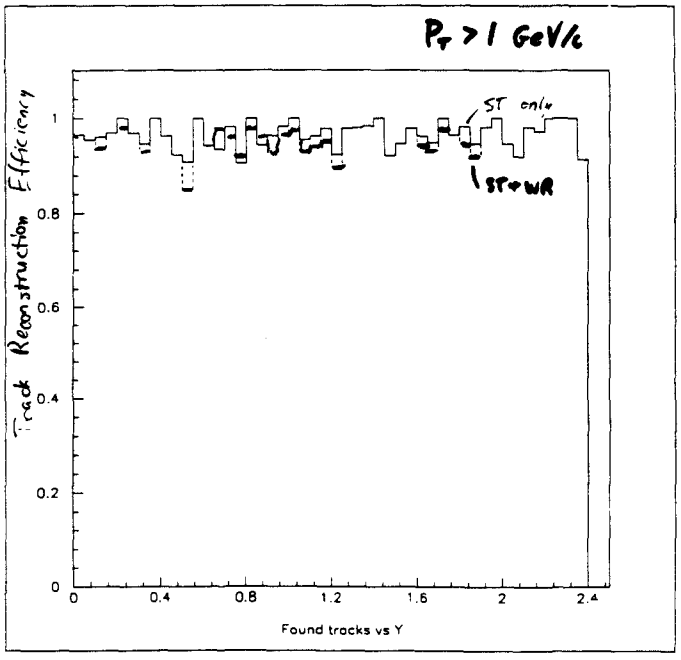

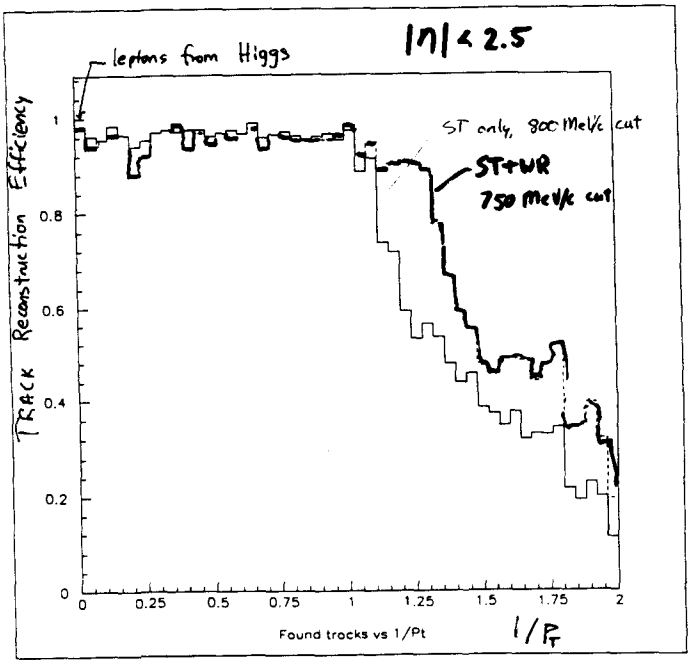

1332

$\langle n \rangle_{back} = 1.6$, for several crossings

7 cm beam σ_z

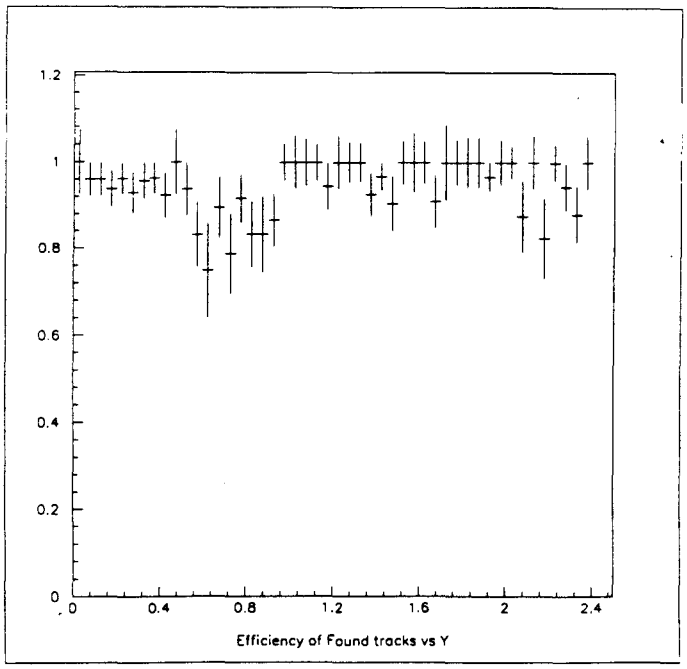

1333

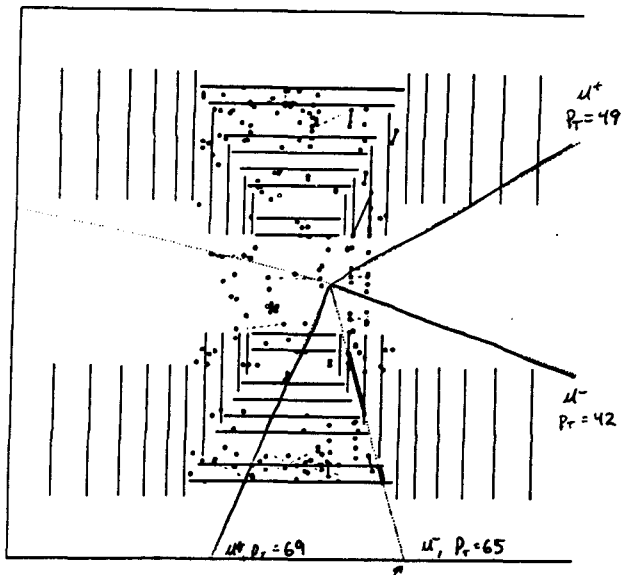

only Higgs lepton not found in 50 events

1334

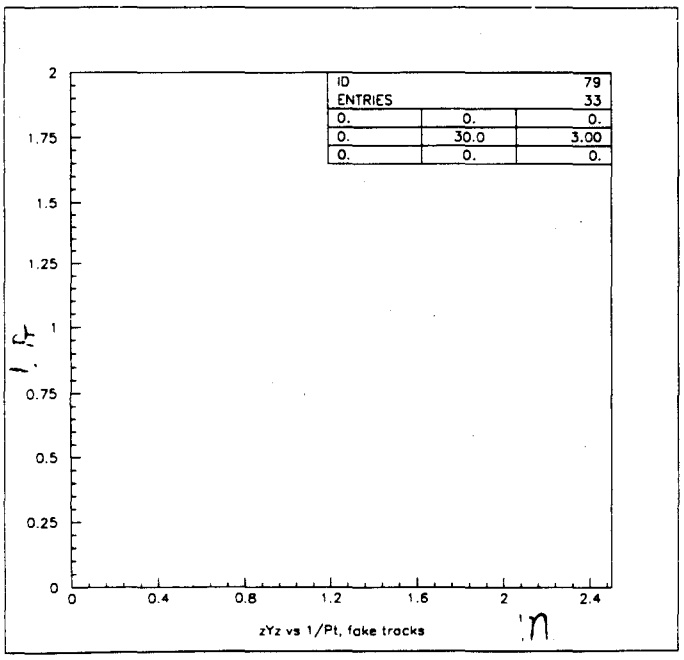

1335

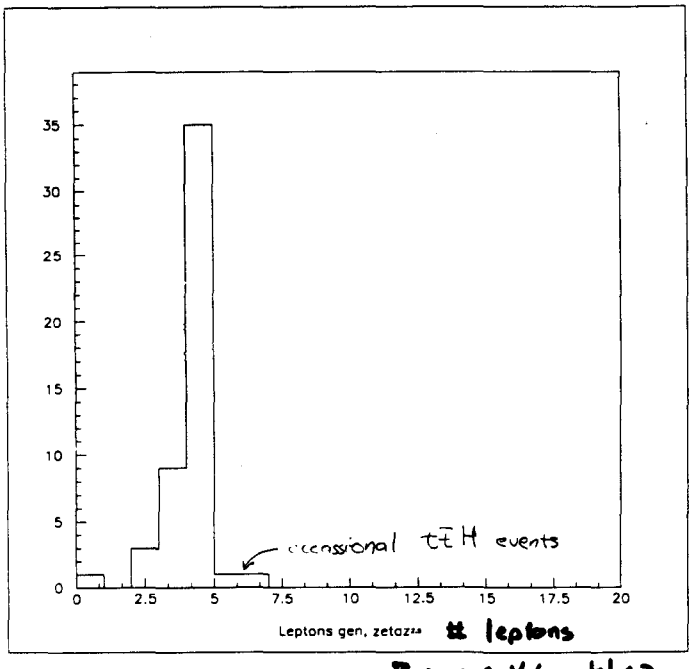

$P_T > 10$ GeV/c, $|\eta| < 2$

1336

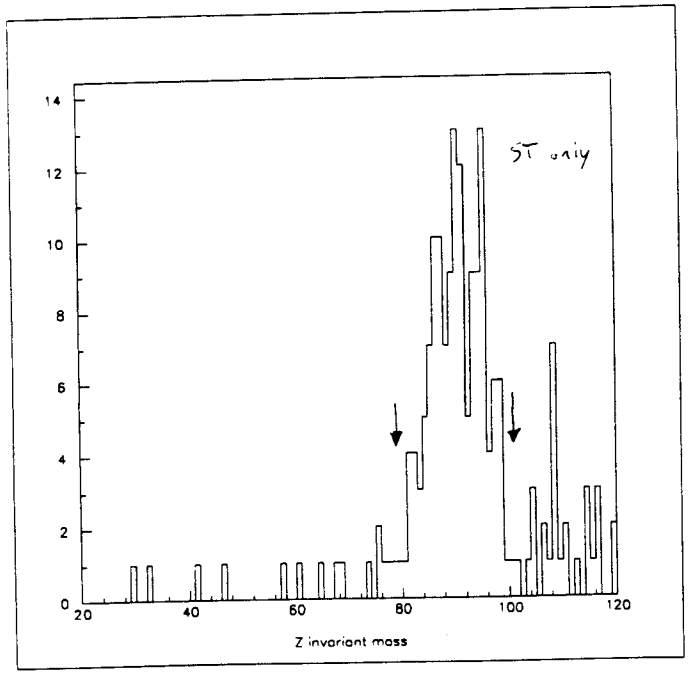

1337

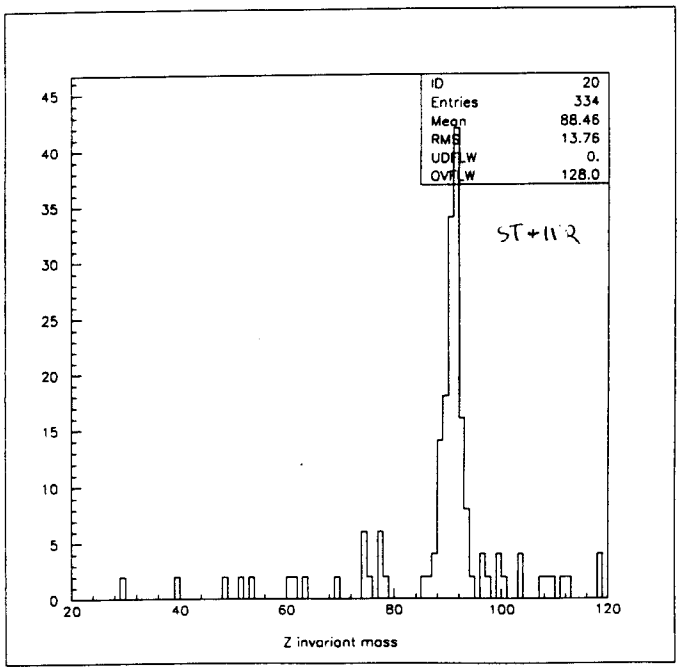

1338

2K design luminosity

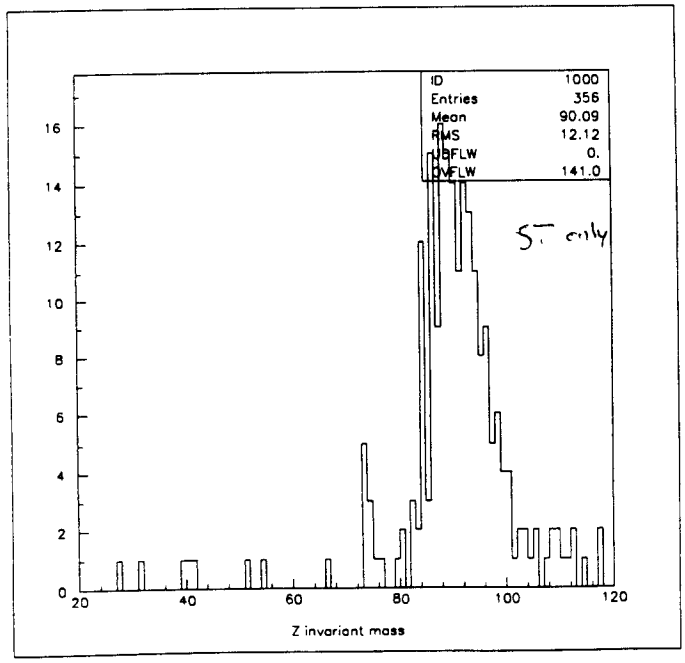

1339

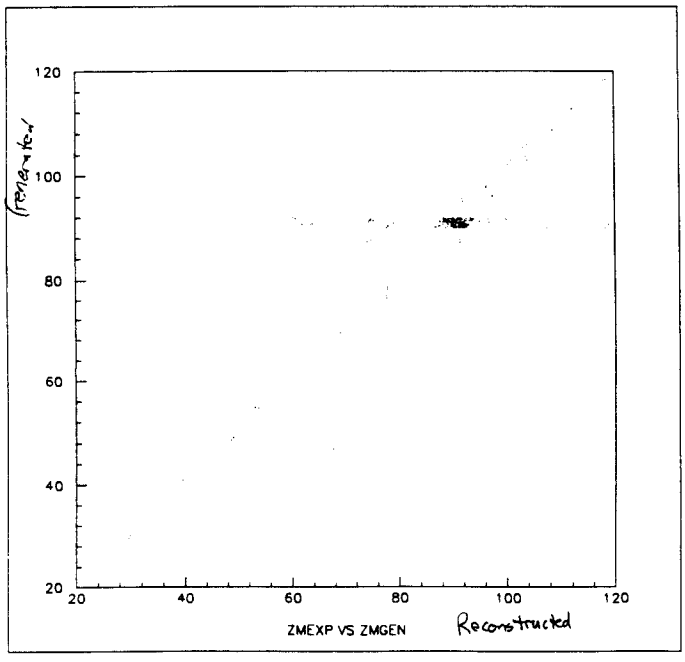

1340

3x design luminosity

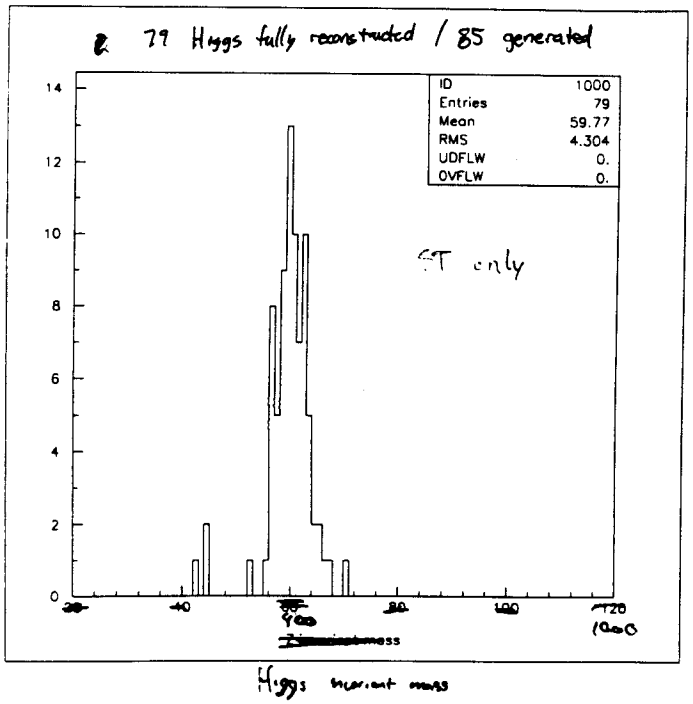

1341

3x design luminosity

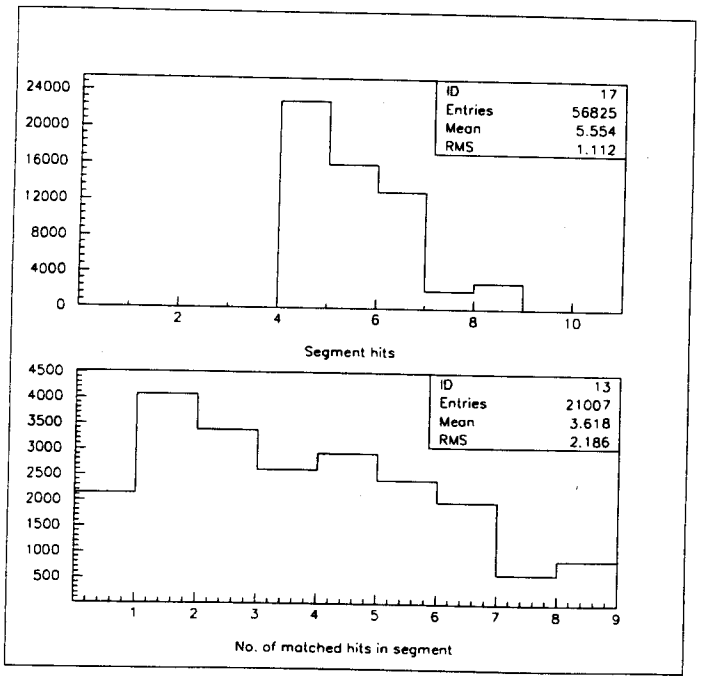

1342

3 x design luminosity

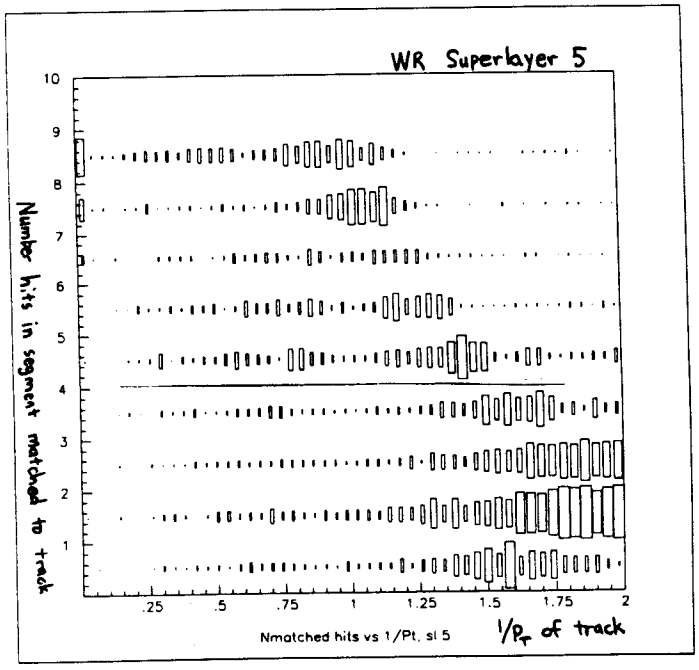

1343

3x design luminosity

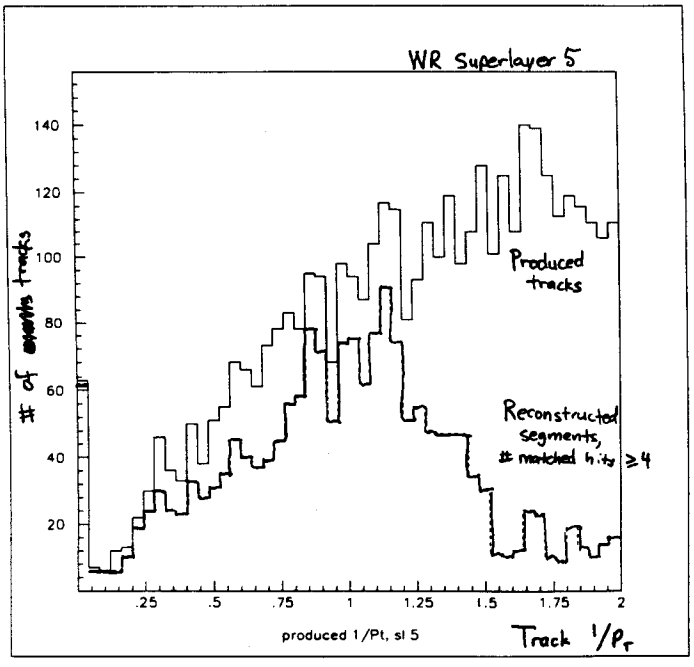

3x design luminosity

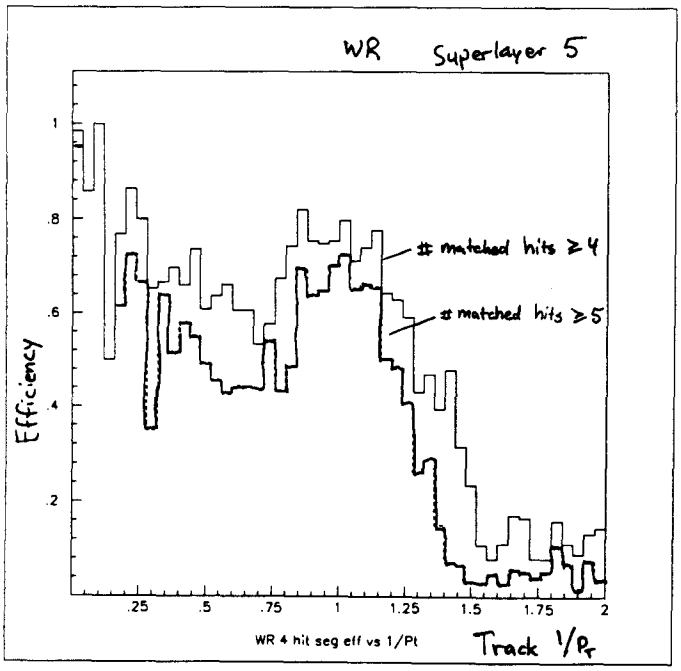

3x design luminosity

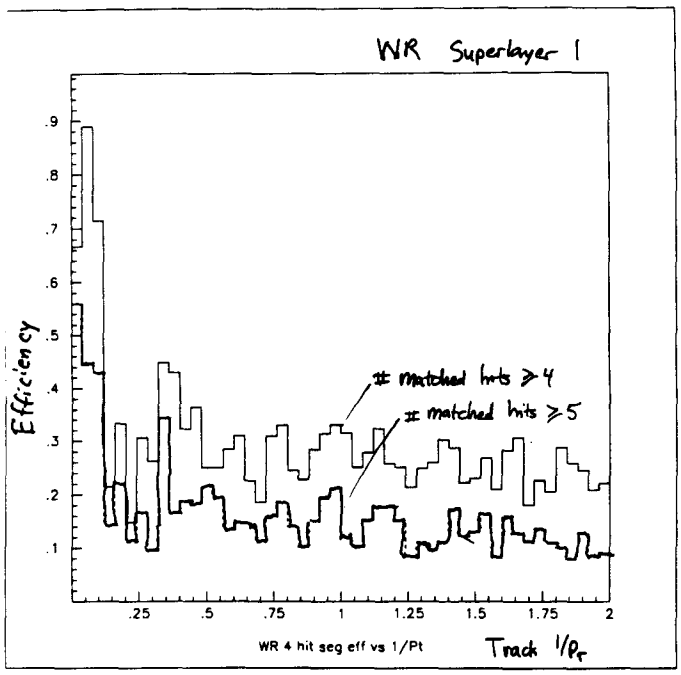

Preliminary conclusions:

- ST + WR resolution as expected
- Concerns about resolution tails in busy events due to improper or confused WR segments
- Higgs efficiency high even at 3 x nominal

Physics studies for CDR + Technical Proposal

A. Higgs → 4 leptons, 2e2μ, 4μ
- determine efficiency for isolated e + μ and resolution from tracking system alone
- Vary luminosity from 0 to 10 x design luminosity
- Vary stereo angle.

B. Jets,
- overall track efficiency vs jet P_T
- work to resolve confusion
- look at fakes, resolution tails

C. Top:
- efficiency for non-isolated leptons from b decay
- impact parameter resolution for b decay leptons + hadrons
- Study b tag efficiency for different algorithms

D. Heavy Z' (4 TeV)
- resolution, assymmetry measurement

Pattern Recognition in a Silicon and Scintillating Fiber SDC Tracking System

D. Adams(Rice)

SDC-91-[illegible]

Pattern Recognition in a Silicon and Scintilleting Fiber SDC Tracking System

1343

D. L. Adams, G. Eppley and J. Skeens
Rice University

11 Nov 1991

Abstract

The proposed SDC silicon and scintillating fiber tracking system has been simulated and tracks reconstructed for a 300 GeV Higgs producing four leptons. The process has been simulated with and without the background expected at SSC design luminosity. Results are presented for occupancies, track reconstruction efficiencies and resolutions for the parameters characterizing the reconstructed leptons.

Introduction

The design of the central tracking system for the SDC detector is a major unresolved issue within the collaboration. Here we report results of simulation and pattern recognition studies carried out with the presently envisioned silicon and scintillating fiber detectors.

Detector

This study makes use of two of the subsystems in the SDC design: the silicon inner tracker and the scintilleting fiber outer tracker. The design of the silicon tracker is similar to that in the LOI [1]. Most relevant to us is the barrel which covers +/-45 deg, i.e., -0.9 < eta < 0.9. There are eight double-sided layers with the innermost at a radius of 9 cm and the outermost at 36 cm. The geometry was taken from the SDCSIM v03 file st_descope3.kumac distributed with that version of the program.

The scifi system is that described in the corresponding CDR [1] and shown in figure 1. Three inner barrels cover |eta| < 2.0 and two additional barrels also provide information for |eta| < 1.6. Three disks on either end extend the coverage to |eta| of 1.5. All barrels have four axial layers (fibers parallel to the beam axis) with relative fiber offsets of 0.0, 0.5, 0.25 and 0.75 fibers. These quarter-fiber offsets provide optimal resolution. The outer layer also has two pairs of stereo layers with half-fiber offsets. The sterso angles are opposite in direction and have a magnitude of 15 degrees.

1350

The scifi disks include four layers: two pairs of half-fiber offset spiral layers. All fibers run from the inner to outer radius beginning in the radial direction and then wrapping around the beam axis so as to remain close-packed. We do not make use of the disks in our present reconstruction. It is worthwhile to note that the fiber count is determined by the inner radius and that a detector made up of purely radial wedges with the same spacing at the inner radius would have the same channel count and occupancy.

Simulation

The simulation and reconstruction were carried out in the framework of the SDC simulation package SDCSIM (the "shell") [3] version v03. Minor changes were made to incorporate the most recent versions of the the packages SF and TR. We provided some additional code, mostly the filling of ntuples, through the standard user interface package US. The analysis was carried out in three stages where each of the latter stages used the SDC data structure output from the previous stage as input. In the first stage events were generated using the SE package, in the second they were tracked through the detector and digitized using SG and in the last the tracks were reconstructed using TR. Each of these steps is described in seperate sections below. The user is referred to the SDCSIM documentation [3] for information about the various packages. We generally did runs of 100 events.

The work described here was carried out on IBM RS6000 machines at Rice. There are two model 530's and one 320 for a total of about 100 MIPS with about 1 Gbyte of available disk space. This system was adequate for studies of single events and events at design luminosity but did not allow us to go to significantly higher luminosities. We have begun to carry out studies at the SSCL computer ranch pdsf but note that one user's "fair" share may not exceed that already available to us. Studies at higher luminosity will require some combination of filtering the generated events, improvements in SDCSIM and increased CPU power and disk space.

Event Generation

We generated Higgs with mass 300 GeV/c using Isajet and required that the Higgs decay into two Z's and that each of the Z's decay into electrons or muons. We also did some runs with a Higgs' mass of 800 GeV and found similar occupancies. The event vertex was fixed to be the origin (r=0, z=0) to provide a uniform geometrical acceptance. Background was generated by using Pythia to generate QCD inelastic events (MSEL = 1). Background at design luminosity was simulated by including 1.6 events/crossing in each of buckets -4 through +2 in arcordance with the conventions of the SDC tracking group. We did runs without background and with this background and three times this background. Disk space and CPU limitations prevented us from tracking runs at the higher luminosity. The SE input files used to generate the Higgs and background events are included as appendixes.

1351

Most of the results discussed here are based on two runs: number 90 including Higgs alone and number 94 with the Higgs plus design luminosity (10**33 /cm**2/sec) background. Each run consists of 100 events but the last nine events of the run with background were lost during the GEANT tracking so only 91 of those events are used. The Higgs alone required 4 CPU-sec/event for generation and the Higgs at design luminosity required 14 CPU-sec/event.

GEANT tracking

Events are tracked through the detector using GEANT interfaced to SDCSIM through the package SG. The subpackages ST and SF were used to define the geometry and evaluate the response of the the silicon and scintillating fiber tracking systems. SG provides a description of the beam pipe (1 mm thick beryllium at a radius of 4 cm) and the solenoid. All tracks were stopped when they reached a radius of 180 cm or |z| of 450 cm to save CPU time. The exact details of the geometry and other adjustable constants may be found in the initialization files st_descope3e.kumac for ST and sf_optc5.dat for SF. These are included as appendices to this paper. All 100 events of run 90 and the first 91 events of run 94 were successfully passed through this stage at rates of 10 and 31 CPU-minutes/event.

Track Reconstruction

We reconstructed the tracks in the event using the track reconstruction package TRF which is contained in the SDCSIM package TR. Calls to TRDEFK, TRINIT and TREVNT were added to the corresponding routines in US. Also an optional call to SGINIT was added to USINIT so that the geometry could be set up without calling SG each event. It is expected that SDCSIM will soon be capable of including geometry data structures as part of the overall saved data structure so that this last addition will not be neccessary.

TRF uses a programmable road-following technique to find the tracks. The user provides instructions in an ascii file often called trf.det. The user chooses a layer in which to start tracks and then extends the tracks to each of the others in the order he chooses. Each time a hit is added to the track, it is refit and the user may delete tracks based on the number of hits or chi-square.

For this study, we reconstructed tracks by starting in the outer layer of the silicon and moving in. In some runs, we then stopped and did a final fit with a vertex constraint or varied the vertex and fit at the distance of closest approach. In other runs we added the scifi layers moving outwards after fitting the silicon and then closed tracks in the same way. We only made use of the barrel layers because the disk-fitting routines are not yet debugged. This restricts our eta range to -0.9 < eta < 0.9. We only searched for tracks with pT > 5 GeV/c to decrease the execution time. We rejected tracks with chi-square above 50 in the silicon or 100 in the combined system.

1352

Each of the two runs was reconstructed four times -- with and without the scifi and with and without the radial vertex constraint. One of the map files is included as an appendix. The longest runs required 2 CPU-min/event for the events without background and 3 min/event for those at design luminosity.

At the end of the reconstruction, each of the reconstructed tracks is compared with the each of the Monte Carlo tracks and the nearest Monte Carlo track is assigned to that reconstructed track. The nearness of tracks is measured in terms of a match chi-square obtained by squaring the difference between the Monte Carlo and reconstructed track vectors weighted by the inverse of the error matrix. Each Monte Carlo track is only assigned to no more than one reconstructed track.

Results

We present results for occupancies, track-finding and reconstruction efficiency and resolution. The data were reduced to two ntuples from which these values were extracted. The first ntuple is filled once for each layer each event and contains the number of channels, digitizations and coordinates. It was used to calculate occupancies. The second ntuple is filled for each charged Monte Carlo track with pT > 2 GeV/c and for each unmatched reconstructed track (i.e., each one without a Monte Carlo track assigned to it). The ntuple contains the Monte Carlo and reconstructed track vectors and is used to calculate efficiencies and resolutions.

Occupancies

Occupancies in the scintillating fiber system were obtained by dividing the number of digitized fibers by the total number of fibers in each superlayer. The silicon values were obtained in a similar way. Results are give in tables 1-3 for the Higgs events with and without the 10**33 background. The silcon occupancies are always well under a percent and the highest scifi occupancy is 3% in the innermost layer.

Efficiencies

Efficiencies were calculated using electrons and muons with pT > 5 GeV/c. There are 60 to 80 of each of these constructed tracks.e track-finding efficiency is defined as the fraction of these tracks which are assigned to one of the reconstructed tracks. This efficiency was 99 or 100% for the silicon alone for both electrons and muons. The track-finding efficiency for muons remains at 99% when the scintillating fibers are added but drops to 92% for the electrons.

The track-finding efficienry does not include any measure of how well the raconstructed tracks match up with the Monte Carlo tracks so we define a reconstruction efficiency for which we require the match chi-square to be less than 100. The match chi-square was defined in the reconstruction section.

With this addition, there is a small decrease in the muon efficiencies which still remain above 95% while the electron efficiencies drop significantly. We assume that the electron inefficiencies are due to bremsstrahlung and expect that much of the loss can be recovered by fitting with a special electron algorithm. This is justified because the electron track-finding efficiency for silicon alone is 99%.

Both track-finding and reconstruction efficiencies are presented in table 4. The efficiencies were not significantly different for the run with 10**33 background and these values are an average of the two. The number of false tracks, i.e. those not assigned to any Monte Carlo track varied from 0 to 2 in the different runs implying giving a false/true ratio of less than 0.01 above our track-finding momentum threshold of 5 GeV/c.

Resolutions

We have evaluated the resolution for various tracking parameters by looking at the difference between their reconstructed and Monte Carlo values. The event sample used for these includes all found leptons that passed the match chi-square criterion used to define the reconstruction efficiency. The resolutions quoted are the RMS deviations from zero for these differences. The mean values of the differences were always small compared to the resolution.

Resolutions for all following are given in table 5. The transverse momentum resolution dpT/pT**2 is calculated from the curvature. The xy direction of motion phi0 is measured at the origin or point of closest approach. The impact parameter r0 is the distance of closest approach in the r-phi plane. The dip angle tan(lambda) = dz/dxy is approximately dz/dr for stiff tracks. The resolution for the z-position of the vertex (z0) is also given. In addition to these parameters which are taken directly from the track vectors, we use the tan(lambda) resolution to estimate the z-resolution at the shower-max and muon systems. This is done by assuming

dz' = (r - rtmax) dtan(lambda)

where r is the radius of the shower-max or muon system (taken to be 250 and 600 cm, respectively) and rtmax is the outer radius of the tracking system taken to be 35 cm for the silicon alone and 165 for the combined system.

We note that the leptons used in this study have a spectrum that peaks around pT = 50 GeV/c with 30% of the tracks below the peak value. Consequently, multiple scattering still plays a significant role and the resolutions can be expected to improve for muons with higher momenta. For example, we find that the momentum resolution for single 4 TeV muons is 1.2 TeV/c corresponding to dpT/pT**2 = 0.08 -- a factor of two better than for the muons here.

Conclusions

We find that the proposed design for the silicon and scintillating fiber tracking systems is very efficient and easily meets the design requirements for the SDC at design luminosity over the rapidity range studied here. We plan to extend these studies to higher luminosities (3 and 10 times design) in the near future. We also expect to implement disk track-finding in TRF so that the full range of rapidity can be covered.

Fig. 1

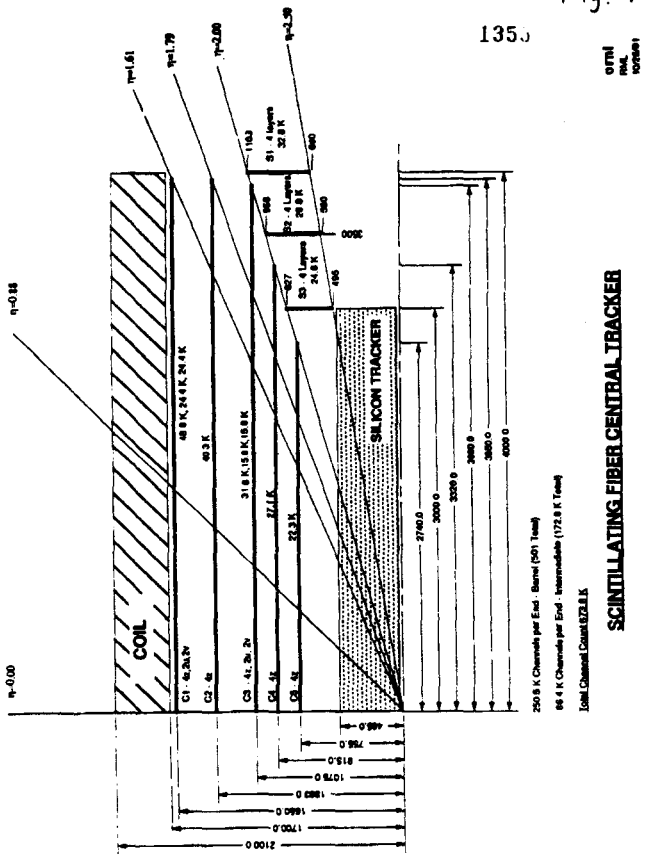

layer	radius (cm)	z max (cm)	eta max	# chan /side	occupancy L = 0	occupancy 10**33
1	9.0	15.0	1.3	58000	.00024	.00032
2	12.0	15.0	1.0	77000	.00032	.00044
3	18.0	18.0	0.9	69000	.00047	.00066
4	21.0	21.0	0.9	81000	.00053	.00073
5	24.0	24.0	0.9	122000	.00077	.00105
6	27.0	27.0	0.9	138000	.00085	.00107
7	33.0	33.0	0.9	211000	.00085	.00115
8	36.0	36.0	0.9	276000	.00132	.00180

Table 1. Silicon barrel geometry and occupancies. The dimensions of each barrel and the number of readout channels on each side of each barrel are listed. The occupancy is calculth Z --> e e, e muhe number of digitizetions by the number of channels. The occupancy is for H --> ZZ with Z --> e e, e mu or mu mu and a Higg's mass of 300 GeV. Occupancies are given for these events alone and these events superimposed on a minimum bias background at design luminosity (10**33 /cm**2/sec).

super layer	radius (cm)	z max (cm)	eta max	# fibers /layer	# fibers total	occupancy L = 0	occupancy 10**33
1	165.2	395.	1.6	11952	186000	.0028	.0045
2	135.3	395.	1.8	9792	78000	.0055	.0085
3	107.4	395.	2.0	7776	62000	.0097	.0159
4	91.5	390.	2.0	6624	53000	.0122	.0216
5	75.5	274.	2.0	5472	44000	.0166	.0295

Table 2. Scifi barrel geometry and occupancies. The number of fibers in an axial layer and the total number in the superlayer (two ends and four or eight layers) are given. Occupancies are calculated as the number of hit fibers divided by the number of fibers in a superlayer. The events used are the same as in table 1.

super layer	z (cm)	r (cm) min	r (cm) max	eta min	eta max	# fibers /layer	# fibers total	occupancy L = 0	occupancy 10**33
1	400.0	66.0	110.3	2.0	2.5	4767	38000	.0034	.0064
2	350.0	58.0	96.6	2.0	2.5	4189	34000	.0041	.0084
3	300.0	49.5	82.7	2.0	2.5	3575	29000	.0038	.0093

Table 3. Scifi intermediate geometry and occupancies. The number of fibers in a layer and the total number in the disks on both ends are given. The occupancies are calculated in the same way as table 2 and the events are those described in table 1.

	Track-finding		Reconstruction	
	e	mu	e	mu
Si alone	0.99	1.00	0.94	1.00
Si + Scifi	0.92	0.99	0.70	0.97

Table 4. Track finding and track reconstruction efficiencies for electrons and muons in the silicon alone and silicon with scintillating fibers.

		Resolution		
particle			Si	Si + Scifi
dpT/pt**2 (/TeV/c)	w/rvc	e	1.1	0.35
		mu	0.8	0.16
	w/o rvc	e	2.3	0.41
		mu	1.6	0.16
phi0 (rad)	w/rvc	e	0.00007	0.00005
		mu	0.00006	0.00003
	w/o rvc	e	0.00027	0.00009
		mu	0.00021	0.00007
r0 (mm)	w/o rvc	e	0.027	0.013
		mu	0.022	0.012
tan(lambda)		both	0.011	0.0007
z0 (mm)		both	2.6	1.1
z-showermax (mm)		both	24.	1.
z-muon (mm)		both	62.	3.

Table 5. Resolutions for various track parameters calculated as the RMS difference between reconstructed and Monte Carlo values. Moments are evaluated with and without a radial vertex constraint (rvc). The last two parameters (z-showermax and z-muon) are not evaluated directly but are estimated from tan(lambda). See the text for details.

Refsrences

1. Letter of Intent by the Solenoidal Detector Collaboration, SSCL, Nov 1990.

2. Outer Tracker Conceptual Design Scintillating Fiber Option, Nov 1991.

3. SHELL_USERS_GUIDE.DOC in the SDCSIM documentation area presently in SSCVX1::USER5:[SDCSHELL.V03.DOC].

Appendicas

A. Higgs event generation file used with SE/Isajet

B. Background event generation file used with SE/Pythia

C. ST geometry description file st_descope3a.kumac

D. SF geometry description file sf_optc5.dat

Appendix A

```
HIGGS DECAY TO Z PAIRS
40000,1000,0,0/
HIGGS
HMASS
300/
QMH
250,400/
JETTYPE1
'Z0'/
JETTYPE2
'Z0'/
WMODE1
'E+','E-'/
WMODE2
'MU+','MU-'/
PT
50,20000,50,20000/
END
STOP
```

Appendix B

```
*-------------------------------------------------------------------
*          -- PYTHIA Control Input Data --
*       Set P-P collider mode with Ecm = 40 TeV
*-------------------------------------------------------------------
*
LULIST = 1            ! Number of events to list by LULIST
*
FRAME = CMS           ! Frame is center-of-mass (Collider)
BEAM  = P             ! Beam is proton
TARGET= P             ! Target is proton
WIN   = 40000.        ! incident energy Ecm=2*Ebeam is 4 TeV
*
LUGIVE:MDCY(C111,1)=0   ! make pi0       stable
LUGIVE:MDCY(C310,1)=0   ! make Ks        stable
LUGIVE:MDCY(C3112,1)=0  ! make sigma+    stable
LUGIVE:MDCY(C3122,1)=0  ! make sigma-    stable
LUGIVE:MDCY(C3222,1)=0  ! make lambda0   stable
LUGIVE:MDCY(C3312,1)=0  ! make Xi0       stable
LUGIVE:MDCY(C3322,1)=0  ! make Xi-       stable
LUGIVE:MDCY(C3334,1)=0  ! make omega0    stable
*
LUGIVE:PMAS(6,1)=150.   ! Set top quark mass to 150 GeV
LUGIVE:PMAS(25,1)=400.  ! Set Higgs mass      to 400 GeV
*
PYGIVE:MSEL=1           ! Set event type by MSEL to QCD inelastic
*PYGIVE:MSEL=16         ! Set event type by MSEL to Higgs production
*
END
```

Appendix C

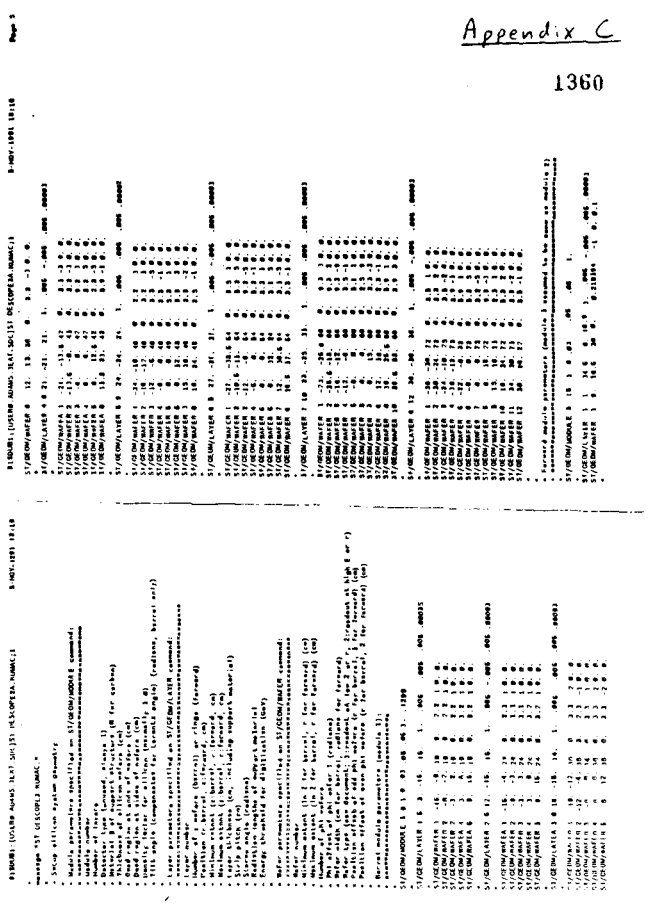

```
$1$DUB1:[USER0.ADAMS.TEXT.SDC]SF_OPTC6.DAT;1          8-NOV-1991 16:20

136.69, 136.86, 0.76, 0.00000      ; r0 , r, offset, stereo slope (rad/cm)
;
; **************** C3 ****************
;
cylinder                        ; volume shape
107.42 107.94 196                 ; min radius, max radius, length (cm)
0. 0. 190.0                     ; location of center of cylinder
4                               ; number of fiber layers
1, 1                               ; fiber shape, readout
0.007, 0.003, 0.0                   ; fiber spacing (cm), width (cm), not used
107.67, 107.57, 0.00, 0.00000       ; r0 , r, offset, stereo slope (rad/cm)
1, 1                               ; fiber shape, readout
0.007, 0.003, 0.0                   ; fiber spacing (cm), width (cm), not used
107.67, 107.76, 0.50, 0.00000       ; r0 , r, offset, stereo slope (rad/cm)
1, 1                               ; fiber shape, readout
0.007, 0.003, 0.0                   ; fiber spacing (cm), width (cm), not used
107.67, 107.86, 0.25, 0.00000       ; r0 , r, offset, stereo slope (rad/cm)
1, 1                               ; fiber shape, readout
0.007, 0.003, 0.0                   ; fiber spacing (cm), width (cm), not used
107.67, 107.61, 0.75, 0.00000       ; r0 , r, offset, stereo slope (rad/cm)
;
cylinder                        ; volume shape
107.47 107.98 196                 ; min radius, max radius, length (cm)
0. 0. 190.0                     ; location of center of cylinder
4                               ; number of fiber layers
1, 1                               ; fiber shape, readout
0.007, 0.003, 0.0                   ; fiber spacing (cm), width (cm), not used
107.67, 107.67, 0.00, 0.00000       ; r0 , r, offset, stereo slope (rad/cm)
1, 1                               ; fiber shape, readout
0.007, 0.003, 0.0                   ; fiber spacing (cm), width (cm), not used
107.97, 107.76, 0.50, 0.00000       ; r0 , r, offset, stereo slope (rad/cm)
1, 1                               ; fiber shape, readout
0.007, 0.005, 0.0                   ; fiber spacing (cm), width (cm), not used
107.87, 107.95, 0.25, 0.00000       ; r0 , r, offset, stereo slope (rad/cm)
1, 1                               ; fiber shape, readout
0.007, 0.003, 0.0                   ; fiber spacing (cm), width (cm), not used
107.67, 107.83, 0.75, 0.00000       ; r0 , r, offset, stereo slope (rad/cm)
;
; **************** C4 ****************
;
cylinder                        ; volume shape
91.47, 92.01, 332.0               ; min radius, max radius, length (cm)
0. 0. -180.0                    ; location of center of cylinder
4                               ; number of fiber layers
1, 1                               ; fiber shape, readout
0.007, 0.003, 0.0                   ; fiber spacing (cm), width (cm), not used
91.72, 91.72, 0.00, 0.00000         ; r0 , r, offset, stereo slope (rad/cm)
1, 1                               ; fiber shape, readout
0.007, 0.003, 0.0                   ; fiber spacing (cm), width (cm), not used
91.72, 91.80, 0.50, 0.00000         ; r0 , r, offset, stereo slope (rad/cm)
1, 1                               ; fiber shape, readout
0.007, 0.003, 0.0                   ; fiber spacing (cm), width (cm), not used
91.72, 91.80, 0.25, 0.00000         ; r0 , r, offset, stereo slope (rad/cm)
1, 1                               ; fiber shape, readout
0.007, 0.003, 0.0                   ; fiber spacing (cm), width (cm), not used
91.72, 91.94, 0.75, 0.00000         ; r0 , r, offset, stereo slope (rad/cm)
;
cylinder                        ; volume shape
91.47, 92.01, 332.0               ; min radius, max radius, length (cm)
0. 0. 180.0                     ; location of center of cylinder
4                               ; number of fiber layers
1, 1                               ; fiber shape, readout
0.007, 0.003, 0.0                   ; fiber spacing (cm), width (cm), not used
91.72, 91.72, 0.00, 0.00000         ; r0 , r, offset, stereo slope (rad/cm)
1, 1                               ; fiber shape, readout
0.007, 0.003, 0.0                   ; fiber spacing (cm), width (cm), not used
91.72, 91.80, 0.50, 0.00000         ; r0 , r, offset, stereo slope (rad/cm)
1, 1                               ; fiber shape, readout
0.007, 0.003, 0.0                   ; fiber spacing (cm), width (cm), not used
91.72, 91.94, 0.26, 0.00000         ; r0 , r, offset, stereo slope (rad/cm)
```

```
$1$DUB1:[USER0.ADAMS.TEXT.SDC]SF_OPTC6.DAT;1          8-NOV-1991 16:20

1, 1                               ; fiber shape, readout
0.007, 0.003, 0.0                   ; fiber spacing (cm), width (cm), not used
91.72, 91.90, 0.75, 0.00000         ; r0 , r, offset, stereo slope (rad/cm)
;
; **************** C5 ****************
;
cylinder                        ; volume shape
76.62, 79.00, 274.0               ; min radius, max radius, length (cm)
0. 0. -137.0                    ; location of center of cylinder
4                               ; number of fiber layers
1, 1                               ; fiber shape, readout
0.007, 0.003, 0.0                   ; fiber spacing (cm), width (cm), not used
76.77, 76.77, 0.00, 0.00000         ; r0 , r, offset, stereo slope (rad/cm)
1, 1                               ; fiber shape, readout
0.007, 0.003, 0.0                   ; fiber spacing (cm), width (cm), not used
76.77, 76.86, 0.50, 0.00000         ; r0 , r, offset, stereo slope (rad/cm)
1, 1                               ; fiber shape, readout
0.007, 0.003, 0.0                   ; fiber spacing (cm), width (cm), not used
76.77, 76.96, 0.35, 0.00000         ; r0 , r, offset, stereo slope (rad/cm)
1, 1                               ; fiber shape, readout
0.007, 0.003, 0.0                   ; fiber spacing (cm), width (cm), not used
76.77, 79.02, 0.75, 0.00000         ; r0 , r, offset, stereo slope (rad/cm)
;
cylinder                        ; volume shape
76.63, 78.90, 274.0               ; min radius, max radius, length (cm)
0. 0. 137.0                     ; location of center of cylinder
4                               ; number of fiber layers
1, 1                               ; fiber shape, readout
0.007, 0.003, 0.0                   ; fiber spacing (cm), width (cm), not used
76.77, 76.77, 0.00, 0.00000         ; r0 , r, offset, stereo slope (rad/cm)
1, 1                               ; fiber shape, readout
0.007, 0.003, 0.0                   ; fiber spacing (cm), width (cm), not used
76.77, 76.86, 0.50, 0.00000         ; r0 , r, offset, stereo slope (rad/cm)
1, 1                               ; fiber shape, readout
0.007, 0.005, 0.0                   ; fiber spacing (cm), width (cm), not used
76.77, 96.96, 0.35, 0.00000         ; r0 , r, offset, stereo slope (rad/cm)
1, 1                               ; fiber shape, readout
0.007, 0.003, 0.0                   ; fiber spacing (cm), width (cm), not used
76.77, 38.03, 0.35, 0.00000         ; r0 , r, offset, stereo slope (rad/cm)
;
; **************** S1 ****************
;
spiral
60.00 110.3 0.44               ; inner, outer radii, thickness
0.0 0.0 -400.00                ; x0, y0, z0
4                              ; number of layers
1 1                            ; fiber shape and readout
0.007, 0.003, 0.0              ; fiber spacing, width, not used
-0.17, 0.0, 60.00, 1           ; x, offset, r0, parity
1 1                            ; fiber shape and readout
0.007, 0.003, 0.0              ; fiber spacing, width, not used
-0.09, 0.5, 60.00, 1           ; x, offset, r0, parity
1 1                            ; fiber shape and readout
0.007, 0.003, 0.0              ; fiber spacing, width, not used
0.01, 0.0, 60.00, 1            ; x, offset, r0, parity
1 1                            ; fiber shape and readout
0.007, 0.003, 0.0              ; fiber spacing, width, not used
0.09, 0.5, 60.00, 1            ; x, offset, r0, parity
;
spiral
60.00 110.6 0.40               ; inner, outer radii, thickness
0.0 0.0 400.00                 ; x0, y0, z0
4                              ; number of layers
1 1                            ; fiber shape and readout
0.007, 0.003, 0.0              ; fiber spacing, width, not used
-0.17, 0.0, 60.00, 1           ; x, offset, r0, parity
1 1                            ; fiber shape and readout
0.007, 0.003, 0.0              ; fiber spacing, width, not used
-0.09, 0.5, 60.00, 1           ; x, offset, r0, parity
1 1                            ; fiber shape and readout
```

1363

```
$1$DUB1:[USER0.ADAMS.TEXT.SDC]ST_DESCOPE1A.KUMAC;1          8-NOV-1991 16:10

ST/GEOM/LAYER  2 2   14.5   9 14.5 1   .005   .005  .005 .00003
ST/GEOM/WAFER  1 A   10.5   30 0       0.186841  -2 0 0.1
ST/GEOM/WAFER  2 14.5 19.1  30 0       0.186841  -1 0. 0.1
*
ST/GEOM/LAYER  3 8   26.5   9 26.5 1   .005  -.005  .005 .00003
ST/GEOM/WAFER  1 4   16.A   30 0       0.214194  -1 .2 -.1
ST/GEOM/WAFER  2 16.5 21.A  40 0       0.141901  -2 0 0.1
ST/GEOM/WAFER  3 21.5 26.5  40 0       0.141901  -1 0 0.1
*
ST/GEOM/LAYER  4 4   31.5   9 31.5 1   .005   .005  .005 .00003
ST/GEOM/WAFER  1 9   16.5   20 0       0.186841  -2 .2 -.1
ST/GEOM/WAFER  2 16.5 19.5  30 0       0.186841  -1 -.2 -.1
ST/GEOM/WAFER  3 16.5 26.5  40 0       0.114421  -2 0 0.1
ST/GEOM/WAFER  4 26.5 31.5  60 0       0.114021  -1 0 0.1
*
* slight edge gap wafers 1,2
*
ST/GEOM/LAYER  5 4   38.0  15. 38.0 1.  .005  -.005  .005 .00003
ST/GEOM/WAFER  1 16  21.0  40 0.      0.1340741  -3 -.2 -.1
ST/GEOM/WAFER  2 21  27.0  40 0.      0.1340741  -1 -.2 -.1
ST/GEOM/WAFER  3 21. 33.0  72 0.      0.0020206  -2 0. 0.1
ST/GEOM/WAFER  4 33  29.0  72 0.      0.0020206  -1 0. 0.1
*
ST/GEOM/LAYER  6 8   40.0  15. 38.0 1.  .005   .005  .005 .00003
ST/GEOM/WAFER  1 16  21.0  40 0.      0.1340741  -2 -.2 -.1
ST/GEOM/WAFER  2 21  27.0  40 0.      0.1340741  -1 -.3 -.1
ST/GEOM/WAFER  3 21  33.0  72 0.      0.0020206  -2 0. 0.1
ST/GEOM/WAFER  4 33. 30.0  72 0.      0.0020300  -1 0. 0.1
*
ST/GEOM/LAYER  7 4   56.0  15. 38.0 1.  .005  -.005  .005 .00003
ST/GEOM/WAFER  1 16  21.0  70 0.      0.1340741  -2 -.2 -.1
ST/GEOM/WAFER  2 21. 27.0  40 0.      0.1340741  -3 -.3 -.5
ST/GEOM/WAFER  3 27. 33.0  72 0.      0.0020206  -2 0. 0.1
ST/GEOM/WAFER  4 33. 20.0  32 0.      0.0020306  -1 0. 0.1
*
ST/GEOM/LAYER  8 4   80.0  15. 38.0 1.  .005   .005  .005 .00003
ST/GEOM/WAFER  1 16. 21.0  40 0.      0.1340741  -2 -.3 -.1
ST/GEOM/WAFER  2 21. 27.0  45 0.      0.1340741  -1 -.2 -.1
ST/GEOM/WAFER  3 27  33.0  72 0.      0.0020206  -2 0. 0.1
ST/GEOM/WAFER  4 53. 59.0  72 0.      0.0020306  -3 0. 0.1
*
ST/GEOM/LAYER  9 4   77.0  15 38.0 1.   .005  -.005  .005 .00005
ST/GEOM/WAFER  1 16. 21.0  45 0.      0.1340741  -2 -.3 -.1
ST/GEOM/WAFER  2 31. 27.0  45 0.      0.1140741  -1 -.2 -.1
ST/GEOM/WAFER  3 27. 31.0  72 0.      0.0020206  -3 0. 0.1
ST/GEOM/WAFER  4 35. 29.0  72 0.      0.0030206  -1 0. 0.1
*
ST/GEOM/LAYER 10 4   81.0  15. 38.0 1.  .005   .005  .005 .00003
ST/GEOM/WAFER  1 16  21.0  40 0.      0.1340741  -2 -.2 -.1
ST/GEOM/WAFER  2 21  27.0  40 0.      0.1340741  -1 -.2 -.1
ST/GEOM/WAFER  3 27  33.0  72 0       0.0020206  -2 0 0.1
ST/GEOM/WAFER  4 43. 56.0  72 0       0.0030206  -1 0. 0.1
*
ST/GEOM/LAYER 11 4  110.0  15. 88.0 1.  .005  -.005  .005 .00003
ST/GEOM/WAFER  1 16  21.0  40 0       0.1340741  -2 -.2 -.1
ST/GEOM/WAFER  2 21. 27.0  40 0.      0.1340741  -1 -.3 -.1
ST/GEOM/WAFER  3 27  33.0  72 0.      0.0020206  -2 0. 0.1
ST/GEOM/WAFER  4 33. 30.0  72 0.      0.0010306  -1 0. 0.1
*
ST/GEOM/LAYER 12 4  130.0  22.5 40.5 1. .005   .005  .005 .00003
ST/GEOM/WAFER  1 22.5 28.5  66 0      0.1049277  -2 -.2 -.1
ST/GEOM/WAFER  2 28.5 2c.5  60 0      0.1049236  -1 .2 -.1
ST/GEOM/WAFER  3 34.5 40.5  90 0      0.0770406  -2 0. 0.1
ST/GEOM/WAFER  4 40.5 46.5  64 0      0.0770406  -1 0. 0.1
*
ST/GEOM/LAYER 13 4  150.0  22.5 40.5 1. .005  -.005  .005 .00003
ST/GEOM/WAFER  1 22.5 28.5  70 0.     0.1049276  -1 -.2 -.1
ST/GEOM/WAFER  2 28.5 34.5  30 0.     0.1049276  -1 -.2 -.1
ST/GEOM/WAFER  3 34.5 40.0  40 0      0.0770406  -3 0. 0.1
ST/GEOM/WAFER  4 40.5 40.5  40 0.     0.0770406  -1 0. 0.1
```

```
$1$DUB1:[USER0.ADAMS.TEXT.SDC]ST_DESCOPE1A.KUMAC;1          8-NOV-1991 16:10

*
ST/GEOM/LAYER 14 2  200.0  64.5 40.5 1  .005   .005  .005 .00002
ST/GEOM/WAFER  1 34.5 40.5  40 0      0.0770405   2 0 0.1
ST/GEOM/WAFER  2 40.5 46.5  40 0      0.0770406   1 0 0.1
*
ST/GEOM/LAYER 16 2  200.0  64.5 40.5 1  .005  -.005  .005 .00005
ST/GEOM/WAFER  1 34.0 40.5  45 0      0.0770406   2 0 0.1
ST/GEOM/WAFER  2 40.5 40.5  45 0      0.0770406  -1 0 0.1
```

136[illegible]

```
$1$DUB1:[USER0.ADAMS.TEXT.SDC]SF_OPTC6.DAT;1          8-NOV-1991 16:20

0.007, 0.003, 0.0              ; fiber spacing, width, not used
0.05, 0.0, 60.00, 1            ; x, offset, r0, parity
1 1                            ; fiber shape and readout
0.007, 0.003, 0.0              ; fiber spacing, width, not used
0.09, 0.5, 60.00, 1            ; x, offset, r0, parity
;
; **************** S2 ****************
;
spiral
60.00 90.0 0.44                ; inner, outer radii, thickness
0.0 0.0 -360.00                ; x0, y0, z0
4                              ; number of layers
1 1                            ; fiber shape and readout
0.007, 0.003, 0.0              ; fiber spacing, width, not used
-0.17, 0.0, 67.00, 1           ; x, offset, r0, parity
1 1                            ; fiber shape and readout
0.007, 0.003, 0.0              ; fiber spacing, width, not used
-0.09, 0.5, 67.00, 1           ; x, offset, r0, parity
1 1                            ; fiber shape and readout
0.007, 0.003, 0.0              ; fiber spacing, width, not used
0.01, 0.0, 67.00, 1            ; x, offset, r0, parity
1 1                            ; fiber shape and readout
0.007, 0.003, 0.0              ; fiber spacing, width, not used
0.05, 0.5, 67.00, 1            ; x, offset, r0, parity
;
spiral
60.00 90.0 0.44                ; inner, outer radii, thickness
0.0 0.0 360.00                 ; x0, y0, z0
4                              ; number of layers
1 1                            ; fiber shape and readout
0.007, 0.003, 0.0              ; fiber spacing, width, not used
-0.17, 0.0, 67.00, 1           ; x, offset, r0, parity
1 1                            ; fiber shape and readout
0.007, 0.003, 0.0              ; fiber spacing, width, not used
-0.09, 0.5, 67.00, 1           ; x, offset, r0, parity
1 1                            ; fiber shape and readout
0.007, 0.003, 0.0              ; fiber spacing, width, not used
0.01, 0.0, 67.00, 1            ; x, offset, r0, parity
1 1                            ; fiber shape and readout
0.007, 0.003, 0.0              ; fiber spacing, width, not used
0.09, 0.5, 67.00, 1            ; x, offset, r0, parity
;
; **************** S3 ****************
;
spiral
45.50 67.7 0.44                ; inner, outer radii, thickness
0.0 0.0 -300.00                ; x0, y0, z0
4                              ; number of layers
1 1                            ; fiber shape and readout
0.007, 0.002, 0.0              ; fiber spacing, width, not used
-0.17, 0.0, 49.50, 1           ; x, offset, r0, parity
1 1                            ; fiber shape and readout
0.007, 0.003, 0.0              ; fiber spacing, width, not used
-0.09, 0.5, 49.50, 1           ; x, offset, r0, parity
1 1                            ; fiber shape and readout
0.007, 0.003, 0.0              ; fiber spacing, width, not used
0.01, 0.0, 49.50, 1            ; x, offset, r0, parity
1 1                            ; fiber shape and readout
0.007, 0.003, 0.0              ; fiber spacing, width, not used
0.09, 0.5, 49.50, 1            ; x, offset, r0, parity
;
spiral
47.50 62.7 0.44                ; inner, outer radii, thickness
0.0 0.0 300.00                 ; x0, y0, z0
4                              ; number of layers
1 1                            ; fiber shape and readout
0.007, 0.003, 0.0              ; fiber spacing, width, not used
-0.17, 0.0, 49.50, 1           ; x, offset, r0, parity
1 1                            ; fiber shape and readout
0.007, 0.002, 0.0              ; fiber spacing, width, not used
```

```
$1$DUB1:[USER0.ADAMS.TEXT.SDC]SF_OPTC6.DAT;1          8-NOV-1991 16:20

-0.09, 0.5, 40.50, 1           ; x, offset, r0, parity
1 1                            ; fiber shape and readout
0.007, 0.003, 0.0              ; fiber spacing, width, not used
0.01, 0.0, 49.50, 1            ; x, offset, r0, parity
1 1                            ; fiber shape and readout
0.007, 0.003, 0.0              ; fiber spacing, width, not used
0.09, 0.5, 49.50, 1            ; x, offset, r0, parity
;
```

1364

```
$1$DUB1:[USER0.ADAMS.TEXT.SDC]SF_OPTC6.DAT;1          8-NOV-1991 16:20          Page 1

                                  SF.DAT

; 8-NOV-91 dla - The previous version of this file was bad. A mistake in the
;           light propagation speed and no fiber digitizations
; 13-OCT-91 dla - modify digitization parameters -- I decreased the light output
;           and fixed the timing so that we no longer lose 0.5 ns on the
;           fast end
; 10-OCT-91 dla - Fix fiber spacing in C2 to be 0.007 instead of 0.009
; Created 20 OCT 91 dla.
;
;     Describes FTC option C as circulated by D. Kaltick. See Figure in
; HA log II-43. Layer spacings are on 31-10.
;     Modified to reflect new drawings circulated 30OCT91. See drawing and
; layer positions on 32-40.
;
;     Contains a description of a scintillating fiber tracking detector for
; use with SSC simulations. A series of volumes are defined by giving a name
; for the shape and then the size, position and orientation.
; The units are cm and radians.
;
; The line beginning with 'digit' is followed with two lines setting the
; parameters used in the digitization:
; FNDTIM  DGOTIM  DGTOFF  DGTRID
; PHNUFY  FINTER  ATTLEN  ATTOPT  QUANEF  VSIG
; The signal is DGTRID ns wide and is sampled FNDTIM times at intervals of
; DGOTIM ns starting at time DGTOFF. The other parameters are:
; PHNUFY = # photons produced in one cm of fiber per GeV of energy deposit
; FINTER = fraction of photons internally reflected = 1 - cos(thtint)
; ATTLEN = attenuation length in the scintillating fiber
; ATTOPT = attenuation in optical fiber and couplings
; QUANEF = quantum efficiency of the photodetector
; VSIG = speed of the signal in the fiber (cm/s)
; Defaults are provided if these lines are missing; they are:
; 1       10.0    39.0    10.0
; 1.e7    0.030   1000.0  0.5     0.0     20.e9
; The following parameters give 10.2 photons at the near end of a fiber and
; <.5 at 4 meters. The timing is set to accept all prompt particles and has
; 6 ns of slop on the slow end.
digitization parameters
1         10.0    31.0    22.0                    ; see log 31-40
9.5e7     0.030   600.0   0.5     0.0    30.0E9   ; see 31-40
;
mother                          ; description of mother volume
170.0, 420.0                    ; outer radius and half-length
;
; ************ C1 ************
;
cylinder                        ; volume shape
106.24 108.18 386.                ; min radius, max radius, length (cm)
0  0  -107.5                    ; location of center of cylinder
8                               ; number of fiber layers
1, -1                              ; fiber shape, readout
0.007, 0.003, 0.0                   ; fiber spacing (cm), width (cm), not used
105.49, 106.49, 0.00, 0.00000       ; r0 , r, offset, stereo slope (rad/cm)
1, 1                               ; fiber shape, readout
0.007, 0.007, 0.0                   ; fiber spacing (cm), width (cm), not used
105.49, 106.67, 0.50, 0.00000       ; r0 , r, offset, stereo slope (rad/cm)
1, -1                              ; fiber shape, readout
0.007, 0.002, 0.0                   ; fiber spacing (cm), width (cm), not used
106.4A, 106.67, 0.35, 0.00000       ; r0 , r, offset, stereo slope (rad/cm)
1, -1                              ; fiber shape, readout
0.007, 0.003, 0.0                   ; fiber spacing (cm), width (cm), not used
106.49, 106.76, 0.76, 0.00000       ; r0 , r, offset, stereo slope (rad/cm)
1, 1                               ; fiber shape, readout
0.007, 0.003, 0.0                   ; fiber spacing (cm), width (cm), not used
106.A6, 106.86, 0.00, 0.00101       ; r0 , r, offset, stereo slope (rad/cm)
1, 1                               ; fiber shape, readout
0.007, 0.003, 0.0                   ; fiber spacing (cm), width (cm), not used
106.86, 106.83, 0.56, 0.00101       ; r0 , r, offset, stereo slope (rad/cm)
```

```
$1$DUB1:[USER0.ADAMS.TEXT.SDC]SF_OPTC6.DAT;1          8-NOV-1991 16:20

0.007, 0.003, 0.0                   ; fiber spacing (cm), width (cm), not used
100.03, 100.02, 0.00,-0.00101       ; r0 , r, offset, stereo slope (rad/cm)
1, -1                              ; fiber shape, readout
0.007, 0.003, 0.0                   ; fiber spacing (cm), width (cm), not used
100.03, 1A0.11, 0.50,-0.00101       ; r0 , r, offset, stereo slope (rad/cm)
;
;
cylinder                        ; volume shape
106.24 108.18 386.                ; min radius, max radius, length (cm)
0. 0. 107.5                     ; location of center of cylinder
8                               ; number of fiber layers
1, 1                               ; fiber shape, readout
0.007, 0.003, 0.0                   ; fiber spacing (cm), width (cm), not used
106.40, 106.40, 0.00, 0.00000       ; r0 , r, offset, stereo slope (rad/cm)
1, 1                               ; fiber shape, readout
0.007, 0.007, 0.0                   ; fiber spacing (cm), width (cm), not used
106.4A, 106.67, 0.00, 0.00000       ; r0 , r, offset, stereo slope (rad/cm)
1, 1                               ; fiber shape, readout
0.007, 0.002, 0.0                   ; fiber spacing (cm), width (cm), not used
106.49, 106.67, 0.22, 0.00000       ; r0 , r, offset, stereo slope (rad/cm)
1, 1                               ; fiber shape, readout
0.007, 0.005, 0.0                   ; fiber spacing (cm), width (cm), not used
106.49, 106.76, 0.75, 0.00000       ; r0 , r, offset, stereo slope (rad/cm)
1, 1                               ; fiber shape, readout
0.007, 0.003, 0.0                   ; fiber spacing (cm), width (cm), not used
106.66, 106.86, 0.00, 0.00101       ; r0 , r, offset, stereo slope (rad/cm)
1, 1                               ; fiber shape, readout
0.007, 0.007, 0.0                   ; fiber spacing (cm), width (cm), not used
106.66, 106.83, 0.60, 0.00101       ; r0 , r, offset, stereo slope (rad/cm)
1, 1                               ; fiber shape, readout
0.007, 0.003, 0.0                   ; fiber spacing (cm), width (cm), not used
100.03, 100.03, 0.00,-0.00101       ; r0 , r, offset, stereo slope (rad/cm)
1, 1                               ; fiber shape, readout
0.007, 0.002, 0.0                   ; fiber spacing (cm), width (cm), not used
100.03, 100.11, 0.50,-0.00101       ; r0 , r, offset, stereo slope (rad/cm)
;
; **************** C2 ****************
;
cylinder                        ; volume shape
133.34 136.90 386.                ; min radius, max radius, length (cm)
0. 0. -107.5                    ; location of center of cylinder
8                               ; number of fiber layers
1, -1                              ; fiber shape, readout
0.007, 0.951, 0.0                   ; fiber spacing (cm), width (cm), not used
133.58, 136.60, 0.00, 0.00000       ; r0 , r, offset, stereo slope (rad/cm)
1, -5                              ; fiber shape, readout
0.007, 0.005, 0.0                   ; fiber spacing (cm), width (cm), not used
133.58, 136.07, 0.50, 0.00000       ; r0 , r, offset, stereo slope (rad/cm)
1, -1                              ; fiber shape, readout
0.007, 0.005, 0.0                   ; fiber spacing (cm), width (cm), not used
133.58, 133.77, 0.25, 0.00000       ; r0 , r, offset, stereo slope (rad/cm)
1, -1                              ; fiber shape, readout
0.007, 0.003, 0.0                   ; fiber spacing (cm), width (cm), not used
133.58, 133.86, 0.75, 0.00000       ; r0 , r, offset, stereo slope (rad/cm)
;
cylinder                        ; volume shape
136.34 136.90 386.                ; min radius, max radius, length (cm)
0. 0. 107.5                     ; location of center of cylinder
8                               ; number of fiber layers
1, 1                               ; fiber shape, readout
0.007, 0.007, 0.0                   ; fiber spacing (cm), width (cm), not used
136.60, 136.70, 0.00, 0.00000       ; r0 , r, offset, stereo slope (rad/cm)
1, 1                               ; fiber shape, readout
0.007, 0.003, 0.0                   ; fiber spacing (cm), width (cm), not used
136.60, 133.67, 0.50, 0.00000       ; r0 , r, offset, stereo slope (rad/cm)
1, 1                               ; fiber shape, readout
0.007, 0.004, 0.0                   ; fiber spacing (cm), width (cm), not used
136.60, 133.77, 0.22, 0.00000       ; r0 , r, offset, stereo slope (rad/cm)
1, 1                               ; fiber shape, readout
```

1362

Appendix D

APPENDIX

LIST OF PARTICIPANTS

LAST NAME	FIRST NAME	INSTITUTION
Adams	David L.	Rice University
Amendolia	Salvator Roberto	INFN-Pisa
Arai	Yasuo	Nat'l Lab. for High Energy Physics (KEK)
Armitage	John	Carleton University
Atac	Muzaffer	University of California - Los Angeles
Avery	Paul R.	University of Florida
Ball	Robert C.	University of Michigan
Barasch	Gene	Texas A&M University
Barnes	Virgil E.	Purdue University
Barnett	R. Michael	Lawrence Berkeley Laboratory
Bartaszek	Larry	Fermilab
Baumbaugh	Alan	Fermilab
Bautz	Pat	Lawrence Berkeley Laboratory
Bellettini	Giorgio	INFN-Pisa
Bensinger	James R.	Brandeis University
Beuville	Eric	CEN-Saclay
Barder	Peter	University of Minnesota
Brissan	Jean Claude	CEN-Saclay
Campbell	Myran	University of Michigan
Carden	Martyn J.	Florida State University
Dainton	John	University of Liverpool
Davissan	Richard	University of Washington
Dougherty	William M.	University of Washington
Durkin	L. Stanley	Ohio State University
Edwards	Michael	Rutherford Appletan Laboratory

LAST NAME	FIRST NAME	INSTITUTION
Einsweiler	Kevin	Lawrence Berkeley Laboratory
Elias	John E.	Fermilab
Emwein	Jean	CEN-Saclay
Feldman	Gary	Harvard University
Ford	William T.	University of Colorado
Frisken	William R.	Lawrence Berkeley Laboratory
Gabriel	Tony A.	Oak Ridge National Laboratory
Gachelin	Olivier	CEN-Saclay
Gaines	Irwin	Fermilab
Gilchriese	Murdock G. D.	Lawrence Berkeley Laboratory
Goshaw	Alfred T.	Duke University
Gourlay	Stephen A.	Fermilab
Green	Dan	Fermilab
Groom	Donald E.	Lawrence Berkeley Laboratory
Hagopian	Vasken	Florida State University
Handler	Thomas	University of Tennessee
Hansan	Gail G.	Indiana University
Hearty	Christopher	Lawrence Berkeley Laboratory
Hill	Norman	Argonne National Laboratory
Hubbard	Bradley	University of California - Santa Cruz
Hubbard	Richard	CEN-Saclay
Inzani	Pierino	INFN-Milano
Iwasaki	Hirayuki	Nat'l Lab. for High Energy Physics (KEK)
Job	Panakkal	Argonne National Laboratory
Kadyk	John A.	Lawrence Berkeley Laboratory

LAST NAME	FIRST NAME	INSTITUTION
Kephart	Robert D.	Fermilab
Kirk	Thomas	Argonne National Laboratory
Kaltick	David S.	Purdue University
Konda	Takahika	Nat'l Lab. for High Energy Physics (KEK)
Lankford	Andrew J.	University of California - Irvine
Larson	Eric T.	Fermilab
LeDû	Patrick	CEN-Saclay
Leitch	Robert M.	Oak Ridge National Laboratory
Levi	Michael	Lawrence Berkeley Laboratory
Lewis	Raymond A.	Pennsylvania State University
Ling	Ta-Yung	Ohio State University
Luehring	Fred	Indiana University
Lyndon	Chris	Louisiana State University
Maki	Akihiro	Nat'l Lab. for High Energy Physics (KEK)
Mantsch	Paul M.	Fermilab
May	Edward	Argonne National Laboratory
Miettinen	Hannu I.	Rice University
Ma	Luke W.	Virginia Polytechnic Institute
Mari	Shigeki	University of Tsukuba
Marani	Luigi	INFN-Milano
Nadulman	Larry	Argonne National Laboratory
Oakham	F. Gerald	Carleton University
Odaka	Shigeru	Nat'l Lab. for High Energy Physics (KEK)
Ogren	Harold	Indiana University
Ohska	Takio	Nat'l Lab. for High Energy Physics (KEK)

LAST NAME	FIRST NAME	INSTITUTION
Ohsugi	Takashi	Hiroshima University
Orr	Robert S.	University of Toronto
Palounek	Andrea	Los Alamos National Laboratory
Partridge	Richard	Brown University
Pedrini	Daniele	INFN-Milano
Pellett	David E.	University of California - Davis
Painsignan	Jean	CEN-Saclay
Pope	William L.	Lawrence Berkeley Laboratory
Price	Lawrence E.	Argonne National Laboratory
Proudfoot	James	Argonne National Laboratory
Rouse	Forest	University of California - Davis
Ruchti	Randy	University of Notre Dame
Rusack	Roger W.	Rockefeller University
Rust	David	Indiana University
Sadrazinski	Hartmut	University of California - Santa Cruz
Sakamata	Hirashi	Nat'l Lab. for High Energy Physics (KEK)
Sala	Silvina	INFN-Milano
Seiden	Abraham	University of California - Santa Cruz
Sill	Alan F.	University of Rochester
Siratenka	Vladimir	Northern Illinois University
Skubic	Patrick L.	University of Oklahoma
Skuja	Andris	University of Maryland
Smith	Wesley H.	University of Wisconsin
Takikawa	Koji	University of Tsukuba
Taras	Paul	Universities de Montreal

LAST NAME	FIRST NAME	INSTITUTION
Terada	Susumu	Nat'l Lab. for High Energy Physics (KEK)
Trilling	George H.	Lawrence Berkeley Laboratory
Trost	Hans-Jochen	Argonne National Laboratory
Vidal	Richard A.	Fermilab
Weinstein	Alan J.	California Inst. of Technology
Williams	Hugh H. (Brig)	University of Pennsylvania
Willis	Suzanne	Northern Illinois University
Wiss	James E.	University of Illinois, Urbana-Champaign
Womble	Ed	Draper Laboratory
Yaussef	Saul	Florida State University
Zhao	Tianchi	University of Washington
Ziock	Hans-Joachim	Los Alamos National Laboratory

LAST NAME	FIRST NAME	INSTITUTION
Dunn	William	Quantum Research Services, Inc.
Elam	Anthony J	IBM Federal Systems
Ennis	Robert	IBM
Flyckt	Esso	Philips International
Kubena	Glenn T.	IBM
Liao	Kenneth	IBM Corp.
Shaffer	Howard	Westinghouse Science & Technology Center
Swensrud	Roger L.	Westinghouse Electric Corporation

LAST NAME	FIRST NAME	INSTITUTION
Adams	Thomas	SSC Laboratory
Bird	Fred	SSC Laboratory
Coupal	David	SSC Laboratory
Frederikson	Soren	SSC Laboratory
Fry	Alan	SSC Laboratory
Henderson	Peggy	SSC Laboratory
Lubatti	Henry	SSC Laboratory
Roe	Byron	SSC Laboratory
Siegrist	James	SSC Laboratory
Thurston	Timothy A.	SSC Laboratory
Turcatte	Marc	SSC Laboratory
Western	Jeffrey	SSC Laboratory